SOVIET PHYSICS

JETP

*A translation of Zhurnal Éksperimental'noĭ i Teoreticheskoĭ Fiziki.*

Vol. 11, No. 5, pp. 981-1193 (Russ. orig. Vol. 38, No. 5, pp. 1361-1656, May, 1969) Nov.,1960

# *ENERGY SPECTRA OF THE ELECTRON-PHOTON COMPONENT IN EXTENSIVE ATMOSPHERIC SHOWERS NEAR THE SHOWER AXIS*

O. I. DOVZHENKO, S. I. NIKOL'SKIĬ, and I. V. RAKOBOL'SKAYA

P. N. Lebedev Physics Institute, Academy of Sciences, U.S.S.R.

Submitted to JETP editor December 18, 1959

J. Exptl. Theoret. Phys. (U.S.S.R.) **38**, 1361-1369 (May, 1960)

A cloud chamber with lead plates was employed to investigate the electron-photon component of extensive atmospheric showers at sea level. Showers containing on the average $8 \times 10^3$, $1.2 \times 10^4$, and $3 \times 10^4$ particles and passing at distances of $0-3$ m from the chamber were selected. Energy spectra of the electron-photon component were derived, and the fraction of high-energy electrons and photons at distances of $0-3$ m and $0-0.3$ m from the shower axis were determined. The lateral distribution of high-energy electrons and photons at distances of $0-0.3$ m from the axis was also obtained.

A study of the energy spectra and of the lateral distribution of the electron-photon component of extensive atmospheric showers (EAS) has previously been carried out both at sea level[1] and at high altitudes.[2,3] In these studies the region between 0 and 10 m from the shower axis was investigated. Comparison of the obtained spectra with those calculated according to the cascade theory, assuming the energy of the generating particle to be infinite,[3] showed that the experimental spectra near the shower axis are poor in high-energy electrons,* particularly at very small distances from the shower axis (mainly $0-1$ m), i.e., in the actual shower core.

However, previous studies[1,2] did not permit a sufficiently accurate separation of shower cores, and few cases in which the EAS passed at a distance up to 1 m from the cloud chamber were registered. Therefore, the energy spectra of the electrons and photons in this region were investigated with insufficient accuracy.

In reference 3 showers with a number of particles $\bar{N} = 2 \times 10^5$ were investigated. For small distances between the shower axis and the cloud chamber a very large particle flux density ($\sim 100$ per $0.15$ m$^2$) was observed in the upper section. Therefore, a separation of discrete particles was difficult, a fact which lowered the precision of the obtained results. The results of references 1 and 3 differ markedly from each other. It became, therefore, essential to investigate in detail the electron and photon energy spectra in EAS at sea level in the region $0-3$ m from the shower axis, choosing showers with a small particle flux density.

## MEASUREMENT METHOD

A rectangular cloud chamber[4] containing lead plates successively 1, 2, 2.5, 2, 2.5, and 1.5 cm thick (a total thickness of 120 g/cm$^2$) was used as the registering device.

The energy of the electrons and photons was determined from the total number of particles in the cascade showers which they produced in the lead plates of the chamber (cf. references 1 and 3). In practice account was taken not of the total number of particles moving forward in all sections within an angle of 180°, but only of particles in the region of the shower maximum. At the shower boundary where one or two particles should have been observed, the latter were strongly scattered in the lead and it was impossible to count them reliably. Owing to the error in counting the number of scattered particles, the electron energy may be about 10% too low.

---

*It must here be noted that the theoretical integral spectra were calculated for electrons only. However, an experimental separation of electrons and photons in the cloud chamber has until now proved impossible because of the large conversion probability in the upper wall of the chamber.

The monitoring device was chosen with a view to making a more efficient separation of EAS with axes close to the cloud chamber possible. Two alternate methods for the selection of showers were employed. (The general plan of the array is shown in Fig. 1.)

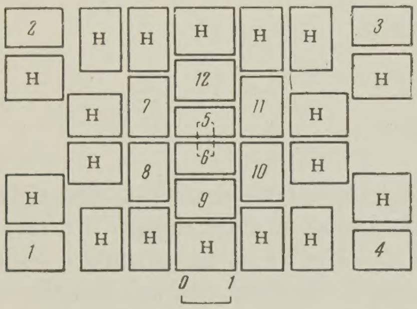

FIG. 1. General plan of the array. The cloud chamber is represented by the dashed rectangle at the center. The counters of the monitoring system are in trays 1–6; H – hodoscopes for the first monitoring system; 7 – 12 are the trays for the second monitoring system.

1. In the first method the EAS was separated from the general flux of cosmic particles with the aid of counters connected to coincidence and anticoincidence circuits. The group of counters 5 – 6 (at the center of the array) was connected to four channels of a coincidence circuit. The area of the counters connected to one channel amounted to 0.16 $m^2$. Each group of counters 1 – 4 (located at a distance of 3 m from the center) was connected to three channels of a triple coincidence circuit; the counter area for each channel was 0.13 $m^2$. A shower was recorded only in the event that a fourfold coincidence in the counters of the group 5 – 6 was not accompanied by a threefold coincidence in any one of groups 1 – 4. To determine the location of the EAS axis and the number of particles in the shower a GK-7 hodoscopic device consisting of 24 groups of 12 hodoscope counters each (counter area $\sigma_c = 330$ $cm^2$) was employed. The hodoscopic device made it possible to pick out showers whose axes passed not further than 3 m from the chamber; the precision in locating the axis was ~ 1 m.

An earlier[5] theoretical calculation distribution of the distances of the EAS axes from the center of the array for a given monitoring system indicated that 50% of all the showers registered by the array should have axes located 0 – 3 m from the chamber. In the experiment, however, 30% of all shower axes were found within a radius of 3 m. Such a discrepancy between the experimental and calculated values can be explained if account is taken of the fact that the number of hodoscopes fired upon passage of showers with $\leq 3 \times 10^3$ particles was insufficient for a determination of the shower-axis location. In the processing of the hodoscopic data this caused such events to be counted among the showers with axes more than 3 m from the chamber.

In Fig. 2 the solid line indicates the distribution of the distances from the cloud chamber to the axes of the showers chosen for processing. Showers with $\bar{N} \sim 8 \times 10^3$ were registered most efficiently.

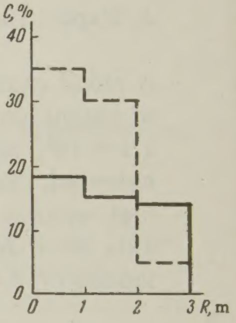

FIG. 2. The distribution of the numbers C of EAS by the distances R of their axes from the cloud chamber. The solid line indicates the experimental distribution for the first monitoring system; the dashed line indicates the distribution for the second monitoring system, obtained by theoretical calculations.

2. In the second method of measurement an extensive atmospheric shower was recorded only when the particle flux density above the cloud chamber (registered by the counters) exceeded the particle flux density registered by counter groups located away from the center.

Groups 1 – 4 contained 12 counters each, while groups 5 and 6 had 18 each (cf. Fig. 1). The area of each counter was 100 $cm^2$ in the first measurement series and 38 $cm^2$ in the second. In the event of an EAS passing through the array, a voltage pulse, of amplitude proportional to the number of counters fired in a given group, was formed in each of the electronic circuits connected to the counter groups 1 – 6. If we denote the number of counters fired in the i-th group by $m_i$, then the condition for the registration of a shower can be expressed as

$$\sum_{i=5}^{6} m_i - \sum_{j=1}^{4} m_j \geqslant 6; \qquad m_5 \geqslant 2, \qquad m_6 \geqslant 2.$$

To determine the total number of particles in the recorded showers, a hodoscopic device, consisting of six groups of 24 counters each (the area of each counter was 100 cm$^2$) was employed. The distribution of the shower-axis distances from the cloud chamber (indicated in Fig. 2 by the dashed line) was calculated for the given monitoring system.[5]

In the first series of measurements the monitoring system registered most efficiently showers with $\overline{N} = 1.2 \times 10^4$, in the second series — showers with $\overline{N} = 3 \times 10^4$ particles.* The axes of 70% of all recorded showers were not farther than 3 m from the chamber.

To check the effect of the passage through the roof over the building in which the measurements were carried out, one tray of counters, connected to the hodoscopic device, was placed on the roof.

## MEASUREMENT RESULTS

In all, 2370 EAS were registered with the first monitoring system, while 1830 showers with $\overline{N} = 1.2 \times 10^4$ particles (after 680 hours of operation) and 436 showers with $\overline{N} = 3 \times 10^4$ (after 420 hours of operation) were registered with the second monitoring system. The mean flux density of charged particles, determined with the aid of the hodoscopes on the roof, was 20% less than the density in the room.

The data from the hodoscopes of the first monitoring system yielded the lateral distribution of charged particles in the showers with $\overline{N} = 9 \times 10^3$, as shown in Fig. 3. It can be seen that this distribution has the form

$$\rho(>0) \sim r^{-n}, \qquad n = 1.0 \pm 0.1.$$

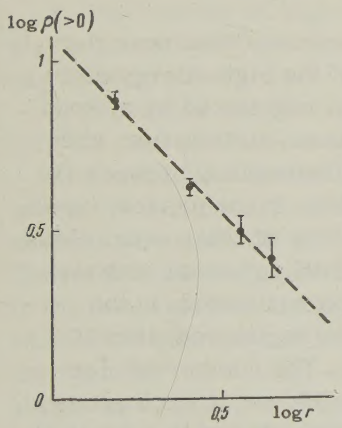

FIG. 3. Lateral distribution of charged particles in showers with $\overline{N} = 9 \times 10^3$; r is the distance from the shower axis in meters, $\rho(>0)$ is the electron flux density per m$^2$.

The measurements yielded the integral energy spectra of the electron-photon component, as shown in Fig. 4. The flux density per square meter of electrons and photons with energies higher than E was determined as follows:

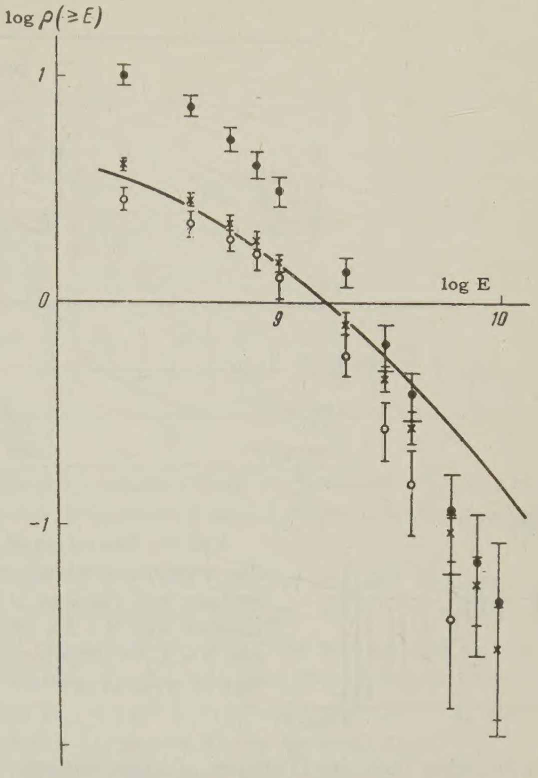

FIG. 4. Integral energy spectra of electrons and photons. $\rho(\geqslant E)$ is the flux density of electrons and photons with energies $\geqslant E$ (per m$^2$) in one shower (the energy E is expressed in ev). The solid curve is the theoretical curve for $s = 1.2$ and $E_0 = 10^{15}$ ev, normalized in terms of the experimental results for $E = 10^9$ ev and $\overline{N} = 1.2 \times 10^4$; ● – $\overline{N} = 3 \times 10^4$, × – $\overline{N} = 1.2 \times 10^4$, and ○ – $\overline{N} = 8 \times 10^3$.

$$\rho(\geqslant E) = N(\geqslant E)/C, \qquad N(\geqslant E) = \int_E^\infty (N(E)/\sigma(E))\, dE,$$

where C is the number of showers, $\sigma(E)$ — the effective area of the chamber for electrons with energy E, and N(E) the number of such electrons and photons.

The electron and photon energy spectrum thus obtained can be represented in the form

$$\rho(\geqslant E) = \text{const}/E^\gamma \quad \begin{array}{ll} \gamma = 0.65 \pm 0.05 & \text{for } E = 2\cdot 10^8 \div 10^9 \text{ ev}, \\ \gamma = 1.8 \pm & \text{for } E = 2\cdot 0^9 - 10^{10} \text{ ev}. \end{array}$$

This agrees with our earlier results,[3] and also with the results of the Japanese authors[6] who, for somewhat larger distances (1 – 5 m), obtained $\gamma = 1$ for energies of $2 \times 10^8 - 10^9$ ev, and $\gamma = 1.5$ to 2 for energies of $10^9 - 5 \times 10^9$ ev.

To check whether the energy spectrum of the particles in a shower varies with the number of particles $\overline{N}$ in the shower, we plotted the ratio of the electron and photon flux density for showers with $\overline{N} = 3.0 \times 10^4$ and $\overline{N} = 1.2 \times 10^4$ (cf. Fig. 5).

---

*This was achieved by decreasing the counter area (by a factor of 2.6) in the monitoring system (we assumed the exponent $\kappa$ in the shower number-of-particles spectrum to be constant).

TABLE I

| | Present work | | | [2] | [3] | [4] |
|---|---|---|---|---|---|---|
| $\overline{N}$ | $8\cdot10^3$ | $1.2\cdot10^4$ | $3\cdot10^4$ | $10^5$—$3\cdot10^6$ | $6.4\cdot10^4$ | $8\cdot10^4$—$3\cdot10^6$ |
| $\rho(\geqslant10^9)$, $m^{-2}$ | 1.32 | 1.90 | 4.08 | | | |
| $\rho(>0)$, $m^{-2}$ | 8 | 13 | 30 | | | |
| $\Delta$, % | 16±4 | 15±3 | 13±3 | 11±5 | 10±1 | 12±1 |

TABLE II

| $r$, m | 0—1 | 1—2 | 2—3 | 3—6 | 6—10 | 10—20 |
|---|---|---|---|---|---|---|
| $\rho$, $m^{-2}$ | 3.66 | 1.01 | 0.48 | 0.185 | 0.027 | 0.008 |
| $\rho C$ | 132 | 30.3 | 2.15 | 0.65 | 0.1 | 0.05 |
| $10^{-4}\rho C\overline{N}$ | 264 | 73 | 8.6 | 6.5 | 3.0 | 2.5 |

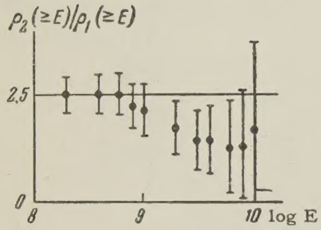

FIG. 5. The ratios of the flux densities of electrons and photons with energies ≥E for showers with $\overline{N} = 3 \times 10^4$ ($\rho_2$) and $\overline{N} = 1.2 \times 10^4$($\rho_1$). The energy is given in ev.

It can be seen that the fraction of high-energy ($E \geq 2 \times 10^9$ ev) electrons and photons is smaller in showers with $\overline{N} = 3 \times 10^4$ than in showers with $\overline{N} = 1.2 \times 10^4$.

In addition, the fraction of high-energy electrons and photons relative to all the electrons in the shower was determined for showers with various numbers of particles. As before, this fraction was found from the ratio of the flux density of electrons and photons with $E \geq 10^9$ ev, obtained from the cloud chamber data to the flux density of all electrons, obtained from the data of the hodoscopic counters:*

$$\Delta = \rho(\geqslant 10^9)/\rho(>0).$$

The value of $\Delta$ obtained is listed in Table I together with data by others, pertaining to a distance $0-3$ m from the shower axis. As can be seen from Table I, all the results obtained for showers with different numbers of particles agree with each other within the limits of the experimental errors.

In working with the second monitoring system, we could not determine the location of the shower axis. To estimate the number of high-energy electrons in the region of $0-3$ m from the chamber, the theoretical lateral distribution of electrons with $E \geq 10^9$ ev, obtained from cascade theory for a value of $s = 1.5$, was employed.

This distribution is listed in Table II (second line). The third line was obtained after taking into account the experimentally observed distribution of the distances of the recorded shower from the cloud chamber. The fourth line includes an allowance for the change in the mean number of particles $\overline{N}$ in a shower with increasing distance from the axis to the chamber. From Table II it can be seen that for this monitoring system no more than 4% of the total of recorded electrons with $E \geq 10^9$ ev will be registered at a distance of more than 3 m from the axis. Using this estimate, we obtained the data listed in Table I for the region of $0-3$ m.

It has been assumed previously[7] that near the EAS axis the fluctuations of the high-energy electron and photon flux density, registered by a cloud chamber, do not have a Poisson distribution, and this partially explains the discrepancy between the results of references 1 and 3. In the present investigation we checked the validity of that assumption. For this purpose the 1800 EAS recorded with the second monitoring system were divided, in the order in which they had been registered, into 36 groups of 50 showers each. The number of electrons and photons with $E \geq 10^9$ ev in each group was calculated, and the distribution of the obtained values, shown in Fig. 6, was then found. The smooth curve in the figure represents Poisson's integral distribution, corresponding to the known mean number of particles per effective chamber area. It is clear that the experiment does not yield a Poisson distribution.

Later we excluded from consideration those

---

*The flux density $\rho(>0)$ was determined from the cloud-chamber measurements. On the average $\rho(>0)$ obtained from the chamber measurements is 20% higher than that obtained from the hodoscopic data. This is explained by the effect of the passage through the upper wall of the chamber. The effect of the passage through the roof of the building is still not accounted for in these calculations; the correction for this effect is introduced in the comparison with the theory.

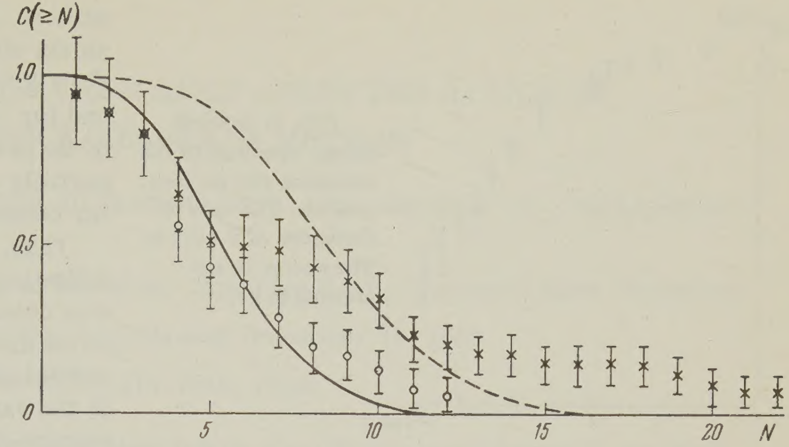

FIG. 6. Integral distribution of 50 EAS by the number N of electrons and photons with energies $\geqslant 10^9$ ev recorded in the cloud chamber; × – experimental points for all showers, o – points obtained on excluding the 12 cases in which the shower core passed through the chamber. The curves are the Poisson distributions for the corresponding cases.

12 cases* in which the EAS cores passed through the chamber, and the distribution, also shown on Fig. 6, was plotted. This turned out to be close to a Poisson distribution. Thus, as was assumed, the main deviation from a Poisson distribution is connected with the fact that in the relatively few cases when an EAS core passes through the cloud chamber, the flux density of the high-energy electrons and photons exceeds the mean flux density of these particles within the investigated distance of 0 – 3 m.

The passage of a core through the cloud chamber was identified by simultaneous satisfaction of three criteria:

1. The electron and photon flux density, determined from the measurements in the chamber, had to exceed at least by one order of magnitude the electron flux densities determined with the aid of the hodoscopes located near the chamber.
2. The number of high-energy ($\geq 10^9$ ev) electrons and photons observed in the chamber had to be greater than 7.
3. Electrons and photons with an energy $\geq 6 \times 10^9$ ev had to be observed in the chamber.

The mean flux density $\rho$ ($\geq 10^9$) of high-energy electrons and photons was 70 $m^{-2}$ in the shower core and 1.25 $m^{-2}$ 0.3 – 3 m from the axis. Therefore, the fraction of high-energy particles ($\Delta$) in the total electron and photon flux depends strongly on whether the events of the passages of cores through the chamber ($\Delta = 15\%$) are included in the general statistics or whether they are not included (in which case $\Delta \approx 10\%$). From this it is clear that the apparent "softening" of the experimental spectrum for showers with $\bar{N} = 3 \times 10^4$ particles compared to showers with $\bar{N} = 1.2 \times 10^4$ can be explained by the fact that in the second series of experiments not even one passage of a shower core through the chamber was registered (the passage of two or three cores was expected from the calculations).

In view of the fact that the number of high-energy electrons and photons $N(\geq E)$ which entered the cloud chamber did not have a Poisson distribution, we did not take the error in the calculation of $N(\geq E)$ to be of the form $\sqrt{N}$, but applied the formulas of the general theory of errors. We considered the number of high-energy electrons $N(\geq E)$ obtained by us to be a linear combination of the form

$$N = \rho_1 n_1 + \rho_2 n_2 + \ldots + \rho_n n_n,$$

where $n_i$ is the number of events when $\rho_i$ electrons with an energy $\geq E$ are observed in the chamber. The mean-square error of the arithmetic mean of the electron flux density is then equal to

$$\sigma = \left[\frac{1}{n(n-1)} \sum_{i=1}^{n} \varepsilon_i^2\right]^{1/2},$$

where $\epsilon_i$ is the deviation of the observed value of $\rho$ from the arithmetic mean: $\epsilon_i = \rho_i - \bar{\rho}$. The value $\sigma$ thus calculated is almost twice as large as the value of $\sqrt{N}/C$.

We plotted the electron and photon energy spectrum in the region of the EAS axis at distances of 0 – 0.3 m from the axis for the 12 cases of the passage of the core through the chamber (cf. Fig. 7). For such small distances the spectrum exponent $\gamma$ is 0.34 ± 0.05 in the $2 \times 10^8$- to $10^9$-ev energy range, and 1.3 ± 0.2 in the $2 \times 10^9$- to $10^{10}$-ev energy range. The fraction of particles with energies $\geq 10^9$ ev for these cases is $\Delta = (56 \pm 14)\%$. The average energy per charged particle is $\bar{E} \sim 3 \times 10^9$ ev in the region of the shower axis and $\bar{E} \sim 4 \times 10^8$ ev at distances of 0.3 – 3 m from the axis.

Using the results of our measurements, we found the lateral distribution of high-energy elec-

---

*This number corresponds to that calculated for the given monitoring system.

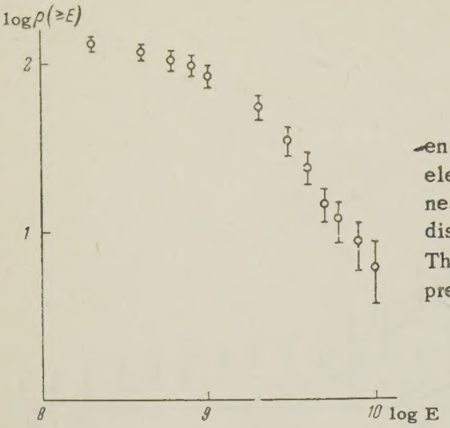

FIG. 7. Integral energy spectrum of the electrons and photons near the EAS axis at distances of 0 – 0.3 m. The energy is expressed in ev.

trons and photons at distances of 0 – 0.3 m from the shower axis. As the shower axis we took the region with the highest energy flux density, which also coincided for the most part with the largest particle density. For electrons and photons with an energy $\geq 10^9$ ev (cf. Fig. 8)

$$\rho(\geqslant 10^9) \sim r^{-n}, \qquad n = 1.2 \pm 0.3.$$

In reference 3 a value n = 1.6 ± 0.3 was obtained for particles of the same energy at distances of 1 – 7 m from the shower axis. In the work of the Japanese authors[6] the lateral distribution of electrons and photons with $E \geq 10^9$ ev at distances of 1 – 7 m from the axis was found to be

$$\rho(\geqslant 10^9) \sim r^{-1.5}.$$

As can be seen, the data obtained in the present paper are in agreement with previous results.

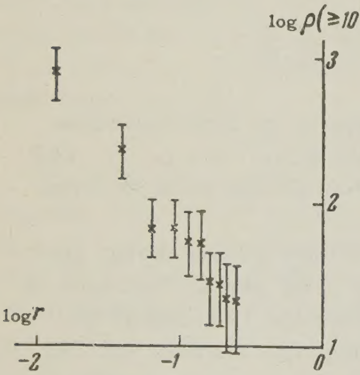

FIG. 8. The lateral distribution of high-energy electrons and photons at distances $r \leqslant 0.3$ m from the shower axis. $\rho(\geqslant 10^9)$ is the flux density of electrons and photons with $E \geqslant 10^9$ ev per m$^2$.

To compare the results obtained with cascade theory, calculations of the energy spectra of the electrons in the shower were carried out. It was assumed that the electron-photon component is in equilibrium with the nuclear-active component, and that the nuclear-active component produces protons with $E = 10^{11}$ ev (or $10^{12}$ ev) with a probability which decreases as $\exp(-\mu t)$. To carry out such calculations we used the results of reference 8. A depth of 30 radiation units was taken as the observation level, and it was assumed that $\overline{s} = 1.2$. The spectra obtained both for $E = 10^{12}$ ev and for $E = 10^{11}$ ev coincide with those calculated by us previously (for s = 1.2) for a generating particle of infinite energy and, as previously, differ considerably from the experimental results.

Thus, on the basis of all that has been said, the following conclusions can be drawn: 1) no change was observed in the fraction of high-energy electrons and photons with increasing total number of particles in the recorded atmospheric showers; 2) the experimentally observed fraction of high-energy electrons and photons is much smaller than its calculated value, obtained for an infinite initial energy and under the assumption of equilibrium between the electron-photon and the nuclear-active component of the shower. The latter conclusion is apparently explained by the fact that the initial conditions of the formation and development of the electron-photon component in an EAS are poorly accounted for in the theoretical calculations.

In conclusion, the authors express their deep gratitude to G. T. Zatsepin, I. P. Ivanenko, and L. I. Sarycheva for a discussion of the obtained results, and also to D. F. Rakitin, O. N. Novoselov, I. A. Ivanovskaya, B. M. Mozhaev, and L. K. Bocharov who took part in the measurements at various stages of the work.

---

[1] Ivanovskaya, Kulikov, Rakobol'skaya, and Sarycheva, JETP **33**, 358 (1957), Soviet Phys. JETP **6**, 276 (1958).

[2] Hazen, Williams, and Randall, Phys. Rev. **93**, 578 (1954).

[3] Danilova, Dovzhenko, Nikol'skiĭ, and Rakobol'skaya, JETP **34**, 541 (1958), Soviet Phys. JETP **7**, 374 (1958).

[4] I. A. Ivanovskaya and A. G. Novikov, J. Tech. Phys. **26**, 209 (1956), Soviet Phys.-Tech. Phys. **1**, 206 (1956).

[5] Dovzhenko, Nikol'skiĭ, and Rakobol'skaya, JETP **36**, 17 (1959), Soviet Phys. JETP **9**, 11 (1959).

[6] Kameda, Toyoda, and Maeda, Cosmic-Ray Research **3**, 470 (1958), in Japanese.

[7] I. A. Ivanovskaya and I. V. Rakobol'skaya, JETP **35**, 1583 (1958), Soviet Phys. JETP **8**, 1108 (1959).

[8] S. Z. Belen'kiĭ and I. P. Ivanenko, Usp. Fiz. Nauk **69**, 591 (1959), Soviet Phys. Uspekhi **2**, 912 (1960).

Translated by Z. Barnea
266

SOVIET PHYSICS JETP VOLUME 11, NUMBER 5 NOVEMBER, 1960

# *YIELD OF PHOTONEUTRONS EMITTED FROM LEAD UNDER THE ACTION OF 10.5 – 20.5 Mev ELECTRONS (THICK-ABSORBER METHOD)*

V. M. GRIZHKO, D. I. SIKORA, V. A. SHKODA-UL'YANOV, A. D. ABRAMENKOV, B. I. SHRAMENKO, and A. N. FISUN

Physico-Technical Institute, Academy of Sciences, Ukrainian S.S.R.; Uzhgorod State University

Submitted to JETP editor August 18, 1959; resubmitted December 19, 1959

J. Exptl. Theoret. Phys. (U.S.S.R.) **38**, 1370-1373 (May, 1960)

The yield of photoneutrons from a thick lead plate totally absorbing a monochromatic electron beam was measured. The experimental curve is compared with the theoretical curves computed with the aid of the Belen'kiĭ-Tamm equilibrium spectrum. The absolute energy calibration of the monochromator was based on the threshold of the $(\gamma, n)$ reaction in oxygen and carbon.

PHOTONEUTRON yields for certain elements, calculated with the aid of the Belen'kiĭ-Tamm equilibrium spectrum, have already been given earlier.[1] The reasons for using the results of the cascade theory to estimate the number of photoneutrons produced under electron-accelerator conditions were also cited there (cf. also reference 2).

The purpose of the present work was the experimental determination of the phontoneutron yield from an essentially infinitely thick lead plate totally absorbing a monochromatic electron beam, and the comparison of the experimental and calculated results.

In setting up the present experiment, we have preserved the basic features of the experimental method proposed by Gol'danskiĭ and Shkoda-Ul'yanov[3] for the determination of photoneutron yields from thick blocks. We note that the results of reference 3 can also be used to estimate the possible number of photoneutrons in experiments with electron accelerators, albeit at higher energies than those considered in this paper.

Figure 1 is a schematic diagram of our experiment. Our experiment differs from that proposed earlier[3] by the fact that a monoenergetic beam of electrons, and not photons, falls directly on the investigated sample and has a bremsstrahlung spectrum. In this way, a Faraday cup can be used simultaneously as the electron-beam monitor and as the photoneutron source (cf. also references 4 and 5).

The linear accelerator of the Physico-Technical Institute of the Ukrainian S.S.R. Academy of Sciences, with a peak output energy of 30 Mev, operating with fifty 1-$\mu$sec current pulses per second, served as the electron source. The monoenergetic beam, 4, obtained with the aid of the magnetic monochromator, 1, located at the accelerator exit and with the aid of the collimator system, 2, was directed at the target, 8, placed at the center of a 80 × 80 × 80-cm paraffin cube. The first collimator, 2, similar to the one used by Brown and Wilson,[6] was a sectional cylinder with an outer diameter of 80 mm, and a total length of 450 mm, consisting of three sections; 150 mm aluminum, 200 mm graphite, and 100 mm lead. The inner opening had a 10 × 20-mm rectangular cross section. The second and third collimators, 4, were made of graphite and had an outer diame-

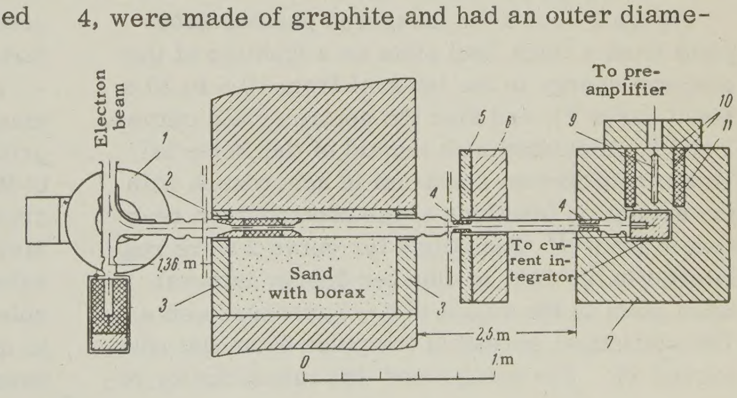

FIG. 1. Experimental setup (schematic).

ter of 50 mm, an inner-opening diameter of 20 mm, and a length of 200 mm.

The energy resolution of the beam extraction system was 0.4%. The target was placed at a distance of 5 m from the monochromator. The collecting collimator was set in a wall aperture and surrounded by sand with an admixture of borax and by a lead shield, 3. Additional shields of lead, 5, and paraffin, 6, were placed around the graphite collimator.

The boron counter, 9, similar to the one proposed by Hanson and McKibben,[7] was used to measure the neutron yield. The counter was placed inside the paraffin cube, 7, and was in addition surrounded by a 50-mm thick boron oxide layer, 11, and by a 2-mm thick cadmium layer. A special electronic circuit switched on the counter only during the time interval between the pulses of the accelerator current, with a 1.5-$\mu$sec delay. This made it possible to avoid counting the gamma quanta and to get rid of the electromagnetic disturbances appearing during the pulse.

The neutron counter worked in the region of direct proportionality between the neutron count and the current incident on the target. The measurements were carried out with currents on the order of $10^{-10}$ amp.

To determine the absolute photoneutron yield, the counter was calibrated against a standard Ra + Be source with a yield of $4.88 \times 10^5 \pm 3\%$ neutrons/sec.

The investigated target, 8, was made in the form of a Faraday cup, whose thick portion, serving as the photoneutron source, had a thickness on the order of 20 radiation units. Thus, the incident electron beam was practically completely absorbed in the investigated target (cf. also references 3 and 5). The Faraday cup was carefully isolated from the vacuum jacket in which it was placed, and was connected by means of a coaxial cable to the precision electron-current integrator, which served as a negative-feedback dc amplifier (cf. also references 8 and 5).

Figure 2 shows the measured photoneutron yield from a thick lead plate as a function of the electron energy in the interval from 10.5 to 20.5 Mev (curve 2), and also the neutron yield curves, 1 and 3, calculated with the aid of the Belen'kiĭ-Tamm equilibrium spectrum in accordance with the excitation functions of the photoneutron reaction in lead.[9,10] The points for curve 2 were registered in the 150- to 400-kev energy interval. Each point is the result of 5 — 7 measurements. The statistical spread of the pulse count did not exceed 2%. The background was measured by removing the Faraday cup, and amounted to 0.5% for energies below and not more than 3% for energies above the threshold of the ($\gamma$,n) reaction in carbon. In the latter case the neutrons were mainly produced in the graphite collimator, 4 ( Fig. 1).

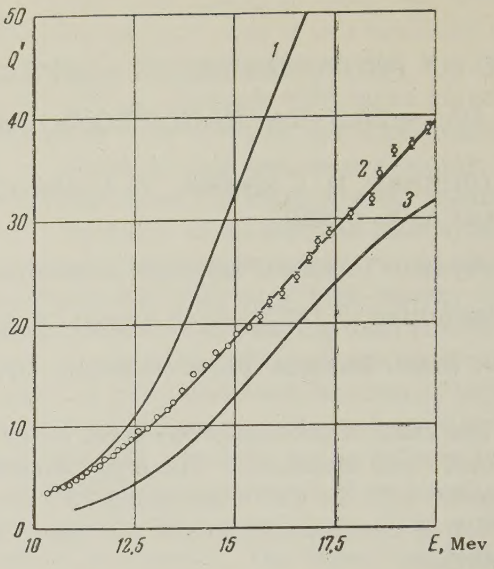

FIG. 2. Photoneutron yield (Q′) as a function of the electron-beam energy. To determine the absolute value of the yield (per electron), Q′ must be multiplied by $10^{-4}$.

The absolute energy calibration was against the ($\gamma$,n) reaction threshold in oxygen and carbon by the activation method; samples of beryllium oxide and polystyrol were used for this. We estimate the calibration accuracy at about 100 kev.

As can be seen from Fig. 2, our experimental data are in better agreement with the results of reference 10 than with those of reference 9. Apparently, the values given in reference 9 for the function of photoneutron production in lead are much too large. Comparison of the experimental and theoretical photoneutron yields in lead permits us to conclude that the Belen'kiĭ-Tamm equilibrium spectrum can be successfully used for the purposes cited in reference 1. True, one must bear in mind that for certain elements the excitation functions of the photoneutron reaction, measured by different authors, give considerably differing absolute values (cf. references 9 and 10).

Following earlier ideas,[3] we have also estimated the integral cross section for photoneutron production in lead, and obtained a value of 2.6 b-Mev. We assumed that the energy for which the cross section attains its maximum value is 13.8 Mev. Our integral cross section agrees with the value of reference 10, 2.17 b-Mev. With the available data on photoneutron yields[4] it is also possible to determine the excitation function of the photoneutron reaction in the investigated element.

However, to obtain reliable results in this case, it is necessary to measure the energy dependence of the photoneutron yield with greater precision and for smaller energy intervals, in view of the need of determining the first and second derivatives.

At present we are making some improvements in the experimental methods. These will obviously not change appreciably the absolute value of the measured yield, but will, we hope, permit a sufficiently precise calculation of the excitation function of the photoneutron reaction in lead from the photoneutron yield curve.

The authors express their gratitude to A. S. Litvinenko, A. I. Charkin, V. A. Skubko, V. L. Auslender, V. I. Gomonaĭ, and A. M. Parlag who took part in the work, and also to A. K. Val'ter and I. A. Grishaev for their interest in the work and for a discussion of the results.

In conclusion, the authors consider it their pleasant duty to thank L. E. Lazarev and V. I. Gol'danskiĭ for their valuable advice and remarks.

---

[1] Gomonaĭ, Krivskiĭ, and Shkoda-Ul'yanov, Атомная энергия (Atomic Energy) 7, 476 (1959).

[2] Chodorow, Ginzton, Hansen, Kyhl, Neal, and Panofsky, Rev. Sci. Instr. **26**, 197 (1955).

[3] V. I. Gol'danskiĭ and V. A. Shkoda-Ul'yanov, JETP **28**, 623 (1955), Soviet Phys. JETP **1**, 579 (1955).

[4] V. A. Shkoda-Ul'yanov, JETP **35**, 1041 (1958), Soviet Phys. JETP **8**, 726 (1959).

[5] Parlag, Sikora, and Shkoda-Ul'yanov, Faraday's Cup as an Electron-beam Monitor and Photoneutron Source, Abstracts of the All-Union Intercollegiate Conference on Electron Accelerators, Tomsk, Sept. 2—7, 1959.

[6] K. L. Brown and R. Wilson, Phys. Rev. **93**, 443 (1954).

[7] A. O. Hanson and J. L. McKibben, Phys. Rev. **72**, 673 (1947).

[8] K. L. Brown and G. W. Tautfest, Rev. Sci. Instr. **27**, 696 (1956).

[9] Montalbetti, Katz, and Goldemberg, Phys. Rev. **91**, 659 (1953).

[10] M. E. Toms and W. E. Stephens, Phys. Rev. **108**, 77 (1957).

Translated by Z. Barnea
267

SOVIET PHYSICS JETP VOLUME 11, NUMBER 5 NOVEMBER, 1960

# *KINETIC ENERGY OF FRAGMENTS FROM THE PHOTOFISSION OF* $U^{238}$

B. A. BOCHAGOV, A. P. KOMAR, and G. E. SOLYAKIN

Leningrad Physico-Technical Institute, Academy of Sciences, U.S.S.R.

Submitted to JETP editor August 26, 1959; resubmitted January 18, 1960

J. Exptl. Theoret. Phys. (U.S.S.R.) **38**, 1374-1380 (May, 1960)

A double ionization chamber was employed to study the energy distribution of $U^{238}$ photofission fragments. Gamma rays with $E_{\gamma\,\max} = 70$ Mev were produced by the synchrotron of the Physico-Technical Institute. A topological plot of the fragment kinetic energy distribution is compared with diagrams representing the fission of heavy elements induced by neutrons of various energies.

## INTRODUCTION

THE photofission of heavy nuclei has not yet been investigated with sufficient thoroughness. Most of the literature (see reference 1, for example) has been concerned with a) fission cross sections, b) the number of neutrons per fission event, c) the mass distribution of fragments, and d) the correlation between the directions of fragments and the gamma-ray beam.

Only two papers have appeared on the energy distribution of fragments,[2,3] which is important both for the understanding of the fission mechanism and for reactor technology.[4] The data presented in references 2 and 3 were obtained by means of pulse ionization chambers with electron collection. The apparatus was able to register the energy of only one fragment per fission. We believe it is extremely important to determine the energy distribution of fragments as completely as in the case of neutron-induced fission.[5-8] A comparison of the distributions for photofission and for neutron-induced fission could be very important for the further development of fission theory.

The present paper reports some results obtained by our laboratory during 1955 in investigations of the photofission of heavy nuclei, particularly $U^{238}$.

## EXPERIMENTAL PROCEDURE

For the measurement of photofission fragment energies we used two pulse ionization chambers with electron collection (Fig. 1). The target material was deposited on the common high-voltage electrode 5 of the chambers, which are more fully described in references 5, 6 and 13. Figure 1 is a block diagram of our apparatus. Voltage pulses from the resistors R were amplified by the preamplifiers 10 and were then fed to the time gate 11, which blocked the amplifier outputs except when gamma rays were passing through the chambers; this was done in order to obviate electrical induction produced by the synchrotron. Pulses passing through the time gate and control circuit 12 reached the MPO-2 loop oscillograph 13 for motion-picture recording. The ionization-chamber electrodes were positioned perpendicular to the direction of the gamma-ray beam.

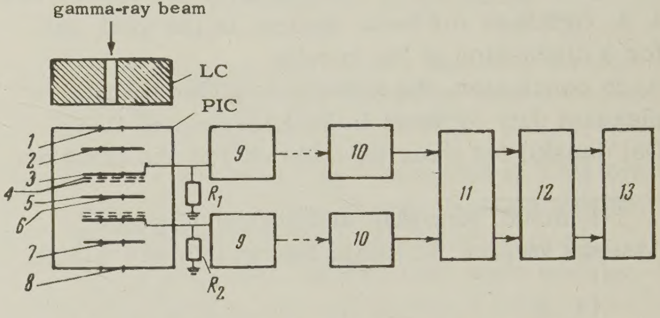

FIG. 1. Block diagram of apparatus. LC – lead collimator, PIC – pulse ionization chamber, 1 – ionization chamber entrance window, 2 – compensating electrode, 3 – collecting electrode, 4 – screening grids, 5 – common high-voltage electrode, 6 – Zapon film bearing layer of uranyl nitrate, 7 – aperture for passage of gamma-ray beam (present in all electrodes); (the second half of the chamber is a mirror image of the first half); 8 – exit window, $R_1$ and $R_2$ – resistors from which voltage pulses are taken, 9 – preamplifiers, 10 – main amplifiers, 11 – time gate, 12 – control circuit of loop oscillograph, 13 – MPO-2 loop oscillograph.

The synchrotron of the Physico-Technical Institute of the USSR Academy of Sciences provided a gamma-ray beam with $E_{\gamma\,\max} = 70$ Mev, which was defined by a lead collimator LC. Compensating electrodes in the ionization chambers served to compensate pulses induced by the gamma radiation. Compensation was facilitated by increasing the duration of gamma-ray pulses from 10 to 1500 μsec. The maximum gamma-ray energy of 70 Mev was selected to produce a greater intensity in the giant resonance region, since photofission is known to result mainly from the absorption of photons in this energy region.

The target was a layer of uranyl nitrate, containing a natural mixture of uranium isotopes, which was deposited on a Zapon film fastened in a brass ring of 40 mm inside diameter. A thin layer of aluminum deposited on each side made the film an electrical conductor; its thickness including the aluminum was 30 μg/cm². The thickness and uniformity of the uranyl nitrate layer were determined from the alpha-particle spectrum of natural uranium. The spectrum registered on the uranyl nitrate side is shown in Fig. 2; the spectrum registered on the film side does not differ essentially. The thickness of the uranyl nitrate deposit was 320 μg/cm². The alpha-particle energy peaks were used as reference values in determining the fission fragment energies.

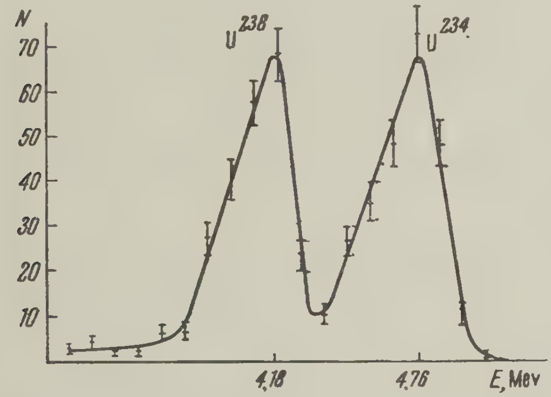

FIG. 2. Alpha-particle spectrum of natural uranium registered on the uranyl nitrate side of the target.

Chuvilo[9] found that all detected fragments from a natural uranium target result, to within 1%, from the fission of $U^{238}$. The film-recorded amplitudes $V_1$ and $V_2$ of heavy and light fragments were proportional to the number of ion pairs produced by each fragment in the chamber, i.e., they were proportional to the kinetic energies $E_1$ and $E_2$ of the fragments. We have assumed that the energy required to produce an ion pair is identical for fragments and alpha particles. We measured the pulse heights on a flat projection obtained by means of a photographic enlarger.

Thus each fission event was associated with two numerical values $E_1$ and $E_2$; the indices 1 and 2 pertain to the chambers (chamber 1 was closer to the synchrotron target). Figure 3 shows $W_{ik} = n_{ik}/n_{ik\,max}$, the distribution (in relative units) of the numbers of cases $n_{ik}$ of different pairs of values for $E_1$ and $E_2$. Corrections for energy losses in the target amounted to 5%. Figure 3 also shows lines representing $E_1/E_2$ = const. All results are given without corrections for source thickness and the ionization defect. Errors in the positions of the maxima in the graphs equal half of the interval width used in plotting.

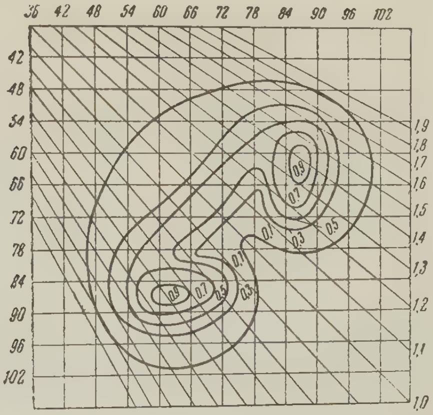

FIG. 3. Topological plot – contour lines of the surface $W_{ik}(E_1, E_2)$. The coordinates represent the energies $E_1$ and $E_2$ of the two fragments in Mev.

## RESULTS AND DISCUSSION

The contour lines of the surface $W_{ik}$ were plotted in Fig. 3 for intervals $\Delta W_{ik} = 0.2$, thus revealing only the most general features of the surface. However, detailed topological information is very important for the understanding of the fission mechanism. Because of the discreteness of the data we studied slices of $W_{ik}$ of finite width in different directions. We found it most useful to consider slices formed by planes parallel to the coordinate planes, perpendicular to the principal diagonal and to the XY plane, and by planes perpendicular to the XY plane and intersecting the latter along lines of constant $E_1/E_2$. We were interested in the dependence of $n_{ik}$ and $N = \Sigma n_{ik}$ on $E_1$ and $E_2$, i.e., on the local topology and "mass" of the slices. We shall show that the type of slice and N are determined by the limitations imposed on i and k.

The main characteristic of the surface $W_{ik}(E_1, E_2)$ is its mirror symmetry with respect to the vertical plane through the principal diagonal ($E_1 = E_2$). This symmetry denotes that either a heavy or a light fragment is ejected in a given direction with equal probability.

Any asymmetry of these fragments would easily be detected in Fig. 4, which represents

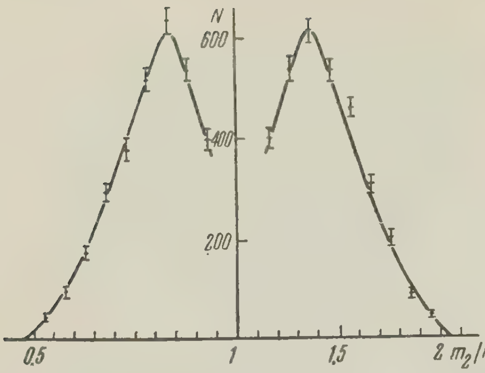

FIG. 4. Photofission fragment yield of $U^{238}$ as a function of the mass ratio $m_2/m_1 = E_1/E_2$.

the total number of cases in slices of type $\Delta(E_1/E_2)$ as a function of $E_1/E_2$. Figure 3 shows that the most probable fragment energies are 87 and 61 Mev, while Fig. 4 indicates that the most probable mass ratio is 1.36. Thus the ratio of the most probable masses, $m_2/m_1 = E_1/E_2 = 1.43$, does not equal the most probable mass ratio. Similar discrepancies are found in the neutron-induced fission of $U^{235}$ and $U^{238}$.[5,6]

If it is assumed that a $U^{238}$ nucleus loses two neutrons in each photofission event, the most probable light and heavy fragment masses will be 100 and 136, thus agreeing, within the limits of error, with radiochemical results for $U^{238}$.[10]

A second important characteristic of $W_{ik}$ is the presence of two pronounced symmetrical hills having ridge lines parallel to the coordinate axes. This indicates constancy of the most probable energies $E_l$ and $E_h$, of light and heavy fragments for different intervals $\Delta E_1$ and $\Delta E_2$.

Similar hills have been found on the corresponding surfaces for the neutron-induced fission of $U^{235}$, $U^{233}$, $Pu^{239}$ and $Pu^{241}$,[5-8] and for the spontaneous fission of $Cf^{252}$.[11] In these cases the median lines of the ridges were curves whose tangents formed small angles with the coordinate axes. Figure 3 clearly shows that when $E_1/E_2 = m_2/m_1 = \text{const}$ there is considerable spread of the combined fragment energy $\Sigma E = E_1 + E_2$ and a smaller spread of the most probable values of this energy. Figure 5 shows the number of instances $n_{ik}$ as a function of $\Sigma E$ for different slices between adjacent planes $E_1/E_2 = \text{const}$. Between $E_1/E_2 = 1.2$ and $E_1/E_2 = 1.1$ the curves exhibit two peaks. For larger values of $E_1/E_2$ the most probable value of the combined energy, corresponding to the left-hand peak in Fig. 5, is reduced. For $E_1/E_2 = 1.5$ to $1.4$ this peak becomes a barely perceptible step, and for $E_1/E_2 = 1.6$ to $1.5$ it disappears completely. The right-hand peak, which is just noticeable for $E_1/E_2 = 1.1$ to $1.0$, is gradually transformed into the only peak with the change of $E_1/E_2$ from $1.6-1.5$ to $1.9-1.8$.

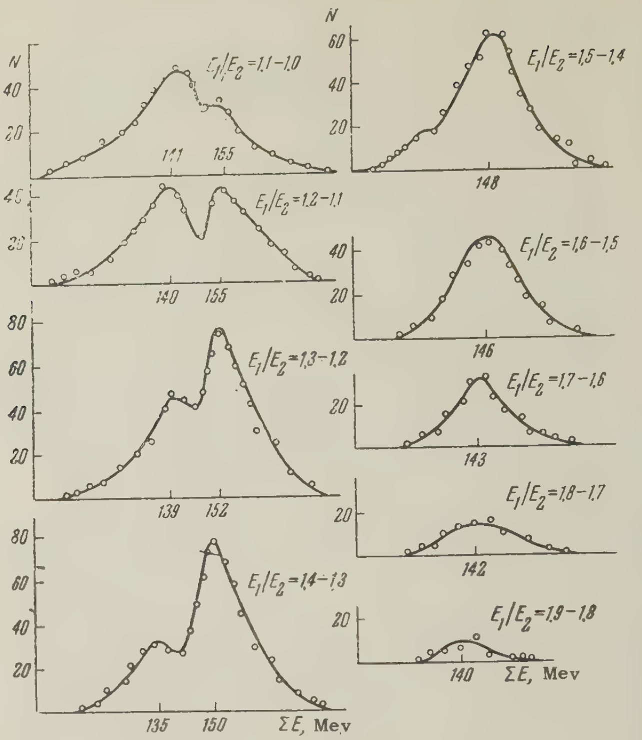

FIG. 5. Total fragment (kinetic) energy $\Sigma E = E_1 + E_2$ in $U^{238}$ photofission for different mass ratios $E_1/E_2$.

Wahl[12] has observed a similar characteristic of the combined-energy distribution for $U^{235}$ fission induced by 14-Mev neutrons, although a clear separation of the two peaks was not observed.

The left-hand peak of the curves in Fig. 5 results from the existence of a bridge connecting the two hills of the $W_{ik}$ surface. This bridge is absent in the spontaneous fission of $Cf^{252}$ and slow-neutron fission of $U^{235}$, but appears with increasing energy of the neutrons that induce $U^{235}$ fission. Fission in which the points of the $W_{ik}$ surface are on the bridge is often called symmetric. We note, however, that not only actually symmetric fission, but many asymmetric fissions are represented by points near the bridge.

Figure 6 shows the total number of fission events corresponding to vertical slices of $\Sigma E = \text{const}$ at 3-Mev intervals. The most probable value, $\Sigma E_{pr}$, was 150 Mev. It is interesting that the bridge on the $W_{ik}$ surface is most pronounced for $\Sigma E < \Sigma E_{pr}$.

We shall now consider the total number of

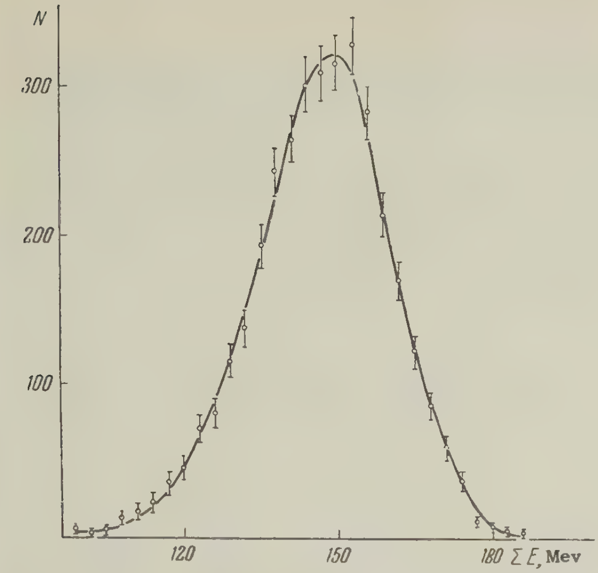

FIG. 6. Total fragment energy from photofission of U$^{238}$.

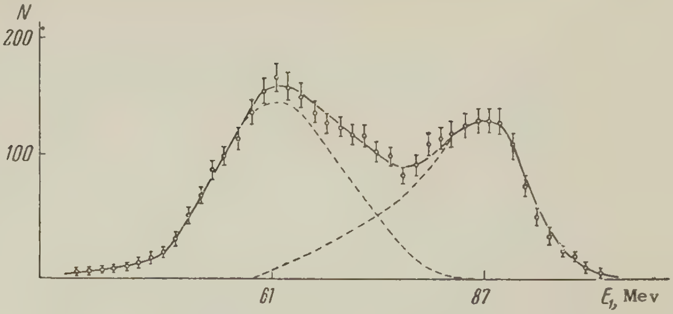

FIG. 7. U$^{238}$ photofission fragment energy $E_1$ measured with a single chamber. The dashed curves represent light and heavy fragment energies measured separately by means of two chambers.

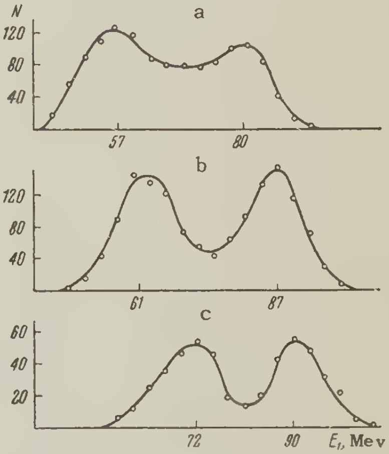

FIG. 8. U$^{238}$ photofission fragment energy $E_1$ in one chamber for three different intervals of total fragment energy: a – $105 < \Sigma E < 135$ Mev; b – $135 < \Sigma E < 165$ Mev; c – $165 < \Sigma E < 195$ Mev.

fissions as a function of $E_1$ for $E_2$ = const at 1.5 -Mev intervals (Fig. 7). This corresponds to the measurement of fragment energies in only one of the two chambers. The dashed curves in Fig. 7 represent the energy distributions of heavy and light fragments as determined by means of both chambers. Our curves are in satisfactory agreement with reference 3 when a correction for target absorption is introduced, but differ considerably from reference 2.

Our data also provided us with the energy spectra of fragments for three intervals of ΣE (Fig. 8). It is here seen that the valley between the peaks in Fig. 7 does not characterize symmetric fission, because each ordinate in Fig. 7 is the sum of the corresponding ordinates for the three curves in Fig. 8, and a peak of the curve in Fig. 8c almost coincides with valleys of curves a and b.

In conclusion, we present a summary of the quantities that usually characterize the energy distribution of fission fragments. The authors wish to thank the synchrotron team of the Physico-Technical Institute for the uninterrupted operation of the synchrotron, and Yu. Morozov and B. K. Gormin for technical assistance.

---

[1] L. E. Lazareva and N. V. Nikitina, Физика деления атомных ядер, (The Physics of Atomic Fission), Atomizdat, 1957, p. 189.

[2] Korotkova, Cherenkov, and Chuvilo, Doklady Akad. Nauk SSSR **106**, 811 (1956), Soviet Phys.-Doklady **1**, 104 (1956).

[3] Kovrigin, Kondrat'ko, and Petrzhak, JETP **36**, 315 (1959), Soviet Phys. JETP **9**, 217 (1959).

| No. | Experimental quantities | Uncorrected | Corrected for source thickness | Correction for ionization defect |
|---|---|---|---|---|
| 1 | Most probable light-fragment energy, Mev | 87±1 | 91.5±1 | +5.6 |
| 2 | Most probable heavy-fragment energy, Mev | 61±1 | 64,5±1 | +6.8 |
| 3 | Ratio of most probable energies | 1,43±0.04 | 1.42±0.04 | |
| 4 | Most probable mass ratio | 1.36±0.04 | 1.36±0.04 | |
| 5 | Half-width of high-energy peak, Mev | 17 | | |
| 6 | Half-width of low-energy peak, Mev | 19 | | |
| 7 | Valley-to-peak ratio for high-energy peak | 0,7 | | |
| 8 | Most probable total (kinetic) energy ΣE, Mev | 150±2 | 157.5±2 | +12.4 |
| 9 | Half-width of total energy peak, Mev | 31 | | |

[4] R. B. Leachman, International Conference on the Peaceful Uses of Atomic Energy, Geneva, August 1955, Vol. 2, Russ. Transl. Goztekhizdat 1958, p. 220.

[5] W. Jentschke and F. Prankl, Z. Phys. **119**, 696 (1942).

[6] D. C. Brunton and G. C. Hanna, Can. J. Research **28A**, 190 (1950).

[7] D. C. Brunton and W. D. Thompson, Can. J. Research **28A**, 498 (1950).

[8] Smith, Friedman, and Fields, Phys. Rev. **106**, 779 (1957)

[9] I. V. Chuvilo, Dissertation, Physico-Technical Inst., Acad. Sci. USSR, 1952.

[10] Katz, Kavanagh, Cameron, Bailey, and Spinks, Phys. Rev. **99**, 98 (1955).

[11] Smith, Friedman, and Fields, Phys. Rev. **102**, 813 (1956).

[12] J. S. Wahl, Phys. Rev. **95**, 126 (1954).

[13] Bogachov, Vorob'ev, and Komar, Izv. Akad. Nauk SSSR, Ser. Fiz., **20**, 1455 (1956), Columbia Tech. Transl. p. 1331.

Translated by I. Emin
268

SOVIET PHYSICS JETP VOLUME 11, NUMBER 5 NOVEMBER, 1960

# INVESTIGATION OF THE MAIN K X-RAY ABSORPTION EDGE IN SELENIUM

D. BALLY and L. MÜLLER

Atomic Physics Institute of Rumania, Bucharest

Submitted to JETP editor October 16, 1959

J. Exptl. Theoret. Phys. (U.S.S.R.) 38, 1381-1382 (May, 1960)

The position and the width of the K x-ray absorption edge of crystalline and amorphous selenium are measured. The dependence of the main absorption edge on the thickness of the absorber is investigated.

THE main K x-ray absorption spectrum of selenium was investigated by a number of authors.[1-3] In stating their experimental methods, the authors did not indicate the structure of the absorbers; apparently they investigated crystalline selenium.

Investigating the L absorption spectrum of selenium, Rudström and Sjöberg[4] found that a transition from the crystalline into the amorphous state leads to a change in the absorption spectrum. In connection with these results, the investigation of the K absorption spectrum of crystalline and amorphous selenium is of interest.

The investigation was carried out with the aid of a bent-crystal Cauchois-type spectrometer with a radius of 41.6 cm. We used the reflecting ($\bar{2}01$) planes of a mica crystal. The absorbers were prepared: a) by vacuum evaporation, and b) by glueing powder onto a mica foil. The thickness of the absorbers varied from 4 to 160 $\mu$.

We found the position of the main absorption edge of crystalline selenium to be K = 12652.6 ev (977.86 xu). This value coincides with the results (12653.4 ev) of other authors.[1,3]

W. H. Zinn determined the width $\Delta K$ of the main absorption edge by Ross' method.[5] The value determined by this method depends on the thickness of the absorber. Therefore, we used Sandström's method[6] for determining the width of the main absorption edge. The value obtained by Sandström's method does not depend on the thickness of the absorber, and amounts to 17.2 ev, i.e. 1.33 xu, instead of 7.9 ev as found by Zinn.

We also observed the structure elements of the main absorption edge which had been observed by Hulubei and Cauchois,[3] namely the "white line" at a distance of 5 ev, and the "black line" at a distance of 13 ev from the main edge.

An increase in the absorber thickness leads to the appearance of "structure" in the main absorption edge. This structure was observed on the short-wave side by Parratt, Hempstead, and Jossem,[7] and by Vaĭnshteĭn,[8] who also explained this effect. Our experiments show that on increasing the absorber thickness, structure also appears on the long-wave side (see the figure). On increasing the absorber thickness to 160 $\mu$ we observed a 1.8-ev shift of the point of inflection of the K absorption edge of selenium, towards shorter wavelengths. Such a shift was predicted by Sandström,[6] and also experimentally shown in other works.[7,8]

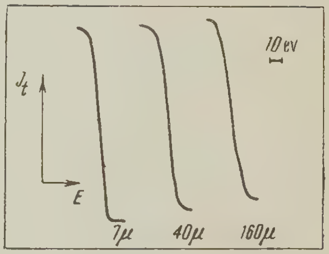

The main K absorption edge in selenium for various absorber thicknesses. $J_t$ is the intensity of the transmitmitted x-ray beam.

The investigation of amorphous selenium led to the results listed in the table, where $\delta$ denotes the distance between the main K absorption edges of crystalline and amorphous selenium. It should be noted that Shiraiwa, Ishimura, and Sawada[9] investigating germanium observed that the transition from the crystalline to the amorphous state caused a 4-ev shift of the point of inflection of the K absorption edge, towards higher energies. This result is analogous with our result.

From the table it can be seen that during a transition from the crystalline to the amorphous state the width of the main edge increases by (4.65 ± 0.5) ev. However, since even an estimate of the error in such measurements is difficult, it seems to us that only the increase itself in the width of the main edge is of interest.

Small amounts of impurities affect both the position of the point of inflection and the width of the main absorption edge of selenium. We ob-

| | $K$ | | $\Delta K$ | |
|---|---|---|---|---|
| | ev | xu | ev | xu |
| Crystalline state | 12652.6 | 977.86 | 17.2 | 1.33 |
| Amorphous state | 12649.8 | 978.08 | 21.8 | 1.69 |
| $\delta$ | 2.8 | —0.22 | —4.6 | —0.36 |

served this effect when investigating 99.9% pure selenium.

---

[1] B. Kievit and G. A. Lindsay, Phys. Rev. **36**, 648 (1930).

[2] W. H. Zinn, Phys. Rev. **46**, 659 (1934).

[3] H. Hulubei et al., Compt. rend. **211**, 316 (1940).

[4] L. Rudström and S. Sjöberg, Arkiv Fysik **13**, 297 (1958).

[5] P. A. Ross, Phys. Rev. **44**, 977 (1933).

[6] A. E. Sandström, Phil. Mag. **22**, 497 (1936).

[7] Parratt, Hempstead, and Jossem, Phys. Rev. **105**, 1228 (1957).

[8] M. M. Kakhana and É. E. Vaĭnshteĭn, Izv. Akad. Nauk SSSR, Ser. Fiz. **21**, 1459 (1957), Columbia Tech. Transl. p. 1447.

[9] Shiraiwa, Ishimura, and Sawada, J. Phys. Soc. Japan **12**, 788 (1957).

Translated by Z. Barnea
269

SOVIET PHYSICS JETP VOLUME 11, NUMBER 5 NOVEMBER, 1960

# *EFFECT OF TEMPERATURE ON CHARACTERISTIC ENERGY LOSSES OF ELECTRONS IN IRON*

I. B. BOROVSKIĬ, A. N. KABANOV, Yu. M. KUSHNIR, and V. V. SHMIDT

Metallurgy Institute, Academy of Sciences, U.S.S.R.

Submitted to JETP editor November 4, 1959

J. Exptl. Theoret. Physics (U.S.S.R.) **38**, 1383-1387 (May, 1960)

It is found that the characteristic energy losses of electrons in Fe exhibit a discontinuity at a first-order phase transition ($\alpha \rightarrow \gamma$-transition). The effect is analyzed on the basis of the plasma model.

## 1. FORMULATION OF THE PROBLEM

INVESTIGATIONS of the fine structure in the principal K absorption edge of x rays in iron[1] have shown that there is a marked change in this structure when the absorber is heated above the temperature of the $\alpha \rightarrow \gamma$-transition (910° C). It has also been shown that there is a connection between the fine structure in the x-ray K edge in Fe and the magnitude of the characteristic energy losses of electrons at room temperature; these have been investigated by Kleinn.[2]

The characteristic energy losses of fast electrons which pass through thin layers of matter or are reflected from bulk samples have been discussed frequently in the literature.[3-12]

In some of this work the following model is assumed: the fast charged particle, passing through the solid body, undergoes an inelastic collision with a valence electron and loses a certain amount of energy in transferring this electron to the next allowed energy band of the solid.

In this analysis the positions of the maxima of the characteristic energy losses are chosen in all investigations (except reference 1) to correspond to the extrema of the fine structure of the x-ray absorption spectrum on the short-wave side of the principal edge. Many of the experimental data are in agreement with this interpretation; in particular, the data are in agreement with the conclusion that the magnitude of the characteristic losses $\epsilon \sim 1/a^2$, where a is the lattice constant of the crystal.[5]

However, a considerable portion of the experimental data is not consistent with this one-electron analysis of the effect. To explain this discrepancy it has been proposed that the charged particle interacts collectively with many valence electrons in the solid (cf. references 8 — 11). This interaction leads to the excitation of collective (plasma) oscillations of the electron gas; the frequency of the plasma oscillations satisfies the dispersion relation $\omega^2 = \omega_p^2 + \alpha k^2$, where $\omega_p = (4\pi n e^2/m)^{1/2}$, n is the number of electrons per unit volume, e is the charge of the electron, m is the effective mass of the electron, k is the wave number for the plasma wave and $\alpha$ is a proportionality factor.

The low-wavelength limit of the plasma oscillations is determined by the mean inter-electronic distance $r_s = (3/4\pi n)^{1/3}$. Consequently there is an upper limit on the wave number: $k \leq k_c$. In metals $\alpha k_c^2 \ll \omega_p^2$. The energy of the photon associated with the plasma oscillations (plasmon), which are excited by a fast charged particle which passes through or is reflected from the metal, is given by

$$\hbar\omega \approx \hbar\omega_p = \hbar\,(4\pi n e^2/m)^{1/2}.$$

This energy agrees with the value of the first characteristic energy loss for such a particle.

We note that there is also a compromise point of view,[12] according to which some of the lines in the characteristic losses are associated with the excitation of plasma oscillations, while others are associated with single-electron transitions between energy bands in the solid.

## 2. EXPERIMENTAL METHOD

We have measured the characteristic losses in iron with an electrostatic electron velocity analyzer of original design.[13,14] The device provides accelerating voltages up to 75 kv and a resolving power of 0.5 ev.

The electron-optical system of the analyzer consists of an illuminating system (cathode, control electrode, anode, illumination iris and electrostatic condenser), which is inclined 8° to the optical axis of the analyzer, a sample holder, an analyzing lens, and a camera. The design of the sample holder is such that the horizontal position of the sample and its inclination with respect to the axis of the instrument can be adjusted. The samples used in this work consist of plates 3 — 4 mm wide, 0.08 — 0.10 mm thick, and 25 mm long. The samples can be heated to 1200° C by passing direct current through them. The analyzing lens provides a dispersion of 0.2 mm/ev at an electron energy of 75 kev. The camera contains a movable magazine with twelve plates (6 × 9 cm) which are used to photograph the energy spectra of the reflected electrons.

In this work we measure the characteristic energy losses of electrons reflected from the sample in the following manner.

An electron beam with an energy of 70 — 75 kev, produced by the illumination system, strikes the sample being investigated at a glancing angle of 4°. The electrons which are reflected at the same angle (angle of observation) strike a narrow slit (width approximately 3 μ) located above the analyzing lens and are analyzed by the latter into an energy spectrum which is recorded on the photographic plate.

A vacuum of $5 \times 10^{-6}$ mm Hg is maintained in the apparatus. The temperature of the sample is measured with an accuracy of approximately 20° by means of an optical pyrometer.

The characteristic losses in Fe have been investigated at temperatures of 20, 800 and 930° C. Two control pictures are taken at 600° C. Each picture at room temperature is taken immediately after the sample is heated to 700 — 800° C. This preliminary heating serves to remove any organic film which may form on the sample; a new film does not have time to form during the exposure time (1.5 min). This procedure is found to be mandatory. On pictures obtained at room temperature with samples which are not preheated, it is impossible to obtain well resolved lines, in spite of careful surface cleaning; the smearing of the lines is due to energy losses in the thin film of organic contaminant which forms on the sample. From 6 to 11 pictures are taken at each temperature. A photometric analysis is then made with an MF-4 recording microphotometer. Typical results of an analysis of this kind are shown in Table I. The photometric curves for Fe at 20 and 930° C are shown in the figure. The position of the line is determined by means of markers made in the ex-

TABLE I

| Number of photograph | T, °C | Characteristic electron energy losses in Fe, ev | | | | |
|---|---|---|---|---|---|---|
| 1 | 20 | — | 13.5 | 20.5 | — | — |
| 2 | | 6.6 | 14.9 | 21.0 | 41 | 53 |
| 3 | | 7.0 | 16.2 | 22.1 | 42 | 55 |
| 4 | | 7.5 | 15.0 | 21.7 | — | 57 |
| 5 | | 8.8 | 14.4 | — | — | 53 |
| 6 | | — | — | 22.3 | 37 | 57 |
| Average over photographs 1–6 | 20 | 7.5±0.7 | 14.8±0.7 | 21.5±0.6 | 40±2 | 55±2 |
| 7 Control photographs | 600 | 7.2 | 12.7 | 19 | — | 54 |
| 8 | | 7.4 | 14.6 | 20.4 | 41 | 55 |
| 9 | 800 | 7.9 | 13.7 | 21.5 | 45 | 58 |
| 10 | | 7.0 | 12.7 | 19.5 | 39 | 54 |
| 11 | | 8.5 | 12.7 | 20.2 | — | 53 |
| 12 | | 8.2 | 13.0 | 20.2 | 42 | 60 |
| 13 | | 7.4 | 14.4 | 21.5 | — | 58 |
| 14 | | 8.6 | 13.9 | 21.5 | 45 | 60 |
| Average over photographs 9–14 | 800 | 8.1±0.5 | 13.2±0.5 | 20.7±0.8 | 43±2 | 57±3 |
| 15 | 930 | 10.3 | 22.7 | 33 | — | 54 |
| 16 | | 10.6 | 23.1 | — | 42 | 54 |
| 17 | | 10.6 | 22.3 | 32 | 44 | 54 |
| 18 | | 9.7 | 24.3 | — | 39 | — |
| 19 | | 10.9 | 24.5 | — | — | — |
| 20 | | 11.2 | 21.3 | 32 | — | 53 |
| 21 | | 11.1 | 22.9 | 33 | 42 | 55 |
| 22 | | 12.3 | 23.3 | — | 43 | — |
| 23 | | 10.4 | 22.3 | — | 53 | 56 |
| 24 | | 12.5 | 26.2 | — | — | 56 |
| 25 | | 11.2 | 21.7 | 34 | — | 54 |
| Average over photographs 15–25 | 930 | 11.0±0.6 | 23±1 | 33±1 | 42±1 | 54±1 |

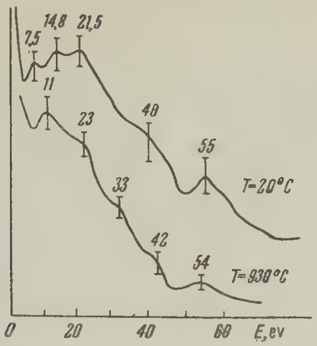

The characteristic energy losses (E) of electrons reflected from Fe. The energy is computed from the line corresponding to elastically-scattered electrons. The numbers on the vertical lines indicate the abscissa of the maxima and give the characteristic losses in electron volts (cf. Table I). The blackening of the photographic plates which record the reflected electrons is plotted along the ordinate axis.

posure at every 9.5 ev. With this procedure it is possible to determine the positions of the maxima of the characteristic losses with an accuracy of 0.5 — 0.8 ev with respect to the zero line (elastic scattering).

## 3. EXPERIMENTAL RESULTS

The experimental results may be summarized as follows. The characteristic losses in $\alpha$-Fe (body-centered cubic, a = 2.86 A) investigated at 20, 600 and 800° C are found to be independent of temperature. The first characteristic loss at 20° C is (7.5 ± 0.7) ev. The next two lines, 14.8 and 21.5 ev may be considered multiples of the first. The difference in the value of the second characteristic loss (13.2 ev) at 800° C (close to the Curie point) as compared with the value at 20° C (14.8 ev) approaches the limiting accuracy of the experiment. In order to verify that there is in fact no change in the characteristic energy losses in transition through the Curie point, we have carried out experiments with a nickel sample ($T_C$ = 330° C). No change is observed in the energy of the characteristic losses as the temperature of the sample is varied from 20 to 500° C; this result can be seen from Table II.

The characteristic energy losses in $\gamma$-Fe (face-centered cubic, a = 3.60 A at 940° C) are considerably different from the energy losses in $\alpha$-Fe. The first characteristic energy loss is (11.6 ± 0.6) ev. The next two lines (23 and 33 ev) can also be considered multiples of the first.

## 4. DISCUSSION OF THE EXPERIMENTAL RESULTS

We first interpret these results on the basis of single-electron transitions. According to this picture, the increase in the lattice constant which occurs in the $\alpha \rightarrow \gamma$-transition should lead to a reduction in the energy losses (because $\epsilon \sim 1/a^2$). This conclusion, however, is in contradiction with the experimental results: the $\alpha \rightarrow \gamma$-transition increases the characteristic losses. Thus, the single-electron transition analysis does not agree with experiment even insofar as determining the sign of the change in the energy of the characteristic losses due to a change in the interactomic distances and a change in the crystal lattice; for this reason we are forced to interpret the experimental results on the basis of a plasma-oscillation picture.

The valence electrons in Fe are 3d and 4s electrons. The latter are conduction electrons. The 3d electrons are usually considered strongly bound, i.e., heavy particles ($m \sim 30$) with wave functions localized at the atoms. Hence we shall assume that only the 4s electrons in Fe participate in the plasma oscillations. Setting the effective mass equal to the mass of the free electron, we use the formula $\hbar\omega_p = \hbar(4\pi ne^2/m)^{1/2}$ to com-

TABLE II

| Number of photograph | T, °C | Characteristic energy losses in Ni, ev | | | |
|---|---|---|---|---|---|
| 1 | 20 | 7.0 | 20 | 27 | 33 |
| 2 | | 10.7 | 22 | 28 | — |
| 3 | | 8.0 | 20 | — | 33 |
| 4 | | 9.0 | 19 | — | — |
| Average over photographs 1–4 | 20 | 9±1 | 20±1 | 27.5 | 33 |
| 5 | 500 | 10.4 | 19.0 | 28 | 33 |
| 6 | | 9.5 | 19.0 | 28 | 33 |
| 7 | | 9.5 | 18.4 | 26 | 35 |
| 8 | | 9.5 | 16.3 | — | 33 |
| Average over photographs 5–8 | 500 | 9.7±0.5 | 18.2±0.9 | 27±1 | 34±1 |

pute the number of 4s electrons for α and γ-Fe. This calculation gives approximately 0.5 electrons at an atom for α-Fe and approximately 1.2 electrons per atom for γ-Fe. This estimate is in agreement with the calculation of the electronic structure of metallic α-Fe made on the basis of a self-consistent field analysis with exchange effects neglected.[15] In this calculation the configuration $3d^{7.2}4s^{0.8}$ is obtained, i.e., metallic α-Fe has 0.8 of a 4s electron per atom.

The marked difference in the number of 4s electrons per atom in α-Fe as compared with that in γ-Fe casts doubt on the validity of setting the effective mass equal to the mass of the free electron in the formula given above.

It would seem more reasonable to explain the observed characteristic energy losses of electrons in iron in terms of excitation of collective oscillations. However, the nature of the characteristic losses in Fe will require additional investigation; this question is far from resolved at present.

The fact remains, however, that an allotropic transformation in iron is accompanied by a change in the characteristic energy losses.

---

[1] N. B. Borovskiĭ and V. V. Shmidt, Dokl. Akad. Nauk SSSR **127**, 997 (1959), Soviet Phys.-Doklady **4**, 855 (1960).

[2] W. Kleinn, Optik **11**, 226 (1954).

[3] E. Rudberg, Phys. Rev. **50**, 138 (1936).

[4] L. B. Leder, Phys. Rev. **103**, 1721 (1956).

[5] A. Ya. Vyatskin, J. Tech. Phys. (U.S.S.R.) **28**, 2217, 2455 (1958), Soviet Phys.-Tech. Phys. **3**, 2083 (1959).

[6] Y. Cauchois, Acta Cryst. **5**, 351 (1952).

[7] Leder, Mendlowitz, and Marton, Phys. Rev. **101**, 1460 (1956).

[8] D. Bohm and D. Pines, Phys. Rev. **82**, 625 (1951).

[9] D. Bohm and D. Pines, Phys. Rev. **92**, 609 (1953).

[10] D. Pines, Phys. Rev. **92**, 626 (1953).

[11] H. Watanabe, J. Phys. Soc. Japan **11**, 112 (1956).

[12] R. Ferrell, Phys. Rev. **101**, 554 (1956).

[13] Kabanov, Milyutin, and Fetisov, Izv. Akad. Nauk SSSR Ser. Fiz. **23**, 459 (1959), Columbia Tech. Transl. p. 443.

[14] A. N. Kabanov and V. I. Milyutin, Радиотехника и электроника, (Radio Engineering and Electronics) **4**, 109 (1959).

[15] F. Stern, Phys. Rev. **104**, 684 (1956).

Translated by H. Lashinsky
270

SOVIET PHYSICS JETP VOLUME 11, NUMBER 5 NOVEMBER, 1960

# *DISINTEGRATION OF EMULSION NUCLEI BY 930-Mev PROTONS*

O. V. LOZHKIN, N. A. PERFILOV, A. A. RIMSKIĬ-KORSAKOV and J. FREMLIN*

Radium Institute, Academy of Sciences, U.S.S.R.

Submitted to JETP editor November 18, 1959

J. Exptl. Theoret. Phys. (U.S.S.R.) 38, 1388-1398 (May, 1960)

The interaction of 930-Mev protons with emulsion nuclei has been investigated, special attention being directed to interactions involving the emission of multiply charged particles with $Z \geq 3$ from the nuclei. The relative yields of isotopes of hydrogen, helium, lithium, and nuclei with $Z \geq 4$ were determined for disintegrations of light and heavy nuclei with three or more prongs. The cross section for the production of lithium isotopes in the disintegration of Ag and Br nuclei was found to be (135 ± 13) mb; for fragments with $Z \geq 4$ the cross section was (62 ± 11) mb. The angular and energy distributions of the fragments, multiplicity of fragment production, dependence of the fragment-production probability on the number of $\alpha$ particles and protons in one disintegration, and other characteristics of the fragmentation process were studied. The fragmentation mechanism is discussed.

## 1. INTRODUCTION

INVESTIGATION of the phenomenon of the emission of multiply charged particles (fragments) in nuclear disintegrations, for various energies of the incident particles and various atomic numbers of the target nuclei, indicates a number of interesting characteristics of this phenomenon: a sharp increase in the cross section for fragment production and an increase in the number of fragments per disintegration with increasing energy of the incident protons, a considerable angular anisotropy of the produced fragments relative to the direction of the incident protons, a connection between the probability of fragment emission and the total energy transferred to the nucleus during the collision, and others. Interest in the phenomenon of fragment production in nuclear disintegrations produced by high-energy particles has considerably increased recently in connection with the question of the existence of correlated clusters of nucleons in nuclei and the presence of collective interactions between the high-energy particles and these clusters.

The data describing the properties of the emitted fragments is at present far from complete, and sometimes contradictory, which leads to great differences in the basic points of view on the nature of the fragmentation process. Some of the known facts prove to be difficult to explain within the framework of generally accepted ideas on various interactions of high-energy particles with nuclei (nuclear cascade, evaporation, fission). However, another basic point of view which envisages the production of fragments by a quite distinct mechanism of nuclear disintegration[1-3] has not yet been supported by sufficiently weighty evidence.

The possibility of direct investigation of many characteristics of the fragments emitted in disintegrations by means of the nuclear emulsion method makes this method very valuable for a study of the fragmentation process.

In this article we present experimental material on the interaction of 930-Mev protons with emulsion nuclei, particular attention being directed to disintegrations accompanied by the emission of fragments with $Z \geq 3$.

## 2. EXPERIMENTAL METHOD

Especially fine-grained type P-R emulsions, used in the experiment and prepared in N. A. Perfilov's laboratory without additional sensitization in triethanolamine, were irradiated in the 930-Mev proton beam of the Birmingham (England) proton synchrotron. Figure 1 shows the sensitometric characteristic of the emulsion for charged particles. As can be seen from the figure, although the emulsion was also sensitive to relativistic electrons, the grain density of relativistic particle tracks was insufficient for a reliable visibility on the random grain back-

---

*Professor at the University of Birmingham (England).

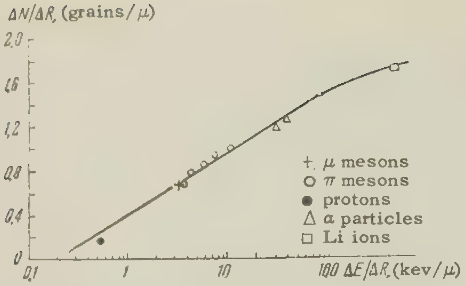

FIG. 1. Sensitometric characteristic of P-R emulsion not sensitized with triethanolamine.

ground, and therefore only protons of energy $\leq$ 500 Mev were reliably recorded. But the low contrast of the emulsion (i.e., the weak variation of dN/dR with dE/dR) leads to the formation of a great number of gaps between grains at the end of the range of tracks produced by particles of charge $Z = 3$, which permits use of the "scale" method[4] for identifying particles of charge $Z = 1$, 2, and 3. The tracks of particles with $Z \geq 4$ had almost no gaps close to the end of the range and, furthermore, were marked by a very noticeable thinning down; therefore they could be reliably distinguished from particles of smaller charge. The charge of particles in the region $Z \geq 4$ was measured by the method[5] of integral track-width measurement* at a given distance from the end of the range.

The "scale method" used in this work to identify particles with $Z = 1$, 2, and 3 was first used by Serebrennikov[6] and later developed by Rimskiĭ-Korsakov.[4] This method is based on studying the track by means of an eyepiece scale with uniform divisions of a given length. When the scale is superimposed over the track image, the grains of the track overlap part of the scale divisions. Each track is characterized by some number G of overlapped scale divisions completely filled by grains of the track at a given distance from the end of the range. This number is a nonlinear function of the grain density dN/dR. The choice of the size of the scale division is determined by the region of values of dN/dR in which the estimate given by the scale most strongly depends on dN/dR, and in this way one can obtain the best separation of the particles in the grain density region of interest to us. For the emulsion used by us, a scale division length of 1.25μ in the plane of the object gave the best separation of particles in the region of 120 — 180 grains per 100μ, which corresponded to particles of charge one to three at the end of the range.

In the analysis of nuclear disintegrations the scale was used for the analysis only of tracks of particles stopping in the emulsion with ranges $\geq 60\mu$ and dip angles $\leq 30°$ to the plane of the emulsion. For particles with $Z \geq 4$, only tracks of length $> 15\mu$ were taken; multiply charged particles of smaller length were regarded as recoil nuclei. The following criteria were used for separating the disintegrations into disintegrations of heavy and light nuclei of the emulsion: 1) total charge of the particles in the disintegration (for $\Sigma Z > 8$ the disintegration was regarded as that of a heavy nucleus); 2) the presence or absence of a recoil nuclei (when there was a recoil nucleus, the disintegration was regarded as that of a heavy nucleus); 3) the presence or absence of short-range α particles or protons of range $< 50\mu$ and $< 100\mu$, respectively (in the case of short-range particles the disintegration was regarded as that of a light particle). Disintegrations which could not be classified by all three criteria, i.e. disintegrations with $\Sigma Z \leq 8$ without a recoil nucleus and not having any short-range particles, were regarded as disintegrations of light nuclei, although some of them may, of course, have been due to disintegrations of heavy nuclei. Since, however, the relative amount of disintegrations not satisfying the above criteria is small, the uncertainty introduced by our separation is also correspondingly small. Indeed, since only disintegrations having three or more prongs (i.e. $\Sigma Z \geq 3$) were studied, the doubtful disintegrations could be only those containing no recoil nuclei and with total particle charge $3 \leq \Sigma Z \leq 8$, which constituted only 14% of all disintegrations. The use of the third characteristic (α-particle and proton energy) reduced this value still further.

## 3. EXPERIMENTAL RESULTS

To determine the nature of particles in the region of Z between 1 and 3, a total of 1054 stars with three or more prongs was analyzed. Of these, 905 stars were classed as disintegrations of heavy nuclei and 149 as disintegrations of light nuclei. The estimate of the fragment yield was obtained from the fact that out of 1430 stars with three or more prongs it was found that the number of stars with fragments of $Z \geq 4$ were 103 and 30 for the heavy and light nuclei, respectively. In order to study the production process for such fragments, an additional 147 stars with fragments of $Z \geq 4$ were found.

---

*The method involves the measurement of the particle's track width on successive segments from the end of its range, and the summation of all the values obtained on the preceding segments.

Among the disintegrations with fragments of $Z \geq 4$, the major part consisted of disintegrations in which one or several fragments of $Z < 12$ were emitted. Sometimes, however, disintegrations were observed with two multiply charged fragments having approximately the same range of the order $8\mu$ and emitted in opposite directions; according to Shamov,[7] such stars should be considered to be cases of the fission of the silver nucleus. Eleven such events were observed, which constituted about 5% of the total number of disintegrations with fragments of $Z \geq 4$.

In Fig. 2 is shown the distribution of the G values, obtained with the aid of the scale, for tracks of particles emitted in the disintegration of light and heavy nuclei. It is seen from the figure that the tracks of singly and doubly charged particles with ranges $\geq 62.5\mu$ are clearly separated; for tracks of Li nuclei and of doubly charged particles of the same range, the separation is much poorer. In the same figure are shown the distributions of the evaluation of G for tracks of known protons in emulsion of the same type; also shown are the mean values of G for tracks of protons, $\alpha$ particles, and Li nuclei. The mean values of G for Li ions were obtained by measuring the tracks of $Li^8$, which give a characteristic T shape in the emulsion; and for the analysis of the $\alpha$-particle tracks we used $\alpha$ particles from the decay of $Be^8$ nuclei.

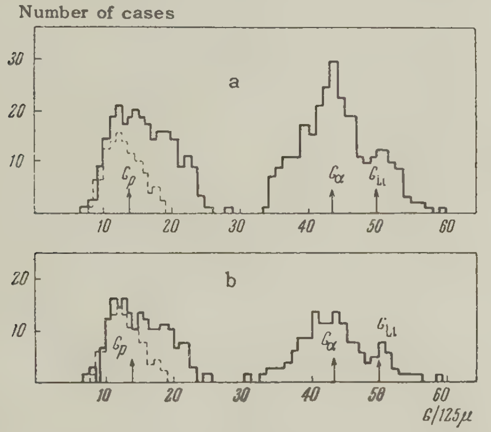

FIG. 2. Distribution of evaluation of G (over $125\mu$ range) obtained by means of the scale method for particles stopped in the emulsion. a) Disintegration products of heavy nuclei of the emulsion; b) light nuclei. The dotted lines indicate the G-value distribution for protons.

The obtained distribution of G values for the nuclear disintegration products clearly shows the presence of some isotopes of hydrogen (heavier than $H^1$) and, possibly, helium. Knowledge of the shape of the G-value distribution curves for $H^1$ and $He^4$ isotopes would permit an analysis of the obtained G-distribution curve and allow one to find the ratio of the isotope yields of singly and doubly charged particles. In the present work, however, it was possible to do this only for the hydrogen isotopes, since we did not have an $\alpha$-particle source of sufficient energy to calibrate the emulsions.

The table gives the characteristics of nuclear disintegrations with three or more prongs analyzed in this work. As seen from the table, a high yield of $H^2$ and $H^3$ isotopes was observed in comparison with $H^1$. The relative number of $Li^8$ isotopes is extremely small in

Characteristics of nuclear disintegrations with three or more prongs

| Characteristics of stars | | Ag, Br | C, N, O |
|---|---|---|---|
| Mean number of particles | H isotopes | 3.7±0.8 | 2.6±0.7 |
| | He isotopes | 0.8±0.1 | 1.7±0.3 |
| | Li isotopes | 0.18±0.04 | 0.10±0.04 |
| | Fragments with $Z \geqslant 4$ | 0.10±0.01 | 0.09±0.03 |
| Cross section, mb | Li isotopes | 135±31 | 20±8 |
| | Fragments with $Z \geqslant 4$ | 62±11 | 18±5 |
| Relative yields | $\frac{He^3 + He^4}{H^1 + H^2 + H^3}$ | 0.22±0.07 | 0.66±0.12 |
| | $\frac{H^2 + H^3}{H^1 + H^2 + H^3}$ | 0.18±0.8 | — |
| | $\frac{Li^8}{Li^6 + Li^7 + Li^8}$ | 0.012±0.009 | 0.03±0.04 |

comparison with the lighter isotopes of lithium.

Figure 3 shows the distribution of 46 measured tracks of particles with $Z \geq 4$ produced in the disintegration of Ag and Br nuclei as a function of their integral width. In the case of tracks with dip angles $\leq 30°$ (in unprocessed emulsion), 7 segments were measured through $3.5\mu$. For the calibration we used the T-shaped tracks, part of which proved to be $Li^8$ and part $B^8$. Shown in the figure are the values of the integral width for particle tracks of various charge relative to the width of the $Li^8$ tracks for an assumed dependence on $Z$ of the integral width of the form $\sqrt{Z}$. The analysis of the distribution shown in Fig. 3 indicates that the ratio of the number of fragments Be : B : C : N : O corresponds approximately to the ratio 15 : 16 : 7 : 6 : 2. It should be noted that the number of recorded Be fragments is considerably reduced, owing to the decay of the $Be^8$ isotope into two $\alpha$ particles immediately after emission from the nucleus.

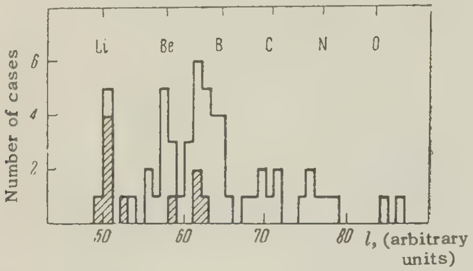

FIG. 3. Distribution of tracks of particles with $Z \geqslant 4$ as a function of the integral width $l$. The shaded area corresponds to T-shaped tracks of $Li^8$ and $B^8$.

The production cross sections for the individual products of nuclear disintegration were evaluated from their frequency in the observed number of disintegrations of emulsion nuclei with three or more prongs on the basis of the production cross section of the latter, which was (859 ± 57) mb (according to the data of Philbert[8]). The cross sections calculated in this way are also shown in the table.

It should be noted that the cross section for the production of $Li^8$ fragments is ~2 mb, in close agreement with the value (1.1 ± 0.3) mb found by Munir[9] for the disintegration of Ag and Br nuclei at the same incident particle energy, but turns out to be considerably larger than that for particles of lower energy. Simultaneously with the increase in the cross section for the production of multiply charged particles, the multiplicity of the fragment production process also increases with the energy of the incident particles. Thus, for 71 disintegrations with one fragment of $Z \geq 4$, there were observed 24 disintegrations with two fragments and 8 disintegrations with three fragments, while for a proton energy $E_0 = 660$ Mev the number of disintegrations with two and three fragments were 4 and 0.8%, respectively, of the number of disintegrations with one fragment.[10]

For disintegrations with fragments of $Z \geq 4$* an additional analysis was made of the various characteristics of nuclear disintegration in order to explain the nature of the fragmentation process. The angular distribution of the fragments with $Z \geq 4$ in the disintegration of Ag and Br nuclei are characterized by a considerable anisotropy with respect to the direction of the incident particles. The forward—backward ratio in the laboratory system turned out in this case to be 2.3 ± 0.7.

The mean number of singly and doubly charged particles in disintegrations with fragments was 8, which is considerably greater than the mean number of particles in ordinary disintegrations.

In Figs. 4 and 5 are shown the relative probability of the emission of fragments with $Z \geq 4$ in stars with various numbers of particles for proton energies $E_p < 30$, $\geq 30$, and $\geq 100$ Mev, relative to the total number of disintegrations with a given number of particles. While the relative probability of the emission of fragments sharply increases with the number of slow particles ($E_p < 30$ Mev) and with the number of particles of cascade origin ($E_p \geq 30$ Mev), the probability of emission of a fragment decreases with an increase in the number of fast "cascade" particles ($E_p \geq 100$ Mev).

Also investigated were the energy and angular distributions of the disintegration products

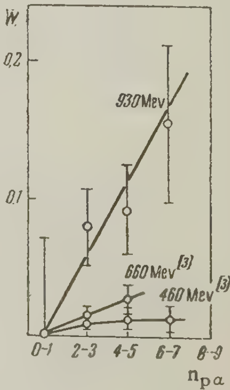

FIG. 4. Dependence of probability W of fragment emission with $Z \geqslant 4$ in disintegrations of Ag and Br nuclei on number of particles $n_{p\alpha}$ in one disintegration with $E_p < 30$ Mev at three energies of incident particles. The data for $E_0 = 460$ and 660 Mev are taken from the work of Lozhkin.[3]

---

*Fragments with $Z = 3$ were not considered, since they could be separated from $\alpha$ particles only statistically.

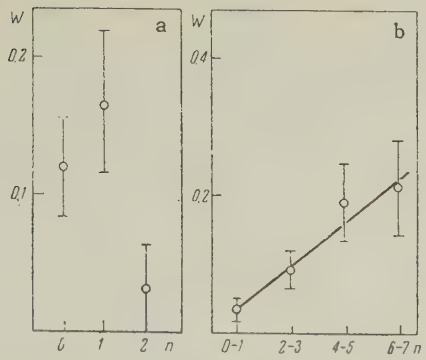

FIG. 5. Dependence of probability W of fragment emission with $Z \geqslant 4$ in disintegrations of Ag and Br nuclei on the number of particles $n_{p\alpha}$ in one disintegration: a) with energy $E_p \geqslant 100$ Mev; b) with energy $E_p \geqslant 30$ Mev.

of the Ag and Br nuclei. For singly and doubly charged particles the results of the present work are in good agreement with the results of Lock et al.[11] for the same incident-proton energy $E_0$.

The energy distribution of Li fragments shown in Fig. 6 was obtained by subtracting the range distribution for helium from the total distribution for helium and lithium; it is in satisfactory agreement with the energy distribution of $Li^8$ reported by Munir,[9] and also with the energy distribution of Li in the disintegration of Ag and Br nuclei by 6.2 Bev protons.[12]

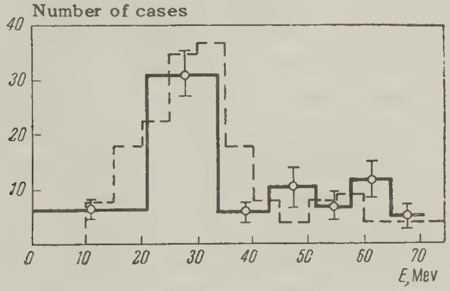

FIG. 6. Energy distribution of Li fragments in disintegrations of Ag and Br nuclei by protons of energy: $E_0 = 930$ Mev (solid line), $E_0 = 6.2$ Bev[12] (dotted line).

A study of the angular correlation between multiply charged particles and fast "cascade" particles led to the dependence portrayed in Fig. 7, which shows a considerable predominance of angles of emission of fragments in the region 30 — 90° with respect to the cascade particle. However, owing to the anisotropy of the distribution of the fragments and of the cascade particles with respect to the direction of the incident particles, such a distribution turns out to be entirely natural. In the same figure is shown the distribution of the angles between the fragments and the cascade particles calculated on the basis of the experimentally found angular distributions of fragments and fast "cascade" particles. Therefore the observed angular correlation between fragments and fast "cascade" nucleons still leads to no conclusions on the existence of genetic ties between these and other particles.

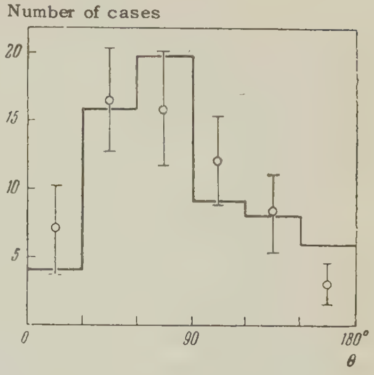

FIG. 7. Distribution of space angle θ between fragments and fast cascade particles ($E_p \geqslant 100$ Mev). Histogram — experimental distribution; the points represent the calculated results.

## 4. DISCUSSION OF RESULTS

A. Cross Sections for the Production of Various Fragments. The use of the scale method for analyzing particles with Z = 1, 2, 3 allowed us to obtain information on the relative yield of hydrogen, helium, and lithium isotopes among the nuclear disintegration products. Moreover, it proved to be possible to estimate the relative number of heavy isotopes among all the isotopes of hydrogen. The comparatively small track length (~60μ) at which the separation of particles of different nature by means of the scale method becomes sufficiently good permits the analysis of practically all particles involved in the disintegration of heavy nuclei and of the greater part of the particles involved in the disintegration of light nuclei. The obtained yield ratio of different isotopes of hydrogen is based on the shape of the G-value distribution curve for protons, which is found experimentally, and on the adopted manner of normalizing the G-value distribution. The accuracy of the results obtained is, moreover, determined by the statistics of the measurements.

The yield ratio of doubly to singly charged particles found in this work, 0.22 ± 0.07, is quite reliable, owing to the complete separation of hydrogen and helium by the scale method. The obtained value of the He/H ratio is somewhat smaller than the ratio $\alpha/p = 0.36$ reported by Lock et al.[11] for the same incident-proton energy. The relative amount of tritium and deuterium among the isotopes of hydrogen, obtained from the analysis of the N(G) curve for singly charged particles, is in agreement with the data published in reference 13 for disintegrations produced by cosmic rays. They give a value of 0.21 — 0.43 for the relative abundance of deuterium and tritium in stars of various numbers of prongs.

The investigation of the lithium isotopes shows that the emission of $Li^8$ makes up a very small part of the total production cross section for lithium, only ~1%, which is characteristic for other incident-particle energies as well.

The charge distribution of fragments with $Z \geq 4$ given above proves to be close to the distribution observed at other energies of the incident particles. In the incident-particle energy range from several hundred Mev to several Bev, as seen from Fig. 8, the distribution of fragments over Z may be described approximately by the exponential expression $P(Z) = \exp(-Z^n)$. For fragments with $Z \geq 4$ the exponent n is very close to unity. The existing differences in the distributions for different incident-particle energies do not exceed the limits of statistical error of the experiments.

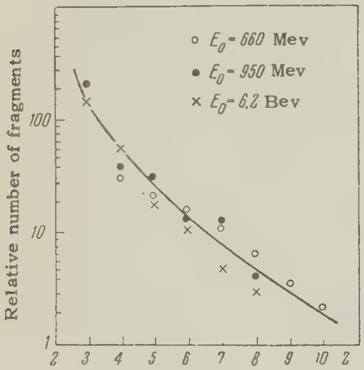

FIG. 8. Charge distribution of fragments for various incident proton energies $E_0$.

B. Characteristics of the Fragmentation Process. We shall consider the experimental data obtained in this experiment for multiply charged particles with $Z \geq 4$. The production cross section for fragments with $Z \geq 4$ in the disintegration of Ag and Br nuclei by 930-Mev protons proves to be much higher than at 660 Mev[14] (Fig. 9). The strongest dependence of the fragmentation process on the incident-particle energy is in the incident-proton energy region close to 1 Bev. This conclusion is in agreement with the data of Caretto, Hudis, and Friedlander[15] on the measurement of the variation of the cross section for the production of $F^{18}$ and $Na^{24}$, with different incident-proton energies $E_0$.

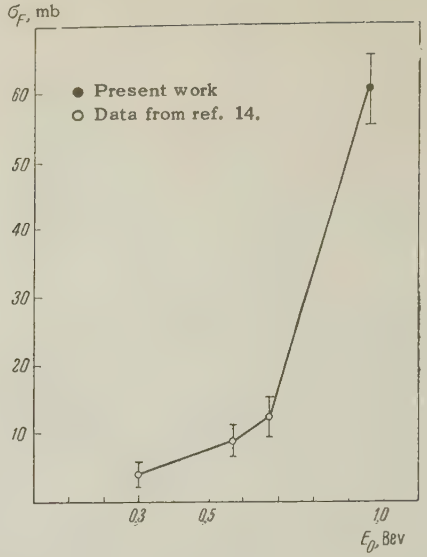

FIG. 9. Dependence of cross section $\sigma_F$ for production of fragments with $Z \geqslant 4$ on proton energy $E_0$.

Together with the increase in the total cross section for fragment production in nuclear disintegrations with an increase in the energy of the incident protons, the relative number of disintegrations with several fragments also increases. Figure 10 shows the dependence of the relative number of disintegrations with fragments on the number of fragments in one disintegration for various incident proton energies, prepared from the available data in the literature.[3, 16] At proton energies above 2 Bev, the disintegrations with more than two fragments ($Z \geq 3$) begin to predominate.

Just like low-energy protons, 930-Mev protons produce fragments primarily in multiprong disintegrations, where the probability of fragment emission increases with the total number of particles in the disintegration. As shown

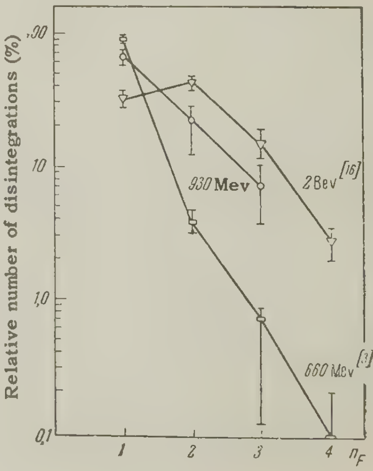

FIG. 10. Dependence of yield of disintegrations with fragments on number of fragments in a disintegration ($n_F$) for various incident proton energies $E_0$.

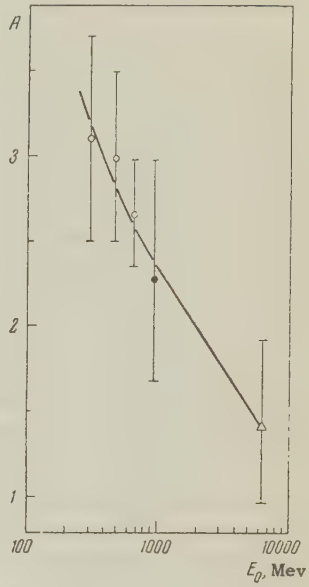

FIG. 11. The anistropy of the angular distribution of fragments as a function of the incident-proton energy. A – the ratio of the number of fragments emitted in the forward and backward hemispheres (relative to the direction of the incident protons); ● – data from the present work, ○ – reference 3, Δ – reference 12.

in Figs. 4 and 5, the probability of the production of fragments in one disintegration is a function of both the number of "cascade" particles with $E_p > 30$ Mev and the number of comparatively slow particles with $E_p < 30$ Mev. The character of this dependence is, in general, in agreement with that obtained at other proton energies.[3,17]

In order to explain the dependence of the probability of fragment emission on the number $n_{\alpha p}$ of slow particles ($E_p < 30$ Mev), Fig. 4 also shows the variation of the fragment production probability with the number of particles $n_{\alpha p}$ for lower proton energies, taken from the work of Lozhkin.[3] From an examination of Fig. 4 it is seen that the relative probability of disintegrations with fragments for an incident proton energy of $E_0 = 930$ Mev and a given number $n_{\alpha p}$ is greater than for 660 and 420 Mev. As is known,[18] the relative number of "cascade" particles among all particles with $E_p < 30$ Mev increases with the energy of the incident particles. Thus, the more rapid increase in the fragment production probability with an increase in the total number of particles in a disintegration produced by high-energy incident protons can be related to the change in the total number of "cascade" particles, while the excitation energy of the residual nucleus even decreases (for a given value of $n_{\alpha p}$) with the increase in the energy of the incident particles.

Another interesting feature of the fragmentation process is the dependence of the anisotropy of the angular distribution of the fragments (with respect to the direction of the incident particles) on their energy. As is known, the angular distribution of fragments in the laboratory system is essentially anisotropic with respect to the forward—backward direction, where the size of this anisotropy can by no means be explained by the velocity transferred from the target nucleus. Figure 11 shows the data describing the change in the anisotropy of the angular distribution with a change in the incident proton energy. The decrease in the angular anisotropy determined from the ratio of the number of fragments emitted in the forward and backward hemispheres with respect to the incident particles is quite clearly seen. Since we know that with an increase in the energy of the incident particles the relative number of "cascade" particles among all particles in the disintegration increases, and, together with this, the angular distribution "spreads out" with respect to the direction of the incident particles, the decrease in the angular anisotropy with increasing energy of the incident protons and the dependence of the fragment yield on $n_{\alpha p}$ can be explained by the interconnection between the cascade-particle and fragment production processes. If the fragments are due to "evaporation," the fragment angular distribution should be all the more anisotropic with an increase in the energy of the incident particles, owing to the increase in the momentum transferred to the nucleus.

The poor statistics of recorded fragments did not allow us to obtain the energy distribution of fragments with $Z \geq 4$. From the results obtained and from comparison with published data[10,17] it can be concluded only that the most probable energy of such fragments almost does not differ from the most probable energy at both lower and higher energies of the incident protons $E_0$. This conclusion can also be made from a comparison of the energy spectra of lithium for various energies of incident protons (see Fig. 6).

C. Remarks on the Mechanism of the Fragmentation Process. Examination of the experimental data on the emission of multiply charged particles in disintegrations obtained in this work and their comparison with data at other incident-particle energies allows us to draw several conclusions on the basic aspects of the fragmentation process. A number of characteristics of the production process for multiply charged particles prove to be functions of the energy of the incident particles $E_0$. With an increase in $E_0$, the cross section for fragment production, the multiplicity of fragment production in one disintegration, the mean number of protons and $\alpha$ particles in disintegrations with fragments, and the probability of fragment emission for a given number of $\alpha$ particles and protons in the disintegration all increase, while the anisotropy of the angular distribution of the fragments with respect to the direction of the incident particles decreases. Moreover, it is known that with increasing incident-proton energy the very shape of the curve of the fragment production cross section vs. atomic weight of the target nucleus changes. At proton energies $E_0 = 300-400$ Mev the production cross section for the $Li^8$, $Be^7$, $C^{11}$, and $F^{18}$ isotopes decreases by almost three orders of magnitude as one goes[19,20] from Al to Pb, while at an energy of $E_0 > 3$ Bev the opposite is observed for the $Be^7$ and $F^{18}$ isotopes, i.e. a certain increase in the cross section with an increase in the atomic weight of the target nucleus.[15]

Along with this, several characteristics of the process of fragment production apparently are either not functions of the energy of the incident particles, or very weakly depend on it. These are, first, the charge distribution of the fragments, which remains constant over a large range of energy of the incident particles, and, second, the energy distribution of the fragments. Although with an increase in the energy of the incident particles the relative number of fragments with energies exceeding the repulsive Coulomb barrier increases, the most probable fragment energy remains almost unchanged and close to the value of the Coulomb barrier of the nucleus.

The above-mentioned features of the fragment production process in nuclear disintegrations, and also all the other features mentioned in this article and known at present from other work, should be explained by some single mechanism of their formation in the nuclear disintegrations. Such a mechanism should also explain the production, in part, of lighter nuclei such as helium or the heavy isotopes of hydrogen, since, in principle, there should be no sharp difference between small and large clusters of nucleons. The results of experiments in which the characteristics of the process of fast $\alpha$-particle production in the disintegration of Ag and Br nuclei were investigated[21, 22] serve as a basis for this.

At the present time the ''cascade-evaporation'' model is generally accepted for the interaction of high-energy particles with nuclei. The occurrence of fragments in the cooling-down process of an excited nucleus has been considered by a large number of authors.[3,9,10,17,23-26] At present it may be considered that the bulk of the experimental data on the production of Li and Be fragments is in sufficiently satisfactory agreement with the calculations based on the theory of evaporation, both as regards the probability of their emission (as compared to protons) and the dependence of this probability on the excitation energy of the residual nucleus and the energy of the incident particles, and as regards the shape of the fragment energy spectrum. When it comes to fragments with $Z \geq 4$, the agreement with the theory of evaporation as to the production probability is far worse. The probability of the production of fragments with $Z \geq 4$ turns out to be higher than that which can be expected from evaporation theory.[3,10] Furthermore, the hypothesis of the production of fragments in some equilibrium process of the evaporation type disagrees with such characteristics of the fragmentation process as the independence of the fragment charge distribution of the incident-particle energy, the increase in the fragment production cross section with increasing atomic number of the target nucleus, the large anisotropy in the angular distributions of the fragments, and the fact that several fragments are emitted in one disintegration.

Therefore, the analysis of the evaporation mechanism does not offer much promise for the further development of views on the fragmentation process. One can also find many contradictions between the known characteristics of the fragmentation phenomenon and the suggestion that fragments are caused by fission of the nuclei. They concern the energy and angular distributions of the fragments produced, as well as the cross sections for both processes, and the mass and excitation energy distributions.[3]

Thus the fission mechanism apparently cannot give results that explain the fragmentation process.

Far more promising is the suggested connection between the fragment-production process and the cascade process in the nucleus. There are direct experimental data indicating the existence of such a connection. These are the dependence of the fragment-production probability on the number of «cascade» particles, the angular anisotropy of the fragments with respect to the direction of the incident particles, and the dependence of the fragment-production probability on the energy of the incident particles for a given number of particles in the disintegration. One can explain from this standpoint such characteristics of the fragmentation process as the fact that the Z distribution of the fragments remains constant for various incident-proton energies $E_0$, the decrease in the anisotropy of the angular distribution of the fragments with increasing energy of the protons, and some others.

To verify the given picture of the occurrence of fragments in nuclear disintegrations, apart from the further accumulation of experimental data, it would be desirable to carry out the corresponding calculations of the nuclear cascade process type by the Monte-Carlo method.[27] In so doing, it would be useful to assume the existence in the nuclei of definite clusters of nucleons with some momentum distribution, and the possibility of quasi-elastic scattering of the cascade nucleons and clusters of nucleons by other nucleons in the nucleus and by their clusters. All this complicates greatly the concepts which serve at the present as the basis of calculations of the nuclear cascade process by the Monte-Carlo method. The difficulty involved in such calculations results from the insufficient knowledge of the differential cross sections for the scattering of fast nucleons on light nuclei, and especially their scattering on one another.

---

[1] P. Kruger and N. Sugarman, Phys. Rev. **99**, 1459 (1955).

[2] Wolfgang, Baker, Caretto, Cumming, Friedlander, and Hudis, Phys. Rev. **103**, 394 (1956).

[3] O. V. Lozhkin, Dissertation, Radium Institute, Academy of Sciences, U.S.S.R. (1957).

[4] A. A. Rimskiĭ-Korsakov and O. V. Lozhkin, Приборы и техника эксперимента, (Instruments and Measurement Engineering), in press.

[5] V. I. Ostroumov and Yu. P. Yakovlev, JETP **35**, 1358 (1958), Soviet Phys. JETP **8**, 949 (1959); Nakagawa, Tamai, Huzita, and Okudaira, J. Phys. Soc. Japan **11**, 191 (1956).

[6] Yu. I. Serebrennikov, Научно-техн. информ. бюлл. Ленинградского политехнического ин-та, (Scientific-Technical Information Bulletin, Leningrad Polytechnical Institute) No. 5 (1957).

[7] V. P. Shamov, JETP **35**, 316 (1958), Soviet Phys. JETP **8**, 219 (1959).

[8] G. Philbert, J. phys. radium **18**, 656 (1957).

[9] B. A. Munir, Phil. Mag. **1**, 355 (1956).

[10] O. V. Lozhkin and N. A. Perfilov, JETP **31**, 913 (1956); Soviet Phys. JETP **4**, 790 (1957).

[11] Lock, March, and McKeague, Proc. Roy. Soc. (London) **A231**, 368 (1955).

[12] Nakagawa, Tamai, Huzita, and Okudaira, J. Phys. Soc. Japan **12**, 747 (1957).

[13] D. H. Perkins, Proc. Roy. Soc. (London) **A203**, 399 (1950).

[14] O. V. Lozhkin, JETP **33**, 354 (1957), Soviet Phys. JETP **6**, 273 (1958).

[15] Caretto, Hudis, and Friedlander, Phys. Rev. **110**, 1130 (1958).

[16] N. A. Perfilov, Материалы совещания по применению радиохимических методов изучения ядерных реакций, (Materials from the Conference on the Use of Radiochemical Methods for Studying Nuclear Reactions), Vol. **1**, Joint Institute of Nuclear Studies, 1958, p. 90; E. Baker and S. Katcoff, Bull. Am. Phys. Soc. Ser. II, **2**, 222 (1957).

[17] Nakagawa, Tamai, and Nomoto, Nuovo cimento **9**, 780 (1958).

[18] V. I. Ostroumov, JETP **32**, 3 (1957), Soviet Phys. JETP **5**, 12 (1957).

[19] L. Marquez, Phys. Rev. **86**, 405 (1952).

[20] S. Wright, Phys. Rev. **79**, 838 (1950).

[21] P. A. Vagonov and V. I. Ostroumov, JETP **33**, 1131 (1957). Soviet Phys. JETP **6**, 871 (1958).

[22] Ostroumov, Perfilov, and Filov, J. Exptl. Theoret. Phys. (U.S.S.R.) **36**, 367 (1959); Soviet Phys. JETP **9**, 254 (1959).

[23] J. Hudis and J. B. Miller, Phys. Rev. **112**, 1322 (1958).

[24] S. Katcoff, Phys. Rev. **114**, 905 (1959).

[25] K. J. LeCouteur, Proc. Phys. Soc. (London) **A63**, 259 (1950).

[26] Goldsack, Lock, and Munir, Phil. Mag. **2**, 149 (1957).

[27] Metropolis, Bivins, Storm, Miller, Friedlander, and Turkevich, Phys. Rev. **110**, 204 (1958).

Translated by E. Marquit
271

SOVIET PHYSICS JETP VOLUME 11, NUMBER 5 NOVEMBER, 1960

# *CHARGE EXCHANGE SCATTERING OF 240 — 330 Mev $\pi^-$ MESONS ON HYDROGEN*

V. G. ZINOV and S. M. KORENCHENKO

Joint Institute for Nuclear Research

Submitted to JETP editor November 17, 1959

J. Exptl. Theoret. Phys. (U.S.S.R.) 38, 1399-1406 (May, 1960)

The results are given of the measurement of the differential cross sections of charge-exchange scattering of 240, 270, 307, and 333-Mev $\pi^-$ mesons on hydrogen.

## 1. EXPERIMENTAL ARRANGEMENT

THE angular distribution of $\pi^0$ mesons was determined from the angular distribution of the $\gamma$ quanta produced in the decay of these mesons.

The geometry of the experiment is shown in Fig. 1. A detailed description of the apparatus employed and the liquid hydrogen target was given in reference 1. The $\gamma$ quanta were detected by means of a telescope consisting of scintillation counters 3, 4, and 6. To increase the efficiency of registration of the $\gamma$ quanta by counter 3, we used a lead plate 7.4 g/cm$^2$ thick, in which these quanta were converted into electron—positron pairs.

Counters 1, 2, 3, and 4 were connected in anticoincidence with counter 6, so that the charged mesons falling in the telescope were not recorded. At the same time, the efficiency of registration of $\gamma$ quanta decreased only slightly ($\sim 1\%$) by conversion in counter 6, which was a Plexiglas container $16 \times 17 \times 1.5$ cm filled with a solution of terphenyl in phenyl cyclohexane (3 g/l). The efficiency of operation of the anticoincidence circuit was continually checked. This could be done because 12346 coincidences were registered side by side with $1234\overline{6}$ anticoincidences. The sum of these coincidences and anticoincidences should be exactly equal to the number of 1234 coincidences.

## 2. EFFICIENCY OF REGISTRATION OF $\gamma$ QUANTA

In determining the efficiency of registration of the $\gamma$ quanta, we made use of a method similar to that used by Anderson et al.[2]

It can be shown that if the c.m.s. angular distribution of the $\pi^0$ mesons is represented in the form of a sum of Legendre polynomials

$$\frac{d\sigma}{d\omega} = \sum_l A_l^0 P_l(\cos\vartheta), \tag{1}$$

then the c.m.s. angular distribution of the $\gamma$ quanta will have the form

$$\frac{d\sigma^\gamma}{d\omega} = \sum_l k_l A_l^0 P_l(\cos\vartheta). \tag{2}$$

The coefficients $k_l$ are determined from the expression

$$k_l = \int_{-1}^{+1} \frac{1-\beta_{\pi^0}^2}{(1-\beta_{\pi^0}\cos x)^2} P_l(\cos x)\, d\cos x, \tag{3}$$

where $\beta_{\pi^0}$ is the velocity of the $\pi^0$ mesons in the c.m. system. Thus a Legendre polynomial of order $l$ in the angular distribution of the $\pi^0$ mesons gives a polynomial of the order $l$ multiplied by the coefficient $k_l$ in the angular distribution of the $\gamma$ quanta. The experimentally observed cross section for $\gamma$ quanta is expressed here through the coefficients of the angular distribution of the $\pi^0$ mesons in the following way:

$$\left(\frac{d\sigma^\gamma}{d\Omega}\right)_{\text{obs}} = \frac{1-\beta^2}{(1-\beta\cos\theta)^2} \sum_l \varepsilon_l(\theta)\, k_l A_l^0 P_l(\cos y). \tag{4}$$

The coefficient $\epsilon_l(\theta)$ is given by the expression

$$\varepsilon_l(\theta) = \frac{\int_{-1}^{+1} \varepsilon\,[E(\theta, x)]\,[(1-\beta_{\pi^0}^2)/(1-\beta_{\pi^0}\cos x)^2]\, P_l(\cos x)\, d\cos x}{\int_{-1}^{+1} [(1-\beta_{\pi^0}^2)/(1-\beta_{\pi^0}\cos x)^2]\, P_l(\cos x)\, d\cos x}. \tag{5}$$

In expressions (4) and (5) $\beta$ is the velocity in the c.m. system, $\theta$ is the angle of flight of the $\gamma$

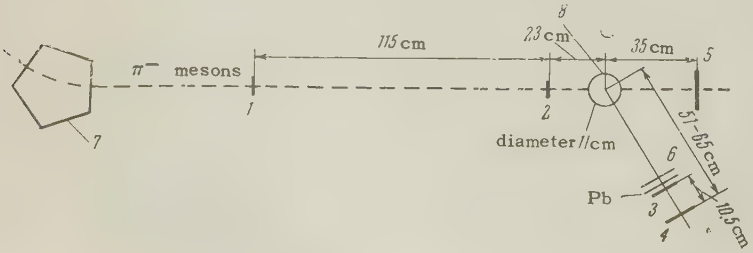

FIG. 1. Geometry of the charge-exchange scattering experiment: 1, 2 — scintillation counters 6×6 cm; 3, 4, 5 — scintillation counters 12.6× 11.5 cm; 6 — scintillation counter 16×17 cm; 7 — deflecting magnet; 8 — liquid hydrogen.

**TABLE I.** Values of Q/D observed in one series of measurements of charge-exchange scattering at 240 Mev

| Angle in lab system, deg | $Q/D \times 10^6$ with H | $Q/D \times 10^6$ without H | Difference for $10^6$ counts of monitor |
|---|---|---|---|
| 15 | 109.6±2.9 | 44.9±2.2 | 64.7±3.7 |
| 30 | 152.3±4.6 | 45.3±2.5 | 107.0±5.3 |
| 45 | 113.5±4.1 | 26.1±2.0 | 87.4±4.6 |
| 60 | 91.3±2.5 | 25.9±1.6 | 65.4±3.0 |
| 80 | 65.3±2.1 | 21.1±1.4 | 44.2±2.5 |
| 100 | 53.0±2.2 | 24.4±1.5 | 28.6±2.7 |
| 125 | 54.9±1.9 | 27.2±1.5 | 27.7±2.4 |
| 150 | 53.6±2.0 | 31.4±1.5 | 22.2±2.5 |

**TABLE II.** Values of Q/D observed in one series of measurements of charge-exchange scattering at 333 Mev

| Angle in lab system, deg | $Q/D \times 10^6$ with H | $Q/D \times 10^6$ without H | Difference for $10^6$ counts of monitor |
|---|---|---|---|
| 15 | 68.3±3.4 | 29.1±2.2 | 39.2±4.1 |
| 30 | 129.0±7.6 | 40.8±2.2 | 88.2±8.0 |
| 45 | 91.9±5.4 | 25.4±1.9 | 66.5±5.7 |
| 60 | 70.0±4.1 | 26.6±1.8 | 43.4±4.5 |
| 80 | 40.6±2.8 | 20.3±1.6 | 20.3±3.2 |
| 112.5 | 29.2±1.8 | 19.8±1.1 | 9.4±2.1 |
| 135 | 29.2±1.6 | 20.4±1.3 | 8.8±2.1 |
| 152 | 19.5±0.7 | 13.0±0.6 | 6.5±0.8 |

quanta in the laboratory system, y is the angle of flight of the $\gamma$ quanta in the c.m. system, $E(\theta, x)$ is the energy of the $\gamma$ quanta, and $\epsilon(E)$ expresses the dependence of the registration efficiency for $\gamma$ quanta on their energy.

As can be seen, to obtain the angular distribution of the $\pi^0$ mesons (in other words, to determine the coefficients $A_l^0$,) it is sufficient to know $(d\sigma^\gamma/d\Omega)_{obs}$ for different angles and $\epsilon(E)$. Indeed, $\epsilon_l(\theta)$, $k_l$, and $P_l$ (cos y) do not depend on the specific form of the angular distribution of the $\gamma$ quanta. They are determined only by the angle $\theta$, the kinematic relations, and the $\epsilon(E)$ curve. The minimum number of angles $\theta$ at which $(d\sigma^\gamma/d\Omega)_{obs}$ should be found depends on the maximum value of $l$.

For further treatment and phase-shift analysis of the results of the study of charge-exchange scattering, it will be more convenient to use, instead of the coefficients of the angular distributions (1) or (4), the differential cross sections for the $\pi \to \gamma$ process. In order to obtain the true cross sections from the experimentally observed cross sections, we should know the mean efficiency $\overline{\epsilon(\theta)}$ of registration of $\gamma$ quanta at a given angle. This mean efficiency is defined by the condition

$$(d\sigma^\gamma/d\Omega)_{\text{obs}} = \overline{\varepsilon(\theta)}\,(d\sigma^\gamma/d\Omega)_{\text{true}}. \tag{6}$$

From (4) and (6), we obtain

$$\frac{1-\beta^2}{(1-\beta\cos\theta)^2}\sum_l \varepsilon_l(\theta)\,k_l A_l^0 P_l(\cos y)$$

$$= \overline{\varepsilon(\theta)}\,\frac{1-\beta^2}{(1-\beta\cos\theta)^2}\sum_l k_l A_l^0 P_l(\cos y), \tag{7}$$

hence

$$\overline{\varepsilon(\theta)} = \frac{\sum\limits_l \varepsilon_l(\theta)\,k_l A_l^0 P_l(\cos y)}{\sum\limits_l k_l A_l^0 P_l(\cos y)}, \tag{8}$$

in agreement with the mean-value superposition rule.

## 3. DIFFERENTIAL CROSS SECTIONS FOR CHARGE-EXCHANGE SCATTERING OF 240-, 270-, 307-, AND 333-Mev $\pi^-$ MESONS ON HYDROGEN

The $\gamma$ quanta produced in the decay of the $\pi^0$ mesons were detected at eight angles. The ratio of the number of $123\overline{4}\overline{6}$ coincidences (Q) to the number of double 12 coincidences (D) was measured. We determined the difference in the ratios Q/D obtained with and without liquid hydrogen in the target. The background conditions during the study of the charge-exchange scattering are illustrated by Tables I and II, which give the respective values of the ratio Q/D observed in one series of measurements at 240 and 333 Mev.

In order to accumulate the necessary statistics, the measurements were made in several series at each energy. The results obtained in the individual series of measurements, after being corrected for errors in the registration of double 12 coincidences, were averaged according to their statistical weight.

In reducing the experimental data, we first calculated the observed differential cross sections from the formula

$$\left(\frac{d\sigma}{d\Omega}\right)_{\text{diff}} = \frac{(Q/D)_{\text{diff}}}{N\Omega f}\cdot 10^{-6}, \tag{9}$$

where $(Q/D)_{\text{diff}}$ is the value of the difference $(Q/D)_{\text{with H}} - (Q/D)_{\text{without H}}$ for $10^6$ monitor counts; N is the mean number of hydrogen atoms per $cm^3$, equal to $0.447 \times 10^{24}$, accurate to ±1%; $\Omega$ is the solid angle subtended by the telescope; f is the summary correction for contamination of the beam by $\mu$ mesons (4.5 — 5.5%), for the finite dimensions of the telescope (to 1.2%), and for the absorption of $\pi^-$ mesons in counter 2, in the front wall of the target, and in the hydrogen (from 2.2 to 3%).

The errors in determining these corrections, and also other factors affecting the calculated values of the differential cross sections, were not

**TABLE III:** Differential cross sections for production of $\gamma$ quanta in charge exchange scattering at 240 Mev on hydrogen

| Angle in lab system, deg | $\Omega$, sr | $(Q/D)$ diff | $f$ | $10^{27}\left(\frac{d\sigma}{d\Omega}\right)_{\text{obs}}$ in lab system cm² sr⁻¹ | $\overline{\epsilon(\theta)}$ including normalization of $\epsilon(E)$ | $10^{27}\left(\frac{d\sigma}{d\Omega}\right)_{\text{lab}}$ cm² sr⁻¹ | Angle in c.m.s. deg | $10^{27}\left(\frac{d\sigma}{d\omega}\right)_{\text{c.m.s.}}$ cm² sr⁻¹ |
|---|---|---|---|---|---|---|---|---|
| 15 | 0.0157 | 62.5±2.9 | 0.921 | 9.67±0,67 | 0,615 | 15.72±1.57 | 19.7 | 9.31±0.93 |
| 30 | 0.0357 | 104.1±3,0 | 0.922 | 7.08±0.43 | 0.597 | 11.86±1.12 | 38,8 | 7.54±0.71 |
| 45 | 0.0437 | 89.9±2,2 | 0.923 | 4,99±0,29 | 0.570 | 8.75±0.80 | 57.2 | 6.20±0.57 |
| 60 | 0.0542 | 63.8±1.8 | 0.928 | 2.84±0.17 | 0,537 | 5.29±0.49 | 74.5 | 4.28±0.40 |
| 80 | 0.0540 | 42.2±1.9 | 0.928 | 1.88±0.13 | 0.491 | 3.83±0.39 | 95.7 | 3.75±0.38 |
| 100 | 0.0538 | 29,2±1.5 | 0.923 | 1.32±0.10 | 0.478 | 2.75±0.29 | 114.9 | 3.24±0.34 |
| 125 | 0.0532 | 25.5±2.2 | 0.922 | 1.16±0.12 | 0.493 | 2.36±0.29 | 136.8 | 3.38±0.42 |
| 150 | 0.0430 | 23.3±1.5 | 0.921 | 1.32±0.11 | 0.509 | 2,59±0.29 | 157.0 | 4.23±0.47 |

**TABLE IV.** Differential cross section for production of $\gamma$ quanta in charge-exchange scattering at 270 Mev on hydrogen

| Angle in lab system, deg | $\Omega$, sr | $(Q/D)$diff | $f$ | $10^{27}\left(\frac{d\sigma}{d\Omega}\right)_{\text{obs}}$ in lab system cm² sr⁻¹ | $\overline{\epsilon(\theta)}$ including normalization of $\epsilon(E)$ | $10^{27}\left(\frac{d\sigma}{d\Omega}\right)_{\text{lab}}$ cm² sr⁻¹ | Angle in c.m.s., deg | $10^{27}\left(\frac{d\sigma}{d\omega}\right)_{\text{c.m.s.}}$ cm² sr⁻¹ |
|---|---|---|---|---|---|---|---|---|
| 15 | 0.0157 | 55.9±2.3 | 0,924 | 8.63±0.58 | 0.622 | 13.88±1.36 | 20.0 | 7.92±0.78 |
| 30 | 0.0357 | 91.5±3.2 | 0.925 | 6.19±0.39 | 0.601 | 10.31±0.97 | 39.6 | 6.36±0.60 |
| 45 | 0.0437 | 74,3±3.0 | 0.926 | 4.11±0.27 | 0,575 | 7.14±0,69 | 58.1 | 4.95±0.48 |
| 60 | 0,0542 | 52,7±2.0 | 0.931 | 2.33±0.15 | 0.535 | 4.35±0.52 | 75.5 | 3.48±0.42 |
| 80 | 0.0540 | 27,7±1,6 | 0.931 | 1.24±0.10 | 0.482 | 2.56±0.26 | 96.8 | 2.52±0.26 |
| 100 | 0.0538 | 20.2±1.2 | 0.927 | 0.906±0.074 | 0.469 | 1.93±0.21 | 115.9 | 2.31±0.25 |
| 125 | 0.0532 | 19.9±1.6 | 0,924 | 0.907±0.086 | 0.493 | 1,84±0.22 | 137.6 | 2.71±0.33 |
| 150 | 0.0430 | 16.8±1.3 | 0,924 | 0,943±0,088 | 0.512 | 1.84±0.22 | 157.4 | 3.12±0.37 |

different from those which were given earlier in Table VIII of reference 4. Since the differential cross sections obtained below were normalized to the total cross section, a number of small corrections (not more than 1%), due primarily to the conversion of the $\gamma$ quanta and weakly dependent on the energy, were not introduced. The values of the quantities entering into formula (9) are given in Tables III—VI.

After calculation of $(d\sigma^{\gamma}/d\Omega)_{\text{obs}}$, the angular distribution of the $\pi^0$ mesons in the c.m.system was found in the form of the sum of the first three Legendre polynomials

$$(d\sigma/d\omega)_{\pi^-\to\pi^0} = A_0^0 + A_1^0 P_1(\cos\vartheta) + A_2^0 P_2(\cos\vartheta). \qquad (10)$$

Formula (4) was used to determine the coefficients $A_l^0$. Since the measurements were made at eight angles, we obtained a system of eight equations with three unknowns, which was solved by the method of least squares. The coefficients $A_l^0$ for all the energies are given in Table VII.

The initial values of $\epsilon_l(\theta)$ were obtained by numerical integration of the right-hand side of (5). In doing so, the values of $\epsilon(E)$ (curve a in Fig. 2) were taken from reference 2. The values of $\epsilon_l(\theta)$ for 240 and 333 Mev are given in Table VIII. For other energies, $\epsilon_l(\theta)$ can be found with sufficient accuracy by linear interpolation.

The analytical expression for the coefficients $k_l$, obtained after integration of (3) has the form

$$k_0 = 2, \qquad k_1 = \frac{2\gamma}{\eta} - \frac{1}{\eta^2}\ln\frac{\gamma+\eta}{\gamma-\eta},$$

$$k_2 = 2 + \frac{6}{\eta^2} - \frac{3\gamma}{\eta^3}\ln\frac{\gamma+\eta}{\gamma-\eta},$$

$$k_3 = \frac{2\gamma}{\eta} + \frac{15\gamma}{\eta^3} - \frac{3}{2\eta^2}\left(\frac{5}{\eta^2}+4\right)\ln\frac{\gamma+\eta}{\gamma-\eta},$$

$$k_4 = 2 + \frac{95}{3\eta^2} + \frac{35}{\eta^4} - \frac{5\gamma}{\eta^3}\left(\frac{7}{2\eta^2}+2\right)\ln\frac{\gamma+\eta}{\gamma-\eta}. \qquad (11)$$

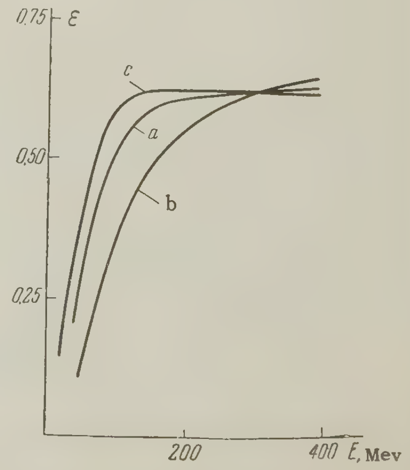

FIG. 2. Variation of efficiency $\varepsilon$ of registration of $\gamma$ quanta with their energy E.

**TABLE V.** Differential cross section for production of $\gamma$ quanta in charge-exchange scattering at 307 Mev on hydrogen

| Angle in lab system, deg | $\Omega$, sr | $(Q/D)_{\text{diff}}$ | $f$ | $10^{27}\left(\frac{d\sigma}{d\Omega}\right)_{\text{obs}}$ in lab system cm² sr⁻¹ | $\overline{\epsilon(\theta)}$ including normalization of $\epsilon(E)$ | $10^{27}\left(\frac{d\sigma}{d\Omega}\right)_{\text{lab}}$ cm² sr⁻¹ | Angle in c.m.s., deg | $10^{27}\left(\frac{d\sigma}{d\omega}\right)_{\text{c.m.s.}}$ cm² sr⁻¹ |
|---|---|---|---|---|---|---|---|---|
| 15 | 0.0120 | 46.3±2.4 | 0.930 | 8.74±0.67 | 0.629 | 13.89±1,46 | 20.5 | 7.60±0.80 |
| 30 | 0.0360 | 101.0±14.0 | 0.931 | 6.74±0.99 | 0.609 | 11.08±1.81 | 40.4 | 6.60±1.08 |
| 45 | 0.0440 | 55.0±5.0 | 0.934 | 2.99±0.31 | 0.582 | 5.13±0,65 | 59.2 | 3.47±0.44 |
| 60 | 0.0550 | 38.8±3.1 | 0.941 | 1.67±0.16 | 0.540 | 3.10±0.36 | 76.8 | 2.45±0.29 |
| 80 | 0.0550 | 19.6±1.6 | 0.942 | 0.846±0.080 | 0.476 | 1.78±0,21 | 98.0 | 1.76±0.21 |
| 112,5 | 0.0550 | 12.6±1.6 | 0.931 | 0.551±0.074 | 0.459 | 1.20±0.18 | 128,1 | 1,66±0.25 |
| 135 | 0.0550 | 10.2±1.4 | 0.930 | 0.447±0.067 | 0.487 | 0.917±0,153 | 146,4 | 1,50±0.25 |
| 152 | 0.0414 | 8.95±0.80 | 0.930 | 0.521±0.054 | 0.513 | 1.015±0.129 | 159.4 | 1.81±0.23 |

**TABLE VI.** Differential cross section for production of $\gamma$ quanta in charge-exchange scattering at 333 Mev on hydrogen

| Angle in lab system, deg | $\Omega$, sr | $(Q/D)_{\text{diff}}$ | $f$ | $10^{27}\left(\frac{d\sigma}{d\Omega}\right)_{\text{obs}}$ in lab system cm² sr⁻¹ | $\overline{\epsilon(\theta)}$ including normalization of $\epsilon(E)$ | $10^{27}\left(\frac{d\sigma}{d\Omega}\right)_{\text{lab}}$ cm² sr⁻¹ | Angle in c.m.s., deg | $10^{27}\left(\frac{d\sigma}{d\omega}\right)_{\text{c.m.s.}}$ cm² sr⁻¹ |
|---|---|---|---|---|---|---|---|---|
| 15 | 0.0120 | 37.4±3.9 | 0.932 | 7.50±0.87 | 0.628 | 11.94±1.64 | 20.8 | 6,33±0.87 |
| 30 | 0.0360 | 97.1±4.2 | 0.932 | 6.48±0,45 | 0,612 | 10.59±1,05 | 41.0 | 6.15±0.61 |
| 45 | 0.0440 | 63.8±5.5 | 0.935 | 3.47±0.35 | 0.586 | 5.92±0,73 | 60.0 | 3.94±0.49 |
| 60 | 0.0550 | 41.6±4.3 | 0.943 | 1.79±0.21 | 0,550 | 3.25±0.44 | 77.7 | 2.56±0.35 |
| 80 | 0.0550 | 21.3±2.4 | 0.945 | 0.915±0.115 | 0.489 | 1.87±0,27 | 99.0 | 1.86±0.27 |
| 112.5 | 0.0550 | 9.16±1.5 | 0.932 | 0.400±0.067 | 0.449 | 0.889±0.163 | 128.8 | 1.25±0.23 |
| 135 | 0.0550 | 10.1±1.6 | 0.932 | 0.440±0.073 | 0.467 | 0.942±0.172 | 146.9 | 1,58±0.29 |
| 152 | 0.0414 | 5.83±0.7 | 0.932 | 0.338±0.046 | 0,481 | 0,703±0.108 | 159.7 | 1,29±0.20 |

**TABLE VII.** Coefficients $A_l^0$ found by solving the system of equations (4) by the method of least squares (in units of $10^{-27}$ cm² sr⁻¹)

| $\pi^-$-meson energy, Mev | $A_0^0$ | $A_1^0$ | $A_2^0$ |
|---|---|---|---|
| 240 | 2.56±0,11 | 1.82±0.28 | 2.19±0.48 |
| 270 | 2.03±0.10 | 1.67±0,24 | 1.97±0.35 |
| 307 | 1.54±0.09 | 1.73±0.23 | 1.53±0,30 |
| 333 | 1.56±0.09 | 1.86±0.22 | 1.23±0,29 |

**TABLE VIII.** Coefficients $\epsilon_l(\theta)$ for 240 and 333 Mev

| Angle in lab system, deg | $E_{\pi^-}$=240 Mev | | | $E_{\pi^-}$=333 Mev | | |
|---|---|---|---|---|---|---|
| | $\varepsilon_0$ | $\varepsilon_1$ | $\varepsilon_2$ | $\varepsilon_0$ | $\varepsilon_1$ | $\varepsilon_2$ |
| 15 | 0.536 | 0.605 | 0.638 | 0.553 | 0.610 | 0.638 |
| 30 | 0,528 | 0.597 | 0.634 | 0.543 | 0.602 | 0.634 |
| 45 | 0.520 | 0.590 | 0.629 | 0.533 | 0.593 | 0.630 |
| 60 | 0.512 | 0.582 | 0.624 | 0.524 | 0.585 | 0.626 |
| 80 | 0.501 | 0.570 | 0.618 | 0.511 | 0.574 | 0.621 |
| 100 | 0.490 | 0.560 | 0.612 | 0.498 | 0.563 | 0.615 |
| 125 | 0.477 | 0.547 | 0.604 | 0,482 | 0.549 | 0.608 |
| 150 | 0.464 | 0.534 | 0.597 | 0,466 | 0.536 | 0.601 |

Here $\eta$ is the c.m.s. momentum of the $\pi^0$ meson in units of $m_{\pi^0}c$; $\gamma$ is the energy of the $\pi^0$ meson in units of $m_{\pi^0}c^2$; correspondingly $\beta_{\pi^0} = \eta/\gamma$. The values of k for 240 — 333 Mev are shown in Table IX.

The three coefficients $A_l^0$ are quite sufficient to determine the values of $\overline{\epsilon(\theta)}$, to the required accuracy, by means of (8). First, the coefficients of the Legendre polynomials of the higher order are small; second, owing to the fact that $\epsilon_l(\theta)$ for different $l$ do not differ from one another by more than 10 — 20%, $\overline{\epsilon(\theta)}$ is weakly dependent on the oscillations of $A_l^0$. Thus an arbitrary 15% variation of the coefficients $A_l^0$ shown in Table VII changes $\overline{\epsilon(\theta)}$ by no more than 1 or 2%.

The correct determination of the "true" differential cross sections depends therefore primarily on the values of $\epsilon_l(\theta)$ and, in the final analysis, on the extent to which the relation found between the registration efficiency for $\gamma$ quanta and their energy is correct.

To gain an idea of how sensitive $\epsilon_l(\theta)$ and the "true" differential cross sections are to the shape of the $\epsilon(E)$ curve, these quantities were calculated by using for $\epsilon(E)$ a curve different from that taken as the most correct. The change in the calculated differential cross sections for a change in the $\epsilon(E)$ curve goes in two directions: first, there is a change in the shape of the angular distribution, i.e., in the ratio of the forward—backward scattering cross sections; second, there is a change in the total cross section for

**TABLE IX.** Coefficients $k_l$ for 240 — 333 Mev

| Energy, Mev | $k_0$ | $k_1$ | $k_2$ | $k_3$ | $k_4$ | Energy, Mev | $k_0$ | $k_1$ | $k_2$ | $k_3$ | $k_4$ |
|---|---|---|---|---|---|---|---|---|---|---|---|
| 240 | 2 | 1.496 | 1.051 | 0.710 | 0.472 | 307 | 2 | 1.577 | 1.173 | 0.858 | 0.602 |
| 270 | 2 | 1.534 | 1.111 | 0.780 | 0.534 | 333 | 2 | 1.598 | 1.207 | 0.893 | 0.625 |

**TABLE X.** Coefficients of angular distribution of $\gamma$ quanta (in units of $10^{-27}$ cm$^2$ sr$^{-1}$)

| $\pi^-$-meson energy, Mev | $A_0^\gamma$ | $A_1^\gamma$ | $A_2^\gamma$ | $M$ | $M_0$ (expected) |
|---|---|---|---|---|---|
| 240 | 4.79±0.21 | 2.54±0.39 | 2.18±0.47 | 1.67 | 5 |
| 270 | 3.79±0.18 | 2.41±0.32 | 2.07±0.37 | 0.15 | 5 |
| 307 | 2.85±0.16 | 2.58±0.33 | 1.77±0.32 | 6.30 | 5 |
| 333 | 2.87±0.17 | 2.81±0.32 | 1.44±0.34 | 3.40 | 5 |

charge-exchange scattering. The latter change is not difficult to calculate, since the total cross section of interaction of $\pi^-$ mesons with hydrogen and the total cross section for elastic scattering are known [to a greater accuracy than the curve of $\epsilon(E)$]. It turned out that if we use curve b, along with curve a (Fig. 2) and if the obtained differential cross sections are normalized to the same total cross section, then the change in the cross sections at different energies, at angles of 30 and 150° in the laboratory system, is +(5 — 8%) and −(5 — 7%). At other angles the change is still smaller. The shape of curve b was calculated in such a way that it differed from curve a more than it differed from the curve obtained by the Monte-Carlo method.[2] A change in the $\epsilon(E)$ in the other direction (curve c) was less probable, and, at the same time, led to relative changes of less than 7% in the differential cross sections.

In connection with the above, the differential cross sections for charge-exchange scattering, obtained by the use of an $\epsilon(E)$ curve taken from reference 2, were then normalized by a factor common to all energies. The normalizing factor was chosen such that the sums of the total cross sections for elastic[4] and charge-exchange scattering at the energies studied would fit best the total cross sections for the interaction between $\pi^-$ mesons and hydrogen measured by the absorption of a $\pi^-$ meson beam in hydrogen[3] at these energies. This factor turned out to be 0.936. The normalization actually meant that the $\epsilon(E)$ curve was normalized, i.e. the efficiency of recording $\gamma$ quanta at all energies was approximately 6% higher than that taken in the preliminary reduction of the data.

In the determination of the errors in the values of the differential cross sections, the error connected with the inexact knowledge of the shape of the $\epsilon(E)$ curve was taken equal to ± 7%, and was added to the statistical error by the usual rule for combining standard deviations. The error associated with the normalization in the determination of the absolute values of the differential cross sections was, for all energies, ~ 5%. It was not taken into account in the subsequent calculations. The values of $\epsilon(\theta)$, with allowance for the normalization of the $\epsilon(E)$ curve and the corresponding differential cross sections for the production of $\gamma$ quanta emitted at a given angle, are listed in Tables III — VI.

To determine the angular distribution of the $\pi^0$ mesons, we now represent the c.m.s. angular distribution of the $\gamma$ quanta in the form of a sum of Legendre polynomials:

**TABLE XI.** Coefficients of angular distribution of $\pi^0$ mesons (in units of $10^{-27}$ cm$^2$ sr$^{-1}$)

| $\pi^-$-meson energy, Mev | $A_0^0$ | $A_1^0$ | $A_2^0$ | Total charge-exchange cross section |
|---|---|---|---|---|
| 240 | 2.39±0.11 | 1.70±0.26 | 2.07±0.45 | 30.0±1.4 |
| 270 | 1.90±0.09 | 1.57±0.21 | 1.86±0.33 | 23.9±1.1 |
| 307 | 1.42±0.08 | 1.64±0.21 | 1.51±0.27 | 17.8±1.0 |
| 333 | 1.43±0.09 | 1.76±0.20 | 1.19±0.28 | 18.0±1.1 |

$$\frac{d\sigma^\gamma}{d\omega} = \sum_l A_l^\gamma P_l(\cos y). \qquad (12)$$

The coefficients $A_l^0$ obtained by the method of least squares are given in Table X for the case $l = 2$.

The values of the sum of the weighted squared deviations indicate that the three Legendre polynomials quite satisfactorily describe, at all energies, the observed angular distribution of the $\gamma$ quanta. The values of M obtained at 240 and 270 Mev were small in comparison with the expected values, possibly because the error of ±7%, due to the inexact knowledge of $\epsilon(E)$, was somewhat exaggerated, while the statistical accuracy of the measurements was sufficiently good (~ 2.5 – 6%).

Knowing the coefficients $A_l^0$, we could determine the coefficients of the angular distribution of the $\pi^0$ mesons. Using the values of $k_l$ included in Table IX, we obtain the coefficients $A_l^0$ listed in Table XI.

The last column of Table XI gives the total cross sections for charge-exchange scattering, obtained by integrating the angular distributions.

A phase-shift analysis of the experimental data is presented in the following article.

---

[1] V. G. Zinov and S. M. Korenchenko, JETP **34**, 301 (1958), Soviet Phys. JETP **7**, 210 (1958).

[2] Anderson, Davidon, Glicksman, and Kruse, Phys. Rev. **100**, 279 (1955).

[3] Ignatenko, Mukhin, Ozerov, and Pontecorvo, JETP **30**, 7 (1956), Soviet Phys. JETP **3**, 10 (1956).

[4] V. G. Zinov and S. M. Korenchenko, JETP **38**, 1099 (1960), Soviet Phys. JETP **11**, 794 (1960).

Translated by E. Marquit
272

SOVIET PHYSICS JETP VOLUME 11, NUMBER 5 NOVEMBER, 1960

# *PHASE SHIFT ANALYSIS OF SCATTERING OF 240–330 Mev PIONS BY HYDROGEN*

V. G. ZINOV, S. M. KORENCHENKO, N. I. POLUMORDVINOVA, and G. N. TENTYUKOVA

Joint Institute for Nuclear Research

Submitted to JETP editor November 17, 1959

J. Exptl. Theoret. Phys. (U.S.S.R.) **38**, 1407-1418 (May, 1960)

Results are presented of a phase-shift analysis of the experimental data on the scattering of pions by nucleons in the energy range from 240 to 330 Mev. Information on phase shifts for the interaction of pions in states with spin $T = \frac{1}{2}$ is of satisfactory accuracy.

## 1. PHASE-SHIFT ANALYSIS EQUATIONS

In the phase-shift analysis of our experimental data[1] we used the formalism of isotopic spin, based on the hypothesis of charge-independence of the nuclear forces. At energies near 300 Mev the states with orbital momenta $l > 1$ and primarily with $l = 2$ are expected to make a noticeable contribution to the scattering. If it is assumed that the phase shifts are real quantities, then the differential scattering cross sections for pions on hydrogen can be written as follows:[2]

$$\begin{aligned}
k^2 (d\sigma/d\omega)_{\pi^+\to\pi^+} = {} & [\sin^2\alpha_3 + (2\sin^2\alpha_{33} + \sin^2\alpha_{31})\cos\vartheta \\
& + (3\sin^2\delta_{35} + 2\sin^2\delta_{33}) P_2(\cos\vartheta)]^2 + \tfrac{1}{4}[\sin 2\alpha_3 \\
& + (2\sin 2\alpha_{33} + \sin 2\alpha_{31})\cos\vartheta \\
& + (3\sin 2\delta_{35} + 2\sin 2\delta_{33}) P_2(\cos\vartheta)]^2 \\
& + \sin^2\vartheta\,\{[\sin^2\alpha_{33} - \sin^2\alpha_{31} + 3\cos\vartheta(\sin^2\delta_{35} - \sin^2\delta_{33})]^2 \\
& + \tfrac{1}{4}[\sin 2\alpha_{33} - \sin 2\alpha_{31} + 3\cos\vartheta(\sin 2\delta_{35} - \sin 2\delta_{33})]^2\};
\end{aligned} \tag{1}$$

$$\begin{aligned}
9k^2 (d\sigma/d\omega)_{\pi^-\to\pi^-} = {} & [\sin^2\alpha_3 + 2\sin^2\alpha_1 \\
& + (2\sin^2\alpha_{33} + 4\sin^2\alpha_{13} + \sin^2\alpha_{31} + 2\sin^2\alpha_{11})\cos\vartheta \\
& + (3\sin^2\delta_{35} + 6\sin^2\delta_{15} + 2\sin^2\delta_{33} \\
& + 4\sin^2\delta_{13}) P_2(\cos\vartheta)]^2 + \tfrac{1}{4}[\sin 2\alpha_3 + 2\sin 2\alpha_1 \\
& + (2\sin 2\alpha_{33} + 4\sin 2\alpha_{13} + \sin 2\alpha_{31} + 2\sin 2\alpha_{11})\cos\vartheta \\
& + (3\sin 2\delta_{35} + 6\sin 2\delta_{15} + 2\sin 2\delta_{33} \\
& + 4\sin 2\delta_{13}) P_2(\cos\vartheta)]^2 \\
& + \sin^2\vartheta\,\{[\sin^2\alpha_{33} + 2\sin^2\alpha_{13} - \sin^2\alpha_{31} - 2\sin^2\alpha_{11} \\
& + 3\cos\vartheta(\sin^2\delta_{35} + 2\sin^2\delta_{15} - \sin^2\delta_{33} - 2\sin^2\delta_{13})]^2 \\
& + \tfrac{1}{4}[\sin 2\alpha_{33} + 2\sin 2\alpha_{13} - \sin 2\alpha_{31} - 2\sin 2\alpha_{11} \\
& + 3\cos\vartheta(\sin 2\delta_{35} + 2\sin 2\delta_{15} - \sin 2\delta_{33} - 2\sin 2\delta_{13})]^2\};
\end{aligned} \tag{2}$$

$$\begin{aligned}
\tfrac{9}{2}k^2 (d\sigma/d\omega)_{\pi^-\to\pi^0} = {} & [\sin^2\alpha_3 - \sin^2\alpha_1 \\
& + (2\sin^2\alpha_{33} - 2\sin^2\alpha_{13} + \sin^2\alpha_{31} - \sin^2\alpha_{11})\cos\vartheta \\
& + (3\sin^2\delta_{35} - 3\sin^2\delta_{15} + 2\sin^2\delta_{33} \\
& - 2\sin^2\delta_{13}) P_2(\cos\vartheta)]^2 \\
& + \tfrac{1}{4}[\sin 2\alpha_3 - \sin 2\alpha_1 + (2\sin 2\alpha_{33} - 2\sin 2\alpha_{13} \\
& + \sin 2\alpha_{31} - \sin 2\alpha_{11})\cos\vartheta \\
& + (3\sin 2\delta_{35} - 3\sin 2\delta_{15} + 2\sin 2\delta_{33} \\
& - 2\sin 2\delta_{13}) P_2(\cos\vartheta)]^2 \\
& + \sin^2\vartheta\,\{[\sin^2\alpha_{33} - \sin^2\alpha_{13} - \sin^2\alpha_{31} + \sin^2\alpha_{11} \\
& + 3\cos\vartheta(\sin^2\delta_{35} - \sin^2\delta_{15} - \sin^2\delta_{33} + \sin^2\delta_{13})]^2 \\
& + \tfrac{1}{4}[\sin 2\alpha_{33} - \sin 2\alpha_{13} - \sin 2\alpha_{31} + \sin 2\alpha_{11} \\
& + 3\cos\vartheta(\sin 2\delta_{35} - \sin 2\delta_{15} - \sin 2\delta_{33} + \sin 2\delta_{13})]^2\}.
\end{aligned} \tag{3}$$

The total cross sections are written in the following manner:

For positive pions

$$\begin{aligned}
\sigma_t^+ = \frac{4\pi}{k^2} & (\sin^2\alpha_3 + 2\sin^2\alpha_{33} + \sin^2\alpha_{31} \\
& + 3\sin^2\delta_{35} + 2\sin^2\delta_{33});
\end{aligned} \tag{4}$$

For negative pions

$$\begin{aligned}
\sigma_t^- = \frac{4\pi}{3k^2} & (\sin^2\alpha_3 + 2\sin^2\alpha_1 + 2\sin^2\alpha_{33} + 4\sin^2\alpha_{13} \\
& + \sin^2\alpha_{31} + 2\sin^2\alpha_{11} + 3\sin^2\delta_{35} + 6\sin^2\delta_{15} \\
& + 2\sin^2\delta_{33} + 4\sin^2\delta_{13}).
\end{aligned} \tag{5}$$

The symbols for the phase shifts are given in Table I.

## 2. METHOD OF CALCULATING PHASE SHIFTS AND THEIR ERRORS

Using the least-squares method, we find an assembly of phase shifts such as to minimize the sum of the weighted squares of deviations

$$M = \sum [(\sigma_{i\,\mathrm{calc}} - \sigma_{i\,\mathrm{exp}}) / \varepsilon_i]^2, \tag{6}$$

TABLE I

| State | $S_{1/2}$ | $P_{1/2}$ | $P_{3/2}$ | $D_{3/2}$ | $D_{5/2}$ |
|---|---|---|---|---|---|
| $T = {}^3/_2$ | $\alpha_3$ | $\alpha_{31}$ | $\alpha_{33}$ | $\delta_{33}$ | $\delta_{35}$ |
| $T = {}^1/_2$ | $\alpha_1$ | $\alpha_{11}$ | $\alpha_{13}$ | $\delta_{13}$ | $\delta_{15}$ |

where $\sigma_{i\,\mathrm{calc}}$ are the differential and total cross sections, calculated from the phase shifts with the aid of Eqs. (1) — (3), $\sigma_{i\,\mathrm{exp}}$ are the corresponding experimental values of the cross sections, and $\epsilon_i$ are the experimental errors in the measured cross sections.

All the calculations were made with the high-speed "Strela" computer.

To reduce the computation time, the minimum value of M was obtained by the gradient method. Corresponding to the minimum value $M = M_{\mathrm{min}}$ is a definite point in the phase-shift hyperspace. The functions M = const form for all values $M > M_{\mathrm{min}}$ a system of hypersurfaces, which are level surfaces of the scalar field $M(\alpha)$. It is obvious that by moving along the gradient of this field it is possible to arrive most rapidly to the point of minimum. Accordingly, we determined the value of $M_1$ and the normal to the hypersurface $M_1 = \mathrm{const}$ at the initial point of the phase-shift hyperspace. All phase shifts were then increased sufficiently to move in the direction of this normal by approximately 1 deg. The value $M = M_2$ at the new point was then calculated and the new value $M_2$ compared with the initial one. If $M_2 < M_1$, the motion along the initial gradient was repeated until the new value of $M_2$ was found to be greater than the preceding one. We then determined a new gradient direction at the point next to the last and the motion then proceeded along this direction at the same spacing as before. This was repeated until the first step no longer led to an increase in M after calculating the gradient. The magnitude of the step was then reduced one half and an analogous calculation performed. The step was then again reduced one half, etc. The calculations were completed after the required step amounted to $2^{-4}$ deg.

After finding the solution $(M = M_{\mathrm{min}})$ we calculated the errors in the phase shifts. An expansion of the function $M(\alpha_1, \alpha_2, \ldots)$ in a Taylor series about $M_0$ yields

$$M = M_0 + \sum_i \frac{\partial M}{\partial \alpha_i} \Delta\alpha_i + \frac{1}{2} \sum_i \sum_j \frac{\partial^2 M}{\partial \alpha_i\, \partial \alpha_j} \Delta\alpha_i\, \Delta\alpha_j + \ldots. \quad (7)$$

At the point of the minimum, the second term vanishes and

$$M - M_{min} \approx \sum_i \sum_j S_{ij}\, \Delta\alpha_i\, \Delta\alpha_j; \quad S_{ij} = \frac{1}{2} \frac{\partial^2 M}{\partial \alpha_i\ \partial \alpha_j}. \quad (8)$$

Expression (8) defines a hyperellipsoid at the minimum point, that is, the matrix of the coefficients $\langle S_{ij} \rangle$ determines the sensitivity $M_{\mathrm{min}}$ to deviations of the phase shifts from the optimum values. Accordingly, the terms of the reciprocal matrix $\langle S_{ij} \rangle^{-1}$ determine the errors in the phase shifts (when $i = j$) and the connection between the phase shifts (when $i \neq j$).[3]

The coefficients $S_{ij}$ can be calculated directly from (8), but this is too cumbersome. We used an approximate finite-difference method. To determine the diagonal element $S_{ii}$ we increased the phase shift $\alpha_i$ by an amount $\Delta\alpha_i$ and determined the value of M. Then, according to (8),

$$S_{ii} = (M - M_{min}) / (\Delta\alpha_i)^2. \quad (9)$$

The calculations were carried out both for positive and for negative increments of $\alpha_i$ and the results averaged.

To find the non-diagonal elements, increments were applied to both phase shifts. Increments of all possible signs were taken and the result was averaged. If we denote the quantities M corresponding to the possible combinations of the signs of the increments $\Delta\alpha_i$ and $\Delta\alpha_j$ as $M_{++}$, $M_{--}$, $M_{+-}$, and $M_{-+}$, we have

$$\begin{aligned}
M_{++} - M_{min} &= S_{ii}(\Delta\alpha_i)^2 + S_{jj}(\Delta\alpha_j)^2 + 2S_{ij}(\Delta\alpha_i)(\Delta\alpha_j),\\
M_{--} - M_{min} &= S_{ii}(-\Delta\alpha_i)^2 + S_{jj}(-\Delta\alpha_j)^2\\
&\quad + 2S_{ij}(-\Delta\alpha_i)(-\Delta\alpha_j),\\
M_{+-} - M_{min} &= S_{ii}(\Delta\alpha_i)^2 + S_{jj}(-\Delta\alpha_j)^2 + 2S_{ij}(\Delta\alpha_i)(-\Delta\alpha_j),\\
M_{-+} - M_{min} &= S_{ii}(-\Delta\alpha_i)^2 + S_{jj}(\Delta\alpha_j)^2 + 2S_{ij}(-\Delta\alpha_i)(\Delta\alpha_j).
\end{aligned} \quad (10)$$

Subtracting the third and fourth equation of (10) from the first and second we obtain (for $\Delta\alpha_i = \Delta\alpha_j = \Delta\alpha$)

$$S_{ij} = \frac{[(M_{++} + M_{--}) - (M_{-+} + M_{+-})]}{8\,(\Delta\alpha)^2}.$$

In all cases, the increment $\Delta\alpha$ amounted to 1 deg.

## 3. PHASE-SHIFT ANALYSIS WITH ALLOWANCE FOR THE S AND P WAVES (SP ANALYSIS)

In carrying out the phase-shift analysis we used a total of 25 experimental points for each value of the pion energy: 8 differential cross sections for elastic scattering of positive pions by protons, 7 differential elastic-scattering cross sections for negative pions, and 8 differential cross sections for exchange scattering of negative pions by hydrogen and the total cross sections for the scattering of positive and negative pions by hydrogen.

The differential cross sections for elastic scattering of positive pions by hydrogen and the total cross sections for the interaction between positive pions and hydrogen, as well as the initial values of the phase shifts for states with $T = {}^3/_2$, were taken from the work by Mukhin et al.[4-7]

The differential cross sections for the scattering of positive pions by hydrogen at 330 Mev were determined by interpolating the data of Mukhin, Ozerova, Pontecorvo,[6] and Grigor'ev and Mitin.[8] In this connection, the result of the phase-shift analysis at 333 Mev cannot be considered as fully independent.

The initial values of the phase shifts for the states with $T = \frac{1}{2}$ were obtained by the graphic method of Ashkin.[9] This method gave two possible sets of phase shifts (variants 1 and 3 of Tables II — VI). Along with these, we used two initial phase-shift assemblies for each energy, in which the phase shift $\alpha_1$ had a sign opposite that obtained graphically (variants 2 and 4) and two assemblies with negative phase shifts of P waves with $T = \frac{1}{2}$ (variants 6 and 7). Such assemblies should agree better with certain data on photoproduction (private communication from A. M. Baldin).

In addition to the data of reference 1, data for 220 Mev, obtained by Ashkin et al.,[10] were also processed.

The initial and calculated values of the phase shifts are given in Tables II — VI.

It is seen from these tables that there are only two stable variants of this solution, observed at all energies. In each of these variants, the same phase shifts differ little from each other at different energies. These are solutions a and b. The

**TABLE II.** Phase shifts (in degrees) at pion energies of 220 Mev (data by Ashkin et al.[10])

| Variant | | 3 | 6 | 1 | 2 | 4 | 7 |
|---|---|---|---|---|---|---|---|
| Initial values | $\alpha_3$ | —12.0 | —19.0 | —12.0 | —12.0 | —12.0 | —19.0 |
| | $\alpha_{31}$ | 0.0 | —5.0 | 0.0 | 0.0 | 0.0 | —5.0 |
| | $\alpha_{33}$ | 107.0 | 125.0 | 107.0 | 107.0 | 107.0 | 125.0 |
| | $\alpha_1$ | 10.0 | 10.0 | 10.0 | —10.0 | —10.0 | —10.0 |
| | $\alpha_{11}$ | 8.0 | —10.0 | —6.0 | —6.0 | 8.0 | —10.0 |
| | $\alpha_{13}$ | —3.0 | —10.0 | 5.0 | 5.0 | —3.0 | —10.0 |
| | $M$ | 36.0 | 687.0 | 109.0 | 88.0 | 122.0 | 1559.0 |
| Solution | | *a* | | *b* | | | |
| Values at the minimum | $\alpha_3$ | —15.8±1.5 | | —17.0 | | | |
| | $\alpha_{31}$ | —2.0±2.9 | | —0.1 | | | |
| | $\alpha_{33}$ | 111.0±1.8 | | 112.0 | | | |
| | $\alpha_1$ | 14.0±4.3 | | —7.0 | | | |
| | $\alpha_{11}$ | 6.2±3.3 | | 16.1 | | | |
| | $\alpha_{13}$ | —5.2±0.8 | | 3.6 | | | |
| | $M$ | 16.1 | | 14.5 | | | |

**TABLE III.** Phase shifts (in degrees) at pion energies of 240 Mev

| Variant | | 1 | 3 | 5 | 4 | 2 | 6 | 7 |
|---|---|---|---|---|---|---|---|---|
| Initial values | $\alpha_3$ | —18.1 | —18.1 | —14,7 | —18.1 | —18.1 | —19.0 | —19.0 |
| | $\alpha_{31}$ | —2,6 | —2.6 | —3.2 | —2.6 | —2.6 | —5.0 | —5.0 |
| | $\alpha_{33}$ | 114,7 | 114,7 | 109.5 | 114.7 | 114,7 | 125.0 | 125.0 |
| | $\alpha_1$ | 10.0 | 10.0 | 8.0 | —10.0 | —10.0 | 10.0 | —10.0 |
| | $\alpha_{11}$ | —6.5 | 8.0 | —5.4 | 8.0 | —6.5 | —10.0 | —10.0 |
| | $\alpha_{13}$ | 4.5 | —2.5 | 3.3 | —2.5 | 4.5 | —10.0 | —10.0 |
| | $M$ | 63.0 | 20.0 | 85.0 | 140.0 | 121.0 | 468.0 | 832.0 |
| Solution | | *a* | | | *c* | *b* | | |
| Values at the minimum | $\alpha_3$ | —18.1±1.3 | | | —18.5 | —19.6 | | |
| | $\alpha_{31}$ | —3.0±2.5 | | | —0.5 | —1.4 | | |
| | $\alpha_{33}$ | 115.0±1.0 | | | 115.0 | 115.0 | | |
| | $\alpha_1$ | 11.2±4.4 | | | 4.8 | —0.3 | | |
| | $\alpha_{11}$ | 10.0±5,4 | | | 16.7 | —2.6 | | |
| | $\alpha_{13}$ | —2.4±1.4 | | | 1.7 | 14.0 | | |
| | $M$ | 18.8 | | | 18.8 | 29.7 | | |

**TABLE IV.** Phase shifts (in degrees) at pion energies of 270 Mev

| Variant | | 3 | 6 | 7 | 4 | 1 | 2 | 5 |
|---|---|---|---|---|---|---|---|---|
| Initial values | $\alpha_3$ | —20.2 | —19.0 | —19.0 | —20.2 | —20.2 | —20.2 | —24.1 |
| | $\alpha_{31}$ | —6.7 | —5,0 | —5.0 | —6.7 | —6.7 | —6,7 | —10,3 |
| | $\alpha_{33}$ | 129,3 | 125.0 | 125.0 | 129.3 | 129.3 | 129.3 | 132.8 |
| | $\alpha_1$ | 11,0 | 10.0 | —10.0 | —11.0 | 11,0 | —11,0 | 9.6 |
| | $\alpha_{11}$ | 10.5 | —10.0 | —10.0 | 10.5 | —17.5 | —17.5 | —10,0 |
| | $\alpha_{13}$ | —7.5 | —10.0 | —10.0 | —7.5 | 10.5 | 10.5 | +10.0 |
| | $M$ | 76.0 | 404,0 | 727.0 | 410,0 | 104.0 | 180.0 | 216.0 |
| Solution | | *a* | | | *c* | *b* | | |
| Values at the minimum | $\alpha_3$ | —20,1±1.3 | | | —19,9 | —20.3 | | |
| | $\alpha_{31}$ | —7,0±1,8 | | | —6.1 | —8.2 | | |
| | $\alpha_{33}$ | 129.0±0.9 | | | 129.2 | 129.7 | | |
| | $\alpha_1$ | 25.7±2,5 | | | 3.0 | 0.2 | | |
| | $\alpha_{11}$ | 5.3±3.0 | | | 27.3 | —9,4 | | |
| | $\alpha_{13}$ | —1,2±1.2 | | | 4,1 | 20.1 | | |
| | $M$ | 9.6 | | | 15.3 | 27.0 | | |

remaining variants either coincide with the aforementioned solutions, or give phase-shift values that are observed only at certain energies (for example, variant 4 at 240 and 270 Mev). Apparently these last solutions are connected with the mathematical aspect of the problem and not with the physical one, i.e., they are accidental.

Only solution a describes the experimental data sufficiently well. Actually, the expected value of M in the SP analysis is 19 (25 experimental points minus 6 phase shifts). In the case of solution b, the value of M is approximately 30 for almost all energies. The probability of obtaining such a value of M is approximately 5%.[11] At 307 Mev, the value of M for solution b reaches 71. The probability of observing such a value of M is negligibly small. At the same time, the values of M obtained in solution a are in good agreement with the expected values.

The angular distributions of the negative pions and photons in elastic and exchange scattering, calculated from the phase shifts of solution a, are shown in Figs. 1—4.

One must point out still another feature of so-

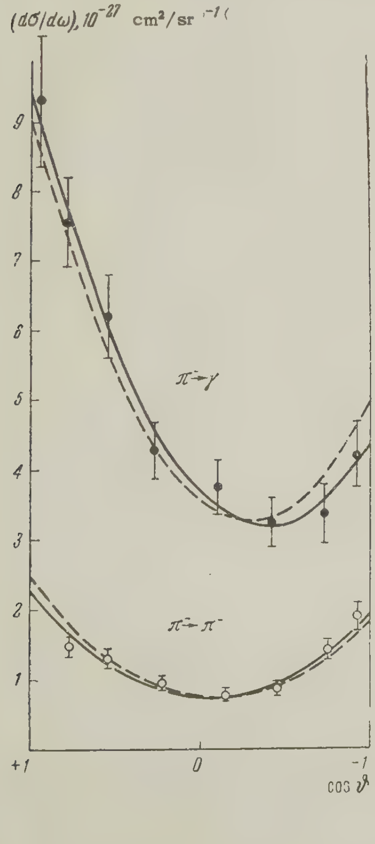

FIG. 1. Differential cross sections (c.m.s.) of the elastic and exchange scattering of 240-Mev pions by hydrogen. Solid curve — distribution of the form $[A_0 + A_1P_1(\cos\vartheta) + A_2P_2(\cos\vartheta)]$; dotted curve — distribution calculated from the SP analysis (solution a).

FIG. 2. Differential cross section (c.m.s.) of elastic and exchange scattering of negative pions with 270-Mev energy on hydrogen. Solid curve — distribution of the form $[A_0 + A_1P_1 \times(\cos\vartheta) + A_2P_2(\cos\vartheta)]$; the dotted curve represents distribution calculated from the SP analysis (solution a).

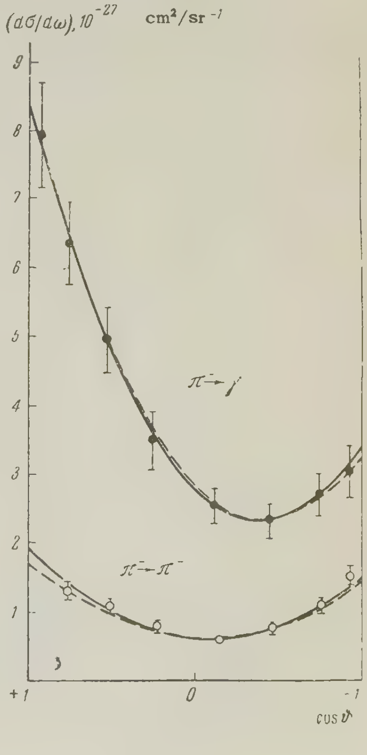

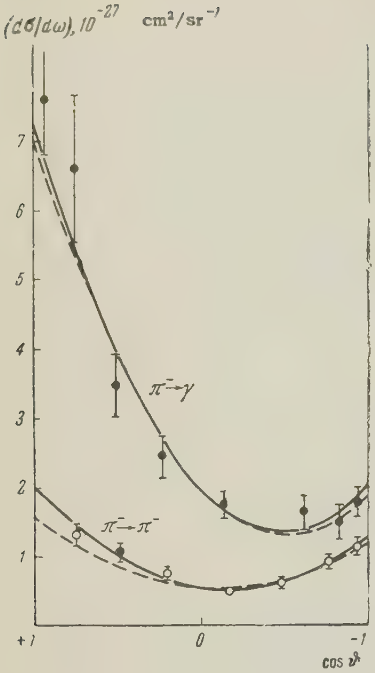

FIG. 3. Differential cross sections (c.m.s.) of elastic and exchange scattering of 307-Mev negative pions by hydrogen. Solid curve – distribution of the form $[A_0 + A_1P_1(\cos\vartheta) + A_2P_2(\cos\vartheta)]$; dotted curve – distribution calculated from SP analysis (solution a).

lution b, namely that on going from 240 to 270 Mev the signs of the phases $\alpha_1$ and $\alpha_{11}$ become reversed. It appears to be little likely that the phase shift $\alpha_1$, which is positive at small energies, reverses its sign twice between 150 and 270 Mev. An additional criterion, which makes it possible to choose between the different solutions, is the result of the experiments on the polarization of recoil protons is the interaction between pions and hydrogen. These experiments were made by Ashkin et al.[12] at a negative-pion energy of 223 Mev and by Vasilevskiĭ and Vishnyakov[13] (preliminary data) at negative-pion energies of 300 Mev. It follows from the experiments that solution a is the more probable.

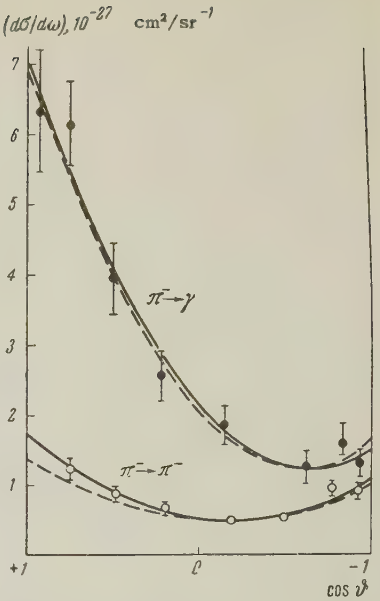

FIG. 4. Differential cross sections (c.m.s.) of elastic and exchange scattering of 333-Mev negative pions by hydrogen. Solid curve – distribution of type $[A_0 + A_1P_1(\cos\vartheta) + A_2P_2(\cos\vartheta)]$; dotted curve – distribution calculated from SP analysis (solution a).

All the foregoing statements lead to the conclusion that the scattering of pions by protons in the energy range above "resonant" is most probably described by solution a. The error matrices for this solution are given in Tables VII – XI. The errors in the phase shifts of solution a, which are given in Tables II – VI, are the diagonal elements of the corresponding matrices.

The phase shifts in the states with isotopic spin $T = 3/2$, given by solution a, actually do not differ from those obtained in experiments with positive mesons.[7]

As regards phase shift in states with isotopic spin $T = 1/2$, we can state the following. The phase shift of the S state is positive. The dependence of the value of this phase on the momentum is shown in Fig. 5. It is seen that, accurate to errors

TABLE V. Phase shifts (in degrees) at pion energies of 370 Mev

| Variant | | 3 | 4 | 6 | 7 | 1 | 2 | 5 |
|---|---|---|---|---|---|---|---|---|
| Initial values | $\alpha_3$ | —25.0 | —25.0 | —25.0 | —25.0 | —25.0 | —25.0 | —24.1 |
| | $\alpha_{31}$ | —10.0 | —10.0 | —12.0 | —12.0 | —10.0 | —10.0 | —10.3 |
| | $\alpha_{33}$ | 133.0 | 133.0 | 135.0 | 135.0 | 133.0 | 133.0 | 132.8 |
| | $\alpha_1$ | 9.0 | —9.0 | 10.0 | —10.0 | 9.0 | —9.0 | 9.6 |
| | $\alpha_{11}$ | 10.0 | 10.0 | —10.0 | —10.0 | —18.5 | —18.5 | —10.0 |
| | $\alpha_{13}$ | —9.0 | —9.0 | —10.0 | —10.0 | 10.0 | 10.0 | 10.0 |
| | $M$ | 56.0 | 217.0 | 379.0 | 505.0 | 151.0 | 159.0 | 228.0 |
| Solution | | *a* | | | | *b* | | |
| Values at the minimum | $\alpha_3$ | —23.9±1.2 | | | | —23.6 | | |
| | $\alpha_{31}$ | —10.0±2.0 | | | | —15.4 | | |
| | $\alpha_{33}$ | 132.4±0.9 | | | | 135.2 | | |
| | $\alpha_1$ | 17.1±5.2 | | | | 4.1 | | |
| | $\alpha_{11}$ | 11.4±3.3 | | | | —22.4 | | |
| | $\alpha_{13}$ | —5.0±1.2 | | | | 14.6 | | |
| | $M$ | 29.0 | | | | 71.0 | | |

**TABLE VI.** Phase shifts (in degrees) at pion energies of 333 Mev

| Variant | | 3 | 4 | 1 | 2 | 5 | 6 | 7 |
|---|---|---|---|---|---|---|---|---|
| Initial values | $\alpha_3$ | —30.0 | —30.0 | —30.0 | —30.0 | —24.1 | —25.0 | —25.0 |
| | $\alpha_{31}$ | —12,0 | —12.0 | —12.0 | —12.0 | —10.3 | —12.0 | —12.0 |
| | $\alpha_{33}$ | 139.0 | 139.0 | 139.0 | 139.0 | 132.8 | 135.0 | 135.0 |
| | $\alpha_1$ | 10.0 | —10.0 | 10.0 | —10.0 | 9.6 | 10.0 | —10.0 |
| | $\alpha_{11}$ | 10.0 | 10.0 | —18.0 | —18.0 | —10.0 | —10.0 | —10.0 |
| | $\alpha_{13}$ | —9.0 | —9.0 | 10.0 | 10.0 | 10.0 | —10.0 | —10.0 |
| | $M$ | 87 | 324 | 179 | 224 | 251 | 3875 | 6706 |
| Solution | | *a* | | *b* | | | *d* | |
| Значения в минимуме | $\alpha_3$ | —26.5±1.4 | | —25.0 | | | —28.0 | |
| | $\alpha_{31}$ | —10.6±2.1 | | —15.7 | | | —10.7 | |
| | $\alpha_{33}$ | 137.2±1.1 | | 140.1 | | | 139.5 | |
| | $\alpha_1$ | 29.2±1.8 | | 11.7 | | | 31.4 | |
| | $\alpha_{11}$ | 8.1±2.9 | | —24.0 | | | —16.3 | |
| | $\alpha_{13}$ | —2.0±1.3 | | 16.0 | | | 10.0 | |
| | $M$ | 22.6 | | 33.1 | | | 94.4 | |

**TABLE VII;** Matrix of phase-shift errors (radians$^2$), $E_\pi = 220$ Mev

| | $10^4\alpha_3$ | $10^4\alpha_{31}$ | $10^4\alpha_{33}$ | $10^4\alpha_1$ | $10^4\alpha_{11}$ | $10^4\alpha_{13}$ |
|---|---|---|---|---|---|---|
| $\alpha_3$ | 6.16 | —5.40 | —0.08 | 0.68 | 7.46 | 1.28 |
| $\alpha_{31}$ | | 22.34 | —0.56 | 3.80 | —12.66 | 1.36 |
| $\alpha_{33}$ | | | 8.54 | 16.38 | — 5.16 | 1.14 |
| $\alpha_1$ | | | | 49.38 | —21.22 | 3.88 |
| $\alpha_{11}$ | | | | | 29.84 | —0.32 |
| $\alpha_{13}$ | | | | | | 0.17 |

**TABLE VIII.** Matrix of phase-shift errors (radians$^2$), $E_\pi = 240$ Mev

| | $10^4\alpha_3$ | $10^4\alpha_{31}$ | $10^4\alpha_{33}$ | $10^4\alpha_1$ | $10^4\alpha_{11}$ | $10^4\alpha_{13}$ |
|---|---|---|---|---|---|---|
| $\alpha_3$ | 4.92 | —1.80 | —0.42 | —3.16 | 7.24 | 1.76 |
| $\alpha_{31}$ | | 17.54 | —0.38 | 2.56 | —10.90 | 0.80 |
| $\alpha_{33}$ | | | 2.56 | 4.46 | —2.52 | —0.82 |
| $\alpha_1$ | | | | 52,34 | —47.10 | —8.52 |
| $\alpha_{11}$ | | | | | 79.72 | 14.64 |
| $\alpha_{13}$ | | | | | | 5.32 |

**TABLE IX.** Matrix of phase-shift errors (radians$^2$), $E_\pi = 270$ Mev

| | $10^4\alpha_3$ | $10^4\alpha_{31}$ | $10^4\alpha_{33}$ | $10^4\alpha_1$ | $10^4\alpha_{11}$ | $10^4\alpha_{13}$ |
|---|---|---|---|---|---|---|
| $\alpha_3$ | 3.70 | —0.20 | —0.40 | —1.86 | 2.38 | 0.44 |
| $\alpha_{31}$ | | 10.28 | —0.42 | 11.98 | —11.40 | 2.74 |
| $\alpha_{33}$ | | | 1.94 | 5.20 | —1.04 | 0.80 |
| $\alpha_1$ | | | | 73.04 | —23.46 | 13.64 |
| $\alpha_{11}$ | | | | | 28.96 | —4.78 |
| $\alpha_{13}$ | | | | | | 3.98 |

**TABLE X.** Matrix of phase-shift errors (radians$^2$), $E_\pi = 307$ Mev

| | $10^4\alpha_3$ | $10^4\alpha_{31}$ | $10^4\alpha_{33}$ | $10^4\alpha_1$ | $10^4\alpha_{11}$ | $10^4\alpha_{13}$ |
|---|---|---|---|---|---|---|
| $\alpha_3$ | 4.48 | —0.28 | 0.10 | 1.00 | 1.52 | 1.26 |
| $\alpha_{31}$ | | 8.62 | —0.28 | 0.68 | —5.28 | 0.82 |
| $\alpha_{33}$ | | | 2.16 | 3.40 | —1.98 | 1.08 |
| $\alpha_1$ | | | | 16.40 | —13.60 | 6.28 |
| $\alpha_{11}$ | | | | | 24.36 | —5.88 |
| $\alpha_{13}$ | | | | | | 3.94 |

**TABLE XI.** Matrix of phase-shift errors (radians$^2$), $E_\pi = 333$ Mev

| | $10^4\alpha_3$ | $10^4\alpha_{31}$ | $10^4\alpha_{33}$ | $10^4\alpha_1$ | $10^4\alpha_{11}$ | $10^4\alpha_{13}$ |
|---|---|---|---|---|---|---|
| $\alpha_3$ | 5.56 | —2.38 | —1.22 | 0.48 | 5.62 | —0.04 |
| $\alpha_{31}$ | | 11.88 | —2.86 | 3.66 | —10.66 | 5.18 |
| $\alpha_{33}$ | | | 3.44 | 1.84 | 2.40 | 0.06 |
| $\alpha_1$ | | | | 8.68 | —8.40 | 4.94 |
| $\alpha_{11}$ | | | | | 22.68 | —7.66 |
| $\alpha_{13}$ | | | | | | 4.60 |

in the determination of its magnitude, the behavior of the phase shift $\alpha_1$ does not contradict the linear dependence observed at small energies ($\alpha_1 = 9.9\,\eta$, where $\eta$ is the momentum of the pion in the c.m.s.).

The value of the phase shift $\alpha_{11}$ does not exceed 10 deg, and its sign is apparently positive.

The phase shift $\alpha_{13}$, as can be seen from Tables II — VI, is small (1 — 5 deg) and apparently negative. It should be noted here that, according to the theory of Chew,[14-16] the phase shift

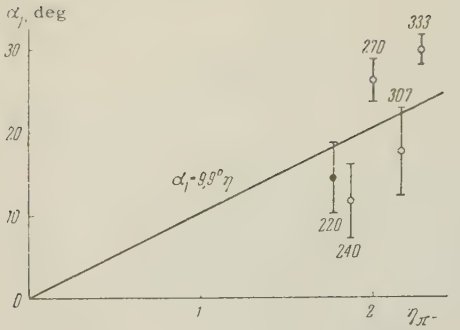

FIG. 5. Dependence of the value of the phase shift $\alpha_1$ on the pion momentum in the c.m.s.

$\alpha_{13}$ should be negative and approximately equal to $\alpha_{31}$. Within the limit of errors, the phase shifts of solution a satisfy this condition. A published paper by Chiu and Lomon[17] gives a phase-shift analysis of the data of Ashkin et al. and of our preliminary data at 370 Mev. In view of the fact that the solution which they consider to be the most reliable coincides with our solution a, we have made some additional calculations. In these calculations we took as the starting data the phase shifts of the solution given by Chiu and Lomon. These led to solution b at all energies (except 240 Mev).

At 307 and 333 Mev, the cross sections for inelastic processes are sizable, and therefore the scattering phase shifts, strictly speaking, can no longer be considered real. In general form, the differential cross sections for the scattering of pions by nucleons in a state with definite isotopic spin can be written in the following manner:

$$\left(\frac{d\sigma}{d\omega}\right)_{\pi^+\to\pi^+} = \left|\sum_{l=0}^{\infty} \frac{a_l}{2ki} P_l(\cos\vartheta)\right|^2 + \left|\sum_{l=0}^{\infty} \frac{b_l}{2ik} P_{l1}(\cos\vartheta)\right|^2, \qquad (12)$$

where k is the momentum of the pion in the c.m.s., while $a_l$ and $b_l$ are given by

$$a_l = (l+1)\exp 2i\alpha^l_{3,\,2l+1} + l\exp 2i\alpha^l_{3,\,2l-1} - (2l+1),$$
$$b_l = \exp 2i\alpha^l_{3,\,2l+1} - \exp 2i\alpha^l_{3,\,2l-1}. \qquad (13)$$

The presence of an imaginary part of the phase shift causes expressions of the form $\beta_l \exp(2i\alpha_l)$ to appear in Eq. (13) instead of expressions of the form $\exp(2i\alpha_l)$, where $\beta_l$ and $\alpha_l$ are real numbers. Using the experimentally obtained cross sections for inelastic processes,[18] we can estimate $\beta_l$ from the general quantum-mechanical theory of inelastic scattering.[19] It is found that for any state, even at 333 Mev, $\beta_l$ differs from unity by not more than 2% or 3%, corresponding to an imaginary part not greater than 0.5 deg. The fact that $\beta_l$ differs little from unity makes maximum phase-shift variation, due to taking the inelastic processes into account (in accordance with the estimates made) not greater than approximately ±3 deg, that is, the accuracy in the determination of the phases. Thus, up to 330 Mev, a phase-shift analysis based on the assumption that the phases are real numbers is apparently a sufficiently good approximation.

## 4. PHASE-SHIFT ANALYSIS WITH ALLOWANCE FOR S, P AND D WAVES (SPD ANALYSIS)

At pion energies near 300 Mev, one can expect a noticeable contribution from D waves ($l = 2$) to the scattering. In this connection, we made a phase-shift analysis with allowance for the D waves for all pion energies. The initial phase shifts for the S and P waves were taken in the SPD analysis to be the phase shifts of solutions a and b, obtained in the SP analysis. The initial values of the phase shifts of the D waves in states with $T = 3/2$, in accordance with the results obtained in experiments with positive pions,[7] were taken to be $\delta_{33} = 6$ deg and $\delta_{35} = -6$ deg. The values of the initial phase shifts of the D waves in states with isotopic spin $T = 1/2$ were taken to have an absolute value of 8 deg. The signs of these phase shifts were taken in all possible combinations, that is, ++, −−, +−, and −+. Thus, we obtained eight versions of the initial values of the phase shift for each energy, four for solution a and four for solution b.

As a result of the calculations performed, the initial versions, which differed only in the signs of the phase shifts $\delta_{13}$ and $\delta_{15}$, yielded one and the same solution. In other words, we obtained two sets of final versions of solution, one for initial solution a and the other for solution b. The values of the phase shifts corresponding to solutions a and b are listed in Tables XII and XIII. These two versions of the solutions will henceforth be called the "$a_{SPD}$ solution" and "$b_{SPD}$ solution."

For 333 Mev we obtained three different variants for solution a. Two of these are listed in Table XII. These solutions give phase-shift values corresponding to those obtained at lower energies.

It is seen from Table XII that when the D waves are taken into account the phase shifts $\alpha_1$, $\alpha_{11}$, and $\alpha_{13}$ of solution a change by not more than a few degrees, that is, they remain unchanged within the limit of errors. This is expected, for the S and P phases alone have already described the experimental data sufficiently well.

The phase shifts $\delta_{33}$ and $\delta_{35}$ of the D waves in states with isotopic spin $T = 3/2$ do not differ

**TABLE XII.** Phase shifts (degrees) at pion energies 240 — 333 Mev. Solution $a_{SPD}$

| Pion energy, Mev | 240 | 270 | 307 | 333 (1) | 333 (2) |
|---|---|---|---|---|---|
| $\alpha_3$ | —20.4±1,9 | —15.0±6.2 | —10.2±3.7 | —22.0±1,6 | —10.5±1.1 |
| $\alpha_{31}$ | —4.2±3.6 | —4.0±3.1 | —3.6±2.2 | —6.3±2.1 | —2.8±1.7 |
| $\alpha_{33}$ | 116.7±2.8 | 128.4±1.0 | 134.7±1.9 | 136.2±1.1 | 139.7±1.5 |
| $\delta_{33}$ | —0.9±3.4 | 3.9±6.6 | 11.1±3.0 | 2.4±1.3 | 12.1±1.8 |
| $\delta_{35}$ | 4.9±5.5 | —5.3±5.1 | —12.0±2.1 | —4.3±1.0 | —13.2±1.0 |
| $\alpha_1$ | 8.1±3.5 | 25.8±2.2 | 23.8±3.3 | 28.9±2,0 | 31.8±1.6 |
| $\alpha_{11}$ | 11.2±3.2 | 4.2±3.8 | 8.0±4.0 | 9.4±3.4 | 4,3±3.5 |
| $\alpha_{13}$ | —1.4±1.45 | —0.4±1.5 | —2.2±1.9 | —2.2±1.0 | 1.0±1.9 |
| $\delta_{13}$ | 3.0±2.1 | 0.8±2.2 | 3.1±1.4 | 2.0±1.1 | 0.8±1.5 |
| $\delta_{15}$ | 2.3±2.5 | 1.3±2.2 | 1.9±2.0 | 1.0±1.0 | 1.8±1.2 |
| $M_{min}$ | 9.7 | 5.9 | 7.0 | 16.2 | 9.6 |

**TABLE XIII.** Phase shifts (degrees) at pion energies 240 — 333 Mev. Solution $b_{SPD}$

| Pion energy, Mev | 240 | 270 | 307 | 333 | Pion energy, Mev | 240 | 270 | 307 | 333 |
|---|---|---|---|---|---|---|---|---|---|
| $\alpha_3$ | —16.8 | —16.0 | —10.1 | —19.8 | $\alpha_1$ | — 0.3 | — 4.8 | — 3.5 | — 3.0 |
| $\alpha_{31}$ | — 1.7 | — 6.3 | — 3.2 | — 9.6 | $\alpha_{11}$ | — 6.9 | —12.9 | 0.0 | —21.9 |
| $\alpha_{33}$ | 115.5 | 128.0 | 134.7 | 136.3 | $\alpha_{13}$ | 7,2 | 9.2 | 6.6 | 15.2 |
| $\delta_{33}$ | 7.1 | 3.6 | 11.3 | 3.6 | $\delta_{13}$ | 6.2 | 9.0 | 15.0 | 2.7 |
| $\delta_{35}$ | — 2.4 | — 5.7 | —11.9 | — 6.1 | $\delta_{15}$ | 3.8 | 3.6 | 4.2 | 4.5 |
| | | | | | $M_{min}$ | 13.9 | 10.1 | 5.3 | 17.5 |

essentially from those obtained earlier by Mukhin and Pontecorvo.[7]

The phase shifts $\delta_{13}$ and $\delta_{15}$ of D waves in states with isotopic spin $T = \frac{1}{2}$ are small, as can be seen from Table XII. The accuracy with which they have been determined does not permit any definite conclusions to be drawn concerning the signs of these phase shifts.

Nothing definite can be said about the solution of $b_{SPD}$. It cannot be discarded completely merely because the corresponding solution b of the SP analysis does not agree with the experimental data. Nor can one exclude the possibility that the poor agreement given by solution b is connected with the need for taking the D waves into account in the analysis. It appears to be little probable, however, that the large D-phase values (up to 15 deg) obtained in the solution $b_{SPD}$ would occur already at 240 — 307 Mev. The dispersion relations described below give additional indications that the solution $b_{SPD}$ is apparently incorrect.

## 5. COMPARISON OF THE PHASE-SHIFT ANALYSIS RESULTS WITH THE DISPERSION RELATIONS

It is well known that the dispersion relations yield the dependence of the real part of the zero-degree scattering amplitude D(0) on the pion energy.

An expression for $D_-(0)$ can be obtained from Eq. (2) for the cross section of elastic scattering of negative pions by hydrogen. This expression represents the sum of the squares of the real and imaginary parts of the scattering amplitude. Then

$$D_-(0) = \tfrac{1}{6}\, k^{-1}(\sin 2\alpha_3 + \sin 2\alpha_{31} + 2\sin 2\alpha_{33} + 2\sin 2\delta_{33} + 3\sin 2\delta_{35} + 2\sin 2\alpha_1 + 2\sin 2\alpha_{11} + 4\sin 2\alpha_{13} + 4\sin 2\delta_{13} + 6\sin 2\delta_{15}). \tag{14}$$

The values of $D_-(0)$ calculated from the phase shifts are shown in Fig. 6. It is seen that solution a is in satisfactory agreement with the curve given by Pontecorvo,[13] with a coupling constant $f^2 = 0.08$ for the meson-nucleon interaction.

In conclusion, the authors consider it their pleasant duty to express sincere gratitude to B. Pontecorvo for constant attention and help with the work; to A. I. Mukhin, L. I. Lapidus, S. N. So-

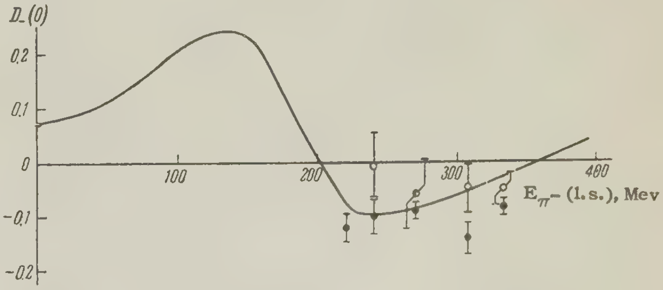

FIG. 6. Dependence of the real part of the amplitude of scattering at zero degrees, $D_-(0)$, in $h/\mu c$ units, on the negative-pion energy: ● — SP analysis (solution a), ○ — SPD analysis (solution $a_{SPD}$). The solid curve is taken from reference 13.

kolov, and N. P. Klepikov for numerous and fruitful discussions, and I. V. Popova and L. A. Chudov for valuable aid in programming the electronic computer.

---

[1] B. G. Zinov and S. M. Korenchenko, JETP **38**, 1099 (1960), Soviet Phys. JETP **11**, 794 (1960); **38**, 1399 (1960), this issue p. 1010.

[2] E. Clementel and C. Villi, Suppl. Nuovo cimento **3**, 474 (1955).

[3] Anderson, Davidon, Glicksman, and Kruse, Phys. Rev. **100**, 279 (1955).

[4] Ignatenko, Mukhin, Ozerov, and Pontecorvo, Dokl. Akad. Nauk SSSR **103**, 45 (1955).

[5] Ignatenko, Mukhin, Ozerov, and Pontecorvo, JETP **30**, 7 (1956), Soviet Phys. JETP **3**, 10 (1956).

[6] Mukhin, Ozerov, and Pontecorvo, JETP **31**, 371 (1956), Soviet Phys. JETP **4**, 237 (1957).

[7] A. I. Mukhin and B. Pontecorvo, JETP **31**, 550 (1956), Soviet Phys. JETP **4**, 373 (1957).

[8] E. L. Grigor'eva and N. A. Mitin, JETP **32**, 440 (1957), Soviet Phys. JETP **5**, 000 (1957).

[9] J. Ashkin and S. H. Vosko, Phys. Rev. **91**, 1248 (1953).

[10] Ashkin, Blaser, Feiner, and Stern, Phys. Rev. **105**, 724 (1957).

[11] I. V. Dunin-Barkovskiĭ and N. V. Smirnov, Теория вероятностей и математическая статистика в технике (Theory of Probability and Mathematical Statistics in Engineering), Gostekhizdat, 1955.

[12] Ashkin, Blaser, Burger, Hunze, and Romanowski, Ann. Intern. Conf. on High-Energy Physics, CERN, 1958.

[13] B. Pontecorvo, Paper at Conference on High-Energy Physics, Kiev, 1959.

[14] G. F. Chew, Phys. Rev. **89**, 591 (1953).

[15] G. F. Chew, Phys. Rev. **95**, 285 (1954).

[16] Chew, Goldberger, Low, and Nambu, Phys. Rev. **106**, 1337 (1957).

[17] H. Y. Chiu and E. L. Lomon, Ann. of Phys. **6**, 50 (1959).

[18] V. G. Zinov and S. M. Korenchenko, JETP **34**, 301 (1958), Soviet Phys. JETP **7**, 210 (1958).

[19] L. D. Landau and E. M. Lifshitz, Квантовая механика (Quantum Mechanics), Gostekhizdat, 1948. (Engl. Transl., Pergamon, 1958).

Transl. by J. G. Adashko
273

SOVIET PHYSICS JETP VOLUME 11, NUMBER 5 NOVEMBER, 1960

# *ANGULAR DISTRIBUTIONS OF 6.8-Mev PROTONS ELASTICALLY SCATTERED BY CHROMIUM, NICKEL, AND COPPER ISOTOPES*

A. K. VAL'TER, I. I. ZALYUBOVSKIĬ, A. P. KLYUCHAREV, M. V. PASECHNIK, N. N. PUCHEROV, and V. I. CHIRKO

Physico-Technical Institute, Academy of Sciences, Ukrainian S.S.R.

Submitted to JETP editor November 17, 1959

J. Exptl. Theoret. Phys. (U.S.S.R.) **38**, 1419-1423 (May, 1960)

The angular distributions of 6.8-Mev protons elastically scattered by $Cr^{52,53}$, $Ni^{58,60,62}$, and $Cu^{63,65}$ isotopes were investigated. Appreciable differences in the variation of the differential cross sections were found in the various isotopes. The results indicate that in scattering studies the individual features of the nuclei should be taken into account.

In recent years, in connection with the development of the optical-model concept of the nucleus, a series of detailed investigations of the angular distributions of nucleons elastically scattered by nuclei was carried out within a wide energy range. Comparison of theory and experiment showed that the optical model of the nucleus is sufficiently effectual for the description of scattering processes.

However, almost all the studies of nucleon scattering were carried out with targets of natural isotope composition. The results obtained refer therefore to the averaged result of scattering by the different isotopes contained in the investigated target. It was difficult or simply impossible to observe in such measurements the peculiarities in the scattering by any individual isotope. Nonetheless, the peculiarities of "isotopic" scattering had been pointed out in a number of papers. Thus, in the investigation of elastically scattered protons by a group of nuclei with $Z = 24$ to 30, a substantial change in the angular distributions was noted from element to element.[1-6] Inasmuch as the mass number of the scattering nuclei changes little, similar results fit the optical-model concepts poorly, since to describe the above group of nuclei they require a considerable and irregular variation of the model parameters. This obviously raises the question of investigating separated isotopes. The first experiments in this direction showed that the angular distributions can change to a large extent from isotope to isotope.[7-10]

At present, the theoretical interpretation of these effects in the scattering of nucleons by nuclei runs into many difficulties. It is therefore desirable to investigate the scattering of nucleons by separated isotopes in a broad energy range. The accumulation and systematization of experimental data will add to our knowledge of the structure of the nucleus and of the interaction of nucleons with nuclei.

The present work is devoted to a study of angular distributions of elastically scattered 6.8-Mev protons by the $Cr^{52,53}$, $Ni^{58,60,62}$, and $Cu^{63,65}$ isotopes.

## EXPERIMENTAL METHOD

Protons with an energy of (6.8 ± 0.1) Mev were obtained in the cyclotron of the Physics Institute of the Ukrainian S.S.R. Academy of Sciences. After extraction from the accelerating chamber, the beam was focused by magnetic quadrupole lenses, deflected by 30°, and passed through collimating diaphragms to the target. The target was placed at the center of a scattering chamber of 1.6 m diameter.

The scattered protons were registered by a scintillation spectrometer consisting of a CsI(Tl) crystal, a FÉU-20 photomultiplier, and of an AIMA-1 (reference 6) 50-channel pulse-height analyzer. The spectrometer in a special jacket was fixed to a mobile bracket in the scattering chamber and could be rotated about the target. The large dimensions of the scattering chamber assured good geometry.

The measurements were carried out every 5° from 20 to 160°. The precision in the setting of the scattering angle amounted to 0.3°. The energy resolution of the scintillation spectrometer at its half-width was 4 — 6%, depending on the effective target thickness. The relative proton flux on the target was measured with the aid of a scintillation counter.

The energy spectrum of the scattered protons was registered at each angle where measurements were carried out. The statistics of the elastically scattered proton group were chosen such that the statistical error should not exceed 2%. The group of elastically scattered protons was segregated in the energy spectrum. The results obtained for each angle were reduced to one and the same value of the monitor reading; the relative angular distribution was thereby determined.

After going over to the center-of-mass system (c.m.s.), the value of the differential cross section (in arbitrary units) was multiplied by $\sin^4(\theta/2)$, and was normalized to unity in the 20° range. Under the natural assumption that in the region of angles on the order of 20° pure Rutherford scattering takes place, the above-mentioned quantity is the ratio of the experimental cross section to the Rutherford cross section.

Targets in the form of thin 3- to 5-$\mu$ self-supporting foils, enriched to contain 93 — 98% of the investigated isotope, were used in the experiment. The composition of the targets is listed in the table.

## MEASUREMENT RESULTS AND DISCUSSION OF THE DATA

For most nuclei studied in this work, the energy resolution of the scintillation spectrometer was sufficient to separate the group of inelastically scattered protons from the group of those elastically scattered. One example of an energy spectrum is shown in Fig. 1

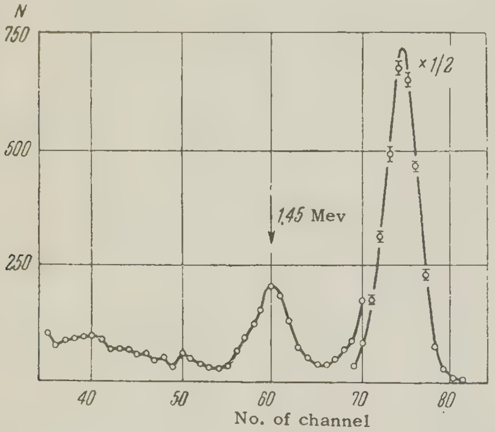

FIG. 1. The energy spectrum of protons scattered at 90° by the $Cr^{52}$ nucleus.

The first 1.44-Mev level[11] of the $Cr^{52}$ nucleus is well separated in the energy spectrum of the scattered protons. This group of protons is easily separated from the group of elastically scattered protons. At the same time, the groups of protons connected with the lower 0.54- and 1.01-Mev levels of the $Cr^{53}$ nucleus may, in view of the insufficient energy resolution, contribute considerably to the elastic scattering, particularly at large scattering angles. The angular distributions of 6.8-Mev protons elastically scattered by chromium isotopes are shown in Fig. 2. In spite of the small shift in the positions of the angular-distribution maxima and minima, our attention is drawn to the considerably larger value of the $Cr^{52}$ cross section compared with that of $Cr^{53}$ in the region of large scattering angles. This difference may really be much larger than appears from our experiments, if the possible contribution of inelastic groups to the elastic scattering by $Cr^{53}$ is taken into consideration. It will be possible to form an opinion about the magnitude of this contribution after additional experiments. Measurement results for the chromium isotopes are in good qualitative agreement with data on the scattering of 5.4-Mev protons (reference 9).

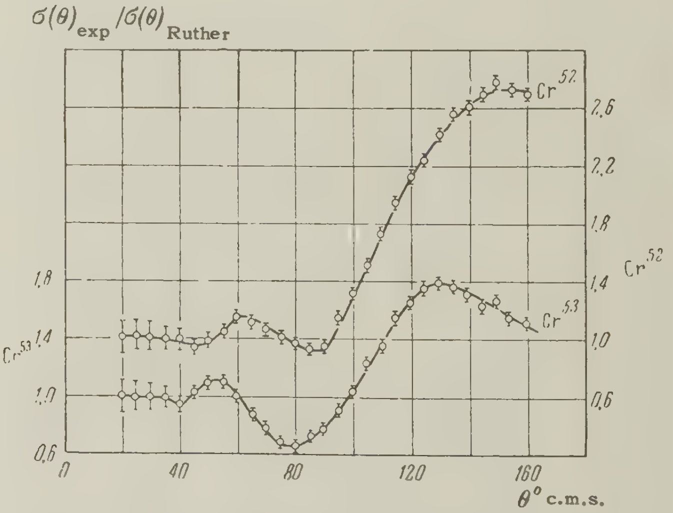

FIG. 2. The angular distribution of protons elastically scattered by chromium isotopes.

| Target | Contents, % | | | | | | | | | | |
|---|---|---|---|---|---|---|---|---|---|---|---|
| | Thickness, $\mu$ | $Ni^{58}$ | $Ni^{60}$ | $Ni^{61}$ | $Ni^{62}$ | $Ni^{64}$ | $Cr^{52}$ | $Cr^{53}$ | $Cr^{54}$ | $Cu^{63}$ | $Cu^{65}$ |
| $Cr^{52}$ | 5 | — | — | — | — | — | 98.7 | 1.23 | <0.1 | — | — |
| $Cr^{53}$ | 6 | — | — | — | — | — | 4.04 | 94.96 | 1.0 | — | — |
| $Ni^{58}$ | 3.5 | 98.6 | 1.0 | 0.2 | 0.1 | <0.1 | — | — | — | — | — |
| $Ni^{60}$ | 3.4 | 1.2 | 97.9 | 0.4 | 0.5 | <0.1 | — | — | — | — | — |
| $Ni^{62}$ | 2.5 | 2 | 0.8 | 1.6 | 94.5 | 1.1 | — | — | — | — | — |
| $Cu^{63}$ | 3.3 | — | — | — | — | — | — | — | — | 98 | 2.0 |
| $Cu^{65}$ | 3.1 | — | — | — | — | — | — | — | — | 2.0 | 98 |

The first excited states of the $Ni^{58}$, $Ni^{60}$, and $Ni^{62}$ isotopes are located above 1 Mev (1.44, 1.33, and 1.17 Mev, respectively). Proton groups corresponding to the above levels are well separated from the elastically scattered proton groups. The angular distributions of $Ni^{58}$ and $Ni^{60}$ (Fig. 3) are similar to each other, and duplicate in the main the result obtained with a natural mixture of nickel isotopes. This is not unexpected, since these two isotopes constitute the main part of the natural isotope mixture. It should be noted that the cross section for $Ni^{60}$ in the range of large angles is somewhat larger than for $Ni^{58}$. This result is in good agreement with the observations made[10] in the scattering of 40-Mev protons by these isotopes.

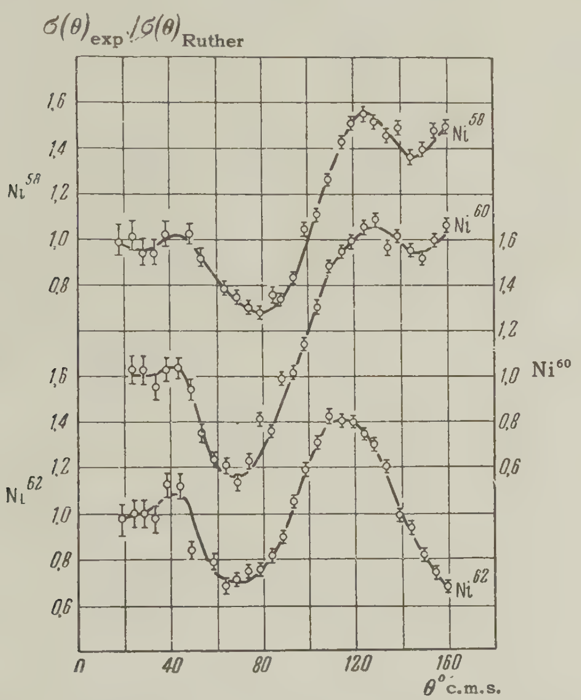

FIG. 3. The angular distribution of protons elastically scattered by nickel isotopes.

The angular distribution for $Ni^{62}$ differs sharply from the analogous curves for the two lighter nickel isotopes. In the range of angles above 120° the differential cross section decreases. If account is taken of the fact that in going over from one isotope to the other the number of neutrons changes only by two, this result is somewhat unexpected. Nonetheless, this effect does not contradict the experimental results with 5.4-Mev protons.[7]

The variation of the cross sections with angle for the $Cu^{63}$ and $Cu^{65}$ isotopes is completely identical (Fig. 4). However, the curve of the heavier copper isotope is shifted towards smaller angles by about 5° relative to the $Cu^{63}$ curve. An

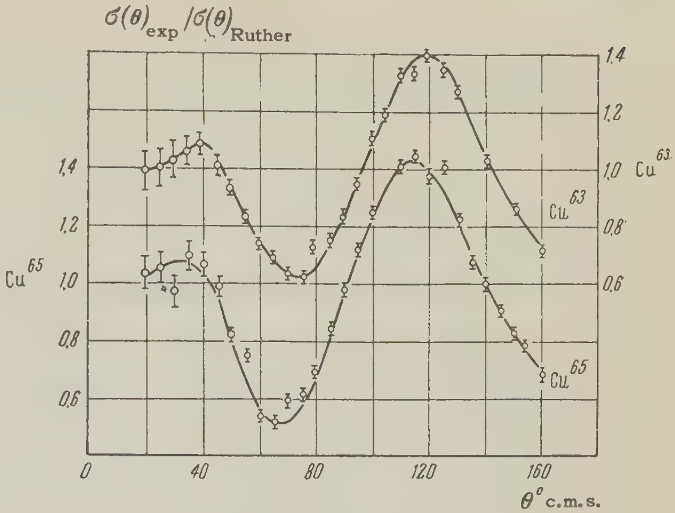

FIG. 4. The angular distribution of protons elastically scattered by copper isotopes.

analogous result is obtained in the scattering of 19.6-Mev protons by the same isotopes.[7] We note that the variation of the cross section with angle for $Ni^{62}$ is in the main analogous to that observed for cobalt and copper isotopes.

It is known that in calculations according to the optical model the change in the imaginary part of the potential W causes a change in the maxima and minima of the differential cross section.[12] On the other hand, the imaginary part of the potential is connected with the value of the absorption. With decreasing W the absorption decreases; at the same time the differential cross section in the region of large angles increases. Thus, it is possible to speak of a possible change in the value of the absorption on going over from one isotope to another. At the same time, one can expect a somewhat different value of the elastic-scattering cross section connected with the formation of a compound nucleus. Taking account of interference effects, one can expect different results for the scattering. A similar set of arguments could serve as an explanation of such a considerable difference in the scattering by neighboring isotopes.

Obviously, the interpretation of the scattering results by separated isotopes, within the frame of the optical model, requires a considerable variation of the model parameters. This refers not only to the value of the imaginary part of W, but also to the real part of the potential V and to the radius R. The two last parameters are connected with the shift of the angular-distribution curves, and, as we have seen, for neighboring isotopes this shift may be considerable.

Apparently, to obtain fuller agreement between theory and experiment, account must be taken in the optical model not only of the spin-orbit interaction of the incident proton but also of the effect of the shell structure of the nucleus on the scattering process.

---

[1] B. L. Cohen and R. V. Neidigh, Phys. Rev. **93**, 282 (1954).

[2] B. B. Kinsey and T. Stone, Phys. Rev. **103**, 975 (1956).

[3] D. A. Bromley and N. S. Wall, Phys. Rev. **102**, 1560 (1956).

[4] W. F. Waldorf and N. S. Wall, Phys. Rev. **107**, 1602 (1957).

[5] Kondo, Yamazaki, Toi, Nakasima, and Yamabe, J. Phys. Soc. Japan **13**, 231 (1958).

[6] N. N. Pucherov, Ukrainian Phys. J. **4**, 313, 318 (1959).

[7] Vanetsian, Klyucharev, and Fedchenko, Compt. rend. (1959); Атомная энергия (Atomic Energy) **6**, 661 (1959).

[8] Rutkevich, Golovnya, Val'ter, and Klyucharev, Dokl. Akad. Nauk SSSR **130**, 1008 (1960), Soviet Phys. - Doklady **5**, 118 (1960).

[9] A. P. Klyucharev and N. Ya. Rutkevich, JETP **38**, 285 (1960), Soviet Phys. JETP **11**, 207 (1960).

[10] M. K. Brussel and J. H. Williams, Phys. Rev. **114**, 525 (1959).

[11] B. S. Dzhelepov and L. K. Peker, Схемы распада радиоактивных ядер Decay Schemes of Radioactive Nuclei, Acad. Sci. Press, 1958.

[12] Glassgold, Cheston, Stein, Schuldt, and Erickson, Phys. Rev. **106**, 1207 (1957).

Translated by Z. Barnea
274

# *INVESTIGATION OF POLARIZATION OF INTERNAL CONVERSION ELECTRONS IN TRANSITIONS FOLLOWING DECAY OF HEAVY ELEMENTS*

M. E. VISHNEVSKIĬ, V. A. LYUBIMOV, E. F. TRETYAKOV, and G. I. GRISHUK

Submitted to JETP editor November 23, 1959

J. Exptl. Theoret. Phys. (U.S.S.R.) 38, 1424-1429 (May, 1960)

Polarization of conversion electrons has been measured for transitions following $\beta^-$ decay in $\mathrm{Tm}^{170}$, $\mathrm{Re}^{186}$, $\mathrm{Hg}^{203}$ and $\mathrm{Pa}^{233}$. The conversion electrons were found to be polarized in the direction of emission of the $\beta^-$ particles for $\mathrm{Tm}^{170}$ and $\mathrm{Re}^{186}$, and in the opposite direction for $\mathrm{Hg}^{203}$ and $\mathrm{Pa}^{233}$. The most probable value of the ground state spin of $\beta^-$-decaying nuclei has been determined for $\mathrm{Hg}^{203}$ and $\mathrm{Pa}^{233}$. Experimental data for $\mathrm{Tm}^{170}$ and $\mathrm{Re}^{186}$, for which all transition constants are known, are compared with the theoretical polarization values.

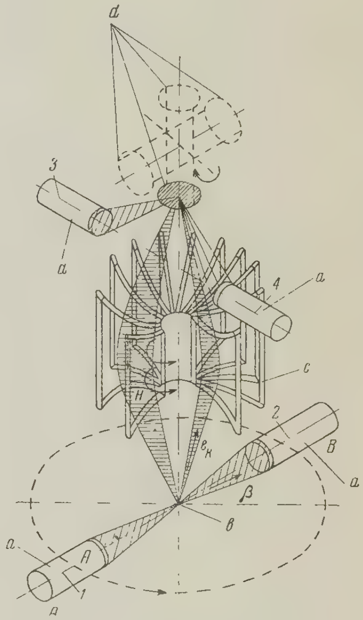

FIG. 1. Diagram of the instrumentation. a – scintillation counters, b – beta source, c – toroidal coil, d – scatterers.

PARITY nonconservation in weak interactions has now been firmly established. In some cases one can use the laws of weak interaction to investigate the characteristics of nuclear transitions.

Thus, old methods of nuclear spectroscopy can be supplemented with new "non-classical" methods (experiments with polarized particles, participating in weak interactions).

One of these methods, particularly suitable for the study of heavy nuclei, is the measurement of the polarization of the electrons in internal conversion following $\beta^-$ decay. The effect of polarization of the conversion electrons following the decay was predicted by A. I. Alikhanov and V. A. Lyubimov (see reference 1), and was experimentally observed by Lyubimov and Vishnevskiĭ.[2] The theory of this phenomenon was developed by V. B. Berestetskiĭ and A. P. Rudik[3] and by B. V. Geshkenbeĭn.[4]

The results of the present paper were reported at the International Conference on High-Energy Physics in Kiev, July 1959.[2]

## DESCRIPTION OF THE APPARATUS

The internal-conversion electrons were polarized in the direction of the nuclear polarization due to the preceding $\beta$ decay. If the conversion electrons emitted at 90 deg to the momentum of the particles are separated, the polarization is found to be transverse, and this greatly facilitates its measurement. Transverse polarization of conversion electrons was determined from the azimuthal asymmetry of the Mott scattering by gold nuclei.

A diagram of the instrument is shown in Fig. 1.

The $\beta$ electrons from a given source b were registered in counters 1 and 2. The conversion electrons emitted after the $\beta$ decay were separated by a toroidal spectrometer after being scattered from gold scatterer d through an average of 135 deg, and registered by counters 3 and 4, connected pairwise for coincidence with $\beta$ counters 1 and 2. Counters 3 and 4 were oriented in a plane perpendicular to the axis of counters 1 and 2

Since the conversion electrons were monochromatic and the transverse component of their polarization exhibited little dependence on the angle $\theta$ between the directions of the $\beta$ and conversion electrons for $\theta$ close to 90 deg, it became possible to separate the conversion electrons from the $\beta$ particles by a wide-angle high-aperture magnetic spectrometer[5] with good energy resolution for the electrons.

Counters 1 and 2 separate the oppositely-directed $\beta$ particles from the source. Thus, depending on which of the $\beta$ counters, 1 or 2, coincides with the pulses from the conversion-electron pulses in counters 3 or 4, one measures the azimuthal asymmetry in the scattering of electrons with opposite spin directions. This is equivalent to replacement of the "right-hand" counter by the "left-hand" one, customarily used to measure scattering asymmetry. In addition, as a check on the measurements, counters 1 and 2 were rotated 180 deg, from position AA to position AB (Fig. 1). In this case asymmetry due to the instrumentation can be excluded without additional measurements. Actually, after subtracting the background, the coincidences between the conversion electrons and the $\beta$ electrons are given by

$$\begin{aligned}
(N_{13})_{AA} &= a(\eta_1\eta_3)_{AA}\eta_{13}(1 - S\langle\sigma\rangle),\\
(N_{14})_{AA} &= a(\eta_1\eta_4)_{AA}\eta_{14}(1 + S\langle\sigma\rangle),\\
(N_{23})_{AA} &= a(\eta_2\eta_3)_{AA}\eta_{23}(1 + S\langle\sigma\rangle),\\
(N_{24})_{AA} &= a(\eta_2\eta_4)_{AA}\eta_{24}(1 - S\langle\sigma\rangle),\\
(N_{13})_{AB} &= a(\eta_1\eta_3)_{AB}\eta_{13}(1 + S\langle\sigma\rangle),\\
(N_{14})_{AB} &= a(\eta_1\eta_4)_{AB}\eta_{14}(1 - S\langle\sigma\rangle),\\
(N_{23})_{AB} &= a(\eta_2\eta_3)_{AB}\eta_{23}(1 - S\langle\sigma\rangle),\\
(N_{24})_{AB} &= a(\eta_2\eta_4)_{AB}\eta_{24}(1 + S\langle\sigma\rangle),
\end{aligned}$$

where a is a proportionality coefficient, $\eta_i$ is the probability of registering an electron by an individual counter (determined by the solid angles, the efficiency of the counter, etc.) and may not be the same in positions AA and AB; $\eta_{ik}$ are the corresponding probabilities, which depend on the counter combination (for example, the efficiency of coincidences in channel ik). The values of $\eta_{ik}$ are independent, with sufficiently good approximation, of the positions of counters AA or AB; S is the asymmetry of single scattering of fully polarized electrons by gold, with allowance for the geometric parameters of the instrument, and $\langle\sigma\rangle$ is the degree of transverse polarization of the electrons.

It is easily seen that one can make up of the measured eight quantities $(N_{ik})_{AB}$ and $(N_{ik})_{AA}$ an expression that depends only on the degree of polarization of the electrons. Actually, the asymmetry coefficient

$$R = \left[\left(\frac{N_{13}N_{24}}{N_{14}N_{23}}\right)_{AA}\left(\frac{N_{14}N_{23}}{N_{13}N_{24}}\right)_{AB}\right]^{1/4} = \frac{1 - S\langle\sigma\rangle}{1 + S\langle\sigma\rangle},\ S\langle\sigma\rangle = \frac{1 - R}{1 + R}$$

does not include the instrumentation asymmetry.

As a rule, to exclude the instrumentation asymmetry, additional measurements are made with a scatterer made of light material. In this case the azimuthal asymmetry due to the polarization of the electrons should be practically zero. In our case there is no direct need for such measurements. Measurements with an aluminum scatterer were made by us only for control purposes and disclosed a high degree of exclusion of the instrumentation asymmetry for all the substances investigated, namely:

| $\beta$ source | $Tm^{170}$ | $Pa^{233}$ ($E_\gamma = 312.6$ kev) |
|---|---|---|
| $R$ | $1.00 \pm 0.02$ | $0.98 \pm 0.02$ |

| $\beta$ source | $Pa^{233}$ ($E_\gamma = 74.8$ kev) | $Hg^{203}$ |
|---|---|---|
| $R$ | $1.01 \pm 0.03$ | $0.97 \pm 0.03$ |

The measurements were made in the following sequence: first with a gold scatterer, then with an aluminum scatterer, and finally with an empty frame (to exclude the cases of scattering from the walls of the instrument and from the frame of the scatterer). The background of random coincidences was measured directly for each case. All the measurements and the interchange of the scatterers were automatic, the result being recorded on corresponding groups of mechanical counters. The measurements were carried out both in position AA and in position AB, at approximately equal times for each measurement. It can be seen from the definition of the asymmetry coefficient R (see also Fig. 1) that if the measured R is greater (less) than unity the internal-conversion electrons following the $\beta$ decay should be polarized against (with) the direction of emission of the $\beta$ particle.

## MEASUREMENT RESULTS

Thulium, $Tm^{170}$. The $\beta$ decay of $Tm^{170}$ is accompanied by strong $\gamma$-ray conversion, and the constants of the transitions of $Tm^{170}$ are well known.[6] This source is therefore very convenient for experimental verification of the theory of conversion-electron polarization. In approximately 24% of the cases, the $\beta$ decay is to the excited level $Yb^{170}$ with E = 84.23 kev, which is then deexcited by the internal-conversion electron with multipolarity E2 in accordance with the scheme

$$1^- \xrightarrow[\beta,864\ \text{kev}]{} 2^+ \xrightarrow[e,\ \gamma,\ 84.2\ \text{kev}]{} 0^+.$$

We measured the polarization of the conversion electrons emitted from the L shell ($E_{eL}$ = 75 kev). The measured asymmetry of scattering by a gold scatterer (0.07 mg/cm$^2$) was

$$R_{Au} = \left[\left(\frac{N_{13}N_{24}}{N_{14}N_{23}}\right)_{AA}\left(\frac{N_{14}N_{23}}{N_{13}N_{24}}\right)_{AB}\right]^{1/4} = 0.83 \pm 0.03.$$

It follows therefore that

$$2S\langle\sigma\rangle = 2(1 - R)/(1 + R) = 0.19 \pm 0.03.$$

The value obtained for the asymmetry S corresponds to conversion electrons polarized in the direction of the emitted $\beta$ electron.

It is necessary to correct the measured asymmetry for the finite thickness of the scatterer. The value of this correction for electrons of different energies, at an identical scatterer placement, was carefully measured by Alikhanov, Eliseev and Lyubimov.[7] Corrected for finite scatterer thickness, the result was

$$(2S\langle\sigma\rangle)_0 = +0{,}22 \pm 0{,}03.$$

Using the data tabulated by Sherman[8] and the corrections for these data from reference 7, we can obtain, allowing for the geometrical parameters of the instrument, the polarization of the conversion electrons

$$\langle\sigma\rangle_{\mathrm{exp}} = (0{,}49 \pm 0{,}06)\ v/c.$$

In this case the average value of v/c for the registered part of the $\beta$ spectrum is 0.78.

According to the theory of Geshkenbeĭn[4] the polarization of conversion electrons from the L level in electrical transitions is

$$\langle\sigma\rangle = \alpha \frac{\mathscr{L}(\mathscr{L}+1) + J_2(J_2+1) - J_3(J_3+1)}{2\mathscr{L}(\mathscr{L}+1) J_1 (1 + |\eta_{L_i}|^2)}$$

$$\times \{(\mathbf{vn})\mathbf{n} + \sqrt{\mathscr{L}(\mathscr{L}+1)}\,\mathrm{Re}\,\eta_{L_i}[\mathbf{v} - (\mathbf{vn})\mathbf{n}]\},$$

where $\alpha$ depends on the same combination of constants and matrix elements as the angular distribution of the electrons in $\beta$ decay of polarized nuclei,

$$\alpha = \frac{\lambda_{J_1J_2} |C_A|^2 |M_{GT}|^2 2\delta_{J_1J_2} \sqrt{J_2(J_2+1)}\,\mathrm{Re}\,C_V C_A^* M_F M_{GT}}{|C_A|^2 |M_{GT}|^2 + |C_V|^2 |M_F|^2},$$

$$\lambda_{J_1J_2} = [J_2(J_2+1) - J_1(J_1+1) + 2]/2(J_2+1);$$

$M_F$ and $M_{GT}$ are the nuclear matrix elements, $\mathscr{L}$ is the multipolarity of the $\gamma$ quantum, $J_1$ is the spin of the nucleus prior to $\beta$ decay, $J_2$ is the spin of the nucleus prior to conversion, $J_3$ is the spin of the nucleus after conversion, $\mathbf{v}$ is the electron velocity, $\mathbf{n}$ is the unit vector in the direction of emission of the conversion electron, $\eta_{L_i}$ is a function of the radial integrals, while $C_A$ and $C_V$ are the interaction constants.

The main contribution to the polarization is made by the electrons from the $L_{II}$ and $L_{III}$ shells.

According to the Geshkenbeĭn calculations, $\eta_{L_{II}} = 0.51 \pm 0.25$ and $\eta_{L_{III}} = 0.534$.

This gives for the polarization

$$\langle\sigma\rangle_{\mathrm{theor}} = +0.488\ v/c,$$

which is in good agreement with the experimental value.

Protactinium, $Pa^{233}$. The decay scheme of protactinium and the characteristics of the transition are given in the book by Dzhelepov and Peker.[6] Principal attention was paid here to a measurement of the polarization of the conversion electrons produced by de-excitation of the 312.6-kev excited level of $U^{233}$, in accordance with the scheme

$$({}^1/{}_2,\ {}^3/{}_2,\ {}^5/{}_2) \xrightarrow[E_\beta = 257\ \text{kev}]{} ({}^3/{}_2)^+ \xrightarrow[E_\gamma = 312.6\ \text{kev}]{} ({}^5/{}_2)^+.$$

We measured directly the polarization of the conversion electrons from the K shell, arising as a result of a type-M1 transition at $E_\gamma = 312.6$ kev. The experimental value of the scattering asymmetry is $R = 1.10 \pm 0.02$, i.e., the electrons are polarized against the direction of the $\beta$-particle momentum.

After introducing corrections for the finite thickness of the scatterer (0.45 mg/cm$^2$) and for the contamination by cascade transitions, we obtained the experimental value of the polarization $\langle\sigma\rangle = (-0.48 \pm 0.14)\,v/c$ (the average value of v/c is 0.56).

For the proposed values of the spin of the ground state of $Pa^{233}$ (½, 3/2, or 5/2), the calculated values of the polarization are respectively

$$\langle\sigma\rangle_{1/2} = -0.334\,v/c,\quad \langle\sigma\rangle_{3/2} = (-0.334 \div +0.200)\,v/c,$$

$$\langle\sigma\rangle_{5/2} = 0.200\ v/c.$$

If the ground state of $Pa^{233}$ has a spin 3/2, the transition is between the levels 3/2 and 3/2. In this case the calculated value of the polarization depends on the combination of the matrix elements of the $\beta$ transition. Figure 2 shows the calculated value of the polarization as a function of the ratio of the matrix element $x = M_F/M_{GT}$ ($C_A = -1.2\,C_V$), and shows also the experimental value of $\langle\sigma\rangle$. Bearing in mind the possible inaccuracies in the intensity of the transitions between the levels of the "daughter" nucleus $Pa^{233}$, as well as experimental errors, our data agree with the theory if a value of ½ or 3/2 is assumed for the spin of the ground state of $Pa^{233}$. In the latter case there is an interference between the Fermi and the Gamow-Teller interactions, and the matrix elements have opposite signs.

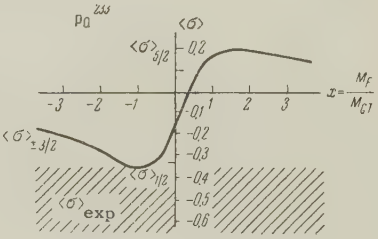

FIG. 2. Polarization $\langle\sigma\rangle$ calculated as a function of the ratios x of the matrix elements of the $\beta^-$ transition $Pa^{233} \to U^{233}$. The shaded area shows the region of possible experimental values of $\langle\sigma\rangle$.

For purposes of control, we measured the polarizations of the conversion electron from the 74.5-kev $\gamma$ quanta produced in the transition between two excited levels of $U^{233}$ in accordance with the scheme

$$(1/2,\ 3/2,\ 5/2) \xrightarrow[E_{\beta^-}=145\text{ kev}]{} (3/2)^+ \xrightarrow[e,\ E_\gamma=74.5\text{ kev}]{} (5/2)^+$$

(excited state). This transition is almost analogous with the previous one and differs in the energies of the $\beta$ particles and of the conversion electrons. The asymmetry obtained is $R = 1.06 \pm 0.04$ and corresponds to the same direction of conversion-electron polarization as in the case of a 312.6-kev $\gamma$ transition.

Mercury, $Hg^{203}$. A study of the polarization of the conversion electrons accompanying the $\beta$ decay of $Hg^{203}$ is of interest, because we can establish here a connection between the spin ($1/2$, $3/2$, or $5/2$) of the ground state of $Hg^{203}$, which is not accurately known (see reference 6). The decay of $Hg^{203}$ is characterized by the fact that the conversion electrons have an energy exceeding the end-point energy of the $\beta$ spectrum. Because of this, the measurements were carried out with a spectrometer of lower resolution (see reference 2). The measurements have shown that the electrons are polarized against the direction of emission of the $\beta$ particles, and the polarization has a value $\langle\sigma\rangle = (-0.32 \pm 0.09)\,\mathbf{v/c}$ at an average $V/C = 0.55$. The calculated values of the polarization are

$$\langle\sigma\rangle_{\pm 1/2} = 0.495\ v/c;\ \langle\sigma\rangle_{\pm 3/2} = (0.495 \text{ to } -0.297)\ v/c;$$
$$\langle\sigma\rangle_{\pm 5/2} = -0.297\ v/c,$$

for spins $\pm 1/2$, $\pm 3/2$, and $\pm 5/2$, respectively.

Figure 3 shows the calculated values and the experimental data of polarization.

The results of the measurements agree with the values of the spin of the ground state of $Hg^{203}$, $\pm 5/2$ and $\pm 3/2$, and disagree with the value $\pm 1/2$.*

In the case of a $3/2 \rightarrow 3/2$ type of transition, there is an interference between the Fermi and the Gamow-Teller interactions. The matrix elements have like signs.

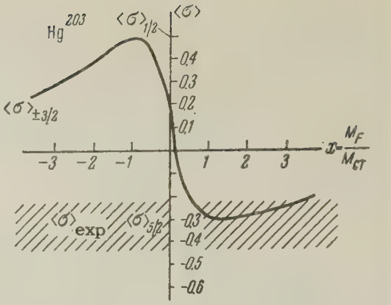

FIG. 3. Polarization $\langle\sigma\rangle$ calculated as a function of the ratios $x$ of the matrix elements of the $\beta^-$ transition $Hg^{203} \rightarrow Tl^{203}$. The shaded area shows the region of possible experimental values of $\langle\sigma\rangle$.

Rhenium, $Re^{186}$. The setup of reference 2 was used to measure the sign of the electrons of the conversion that follows the beta decay of $Re^{186}$. The decay of $Re^{186}$ is similar to the decay of $Tm^{170}$. As in the decay of $Tm^{170}$, the electrons of the conversion following the beta decay of $Re^{186}$ are polarized in the direction of the beta-particle momentum.

The authors are grateful to Academician A. I. Alikhanov for continuous interest and attention to the work, and to B. V. Geshkenbeĭn for fruitful collaboration and a discussion of the results. The authors are also grateful to V. N. Markizov for help with the work.

---

*The results of the experiments were interpreted differently earlier.[2] The experimental data were compared with the Geshkenbeĭn formulas,[4] in which the sign of polarization was in error. The error in the formula was discovered by Geshkenbeĭn after we measured the polarization of the conversion electrons in $Tm^{170}$, where all the characteristics of the transitions were known, and the result had a sign opposite that of the theoretical value computed with the old formula.

---

[1] A. I. Alikhanov, Paper delivered at the International Conference on High-Energy Physics, Kiev, July 1959, in press.

[2] V. A. Lyubimov and M. E. Vishnevskiĭ, JETP **35**, 1577 (1958), Soviet Phys. JETP **8**, 1103 (1959).

[3] V. B. Berestetskiĭ and A. P. Rudik, JETP **35**, 159 (1958), Soviet Phys. JETP **8**, 111 (1959).

[4] B. V. Geshkenbeĭn, JETP **35**, 1235 (1958), Soviet Phys. JETP **8**, 865 (1959).

[5] Tret'yakov, Gol'din, and Grishuk, Приборы и техника эксперимента (Instrum. and Meas. Engg.) No. 6, 22 (1957).

[6] B. S. Dzhelepov and L. K. Peker, Схемы распада радиоактивных ядер (Decay Schemes of Radioactive Nuclei), Acad. Sci. Press, 1958.

[7] Alikhanov, Eliseev, and Lyubimov, JETP **34**, 1045 (1958).

[8] N. Sherman, Phys. Rev. **103**, 1601, (1956).

Translated by J. G. Adashko
275

SOVIET PHYSICS JETP VOLUME 11, NUMBER 5 NOVEMBER, 1960

# *OBSERVATION OF ION OSCILLATIONS IN A PLASMA*

M. D. GABOVICH, L. L. PASECHNIK, and V. G. YAZEVA

Submitted to JETP editor November 23, 1959

J. Exptl. Theoret. Phys. (U.S.S.R.) **38**, 1430-1433 (May, 1960)

Ion oscillations have been observed against the noise background of a discharge plasma (charge density approximately $10^{10}\,\mathrm{cm}^{-3}$). The results which have been obtained can be interpreted if it is assumed that the probe selectively detects oscillations characterized by a wavelength approximately equal to the radius of the ion sheath which surrounds the probe.

As is well known, ion oscillations with a limiting frequency

$$f_0 = \sqrt{ne^2/\pi M} \tag{1}$$

have been observed in electron beams with compensated space charge.[1,2] However, no one has as yet been successful in observing oscillations of this kind in a gas-discharge plasma.[3] The existence of resonance effects at frequencies close to $f_0$ has been indicated by Rutgaizer and Kononenko.[4] In the present paper we describe a possible direct experimental observation of self-sustaining ion oscillations in a gas discharge plasma.

A plasma is formed in an arc discharge in mercury vapor (pressure approximately $10^{-3}$ mm) in a discharge tube 1 (cf. Fig. 1); the charge density in the plasma can be varied as required by changing the discharge current. The plasma contains a cylindrical probe 2 (diameter 100 $\mu$ and length 5 mm). If necessary it is possible to insert a similar fixed probe 3 near the first and the distance between these probes can be varied from 0 to 15 mm.

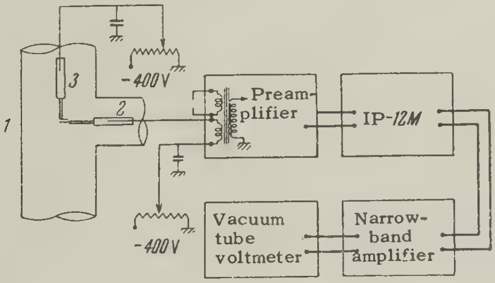

FIG. 1

An important factor in the observation of oscillations is the detection system. The signal picked up by the probe is fed to a preamplifier with transformer input and then to a superheterodyne amplifier (IP — 12M) and a special narrow-band amplifier[5] (band width approximately 100 cps) which consists of three stages with quartz filters (frequency 455 kcs). The sensitivity of the entire amplifier is approximately $2 \times 10^{-8}$ v.

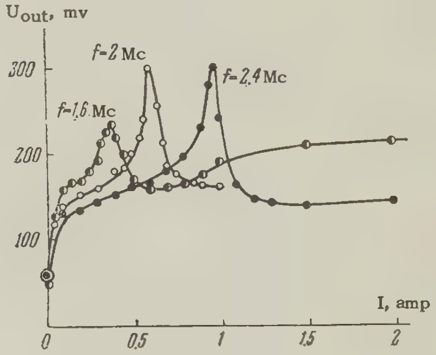

FIG. 2

The measurements are carried out as follows. The amplifier is tuned to a fixed frequency f and the dependence of the signal at the output of the amplifier on discharge current I (i.e., charge density in the plasma) is determined (Fig. 2). The signal at the output of the amplifier increases abruptly when the discharge is fired, and then increases more or less sharply as the discharge current is increased to approximately 0.1 amp; the signal variation then becomes a sensitive function of probe potential. If the negative potential of the probe is small (less than 30 — 40 v), the signal increases monotonically with further increase in discharge current. For negative probe potentials of large absolute value, however, the dependence of signal on discharge current exhibits a more or less clearly defined maximum. The position of this maximum depends primarily on the frequency f to which the amplifier is tuned; when f is increased the maximum is displaced in the direction of higher plasma charge densities (cf. Fig. 2).

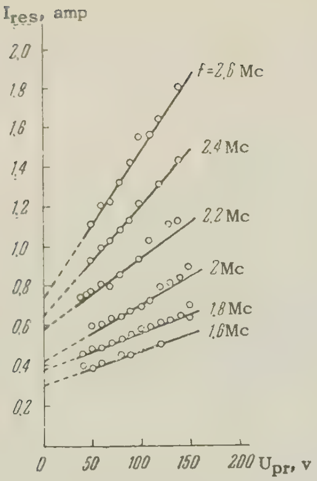

FIG. 3

It is reasonable to explain the results described above in the following manner. The signal, which increases monotonically with increasing discharge current, is due to plasma noise; the plasma ion oscillations must be detected against this background. A reduction in the bandwidth of the amplifier and an appropriate choice of the negative probe potential makes it possible to observe these oscillations, which appear in the form of maxima such as those shown, for example, in Fig. 2. An increase in the negative probe potential reduces the probe current component associated with the fast plasma electrons and thus reduces the noise signal picked up by the probe as long as the negative probe potential remains within proper limits. The important role played by the probe potential is indicated by the dependence of resonance current (we shall call the discharge current at which the indicated maximum in the output signal is observed the resonance current) on probe potential. In Fig. 3 we show the dependence of resonance current $I_{res}$ on probe potential $U_{pr}$ obtained at various frequencies f. These curves can be obtained (indicating oscillations) only in the frequency range 1 – 3 Mcs, and only for a definite range of probe potentials. One of the reasons for the limited frequency range is the characteristic of the amplifier system which is used. The ratio of the signal to intrinsic noise in this device has a maximum in the region of 2 Mcs and falls off away from this frequency.

In order to explain the dependence of resonance current on frequency f and probe potential we turn to the familiar expression for the frequency of ion oscillations (cf. reference 6)

$$f = f_0/\sqrt{1 + ne^2\lambda^2/\pi kT_e}, \tag{2}$$

where $f_0$ is the limiting frequency given by Eq. (1) and $\lambda$ is the wavelength. From Eq. (2) we can get an expression for the plasma charge density n, which is determined by the discharge current, for given values of f and $\lambda$:

$$n = f^2/(e^2/\pi M - e^2 f^2\lambda^2/\pi kT_e). \tag{3}$$

We shall not try to justify here the assertion that the probe exhibits a selective response to oscillations at a wavelength $\lambda$ close to the order of magnitude of the radius of the ion sheath that surrounds the probe; we can only call attention to the fact that this assertion allows a qualitative interpretation of the relations shown in Fig. 3. Since the radius of the ion sheath increases with increasing probe potential, the quantity n and consequently the resonance current should increase with increasing frequency f and with increasing negative probe potential $U_{pr}$. This effect is observed in the present experiments.

Furthermore, the following inequality follows from Eq. (3):

$$\lambda^2 < kT_e/Mf^2, \tag{4}$$

this inequality indicates a limit on the negative potential of the probe, as has been observed in the experiments described above. To compare the relation in (4) with experiment, we give the following example. Under the present conditions ($T_e = 3.8 \times 10^4$°K) with $f = 2 \times 10^6$ cps, computed by means of Eq. (4), we have $\lambda_{max} = 6.4 \times 10^{-2}$ cm. The experiment indicates (cf. Fig. 3) that when $f = 2 \times 10^6$ cps it is impossible to observe oscillations at a negative probe potential greater than 150 v; the resonance current for this potential is 0.9 amp. The calculation shows that with this plasma (anode current 0.9 amp) an ion sheath with a radius of $6.4 \times 10^{-2}$ cm is formed at approximately 130 v. The fact that the experimental and calculated values of the maximum probe potential are of the same order of magnitude is also evidence in favor of the assertion made above concerning the selective effect of the ion sheath at the probe.

It follows from Fig. 3 that the concentration $n_0$ and, consequently, the resonance current $I_{0res}$ corresponding to the limiting frequency $f_0$ should be determined for $\lambda \rightarrow 0$, i.e. by extrapolation of the curves in Fig. 3 to zero probe potential. In Fig. 4 we show the dependence of $\sqrt{I_{0res}}$ on frequency obtained by extrapolation of a number of experimental lines. Here we also give the calculated line obtained by means of Eq. (1) and the experimentally determined depend-

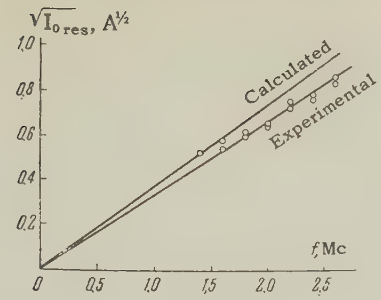

FIG. 4

ence of charge density in the plasma on discharge current: $n = 3.1 \times 10^{10}\,I$ (I in amperes). It is apparent that the discrepancy between the experimental and calculated lines does not exceed the differences frequently observed in investigations of electron plasma oscillations; this discrepancy may be attributed to experimental errors, errors in the extrapolation procedure, etc.

The comparison shown in Fig. 4, together with the facts indicated above, would seem to indicate that in the present experiments we have actually observed ion oscillations and have qualitatively verified the relation given in Eq. (2).

The complexity of the effects which attend the detection of oscillations by the probe also appear in the following interesting fact. If a second probe is placed in line with the measurement probe and the second probe is kept at a negative potential, the ion-oscillation signal is increased — the signal-to-noise ratio reaches 10 — 20 under these conditions. However, the dependence of resonance current on the potentials of the two probes is complicated and has not yet been interpreted.

---

[1] K. G. Hernqvist, J. Appl. Phys. **26**, 544, 1029 (1955).

[2] E. G. Linder and K. G. Hernqvist, J. Appl. Phys. **21**, 1088 (1950).

[3] Armstrong, Emeleus, and Neill, Proc. Irish Acad. **54**, 291 (1951).

[4] V. D. Rutgaizer and K. I. Kononenko, Уч. зап. Харьковского гос. ун-та, (Sci. Notes, Khar'kov State University) **64**, 203 (1955).

[5] D. E. Hildreth, Electronics **28**, 166 (December, 1955).

[6] L. Tonks and I. Langmuir, Phys. Rev. **33**, 195 (1929).

Translated by H. Lashinsky
276

SOVIET PHYSICS JETP VOLUME 11, NUMBER 5 NOVEMBER, 1960

# ANGULAR DISTRIBUTION OF ELASTICALLY SCATTERED NEUTRONS

G. N. LOVCHIKOVA

Submitted to JETP editor December 1, 1959

J. Exptl. Theoret. Phys. (U.S.S.R.) **38**, 1434-1435 (May 1960)

The differential cross sections for the elastic scattering of neutrons from a $Na^{24}(\gamma,n)D_2O$ source by Pb, Bi, Sn, Fe, and Al nuclei have been measured over the range of angles from 30° to 150°. The total elastic cross section, the transport cross section, and the mean value of the cosine of the scattering angle were obtained from the measured angular distributions.

WE have studied the angular distributions of neutrons elastically scattered from Bi, Pb, Fe, Sn, and Al nuclei. A $Na^{24}(\gamma,n)D_2O$ photoneutron source was used for this purpose. The $\gamma$ rays were emitted from a thin-walled nickel capsule with an internal diameter of 29 mm, containing compressed sodium fluoride. This source was placed in another nickel capsule consisting of two halves filled with heavy water to a layer thickness of 8 mm. The mean energy of the neutrons from a source with this same thickness of heavy water, according to Wattenberg's results,[1] was 220 kev. A proportional counter with an active volume 80 mm in length, filled with $BF_3$ and surrounded with layers of paraffin and boron carbide, served as the detector. Rings of various diameter and thickness, according to the scattering angle, were used as the scattering samples.

In reducing the experimental data, it was kept in mind that the sensitivity of the counter circuit was different for neutrons which arrived directly and those which had been scattered from the sample. Allowance was made for the fact that the direct and scattered neutrons fall on the detector at different angles to the detector — source symmetry axis. The angular sensitivity of the detector was determined experimentally; the corresponding corrections were applied. Allowance for the effects of attenuation and multiple scattering was made in the course of the calculation by the method of Turchin.[2] A measurement was also made of the effect of the shielding screen on the number of neutrons scattered from the sample. Throughout the work, elaborate checks were carried out on the influence of $\gamma$ radiation on the results.

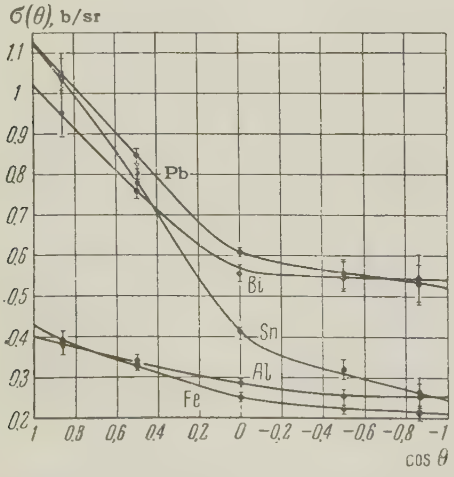

Angular distribution of elastically scattered neutrons.

To provide a correction for the decay of the source, and also as a check on the stability of the operation of the apparatus, the half-life of the $Na^{24}$ source was measured and found to be 14.93 ± 0.08 hours.

The differential cross sections for elastic scattering of neutrons, measured by the method described above, are shown in the figure. They are given as functions of the cosine of the scattering angle in the laboratory system of coordinates. The mean-square statistical errors are different for different angles, and lie between the limits of 2% and 7%. At 150° (reversed geometry) they are somewhat larger, amounting to about 10% on the average. The statistical errors of the measured corrections are very small, and amount to less than a percent each. On the average, the total error of the results, for all values of cross sections, did not exceed 15%.

The elastic scattering was measured every 30° over the range of angles from 30° to 150°. The average angular resolution was ±10°. The variation of the scattering angle $\theta$ was accomplished by varying the distance

Values of elastic, transport, and total cross sections (in barns)

| Element | $\sigma_e$ | $\sigma_{tr}$ | $\sigma_t$ | $\overline{\cos\theta}$ | Element | $\sigma_e$ | $\sigma_{tr}$ | $\sigma_t$ | $\overline{\cos\theta}$ |
|---|---|---|---|---|---|---|---|---|---|
| Al | 3.75 | 3.43 | 3.76 | 0.086 | Pb | 8.79 | 7.62 | 8.80 | 0.134 |
| Fe | 3.49 | 3.10 | 3.50 | 0.116 | Bi | 8.23 | 7.37 | 8.23 | 0.104 |
| Sn | 6.80 | 4.90 | 6.85 | 0.285 | | | | | |

between the source and the detector, and also by the use of rings of different diameters. In order to increase the scattering effect, thicker rings were used at 30° and 150° than at the other angles.

Since no inelastic scattering is observed in the elements studied at the neutron energies used, the differential cross sections are the cross sections for the elastic scattering only.

In the table are shown the total elastic cross-sections $\sigma_e$, the transport elastic cross sections $\sigma_{tr}$, the total cross sections including the decay cross section ($\sigma_t$), and also the mean value of the cosine of the scattering angle. The decay cross section is taken for the same neutron source from the work of Belanova.[3]

The total elastic scattering cross section was obtained by integrating the differential cross-section curve over the total solid angle. In a case where there is no inelastic scattering, the formula

$$\sigma_{tr} = \sigma_t (1 - \overline{\cos\theta}).$$

was used in calculating $\sigma_{tr}$.

Translated by D. C. West
277

---

[1] A. Wattenberg, Phys. Rev. **71**, 497 (1947).

[2] V. F. Turchin, Атомная энергия, (Atomic Energy) **4**, 244 (1958).

[3] T. S. Belanova, JETP **34**, 574 (1958), Soviet Phys. JETP **7**, 397 (1958).

SOVIET PHYSICS JETP VOLUME 11, NUMBER 5 NOVEMBER, 1960

# INVESTIGATION OF THE ALPHA DECAY OF $U^{236}$

A. P. KOMAR, G. A. KOROLEV, and G. E. KOCHAROV

Leningrad Physico-Technical Institute, Academy of Sciences, U.S.S.R.

Submitted to JETP editor December 15, 1959

J. Exptl. Theoret. Phys. (U.S.S.R.) 38, 1436-1438 (May, 1960).

The $\alpha$ spectrum of $U^{236}$ has been studied with the aid of an ionization chamber containing a grid. The energy of the fundamental group of $\alpha$ particles, after corrections for ionization, imperfect grid shielding, and pulse rise time have been applied, is equal to 4.488 ± 0.003 Mev. The energies and intensities of the transitions to the $2^+$ and $4^+$ levels of the daughter nucleus were also determined.

INFORMATION about the excited levels of $Th^{232}$ has been obtained chiefly from Coulomb excitation experiments; the excitation of levels with energies of 50 and 790 kev has been observed.[1,2] The existence of the 50-kev level, which appears to be the first level of the fundamental rotation band, has also been confirmed by measurements of the conversion electron spectrum in photo-emulsions.[3] The 790-kev level is de-excited by the emission of $\gamma$ quanta with energies of 790, 740, and 613 kev, which apparently correspond to transitions to the $0^+$, $2^+$, and $4^+$ levels of the fundamental rotation band. It is known that the $0^+$, $2^+$, and $4^+$ levels in even-even nuclei are also excited during $\alpha$ decay. Hence the study of the fine structure of the $U^{236}$ $\alpha$ spectrum is of considerable interest.

We have carried out a study of the $U^{236}$ $\alpha$ spectrum in an ionization $\alpha$ spectrometer of high resolution.

An ionization chamber permits one to determine the number of ion pairs produced by an $\alpha$ particle within the active volume of the chamber. The number of ion pairs N and the energy E of the $\alpha$ particle are connected by the relation $E = Nw$, where w is the mean energy required for the formation of a single ion pair. w depends on the working gas in the chamber and also, generally speaking, on the $\alpha$-particle energy. In the case of argon there are contradictory opinions in the literature about the dependence of w on the $\alpha$-particle energy. However, for $\alpha$-particle energies above 4 Mev, w can be assumed, on the basis of experimental results, to be independent of the energy. Under these conditions the relation of $\alpha$-particle energy to the total number of pairs is given by the formula $E = Nw_0 + \epsilon_0$, where $w_0$ is the mean energy going into the formation of a single ion pair when $E > 4$ Mev, and $\epsilon_0$ is a parameter depending on the nature of the gas. For a mixture of argon and methane, $\epsilon_0 = 83$ kev.[4]

The $U^{236}$ $\alpha$-particle energies were measured by a comparison of the pulse amplitudes from $U^{236}$ $\alpha$ particles with the pulse amplitudes from a reference $\alpha$ source, $U^{234}$, whose energy was taken equal to 4.768 Mev.[5] The amplitude comparison was accomplished with the aid of a precision generator, whose pulses were applied to the input of the preamplifier. The pulse amplitudes were measured by a method described previously.[6] The energy of the $U^{236}$ $\alpha$ particles was determined from the relationship

$$E_{236} = aE_{234} + \varepsilon_0 (1 - a),$$

where a is the ratio of the pulse amplitudes of the $\alpha$ particles from $U^{236}$ and $U^{234}$.

After correcting for imperfect screening by the grid and for the pulse rise time, the energy of the $U^{236}$ $\alpha$ particles was found to be $E = 4.488 \pm 0.003$ Mev. No correction was applied for the source thickness, since the $\alpha$-particle energies of $U^{236}$ and $U^{234}$ are close together, and the source was one and the same. Previously measured values for the energy have been 4.5 Mev[7] and 4.499 ± 0.004 Mev.[8] It should be observed that reference 8 gives not the measurement error, but the deviation from the mean of 9 measurements. The error of these measurements must have been high (about 10 kev), judging from the large half-width of the $\alpha$ lines, the considerable "tail" of $U^{234}$ $\alpha$ particles, and the inaccurate values of energies for the reference standards used. The $U^{236}$ $\alpha$-particle energy measured in reference 8 is high because corrections were not applied for imperfect grid screening and for pulse rise time. When these corrections are taken into

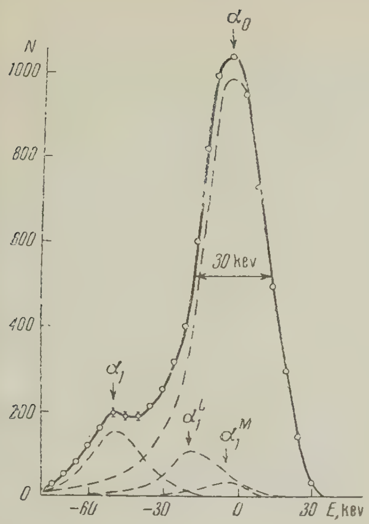

FIG. 1

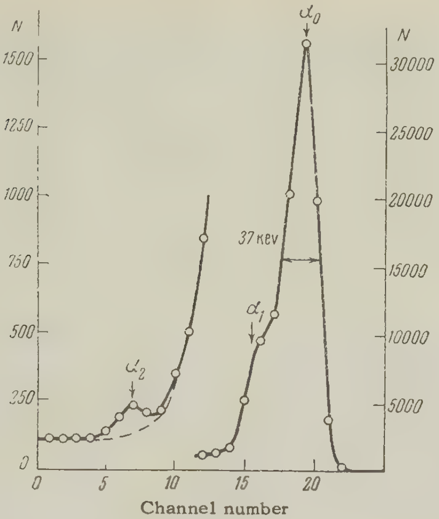

FIG. 2

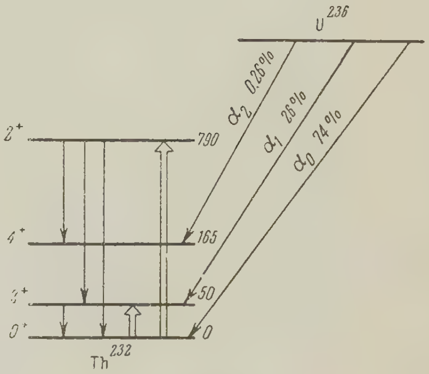

FIG. 3

FIG. 1. Spectrum of $U^{236}$ $\alpha$ particles. Channel width 5 kev. The resolution of the curve is shown by dashed lines. $\alpha_0$ is the group of $\alpha$ particles corresponding to a transition to the $0^+$ level of the daughter nucleus, and $\alpha_1$ to the $2^+$ level. The groups $\alpha_1^L$ and $\alpha_1^M$ correspond to the cases in which the $\alpha$ particles of group $\alpha_1$ are accompanied by conversion electrons from the L and M shells, which introduce an additional ionization; in half the cases the electrons do not traverse the active volume of the chamber (group $\alpha_1^0$).

FIG. 2. Energy spectrum of $U^{236}$ $\alpha$ particles, taken with a channel width of 13.9 kev. The groups $\alpha_0$, $\alpha_1$, and $\alpha_2$ correspond to transitions to the $0^+$, $2^+$, and $4^+$ levels of the $Th^{232}$ nucleus.

FIG. 3. Decay scheme of $U^{236}$.

account, the value of energy measured in reference 8 does not disagree with our result, within the errors of measurement.

In Fig. 1 is shown the $\alpha$ spectrum of $U^{236}$, obtained with the use of electrical collimation. In carrying out the resolution of the curve, the distortion of the spectrum due to the conversion electrons was taken into account. The intensity of the $\alpha_1$ line was $26 \pm 4\%$. The separation between the $\alpha_0$ and $\alpha_1$ lines is $50 \pm 5$ kev.

Figure 2 represents the $\alpha$ spectrum of $U^{236}$ taken with a greater channel width. A group of $\alpha_2$ particles can be seen at a separation of 160 kev from the main line, with an intensity of $0.26 \pm 0.1\%$. In determining the intensities of the $\alpha$ lines, account has been taken of the intensity distortions introduced by the electrical collimation. The $\alpha_2$ group apparently corresponds to the transition to the excited state $4^+$ of the $Th^{232}$ nucleus.

The decay scheme for $U^{236}$ is shown in Fig. 3.

The authors take this opportunity to express sincere thanks to Prof. S. A. Baranov for kindly furnishing the $U^{236}$.

---

[1] Davis, Divatia, Lind, and Moffat, Phys. Rev. **103**, 1801 (1956).

[2] F. K. McGowan and P. H. Stelson, Bull. Am. Phys. Soc., Ser. II, **2**, 207 (1957).

[3] D. Dunlavey and G. Seaborg, Phys. Rev. **87**, 165 (1952).

[4] Harvey, Jackson, Eastwood, and Hanna, Can. J. Phys. **35**, 258 (1957).

[5] Gol'din, Tret'yakov, and Novikova, Сессия АН СССР по мирному использованию атомной энергии, серия физ.-мат.,(Conf. Acad. Sci. U.S.S.R. on Peaceful Uses of Atomic Energy, Phys. & Math. Section) July 1955, page 226.

[6] Vorob'ev, Komar, Korolev, and Solyakin, JETP **37**, 546 (1959), Soviet Phys. JETP **10**, 386 (1960).

[7] Ghiorso, Brittain, Manning, and Seaborg, Phys. Rev. **82**, 558 (1951).

[8] Jaffey, Diamond, Hirsch, and Mech, Phys. Rev. **84**, 785 (1951).

Translated by D. C. West
278

SOVIETY PHYSICS JETP VOLUME 11, NUMBER 5 NOVEMBER, 1960

# INVESTIGATION OF FAST ELECTRONS IN POWERFUL PULSED DISCHARGES

N. G. KOVAL'SKIĬ, I. M. PODGORNYĬ, and M. M. STEPANENKO

Institute of Nuclear Physics, Moscow State University

Submitted to JETP editor December 19, 1959

J. Exptl. Theoret. Phys. (U.S.S.R.) 38, 1439-1445 (May, 1960)

The properties of fast electrons (50 — 300 kev), which produce hard x rays in powerful pulsed discharges, are investigated. The dependence of the peak energy of the electron spectrum on the initial pressure and on the initial voltage is derived. The effect of an external longitudinal magnetic field on the electron energy is studied. The experiments were carried out in hydrogen, deuterium, and inert gases.

## INTRODUCTION

In 1952, hard x rays were observed during the course of investigations devoted to attempts at realizing controllable thermonuclear reactions in high-power gas discharges. In particular, a study was made[1,2] of the basic properties of hard x rays produced in discharges in cylindrical chambers. It was shown later on that the electrons responsible for this radiation are accelerated along the axis of the discharge chamber towards the electrode which is under positive potential at the initial instant of time (“anode”). The maximum energy of the fast electrons diverted from the discharge through the aperture in the “anode” was found to be (300 ± 20) kev at the initial voltage of 40 kv in the discharge chamber.[3]

It is well known[4] that a high-power pulsed discharge in deuterium is accompanied by the emission of neutrons. The neutron emission is due to a group of deuterons accelerated to energies of order 200 kev along the discharge axis towards the “cathode.”[5,6] Thus, during the development of a powerful pulsed discharge, strong electric fields are produced and favorable conditions are created for acceleration of charged particles in the axial direction. The occurrence of a non-equilibrium group of fast particles in the plasma is not only of interest in itself, but may be significant in the explanation of the nature of bursts of cosmic radiation. The lack of sufficient experimental material and the complexity of the phenomenon have made it impossible until now to explain fully the mechanism of acceleration of charged particles.

In the present paper we report the results of an investigation of fast electrons produced in a powerful discharge.

## EXPERIMENTAL SETUP AND MEASUREMENT PROCEDURE

The construction of the experimental setup is similar in its main outlines to the generators used previously in work on powerful pulsed discharges in cylindrical chambers. The capacitor bank consisted of 12 IM-3/50 capacitors, with a total capacity of 36 μf. The discharges were produced in a porcelain chamber 170 mm in diameter and 1,000 mm long. The discharge chamber was placed in a coaxial feeder. The parisitic inductance of the external circuit amounted to 0.5 microhenry. The capacitor bank could be charged with a high-voltage rectifier to 45 kev. The circuit was closed by applying an igniting pulse to a thyratron. After each discharge, the chamber was pumped out to a high vacuum and filled with a new batch of gas. When working with hydrogen and deuterium, the chamber was filled through a nickel gas-leak valve. In experiments with inert gases, the gases were spectrally pure. The time characteristics of the discharge were investigated by means of a type OK-17M double-beam pulse oscillograph. The current flowing in the main resonant circuit of the pulse generator was measured with a Rogovsky belt with an RL integrating network. In the case of hydrogen, the maximum in the discharge chamber was 200 kiloamp at a pressure of $6 \times 10^{-2}$ mm Hg and 40 kv on the capacitor bank.

To divert the electron beam from the discharge, a hole was drilled through the center of the “anode.” The energy of the electrons accelerated along the axis of the discharge was measured with a direct-deflection spectrograph, located directly behind the hole in the “anode.” The electromagnet of the spectrograph was fed with direct current from a storage battery. The electrons were registered with sensitive Agfa x-ray film, wrapped in aluminum foil 6 micron thick (to protect it against visible light). In the first experiment on the extraction of the fast-electron beam,[3] the exposure amounted to several tens of discharges. In order to reduce the exposure, we decreased considerably the distance from the hole in the electrode to the input slit of the spectrograph. To separate the vacuum volume of the spectrograph from the discharge chamber during the reloading of the film cassette, a special vacuum valve was used. After thorough adjustment of the spectrograph we succeeded in reducing the exposure to three or four discharges, and sometimes even to one discharge.

To determine the electron energy, the x-ray film was exposed without a magnetic field, and then, without changing the film, several discharges were made at 200 oe. This procedure produced on the same film both the energy spectrum of the electrons and a reference line corresponding to the undeflected beam. The density of the film was measured with a MF-4 microphotometer. The spectrograph dispersion curve was obtained by graphically plotting the electron trajectories. By using this curve and by measuring on the microphotogram the distance between the reference line and the boundary of the blackening due to the electrons deflected in the magnetic field, it is easy to obtain the maximum energy of the electron spectrum

The correctness of the plotted electron trajectories was verified with a 100-kev electron beam. In addition, the spectrograph was calibrated against the blackening of the film by the electrons ''shot through'' at the beginning of the discharge. At a pressure of $1.5 \times 10^{-2}$ mm Hg and an exposure of one or two discharges, these electrons produce on the x-ray film a black sharp line. The energy of the electrons, obtained by measuring the difference in potentials, coincided within 3% or 4% with the energy obtained from the dispersion curve. In determining the end-point energy of the electron spectrum, an additional error of approximately 3% must be taken into account, due to the fact that the boundary of the blackened part of the x-ray film is somewhat smeared. The overall relative error in the determination of the end-point energy of the electron spectrum did not exceed 8%.

The instant at which the electron pulse occurs and its relative intensity under different initial discharge conditions was determined by a scintillation recorder feeding an oscillograph, the second beam of which recorded the discharge-current curve. In these experiments the hole in the ''anode'' was covered with a 6-micron aluminum foil. Located behind the foil was a luminescent stilbene crystal. To reduce the sensitivity to the hard x rays, a thin crystal (approximately 1 mm) was used. The optical connection between the crystal and the FÉU-19 photomultiplier was provided by a light pipe of organic glass.

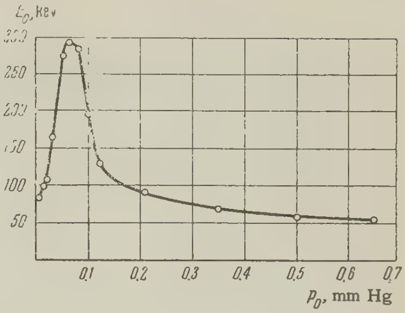

FIG. 1. Dependence of the end-point energy of the electron spectrum, $E_0$, on the initial pressure $p_0$ of the hydrogen in the discharge chamber ($U_0 = 40$ kv).

## MEASUREMENT RESULTS

1. The dependence of the end-point energy of the electron spectrum on the initial hydrogen pressure $p_0$ in the discharge chamber was determined with the direct-deflection magnetic spectrograph described above. The experiments were carried out with $p_0$ ranging from $4 \times 10^{-3}$ to $6 \times 10^{-1}$ mm Hg (the gas in the discharge chamber did not break down at $p_0 < 4 \times 10^{-3}$ mm Hg). A capacitor-bank voltage $U_0$ of 40 kv was used in these experiments. The dependence of the electron end-point energy $E_0$ on the pressure $p_0$ is shown in Fig. 1. The energy $E_0$ was determined by averaging the results of five individual experiments (the dispersion of the results of the individual experiments did not exceed 8% for each value of $p_0$). As can be seen from Fig. 1, when $p_0$ ranges from $2 \times 10^{-2}$ to $1.3 \times 10^{-1}$ mm Hg there is a sharply pronounced maximum, in which the electron energy reaches 295 kev.

The dependence obtained is similar to the dependence of the neutron yield on the initial pressure in discharges in deuterium, but differs somewhat from the corresponding dependence for the intensity of the hard x rays. This is apparently due to the fact that the electrons and deutrons, being accelerated in the same electric fields, acquire identical energies. The yield of neutrons depends exponentially on the energy of the deuterons accelerated along the discharge axis:[7]

$$\sigma_{dd} = (288/E_d) \exp[-45.8 E_d^{-1/3}],$$

where $\sigma_{dd}$ is the cross section of the (d,d) reaction in barns, while $E_d$ is the deuteron energy in kev. At electron energies not greater than 500 kev the yield of x-ray quanta is, as is well known, directly proportional to the electron energy. As a result, with $p_0$ greater than $7 \times 10^{-2}$ mm Hg, when the energy of the charged particles accelerated along the discharge axis diminishes rapidly, the neutron yield diminishes much more rapidly than the intensity of the hard x rays.

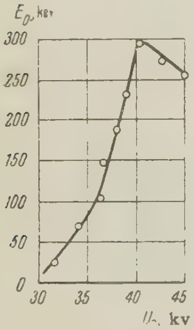

FIG. 2. Dependence of the end-point energy $E_0$ on the initial voltage $U_0$ ($p_0 = 7 \times 10^{-2}$ mm Hg).

2. We measured the dependence of the end-point energy $E_0$ on the initial voltage $U_0$ at an initial hydrogen pressure of $7 \times 10^{-2}$ mm Hg (see Fig. 2). As in Fig. 1, the experimental points of Fig. 2 represent average values of several individual experiments. At initial voltages $U_0 < 30$ kv the intensity of the electron beam diminishes rapidly, since even an exposure of 15 or 20 discharges is insufficient for registration. The dependence considered here is also analogous to the dependence of the neutron yield on the initial voltage in discharges in deuterium. The reduction in the fast-electron energies at voltages $U_0 > 40$ kv can be attributed to the intense liberation of gas and evaporation of the wall material at the initial stages of very powerful discharges. Actually, the evaporation from the walls increases the mass of the gas-discharge column, slows down its compression, and consequently reduces the electric induction fields which can accelerate the charged particles.

3. In connection with the suggested possibility of accelerating the charged particles during the development of an unstable plasma pinch of the "neck-in" type, we investigated the dependence of the electron end-point energy $E_0$ on the intensity of the external longitudinal magnetic field.

For this purpose, the coaxial feeder surrounding the discharge chamber was placed in a solenoid. The solenoid winding consisted of 180 turns, uniformly distributed over the entire length of the discharge chamber. The solenoid was fed with direct current from a motor generator electronically stabilized to within 0.5% of the excitation current. The electron energies were measured with a direct-deflection magnetic spectrograph with the magnetic field intensity H on the solenoid axis ranging from 0 to 150 oe at the optimum initial discharge conditions ($p_0 = 10^{-2}$ mm Hg, $U_0 = 40$ kv). The results obtained are shown in Fig. 3. When the current in the solenoid winding is reversed, the plot of $E_0$ vs. H remains the same. As can be seen from Fig. 3, the electron end-point energy diminishes sharply (from 300 to 150 kev) as the magnetic field intensity is increased from 0 to 25 or 30 oe. Further increase in the magnetic field causes the electron energy to diminish much more slowly.

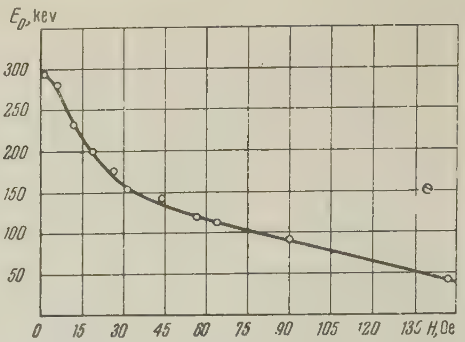

FIG. 3. Dependence of the end-point energy $E_0$ on the intensity of the external longitudinal magnetic field H ($p_0 = 7 \times 10^{-2}$ mm Hg; $U_0 = 40$ kv).

If it is assumed that the plasma in the discharge has an infinite conductance and consequently the force lines of the magnetic field are "frozen-in" and completely entrained by the plasma, the longitudinal magnetic field $H_z$ inside a pinch of radius r should increase as $r^{-2}$ upon compression. The magnetic field $H_\varphi$ of the discharge current increases as $r^{-1}$ upon compression of the plasma pinch. At a radius $r_m$ corresponding to the instant of maximum compression (approximately 1 to 2 cm) we have $H_\varphi \gg H_z$ (if $H_z = 30$ oe initially). It is therefore difficult to expect the presence of so weak an external magnetic field to influence noticeably the compression of the current column. However, the fields $H_z$ and $H_\varphi$ become comparable in magnitude when the plasma pinch radius becomes of order 0.2 — 0.5 cm. Since the application of an external magnetic field $H \sim 30$ oe reduces the electron energy from 300 to 150 kev, it is obvious that the electrons acquire these high energies by acceleration in the electric field produced when the radius of the plasma pinch is reduced to 0.2 or 0.5 cm. A plasma pinch can have so small a radius where an instability of the "neck-in" type occurs.

4. The radial distribution of fast electrons accelerated along the discharge axis was investigated with a specially prepared collimator (see Fig. 4). The x-ray film was placed directly behind the collimator and could be covered with aluminum filters of different thickness. The experiments were

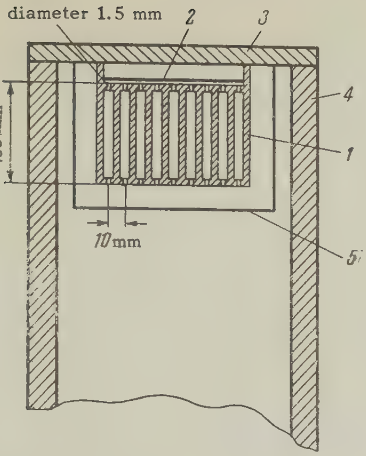

FIG. 4. Arrangement and placement of the collimator. 1 – collimator, 2 – cassette with x-ray film, 3 – "anode" of discharge chamber, 4 – side walls of the chamber, 5 – protective cover.

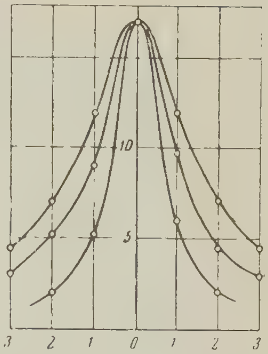

FIG. 5. Radial distribution of the intensity of the electron beam at the outlet of the collimator. Ordinates – film density (relative units), abscissas – distance from the tube axis (centimeters); the upper, middle, and lower curves are for filter thicknesses of 30, 54, and 75 microns, respectively.

carried out at $U_0 = 40$ kv. In the region of low initial hydrogen pressures, approximately $7 \times 10^{-3}$ mm Hg, the intensity of the "shot through" electrons produced at the start of the discharge exceeds considerably the intensity of the electrons responsible for the hard x rays. Under these conditions an exposure of ten discharges produced no blackening of the film placed behind an aluminum filter 30 microns thick. At the same initial pressure and at a filter thickness of 12 microns, the same blackening was obtained on x-ray films placed opposite each opening of the collimator. It follows therefore that the electrons, with energies several times ten kev, produced at the start of the discharge, are uniformly distributed over the cross section of the discharge chamber.

The radial distribution of fast electrons responsible for the hard x rays was investigated at $p_0 = 10^{-2}$ mm Hg. Figure 5 shows the film density distribution after an exposure of 10 discharges with aluminum filters 30, 54 and 75 microns thick. According to the experimental data, electrons with energies 80, 110 and 140 kev have average ranges of 30, 54 and 75 microns in aluminum, respectively. As can be seen from Fig. 5, as the filter thickness is increased the half-width of the radial distribution of the film density decreases. The results of these experiments indicate that the non-equilibrium group of fast electrons is accelerated in the immediate vicinity of the axis of the discharge chamber.

Calibration experiments, in which the densities of x-ray film exposed to electron beams of known intensity were measured, made it possible to estimate the number of fast electrons accelerated along the discharge axis. At optimum initial conditions ($p_0 = 7 \times 10^{-2}$ mm Hg, $U_0 = 40$ kv), the total number of 140-kev electrons amounts to approximately $10^{13}$ electrons per discharge.

## INVESTIGATION OF FAST ELECTRONS IN DEUTERIUM AND INERT GASES

For all the investigated gases, with the exception of krypton and xenon, there exists a minimum pressure $p_{min}$, below which no electron pulses are observed. These values of $p_{min}$ are listed in the second column of the table.

As the pressure increases above $p_{min}$, the amplitude of the electron pulse increases, reaches a maximum value, and starts diminishing with further increase in pressure. The third column of the table lists the values of the pressure $p_1$ corresponding to the maximum amplitude of the electron pulse. For krypton and xenon, the intensity of the electron pulse increases down to $3 \times 10^{-3}$ mm Hg, below which these gases do not break down in the discharge chamber. It must be noted that in heavy gases the electron pulses appear both near the first and near the second singularity of the current oscillogram. On the other hand, in light gases (hydrogen, deuterium, or helium) the electron-pulse time coincides as a rule, with the second singularity of the discharge-current curve. When the polarity of the voltage applied to the discharge chamber is reversed, no electron pulses are observed on the oscillogram even when the sensitivity of the photomultiplier is increased by two orders of magnitude.

| Gas | Minimum pressure, $p_{min}$ $10^{-2}$ mm Hg | Pressure $p_1$ at maximum electron energy, $10^{-2}$ mm Hg | Maximum electron energy registered, kev | Gas | Minimum pressure, $p_{min}$ $10^{-2}$ mm Hg | Pressure $p_1$ at maximum electron energy, $10^{-2}$ mm Hg | Maximum electron energy registered, kev |
|---|---|---|---|---|---|---|---|
| $H_2$ | 2.5 | 7 | 295 | Ar | 0.4 | 4 | 105 |
| $D_2$ | 2,0 | 6 | 290 | Kr | 0,3 | 0,5 | 50 |
| He | 1.5 | 5 | 290 | Xe | 0.3 | — | <40 |
| Ne | 1,0 | 7 | 210 | | | | |

The end-point energy $E_0$ of the electrons accelerated along the discharge axis was measured for each gas at initial pressures $p_1$ corresponding to the maximum intensity of the electron pulse. The results obtained are listed in the fourth column of the table.

The data listed in the table agree qualitatively with the assumption that inertial forces play a predominant role in the process of the constriction of the plasma pinch.[8] No accurate calculations can be made, however, because of the differences in the effective cross sections for the interactions between the ions and the electrons of the plasma with the neutral atoms.

## CONCLUSION

Analyzing the dependence of the end-point energy of the electron spectrum on the intensity of the external magnetic field and on the initial pressure, as well as the radial distribution of the fast electrons, we can conclude that there exist two groups of nonequilibrium electrons in powerful pulsed discharges. The first group of fast electrons, with energies up to 100 kev, is apparently accelerated in the electric field produced when the current becomes redistributed during the constriction of the plasma pinch. The second group of fast electrons, with energies up to 300 kev, is apparently accelerated in the local electric field, due for example to the development of plasma pinch instabilities of the neck-in type. The corresponding estimates[5] lead to a voltage drop of approximately 50 kv for each "neck-in." Assuming a mechanism of successive acceleration of particles in several "neck-in" spots, one would expect a discrete spectrum of the fast electrons extracted along the discharge axis. Experiments have shown, however, that the electron spectrum has no such discrete nature.

The authors express their gratitude to S. Yu. Luk'yanov for discussing the results obtained.

---

[1] S. Yu. Luk'yanov and I. M. Podgornyĭ, Атомная энергия,(Atomic Energy) No. 3, 97 (1956).

[2] Koval'skiĭ, Podgornyĭ, and Khvashchevskiĭ, JETP **35**, 940 (1958), Soviet Phys. JETP **8**, 656 (1959).

[3] Podgornyĭ, Koval'skiĭ, and Pal'chikov, Dokl. Akad. Nauk SSSR **123**, 825 (1958), Soviet Phys.-Doklady **3**, 1208 (1959).

[4] Artsimovich, Andrianov, Dobrokhotov, Luk'yanov, Podgornyĭ, Sinitsyn, and Filippov, Атомная энергия,( Atomic Energy), No. 3, 84 (1956).

[5] Anderson, Baker, Colgate, Ise, and Pyle, Proc. III Int. Conf. Ioniz. Phenomena in Gases, Venice, 1957.

[6] Andrianov, Bazilevskaya, Braginskiĭ, Brezhnev, Koval'skiĭ, Podgornyĭ, Prokhorov, Filippov, Filippova, Khvashchevskiĭ, and Khrabrov, Paper delivered at Second Geneva Conference, 1958.

[7] R. Post, Usp. Fiz. Nauk **61**, 491 (1957).

[8] M. A. Leontovich and S. M. Osovets, Атомная энергия,(Atomic Energy) No. 3, 81 (1956).

Translated by J. G. Adashko
279

SOVIET PHYSICS JETP VOLUME 11, NUMBER 5 NOVEMBER, 1960

# *DETERMINATION OF THE SPINS OF* $\mathrm{PT}^{196}$ *NUCLEAR LEVELS ON THE BASIS OF GAMMA RAYS EMITTED IN THE CAPTURE OF RESONANCE NEUTRONS*

N. D. GALANINA, B. F. SHVARTSMAN, and A. YA. DIAMENT

Submitted to JETP editor December 18, 1959

J. Exptl. Theoret. Phys. (U.S.S.R.) 38, 1446-1450 (May, 1960)

Gamma rays produced in the capture of resonance neutrons are investigated. The spin of the compound-nucleus levels is determined from the presence of the ground transition in the $\gamma$-ray spectrum. It is found that the spin of the $\mathrm{Pt}^{196}$ nucleons is 1 for levels with neutron energies of 11.9 and 68.2 ev and 0 for a level energy of 19.6 ev.

MEASUREMENT of the total neutron cross section yields all the parameters of the excited level of the nucleus, with the exception of the spin. To determine the spin it is necessary to measure, in addition to the total cross section, one of the partial cross sections, for example the radiative-capture cross section or the scattering cross section. Another method of determining the spin is also possible, based on the study of the spectrum of $\gamma$ rays emitted in the capture of neutrons at different levels. The use of the method is particularly simple in those cases when the radiative transition from the excited state into the ground state is possible only for one value of the excited-state spin. This is the situation in the case of even-odd nuclei with spin $1/2$. In this case one obtains upon capture of a neutron an even-even compound nucleus, in which the spin of the ground state is 0 and the spin of the excited state may be either 0 or 1. Since the $0 \rightarrow 0$ transition is forbidden, the presence in this case of $\gamma$ rays of energy corresponding to the ground-state transition will determine uniquely that the spin of the excited state is 1, while the absence of $\gamma$ rays of the ground-state transition will correspond to a spin of 0.

Using such measurements, the spins were determined[1-4] for a series of levels of $\mathrm{Hg}^{199}$ and $\mathrm{W}^{183}$. In the present investigation, this method was used to determine the values of the spin for several levels of platinum. The nucleus of $\mathrm{Pt}^{195}$ is even-odd and has a spin $1/2$, i.e., it is included among the nuclei whose spin levels are completely determined by the $\gamma$ rays of the ground-state transition.

The arrangement of the apparatus is shown in Fig. 1. The neutron source was a cyclotron with a "pulsed" beam. The duration of the neutron pulse was 2 to 3 microseconds. The energy of the neutrons was determined by means of a time analyzer[5] from the time required to cover the 10-cm base. The width of the electronic channel was 2 microseconds. The $\gamma$ rays produced by neutron capture in the sample were detected with two NaI(Tl) crystals and FÉU-24 photomultipliers. The crystal dimensions were 8 cm high and 10 and 7 cm in diameter. The $\gamma$-ray detectors were placed in a shield made of lead and boron carbide. The crystals were protected by filters made of boron carbide, 2 cm thick, against neutrons scattered by the sample.

The pulses from the photomultipliers were fed to cathode followers, linear amplifiers, and an amplitude discriminator, with which the necessary $\gamma$-ray energy interval $E_\gamma$ was selected. The pulses were then analyzed by a time analyzer. The amplitudes of the pulses in the crystal were calibrated by measuring the energies of the $\gamma$ rays from $\mathrm{Co}^{60}$ (1.17 and 1.33 Mev) and from Po + Be (4.45 Mev). The measurements were made

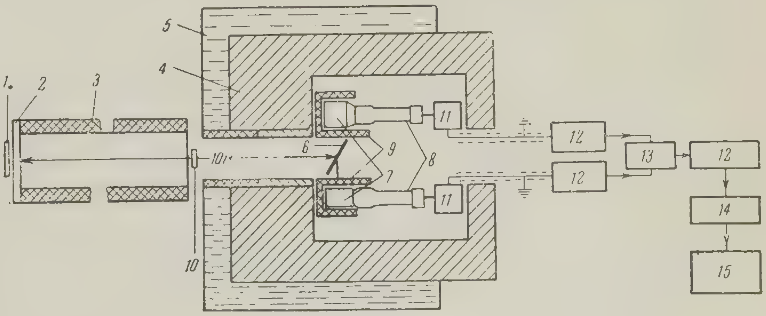

FIG. 1. Diagram of the setup: 1 – cyclotron target, 2 – paraffin moderator, 3 – boron-carbide neutron collimator, 4 – lead shield, 5 – boric-acid shield, 6 – specimen, 7 – NaI(Tl) crystals, 8 – FEU-24 photomultipliers, 9 – boron-carbide filter, 10 – monitoring neutron counter with $\mathrm{BF}_3$, 11 – cathode followers, 12 – amplifiers, 13 – adder, 14 – discriminator, 15 – time analyzer.

with a multi-channel amplitude analyzer.

It must be noted that the crystals did not have sufficiently good resolution. The forms of the spectra of the $\gamma$ rays from the $Co^{60}$ and Po + Be are shown in Fig. 2. As can be seen from the figure, the distribution of the amplitudes for monochromatic 4.45-Mev $\gamma$ rays is rather complicated. In addition to the maximum corresponding to total absorption of the energy, two other maxima are observed, corresponding to one of the two annihilation quanta going outside the crystal. In addition, relatively many low-amplitude pulses are abserved. Such a pulse distribution is probably due both to insufficient crystal size (for total absorption of the $\gamma$ rays) and to rather poor quality of the crystal, with respect to uniformity of the light yield and the gathering of the light over the volume of the crystal. Under such conditions only the lower limit of the registered energy can be established more or less accurately, and the efficiency of registration of $\gamma$ rays of high energies is substantially reduced.

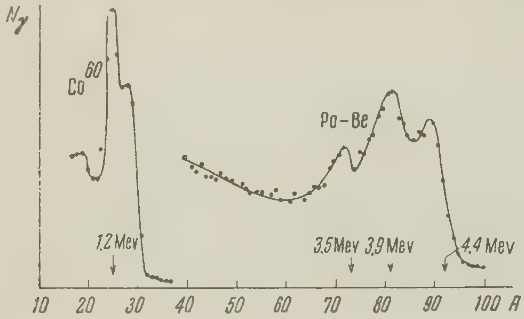

FIG. 2. Calibration curves for NaI(Tl) crystals. A – pulse amplitude in relative units, $N_\gamma$ – number of pulses in relative units.

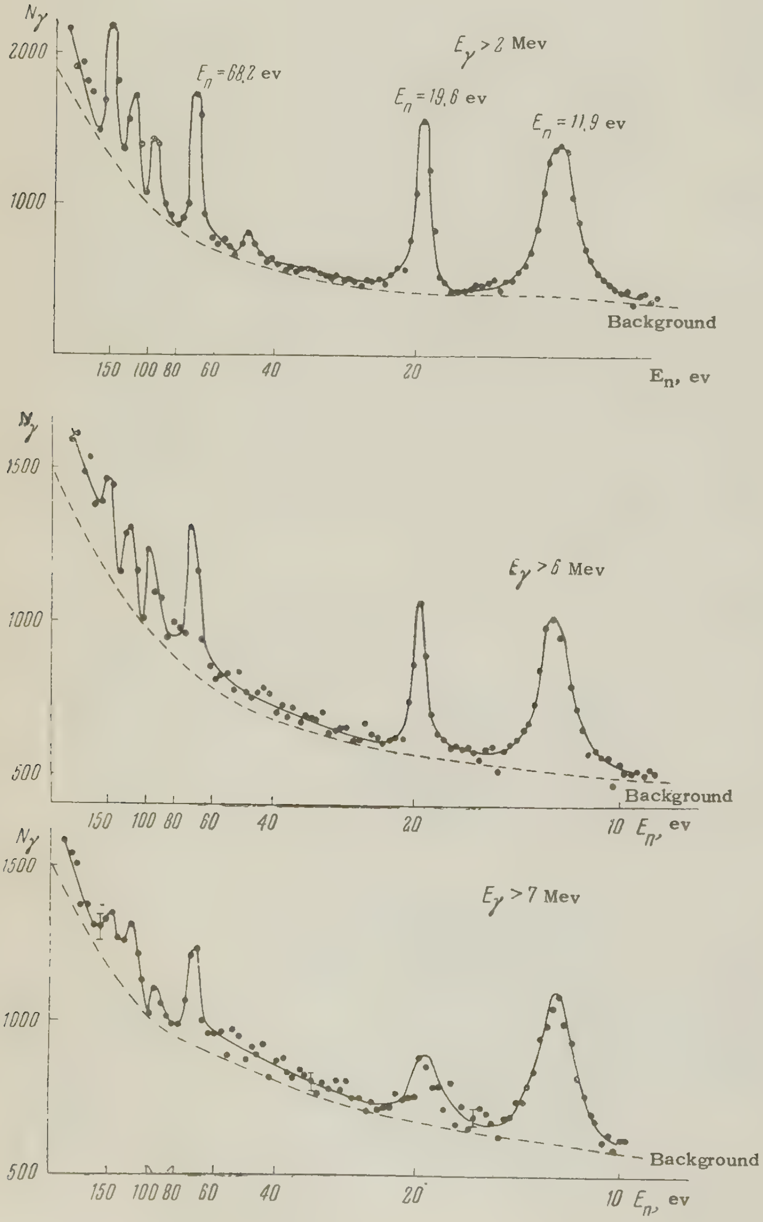

FIG. 3. Intensity of resonances of $Pt^{195}$ at different energies of registered capture $\gamma$ rays, $N_\gamma$ – number of pulses.

The measured dependence of the intensity of the $\gamma$ rays due to neutron capture on the neutron energy $E_n$, for a sample of platinum, are shown in Figs. 3 and the table.

Comparison of the intensities of the neutron resonances for different energies of registered capture $\gamma$ rays

| **Resonance energy, ev** | 11.9 | 19.6 | 68.2 | 95 |
|---|---|---|---|---|
| $N\,(E_\gamma > 6\text{Mev})/N\ \ (E_\gamma > 2\text{Mev})$ | 1 | 0.9 | 1.1 | 1.0 |
| $N\,(E_\gamma > 7\text{Mev})/N\ \ (E_\gamma > 2\text{Mev})$ | 1 | 0.56 | 0.9 | 0.36 |

The counting rate of the capture $\gamma$ rays at $E_\gamma > 2$ Mev is sufficiently large under our conditions, and within two or three hours one can obtain a curve with a statistical accuracy of nearly 3% (Fig. 3). However, when changing to energies $E_\gamma > 6$ or 7 Mev, the counting rate decreases sharply, and a time 10 or 15 times longer is necessary to obtain the same accuracy.

At $\gamma$-ray energies above 2 Mev (see Fig. 3), all the neutron resonances, which are well known[6] for this energy range in platinum, appear. It is known that three levels corresponding to the neutron energies ($E_n$) 11.9, 19.6 and 68.2 ev belong to the isotrope ${}_{78}Pt^{195}$, while the 95-ev level belongs to ${}_{78}Pt^{198}$. At higher neutron energies, the individual resonances cannot be resolved by our system.

On going to $\gamma$-ray energies greater than 6 Mev (Fig. 3), the same resonances are observed, but, as can be seen from the table, the ratio of the intensities remains the same as for the lower $\gamma$-ray energies. Upon further increase of the lower threshold of registered $\gamma$ rays, to 7 Mev, a noticeable change is observed in the relative intensities of the maxima.

From the form of the $\gamma$-ray spectrum upon capture of thermal neutrons, and from the binding energies of the isotopes of platinum,[7] one would expect the neutron-energy maximum at 95 ev to disappear for $\gamma$ rays with $E_\gamma > 7$ Mev, since the binding energy of the neutron in the compound nucleus $Pt^{199}$ amounts to 6.5 Mev. Experimentally, however, a noticeable reduction in this maximum is observed. The fact that it does not vanish completely is apparently explained by the inaccuracy in calibration of the apparatus in $\gamma$-ray energies, due to the poor resolution of the crystals, and also by a certain instability of the threshold of registration of $\gamma$ rays in prolonged measurements.

Next, when the $\gamma$-ray lower energy threshold is approximately 7 Mev, transitions should be registered for the isotope $Pt^{195}$, both to the ground state, with energy 7.9 Mev, and to the lower levels, with energies 7.6 and 7.26 Mev. Both lower levels have spin 2. Therefore all three transitions should take place from excited levels with spin 1 and should be forbidden (or have very low probability) for excited levels with spin 0.

In our experiment (see Fig. 3), as can be judged from the incomplete vanishing of the maximum with neutron-resonance energy 95 ev, the true threshold of the registered $\gamma$-ray energy is found to be not 7 Mev, but approximately 6 Mev. Therefore, even in the absence of the ground-state and the two neighboring transitions, one could hardly achieve total vanishing of the resonance, because of the partial registration of transitions with lower energy.

Thus, the observed resonance-intensity ratio can be explained in the following manner. For levels corresponding to neutron energies 11.9 and 68.2 ev, a ground-state transition is observed, and therefore the spins of these levels should be 1. For the level corresponding to $E_n = 19.6$ ev, the reduction in the intensity corresponds apparently to the absence of a ground-state transition, and corresponds therefore to spin 0.

Unfortunately, our apparatus cannot as yet operate at high $\gamma$-ray energies, owing to the poor resolution of the crystals and the low intensity, and we cannot establish precisely the absence of a ground-state transition for the 19.6-ev level. Nor can we deny, until such an experiment is carried out, the other possible explanation of the observed effect, namely that the intensity change obtained may be due to fluctuations of the partial radiation widths of the levels under consideration. In this case the deduced value of the spin of the 19.6-ev level may be incorrect.

We have also attempted to detect the presence of a ground-state transition by direct observation of the spectrum of the $\gamma$ rays emitted upon capture of 11.9- and 19.6-ev neutrons. For this purpose we chose the necessary neutron-energy interval in the maximum region and analyzed the $\gamma$-ray spectrum with a multi-channel amplitude analyzer.

Figure 4 shows an overall view of the spectra obtained. As can be seen, the intensity of the $\gamma$ rays diminishes sharply at high energies for both levels, and it becomes very difficult to compare the spectra in our region, owing both to the low intensity and to the fact that the effect little exceeds the background. In addition, the spectra are not measured simultaneously for the two levels, and

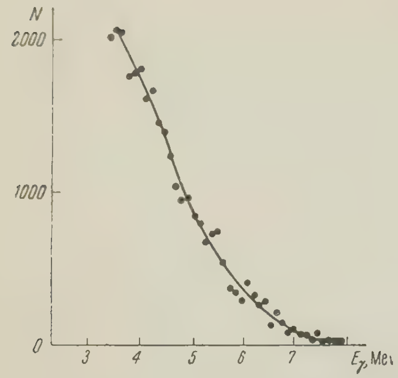

FIG. 4. Form of $\gamma$-ray spectrum.

therefore more stringent requirements are imposed on the stabilities of the amplitudes.

Nevertheless, our comparison of the two spectra, shown in Fig. 5, confirms qualitatively the result previously obtained, that in the $\gamma$-ray energy region 6.5 — 7 Mev the intensity of the spectrum for the 19.6-ev resonance drops approximately to half the intensity of the $\gamma$ rays for the 11.9-ev resonance.

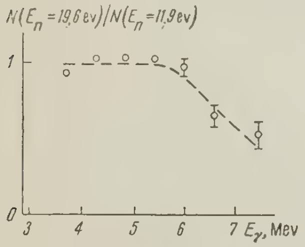

FIG. 5. Comparison of intensity of $\gamma$-ray spectra for the 19.6- and 11.9-ev resonances.

To confirm the final conclusions regarding the spins of the levels under consideration, it would be desirable to perform further measurements with better resolution for $\gamma$ rays of higher energy.

---

[1] H. H. Landon and E. R. Rae, Phys. Rev. **107**, 1333 (1957).

[2] J. R. Bird, Second Geneva Conference, 1958.

[3] Fox, Zimmerman, Hughes, Palevsky, Brussel, and Chrien, Phys. Rev. **110**, 1473 (1958).

[4] Vinh-Dinh Huynh, Julien, Corge, Netter, and Simic, Compt. rend. **248**, 2330 (1959).

[5] V. V. Okorokov, Приборы и техника эксперимента (Instrum. and Meas. Engg.) No 6, 63 (1958).

[6] D. J. Hughes and B. B. Schwartz, Neutron Cross Section, BNL-325, 1958.

[7] Groshev, Demidov, Lutsenko, and Pelekhov, Атлас спектров $\gamma$-лучей радиационного захвата тепловых нейтронов, (Atlas of Spectra of Gamma Rays from Radiative Capture of Thermal Neutrons), Atomizdat, M., 1958.

Translated by J. G. Adashko
280

SOVIET PHYSICS JETP VOLUME 11, NUMBER 5 NOVEMBER, 1960

# *TRIPLE SCATTERING OF 660-Mev PROTONS II. ANGULAR DEPENDENCE OF DEPOLARIZATION*

YU. P. KUMEKIN, M. G. MESHCHERYAKOV, S. B. NURUSHEV, and G. D. STOLETOV

Joint Institute for Nuclear Research

Submitted to JETP editor December 25, 1959

J. Exptl. Theoret. Phys. (U.S.S.R) **38**, 1451-1455 (May, 1960)

Results are presented on the measurement of the depolarization parameter for the scattering of a polarized beam of 640-Mev protons through 54, 72, 108, and 126° in the c.m.s. In scattering through 54, 72, and 90° the normal polarization component of the proton beam is changed slightly. The sum and difference of the values of the depolarization parameter for scattering angles that are symmetric about the 90° direction are interpreted in terms of the amplitude of the p-p scattering matrix.

OUR previous experiments[1] showed that the scattering of a polarized beam of 640-Mev protons by protons through an angle of 90° in the c.m.s. causes a weak depolarization of the beam. This result is evidence of the fact that at this energy the p-p interaction associated with elastic scattering at large angles is relatively rarely accompanied by a change in the spin orientation. Further information on the character of the p-p interaction can be obtained from experiments in which the depolarization parameter is measured at c.m.s. scattering angles both smaller and larger than 90°, which was done in this experiment. The results of such measurements give two independent relations between the amplitudes of the p-p scattering matrix supplemented by two relations embodying the data on the angular dependence of the differential cross sections and polarization.

The experiments described below were carried out on the six-meter synchrocyclotron of the Joint Institute for Nuclear Research as part of the program for studying the p-p interaction at ~660 Mev.

## MEASUREMENT PROCEDURE AND RESULTS

The experimental arrangement is shown in the figure, its general features being the same as in the previous measurements (see Fig. 1a of reference 1). We used a proton beam with a degree of polarization $P_1 = 0.58 \pm 0.03$ and energy (640 ± 12) Mev, scattered inside the synchrocyclotron chamber to the left by an angle of 9° in a beryllium target-polarizer. The second scattering took place in a cylindrical vessel of diameter 12 cm filled with liquid hydrogen. The mean proton energy in the center of the liquid hydrogen target was 635 Mev, the intensity of the beam in a 3 cm diameter was $7 \times 10^5$ protons/cm$^2$-sec.

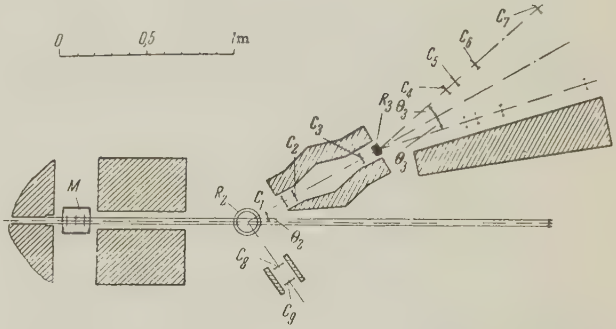

Experimental setup (in plane of scattering). M – monitor; $R_2$ – second scatterer (vessel with liquid hydrogen); $R_3$ – third scatterer (graphite block 5×5 cm, 6 cm thick; $C_1$–$C_9$ – scintillation counters of dimensions (the first figure gives the horizontal dimension, and the second the vertical) 6.5×6.5; 6×7; 6×7; 6×6; 6×6.5; 6.5×7; 6.5×6.5; 7.5×12; and 8.5×13 cm and thickness 6 mm. The depolarization measurements at 126° were made without counters $C_2$ and $C_5$; a third scatterer of cross section 5×5 cm and thickness 3 cm was used here. The shaded areas indicate the position of the lead shielding.

The depolarization parameter D was measured every 18° over the scattering angle $\theta_2$, beginning at 54° and ending at 126°. The beam of protons doubly scattered through an angle $\theta_2$ on the same side (to the left) was picked up by a telescope consisting of three counters $C_1$, $C_2$, and $C_3$. In order to separate elastic p-p scattering from accompanying inelastic processes taking place in the liquid hydrogen target, the scattered protons and recoil protons were registered by telescopes ($C_1C_2C_3$) and ($C_8C_9$) working together, the angle between them corresponding to the kinematics of elastic p-p collisions.

The normal component of the polarization vector of the doubly scattered protons was determined by measurements of the left-right asymmetry $\epsilon_{3n}$ of the emitted charged particles in the direction $\theta_3 = 12°$ (in the laboratory system) from a carbon target-analyzer $R_3$. These measurements involved the registration of nine-fold coincidences of counter pulses grouped in telescopes ($C_1C_2C_3$), ($C_8C_9$), and ($C_4C_5C_6C_7$), the last registering triply scattered protons. Corrections to the number of nine-fold coincidences took into account chance nine-fold coincidences ($\sim 1\%$) and the effect of the empty vessel ($\sim 3\%$). In order to check that the angles $\theta_3$ measured to the left and right were actually equal to one another, and therefore to exclude the possibility of the appearance of a false asymmetry owing to the zero mark on the $\theta_3$ angular scale not coinciding with the effective axis of the secondary beam, the "profile" of the beam of doubly scattered protons was measured carefully for all angles. The procedure involved in these measurements was similar to that used earlier by the Berkeley group.[2]

The value of the depolarization parameter $D(\theta_2)$ was found from the relation[3]

$$D = \frac{\varepsilon_{3n}}{\varepsilon_3}(1 + P_1P_2) - \frac{P_2}{P_1}, \qquad (1)$$

where $P_1$ is the initial polarization of the beam, and $P_2$ is the polarization arising in the scattering on hydrogen of an unpolarized proton beam through a given angle $\theta_2$. The value and angular dependence of $P_2$ are known from previous measurements.[4]

The value of $\epsilon_3$ represents the experimentally observed left-right asymmetry of emission from the carbon target of charged particles under the action of a proton beam of polarization $P_1$ and energy equal to the energy of the protons scattered in hydrogen through an angle $\theta_2$. In measuring the value of this asymmetry, we used the same apparatus as in the measurements of $\epsilon_{3n}$. Counters $C_1$, $C_2$, $C_3$ and the carbon target were set in the primary polarized proton beam whose energy was degraded, by means of a filter consisting of lead and polyethylene plates, to the energy of the doubly scattered proton beam. Particles emitted from the carbon target in the direction of ± 12° were registered by the telescope ($C_4C_5C_6C_7$) connected in coincidence with the telescope ($C_1C_2C_3$); the intensity of the primary beam was reduced here to 1/50 — 1/100 of its former value. It should be noted that measurements made with filters having different ratios of thickness of lead and polyethylene layers were in agreement, within the limits of standard deviations of the value of $\epsilon_3$.

At each angle of observation, of the depolarization, we made 10 — 12 independent repeated measurements of the asymmetries $\epsilon_{3n}$ and $\epsilon_3$. In the overwhelming majority of cases the results of the repeated measurements were in agreement, within the limits of error, with the mean values. The data on the mean energies, and also the angular and energy spread of the protons in the secondary beam, are given in the table, along with the values found for the asymmetries $\epsilon_{3n}$ and $\epsilon_3$ and their statistical errors. The table lists also the values obtained for the depolarization parameter, for various scattering angles.

## DISCUSSION OF RESULTS

According to Wolfenstein,[3] the depolarization parameter can vary in the limits of $-1 + 2|P_2| \leq D \leq +1$. The results obtained in our experiment indicate that the depolarization parameter corresponding to p-p scattering through 54, 72, 90, 108, and 126° is a positive quantity. Moreover, for scattering angles of 54, 72, and 90° the depolarization parameter was found to be close to +1. By comparing the asymmetries $\epsilon_{3n}$ and $\epsilon_3$ obtained for angles of 54, 72, and 90°, it can be seen that in p-p scattering at those angles the normal component of the polarization does not undergo large changes.

Thus far, systematic measurements of the depolarization parameter in p-p scattering were

Values of the Asymmetries $\epsilon_{3n}$ and $\epsilon_3$ and Depolarization D
(the results for 90° are taken from ref. 1)

| $\theta_2 \pm \Delta\theta_2$, deg | $E_2 \pm \Delta E_2$, Mev | $\varepsilon_3 \pm \Delta\varepsilon_3$ | $\varepsilon_{3n} \pm \Delta\varepsilon_{3n}$ | $D \pm \Delta D$ |
|---|---|---|---|---|
| 54±4 | 490±20 | 0,121±0,005 | 0.161±0,024 | 0,99±0.25 |
| 72±4 | 416±21 | 0,173±0,008 | 0.1[illegible]4±0,029 | 0.69±0,20 |
| 90±5 | 315±20* | 0,216±0,012 | 0,200±0,032 | 0,93±0,17 |
| 108±5 | 219±27 | 0,198±0,011 | —0,023±0,033 | 0,28±0,16 |
| 126±5 | 125±21 | 0,157±0,015 | —0.009±0.036 | 0,57±0,20 |

---

*In the previous work[1] the energy spread of the protons was erroneously given as ±40 Mev.

carried out at energies of 315 (reference 5) and 143 (reference 6) Mev for angles less than 90°. In both cases the values obtained for the depolarization parameter were of positive sign.* Comparison of the available data for triple scattering of protons indicates that the depolarization parameter discloses a tendency to increase with an increase in energy from 143 to 635 Mev in the scattering angle interval $50° \leq \theta_2 \leq 90°$. This characteristic of p-p interactions in the considered energy region would be brought out still more convincingly if the depolarization parameter were to be measured with greater accuracy and over smaller energy intervals.

In the notation of Wolfenstein,[3] the p-p scattering matrix can be written

$$M = BS + C(\sigma + \sigma_t)\mathbf{n} + \tfrac{1}{2}G[(\sigma\mathbf{k})(\sigma_t\mathbf{k}) + (\sigma\mathbf{p})(\sigma_t\mathbf{p})]T$$

$$+ \tfrac{1}{2}H[(\sigma\mathbf{k})(\sigma_t\mathbf{k}) - (\sigma\mathbf{p})(\sigma_t\mathbf{p})]T + N(\sigma\mathbf{n})(\sigma_t\mathbf{n})T, \quad (2)$$

and the differential cross section $\sigma_0(\theta)$ for the scattering of an unpolarized beam of protons on protons and the depolarization parameter $D(\theta)$ can be expressed in terms of the complex amplitudes B, C, G, H, N in the following way:

$$\sigma_0(\theta) = \tfrac{1}{4}|B|^2 + 2|C|^2 + \tfrac{1}{4}|G - N|^2 + \tfrac{1}{2}|N|^2 + \tfrac{1}{2}|H|^2, \quad (3)$$

$$\sigma_0(\theta)[1 - D(\theta)] = \tfrac{1}{4}[G - N - B]^2 + |H|^2. \quad (4)$$

Then, since B, $C/\sin\theta$, and H is an even function of $\cos\theta$, while G and N are odd, it is not difficult to show that the values of the depolarization parameter for angles symmetric with respect to the 90° direction are connected with the scattering matrix amplitudes by the two following independent relations:

$$\sigma_0(\theta)[D(\theta) + D(\pi - \theta)] = 4|C|^2 + |N|^2 - |H|^2, \quad (5)$$

$$\sigma_0(\theta)[D(\theta) - D(\pi - \theta)] = \mathrm{Re}\{[G - N]B^*\}. \quad (6)$$

From this it is seen that the product of the differential cross section $\sigma_0(\theta)$ and the sum $[D(\theta) + D(\pi - \theta)]$ is represented in terms of the triplet amplitudes C, N, and H, while the product of the differential cross section $\sigma_0(\theta)$ and the difference $[D(\theta) - D(\pi - \theta)]$ depends only on the singlet-triplet interference.

On the basis of the results of the present experiment, it may reliably be shown that in p-p scattering at 640 Mev the sum $[D(\theta) + D(\pi - \theta)]$ is not equal to zero. This means that the basic role in the p-p scattering matrix is played by the triplet terms $C(\sigma + \sigma_t)\mathbf{n}$, $H[(\sigma\mathbf{k})(\sigma_t\mathbf{k}) - (\sigma\mathbf{p})(\sigma_t\mathbf{p})]$, $N(\sigma\mathbf{n})(\sigma_t\mathbf{n})$. As has already been noted,[1] from the fact that $D(90°)$ is close to +1 it follows that the main contribution to scattering at an angle of 90° is given by the term $C(\sigma + \sigma_t)\mathbf{n}$.

In order to see if the observed difference between the values of $D(\theta)$ and $D(\pi - \theta)$ are significant or accidental, it was necessary to analyze the character of the distributions of all the errors of measurement of the asymmetries $\epsilon_{3n}$ and $\epsilon_3$ and polarizations $P_1$ and $P_2$. The results of the statistical analysis were that the probabilities of non-zero differences in moduli $[D(54°) - D(126°)]$ and $[D(72°) - D(108°)]$ are 80 and 86%, respectively. Both differences between the observed values of the depolarization parameter are practically independent of each other and the probability that both these differences are simultaneously chance deviations from a mean value of zero is only ~3%.

Thus, although the data of the present experiment are not marked by a high accuracy, they all indicate that in the energy region and scattering angles under consideration singlet-triplet interference occurs. It thus follows that the final state of the p-p system includes some mixture of the singlet states.

The authors express their gratitude to Ya. A. Smorodinskiĭ, S. N. Sokolov, N. P. Klepikov, and R. M. Ryndin for helpful discussions.

---

*The Harwell group[7] carried out observations of the depolarization in p-p scattering at 142 Mev and found negative values of the depolarization parameter for angles in the interval $50° \leq \theta_2 \leq 90°$. This result, however, has not been confirmed (see reference 6). It should be noted that the sign of the depolarization parameter is extremely sensitive to the model used for the nuclear potentials. Thus, the values of the depolarization parameter found in reference 6 are in agreement with the results of the calculations of Gammel and Thaler,[8] who used the statistical potential with the addition of an LS term, while use of the Signell–Marshak potential[9] leads to values of the depolarization parameter differing even in the sign from that given by experiment.

[1] Kumekin, Meshcheryakov, Nurushev, and Stoletov, JETP **35**, 1398 (1958), Soviet Phys. JETP **8**, 977 (1959).

[2] Chamberlain, Segrè, Tripp, Wiegand, and Ypsilantis, Phys. Rev. **102**, 1659 (1956).

[3] L. Wolfenstein, Phys. Rev. **96**, 1654 (1954).

[4] Meshcheryakov, Nurushev, and Stoletov, JETP **33**, 37 (1957), Soviet Phys. JETP **6**, 28 (1958).

[5] Chamberlain, Segrè, Tripp, Wiegand, and Ypsilantis, Phys. Rev. **105**, 288 (1957).

[6] Hwang, Ophel, Thorndike, Wilson, and Ramsey, Phys. Rev. Letters **2**, 310 (1959).

[7] A. Taylor and I. Wood, 1958 Annual International Conference on High-Energy Physics, CERN, Geneva, 1958, p. 56.

[8] J. Gammel and R. Thaler, Phys. Rev. **108**, 163 (1957).

[9] Signell, Zinn, and Marshak, Phys. Rev. Letters **1**, 416 (1958).

Translated by E. Marquit

SOVIET PHYSICS JETP VOLUME 11, NUMBER 5 NOVEMBER, 1960

# *ANISOTROPY OF SURFACE TENSION AT THE BOUNDARY BETWEEN THE SUPERCONDUCTING AND NORMAL PHASES OF TIN*

Yu. V. SHARVIN and V. F. GANTMAKHER

Institute for Physical Problems of the Academy of Sciences, U.S.S.R.

Submitted to JETP editor December 31, 1959

J. Exptl. Theoret. Phys. (U.S.S.R.) **38**, 1456-1470 (May, 1960)

The anisotropy of surface tension at the boundary between the s and n phases of tin was investigated by two methods. In the first, the structures of the intermediate state, revealed by using a ferromagnetic powder, were observed in specimens with different crystal orientations. In the second method, the moment of the forces acting on a spherical specimen in a magnetic field was measured. There was agreement between the results obtained by both methods. The form of the dependence of surface tension on the direction of the normal to the phase interface, the absolute order of magnitude of the effect and its temperature dependence were determined.

THERE is little known at present about the anisotropy of the properties of superconductors. In particular, the anisotropy of surface tension Δ* at the boundary between the superconducting (s) and normal (n) phases has not been studied. A comparison between the anisotropy of Δ and the anisotropy of other quantities characterizing the electronic state of a metal is interesting, in that the method of studying the anisotropy of Δ has some advantages over the study of the anisotropy of other parameters of superconductors.

The boundary separating the s and n phases extends into the body of the metal. In studying Δ, therefore, we do not encounter the difficulties met in measuring the penetration depth of a magnetic field into a superconductor and the high-frequency impedance, where the results depend appreciably on the state of the surface of the metal.

On the other hand, we should point out that in measuring Δ the specimens must satisfy stringent requirements as to the perfection of the crystal lattice. It is essential that the phase boundary be able to move freely and take up the position corresponding to thermodynamic equilibrium. This condition gives rise to serious difficulties in the case of boundary movement in a solid. Any irregularities in the metal lattice give rise to "dry friction" in the movement of an ns boundary, i.e. to forces preventing the motion of the boundary, which do not tend to zero as the movement slows down.

In our work we were up against the fact that in single-crystal tin with less than $6 \times 10^{-5}$% impurity, treated with the greatest care to avoid mechanical deformation, these forces nevertheless do not disappear and noticeably affect the regularity and reproducibility of the structures of the intermediate state. The form of the structures always depends, to a known extent, on the previous history of the specimen, i.e., on how the magnetic field and temperature were changed in the preceding moments.

This made investigation of the anisotropy of Δ considerably more difficult, especially as it turned out to be relatively small.

In order to obtain a qualitative picture of the phenomenon, we used two independent differential methods, which allowed direct comparison to be made between the values of Δ for different orientations of the ns boundary, under conditions which excluded, as far as possible, the influence of "dry friction" on the results.

## 1. THE "FROZEN-IN FLUX" METHOD

The object of this part of the work was to obtain information on the anisotropy of Δ from an analysis of the structures of the intermediate state, which can easily be observed by sprinkling a fine ferromagnetic powder on the surface of the specimen.[1,2] The existence of an anisotropy in Δ should lead to a preferential orientation of the phase boundaries along directions for which Δ is

---

*We denote by Δ, as usual, a quantity with the dimensions of length, which is related to the magnitude of the surface free energy $\sigma_{ns}$ by the relation $\sigma_{ns} = \Delta H_c^2/8\pi$.

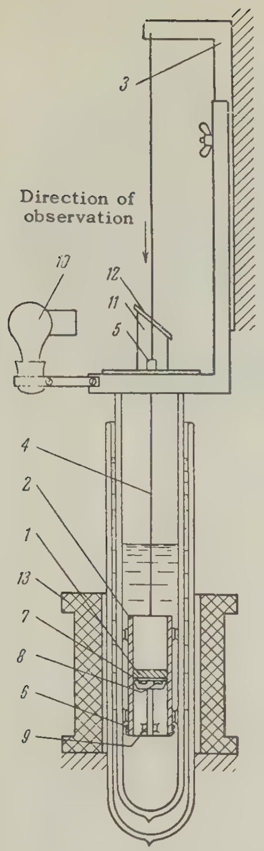

FIG. 1. Diagram of apparatus: 1 – specimen; 2 – lead tube, hung from the stand 3 by two threads 4, passing through the seal 5; 6 – lead resistance thermometer for monitoring the temperature of the tube; 7 – carbon thermometer; 8 – bismuth for measuring the field; 9 – heater; 10 – lamp; 11 – glass tube; 12 – flat window; 13 – solenoid.

a minimum, assuming of course that other factors that determine the arrangement of s and n domains are sufficiently unimportant.

First of all it is essential to remove all factors, related to the geometry of the field or of the specimen, which could affect the arrangement of the regions. Ideally the experiment would be carried out on an infinite plane-parallel plate of superconductor, in a uniform magnetic field perpendicular to its surface. We realized this case in practice by containing the specimen (a flat round single crystal of tin, 37 mm in diameter and 10 mm thick) — in a long lead tube (16 cm long) fitting the specimen closely (see Fig. 1). Since the critical field is considerably higher for lead than for tin at all temperatures, the lead tube acted as an ideal "magnetic mirror", thanks to which the specimen was equivalent to an infinite disc in an electrodynamic sense.

The uniform magnetic field, produced by a solenoid, penetrated the lead tube when its temperature was above the critical temperature for lead. A Dewar with liquid helium, which could be moved vertically, was first placed in its lower position. The Dewar was then raised, the lead tube immersed in the helium and cooled, and the magnetic flux became "frozen" in the tube. On lowering the temperature further (by pumping the helium) the tin specimen went over into the intermediate state. As the magnetic flux in the specimen stayed constant, the transition occurred under the condition $\mathbf{B} = \text{const}$ ($\mathbf{B}$ is the magnetic induction in the specimen, averaged over the volume, which contained a considerable number of s and n domains). It was essential for our purpose that this condition be fulfilled, since eddy currents would otherwise be induced on the surface of the specimen at the moment of transition, flowing round the whole specimen and exerting an orienting action on the position of the boundaries. It is known that this effect causes a marked 'radial' structure to appear in a spherical or plane cylindrical specimen when a field is suddenly trapped.[3,1] In our case the edge and center of the specimen were in practically the same states, and no radial structures were observed.

The technique for introducing the ferromagnetic powder was the same as in the previous work[2] (the apparatus for sprinkling is not shown in Fig. 1). The illumination of the surface of the specimen was produced by an opal bulb, the light from which was reflected from the mirror surface of the specimen.

We obtained photographs of the structures of the intermediate state for nine tin single-crystal specimens, containing not more than $10^{-4}\%$ impurity. The crystallographic orientations of the specimens are shown in Fig. 2. Most of the pictures were taken at 3°K, and for some specimens the temperature dependence of the structures was followed up to 3.6°. The concentration $C_S$ of the superconducting phase in the specimen was determined from the value of the frozen-in field B by the relation $C_S = 1 - B/H_C$.

The most convenient structures for interpretation were obtained with concentrations $C_S$ in the range 0.05 – 0.2. The s domains then appeared

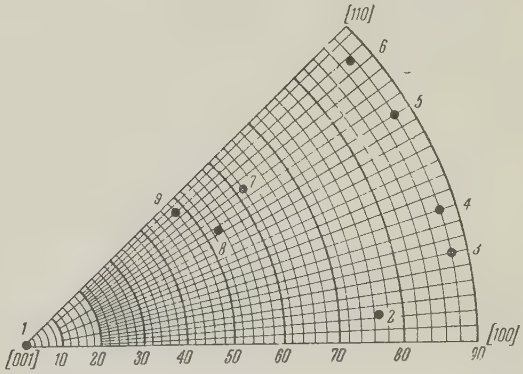

FIG. 2. Stereographic projection of the directions of the normals to the plane surfaces of the specimens.

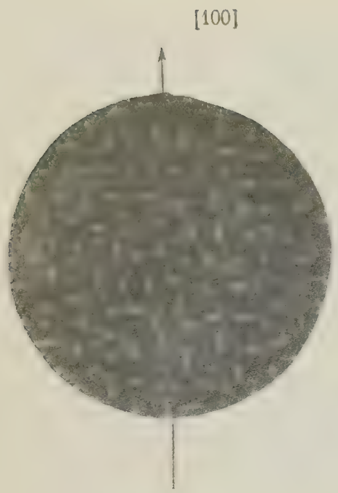

FIG. 3

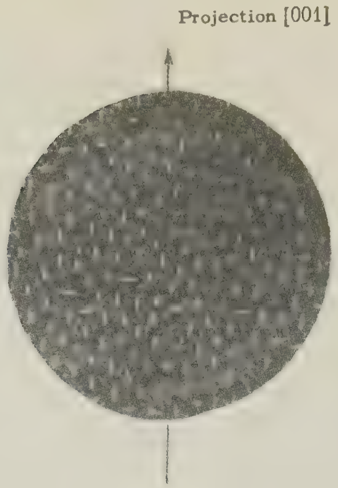

FIG. 4

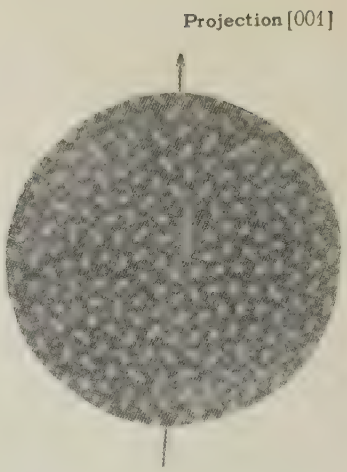

FIG. 5

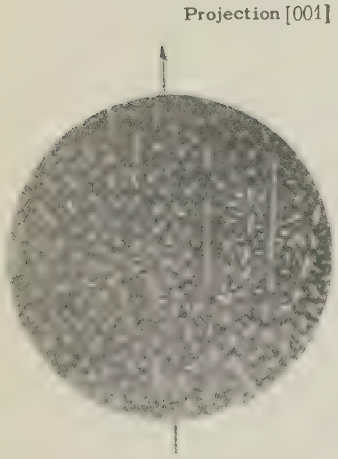

FIG. 6

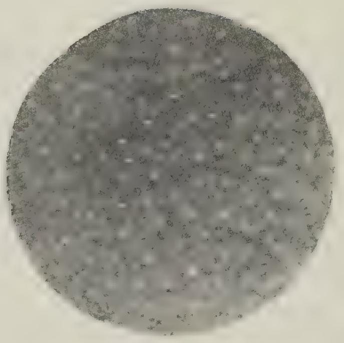

FIG. 7

FIGS. 3–7. Photographs of structures of the intermediate state. White regions are superconducting. Field of view 1.4 cm in diameter. The arrows denote the projections of the crystallographic axes onto the plane of the specimen.

FIG. 3. Specimen 1. $T = 3.04^\circ$, $C_s = 0.08$.

FIG. 4. Specimen 2. $T = 3.24^\circ$, $C_s = 0.17$

FIG. 5. Specimen 9. $T = 3.00^\circ$, $C_s = 0.17$

FIG. 6. Specimen 9. $T = 3.00^\circ$, $C_s = 0.17$. The transition to the intermediate state produced by cooling.

FIG. 7. Filament-like s domains. $T = 3.00^\circ$, $C_s = 0.06$.

on the surface of the specimen as elongated spots, having one or several directions of preferred orientation (Figs. 3–5).

From the condition that the free energy of the system should be a minimum, it follows that in the body of the specimen the s domains must have a cross section approaching circular (with minimum surface area), flattening only at the surface of the specimen (like the end of a screwdriver). This is due to the reduced magnetic field energy, compared with the case of cylindrical regions with the same cross section. For $C_s \to 0$ the observed dimensions of the s domains decrease and no flattening takes place near the surface (see Fig. 7).

When $C_s$ increases, small specks of s phase appear in the structures (the white dots in Figs. 4–6), which are, apparently, a peculiar form of branched structure, also leading to a reduction of magnetic energy.[4]

For $C_s > 0.2$ the structures take on a more involved character, going over for $C_s \to 1$ to a system of wrinkled n domains.[1]

To explain the results obtained we must first discuss the factors that can affect the orientation of the s domains, apart from the anisotropy of $\Delta$ which interests us.

1. The movement of the ns boundaries leads to the production of local eddy currents flowing near the boundaries and hindering the movement. In pure metals, as Faber has shown,[5] the electron mean free path exceeds the thickness of the layer in which the eddy currents flow, i.e., the conditions are analogous to the conditions for the anomalous skin effect. The anisotropy in the rate of growth of the s domains will therefore be related to the anisotropy of the anomalous skin effect in a given metal.

We can judge the influence of this factor by comparing Figs. 5 and 6. In one case (Fig. 6) the specimen was brought into the intermediate state from the normal state. The supercooling produced a rapid growth of long s filaments parallel to the [001] axis. In the second case (Fig. 5) the specimen was originally in the intermediate state, with larger $C_s$ and with a finely dispersed structure. On heating to the required temperature the s domains gradually "crystallized out" in the presence of sufficient nuclei. In this case layers parallel to the [001] axis were encountered very rarely. We made analogous observations on other specimens. We then have grounds for saying that for such a transition the influence of eddy currents on the anisotropy of the structure is small.

We therefore used the second method of transition in all the remaining cases, sometimes also applying a slow temperature oscillation with amplitude ~0.01°, which improved the regularity of the structures.

2. One can also assume an ordering of the structure to result from a correlation in the orientation of the s domains relative to one another, i.e., some "packing" of the domains due to their magnetic interaction. The following facts, however, contradict this suggestion: a) the structures in specimens with different crystal orientations differ from one another, b) in structures of the type shown in Fig. 3, one finds neighboring regions oriented perpendicular to one another as often as parallel, c) the orientation of the s domains is related to the direction of the crystal axes in the specimen.

From the above we deduce that the observed preferred orientation of the s domains is determined primarily by the anisotropy of $\Delta$.

Results obtained with the "frozen-in flux" method. We counted on the photographs the number of regions whose directions lay in consecutive equal intervals of angle, and plotted polar diagrams (Figs. 8 — 10 and 13 — 15) showing the corresponding number in the direction of the normal to the elongated side of the s domain (this direction will be referred to as **n** in what follows). The part of the diagram between 180 and 360° is just a duplicate of the 0 — 180° part. The scale for the number of regions is shown along one of the radii. The appearance of the diagram is independent of $C_s$ for a given specimen.

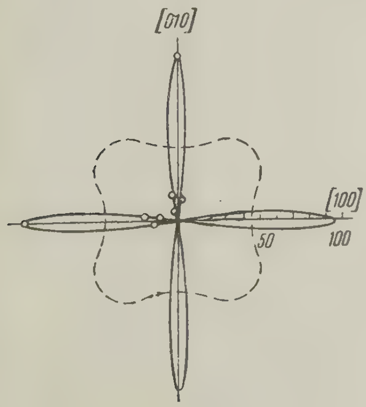

FIG. 8. Specimen 1. T = 3.04°, $C_s$ = 0.08. Angular interval 10°.

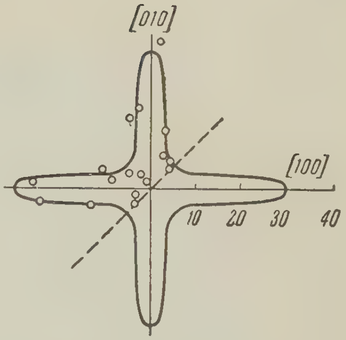

FIG. 9. Specimen 1. T = 3.52°, $C_s$ = 0.12. Angular interval 10°.

We shall consider first the results of experiments for the simplest orientations of the crystallographic axes relative to the specimen surface, and at a temperature relatively far from the critical temperature (T ~ 3°K).

1. Specimen 1. The normal to the surface of the specimen **N** directed along the 4-fold crystal axis [001]. The s domains are equally divided between the equivalent directions [100] and [010] (Figs. 3 and 8). The corresponding polar diagram for $\Delta(\mathbf{n})$ must have two identical minima in these directions, i.e., it must have the form of the dashed curve shown in Fig. 8.

2. Specimen 2 (Fig. 4). The normal **N** close to the [100] axis in direction. The greater part of the s domains is elongated along the [001] axis, but about 15% have a perpendicular direction. It is natural to assume that the polar diagram for $\Delta$ would have, in this case, two minima, one of which is wider and deeper than the other.

3. Specimen 6. The normal **N** parallel to the [110] axis. There are again two preferred orientations along the [001] and [110] directions with roughly the same number of domains.

Figure 11 shows how the structure changes as **N** varies from the [100] to the [110] direction.

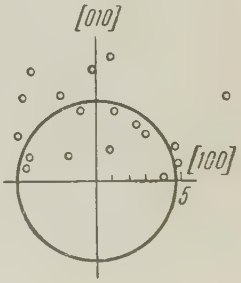

FIG. 10. Specimen 1. T = 3.60°, $C_s$ = 0.16. Angular interval 10°.

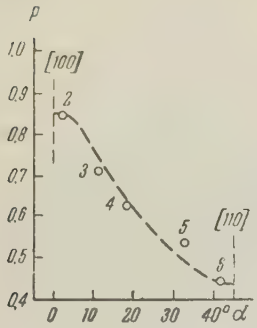

FIG. 11. p – the ratio of the number of domains elongated along the [001] axis, to the total number. The domains are oriented either along the [001] axis or perpendicular to it. The numbers at the points denote the specimen number. T = 3° K, $C_s = 0.1$–$0.2$, α is the angle between the [100] axis and the surface of the specimen.

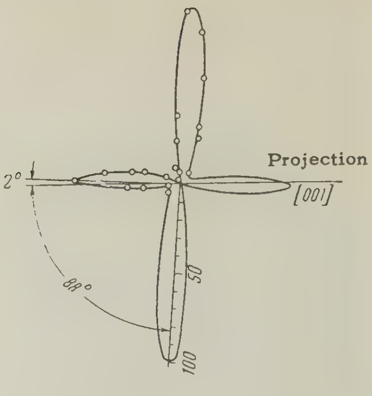

FIG. 13. Specimen 7. T = 3°. Data from four photographs: $C_s = 0.16$; 0.14; 0.14; 0.13. Angular interval 5°.

The magnitude of Δ must in general depend on the direction of the normal **n** to the ns boundary and the direction **i** of the superconductivity current in the boundary layer, i.e., on three angular parameters, in so far as $\mathbf{i} \perp \mathbf{n}$.

Each of the experiments described makes possible a comparison of the values of Δ, for a given direction of **N**, associated with ns boundaries when $\mathbf{n} \perp \mathbf{N}$ and $\mathbf{i} \perp \mathbf{N}$.

We must have additional data, obtained by other methods, in order to connect together the data for specimens with different **N**. In the second part of this work we shall return to this question, but for now, to systematize our qualitative data, we shall make the simplifying assumption that the dependence $\Delta(\mathbf{i})$ for a given **n** is small and can be neglected compared with the variation of $\Delta(\mathbf{n})$.

With this assumption we can describe the $\Delta(\mathbf{n})$ surface qualitatively from our data. Its central sections by planes parallel to the surfaces of the specimen must look like the polar diagrams of Δ for the corresponding experiments.

There is apparently a minimum on the $\Delta|\mathbf{n}|$ surface for $\mathbf{n} \parallel [100]$, since there are minima at this point for two mutually perpendicular sections of the surface by its plane of symmetry (see above, items 1 and 2).

It follows in an analogous way from item 2 (or 3) that for $\mathbf{n} \parallel [001]$ there is a shallower minimum on the surface i.e. $\Delta_{[001]} > \Delta_{[100]}$. These minima are indicated by full circles in the stereographic projection of Fig. 12. The point [110] on the $\Delta(\mathbf{n})$ surface must be the saddle point, according to items 1 and 3.

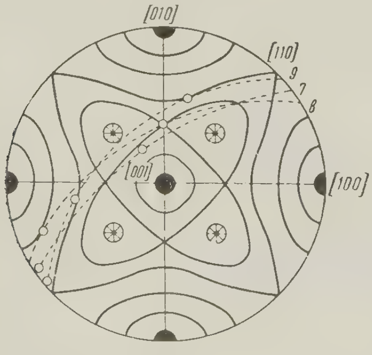

FIG. 12

We should point out that an attempt to represent the results by using the $\Delta(\mathbf{i})$ surface, neglecting the dependence of $\Delta(\mathbf{n})$, would immediately lead to an inconsistency, since then

from item 1 it follows that $\Delta^{[110]} > \Delta^{[100]}$
" " 3 " " " $\Delta^{[110]} \approx \Delta^{[001]}$
" " 2 " " " $\Delta^{[001]} < \Delta^{[100]}$

where the superscript to Δ denotes the direction of the superconductivity current.

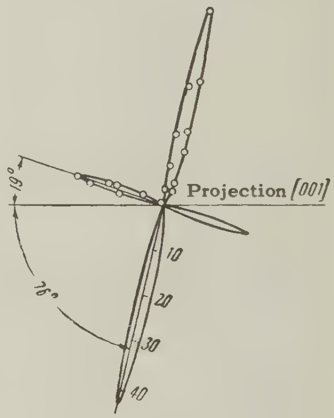

FIG. 14. Specimen 8. T = 2.95°. $C_s = 0.14$. Angular interval 2°.

The form of the $\Delta(\mathbf{n})$ surface can be determined on the basis of experiments with specimens 7, 8, and 9 (Figs. 13 – 15). The circuits corresponding to the surfaces of these specimens are

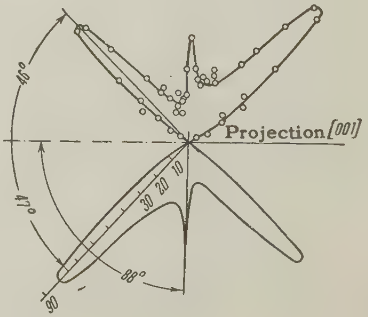

FIG. 15. Specimen 9. T = 3°. Data from four photographs: $C_s = 0.17$; 0.15; 0.09; 0.08. Angular interval 3°.

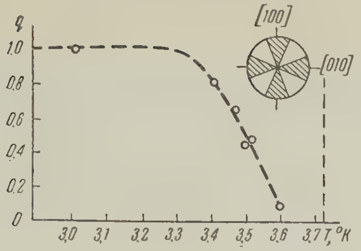

FIG. 16. Specimen 1. $q = (a - b)/(a + b)$, where a is the number of s domains with normals making angles of less than 22.5° with the [100] or [010] axis, i.e., falling within the shaded sectors of the diagram; b is the number of remaining s domains. $C_s = 0.1 - 0.2$.

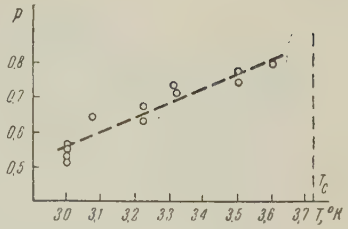

FIG. 17. Specimen 5. p is the ratio of the number of domains elongated along the [001] axis to the total number; p = 0.5 corresponds to equal probability of the two different directions. $C_s = 0.1 - 0.2$.

shown by dashes in Fig. 12, and the points for the relative minima of $\Delta$ in these sections (corresponding to the peaks of Figs. 13 — 15) are shown by the small circles. If we represent the dependence $\Delta(\mathbf{n})$ by using lines of constant $\Delta$, then these lines must touch the dashed curves at the points of relative minimum.

The arbitrariness in drawing the lines of constant $\Delta$ turns out to be insignificant in practice.

The lines of equal $\Delta$, shown in Fig. 12 and obtained from the data on the positions of the peaks in Figs. 13 — 15, also explain a number of other features of these diagrams. For example, the large difference in height between the peaks in Fig. 14 is related to the fact that one of the minima for specimen 8 in Fig. 12 (near the saddle point) lies between two close maxima, and the probability of the s domain falling in this narrow angular interval is small.

The diffuseness and the sharp asymmetry in the form of the peaks in Fig. 15 are related to the fact that the circuit for specimen 9 in Fig. 12 runs almost exactly along a line of constant $\Delta$ far from the [001] axis, and spreads through the maximum in the region between the peaks near the [001] axis.

Let us examine the temperature dependence of the anisotropy of $\Delta$. The data obtained with specimen 1 ($\mathbf{N} \parallel [001]$) show that the anisotropy in this section gradually decreases as $T \to T_c$. With increasing temperature, the polar diagrams of the distribution of s domains become ever more diffuse (see Figs. 8 — 10 and 16). At T = 3.6°K the distribution is practically isotropic, since the disordering action of other factors predominates over the anisotropy of $\Delta$ at this temperature.

On the other hand, we found no noticeable temperature dependence for the structures obtained for $\mathbf{N} \parallel [100]$ up to 3.6°K. The structures obtained with $\mathbf{N} \parallel [110]$ approach the structures for $\mathbf{N} \parallel [100]$ for $T \to T_c$ (see Fig. 17) and become practically identical at T = 3.6°. It became difficult to observe the structures at T = 3.6° because of the small contrast in the pictures (due to the small field $H_c$), and it was not possible to raise the temperature further.

From our observations we can deduce that for $T \to T_c$ the $\Delta(\mathbf{n})$ surface takes on the symmetry of a body of rotation and has a line of minima on the equator. The question of whether the small minimum at the pole is preserved or merges into the maximum is still open.

We will return to a discussion of these results after presenting the second part of the work.

## 2. TORSION BALANCE METHOD

An anisotropy in $\Delta$ must lead to a dependence of the free energy, F, of the specimen in the intermediate state on the direction of the magnetic field relative to the crystallographic axes of the specimen.

If the specimen is hung on a taut thread in a horizontal magnetic field, then by measuring the angle turned through by the thread at equilibrium the mechanical moment $M = -\partial F/\partial\alpha$ can be determined, where $\alpha$ is the angle turned through by the specimen around a vertical axis. The magnitude of M must be related to the anisotropy of $\Delta$ if, of course, the specimen is sufficiently uniform and the "dry friction" forces and irregularities in the external shape of the specimen have no effect.

In our experiments we studied single crystal specimens of tin which were close to spherical in shape. The specimens were cast in a glass former and the deviations from spherical were 2 – 3 $\mu$ in diameter for a mean diameter of about 12.6 mm. After cooling to helium temperatures the specimens approximated to an oblate ellipsoid of revolution with axes differing by 0.1 mm.

The torsion balance, used for measuring the mechanical moment in the intermediate state, was also used to measure the conductivity of metal specimens at helium temperatures (including all the specimens mentioned below) and has been described elsewhere.[6]

TABLE I.

| Specimen No. | | $10^{10}\rho_0$, Ω·cm | Impurity Content, % | $10^4 \mid m \mid_{max}$ (at $T = 3{,}69°$) |
|---|---|---|---|---|
| I | 1c | 0,4 | $<6\cdot10^{-5}$ | 4 |
| | 2c | 0,5 | $8\cdot10^{-5}$ | 3 |
| | 3c | 1,8 | $3\cdot10^{-4}$ | 5 |
| | 4c | 1,6 | $3\cdot10^{-4}$ | 3 |
| II | 5c | 0,4 | $<6\cdot10^{-5}$ | 11, 14* |
| | 6c | 0,5 | $8\cdot10^{-5}$ | 8 |
| | 7c | 0,7 | $1\cdot10^{-4}$ | 10 |
| | 8c | 13 | $2\cdot10^{-3}$ | 12 |
| | 9c | 18 | $3\cdot10^{-3}$ | 8 |

*Two measurements on different days.

The measurements were carried out in the following way. After the required temperature had been established, a small field $H_s$ was switched on and the mechanical moment in the superconducting state, $M_s$, was determined. This moment is related to the deviation of the specimen from a spherical shape, already mentioned. We then determined the critical field $H_c$ by reducing the field gradually to a value $(2/3)H_c$, at which the specimen went over from the intermediate into the superconducting state. This transition was determined by finding when the specimen ceased being carried by the slowly rotating field which induces eddy currents in the normal phase. The specimen was then put into the intermediate state and the moment of the forces acting on it was measured for different directions of the magnetic field in the horizontal plane. All but some preliminary measurements were made at the concentration $C_s = 0.5$, i.e. for $H = (5/6)H_c$.

We took each point twice in order to annul the influence of "dry friction." In one case the specimen, previously inclined to the position of equilibrium, approached it by turning in a clockwise direction, and in the other case by turning in the opposite direction. As far as possible, all conditions were symmetrical in both cases. The approach to the equilibrium position was made very slowly (to prevent eddy currents) and usually took 5 — 6 min. The position reached by the specimen when approaching from different directions did not coincide, and this served as a measure of the magnitude of the "dry friction." We took the mean of the results of the two measurements as the position for true thermodynamic equilibrium. From the value of the moment M obtained, we subtracted the part $M_e$ which was caused by the specimen not being spherical. $M_e$ was determined from the moment $M_s$ in the superconducting state for the same magnetic field direction, using the formula $M_e = 4M_s\,(H_c - H)^2/H_s^2$, which can easily be derived by assuming the specimen to be an ellipsoid that differs little from a sphere. The difference obtained $M - M_e = M_i$ is the quantity required, related to the anisotropy of the structure in the intermediate state. The effect observed was small, so that $M_e$ and $M_i$ were of the same order of magnitude. The deflection of the light spot of the torsion balance was usually not more than 5 — 10 mm and its position was determined with an accuracy of 0.1 to 0.2 mm.

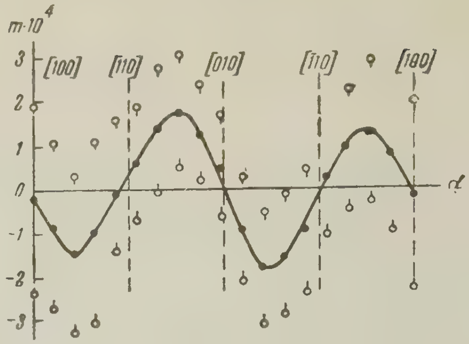

FIG. 18. Spherical specimen 1c. Axis of rotation along [001], T = 3.11°.

Results obtained with the torsion-balance method. We studied nine specimens, the residual resistance $\rho_0$ and the presumed purity of which are shown in the first and second columns of Table I. It appeared that the specimens could be divided into two qualitatively different groups according to the type of curves obtained (group I comprising speciments 1c — 3c and group II specimens 5c — 9c). Within the groups, the differences were more of a quantitative nature.

Specimen 4c was intermediate in its properties.

We shall discuss the properties of specimens of the first group, which appear to approximate more closely to the properties of an ideal uniform single crystal. Specimens 1c and 2c were comparatively similar and gave results in close agreement.

One of the curves obtained with specimen 1c is shown in Fig. 18. The specimen was hung so that the [001] axis was vertical. The abscissa represents the angle, α, between the [100] axis and the magnetic field. The orientation of the specimen relative to the balance was determined by x-ray diffraction. The ordinate gives the mechanical moment $m = 8\pi M_i/H_c^2 V$, where V is the volume of the specimen. The circles show the results of measurement when the equilibrium position is approached from two directions (with a correction for departures from sphericity) and

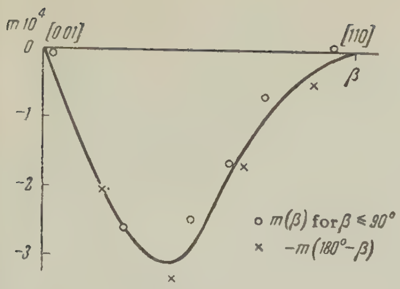

FIG. 19. Spherical specimen 1c. Axis of rotation along $[1\bar{1}0]$, T = 3.13°. Points obtained by averaging over the approach from the left and from the right.

the solid dots and the curve represent the mean. It can be seen from the figure that the moment of the "dry friction" forces $\Delta m$ (i.e., the distance between the upper and lower points) does not depend on direction in a regular way, while the mean moment changes with angle smoothly and is symmetrical with respect to the crystallographic directions.

Assuming that the mean value of m is the equilibrium value, we obtain, apart from an arbitrary constant, $f(\alpha) = -\int m d\alpha$, where f is the free energy of the specimen divided by $VH_c^2/8\pi$. For $\mathbf{H} \| [110]$ f is a maximum; it is a minimum for $\mathbf{H} \| [100]$. For specimen 1c at $T = 3.11°$ $f_{[110]} - f_{[100]} = 7.4 \times 10^{-5}$, where the subscript denotes the direction of the magnetic field.

Figures 19 and 20 show the curves obtained on the same specimen at 3.13° for the cases where the [110] and [100] axes were vertical. Integrating these curves gives $f_{[1\bar{1}0]} - f_{[001]} = 25 \times 10^{-5}$ and $f_{[010]} - f_{[001]} = 21 \times 10^{-5}$. The difference between these two values is $4 \times 10^{-5}$, which agrees in sign and order of magnitude with the value $7.4 \times 10^{-5}$, derived from Fig. 18. For specimen 2c at $T = 3.13°$ the difference $f_{[010]} - f_{[001]} = 23.6 \times 10^{-5}$.

In order to connect these results with the anisotropy of $\Delta$, we have to make some assumptions about the structure of the intermediate state of spherical specimens.

Experiments made by the powder method[1] have shown that a sphere in the intermediate state with $C_S = 0.5$ has a radial layer structure in the region of the magnetic equator and a complicated wrinkled structure elsewhere.

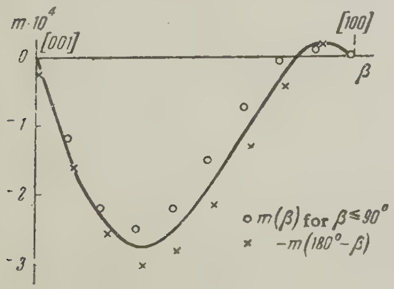

FIG. 20. Spherical specimen 1c. Axis of rotation along [010], T = 3.13°. Points obtained by averaging over the approach from the left and from the right.

If we construct the normals to all the surfaces of separation of the phases within the sphere, their traces on a stereographic projection will appear in a narrow band running along the magnetic equator, since it is known that inside a sphere the field has a constant direction at all points. In what follows we shall assume that the normals lie exactly in the plane of the magnetic equator, that all directions in this plane are equally represented, and that the free energy in the intermediate state is determined by the value of $\overline{\Delta(\mathbf{n})}$, averaged over these directions. It is not difficult to see that with these assumptions the data for f are in qualitative agreement with the form of the $\Delta(\mathbf{n})$ surface, shown in Fig. 12, since averaging $\Delta$ over the great circle (110) must lead to a larger value of $\Delta$ than the circle (100), and the average over (001) to a smaller value of $\Delta$.

For a quantitative measure of the anisotropy of $\Delta$ we need the absolute value of the free energy in the intermediate state. Using Landau's model for the structure of the intermediate state,[7] an expression can be derived for the free energy of a sphere: $f = 2\sqrt{2\varphi\Delta/R}$, where R is the radius of the sphere and $\varphi = 0.0221$ for $C_S = 0.5$*. Substituting $\Delta$ for tin here, equal to $2.3 \times 10^{-5}(1 - T/T_c)^{-1/2}$ cm (see references 2 and 8), we obtain $f = 2.6 \times 10^{-3}(1 - T/T_c)^{-1/4}$. For specimen 1c at 3.13°, for example, we then derive $(f_{[100]} - f_{[001]})/f \approx 6\%$. Since $f \sim \sqrt{\bar{\Delta}}$, the corresponding relative change in $\bar{\Delta}$ must be twice as great i.e. 12%. The change in the unaveraged value of $\Delta$ must be even greater. A rough calculation based on the assumptions about the way of averaging $\Delta$ shows that the relative difference between the maximum value, at the points shown in Fig. 12 by stars, and the minimum at the points [100] is 20 — 25% at 3.1°K.

---

*For the calculation it was assumed that the n domains in a sphere are not branched and are distributed in a radial direction. It was also taken into account that the lines of force make an angle with the surface of the sphere which depends on the magnetic latitude. If the sphere is divided into strips by coaxial cylinders, then the energy enclosed in such a strip per unit surface of the sphere is $F = (H_c^2/2\sqrt{2}\pi) \times \sqrt{\varphi(C_s)\Delta R}\,\sin^2\vartheta$, where $\vartheta$ is the latitude (see reference 2). Integration of this expression gives the formula above. Calculation according to reference 4 shows that neglecting the branching of the layers does not lead to any appreciable error in our case in calculating the free energy (an error of ~10% in the worst conditions, far from $T_c$). We obtain for the period of the structure the expression $a = \sqrt{2R\Delta\varphi}$, independent of latitude. This expression also holds for a cylinder in a transverse field.

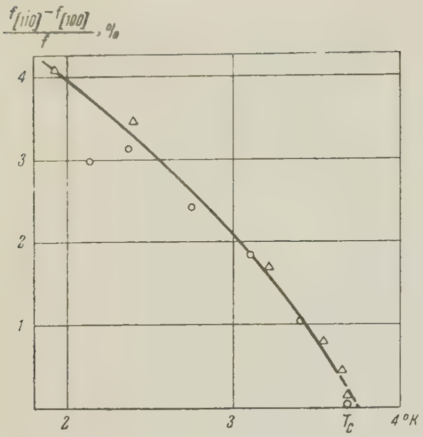

FIG. 21. Rotation about the [001] axis. ○ – specimen 1c, △ – specimen 2c.

The temperature dependence of the effect was different for the various orientations of the specimen in the balance. For rotation around the [001] axis the shape of the curves did not change appreciably with temperature, while the amplitude of the curves and the ratio $(f_{[110]} - f_{[100]})/f$ tended to zero for $T \to T_c$ (see Fig. 21). The curve of Fig. 21 represents, in more accurate form, the behavior also derived by the "frozen-in flux" method (see Fig. 16).

For rotation about the [100] and [110] axes the shape of the curves was slightly different at temperatures far from and close to $T_c$. The ratios $(f_{[010]} - f_{[001]})/f$ and $(f_{[1\bar{1}0]} - f_{[001]})/f$ were little dependent on temperature and apparently tended to a limiting value for $T \to T_c$ (see Table II). We should note that the experimental conditions for a temperature near $T_c$ were worse than for a temperature far from it, and the reproducibility and accuracy of the curves deteriorated. The difference of $2 \times 10^{-2}$ between $(f_{[1\bar{1}0]} - f_{[001]})/f$ and $(f_{[010]} - f_{[001]})/f$ at $T = 3.69°$ comes from the poor reproducibility of the data, in so far as careful direct measurements give $(f_{[110]} - f_{[100]})/f < 0.3\%$. The reason for these disagreements is apparently related to the presence of some sort of lattice defects, the influence of which is more apparent near $T_c$. An analogous phenomenon was found in the same form with the specimens of group II (5c – 9c).

The rather complicated behavior of the specimens of group II is apparently connected with their imperfection, and we will only discuss them briefly to help in substantiating the results obtained with specimens of group I.

The curves obtained for specimens 5c – 9c at $T = 3.69°$ with rotation about the [100] axis were very different from the corresponding curves for the specimens of group I. The value of $m$ became zero in the [001] and [010] directions and at an intermediate point, $\beta = 30 - 40°$ ($\beta$ is the angle with the [001] axis), which was a point of stable equilibrium. The maximum value of $|m|$ was 2 – 4 times greater than $|m|_{max}$ for the specimens of group I (see Table I).

The resemblance between the curves obtained with some of the group II specimens led us at first to the incorrect conclusion[9] that the effect is related to the anisotropy of $\Delta$. It was only after we had managed to obtain the group I specimens that we finally established that the real reason for these curves is apparently the chance plastic deformation of the specimens and the formation of regions with somewhat different values of $H_c$.

This conclusion is borne out by the following facts:

a) For $T \sim 3°$, far from $T_c$, this effect disappears and the curves for rotation about the [100] and [001] axes agree well with the corresponding curves for group I specimens. The relative indeterminacy in the value of $H_c$ must, in fact, decrease with decreasing temperature, since its absolute value is little dependent on $T$ (cf. the data of reference 10).

b) The effect stays at an appreciable magnitude for $C_s \ll 0.5$ (being halved only at $C_s = 0.04$) and is thus connected with a small fraction of the volume of the specimen.

c) A small plastic deformation (rolling it

TABLE II.

| $T°$, K | Specimen No. | Rotation about the [001] axis | | | Rotation about the [110] axis | | |
|---|---|---|---|---|---|---|---|
| | | $10^4 \lvert m \rvert_{max}$ | $10^4 \overline{\Delta m}$ * | $(f_{[010]} - f_{[001]})/f$, % | $10^4 \lvert m \rvert_{max}$ | $10^4 \overline{\Delta m}$ * | $(f_{[110]} - f_{[001]})/f$, % |
| 3.69 | 1c | 4 | 1 | 4.1 | 4.5 | 3.4 | 6,2 |
| 3.69 | 2c | 3 | 1.1 | 3.7 | — | — | — |
| 3.69 | 3c | 5 | 6 | 5.4 | — | — | — |
| 3.13 | 1c | 2,7 | 1.5 | 5.1 | 3,1 | 1,6 | 6.1 |
| 3.13 | 2c | 3 | 0.9 | 5.7 | — | — | — |
| 2.08 | 1c | — | — | — | 3 | 3.8 | 4.7 |

*$\overline{\Delta m}$ is the average value of the "dry friction" forces, i.e., the mean of the difference in the values of m when the equilibrium position is approached from different directions.

lightly on the top of a table) of specimen 4c led to an increase of $|m|_{\max}$ at T = 3.69° to $50 \times 10^{-4}$, i.e. a 16-fold increase.

The observations described lead us to suppose that the anomalous behavior of the group II specimens is to be explained by the existence of some regions of twinning in them. The mechanical twinning plane in tin (301) lies at an angle of ~30° to the [001] axis, which is close to the equilibrium direction of the domains in the specimens of group II.

It seems that measurement of the forces acting on a specimen in the intermediate state might be applicable for showing up small lattice defects, which can not be found by other methods.

The difference between the properties of specimens of groups I and II for T close to $T_c$ serves as some confirmation that the anisotropy of the group I specimens in the intermediate state is not related to lattice imperfections, and is due to the anisotropy of surface tension.

## 3. DISCUSSION OF RESULTS

A. Comparison of the different methods of studying the anisotropy of Δ. A comparison of the results obtained by the two methods described above shows that they are in satisfactory agreement and partly complement each other. The "frozen-in flux" method enables one to build up a qualitative picture of the anisotropy of Δ at temperatures far from $T_c$, which is confirmed by the data obtained with the torsion balance. We should point out that these two methods are independent, since in the first the energies of separate s domains within one structure are compared for a given magnetic field direction, while in the second the energies of a structure as a whole are compared for different field directions.

A consideration of the results obtained by both methods leads to the conclusion that, in the temperature range studied, the dependence of Δ on the direction of the normal to the surface of separation is greater than the dependence on the current direction. In any case, the dependence $\Delta(\mathbf{n})$ derived is quite enough to explain all the observations, while consideration of the dependence $\Delta(\mathbf{i})$ alone, neglecting the dependence on **n**, leads to inconsistencies. This deduction, for a temperature of 3°K, was made in the first part of this work. Near $T_c$ the "frozen-in flux" method shows only that the orientation of layers with $\mathbf{n} \perp [001]$ and $\mathbf{i} \parallel [001]$ are more favorable, i.e., that the surface of $\Delta(\mathbf{n})$ is prolate, or that of $\Delta(\mathbf{i})$ is oblate, in the [001] direction. The torsion balance method yields $f_{[100]} - f_{[001]} > 0$, from which it follows that the surface of $\Delta(\mathbf{n})$ or $\Delta(\mathbf{i})$ is drawn out. For agreement between the results we must therefore introduce a dependence $\Delta(\mathbf{n})$.

The nature and magnitude of the dependence of Δ on the current direction can only be decided experimentally from a more detailed and exact quantitative investigation of the anisotropy of Δ. In principle this could be achieved by measuring the period of the structures in a flat specimen located in an inclined magnetic field. It would be a fairly difficult task to carry out these measurements with sufficient accuracy and completeness, and might only be undertaken after a preliminary qualitative study.[3]

B. Comparison of the results with theory. It seems to us that the most important result from the theoretical point of view is the anisotropy of Δ found in the (001) plane, perpendicular to the four-fold symmetry axis of the crystal. A theory based on the existence of a local tensor relation between current and field, should for such a high degree of symmetry lead to the absence of anisotropy in this plane (see Ginzburg and Landau[11,12]). The existence of anisotropy is evidence of the existence of a non-local correlation between current and field in a superconductor.

The existence of such a correlation, predicted by Pippard,[13] is one of the main points of the microscopic theory of superconductivity due to Bardeen, Cooper, and Shrieffer[14] and to Bogolyubov.[15] The electrodynamics of anisotropic superconductors, taking into account such a correlation, has not yet been worked out. We cannot, therefore, compare our results with data on the anisotropy of other properties of superconductors, especially since such information is very scanty. Bezuglyi et al.[16] and Morse et al.[17] have investigated the anisotropy in the absorption of sound in tin, and Pippard[18] and Schawlow and Devlin[19] have studied the anisotropy of penetration depth δ.

It appears that the gradual disappearance of the anisotropy of Δ in the (001) plane, as the temperature approaches $T_c$, is related to the increase in thickness of the transition layer between the phases, equal to Δ in order of magnitude, as compared with the parameter ξ that characterizes the distance over which a non-local correlation exists. In so far as ξ is independent of temperature, $\xi/\Delta \sim \sqrt{T_c - T}$ for $T \to T_c$. As can be seen from Fig. 21, $(f_{[110]} - f_{[100]})/f$ tends to zero apparently linearly with $T_c - T$. Thus

$$(\Delta_{[110]} - \Delta_{[100]})/\Delta \sim (\xi/\Delta)^2 \text{ for } T \to T_c.$$

For small $\xi/\Delta$ the connection between current and field can be considered local and the relation between the anisotropy of $\Delta$ and $\delta$ can be found from the phenomenological theory of Ginzburg and Landau. The anisotropy of superconductivity can then be described by introducing the effective mass tensor for the superconducting electrons.[12] We confine ourselves to the simplest case, when the normal to the phase boundary is directed along one of the principal axes of the mass tensor, z, and the current flows along another principal axis x.

In the isotropic case $\Delta = \delta_0\alpha(\kappa)/\kappa$ where $\delta_0$ is the penetration depth for $H \rightarrow 0$, and[20] $\kappa = 4.32 \times 10^7 H_c\delta_0^2$. Values of $\alpha(\kappa)/\kappa$ were tabulated by Ginzburg,[21] and $\alpha(\kappa) \rightarrow 1.89$ for $\kappa \rightarrow 0$.

It can be shown easily that in the anisotropic case

$$\Delta_z^x = \delta_{0x}\alpha(\varkappa\ _z)/\varkappa_{xz},$$

where $\kappa_{xz} = 4.32 \times 10^7 H_c\delta_{0x}\delta_{0z}$, $\delta_{0k} = (m_k c^2/4\pi e^2 n_s)^{1/2}$, $m_k$ is the effective mass along the principal axis k, and $n_s$ is the concentration of superconducting electrons. Thus $\Delta_z^x \sim \alpha(\kappa_{xz})\delta_{0z}$ and since $\alpha$ is relatively weakly dependent on $\kappa$, $\Delta_z^x$ is mainly determined by the effective mass and by the direction of the normal to the phase interface.

For tin

$$\frac{\partial\Delta_z^x}{\partial\delta_{0z}}\,\delta_{0z} \Big/ \frac{\partial\Delta_z^x}{\partial\delta_{0x}}\,\delta_{0x} \approx 3.5,$$

i.e. the dependence of $\Delta_z^x$ on $\delta_{0x}$ is 3 — 4 times less than the dependence on $\delta_{0z}$. Our data confirm this result qualitatively.

It will be possible to compare our results quantitatively with these relations when we have data on the temperature dependence of the anisotropy of $\Delta$ for $T_c - T \sim 0.1 - 0.01°$, where the tensor representation of the anisotropy is applicable.

We are very grateful to Academician P. L. Kapitza for his interest in the work and to A. I. Shal'nikov for a detailed discussion of the results.

[1] B. M. Balashova and Yu. V. Sharvin, JETP **31**, 40 (1956), Soviet Phys. JETP **4**, 54 (1957).

[2] Yu. V. Sharvin, JETP **33**, 1341 (1957), Soviet Phys. JETP **6**, 1031 (1958).

[3] A. G. Meshkovskiĭ, JETP **19**, 54 (1949).

[4] E. M. Lifshitz and Yu. V. Sharvin, Dokl. Akad. Nauk. SSSR **79**, 783 (1951).

[5] T. E. Faber, Proc. Roy. Soc. **A223**, 174 (1954).

[6] V. B. Zernov and Yu. V. Sharvin, JETP **36**, 1038 (1959), Soviet Phys. JETP **9**, 737 (1959).

[7] L. D. Landau, JETP **7**, 371 (1937).

[8] Yu. V. Sharvin, JETP **38**, 1 (1960).

[9] Yu. V. Sharvin and V. L. Sedov, JETP **29**, 897 (1955), Soviet Phys. JETP **2**, 771 (1956).

[10] Kan, Lazarev, and Sudovtsov, JETP **18**, 825 (1948).

[11] V. L. Ginzburg and L. D. Landau, JETP **20**, 1064 (1950).

[12] V. L. Ginzburg, JETP **23**, 236 (1952).

[13] A. B. Pippard, Proc. Roy. Soc. **A216**, 547 (1953).

[14] Bardeen, Cooper, and Schrieffer, Phys. Rev. **108**, 1175 (1957).

[15] N. N. Bogolyubov, JETP **34**, 58 (1958), Soviet Phys. JETP **7**, 41 (1958).

[16] Bezuglyi, Galkin, and Korolyuk, JETP **36**, 1951 (1959), Soviet Phys. JETP **9**, 1388 (1959).

[17] Morse, Olsen, and Gavenda, Phys. Rev. Letters **3**, 15 (1959).

[18] A. B. Pippard, Proc. Roy. Soc. **A203**, 98 (1950).

[19] A. L. Schawlow and G. E. Devlin, Bull. Am. Phys. Soc. **4**, 224 (1959).

[20] L. P. Gor'kov, JETP **36**, 1918 (1959), Soviet Phys. JETP **9**, 1364 (1959).

[21] V. L. Ginzburg, JETP **30**, 593 (1956), Soviet Phys. JETP **3**, 621 (1956).

Translated by R. Berman
282

SOVIET PHYSICS JETP VOLUME 11, NUMBER 5 NOVEMBER, 1960

# *ELASTIC SCATTERING OF 8.5-Bev PROTONS ON PROTONS*

P. K. MARKOV, É. N. TSYGANOV, M. G. SHAFRANOVA, and B. A. SHAKHBAZYAN

Joint Institute for Nuclear Research

Submitted to JETP editor December 31, 1959

J. Exptl. Theoret. Phys. (U.S.S.R.), **38**, 1471-1475 (May, 1960)

Elastic pp scattering at 8.5 Bev was studied by the emulsion technique. The irradiation geometry employed was such that the incident-proton beam was perpendicular to the emulsion plane. A total of 145 elastic scattering events were detected, of which 66 have been previously reported.[1] The contribution of scattering on quasi-free photons and of other "background" events comprises approximatelt 1%. The total elastic cross section in the c.m.s. is found to be ( 8.6 ± 0.8 ) mb. A differential cross section down to one degree in the c.m.s. has also been obtained. The results can be made consistent with the model of a homogeneous semi-transparent ball with a refractive index not equal to unity.

## SETUP OF THE EXPERIMENT

PRELIMINARY data on elastic pp scattering at 8.5 Bev have been published earlier.[1] The present work was performed with a $10 \times 10 \times 2$ cm chamber made up of type NIKFI-BR emulsions 400 microns thick and irradiated in the Joint Institute proton synchrotron by the internal 8.5-Bev proton beam, incident perpendicular to the emulsion plane. Special analyses made for the hydrogen content in control emulsions have shown that the hydrogen content was $(2.90 \pm 0.06) \times 10^{22}$ atoms per cubic centimeter of exposed emulsion.

Area scanning was carried out with an immersion objective at a magnification 630×, in the $2 \times 2$ cm central portion of the emulsion. The average flux density in this zone was $(1.97 \pm 0.05) \times 10^5$ particles per square centimeter. A total of 3.35 cubic centimeters of emulsion was scanned.

To determine the effectiveness of finding the investigated events and to increase the reliability of the results, the aforementioned volume was scanned twice. The stars outwardly resembling elastic pp scattering were separated from all the obtained two-prong stars. Their number was 799. These events were divided in the following three groups, depending on the range of the slow proton: 1) $10\,\mu \leq R < 100\,\mu$, 2) $100\,\mu \leq R < 20{,}000\,\mu$, 3) $R \geq 20{,}000\,\mu$.

The tracks of the slow protons in the first two groups were practically "black," since the sensitivity of the emulsion was high ( $J/J_{\min} = 40$ grains/100 $\mu$). The efficiency of the double scanning was found to be ( 85 ± 3 ) %, ( 92.5 ± 0.8 ) %, and ( 78 ± 5 ) % for events in the first, second, and third groups respectively.

## ANALYSIS OF THE DETECTED EVENTS AND MEASUREMENT PROCEDURE

The following criteria were used to identify the cases of elastic scattering on free hydrogen:

1. The relation between the range R of the recoil proton and its angle with the direction of the primary photon, $\varphi$, satisfies the kinematics of elastic scattering.
2. The angle $\gamma$ between the planes passing through the direction of the primary proton and the direction of emergence of the secondary particles is zero ( coplanarity condition ).
3. The relation between the range of the recoil proton and the angle $\psi$ that the scattered proton makes with the direction of the primary particle satisfies the kinematics of elastic scattering.
4. No recoil nucleus or $\beta$ electron is observed at the point of scattering.

The relation between the angle of the scattered proton and the angle of the recoil proton, which holds for elastic scattering, was used when the recoil proton did not stop in the chamber and its momentum, determined by ionization measurements, was known to be in considerable error.

The range of the recoil proton was measured accurate to 5%.

The principal error in the determination of the angle of emission of the recoil proton was due to the inaccuracy in the measurement of the dip angle. On the average this error does not exceed 1.5 or 2 deg, for cases when the recoil proton has a short range ( $R < 500\,\mu$ ).

The angle of emission of the scattered proton, $\psi$, was measured in the following manner. A reference track of a primary proton that did not experience interaction was selected within 20 or 30 microns of the point of scattering. To determine the scattering angle $\psi$, four measurements were made of the x and y projections of the distance from the reference track to the scattered track, in the plane of the emulsion (parallel to the marker lines). We made two measurements to the point of scattering on a $2000\text{-}\mu$ base (that is, through five emulsions), and two past this point, on the same base. The accuracy with which the projections were measured was approximately $1\,\mu$, so that these scattering angles could be measured accurate to 2′ or 3′. To exclude random errors, independent measurements were made relative to the three reference tracks.

The angle of non-coplanarity $\gamma$ was determined from these measurements. The error in $\gamma$ was due essentially to the error of measurement of the angle of the scattered proton, and dependent on the value of this angle. Thus, for $\psi = 1$ deg, the error in the non-coplanarity angle is 3 deg if $\Delta\psi = 3'$. As shown earlier,[1] at the prevailing measurement accuracies the contribution of the number of quasi-elastic scatterings should be approximately 1%.

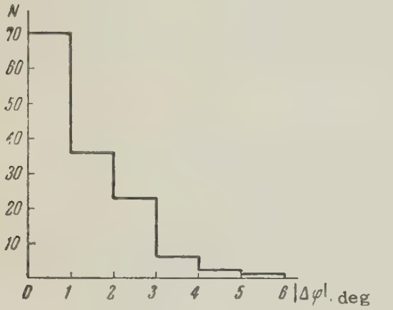

FIG. 1. Distribution of |Δφ| in scattering events: Δφ – difference between the measured angle of the recoil proton and the angle that corresponds to its range in the elastic scattering kinematics.

The measurement errors were estimated for each measured event and the events satisfying the kinematics of elastic scattering within the tripled errors were selected. Figures 1 to 3 show the distributions of $|\Delta\varphi|$, $\Gamma = |\gamma/\Delta\gamma|$, and $|\Delta\psi|$ for these events. It follows from Fig. 1 that the mean-square error in the measurement of $\varphi$ amounts to ~ 2 deg.

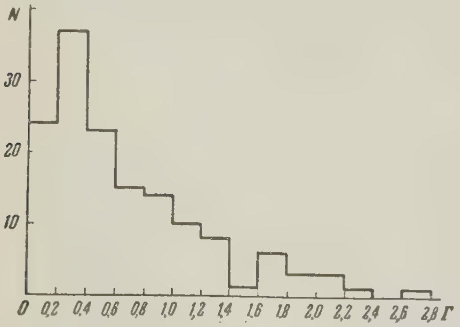

FIG. 2. Distribution of $\Gamma = |\gamma/\Delta\gamma|$ in elastic scattering events; where $\gamma$ is the non-coplanarity angle and $\Delta\gamma$ is the error in its determination.

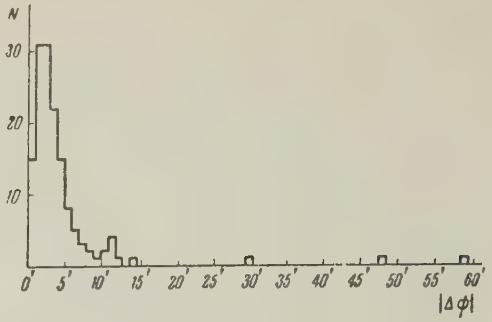

FIG. 3. Distribution of $|\Delta\psi|$ in events chosen in accordance with the first two criteria (ratio of R to $\psi$ and the coplanarity). $\Delta\psi$ – difference between the angle of the scattered proton and the angle corresponding to the range of the recoil proton in the elastic scattering kinematics.

From the distribution of $\Gamma$ in the selected cases it is seen that the errors in the distributions of the non-coplanarity angle $\Delta\gamma$ have been correctly estimated. For the histogram of Fig. 3, we selected, by the first two criteria, the cases satisfying the kinematics of elastic scattering within the limits of the tripled mean-square error. The histogram includes also those cases of scattering by quasi-elastic protons, for which the momentum lies in the scattering plane and is perpendicular to the incident proton, inasmuch as such cases were not identified by the first two criteria. A considerable fraction of such cases falls within the region $|\Delta\varphi| > 12'$ (that is, past the tripled half-width of the distribution), where there are no cases of scattering by free protons. From the number of such events one can estimate the contribution of quasi-elastic cases and other background in the region $|\Delta\varphi| < 12'$. This contribution is found to be approximately 1%.

## RESULTS AND DISCUSSION

The technique employed (irradiation of emulsions at right angle to their plane) and the corresponding measurement procedure have made it possible to obtain the c.m.s. differential cross sections down to 1 deg, to separate reliably the quasi-elastic events from the background, and to accumulate considerable data in a relatively short time.

A total of 145 events satisfied the selection criteria within the limit of tripled mean-squared errors. This is several times more than in other emulsion investigations of elastic scattering in the energy range ≳ 1 Bev (see references 2 – 4).

After estimating the contribution of quasi-elastic processes, discarding the cases of scattering by small angles (≤ 1 deg in the c.m.s.), and estimating the scanning efficiency, the value obtained for the cross section of elastic interaction was found to be $\sigma_{\mathrm{el}} = 8.5 \pm 0.8$ mb.

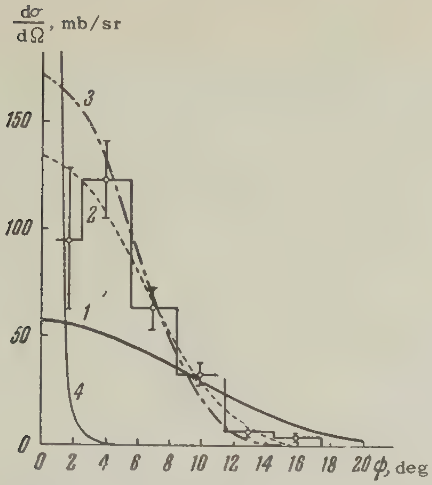

FIG. 4. Differential cross section of elastic pp scattering at 8.5 Bev (histogram). $\psi$ – scattering angle in c.m.s. Calculated curves: 1 – Coulomb scattering, 2 – disc for R = 0.94 f and a = 0.453; 3 – homogeneous semi-transparent sphere, R = 1.5 f, $k = 0.12 \times 10^{13}$ cm$^{-1}$, $k_1 = 0.15 \times 10^{13}$ cm$^{-1}$, U = 34 Mev, and V = 27 Mev; 4 – homogeneous semi-transparent sphere, R = 1.7 f, $k = 0.12 \times 10^{13}$ cm$^{-1}$, $k_1 = 0.12 \times 10^{13}$ cm$^{-1}$, U = 22 Mev, and V = 22 Mev.

Figure 4 shows, in the form of a histogram, the differential cross section for elastic pp scattering in the c.m.s. The heavy solid curve shows the angle of distribution obtained by using the model of a purely-absorbing disc with the following parameters: disc radius $R = 0.94 \times 10^{-13}$ cm, amplitude of passing wave A = 0.453, cross sections for elastic and inelastic interaction $\sigma_{el} = 8.5$ mb and $\sigma_{in} = 22$ mb. It is seen from the figures that the experimental data cannot be explained within the framework of this model. Nor can these data be explained by any other model of a purely absorbing proton, when, without allowance for the spin dependence, the differential cross section at zero angle is given by the optical theorem

$$|\operatorname{Im} f(0)|^2 = (\sigma_t / 4\pi\lambda\!\!\!^-)^2$$

and is found to be considerably less than the experimental value. In this respect, our results disagree with the conclusions of other experiments carried out at lower energies. Thus, for example, in the work by Cork et al.,[5] in which elastic scattering at 6.15 Bev is investigated, the differential cross section is extrapolated from 7.6 deg to the value for 0 deg given by the optical theorem. However, if we plot $k_c \sin\theta$ vs. $k_c^{-2} d\sigma/d\Omega$ instead of our differential cross section (as is usually done to compare experiments at different energies) the experimental data of reference 5 and ours are found to be in satisfactory agreement. The point is that our experimental data disagree with the proton model proposed by the authors of reference 5 only in the range of angles from 0 to 7.6 deg, for which there are no experimental data in reference 5.

The agreement with the data of Kalbach et al.[3] and the model of the purely-absorbing disc may be due to the insufficient statistical accuracy.

In view of the results obtained, we see no full justification for approaching the analysis of the data on elastic scattering of protons by protons by assuming a pure imaginary scattering amplitude.[6]

In reference 7 it has been shown that the model of the purely absorbing proton, in the energy range above 6 Bev, does not contradict the available experimental data. Our data, obtained at smaller scattering angles, indicate that it is also necessary to take into account the real part of the scattering amplitude.

We have performed the calculations using the model of the homogeneous sphere with a complex coefficient of refraction.[6] As seen from Fig. 4, the experimental data are in satisfactory agreement with the calculations for a sphere having the following parameters:

$$R = (1.5 \text{ to } 1.7) \cdot 10^{-13}\,\text{cm}$$
$$k = (0.191 \text{ to } 0.125) \cdot 10^{13}\text{cm}^{-1}, \quad k_1 = (0.155 \text{ to } 0.125) \cdot 10^{13}\text{cm}^{-1},$$
$$U = (34.1 \text{ to } 22.3)\,\text{Mev}, \quad V = (27.5 \text{ to } 21.8)\,\text{Mev},$$

where R is the radius of the sphere, k and $k_1$ describe the absorption and refraction coefficients respectively, and U and V are the imaginary and real parts of the potential inside the sphere.

Figure 4 shows also the differential cross section of the Coulomb interaction (thin solid line). It is seen that at angles greater than 2.5 deg the effect of the Coulomb interaction is very small and can be neglected. In the interval from 1.0 to 2.5 deg, experiment yields a differential cross section somewhat smaller than that predicted by the model of the homogeneous sphere, although the efficiency of finding the scattering is sufficiently high here and is known with good accuracy. If the result is confirmed after the statistical errors have been reduced, it will be possible to attribute it to the interference of the Coulomb interaction with the nuclear interaction.

The large value of the differential cross section at 0 deg does not contradict the model of a purely absorbing proton, if a great difference is assumed in the interaction cross sections for the singlet and triplet states. It is therefore of interest to investigate the role of the spin interactions in elastic pp scattering at 8.5 Bev. This has been done in simplest form by one of the authors (Shakhvazyan)[9] for the model of a purely absorbing proton (pure imaginary scattering phase shifts) with allowance for the spin-spin interaction.

In this case the scattering matrix is independent of the total angular momentum J (see reference 6) and has the form

$$R_l = \eta_l - 1, \quad 0 \leqslant \eta_l \leqslant 1.$$

The last inequality yields expressions for the upper limits of the coefficients of the curve that approximates the experimental points. A phase-shift analysis[9] carried out under the same assumptions both for different mixtures of singlet and triplet states, and for purely singlet states, leads to values of $\eta_l$ which do not satisfy the inequality. This circumstance allows us to state that in the approximation of reference 6 the experimental results cannot be explained by the model of a purely absorbing proton which allows for the spin-spin interaction.

The authors are very pleased to express deep gratitude to D. I. Blokhintsev, V. I. Veksler, M. Danysz, M. I. Podgoretskiĭ, I. Ya. Pomeranchuk, Ya. A. Smorodinskiĭ, and K. D. Tolstov for numerous valuable discussions of the results and for interest in the work. The authors thank the proton synchrotron crew of the Joint Institute for Nuclear Research for irradiating the emulsion chamber, and the staff of the emulsion scanning section of the High-Energy Laboratory of the Joint Institute for Nuclear Research. The authors also thank L. G. Popova, V. A. Nikitin, and V. A. Sviridov for aid in processing the experimental data, to the crew of the "Ural" computer (Laboratory of Technical Physics, Joint Institute for Nuclear Research) and also T. F. Grabovskaya and O. A. Ignatenko for scanning and measurements.

[1] Lyubimov, Markov, Tsyganov, Cheng, and Shafranova, JETP **37**, 310 (1959), Soviet Phys. JETP **10**, 219 (1960). Preprint, Joint Inst. Nuc. Res. R-339.

[2] W. D. Walker, Phys. Rev. **108**, 872 (1957). W. D. Walker and J. Crussard, Phys. Rev. **98**, 1416 (1955); Phys. Rev. **104**, 526 (1956).

[3] Kalbach, Lord, and Tsao, Phys. Rev. **113**, 330 (1959).

[4] Duke, Lock, March, Gibson, McEwen, Hughes, and Muirhead, Phil. Mag. **2**, 204 (1957).

[5] Cork, Wenzel, and Causey, Phys. Rev. **107**, 859 (1957).

[6] Ito, Minami, and Tanaka, Nuovo cimento **8**, 135 (1958); **9**, 208 (1958). V. G. Grishin and I. S. Saitov, JETP **33**, 1051 (1957), Soviet Phys. JETP **6**, 809 (1958). V. G. Grishin, JETP **35**, 501 (1958), Soviet Phys. JETP **8**, 345 (1959).

[7] Grishin, Saitov, and Chuvilo, JETP **34**, 1221 (1958), Soviet Phys. JETP **7**, 844 (1958). V. S. Barashenkov and Huang Nen-Ning, JETP **36**, 832 (1959), Soviet Phys. JETP **9**, 587 (1959).

[8] Fernbach, Serber, and Taylor, Phys. Rev. **75**, 1352 (1949).

[9] B. A. Shakhbazyan. Analysis of Elastic Proton-Proton Scattering at 8.5 Bev. Preprint, Joint Inst. Nuc. Res. D-450, 1959.

Translated by J. G. Adashko
283

SOVIET PHYSICS JETP VOLUME 11, NUMBER 5 NOVEMBER, 1960

# THE EINSTEIN STATICS IN CONFORMAL SPACE

V. A. FOCK

Physical Institute, Leningrad University

Submitted to JETP editor December 21, 1959

J. Exptl. Theoret. Phys. (U.S.S.R.) **38**, 1476-1485 (May, 1960)

A new definition is proposed for a three-dimensional spatial metric that corresponds to a given four-dimensional space-time metric. The space with a metric so defined is called conformal space. It is shown that the equations of the Einstein statics in conformal space are simple in form and lead to definite expressions for the energy density and for the gravitational tensions. Cases of spherical and axial symmetry are considered. It is pointed out that the concept of conformal space can be useful in the general non-static case as well.

## INTRODUCTION

IN the Einstein theory of gravitation, the static is characterized, as is well known, by the fact that the fundamental tensor does not depend upon time and its mixed coefficient components are equal to zero. In this case, the time coordinate is determined uniquely (it is harmonic). For the spatial coordinates, there remains the group of their transformations among themselves. Therefore, it is natural here to make use of the apparatus of three-dimensional tensor analysis and to write the equations of gravity in corresponding fashion. This has also been done by Levi-Civita.[1] However, no attention was paid in these researches to the fact that complete separation of space and time, which is possible in the static case, can be achieved by different means. Usually a metric corresponding to the spatial part of $ds^2$ is attributed to the space. In other words, it is tacitly assumed that the square of the spatial interval must enter into the expression for the square of the four-dimensional interval with the coefficient $(-1)$. But one can introduce another assumption. In the present paper, we shall show that the most natural one is this capability of separation of space and time, in which the metric of the space is conformally connected with the metric usually employed, in such a way that the coefficient mentioned will not be constant but will be a quantity inversely proportional to the coefficient in front of the square of the differential of the time.

A space with a metric defined in such a fashion — we shall call it conformal space — posseses many significant properties. First of all, it is approximately Euclidean; one can assume it to be Euclidean with much greater accuracy than in the usual definition of the spatial metric. In this case, the coordinates, harmonic in a four-dimensional sense, will be harmonic also in a three-dimensional sense (which, as is well known, does not hold in the usual definition of the metric of space). The well-known previous solutions of the equations of Einstein with spherical and axial symmetry (the solutions of Schwartzschild, Weyl, and Levi-Civita) are obtained in especially simple fashion if one starts out from the equations of gravity in conformal space. A further advantage of conformal space is the fact that the equations of Einstein written for it, without any artificial hypothesis, lead to definite expressions for the energy density and for gravitational tensions.

## 1. THE TRANSFORMATION OF LEVI-CIVITA

Let us consider the formulation of the Einstein statics proposed by Levi-Civita (see references 1 and 2).

The static case is characterized by the well-known equations*

$$\frac{\partial g_{\mu\nu}}{\partial t}=0, \qquad g_{0i}=0, \qquad (x_0=t), \tag{1.1}$$

such that if we set†

$$g_{00}=c^2V^2, \qquad g_{ik}=-a_{ik}, \tag{1.2}$$

then one can write the quantity $ds^2$ in the form

$$ds^2=c^2V^2\,dt^2-a_{ik}\,dx_i\,dx_k. \tag{1.3}$$

---

*The Greek letters $\mu$, $\nu$, etc., take on the values 0, 1, 2, 3; the Latin letters i, k, etc., take on the values 1, 2, 3.

†In distinction from the notation used in references 1 and 2, we now write the coefficient for $dt^2$ in the form $c^2V^2$, and not in the form $V^2$.

Levi-Civita proposed to express all the four-dimensional quantities entering into the Einstein equations in terms of three-dimensional quantities referred to a space with the square of the linear element

$$dl^2 = a_{ik}\,dx_i\,dx_k. \tag{1.4}$$

By this means, in particular, a relation is obtained between the four-dimensional curvature tensor $(R_{\mu\nu})_g$, constructed from the fundamental tensor $g_{\mu\nu}$ and the three-dimensional curvature tensor $(R_{ik})_a$ constructed from the $a_{ik}$. For the spatial components, we have

$$(R_{ik})_g = (R_{ik})_a + \frac{(V_{ik})_a}{V}, \tag{1.5}$$

where $(V_{ik})_a$ is the second covariant derivative of $V$ in the sense of the metric (1.4). The mixed components are equal to zero, while the time component is equal to

$$R_{00} = -c^2V(\Delta V)_a, \tag{1.6}$$

where

$$(\Delta V)_a = a^{ik}(V_{ik})_a \tag{1.7}$$

is the Laplace operator in the sense of (1.4). The gravitational equations of Einstein can be transformed by means of these expressions. The corresponding formulas are given in the book of Levi-Civita,[1] and also in our book.[2]

## 2. TRANSITION TO CONFORMAL SPACE

In contrast with Levi-Civita, we represent the square of the four-dimensional interval in the form

$$ds^2 = c^2V^2\,dt^2 - \frac{1}{V^2}h_{ik}\,dx_i\,dx_k \tag{2.1}$$

and write the spatial metric

$$d\sigma^2 = h_{ik}\,dx_i\,dx_k, \tag{2.2}$$

so that

$$ds^2 = c^2V^2dt^2 - \frac{1}{V^2}d\sigma^2. \tag{2.3}$$

Thus, we have

$$g_{00} = c^2V^2, \qquad g_{0i} = 0, \qquad g_{ik} = -\frac{h_{ik}}{V^2}, \tag{2.4}$$

and also

$$g^{00} = \frac{1}{c^2V^2}, \qquad g^{0i} = 0, \qquad g^{ik} = -V^2h^{ik} \tag{2.5}$$

and, finally,

$$\sqrt{-g} = \frac{c}{V^2}\sqrt{h}, \tag{2.6}$$

where $h$ is the determinant composed of the $h_{ik}$. All the three-dimensional quantities will be related to the metric (2.2). From a comparison of (1.3) with (2.1), we obtain

$$dl^2 = \frac{1}{V^2}d\sigma^2 \tag{2.7}$$

and, consequently,

$$a_{ik} = \frac{1}{V^2}h_{ik}, \qquad a^{ik} = V^2h^{ik}. \tag{2.8}$$

Thus, both the spaces (1.4) and (2.2) are conformal to one another. According to the general formula of Finzi (see reference 1), for two such spaces, the covariant components of the curvature tensor of fourth rank are related by the equation

$$V^2(R_{kj,\,li})_a = R_{kj,\,li} + h_{kl}\frac{V_{ij}}{V} - h_{ki}\frac{V_{lj}}{V} + h_{ij}\frac{V_{kl}}{V} - h_{li}\frac{V_{ik}}{V} + (h_{ki}h_{jl} - h_{kl}h_{ji})\frac{V_mV^m}{V^2}. \tag{2.9}$$

On the right hand side of this formula, as in the following formulas, all the three-dimensional tensor symbols refer to the metric (2.2). It follows from Eq. (2.9) that

$$(R_{ik})_a = R_{ik} - \frac{V_{ik}}{V} + h_{ik}\left(-\frac{\Delta V}{V} + 2\frac{V_jV^j}{V^2}\right). \tag{2.10}$$

On the other hand, for the second covariant derivatives of some quantity W, we have

$$(W_{ik})_a = W_{ik} + \frac{V_i}{V}W_k + \frac{V_k}{V}W_i - h_{ik}\frac{V^jW_j}{V} \tag{2.11}$$

and, if W = V,

$$(V_{ik})_a = V_{ik} + \frac{2V_iV_k}{V} - h_{ik}\frac{V^jV_j}{V}. \tag{2.12}$$

Then,

$$(\Delta V)_a = V^2\left(\Delta V - \frac{V_jV^j}{V}\right). \tag{2.13}$$

With the help of (2.10) and (2.12), Eq. (1.5) gives the following expression for the spatial components of the four-dimensional curvature tensor of second rank

$$(R_{ik})_g = R_{ik} + \frac{2V_jV_k}{V^2} + h_{ik}\left(-\frac{\Delta V}{V} + \frac{V_jV^j}{V^2}\right). \tag{2.14}$$

In accordance with (1.6), the time component is equal to

$$(R_{00})_g = c^2V^2(-V\Delta V + V_jV^j). \tag{2.15}$$

The mixed components are equal to zero, as has already been pointed out. The four-dimensional invariant is equal to

$$(R) = 2V\Delta V - 4V_jV^j - V^2R. \tag{2.16}$$

Hence we obtain for the components of the Einstein tensor

$$G_{\mu\nu} = (R_{\mu\nu})_g - \tfrac{1}{2}g_{\mu\nu}(R)_g \tag{2.17}$$

the following expressions

$$G_{ik} = H_{ik} + 2\frac{V_i V_k}{V^2} - h_{ik}\frac{V_j V^j}{V^2}, \qquad (2.18)$$

$$G_{00} = c^2 V^2 \{-V^2 H - 2V\Delta V + 3V_j V^j\}. \qquad (2.19)$$

Here $H_{ik}$ is the three-dimensional conservative tensor of conformal space, and H is its invariant

$$H_{ik} = R_{ik} - \tfrac{1}{2} h_{ik} R, \qquad H = -\tfrac{1}{2} R. \qquad (2.20)$$

In this case

$$R_{ik} = H_{ik} - h_{ik} H. \qquad (2.21)$$

We also write down the expression for the four-dimensional D'Alembert operator

$$\Box\psi = \frac{1}{c^2 V^2}\frac{\partial^2\psi}{\partial t^2} - V^2 \Delta\psi. \qquad (2.22)$$

Here $\Delta\psi$ denotes the Laplace operator in conformal space, as before,

$$\Delta\psi = \frac{1}{\sqrt{h}}\frac{\partial}{\partial x_i}\left(\sqrt{h}\, h^{ik}\frac{\partial\psi}{\partial x_k}\right). \qquad (2.23)$$

It is then seen that the coordinates which are harmonic in a four-dimensional sense will be harmonic also in the sense of three-dimensional conformal space.

An important difference between our formulas (2.18) for the spatial components of the conservative tensor and the formulas of Levi-Civita following from (1.5) and (1.6) is the fact that our formulas, which are written for conformal space, do not contain second derivatives of the quantity V.

## 3. THE EINSTEIN EQUATIONS IN CONFORMAL SPACE

Introducing the expressions (2.15) and (2.16) for the Einstein tensor in the equation of gravity

$$G_{\mu\nu} = -\varkappa T_{\mu\nu}, \qquad \varkappa = \frac{8\pi\gamma}{c^2}, \qquad (3.1)$$

we obtain

$$H_{ik} + 2\frac{V_i V_k}{V^2} - h_{ik}\frac{V_j V^j}{V^2} = -\varkappa T_{ik}, \qquad (3.2)$$

$$H + 2\frac{\Delta V}{V} - 3\frac{V_j V^j}{V^2} = \frac{1}{c^2 V^4}\varkappa T_{00} = \varkappa c^2 T^{00} \qquad (3.3)$$

Eliminating the quantity H from (3.3) by means of (3.2), we can write

$$2\left(\frac{\Delta V}{V} - \frac{V_j V^j}{V^2}\right) = \varkappa\mu, \qquad (3.4)$$

where

$$\mu = c^2 T^{00} + h^{ik} T_{ik} \qquad (3.5)$$

or

$$\mu = \frac{1}{V^2}(T_0^0 - T_1^1 - T_2^2 - T_3^3). \qquad (3.6)$$

In the last equation, the quantities $T_\beta^\alpha$ are also understood in the four-dimensional space. The physical meaning of the quantity $\mu$ is the mass density in conformal space.*

In what follows it is advantageous to replace the quantity V by $\Phi$ through the formula

$$V = e^{-\Phi}, \qquad (3.7)$$

so that the connection of the metric of space-time with the metric of conformal space will have the form

$$ds^2 = c^2 e^{-2\Phi} dt^2 - e^{2\Phi} d\sigma^2. \qquad (3.8)$$

As a consequence of

$$\Phi_i = -\frac{V_i}{V}, \qquad \Delta\Phi = -\frac{\Delta V}{V} + \frac{V_j V^j}{V^2}, \qquad (3.9)$$

the equations of gravity are written

$$H_{ik} = -2\Phi_i\Phi_k + h_{ik}\Phi_j\Phi^j - \varkappa T_{ik}, \qquad (3.10)$$

$$\Delta\Phi = -\tfrac{1}{2}\varkappa\mu. \qquad (3.11)$$

Since $\mu$ is the mass density, and the Einstein constant $\kappa$ is connected with the Newtonian constant $\gamma$ by the relation (3.1), the the latter equation is essentially the equation for the Newtonian potential U. We can write approximately

$$\Phi = \frac{U}{c^2} \qquad (3.12)$$

and, consequently,

$$\Phi_i = \frac{g_i}{c^2}, \qquad (3.13)$$

where $g_i$ is the component of the acceleration due to gravity.

We shall now make clear the physical meaning of Eq. (3.10). We set

$$Q_{ik} = \frac{1}{\varkappa}(2\Phi_i\Phi_k - h_{ik}\Phi_j\Phi^j) \qquad (3.14)$$

and write the equation (3.10) in the form

$$H_{ik} = -\varkappa(Q_{ik} + T_{ik}). \qquad (3.15)$$

The divergence of the tensor $Q_{ik}$ is equal to

$$\nabla^k Q_{ik} = \frac{2}{\varkappa}\Phi_i\Delta\Phi = -\mu\Phi_i \qquad (3.16)$$

by virtue of (3.11). On the other hand, since $H_{ik}$ is the conservative tensor of conformal space, then its divergence is equal to zero. Therefore, it follows from Eq. (3.15) that

$$\nabla^k T_{ik} = \mu\Phi_i. \qquad (3.17)$$

It is not difficult to see that this equation represents a generalization of the ordinary equations of the statics of an elastic body in a gravitational field. It is natural to explain the expression $Q_{ik}$ as the spatial part of the energy-momentum tensor of the gravitational field or, inasmuch as we are dealing with statics here, as a quantity proportional to the tensor of gravitational tension. From this viewpoint the equations (3.15) written down for conformal space form an analogue with the Einstein equations (3.1) written down for space-time. In the present and other equations, the left hand side is a conservative tensor while the right hand is the energy-momentum tensor or the stress tensor. Here the gravitational stresses appear in explicit form only after separation of space from time and after a transition to conformal space.

---

*The value obtained for $\mu$ agrees with the well-known expression of Tolman (see the book of Moeller,[3] page 341).

The gravitational equations in the form (3.10) show that conformal space will be almost Euclidean. In fact, as is seen from (3.13), the right hand side of (3.10) will be of the order of $g_i^2/c^4$; this leads to the result that the deviation of $h_{ik}$ from the Euclidean values will be of the order of $U^2/c^4$, and not of order $U/c^2$, as for a space with the metric (1.4).

All the formulas of this section [except the estimates (3.12) and (3.13)] contain no approximations if we do not consider the approximation of the static character of the field. All our equations are covariant relative to choice of coordinates in conformal space.

For empty space $T_{\alpha\beta} = 0$ we shall have $\mu = 0$ and Eq. (3.11) will be the consequence of (3.10).

## 4. SCHWARTZSCHILD'S SOLUTION IN CONFORMAL SPACE

In the case of spherical symmetry we can set

$$d\sigma^2 = dr^2 + \rho^2 (d\vartheta^2 + \sin^2\vartheta d\varphi^2). \tag{4.1}$$

We shall assume the coefficient of $dr^2$ equal to unity, which presents no limitations. The quantity $\rho$ is a function of the single variable r. The Laplace operator in a space with the metric (4.1) is written

$$\Delta\psi = \frac{1}{\rho^2}\left(\frac{\partial}{\partial r}\left(\rho^2 \frac{\partial\psi}{\partial r}\right) + \Delta^*\psi\right), \tag{4.2}$$

where $\Delta^*\psi$ is the Laplace operator on a sphere. Combining the quantities $H_{ik}$, we obtain

$$H_{rr} = \frac{1-\rho'^2}{\rho^2}, \qquad H_{\vartheta\vartheta} = -\rho\rho'', \quad H_{\varphi\varphi} = -\rho\rho''\sin^2\vartheta, \tag{4.3}$$

while the nondiagonal elements $H_{ik}$ are equal to zero. The equation for empty space has the form

$$H_{rr} = -\Phi_r^2, \qquad H_{\vartheta\vartheta} = \rho^2\Phi_r^2. \tag{4.4}$$

Since we have $\Delta\Phi = 0$, then

$$\rho^2\Phi_r = -\alpha, \tag{4.5}$$

where $\alpha$ is a constant (the gravitational mass radius). As a result of (4.3) and (4.5), the first equation of (4.2) gives

$$\rho'^2 = 1 + \frac{\alpha^2}{\rho^2}, \qquad \rho\rho' = \sqrt{\rho^2+\alpha^2}. \tag{4.6}$$

Since

$$\rho\rho'' + \rho'^2 = 1, \tag{4.7}$$

the second equation here is also satisfied. Hence

$$r = \sqrt{\rho^2+\alpha^2}, \qquad \rho = \sqrt{r^2-\alpha^2}. \tag{4.8}$$

We shall set the additive constant equal to zero. Then,

$$d\sigma^2 = dr^2 + (r^2-\alpha^2)(d\vartheta^2 + \sin^2\vartheta d\varphi^2). \tag{4.9}$$

With the help of (4.2), it is easy to prove that the coordinates

$$x_1 = r\sin\vartheta\cos\varphi, \qquad x_2 = r\sin\vartheta\sin\varphi,$$
$$x_3 = r\cos\vartheta \tag{4.10}$$

will be harmonic. In order to derive the solution of the equations, it suffices to find C. We have from (4.5)

$$\frac{d\Phi}{dr} = -\frac{\alpha}{r^2-\alpha^2}, \qquad \Phi = \frac{1}{2}\log\frac{r+\alpha}{r-\alpha}, \tag{4.11}$$

since for $r = \infty$, $\Phi$ should be equal to zero. Thus, finally,

$$ds^2 = c^2\frac{r-\alpha}{r+\alpha}dt^2 - \frac{r+\alpha}{r-\alpha}d\sigma^2, \tag{4.12}$$

where $d\sigma^2$ has the form (4.9).

The computations that have been written out have the purpose of showing how the Schwartzschild problem is easily solved in conformal space.

## 5. WEYL'S SOLUTION IN CONFORMAL SPACE

For axial symmetry the value of $d\sigma^2$ can be written in the form

$$d\sigma^2 = f^2(dz^2 + dr^2) + \rho^2 d\varphi^2, \tag{5.1}$$

where f and $\rho$ are functions of z and r, but not of $\varphi$. Computing the quantities $H_{ik}$, we have

$$H_{zz} = -\frac{1}{\rho}\frac{\partial^2\rho}{\partial z^2} - \frac{1}{f}\frac{\partial f}{\partial r}\cdot\frac{1}{\rho}\frac{\partial\rho}{\partial r} + \frac{1}{f}\frac{\partial f}{\partial z}\cdot\frac{1}{\rho}\frac{\partial\rho}{\partial z},$$

$$H_{rr} = -\frac{1}{\rho}\frac{\partial^2\rho}{\partial r^2} + \frac{1}{f}\frac{\partial f}{\partial r}\cdot\frac{1}{\rho}\frac{\partial\rho}{\partial r} - \frac{1}{f}\frac{\partial f}{\partial z}\cdot\frac{1}{\rho}\frac{\partial\rho}{\partial z},$$

$$H_{rz} = \frac{1}{\rho}\frac{\partial^2\rho}{\partial r\,\partial z} - \frac{1}{f}\frac{\partial f}{\partial r}\cdot\frac{1}{\rho}\frac{\partial\rho}{\partial z} - \frac{1}{f}\frac{\partial f}{\partial z}\cdot\frac{1}{\rho}\frac{\partial\rho}{\partial r}, \tag{5.2}$$

$$H_{\varphi\varphi} = -\frac{\rho^2}{f^2}\left\{\frac{\partial}{\partial r}\left(\frac{1}{f}\frac{\partial f}{\partial r}\right) + \frac{\partial}{\partial z}\left(\frac{1}{f}\frac{\partial f}{\partial z}\right)\right\}. \tag{5.3}$$

It then follows that

$$R_{\varphi\varphi} = \frac{\rho}{f^2}\left(\frac{\partial^2 \rho}{\partial r^2} + \frac{\partial^2 \rho}{\partial z^2}\right). \tag{5.4}$$

If $R_{\varphi\varphi} = 0$, then we can replace $z$ by such a function $\zeta(z, r)$ that $\zeta + i\rho$ would be a function of the complex variable $z + ir$. Then the quantity $d\sigma^2$ takes the form

$$d\sigma^2 = F^2(d\zeta^2 + d\rho^2) + \rho^2 d\varphi^2. \tag{5.5}$$

The variables $\zeta$ and $\rho$ represent the cyclindrical coordinates of Weyl (see Sec. 35 of Weyl's book[4]). In these coordinates, the expressions for $H_{ik}$ are simplified and can be written

$$H_{\zeta\zeta} = -H_{\rho\rho} = \frac{1}{\rho F}\frac{\partial F}{\partial \rho}, \qquad H_{\rho\zeta} = -\frac{1}{\rho F}\frac{\partial F}{\partial \zeta}, \tag{5.6}$$

$$H_{\varphi\varphi} = -\frac{\rho^2}{F^2}\left\{\frac{\partial}{\partial \rho}\left(\frac{1}{F}\frac{\partial F}{\partial \rho}\right) + \frac{\partial}{\partial \zeta}\left(\frac{1}{F}\frac{\partial F}{\partial \zeta}\right)\right\}. \tag{5.7}$$

The corresponding metric (5.5) of the Laplace operator is equal to

$$\Delta\psi = \frac{1}{F^2}\left\{\frac{\partial^2\psi}{\partial\rho^2} + \frac{1}{\rho}\frac{\partial\psi}{\partial\rho} + \frac{\partial^2\psi}{\partial\zeta^2}\right\} + \frac{1}{\rho^2}\frac{\partial^2\psi}{\partial\varphi^2} \tag{5.8}$$

and for functions which do not depend upon $\varphi$, the Laplace equation will have the same form as in Euclidean space.

Let us write down the conditions for the stress tensor, which follow from our assumption that $R_{\varphi\varphi} = 0$ and that the function $\Phi$ entering into (3.10) does not depend on $\varphi$. We must then have

$$T_\rho^\rho + T_\zeta^\zeta = T_r^r + T_z^z = 0, \qquad T_\varphi^\varphi = 0. \tag{5.9}$$

Moreover, the stress tensor must apparently satisfy the equations of statics (3.17).

For empty space, the equations of gravity (3.10) take the form

$$\frac{1}{F}\frac{\partial F}{\partial \rho} = \rho(\Phi_\rho^2 - \Phi_\zeta^2), \qquad \frac{1}{F}\frac{\partial F}{\partial \zeta} = 2\rho\Phi_\rho\Phi_\zeta, \tag{5.10}$$

where $\Phi$ is the solution of the equation

$$\frac{\partial^2\Phi}{\partial\rho^2} + \frac{1}{\rho}\frac{\partial\Phi}{\partial\rho} + \frac{\partial^2\Phi}{\partial\zeta^2} = 0. \tag{5.11}$$

When $\Phi$ is given, the function $F$ is obtained from (5.10) by integration of the total differential (under the condition that $F = 1$ when $\rho = 0$). The Weyl solution consists of this also. We shall see that, in conformal space, this solution is obtained in an extremely simple way.*

## 6. CONNECTION BETWEEN THE WEYL AND THE SCHWARTZSCHILD SOLUTIONS

Let us express the solution with spherical symmetry considered earlier in the Weyl coordinates. If we mean by $\rho$, $\vartheta$, $\varphi$ the spherical coordinates of Sec. 4, and by $\zeta$, $\rho$, $\varphi$ the Weyl coordinates, then obviously $\varphi$ will be the same in both cases. As a consequence of (5.8), $\zeta = r\cos\vartheta$ since the coordinate $\zeta$ is harmonic. The value of $\rho$ can be obtained by equating the coefficients for $d\varphi^2$ in (5.5) and (4.8). Then

$$\zeta = r\cos\vartheta, \qquad \rho = \sqrt{r^2 - \alpha^2}\sin\vartheta. \tag{6.1}$$

Conversely,

$$r = \frac{1}{2}\left(\sqrt{\rho^2 + (\zeta+\alpha)^2} + \sqrt{\rho^2 + (\zeta-\alpha)^2}\right),$$

$$\alpha\cos\vartheta = \frac{1}{2}\left(\sqrt{\rho^2 + (\zeta+\alpha)^2} - \sqrt{\rho^2 + (\zeta-\alpha)^2}\right). \tag{6.2}$$

Spheres in harmonic coordinates will correspond to ellipsoids of revolution in Weyl coordinates with foci at the points $\rho = 0$, $\zeta = \alpha$, and $\zeta = -\alpha$. If we set

$$r = \alpha\cosh u, \tag{6.3}$$

then $u$, $\vartheta$ will be the ordinary ellipsoidal coordinates. In these coordinates, Eq. (5.11) is written

$$\frac{\partial^2\Phi}{\partial u^2} + \frac{\partial^2\Phi}{\partial\vartheta^2} + \coth u\frac{\partial\Phi}{\partial u} + \cot\vartheta\frac{\partial\Phi}{\partial\vartheta} = 0. \tag{6.4}$$

The desired solution will be a function depending only on $u$, namely

$$\Phi = \frac{1}{2}\log\frac{\cosh u + 1}{\cosh u - 1}. \tag{6.5}$$

This solution coincides with (4.11). Integration of the total differential gives

$$F^2 = \frac{\sinh^2 u}{\sinh^2 u + \sin^2\vartheta}, \tag{6.6}$$

and, since

$$d\rho^2 + d\zeta^2 = \alpha^2(\sinh^2 u + \sin^2\vartheta)(du^2 + d\vartheta^2), \tag{6.7}$$

then

$$d\sigma^2 = \alpha^2\sinh^2 u\,(du^2 + d\vartheta^2 + \sin^2\vartheta\,d\varphi^2). \tag{6.8}$$

We see that in the Weyl coordinates the spherical symmetry is lost and is replaced by axial symmetry. If we take the solution in which $\Phi$ is spherically symmetric in the Weyl coordinates,

$$\Phi = \frac{\alpha}{\sqrt{\rho^2 + \zeta^2}}, \qquad \log F = -\frac{\alpha^2\rho^2}{2(\rho^2 + \zeta^2)^2},$$

then it is shown that it has a singularity in the plane $\zeta = 0$ for $\rho \to 0$, which it is difficult to explain physically. Therefore, in the given case, the Weyl coordinates correspond less to the character of the problem than the harmonic coordinates.

---

*Here it is appropriate to turn our attention to the fact that in the well-known book of Weyl[4] there are typographical errors in the equations for the axially symmetric solution which can lead to misunderstandings, inasmuch as the derivation of the formula is not given in the book.

## 7. CONCLUDING REMARKS

The possibility of a simple physical interpretation of the gravitational equations, which are written down for conformal space, the simplicity of these equations and their solution speak in convincing fashion on behalf of the expediency of the introduction of the concept of conformal space. To this one can add the fact that this concept makes it possible to interpret very simply the known fact that the deviation of a light ray passing by a heavy mass is twice as great as one would expect on the basis of the so-called principle of equivalence. This fact is explained simply in this way, that, according to (2.22), the velocity of light in conformal space is equal to $cV^2$, and not to $cV$ as in the ordinary definition of the spatial metric.

In the present work we have considered only the static case. For the non-static case the transformation of the Einstein equations to the three-dimensional form (without transition to conformal space) was carried out by Zel'manov.[5] The transition to conformal space in this case is not entirely unique, since it depends on the choice of the time coordinate. For corresponding additional conditions laid on the time coordinate, such a transition can nevertheless be shown to be expedient, especially in approximate calculations, when the fact that the conformal space is almost Euclidean can introduce material simplifications.

An attempt to construct a theory of the gravitational field with a single function similar to our function $\Phi$ has been made by Papapetrou.[6] The theory of Papapetrou corresponds to the assumption that the conformal space is Euclidean. There is no doubt that in the static case, the theory of Papapetrou represents a reasonable approximation to the Einstein theory. However, in the general, non-static case, a one field function is clearly insufficient. As a subsequent calculation, one could introduce four functions — the scalar and vector potentials of gravity. The approximate solutions of the gravitational equations given by us in reference 2 demonstrates this. There it was shown that, with the relative error of the order of $U^2/c^4$ in $g_{ik}$, and of the order of $U^3/c^6$ in $g_{00}$, the gravitational field can be expressed in terms of four functions $U^*$ and $U_i$, which satisfy the equations

$$\Delta U^* - \frac{1}{c^2}\frac{\partial^2 U^*}{\partial t^2} = -4\pi\gamma\,(c^2 T^{00} + T^{kk}), \qquad (7.1)$$

$$\Delta U_i = -4\pi\gamma\,\rho v_i, \qquad (7.2)$$

where $\rho v_i$ is the density of mass flow [Eqs. (68.30) and (68.19) in reference 3]. Equation (7.1) corresponds in the static case to Eq. (3.11), while the right-hand side of (7.1) is proportional to the quantity $\mu$ from (3.05). In the given approximation, the conformal space is Euclidean and we have

$$g_{00} \approx c^2 \frac{c^2 - U^*}{c^2 + U^*}, \qquad g_{0i} \approx \frac{4}{c^2} U_i. \qquad (7.3)$$

It is not excluded that the concept of conformal space can find application in an exact non-static theory.

---

[1] T. Levi-Civita, The Absolute Differential Calculus (London, 1927).

[2] V. A. Fock, Теория пространства, времени и тяготения, (Theory of Space, Time and Gravitation) (Moscow, Gostekhizdat, 1955; Pergamon Press, London, 1959).

[3] C. Moeller, The Theory of Relativity, (Oxford, 1952).

[4] H. Weyl, Raum, Zeit, Materie (Space, Time and Matter) (Berlin, 1923).

[5] A. L. Zel'manov, Dokl. Akad. Nauk SSSR **107**, 815 (1956), Soviet Phys. Doklady **1**, 227 (1956).

[6] A. Papapetrou, Z. Physik **139**, 518 (1954).

Translated by R. T. Beyer
284

SOVIET PHYSICS JETP VOLUME 11, NUMBER 5 NOVEMBER, 1960

# INFLUENCE OF COULOMB ATTRACTION ON THE CROSS SECTION FOR ABSORPTION OF ANTIPROTONS BY NUCLEI

P. É. NEMIROVSKIĬ and YU. D. FIVEĬSKIĬ

Submitted to JETP editor August 12, 1959

J. Exptl. Theoret. Phys. (U.S.S.R.) 38, 1486-1488 (May, 1960)

We investigate the effect of the Coulomb attraction of the nucleus on the cross section for the absorption of antiprotons whose energy is small compared with the Coulomb energy on the boundary of the nucleus. The interaction of antiprotons with nuclei is analyzed in the optical model. The calculations are carried out for C, Cu, and Pb, with attraction and repulsion potentials. It is shown that because of the Coulomb attraction the cross section for antiproton absorption, at energies below Coulomb values, is 4 to 10 times greater than the cross section for antineutrons at the same energy.

IT is known[1] that the cross sections for the interaction of antinucleons with nuclei exceed considerably the nuclear cross sections for protons and neutrons. Starting with the cross sections for the elementary nucleon-antinucleon act, we can explain the interaction between fast antinucleons and nuclei with the aid of the optical model. For antiprotons with energies comparable with the Coulomb energy on the boundary of the nucleus, the cross sections for absorption by the nucleus are substantially increased because the Coulomb field focuses the trajectories of the antiprotons in the region of the nucleus. This effect can be calculated within the framework of the optical model of the nucleus.

The calculations that follow can be used for all negatively charged particles which are strongly absorbed, particularly those for which the wavelength $\lambda\!\!\!^-$ at energies on the order of the Coulomb energy $V_C$ on the boundary of the nucleus is small compared with the nuclear radius $R$:

$$\lambda\!\!\!^-(R) = \hbar/\sqrt{2\mu V_c(R)} \ll R \qquad (1)$$

($\mu$ — reduced mass of the particle and nucleus).

The antiproton is acted upon inside the nucleus by a complex potential, whose dependence on the radius $r$ can be assumed to be identical with the dependence of the nucleon-nucleus complex potential on $r$. In the present investigation we consider both the nuclear attractive potential (negative real part of the complex potential), and the nuclear potential of repulsion (positive real part). We consider attraction first.

The nuclear potential diminishes on the boundary of the nucleus gradually.[2,3] This is due to the finite radius of the NN and N$\bar{\text{N}}$ interaction and to the gradual decrease in nuclear density on the boundary of the nucleus. Such a potential leads to a larger coefficient of adhesion of the antiproton than a potential with a sharp edge. However, when $E \ll V_C \times (R)$ ($E$ is the total energy of the antiproton in the c.m.s. of the antiproton and nucleus), the presence of a Coulomb interaction decreases the difference between these two cases. A calculation of the adhesion coefficient for the S-wave shows that a potential of the type

$$W = \begin{cases} -U_0(1+i\zeta) & 0 \leqslant r \leqslant r_0, \\ -U_0 e^{-\alpha(r-r_0)} & r_0 \leqslant r \leqslant R, \\ -Ze^2/r & R \leqslant r, \end{cases}$$

$$1/\alpha = 0.7 \cdot 10^{-13}\ \text{cm},\ r_0 = R - 1/\alpha, \qquad U_0 = \text{const} \qquad (2)$$

($U_0$ includes in addition to the nuclear potential also the electrostatic potential of the antiproton in the nucleus) and

$$W = \begin{cases} -U_0(1+i\zeta) & 0 \leqslant r \leqslant R, \\ -Ze^2/r & R \leqslant r \end{cases} \qquad (3)$$

leads to results that differ by not more than 10%. At the same time, one can obtain for the potential (3) (rectangular well) an exact solution of the Schrödinger equation within the region of the nucleus.

The imaginary part of the complex potential should be much greater for antiprotons than for nucleons. Actually, when slow nucleons interact with the nucleus, the exclusion principle limits the possibility of momentum transfer to the intranuclear nucleons. This limitation is inessential in the case of antinucleons, for which annihilation plays the decisive role (it appears partially only in non-annihilation collisions).

The calculation has been made with the potential (3), using $R = 1.25 \times 10^{-13} A^{1/3}$ cm for the radius of the nucleus. The imaginary part of the potential was set equal to $-(U_0 - V_C)$, and the Coulomb potential was replaced by its value on the boundary of the nucleus. This simplification barely affects the result, which depends little on the real part of the potential.

When $r \leq R$, the solution of the Schrödinger equation can be expressed in terms of spherical Bessel functions. When $r \geq R$ the solution can be written in the quasi-classical approximation in the form

$$\Psi(r,\theta) = \sum_{l=0}^{\infty} \frac{B_l}{\sqrt{rP_r(r)}} \left\{ \exp\left[-\frac{i}{\hbar}\int P_r(r)\,dr\right] - \eta_l \exp\left[\frac{i}{\hbar}\int P_r(r)\,dr\right]\right\} Y_{l0}(\theta), \quad (4)$$

$$P_r(r) = \{2\mu[E - W(r) - \hbar^2(l + {}^1/_2)^2/2\mu r^2]\}^{1/2}. \quad (4')$$

The amplitude $\eta_l$ of the scattered antiproton wave is found by fitting together the logarithmic derivatives of the wave functions with indices $l$.

In the case of a Coulomb potential, the quasi-classical approximation is applicable down to small distances, determined by the centrifugal potential. The condition for a quasi-classical solution on the nuclear boundary at zero energy of the incoming particle can be written in the form

$$R > \frac{\hbar}{2\mu C}\left(\frac{\hbar C}{e^2}\right)\frac{l(l+1)+1}{Z} \approx 1.37\cdot 10^{-12}\,\frac{l(l+1)+1}{Z}\,\text{cm}, \quad (5)$$

from which we obtain for C, Cu, and Pb $l \leq 0$, $l \leq 2$, and $l \leq 5$, respectively. When $E > 0$, solution (4) is applicable for the indicated values of $l$ down to $r = R$.

The absorption cross section can be estimated also for values of $l$ that do not satisfy condition (5). Let us consider an uncharged particle with energy equal to the kinetic energy of the antiproton on the boundary of the nucleus, that is, with $E' = E + Ze^2/R$. The coefficient of adhesion of a particle with energy $E'$ and a momentum $l$ will be somewhat greater than for an antiproton of energy E, owing to the greater perveance of the centrifugal barrier in the former case. It follows therefore that this method of calculating the coefficients of adhesion gives the upper limit of the partial cross sections.

Calculation shows that in the case of carbon the values of $l$ that do not satisfy (5) can yield a large contribution. Their contribution for copper, and particularly for lead, is insignificant.

Table I lists the calculated cross sections for the absorption of antiprotons by nuclei at E = 0.5 Mev.

For comparison, we calculated the absorption cross sections of antineutrons with E = 0.5 Mev. The parameters of the complex potential were taken to be the same as for the antiprotons, and there was no Coulomb field. The results of the calculation are listed in Table II. It should be noted that the adhesion coefficient for antiprotons remains practically constant for energies less than 0.5 Mev.

TABLE I

| Nucleus | $U_0$, Mev | Value of $l$ contributing to the cross section | $\sigma_c^{max}$, b |
|---|---|---|---|
| $C^{12}$ | 33 | $\leqslant 1$ | 3.2 |
| $Cu^{63}$ | 38 | $\leqslant 3$ | 11.2 |
| $Pb^{208}$ | 43 | $\leqslant 5$ | $\gtrsim 18$ |

TABLE II

| Nucleus | $U_0$, Mev | Value of $l$ contributing to the cross section | $\sigma_c$, b | $\frac{\sigma_c^{max}(\bar{p})}{\sigma_c(\bar{n})}$ |
|---|---|---|---|---|
| $C^{12}$ | 30 | $\leqslant 1$ | 0.82 | 4 |
| $Cu^{63}$ | 30 | $\leqslant 2$ | 1,12 | 10 |
| $Pb^{208}$ | 30 | $\leqslant 3$ | 2 | $\sim 10$ |

The relation $\sigma_C = \text{const.}\ v^{-2}$ is satisfied for this energy interval, in agreement with the general quantum-mechanical premises for inelastic processes.[4]

The antiprotons moving in matter collide not with the nuclei, but with the atoms. Therefore, for very slow antiprotons with wavelengths on the order of the radii of the first atomic shells, the nuclear charge is partially screened and antiprotons with orbital momenta other than zero are no longer focused by the Coulomb field. However, the antiproton energy below which partial screening takes place is very low. Thus, for antiprotons with $l = 1$, in the case of lead, this energy is 100 ev, since $\bar{\lambda}$ of the antiproton is equal to the radius of the K shell of lead at 100 ev.

We consider now the absorption cross section for copper under the assumption that the real part of the nuclear potential is positive. We assume here that $U_0 + V_C = 30$ Mev, and retain the same imaginary part, that is, $-30$ Mev. The absorption cross section of antiprotons for E = 0.5 Mev is found here to be 6 barns instead of 10 barns for the attraction potential. Thus, in the presence of a reasonable repulsion potential, the absorption cross section is still much greater than the geometrical cross section.

---

[1] Agnew, Chamberlain, Keller, Mermod, Rogers, Steiner, and Wiegand, Phys. Rev. **108**, 1545 (1957).

[2] A. E. Glassgold, Phys. Rev. **110**, 220 (1958).

[3] P. É. Nemirovskiĭ, Dokl. Akad. Nauk SSSR **112**, 411 (1957), Soviet Phys.-Doklady **2**, 45 (1957).

[4] L. D. Landau and E. M. Lifshitz, Квантовая механика (Quantum Mechanics) 1948, p. 497 (Engl. Transl., Pergamon, 1958).

Translated by J. G. Adashko
285

SOVIET PHYSICS JETP VOLUME 11, NUMBER 5 NOVEMBER, 1960

# *THE RELATIVISTICALLY COVARIANT SPIN STRUCTURE OF THE S MATRIX*

V. I. RITUS

P. N. Lebedev Physics Institute, Academy of Sciences, U.S.S.R.

Submitted to JETP editor September 19, 1959

J. Exptl. Theoret. Phys. (U.S.S.R.) **38**, 1489-1498 (May, 1960)

The relativistically covariant spin structure of the S matrix is examined for the reactions $a + b \rightarrow a' + b'$, $\gamma + b \rightarrow a' + b'$, $\gamma + b \rightarrow \gamma' + b'$, and $a + b \rightarrow 2\gamma$. The S matrix is represented in a form in which its individual terms correspond to transitions between states with definite initial and final spins of the system.

## 1. THE KINEMATICAL VARIABLES

LET us consider a reaction of the type $a + b \rightarrow a' + b'$. The state of a system of two particles a, b is completely determined by the three-dimensional momenta **p**, **q** and spin projections $\mu$, $\nu$ of these particles. Instead of the momenta **p**, **q** (six independent variables) we can introduce the four-momenta* p, q, remembering the condition that their lengths are equal to the masses of the corresponding particles:

$$|p| = m_a, \qquad |q| = m_b. \tag{1}$$

Finally, instead of p, q we can use the four-momentum t of the system

$$t = p + q \tag{2}$$

and the four-momentum k

$$k = \tfrac{1}{2}(p - q) - \tfrac{1}{2}(p + q)(p^2 - q^2)/(p + q)^2, \tag{3}$$

which satisfy the invariant conditions

$$k^2 = [p^2q^2 - \tfrac{1}{4}(t^2 - p^2 - q^2)^2]t^{-2}, \qquad (tk) = 0 \tag{4}$$

and which, like the set of variables p and q, contain six independent variables. We note that the vector t is timelike and the vector k is spacelike; in the center-of-mass system (c.m.s.) t reduces to the total energy of the system and k to the relative momentum,

$$t_c = (0, i(p_{0c} + q_{0c})), \qquad k_c = (\mathbf{k}_c, 0). \tag{5}$$

In what follows we shall describe a system of particles a, b by the spin projections $\mu$, $\nu$ and by the momenta p, q satisfying the conditions (1) or the momenta t, k satisfying the conditions (4). We shall describe the system a′, b′ by analogous quantities with a prime. If a particle is a photon, we shall describe its spin state not by the spin projection, but by the polarization four-vector $e_\mu$. In virtue of gauge invariance we can require that the vector potential $A_\mu$ satisfy the Lorentz gauge condition $\partial A_\mu/\partial x_\mu = 0$, and choose its fourth component equal to zero in the c.m.s. Then the polarization vector $e_\mu$ will satisfy the invariant conditions

$$(ep) = (et) = 0, \tag{6}$$

where p is the four-momentum of the photon, and consequently also the condition

$$(ek) = 0. \tag{7}$$

In the c.m.s. the spacelike vector $e_\mu$ reduces to the three-dimensional vector **e** satisfying the condition $\mathbf{e}\cdot\mathbf{k} = 0$. It is also convenient to introduce a spacelike four-vector $s_\mu$:

$$s_\mu = -i\varepsilon_{\mu\nu\lambda\sigma}k_\nu e_\lambda t_\sigma^0, \qquad t_\sigma^0 = t_\sigma|t|^{-1}, \tag{8}$$

which satisfies the conditions

$$(se) = (sk) = (st) = (sp) = 0 \tag{9}$$

and reduces in the c.m.s. to the vector $\mathbf{s} = \mathbf{k} \times \mathbf{e}$.

Choosing the vectors t, k and t′, k′ to describe the reaction $a + b \rightarrow a' + b'$ and recalling the energy-momentum conservation law $t = t'$

$$t = p + q = p' + q', \tag{10}$$

we see without difficulty that we can describe the reaction $a + b \rightarrow a' + b'$ by only three independent four-vectors k, k′, t, which in virtue of the relations (4) contain only eight independent variables. Since the conditions (4) are of invariant character, we can construct from the vectors k, k′, t only two independent scalars*

---

*The following notation is used:

$a = (\mathbf{a}, a_4)$, $\quad a_4 = ia_0$, $\quad (ab) = a_\mu b_\mu = \mathbf{ab} + a_4b_4$,

$\hat{a} = \gamma_\mu a_\mu$, $\quad \gamma_\mu\gamma_\nu + \gamma_\nu\gamma_\mu = 2\delta_{\mu\nu}$, $\quad \gamma_\mu^+ = \gamma_\mu$, $\quad \gamma_5 = \gamma_1\gamma_2\gamma_3\gamma_4$.

*In the general case one can construct from n independent vectors $n(n + 1)/2$ independent scalars; but if m invariant conditions are imposed on the n vectors, then the number of independent scalars is $n(n + 1)/2 - m$.

$$t^2,\ (k'k). \tag{11}$$

These scalars have good physical meanings: $\epsilon = (-t^2)^{1/2}$ is the total energy of the system in the c.m.s. and $x = (\mathbf{k}\mathbf{k}')/|\mathbf{k}||\mathbf{k}'|$ is equal to the cosine of the scattering angle in the c.m.s.

From the vectors $k$, $k'$, $t$ we can construct a spacelike pseudovector $n_\mu$:

$$n_\mu = -i\varepsilon_{\mu\nu\lambda\sigma} k'_\nu k_\lambda t^0_\sigma, \tag{12}$$

which is orthogonal to the vectors $k$, $k'$, $t$:

$$(nk) = (nk') = (nt) = 0, \tag{13}$$

and consequently also to $p$, $q$, $p'$, $q'$, and reduces in the c.m.s. to the vector normal to the plane of the scattering, $\mathbf{n} = \mathbf{k} \times \mathbf{k}'$.

## 2. THE INVARIANT PROPERTIES OF THE S MATRIX AND OF THE OPERATOR $\mathfrak{S}(p'q';pq)$

The matrix element of the S matrix for the process $a + b \rightarrow a' + b'$ in which particles a, b with momenta $\mathbf{p}$, $\mathbf{q}$ and spin projections $\mu$, $\nu$ collide and particles a′, b′ with momenta $\mathbf{p}'$, $\mathbf{q}'$ and spin projections $\mu'$, $\nu'$ emerge in one of three forms

$$S(\mathbf{p}'\mathbf{q}'\mu'\nu';\ \mathbf{p}\mathbf{q}\mu\nu) = \bar{u}(\mathbf{p}'\mu')\bar{u}(\mathbf{q}'\nu')\mathfrak{S}(p'q';\ pq)u(\mathbf{p}\mu)u(\mathbf{q}\nu), \tag{14a}$$

$$S(\mathbf{p}'\mathbf{q}'\mu'\nu';\ \mathbf{p}\mathbf{q}\mu\nu) = \bar{v}(\mathbf{p}\mu)\bar{v}(\mathbf{q}\nu)\mathfrak{S}(p'q';\ pq)v(\mathbf{p}'\mu')v(\mathbf{q}'\nu'), \tag{14b}$$

$$S(\mathbf{p}'\mathbf{q}'\mu'\nu';\ \mathbf{p}\mathbf{q}\mu\nu) = \bar{u}(\mathbf{p}'\mu')\bar{v}(\mathbf{q}\nu)\mathfrak{S}(p'q';\ pq)u(\mathbf{p}\mu)v(\mathbf{q}'\nu'), \tag{14c}$$

where $u(\mathbf{p}\mu)$, $\bar{u}(\mathbf{p}\mu)$ and $v(\mathbf{p}\mu)$, $\bar{v}(\mathbf{p}\mu)$ are the spin functions of the particle (u) and antiparticle (v) with momentum $\mathbf{p}$ and spin projection $\mu$ in the initial ($u$, $\bar{v}$) and final ($\bar{u}$, $v$) states, and $\mathfrak{S}(p'p';\ pq)$ is an operator in the spin space of the particles which depends on the momenta of the particles. For particles with spin 0 all the u, v are equal to unity, and for particles with spin ½

$$u(\mathbf{p},\ \pm{}^1/_2) = N_p\begin{pmatrix} 1 \\ \sigma\mathbf{p}/(p_0 + |p|)\end{pmatrix},$$

$$v(\mathbf{p},\ \mp{}^1/_2) = N_p\begin{pmatrix} \sigma\mathbf{p}/(p_0 + |p|) \\ 1\end{pmatrix},$$

$$\bar{u} = u^+\gamma_4, \qquad N_p = \sqrt{(p_0 + |p|)/2|p|}.$$

Taken as a matrix in the indices $\mu'$, $\nu'$, $\mu$, $\nu$, the elements $S(\mathbf{p}'\mathbf{q}'\mu'\nu';\ \mathbf{p}\mathbf{q}\mu\nu)$ form a matrix $S(\mathbf{p}'\mathbf{q}';\ \mathbf{p}\mathbf{q})$, whose structure has been well studied in the c.m.s. The right members of the equations (14) also form matrices in the indices $\mu'$, $\nu'$, $\mu$, $\nu$, which we denote by $M(\mathbf{p}'\mathbf{q}';\ \mathbf{p}\mathbf{q})$, $M(\mathbf{p}\mathbf{q};\ \mathbf{p}'\mathbf{q}')$, and $M(\mathbf{p}'\mathbf{q};\ \mathbf{p}\mathbf{q}')$, respectively. It is obvious that with the exception of $M(\mathbf{p}'\mathbf{q}';\ \mathbf{p}\mathbf{q})$ these matrices are not in general the same as the matrices $S(\mathbf{p}'\mathbf{q}';\ \mathbf{p}\mathbf{q})$. One can, however, obtain the matrices $M(\mathbf{p}\mathbf{q};\ \mathbf{p}'\mathbf{q}')$ and $M(\mathbf{p}'\mathbf{q};\ \mathbf{p}\mathbf{q}')$ in a simple way from the corresponding matrices $S(\mathbf{p}'\mathbf{q}';\ \mathbf{p}\mathbf{q})$. Our problem is to find the structure of the operator $\mathfrak{S}(p'q';\ pq)$ from the structure of the matrix $S(\mathbf{p}'\mathbf{q}';\ \mathbf{p}\mathbf{q})$ in the c.m.s. or from the structure of the corresponding matrix M. The analogous problem for a narrow class of reactions has been treated by Stapp[1] and also by Kawaguchi and Mugibayashi;[2] we note that the results of the latter authors are incorrect (see further discussion here, and reference 3).

We shall assume that the operator $\mathfrak{S}$ is invariant under Lorentz transformations, spatial rotations, reflections, and time reversal. The invariance of $\mathfrak{S}$ under the first three transformations means that the operator $\mathfrak{S}(p'q';\ pq)$ of a physical system K is connected with the analogous operator $\mathfrak{S}(p'_c q'_c;\ p_c q_c)$ of the transformed system $K_c$ by relation

$$\mathfrak{S}(p'q';\ pq) = F_{a'}^{-1}F_{b'}^{-1}\mathfrak{S}(p'_c q'_c;\ p_c q_c)F_a F_b, \tag{15a}$$

$$\mathfrak{S}(p'q';\ pq) = F_a^{-1}F_b^{-1}\mathfrak{S}(p'_c q'_c;\ p_c q_c)F_{a'} F_{b'} \tag{15b}$$

$$\mathfrak{S}(p'q';\ pq) = F_{a'}^{-1}F_b^{-1}\mathfrak{S}(p'_c p'_c;\ p_c q_c)F_a F_{b'}, \tag{15c}$$

where $F_a$ is the operator in the spin space of particle a that transforms the system K into the system $K_c$.

In what follows we shall present only relations of type a), since the corresponding relations of types b) and c) can be obtained from those of type a) by obvious interchanges [cf. Eqs. (14) and (15)].

The function $Fu(\mathbf{p}\mu)$ obtained by the action of the operator F on the function $u(\mathbf{p}\mu)$ of the system K can be expressed in terms of the function $u(\mathbf{p}_c\mu_c)$ of the system $K_c$:

$$Fu(\mathbf{p}\mu) = \sum_{\mu_c} u(\mathbf{p}_c\mu_c)f(\mathbf{p}_c\mu_c;\ \mathbf{p}\mu),$$

$$\bar{u}(\mathbf{p}\mu)F^{-1} = \sum_{\mu_c} f^{-1}(\mathbf{p}\mu;\ \mathbf{p}_c\mu_c)\bar{u}(\mathbf{p}_c\mu_c). \tag{16}$$

In the indices $\mu_c$, $\mu$ the coefficients $f(\mathbf{p}_c\mu_c;\ \mathbf{p}\mu)$ form a certain matrix $f(\mathbf{p}_c;\ \mathbf{p})$.

From the invariance of $\mathfrak{S}$ under the transformations F it follows that

$$M(\mathbf{p}'\mathbf{q}';\ \mathbf{p}\mathbf{q}) = f^{-1}(\mathbf{p}',\ \mathbf{p}'_c)f^{-1}(\mathbf{q}';\ \mathbf{q}'_c)M(\mathbf{p}'_c\mathbf{q}'_c;\ \mathbf{p}_c\mathbf{q}_c)f(\mathbf{p}_c;\ \mathbf{p})f(\mathbf{q}_c;\ \mathbf{q}). \tag{17a}$$

For spinless particles $F = f = 1$, and for particles of spin ½ the Lorentz operator is

$$L(v_c) = \exp[{}^1/_2 i\chi\gamma_4\gamma\mathbf{n}]$$

(where $\mathbf{v}_c$ is the velocity of system $K_c$ relative to K, $\tanh\chi = v_c$, $\mathbf{n} = \mathbf{v}_c/v_c$); the operator for rotation of the physical system around the axis $\mathbf{n}$ by the angle $\varphi$ is

$$R(\mathbf{n}, \varphi) = \exp[{}^1/_2\varphi\gamma_4\gamma_5\boldsymbol{\gamma}\mathbf{n}];$$

the reflection (inversion) operator is $P = \gamma_4$; and the corresponding matrixes $l$, r, p are

$$l(\mathbf{p}_c; \mathbf{p}) = \frac{(p_{0c} + |p|)(p_0 + |p|) + (\sigma\mathbf{p}_c)(\sigma\mathbf{p})}{[2(p_{0c} + |p|)(p_0 + |p|)(p_{0c}p_0 + |p|^2 + \mathbf{p}_c\mathbf{p})]^{1/2}}, \quad (18)$$

$$r(\mathbf{p}_c; \mathbf{p}) = \exp[-\tfrac{1}{2}i\varphi(\sigma\mathbf{n})], \quad p(\mathbf{p}_c; \mathbf{p}) \equiv p(-\mathbf{p}; \mathbf{p}) = 1. \quad (19)$$

We note that the matrix $l(\mathbf{p}_C; \mathbf{p})$ has the following properties:

1) it is Hermitian, $l^+(\mathbf{p}_C; \mathbf{p}) = l(\mathbf{p}; \mathbf{p}_C)$;

2) $l(\mathbf{p}; \mathbf{q})\, l^+(\mathbf{r}; \mathbf{q}) = l(\mathbf{p}; \mathbf{q})\, l(\mathbf{q}; \mathbf{r}) = l(\mathbf{p}; \mathbf{r})$;

3) $l(\mathbf{p}; \mathbf{q}) = 1$ if $\mathbf{q}$ is parallel or antiparallel to $\mathbf{p}$;

4) $l^{-1}(\mathbf{p}; \mathbf{q}) = l(\mathbf{p}; \mathbf{q})$, and by definition $l^{-1}(\mathbf{p}; \mathbf{q}) = [l(\mathbf{q}; \mathbf{p})]^{-1}$.

The invariance of $\mathfrak{S}$ with respect to time reversal, under which the momentum $p = (\mathbf{p}, ip_0)$ goes over into $p_C = (-\mathbf{p}, ip_0)$, and so on, means that

$$\mathfrak{S}^*(p'q'; pq) = T_{a'}^{-1}T_{b'}^{-1}\mathfrak{S}^+(p_cq_c; p_c'q_c')\, T_aT_b, \quad (20a)$$

where T is the time-reversal operator, which transforms the function $u(\mathbf{p}\mu)$ into the function $u(-\mathbf{p}\ -\mu)$:

$$Tu^*(\mathbf{p}\mu) = \sum_{\mu_c} \bar{u}^+(\mathbf{p}_c\mu_c)\, t(\mu_c; \mu),$$

$$\bar{u}^*(\mathbf{p}\mu)\, T^{-1} = \sum_{\mu_c} t^{-1}(\mu; \mu_c)\, u^+(\mathbf{p}_c\mu_c). \quad (21)$$

From the invariance of $\mathfrak{S}$ with respect to time reversal it follows that

$$M^*(\mathbf{p}'\mathbf{q}'; \mathbf{pq}) = t_{a'}^{-1}t_{b'}^{-1}M^+(\mathbf{p}_c\mathbf{q}_c; \mathbf{p}_c'\mathbf{q}_c')\, t_at_b. \quad (22a)$$

For particles with spin zero $T = t = 1$, and for particles with spin ½ we have $T = i\gamma_4\gamma_5C$, $t = \pm i\sigma_2$ (the signs ± correspond to the functions u, v).

Let us now go on to the construction of the operator $\mathfrak{S}$ which satisfies the invariance conditions (15), (20) in terms of the S matrix in the c.m.s. (or of the M matrix in the c.m.s.), which satisfies the invariance conditions (17) and (22). For this purpose we write the right member of Eq. (14a) in the form

$$\bar{u}(0\mu')\,\bar{u}(0\nu')\, L^{-1}(\mathbf{p}'/p_0')\, L^{-1}(\mathbf{q}'/q_0')$$
$$\times\, \mathfrak{S}(p'q'; pq)\, L(\mathbf{p}/p_0)\, L(\mathbf{q}/q_0)\, u(0\mu)\, u(0\nu),$$

where $L(\mathbf{p}/p_0)$ is the Lorentz operator which transforms the spin function of a particle at rest into that of a particle with the momentum $\mathbf{p}$:

$$L(\mathbf{p}/p_0)\, u(0\mu) = u(\mathbf{p}\mu). \quad (23)$$

It is obvious that the operator $L^{-1}(\mathbf{p}'/p_0') \times L^{-1}(\mathbf{q}'/q_0')\, \mathfrak{S}(p'q'; pq)\, L(\mathbf{p}/p_0)\, L(\mathbf{q}/q_0)$ transforms the spin functions of the particles a, b at rest into those of the particles a′, b′ at rest. Since for a particle at rest $u_\alpha(0\mu) = \delta_{\alpha\mu}$, the matrix $M(\mathbf{p}'\mathbf{q}'; \mathbf{pq})$ with the matrix elements

$$\bar{u}(\mathbf{p}'\mu')\,\bar{u}(\mathbf{q}'\nu')\, \mathfrak{S}(p'q'; pq)\, u(\mathbf{p}\mu)\, u(\mathbf{q}\nu)$$

is equal to the matrix of the operator

$$L^{-1}(\mathbf{p}'/p_0')\, L^{-1}(\mathbf{q}'/q_0')\, \mathfrak{S}(p'q'; pq)\, L(\mathbf{p}/p_0)\, L(\mathbf{q}/q_0),$$

namely

$$M(\mathbf{p}'\mathbf{q}'; \mathbf{pq})$$
$$= L^{-1}(\mathbf{p}'/p_0')\, L^{-1}(\mathbf{q}'/q_0')\, \mathfrak{S}(p'q'; pq)\, L(\mathbf{p}/p_0) L(\mathbf{q}/q_0) \quad (24a)$$

Using the explicit expression for the matrix $M(\mathbf{p}_C\mathbf{q}_C; \mathbf{p}_C\mathbf{q}_C)$ in the c.m.s., we can find the operator $\mathfrak{S}(p_C'q_C'; p_Cq_C)$:

$$\mathfrak{S}(p_c'q_c'; p_cq_c) = L(\mathbf{p}_c'/p_{0c}')\, L(\mathbf{q}_c'/q_{0c}')$$
$$\times\, M(\mathbf{p}_c'\mathbf{q}_c'; \mathbf{p}_c\mathbf{q}_c)\, L^{-1}(\mathbf{p}_c/p_{0c})\, L^{-1}(\mathbf{q}_c/q_{0c}), \quad (25a)$$

which has as its only elements (14) different from zero the elements (14a).

We now note that the matrix M and the operators L are not relativistically invariant in structure, whereas the expression (25a) as a whole must be of invariant structure. Therefore, if by means of the explicitly noninvariant expressions for the matrix $M(\mathbf{p}_C'\mathbf{q}_C'; \mathbf{p}_C\mathbf{q}_C)$ and the operators $L(\mathbf{p}_C/p_{0C})$, etc., we construct corresponding auxiliary relativistically-invariant operators $\mathfrak{M}(p'q'; pq)$ and $L(p, t)$, etc., which coincide with $M(\mathbf{p}_C'\mathbf{q}_C'; \mathbf{p}_C\mathbf{q}_C)$ and $L(\mathbf{p}_C/p_{0C})$, etc., then by substituting these relativistically-invariant operators into Eq. (25a) we shall get a relativistically-invariant expression for the operator $\mathfrak{S}(p'q'; pq)$. Thus in the construction of the relativistically-invariant operator $\mathfrak{S}(p'q'; pq)$ we can work from the formula

$$\mathfrak{S}(p'q'; pq)$$
$$= L(p', t)\, L(q', t)\, \mathfrak{M}(p'q'; pq)\, L^{-1}(p, t)\, L^{-1}(q, t), \quad (26a)$$

where $\mathfrak{M}(p'q'; pq)$, $L(p, t)$, etc., are auxiliary relativistically-invariant operators that coincide in the c.m.s. with the matrix $M(\mathbf{p}_C'\mathbf{q}_C'; \mathbf{p}_C\mathbf{q}_C)$ and the Lorentz operators $L(\mathbf{p}_C/p_{0C})$, etc.

## 3. THE STRUCTURES OF THE MATRIX S(p′q′; pq) AND THE OPERATOR $\mathfrak{S}$(p′q′; pq)

For particles with spins 0 and ½ the Lorentz operators $L(\mathbf{v})$ are respectively unity and $\exp[i\frac{1}{2}\chi\gamma_4\boldsymbol{\gamma}\mathbf{n}]$. If $\mathbf{v} = \mathbf{p}/p_0$, where $p_0 = (\mathbf{p}^2 + |p|^2)^{1/2}$, then we can write the operator $L(\mathbf{p}/p_0)$ for a particle with spin $\frac{1}{2}$ in the form

$$L(\mathbf{p}/p_0) = (-i\hat{p}\gamma_4 + |p|)/\sqrt{2|p|(p_0 + |p|)}. \quad (27)$$

It is obvious that the corresponding relativistically-invariant operator $L(p, t)$ that coincides with $L(\mathbf{p}/p_0)$ in the c.m.s. is the operator

$$L(p, t) = (-\hat{p}\hat{t} + |t||p|)/\sqrt{2|t||p|(|p||t| - (pt))}. \tag{28}$$

In the spin space of the system the matrix $S(\mathbf{p}'\mathbf{q}'; \mathbf{pq})$ has the structure

$$S(\mathbf{p}'\mathbf{q}'; \mathbf{pq}) = A + \sigma\mathbf{A}, \tag{29}$$

if the spin of the system is half-integral (i.e., is equal to $\frac{1}{2}$), and

$$S(\mathbf{p}'\mathbf{q}'; \mathbf{pq}) = (1 - \tfrac{1}{2}\mathbf{S}^2)A + \mathbf{T}_{01}\mathbf{B} + \mathbf{T}_{10}\mathbf{C}$$

$$+ \tfrac{1}{2}\mathbf{S}^2 D + \mathbf{SD} + (S_iS_j + S_jS_i - \tfrac{2}{3}\mathbf{S}^2\delta_{ij})D_{ij}, \tag{30}$$

if the spin of the system is integral (i.e., is equal to 0 or 1). In the latter case the term in $A$ corresponds to singlet-singlet transitions, the terms in $\mathbf{B}$ and $\mathbf{C}$ to triplet-singlet and singlet-triplet transitions, and the terms in $D$, $\mathbf{D}$, and $D_{ij}$ to triplet-triplet transitions. The functions $A$, $\mathbf{A}$, $\mathbf{B}$, $\mathbf{C}$, $D$, $\mathbf{D}$, $D_{ij}$ depend on the vectors $\mathbf{k}$, $\mathbf{k}'$, $\mathbf{e}$ and the total energy of the system and are so constructed that the entire matrix $S(\mathbf{p}'\mathbf{q}'; \mathbf{pq})$ is a scalar or pseudoscalar, depending on whether the intrinsic parity of the system is conserved or changes in the reaction. Namely, if the intrinsic parity of the system is conserved, then

$$A = A_1, \qquad \mathbf{A} = i\mathbf{n}A_2 \qquad (\text{spin}\,{}^1/_2); \qquad A = A_1,$$

$$\mathbf{B} = i\mathbf{n}B_1, \qquad \mathbf{C} = i\mathbf{n}C_1, \qquad D = D_1, \qquad \mathbf{D} = i\mathbf{n}D_2,$$

$$D_{ij} = (k_i'k_j' - \tfrac{1}{3}\mathbf{k}'^2\delta_{ij})D_3 + (k_ik_j - \tfrac{1}{3}\mathbf{k}^2\delta_{ij})D_4$$

$$+ (k_i'k_j + k_j'k_i - \tfrac{2}{3}(\mathbf{k}'\mathbf{k})\delta_{ij})D_5 \qquad (\text{spin}\,0, 1).$$

If, on the other hand, the parity changes, then

$$A = 0, \qquad \mathbf{A} = \mathbf{k}'A_1 + \mathbf{k}A_2 \qquad (\text{spin}\,{}^1/_2);$$

$$A = 0, \qquad \mathbf{B} = \mathbf{k}'B_1 + \mathbf{k}B_2, \qquad \mathbf{C} = \mathbf{k}'C_1 + \mathbf{k}C_2,$$

$$D = 0, \qquad \mathbf{D} = \mathbf{k}'D_1 + \mathbf{k}D_2,$$

$$D_{ij} = (k_i'n_j + k_j'n_i)D_3 + (k_in_j + k_jn_i)D_4 \qquad (\text{spin}\,0, 1).$$

For details of the structure of the matrix $S(\mathbf{p}'\mathbf{q}'; \mathbf{pq})$ see reference 4.

An investigation shows that if the matrix $S(\mathbf{p}'\mathbf{q}'; \mathbf{pq})$ is put in the form (29) or (30), then the matrix $M$ associated with it has the forms shown below for the three cases of Eq. (14). In these formulas the signs + or − placed on the two-rowed matrices $I$ and $\sigma$ indicate that the corresponding indices on the elements of these matrices refer to the particle (+) or the antiparticle (−); for example, $\sigma_{-+}$ denotes a Pauli matrix for whose elements $(\sigma_{-+})_{\mu\nu}$ the index $\mu$ refers to the antiparticle and $\nu$ to the particle; $\sigma^1$ and $\sigma^2$ connect the particles a, a′ and b, b′ [see Eqs. (32, a, b, c) below] or the particles a, b and a′, b′ [see Eq. (32c′)].

Case a

$$M(\mathbf{p}'\mathbf{q}'; \mathbf{pq}) = A + \sigma_{++}\mathbf{A}; \tag{31a}$$

$$M(\mathbf{p}'\mathbf{q}'; \mathbf{pq}) = \tfrac{1}{4}(1 - \sigma^1_{++}\sigma^2_{++})A + \tfrac{1}{4}(\sigma^1_{++} - \sigma^2_{++}, \mathbf{B} + \mathbf{C}) - \tfrac{1}{4}i([\sigma^1_{++}, \sigma^2_{++}], \mathbf{B} - \mathbf{C}) + \tfrac{1}{4}(3 + \sigma^1_{++}\sigma^2_{++})D$$

$$+ \tfrac{1}{2}(\sigma^1_{++} + \sigma^2_{++}, \mathbf{D}) + \tfrac{1}{2}[\sigma^1_{++i}\sigma^2_{++j} + \sigma^1_{++j}\sigma^2_{++i} - \tfrac{2}{3}(\sigma^1_{++}\sigma^2_{++})\delta_{ij}]D_{ij}. \tag{32a}$$

Case b

$$M(\mathbf{pq}; \mathbf{p}'\mathbf{q}') = A - \sigma_{--}\mathbf{A}; \tag{31b}$$

$$M(\mathbf{pq}; \mathbf{p}'\mathbf{q}') = \tfrac{1}{4}(1 - \sigma^1_{--}\sigma^2_{--})A + \tfrac{1}{4}(-\sigma^1_{--} + \sigma^2_{--}, \mathbf{B} + \mathbf{C}) - \tfrac{1}{4}i([\sigma^1_{--}, \sigma^2_{--}], \mathbf{B} - \mathbf{C}) + \tfrac{1}{4}(3 + \sigma^1_{--}\sigma^2_{--})D$$

$$- \tfrac{1}{2}(\sigma^1_{--} + \sigma^2_{--}, \mathbf{D}) + \tfrac{1}{2}[\sigma^1_{--i}\sigma^2_{--j} + \sigma^1_{--j}\sigma^2_{--i} - \tfrac{2}{3}(\sigma^1_{--}\sigma^2_{--})\delta_{ij}]D_{ij}. \tag{32b}$$

Case c

$$M(\mathbf{p}'\mathbf{q}; \mathbf{pq}') = A + \sigma_{++}\mathbf{A} \text{ or } A - (\sigma_{--}\mathbf{A}); \tag{31c}$$

$$M(\mathbf{p}'\mathbf{q}; \mathbf{pq}') = \tfrac{1}{4}(1 + \sigma^1_{++}\sigma^2_{--})A + \tfrac{1}{4}(\sigma^1_{++} + \sigma^2_{--}, \mathbf{B} + \mathbf{C}) + \tfrac{1}{4}i([\sigma^1_{++}, \sigma^2_{--}], \mathbf{B} - \mathbf{C}) + \tfrac{1}{4}(3 - \sigma^1_{++}\sigma^2_{--})D$$

$$+ \tfrac{1}{2}(\sigma^1_{++} - \sigma^2_{--}, \mathbf{D}) - \tfrac{1}{2}[\sigma^1_{++i}\sigma^2_{--j} + \sigma^1_{++j}\sigma^2_{--i} - \tfrac{2}{3}(\sigma^1_{++}\sigma^2_{--})\delta_{ij}]D_{ij} \tag{32c}$$

or

$$M(\mathbf{p}'\mathbf{q}; \mathbf{pq}') = \frac{1}{\sqrt{2}}I_{-+}A + \frac{1}{\sqrt{2}}\sigma_{-+}\mathbf{B} \text{ or } \frac{1}{\sqrt{2}}I_{+-}A + \frac{1}{\sqrt{2}}\sigma_{+-}\mathbf{C}; \tag{31c′}$$

$$M(\mathbf{p}'\mathbf{q}; \mathbf{pq}') = \tfrac{1}{2}I^1_{-+}I^2_{+-}A + \tfrac{1}{2}\sigma^1_{-+}\mathbf{B} + \tfrac{1}{2}\sigma^2_{+-}\mathbf{C} + \tfrac{1}{2}\sigma^1_{-+}\sigma^2_{+-}D + \tfrac{1}{2}i([\sigma^1_{-+}, \sigma^2_{+-}]\mathbf{D})$$

$$- \tfrac{1}{2}[\sigma_{-+i}\sigma^2_{+-j} + \sigma^1_{-+j}\sigma^2_{+-i} - \tfrac{2}{3}(\sigma^1_{-+}\sigma^2_{+-})\delta_{ij}]D_{ij}. \tag{32c′}$$

The matrices (31, a, b, c) refer to half-integral spin of the system, and the matrices (32, a, b, c, c′) and (31c′) to integral spin.

Each matrix M is two-rowed if only two of the particles in the reaction $a + b \rightarrow a' + b'$ have spin $\frac{1}{2}$ [see Eqs. (31, a, b, c, c′)], and is the direct product of two two-rowed matrices if all of the particles have spin $\frac{1}{2}$ [see Eqs. (31, a, b, c, c′)]. The corresponding relativistically invariant matrix $\mathfrak{M}$ will obviously be a four-rowed matrix or the direct product of two four-rowed matrices, and in the c.m.s. these four-rowed matrices reduce to the left upper (++) two-rowed matrices for processes of type a, to the right lower (− −) matrices for processes of type b, to the left upper or right lower for processes of type c, and to the left lower (−+) or right upper (+−) for processes of type c′. In accordance with this, to construct the relativistically invariant operators $\mathfrak{M}(p'q'; pq)$, etc., that coincide in the c.m.s. with the matrices $\mathbf{M}(\mathbf{p'q'}; \mathbf{pq})$, etc., we have only to replace in the matrix $\mathbf{M}(\mathbf{p'q'}; \mathbf{pq})$ the three-dimensional vectors **k**, **k′**, **n**, **e**, **s** by the four-dimensional vectors k, k′, n, e, s and replace the two-rowed matrices $I_{\pm\pm}$, $I_{\pm\mp}$, $\boldsymbol{\sigma}_{\pm\pm}$, $\boldsymbol{\sigma}_{\pm\mp}$ by the respective four-rowed matrices

$$-\Lambda_{\pm}(t), \qquad -\Lambda_{\pm}(t)\gamma_5\Lambda_{\mp}(t) = -\gamma_5\Lambda_{\mp}(t),$$

$$\pm\Lambda_{\pm}(t)\, i\gamma_5\gamma_\mu\Lambda_{\pm}(t) = \pm i\gamma_5(\gamma_\mu \mp it^0_\mu)\Lambda_{\pm}(t),$$

$$\pm\Lambda_{\pm}(t)\, i\gamma_\mu\Lambda_{\mp}(t) = \pm i(\gamma_\mu \mp it^0_\mu)\Lambda_{\mp}(t).$$

The operators $\Lambda_{\pm}(t)$ are defined in the following way

$$\Lambda_{\pm}(t) = (|t| \mp i\hat{t})/2|t|, \qquad \Lambda^2_{\pm}(t) = \Lambda_{\pm}(t),$$

$$\Lambda_{\pm}(t)\Lambda_{\mp}(t) = 0, \quad \Lambda_{\pm}(t) + \Lambda_{\mp}(t) = 1 \tag{33}$$

and in the c.m.s. are equal to $\frac{1}{2}(1 \pm \beta)$. The signs ± for the operators $\Lambda_{\pm}(t)$ must be chosen in accordance with the form of the matrix M [cf. Eqs. (31) and (32)] and the statements made above.

Using now the formula (26) and the relation

$$\Lambda_{\pm}(t)L^{-1}(p,t) = K_p\Lambda_{\pm}(t)\Lambda_{\pm}(p),$$

$$K_p = [2|t|\,|p|/(|t|\,|p| - (tp))]^{1/2}, \tag{34}$$

we get the final formulas for the matrix $\mathfrak{S}(p'q'; pq)$ (we have further $K_{p'p} = K_{p'}K_p$, etc.):

$$\mathfrak{S}(p'q';\; pq) = K_{p'p}\Lambda_+(p')\Lambda_+(t)\mathfrak{N}(p'q';\; pq)\Lambda_+(t)\Lambda_+(p), \tag{35a, c}$$

$$\mathfrak{S}(p'q';\; pq) = K_{p'p}\Lambda_-(p)\Lambda_-(t)\mathfrak{N}(pq;\; p'q')\Lambda_-(t)\Lambda_-(p), \tag{35b, c}$$

$$\mathfrak{S}(p'q';\; pq) = K_{pq}\Lambda_-(q)\Lambda_-(t)\mathfrak{N}(q'p;\; pq')\Lambda_+(t)\Lambda_+(p)$$

or

$$K_{p'q'}\Lambda_+(p')\Lambda_+(t)\mathfrak{N}(qp';\; pq')\Lambda_-(t)\Lambda_-(q'), \tag{35c′}$$

if only two particles have spin $\frac{1}{2}$, and

$$\mathfrak{S}(p'q';\; pq) = K_{p'q'pq}\Lambda_+(p')\Lambda_+(t)\Lambda_+(q')\Lambda_+(t)\mathfrak{N}(p'q'; pq)$$
$$\times\Lambda_+(t)\Lambda_+(p)\Lambda_+(t)\Lambda_+(q), \tag{36a}$$

$$\mathfrak{S}(p'q';\; pq) = K_{p'q'pq}\Lambda_-(p)\Lambda_-(t)\Lambda_-(q)\Lambda_-(t)\mathfrak{N}(pq; p'q')$$
$$\times\Lambda_-(t)\Lambda_-(p')\Lambda_-(t)\Lambda_-(q'), \tag{36b}$$

$$\mathfrak{S}(p'q';\; pq) = K_{p'q'pq}\Lambda_+(p')\Lambda_+(t)\Lambda_-(q)\Lambda_-(t)\mathfrak{N}(p'q;\; pq')$$
$$\times\Lambda_+(t)\Lambda_+(p)\Lambda_-(t)\Lambda_-(q), \tag{36c}$$

$$\mathfrak{S}(p'q';\; pq) = K_{p'q'pq}\Lambda_-(q)\Lambda_-(t)\Lambda_+(p')\Lambda_+(t)\mathfrak{N}(qp';\; pq')$$
$$\times\Lambda_+(t)\Lambda_+(p)\Lambda_-(t)\Lambda_-(q), \tag{36c′}$$

if all the particles have spin $\frac{1}{2}$; the matrix $\mathfrak{N}$ is obtained from the matrix M [see Eqs. (31), (32)] by replacing the three-dimensional vectors **k**, **k′**, **n**, **e**, **s** by the four-vectors k, k′, n, e, s and the two-rowed matrices $I_{\pm\pm}$, $I_{\pm\mp}$, $\sigma_{\pm\pm}$, $\sigma_{\pm\mp}$ by the four-rowed matrices I, $-\gamma_5$, $\pm i\gamma_5\gamma_\mu$, $\pm i\gamma_\mu$.*

We shall present the form of the matrices $\mathfrak{N}$ for the reactions $a + b \rightarrow a' + b'$, $\gamma + b \rightarrow a' + b'$, $\gamma + b \rightarrow \gamma' + b'$, $a + b \rightarrow 2\gamma$, in which the spins of the particles do not exceed $\frac{1}{2}$. The matrices for reactions with conservation and with change of the intrinsic parity of the system are denoted respectively by $\mathfrak{N}^{(\pm)}$. We have also introduced the notation $\hat{a}^{1,2} = \gamma^{1,2}_\mu a_\mu$.

### The Reaction $a + b \rightarrow a' + b'$

1) If the spins of all particles are zero, $s_a = s_b = s_{a'} = s_{b'} = 0$, then

$$\mathfrak{N} = A(\varepsilon,\; x); \tag{37a, b, c}$$

2) $s_a = s_{a'} = \frac{1}{2}$, $s_b = s_{b'} = 0$,

$$\mathfrak{N}^{(+)} = A_1 - \gamma_5\hat{n}A_2, \tag{38a, b, c}$$

$$\mathfrak{N}^{(-)} = i\gamma_5\hat{k}'A_1 + i\gamma_5\hat{k}A_2; \tag{39a, b, c}$$

3) $s_a = s_b = \frac{1}{2}$, $s_{a'} = s_{b'} = 0$,

$$\mathfrak{N}^{(+)} = -\frac{1}{\sqrt{2}}\gamma_5A_1 + \frac{1}{\sqrt{2}}\hat{n}B_1, \tag{40c′}$$

$$\mathfrak{N}^{(-)} = -\frac{1}{\sqrt{2}}i\hat{k}'B_1 - \frac{1}{\sqrt{2}}i\hat{k}B_2, \tag{41c′}$$

4) $s_a = s_b = s_{a'} = s_{b'} = \frac{1}{2}$,

---

*We note that in Eqs. (35), (36) we may strike out the operators $\Lambda_{\pm}(t)$ on the left (or on the right) of $\mathfrak{N}$ if we replace $\gamma_\mu$ in $\mathfrak{N}$ by $\gamma_\mu \pm it^0_\mu$, which is equivalent to the replacement

$$(\gamma^1\gamma^2) \rightarrow (\gamma^1\gamma^2) - 1 \quad \text{in cases a, b,}$$
$$(\gamma^1\gamma^2) \rightarrow (\gamma^1\gamma^2) + 1 \quad \text{in cases c, c}'.$$

$$\mathfrak{N}^{(+)} = \tfrac{1}{4}(1+\gamma_5^1\gamma_5^2(\gamma^1\gamma^2))A_1 - \tfrac{1}{4}(\gamma_5^1\hat{n}^1 - \gamma_5^2\hat{n}^2)(B_1+C_1) - \tfrac{1}{4}i\gamma_5^1\gamma_5^2\varepsilon_{\mu\nu\lambda\sigma}n_\mu\gamma_\nu^1\gamma_\lambda^2 t_\sigma^0(B_1-C_1) + \tfrac{1}{4}(3-\gamma_5^1\gamma_5^2(\gamma^1\gamma^2))D_1$$
$$-\tfrac{1}{2}(\gamma_5^1\hat{n}^1+\gamma_5^2\hat{n}^2)D_2 - \gamma_5^1\gamma_5^2[\hat{k}'^1\hat{k}^2+\hat{k}^1\hat{k}'^2-\tfrac{2}{3}(\gamma^1\gamma^2)(k'k)]D_3 - \gamma_5^1\gamma_5^2[\hat{k}'^1\hat{k}'^2-\tfrac{1}{3}(\gamma^1\gamma^2)k'^2]D_4$$
$$-\gamma_5^1\gamma_5^2[\hat{k}^1\hat{k}^2-\tfrac{1}{3}(\gamma^1\gamma^2)k^2]D_5 \qquad (42a, b, c)$$

or

$$\mathfrak{N}^{(+)} = \tfrac{1}{2}\gamma_5^1\gamma_5^2A_1 - \tfrac{1}{2}\hat{n}^1\gamma_5^2B_1 + \tfrac{1}{2}\gamma_5^1\hat{n}^2C_1 + \tfrac{1}{2}(\gamma^1\gamma^2)D_1 + \tfrac{1}{2}i\varepsilon_{\mu\nu\lambda\sigma}n_\mu\gamma_\nu^1\gamma_\lambda^2t_\sigma^0D_2 - \left[\hat{k}'^1\hat{k}^2+\hat{k}^1\hat{k}'^2-\tfrac{2}{3}(\gamma^1\gamma^2)(k'k)\right]D_3$$
$$-\left[\hat{k}'^1\hat{k}'^2-\tfrac{1}{3}(\gamma^1\gamma^2)k'^2\right]D_4 - \left[\hat{k}^1\hat{k}^2-\tfrac{1}{3}(\gamma^1\gamma^2)k^2\right]D_5 \qquad (43c')$$

(for elastic reactions it follows from the invariance of the interaction under time reversal that $B_1 = C_1$, $D_4 = D_5$), and

$$\mathfrak{N}^{(-)} = \tfrac{1}{4}i(\gamma_5^1\hat{k}'^1-\gamma_5^2\hat{k}'^2)(B_1+C_1) + \tfrac{1}{4}i(\gamma_5^1\hat{k}^1-\gamma_5^2\hat{k}^2)(B_2+C_2) - \tfrac{1}{4}\gamma_5^1\gamma_5^2\varepsilon_{\mu\nu\lambda\sigma}k'_\mu\gamma_\nu^1\gamma_\lambda^2t_\sigma^0(B_1-C_1) - \tfrac{1}{4}\gamma_5^1\gamma_5^2\varepsilon_{\mu\nu\lambda\sigma}k_\mu\gamma_\nu^1\gamma_\lambda^2t_\sigma^0(B_2-C_2)$$
$$+\tfrac{1}{2}i(\gamma_5^1\hat{k}'^1+\gamma_5^2\hat{k}'^2)D_1 + \tfrac{1}{2}i(\gamma_5^1\hat{k}^1+\gamma_5^2\hat{k}^2)D_2 - \gamma_5^1\gamma_5^2(\hat{k}'^1\hat{n}^2+\hat{n}^1\hat{k}'^2)D_3 - \gamma_5^1\gamma_5^2(\hat{k}^1\hat{n}^2+\hat{n}^1\hat{k}^2)D_4 \qquad (44a, b, c)$$

or

$$\mathfrak{N}^{(-)} = -\tfrac{1}{2}i\hat{k}'^1B_1 - \tfrac{1}{2}i\hat{k}^1B_2 + \tfrac{1}{2}i\hat{k}'^2C_1 + \tfrac{1}{2}i\hat{k}^2C_2 + \tfrac{1}{2}\varepsilon_{\mu\nu\lambda\sigma}\gamma_\nu^1\gamma_\lambda^2t_\sigma^0(k'_\mu D_1+k_\mu D_2) - (\hat{k}'^1\hat{n}^2+\hat{n}^1\hat{k}'^2)D_3 - (\hat{k}^1\hat{n}^2+\hat{n}^1\hat{k}^2)D_4. \qquad (45c')$$

### The Reaction $\gamma + b \to a' + b'$

We present the matrices $\mathfrak{N}^{(+)}$ that correspond to reactions in which the intrinsic parities of the particle b and the system a′ + b′ are the same, since the matrices $\mathfrak{N}^{(-)}$ that correspond to reactions in which these parities are opposite are obtained from those presented here by the interchange $e \rightleftarrows -is$.

1) For $s_b = s_{a'} = s_{b'} = 0$

$$\mathfrak{N}^{(+)} = (k'e)A_1; \qquad (46a, b, c)$$

2) $s_b = s_{b'} = \frac{1}{2}$, $s_{a'} = 0$

$$\mathfrak{N}^{(+)} = (ns)A_1 + \gamma_5\hat{s}A_2 + \gamma_5\hat{k}'(k's)A_3 + \gamma_5\hat{k}(k's)A_4; \qquad (47a, b, c)$$

3) $s_b = 0$, $s_{a'} = s_{b'} = \frac{1}{2}$

$$\mathfrak{N}^{(+)} = -\frac{1}{\sqrt{2}}\{\gamma_5(k'e)A_1 - i\varepsilon_{\mu\nu\lambda\sigma}\gamma_\mu k'_\nu e_\lambda t_\sigma^0C_1 + \hat{s}C_2 + \hat{n}(k'e)C_3\}. \qquad (48c')$$

### The Reaction $\gamma + b \to \gamma' + b'$

We present the matrices $\mathfrak{N}^{(+)}$ that correspond to reactions in which the intrinsic parities of the particles b and b′ are the same, since the matrices $\mathfrak{N}^{(-)}$ that correspond to reactions in which these parities are opposite are obtained from those given here by the interchange $e \rightleftarrows -is$ or $e' \rightleftarrows -is'$.

1) For $s_b = s_{b'} = 0$

$$\mathfrak{N}^{(+)} = (e'e)A_1 + (s's)A_2; \qquad (49a, b, c)$$

2) $s_b = s_{b'} = \frac{1}{2}$

$$\mathfrak{N}^{(+)} = (e'e)A_1 + (s's)A_2 + i\gamma_5\varepsilon_{\mu\nu\lambda\sigma}\gamma_\mu e'_\nu e_\lambda t_\sigma^0A_3 + i\gamma_5\varepsilon_{\mu\nu\lambda\sigma}\gamma_\mu s'_\nu s_\lambda t_\sigma^0A_4 - \gamma_5\hat{k}'(e's)A_5 - \gamma_5\hat{k}(s'e)A_6 - \gamma_5\hat{k}'(s'e)A_7 - \gamma_5\hat{k}(e's)A_8. \qquad (50a, b, c)$$

For elastic reactions it follows from time-reversal invariance that $A_6 = -A_5$, $A_8 = -A_7$.*

### The Reaction $a + b \to \gamma_1 + \gamma_2$

1) In the case $s_a = s_b = 0$

$$\mathfrak{N}^{(+)} = (e_1e_2)A_1 + (ke_1)(ke_2)A_2, \qquad (51a, b, c)$$

$$\mathfrak{N}^{(-)} = \varepsilon_{\mu\nu\lambda\sigma}k'_\mu e_{1\nu}e_{2\lambda}t_\sigma^0A_1 + i[(ks_1)(ke_2)+(ks_2)(ke_1)]A_2; \qquad (52a, b, c)$$

2) $s_a = s_b = \frac{1}{2}$

$$\mathfrak{N}^{(+)} = -\frac{1}{\sqrt{2}}\{\gamma_5(e_1e_2)A_1 + \gamma_5(ke_1)(ke_2)A_2 + \hat{k}'(s_1e_2)C_1 + \hat{k}(s_1e_2)C_2 + [\hat{s}_1(ke_2)+\hat{s}_2(ke_1)]C_3 + \hat{k}'[(ks_1)(ke_2) + (ks_2)(ke_1)]C_4 + \hat{k}[(ks_1)(ke_2)+(ks_2)(ke_1)]C_5\}, \qquad (53c')$$

$$\mathfrak{N}^{(-)} = i\frac{1}{\sqrt{2}}\{-\gamma_5(s_1e_2)A_1 - \gamma_5[(ks_1)(ke_2)+(ks_2)(ke_1)]A_2 + \hat{k}'(e_1e_2)C_1 + \hat{k}(e_1e_2)C_2 + [\hat{e}_2(ke_1)+\hat{e}_1(ke_2)]C_3 + \hat{k}'(ke_1)(ke_2)C_4 + \hat{k}(ke_1)(ke_2)C_5 + \hat{n}(s_1e_2)C_6\}. \qquad (54c')$$

Thus the relativistically-invariant spin structure of the operator $\mathfrak{S}(p'q'; pq)$ defined by Eqs. (35) – (54) is closely connected with the spin structure of the matrix $\mathbf{S}(\mathbf{p'q'}; \mathbf{pq})$ in the c.m.s. The functions $A_i$, $B_i$, $C_i$, $D_i$ are scalar functions of the variables $x$ and $\epsilon$, which in the c.m.s. are the cosine of the scattering angle and the total energy of the system. In the general case the number of such scalar functions that characterize the operator $\mathfrak{S}(p'q'; pq)$ is given by (cf. references 3 and 4)

$$r = \sum_{S',S} r_{S'S}, \qquad r^0 = \frac{1}{2}\sum_{S'\neq S} r_{S'S} + \sum_{S} r^0_{SS} \qquad (55)$$

---

*We note that the ten spin invariants for this reaction presented in reference 2 are actually not independent, and reduce to eight invariants.

for inelastic and elastic reactions, respectively, where $r_{S'S}$ is the number of scalar functions that correspond in the c.m.s. to a transition from a state in which the spin of the system is S to one in which it is S′. We have as the formulas for the numbers $r_{S'S}$ and $r^0_{SS}$:

1) for the reaction $a + b \rightarrow a' + b'$ (S, S′ and i, i′ are the spins and intrinsic parities of the systems $a + b$, $a' + b'$):

$$r_{S'S} = \tfrac{1}{2}(2S'+1)(2S+1) + \tfrac{1}{2}i'i\,(-1)^{S'-S},$$
$$r^0_{SS} = (S+1)^2 \quad (S, S' \text{—integral}), \tag{56}$$
$$r_{S'S} = \tfrac{1}{2}(2S'+1)(2S+1),$$
$$r^0_{SS} = (S+1)^2 - {}^1\!/_4 \quad (S, S' \text{— half-integral}),$$

2) for the reaction $\gamma + b \rightarrow a' + b'$ (S, S′ are the spins of particle b and system $a' + b'$):

$$r_{S'S} = (2S'+1)(2S+1); \tag{57}$$

3) for the reaction $\gamma + b \rightarrow \gamma' + b'$ (S, S′ are the spins of particles b, b′):

$$r_{S'S} = 2(2S'+1)(2S+1), \qquad r^0_{SS} = 2(2S+1)(S+1); \tag{58}$$

4) for the reaction $a + b \rightarrow 2\gamma$ (S is the spin of the system $a + b$):

$$r_S = 2(2S+1). \tag{59}$$

The operator $\mathfrak{S}(p'q'; pq)$ and the matrix $M(\mathbf{p}'\mathbf{q}'; \mathbf{pq})$ discussed in this paper can be used in the relativistic theory of reactions with polarized particles, in the construction of dispersion relations, and in other problems.

---

[1] H. P. Stapp, Phys. Rev. **103**, 425 (1956).

[2] M. Kawaguchi and N. Mugibayashi, Progr. Theoret. Phys. **8**, 212 (1952).

[3] V. I. Ritus, JETP **35**, 1485 (1958), Soviet Phys. JETP **8**, 1035 (1959).

[4] V. I. Ritus, JETP **33**, 1264 (1957), Soviet Phys. JETP **6**, 972 (1958).

Translated by W. H. Furry
286

SOVIET PHYSICS JETP VOLUME 11, NUMBER 5 NOVEMBER, 1960

# *ON THE THEORY OF NUCLEAR MATTER*

G. M. VAGRADOV and D. A. KIRZHNITS

P. N. Lebedev Physics Institute, Academy of Sciences, U.S.S.R.

Submitted to JETP editor November 4, 1959; resubmitted January 16, 1960

J. Exptl. Theoret. Phys. (U.S.S.R.) 38, 1499-1506 (May, 1960)

A simple method is proposed for quantitative description of the ground state of nuclear matter. It is shown that the gas approximation with a modified nucleon dispersion law can be employed. The error of the method does not exceed that of the empirical quantities.

1. Nuclear matter is usually pictured as a uniform infinite system of protons and neutrons having equal density and bound by nuclear forces alone. This obviously idealized model accounts essentially for the most important properties of atomic nuclei. The development of a microscopic theory of real nuclei must begin with an explanation of the fundamental properties* of nuclear matter through the assumption of some interaction potential between isolated nucleons.

The specific character of the many-particle problem of nuclear matter is based on the nature of the nuclear forces — the strong short-range repulsion (with range c) and the relatively weak long-range attraction. The problem is clearly defined by two very important qualitative restrictions. In nucleonic interactions a very important part is played by the Pauli exclusion principle, which forbids virtual transitions into the Fermi sphere and thus effectively suppresses interactions. Also, because of the smallness of the parameter $\rho c^3$ simultaneous collisions† of three or more nucleons are unlikely; therefore collisions are governed by pair correlations.

In the present paper we attempt to construct a simple quantitative scheme which will take both of the foregoing factors into account as completely as possible and will thus provide a quantitative justification for the simplifications that are introduced.

The fundamental investigations of Brueckner and his collaborators (in reference 1, for example) have produced a theoretical apparatus which yields results that are quite close to experimental data, but which is extremely complex and cumbersome. This complexity does not appear to be justified. Brueckner's scheme is a direct extension of the Hartree-Fock method to a case in which pair correlations of particles must be taken into account. Therefore an exact description is given of the interaction of each pair of particles moving in the self-consistent field of the remaining particles. The Brueckner scheme thus reflects the second of the foregoing circumstances (the possibility of neglecting triple and higher correlations).

However, this scheme does not utilize the possible simplification associated with the exclusion principle. It is equally significant that the problem of pair correlations is solved exactly in terms of the parameter $\rho c^3$. Thus higher-order terms in this parameter are taken into account although they are unimportant to the extent to which triple or more complex correlations can be neglected.*

Weisskopf and his co-workers[2] have clearly shown the possibility of simplifying the theory, but despite the convincing qualitative arguments the program is essentially incomplete. This results to a considerable extent from the important part played in Weisskopf's argument by a very indefinite quantity, the so-called "healing distance." Therefore the method of the indicated authors[2] is too complicated. It will be shown below that we do not need to analyze and solve the Bethe-Goldstone equation by the complicated self-consistent procedure to derive the nucleon dispersion law etc.

2. In presenting the results we shall first discuss the choice of an interaction potential. The theory of nuclear matter is usually based on an empirical potential for nucleons interacting pair-

---

*The fundamental properties of nuclear matter are the nucleon density (corresponding to $p_0 \approx 1.5 f^{-1}$) and the binding energy $\varepsilon \approx 15$ Mev/nucleon. The Fermi momentum $p_0$ is related to the nucleon number density $\rho$ by $p_0 = (3\pi^2\rho/2)^{1/3}$ We shall assume $\hbar = 1$.

†By collisions we mean the entrance of particles within the range of repulsive forces.

*It may be necessary to use Brueckner's method when pair correlations are especially distinguished in some sense, as, perhaps, in the superfluidity of nuclear matter.

wise. The many-body forces which arise are not taken into account and their magnitude is still an open question.

Following Weisskopf et al.[2] we shall limit ourselves here to the simplified Hamiltonian

$$\hat{H} = \sum_i \hat{p}_i^2 / 2M + \sum_{i<j} v_{ij}. \tag{1}$$

The potential v consists of the "hard-core" potential

$$v_c = \infty \quad (r < c), \qquad v_c = 0 \quad (r > c) \tag{2}$$

and the attractive potential

$$v_a = -V_0 \quad (c < r < a), \qquad v_a = 0 \quad (r < c,\ r > a), \tag{3}$$

where $c = 0.4\,\mathrm{f}$, $a = 2.3\,\mathrm{f}$, $V_0 = \pi^2/4M(a-c)^2 = 28.4$ Mev. The attractive forces are of the Serber type

$$v_{ij} = v_c(r_{ij}) + v_a(r_{ij})\hat{S}_{ij}, \tag{4}$$

where $\hat{S} = (1 + \hat{P})/2$ is the appropriate exchange operator.

The assumed Hamiltonian neglects tensor and spin-orbit forces as well as the dependence of the interaction on spin states. However, as a result of averaging these effects play a much smaller part in nuclear matter than in interactions between isolated nucleons. Results which have been obtained by using a more exact Hamiltonian will be published in the near future.

**3.** We wish to determine the energy $\epsilon$ per nucleon as a function of the maximum momentum $p_0$. Minimization of $\epsilon(p_0)$ will then yield the equilibrium values of $p_0$ and the binding energy.*

The total energy $\epsilon$ consists of two parts, with the kinetic energy of an ideal nucleonic gas given by the familiar expression

$$\varepsilon_1 = 3p_0^2/10\,M. \tag{5}$$

We shall now calculate the interaction energy including kinetic-energy corrections for a nonideal gas. It has been erroneously believed that the problem of nuclear matter does not depend on small parameters, whereas there are actually two such parameters, $\rho c^3$ and $(\rho a^3)^{-1}$, whose smallness corresponds to the simplifying factors discussed in Sec. 1.†

We shall now consider two ancillary problems, the first of which concerns the potential (2) ($v_a = 0$). We have here $\gamma = cp_0 = 0.59 < 1$, representing a comparatively rarefied Fermi gas. We can here apply the so-called gas approximation,[3] which means physically that in a rarefied nonideal gas such characteristics of interactions between isolated pairs of particles as the scattering amplitude etc. will be conserved and can be used to express corrections for a nonideal gas. The gas approximation thus accounts for the larger part (with respect to the parameter $\gamma$) of the pair correlations.

It has been shown by several authors[3] that the true interaction potential $v_c$ may be replaced by the pseudopotential

$$\hat{U} = \frac{4\pi c}{M}\delta(\mathrm{r})\left(1 + r\frac{\partial}{\partial r}\right) + O(c^3). \tag{6}$$

Expanding the energy of the system in a series with respect to c (in the general case with respect to the scattering amplitude[4]), we obtain the following expression for the interaction energy:

$$\varepsilon_2 = \frac{p_0^2}{M}\left\{\frac{\gamma}{\pi} + \frac{6(11 - 2\ln 2)}{35\pi^2}\gamma^2 + \left(0{,}13 + \frac{1}{2\pi}\right)\gamma^3 + \ldots\right\}. \tag{7}$$

The error resulting from the neglect of three-body correlations is*

$$\delta_1\varepsilon = 0.1 p_0^2\gamma^3/M \sim 2 \text{ MeV}. \tag{8}$$

In the second problem we assume $v_a \neq 0$ ($v_c = 0$). We now have $\xi = ap_0 = 3.4 > 1$, corresponding to a compressed Fermi gas, for which the Hartree-Fock method is sufficiently accurate.[5] Virtual processes are strongly inhibited by the exclusion principle so that only a small part is played by correlation terms corresponding to higher-order perturbations for $v_a$. This effect becomes more pronounced as the parameter $\xi$ increases, so that the latter is a more natural measure of the exclusion-principle effect than the healing distance.

The Hartree-Fock approximation is represented by the substitution

$$\sum_{i<j} v_a\hat{S} \to \sum_i \hat{V}, \tag{9}$$

where the single-particle potential V is given by

$$\hat{V}_i = \sum_j \langle j|v_a\hat{S}(1 - \hat{T})|j\rangle - N^{-1}\sum_{j<k}\langle jk|v_a\hat{S}(1 - \hat{T})|jk\rangle,$$

$\hat{T}$ is the coordinate-permutation operator and N is the total number of particles.

The following self-consistent Hamiltonian is obtained:

---

*This is not an approximate statement of the problem. To check this one need only imagine the system to be inclosed in a large box with movable walls and to consider that at the minimum point the pressure on the walls disappears.

†It is also significant that the correction terms [see (8) and (17) below] are small and that these terms differ in sign.

*See reference 2. The positive sign in (8) [as in (7)] is associated with a reduction of the effective volume of the system due to repulsion.

$$\hat{H}_0 = \sum_i (\hat{p}_i^2/2M + \hat{V}_i) \equiv \sum_i (\hat{p}_i^2/2M + W(\hat{p}_i)) + C(p_0), \tag{10}$$

$$W(p) = \frac{3V_0}{\pi}\left\{\frac{\sin\eta\cdot\sin\xi}{\eta} - \frac{1}{2}[\mathrm{Si}(\xi+\eta) + \mathrm{Si}(\xi-\eta)] - \sin\xi + \mathrm{Si}\,\xi\right\}, \tag{11}$$

where $\eta = ap$. The expression for $C(p_0)$ will not be given.

The interaction energy in this approximation is

$$\varepsilon_3 = N^{-1}\sum_{i<j}\langle ij\,|\,v_a\hat{S}(1-\hat{T})\,|\,ij\rangle = -\frac{V_0}{6\pi}\left\{\xi^3 - \gamma^3 + 9\,\mathrm{Si}\,2\xi - \frac{9}{2\xi}(3-\cos 2\xi) + \frac{9}{\xi^2}\sin 2\xi\right\}. \tag{12}$$

The error resulting from the substitution (9), that is, the correlation energy, can be calculated by regarding the difference

$$\hat{H}' = \sum v_a\hat{S} - \sum\hat{V} \tag{13}$$

as a perturbation. The first order for $H'$ gives

$$\langle\psi_0\,|\,\hat{H}'\,|\,\psi_0\rangle \equiv 0;$$

this expresses the self-consistency of the problem [$\psi_0$ is the wave function of the system with the Hamiltonian (10)]. The sum of important higher-order terms, which was obtained in reference 5, is*

$$\delta_2\varepsilon = -\frac{3(1-\ln 2)}{16\pi^2}V_0^2Ma^2\ln\frac{p_0}{V_0Ma^2} \sim -1\ \text{Mev}. \tag{14}$$

**4.** We shall utilize the foregoing results to solve the basic problem with the potential (4).

We shall show that even when the potential $v_c$ does not vanish the Hartree-Fock approximation may be used for $v_a$, that is, the original Hamiltonian (1) can be replaced by

$$\hat{H}_1 = \hat{H}_0 + \sum_{i<j} v_c, \tag{15}$$

where $\hat{H}_0$ is, as previously, given by (10) and (11). The resulting error is determined by the procedure explained above. The difference between $\hat{H}$ and $\hat{H}_1$ is again found through (13), although the first-order correction no longer disappears since the wave function $\psi_1$ of the Hamiltonian (15) is not now consistent with the single-particle potential $\hat{V}$ (calculated by means of $\psi_0$).

The average difference between $\psi_1$ and $\psi_0$ is insignificant because $\gamma$ is small, as well as because of the exclusion principle. Therefore the first-order correction in $\hat{H}'$ resulting from the interference of $v_c$ and $v_a$ is

$$\delta_3\varepsilon = N^{-1}\langle\psi_1\hat{H}'\psi_1\rangle \approx 2N^{-1}\,\mathrm{Re}\,\langle\psi_0\hat{H}'\delta\psi\rangle,$$

where $\delta\psi = \psi_1 - \psi_0$. The pseudopotential (6) is used to determine $\delta\psi$.* We thus obtain

$$\delta_3\varepsilon = \frac{8\pi c}{MN}\,\mathrm{Re}\sum_n{}'\,\langle 0\,|\,H'\,|\,n\rangle\langle n\,|\,\delta(\mathbf{r})\,|\,0\rangle/(E_0 - E_n).$$

When only the important terms are retained we finally have

$$\delta_3\varepsilon = -V_0\left(\frac{\gamma^3}{\pi} - \frac{6(1-\ln 2)}{\pi^2}\frac{\gamma}{\xi}\right) \sim -1\ \text{Mev}. \tag{16}$$

For high-order terms in $H'$ the difference between $\psi_1$ and $\psi_0$ may be altogether neglected; (14) may therefore be used. The total error resulting from the replacement of $\hat{H}$ by $\hat{H}'$ is

$$\delta_2\varepsilon + \delta_3\varepsilon \sim -2\ \text{Mev}. \tag{17}$$

**5.** In the preceding section we arrived at the approximate Hamiltonian

$$\hat{H}_1 = \sum_i E(\hat{p}_i) + \sum_{i<j} v_c(r_{ij}) + C(p_0), \tag{18}$$

$$E(p) = p^2/2M + W(p). \tag{19}$$

In order to determine the corresponding ground-state energy the gas approximation equations must be extended to the case of a nonquadratic dispersion law [see (19)]. A pair interaction will then depend on the combined momentum of the two particles. Following the procedure used in references 3 and 4, the energy is expanded in terms of the scattering amplitude (or, more precisely, the $t$-operator introduced below) for a pair of isolated nucleons interacting through the potential $v_c$. The wave function of this system satisfies the equation

$$\psi_{12} = \psi_{12}^0 - \hat{Q}^{-1}v_c\psi_{12}, \tag{20}$$

where

$$\hat{Q} = F(\hat{p}_1) + E(\hat{p}_2) - E(p_1) - E(p_2),$$

$$\psi_{12}^0 = \exp\{i(\mathbf{p}_1\mathbf{r}_1 + \mathbf{p}_2\mathbf{r}_2)\},$$

and $\mathbf{p}_{1,2}$ represent initial nucleon momenta. (Here and hereinafter the principal values of inverse operators will be understood.) The new operator $\hat{t}$ is introduced through

$$\psi_{12} = (1 - \hat{Q}^{-1}\hat{t})\,\psi_{12}^0. \tag{21}$$

Unlike the case of $v_0$ the matrix elements of this operator are finite and are related simply to the scattering amplitude. By combining (20) and (21) we obtain

---

*The negative sign in (14) follows from the variation principle; the wave function in the form of a determinant results in a higher energy value.

*In these computations we ignore the change of the dispersion law for nucleons since mass does not appear in the final expression (16).

$$v_c = \hat{t}\,(1 - \hat{Q}^{-1}\hat{t})^{-1}.$$

Substitution of this expression in (18) followed by an expansion in terms of $\hat{t}$ yields the following correction to the pair energy:

$$\delta E_{12} = \langle 12 | t | 12 \rangle + \sum_{i,k} \frac{\langle 12 | t | ik \rangle \langle ik | t | 12 \rangle}{E_1 + E_2 - E_i - E_k} [(1 - N_i)(1 - N_k) - 1] + \ldots. \tag{22}$$

where $N_i$ is the occupation number.

We now proceed to determine the operator $\hat{t}$ for the potential (2). The wave function of a pair satisfies

$$\hat{Q}\psi_{12} = 0 \quad (r_{12} > c), \qquad \psi_{12} = 0 \quad (r_{12} \leqslant c). \tag{23}$$

From (21) and (23) we obtain two conditions which must be satisfied by $\hat{t}$:

a) $\hat{t}\psi^0_{12} = 0$ for $r_{12} > c$, b) $\psi^0_{12} = \hat{Q}^{-1}\hat{t}\,\psi^{\,0}_{12}$ for $r_{12} = c$ [9]. *

We shall obtain $\hat{t}$ in the form

$$\hat{t} = A\delta(\mathbf{r}_{12}) + \mathbf{B}\nabla\delta(\mathbf{r}_{12}) + \ldots, \tag{24}$$

which corresponds to condition a).

In the center-of-mass system with the notation

$$\mathbf{p}_1 + \mathbf{p}_2 = \mathbf{P}, \quad \mathbf{p}_1 - \mathbf{p}_2 = 2\mathbf{k},$$

$$q(\hat{p}) = E(\hat{p} + \mathbf{P}/2) + E(\hat{p} - \mathbf{P}/2) - E(\mathbf{k} + \mathbf{P}/2) - E(\mathbf{k} - \mathbf{P}/2)$$

condition b becomes

$$e^{i\mathbf{kn}c} = (2\pi)^{-3} \int d\mathbf{p}\, q^{-1}(\mathbf{p})\,(A + i\mathbf{p}\mathbf{B} + \ldots)\, e^{i\mathbf{pn}c}; \tag{25}$$

$\mathbf{n}$ is the unit vector of $\mathbf{r}_{12}$.

It is significant that, in accordance with (11) and (19), for high momentum $E \rightarrow p^2/2M$, this corresponds to the "stripping" of a fast nucleon. Since in (24) $p \sim c^{-1}$ is large a nonquadratic dispersion law affects only high-order terms in c. Therefore when (25) is expanded in spherical harmonics with respect to $\mathbf{n}$ the nonquadratic character of the dispersion law must be taken into account only for the term with $l = 0$, since the term with $l = 1$ [corresponding to the second term in (24)] leads to $\mathbf{B} \sim c^3$.† We therefore have

$$A^{-1} = \frac{k}{(2\pi)^3 \sin kc} \int d\mathbf{p}\, p^{-1} q^{-1}(p) \sin pc. \tag{26}$$

As already mentioned the coefficient $\mathbf{B}$ remains the same as for the quadratic dispersion law. Additional terms in the expansion of (25) lead to quantities of the order $\sim c^5$ and may be neglected.

6. The results obtained in the preceding section are sufficient for a solution of the problem in principle. Insertion of the dispersion law (11) leads to integrals which can be solved only numerically. Because of the approximate character of the potential (4) that we are employing we shall limit ourselves to an approximate analytic calculation. The dispersion law must now be simplified, but this will not introduce a large error into the binding energy. The numerical results show that the effects of a nonquadratic dispersion law contribute only about 25% to the energy $\epsilon_2$. Equation (11) will be approximated by means of

$$E(p) = p^2(1 + \mu)/2M, \quad p < \lambda p_0,$$

$$E(p) = p^2/2M + p_0^2\lambda^2\mu/2M, \quad p > \lambda p_0.$$

The parameters $\mu(p_0)$ and $\lambda(p_0)$ are obtained by the method of least squares. We also introduce the notation [see (26) and the Appendix]

$$A = 4\pi \tan(kc)/kM^*.$$

$M^*(\mathbf{p}_1\mathbf{p}_2, \mathbf{p}_0)$ is slightly dependent on $\mathbf{p}_{1,2}$ with a maximum variation of 8%; its average with respect to $\mathbf{p}_{1,2}$ may be regarded as a constant. Omitting the intermediate steps, we present the final expression

$$M/M^* = 1 + \gamma\Phi(p_0),$$

$$\Phi = \frac{2}{\pi}\left\{\left[\frac{\mu}{1+\mu} + \sqrt{\mu}\left(\frac{\pi}{2} - \tan^{-1}\frac{1}{\sqrt{\mu}}\right)\right] - \left[\lambda - \frac{3}{10\lambda}\left(1 + \frac{1}{2\mu}\right)\right] + \frac{3 + 2\mu}{10\lambda(1+\mu)^2}\right\}.$$

The second-order term in $\gamma$ contributes $\sim 0.01$ and may be neglected. Furthermore, in view of the fact that in (22) integration over intermediate momenta is actually performed in a narrow region near the Fermi boundary we use the substitution

$$E_1 + E_2 - E_i - E_k \rightarrow (p_1^2 + p_2^2 - p_i^2 - p_k^2)/2M_0,$$

where

$$\frac{M}{M_0} = \frac{M}{p_0}\frac{\partial E(p)}{\partial p}\bigg|_{p_0} = 1 + \frac{3}{2\pi}\frac{V_0 Ma^2}{\xi}\left(1 + \frac{\sin 2\xi}{2\xi} - \frac{2\sin^2\xi}{\xi^2}\right).$$

We now finally have

---

*A similar condition holds true for $r_{12} < c$. However, it is shown in the Appendix that violation of this condition affects only higher terms of the expansion in c.

†According to reference 2, for a quadratic dispersion law $\varepsilon_2$ may be confined to the three terms of the expansion with respect to $\gamma$ that are given in (7). We are utilizing here this approximation.

$$\varepsilon_2 = \frac{p_0^2}{M}\left\{\frac{\gamma}{\pi}\left(\frac{M}{M^*}\right) + \frac{6\,(11 - 2\ln 2)}{35\,\pi^2}\,\gamma^2\left(\frac{M}{M^*}\right)^2\frac{M_0}{M} + 0.13\,\gamma^3\left(\frac{M}{M^*}\right)^3\left(\frac{M_0}{M}\right)^2 + \frac{1}{2\pi}\gamma^3 + \ldots\right\}. \qquad (27)$$

Minimizing the sum of (15), (12) and (27), we obtain for the binding energy and equilibrium value of $p_0$:

$$\varepsilon \approx -11 \text{ Mev/nucleon} \quad p_0 \approx 1.4 \text{ f}^{-1}.$$

With this value of $p_0$ we obtain $\mu \approx 0.75$, $\lambda = 1.3$, $M/M^* \approx 1.40$, $M/M_0 \approx 1.54$; the separate energy components have the values

$$\varepsilon_1 \approx 25, \quad \varepsilon_2 \approx 32, \quad \varepsilon_3 \approx -68 \text{ Mev}.$$

The terms in $\epsilon_2$ have the values 21, 6.0, 2.5, and 2.5 Mev respectively [in the same order as (27)].

The foregoing results pertain to the ground state of the Hamiltonian (18). In order to estimate the error resulting from the difference between (18) and the exact Hamiltonian (1) we add (8) and (17) and find that even when the effective mass is introduced into (8) the error of our method does not exceed 1 Mev/nucleon. The binding energy of nuclear matter is known to the same degree of accuracy. We have thus justified the replacement of the exact Hamiltonian (1) by the simplified form (18) which permits a much less complicated calculation.

In our opinion the simplification of the mathematical apparatus is one of the principal problems of the microscopic theory of nuclear matter. Calculations of different effects can then be performed to test the validity of using an interaction potential for isolated nucleons.

The authors are indebted to I. E. Tamm, V. L. Ginzburg, A. S. Davydov for discussions and valuable comments, and to L. V. Pariĭskaya for calculations.

## APPENDIX

We shall show that although the operator (24) violates the condition $\psi_{12}^0 = \hat{Q}^{-1}\hat{t}\psi_{12}^0$ for $r_{12} < c$ only the terms of the order $c^4$ and higher are affected. Since this is the region of high momentum we may confine ourselves to the quadratic dispersion law. For the same reason we consider only the S state and obtain from (24) and (26) [see (6)]

$$\hat{t}_0 = \frac{4\pi}{M}\frac{\tan kc}{k}\,\delta(\mathbf{r}).$$

On the other hand, we use the familiar exact expression $\psi_{12} = \exp[iP(r_1 + r_2)/2]\,\varphi(r)$, where $\varphi(r) = \sin k(r - c)/r\cos kc$, $r > c$; $\varphi(r) = 0$, $r \leqslant c$.

From (21) we have $\hat{Q}\psi_{12} = -\hat{t}\psi_{12}^0$, whence

$$\hat{t}\,\frac{\sin kr}{r} = -\frac{\hat{p}^2 - k^2}{M}\,\varphi(r).$$

Thus the exact expression for $\hat{t}$ is

$$\hat{t} = \frac{\tan kc}{Mkr^2}\,\delta(r - c). \quad \text{formula}$$

Calculation the Fourier transforms of $\hat{t}$ and $\hat{t}_0$, we obtain $(p \sim p_0)$

$$t_p - t_{0p} = \frac{1}{2\pi^2 M}\,\frac{\tan kc}{k}\left(\frac{\sin cp}{cp} - 1\right) \sim c^3.$$

It is easily seen that $< 12\,|\,\hat{t} - t_0\,|\,12 >$. In view of (22) our statement is therefore proved.

---

[1] K. A. Brueckner and J. L. Gammel, Phys. Rev. **109**, 1023 (1958); K. A. Brueckner, Revs. Modern Phys. **30**, 561 (1958).

[2] Gomes, Walecka, and Weisskopf, Ann. Phys. **3**, 241 (1958); A. de-Shalit and V. F. Weisskopf, Ann. Phys. **5**, 282 (1958).

[3] K. Huang and C. N. Yang, Phys. Rev. **105**, 767 (1957); T. D. Lee and C. N. Yang, Phys. Rev. **105**, 1119 (1957); C. De Dominicis and P. C. Martin, Phys. Rev. **105**, 1417 (1957).

[4] A. A. Abrikosov and I. M. Khalatnikov, JETP **33**, 1154 (1957), Soviet Phys. JETP **6**, 888 (1958); V. M. Galitskiĭ, JETP **34**, 151 (1958), Soviet Phys. JETP **7**, 104 (1958).

[5] D. A. Kirzhnits, JETP **37**, 585 (1959), Soviet Phys. JETP **10**, 414 (1960).

Translated by I. Emin
287

SOVIET PHYSICS JETP VOLUME 11, NUMBER 5 NOVEMBER, 1960

# *FLUCTUATIONS IN THE ANGULAR DISTRIBUTION OF SECONDARY PARTICLES OF EXPLOSIVE SHOWERS*

B. A. NIKOL'SKIĬ and A. P. MISHAKOVA

Submitted to JETP editor November 6, 1959

J. Exptl. Theoret. Phys. (U.S.S.R.) **38**, 1507-1511 (May, 1960)

Calculations are carried out on the fluctuations in the angular distribution of shower particles which imitate the "two-center" shower production mechanism. It is concluded that most experimentally observed showers possessing a "two-center" angular distribution can be explained by natural statistical fluctuations in the angular distribution. The calculations are performed by the Monte Carlo method.

In recent literature there has been a rather broad discussion on the so called "two-center" model for the production of shower particles in explosive showers of high energy ($10^{10}-10^{14}$ ev).[1-7] According to this model, the secondary particles of the explosive shower originate in the decay of two "excited centers" produced in the collision of the primary particles and moving in opposite directions (in the c.m. system), the angular distribution of the secondary particles in the rest system of the excited center being isotropic. The experimental basis of the "two-center" model for the production of explosive showers was provided by the characteristic shape of the angular distribution of the secondary particles observed in a number of showers. The clearest "two-center" shape of the angular distribution is disclosed when drawn in the coordinates $\log[F/(1-F)] = f(\lambda)$, where we use the following notation: $\lambda = \log\tan\vartheta$; $\vartheta$ is the angle of emission of the shower particle in the laboratory system of coordinates, $F(\vartheta)$ is the fraction of shower particles with angles smaller than the given angle. In these coordinates an angular distribution isotropic in the c.m. system is represented in the form of a straight line making an agle of $\alpha = 65°$ with the axis of abscissas.

The anisotropy in the angular distribution of the shower particles in the c.m. system (which corresponds to that experimentally observed — see Fig. 3 below) is represented by a line whose slope $\alpha$ decreases with an increase in the fraction of shower particles emitted at angles close to 0° and 180° in the c.m. system, i.e. with a greater anisotropy. The "two-center" angular distribution is represented in these coordinates by a stepped curve with a more or less distinct horizontal segment dividing the angular distribution curve into two parts. This horizontal segment reflects the absence of shower particles in some angular interval separating the "narrow" and "wide" cones of the shower particles in the laboratory system. It is assumed that the "narrow" and "wide" cones separated in this way consist of shower particles produced in the decay of the two "excited centers." According to the "two-center" model of shower production, the angular distribution of the particles of the "narrow" and "wide" cones, when drawn separately, should be isotropic in their respective c.m. systems, i.e. in the coordinates $\log[F/(1-F)] = f(\lambda)$ they should be represented by straight lines of slope $\alpha = 63°$.

Figure 1 shows characteristic examples of "two-

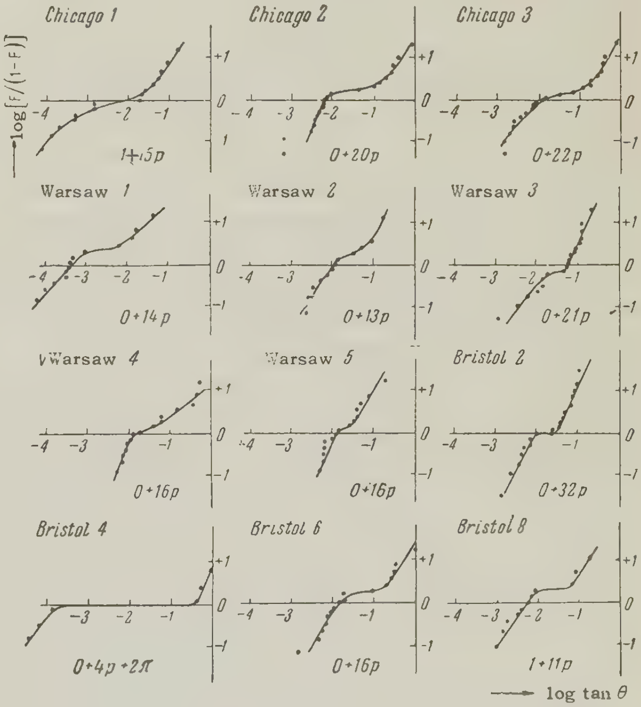

FIG. 1. Experimentally observed "two-center" angular distributions of shower particles.[6]

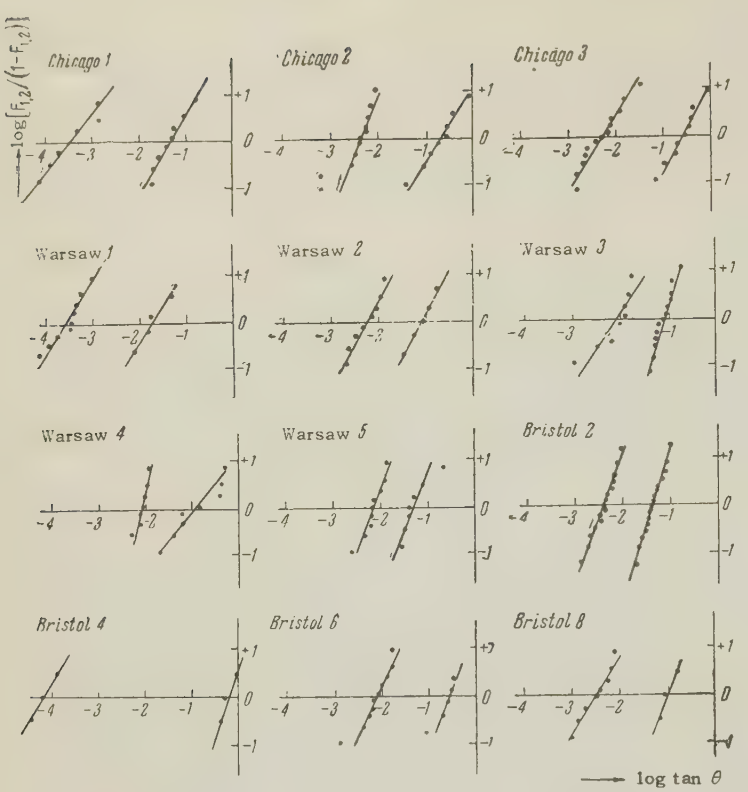

FIG. 2. Angular distributions of "narrow" and "wide" parts of the experimentally observed[6] "two-center" showers shown in Fig. 1.

center" angular distributions observed in various laboratories.

Figure 2 shows graphs of the two parts of these showers, corresponding to the narrow and wide cones in the laboratory system, which may be interpreted as the isotropic decay of two "excited centers."*

It should, however, be pointed out that the interpretation of the angular distribution of the individual showers should take into account the natural statistical fluctuations, which may lead to significant deformations of the angular distribution curves. In particular, the angular distributions of the shower particles shown in Fig. 1 may be the result of such fluctuations. In order to estimate the probability that statistical fluctuations lead to angular distributions imitating the "two-center" mechanism of shower production, we carried out a calculation by the method of random samples (Monte Carlo method). As the initial angular distribution of shower particles we took the experimentally observed distribution $f(\vartheta)$ which has been based on a large number of showers.[8] Figure 3 shows the distribution $f(\vartheta)$ in the c.m. system of the colliding particles $(\gamma_c = \cot\vartheta_{1/2})$. In the same figure the experimental angular distribution curve is also given in the coordinates $\log[F/(1-F)] = f(\lambda)$ for a half angle $\vartheta_{1/2}$

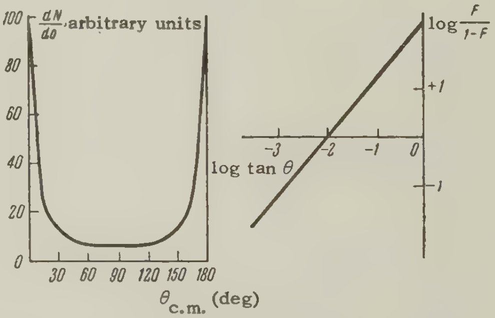

FIG. 3. Experimental angular distribution of shower particles according to data from a large number of showers of energies $10^{11}$ ev.[8]

$= 0.01$ rad. From this distribution were drawn 100 random samples of angular distributions consisting of $n_s = 20$ shower particles and another 100 with $n_s = 10$.

From the 200 angular distribution curves obtained in this way, we chose 16 curves for the case $n_s = 20$ and 19 curves for the case $n_s = 10$. These imitated to a satisfactory degree, the angular distributions of the "two-center" model. Nine of the angular distributions that were chosen are shown in Fig. 4 in the coordinates $\log[F/(1-F)] = f(\lambda)$ for the case $n_s = 20$. In Fig. 5 are shown the corresponding angular distributions drawn separately for the two parts of these showers ("narrow" and "wide" cones in the laboratory system). The 19 curves of the "two-center" angular distribution for the case $n_s = 10$ are of similar shape.

---

*The curves in Figs. 1 and 2 were taken from the report of Piccioni at the 8th Conference on High-Energy Physics.

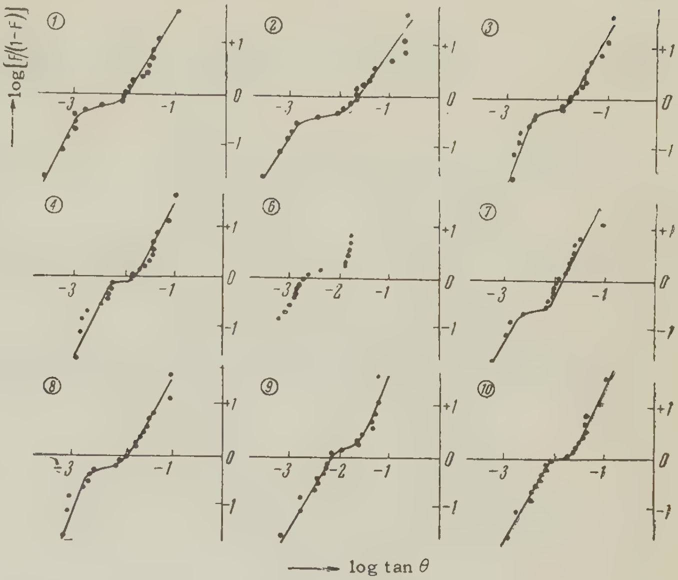

FIG. 4. Results of the calculation by the Monte Carlo method for shower particles imitating the "two-center" mechanism of production of showers for the case $n_s = 20$ (the numbers in the circles are for identification purposes).

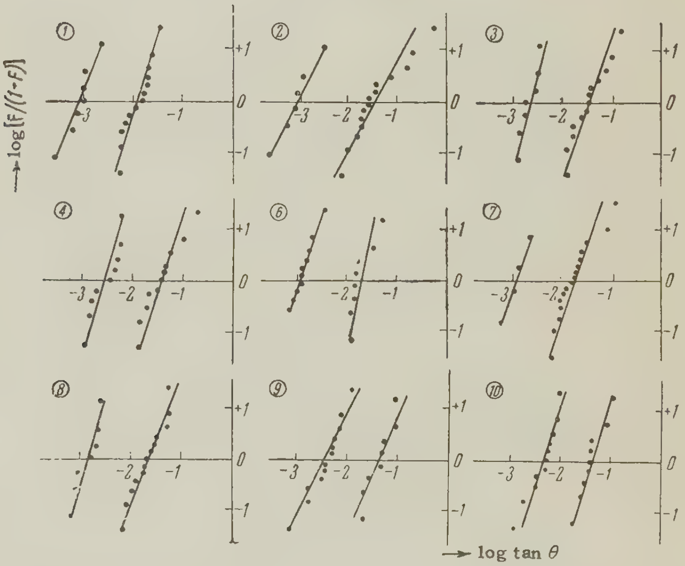

FIG. 5. Angular distribution of "narrow" and "wide" parts of calculated showers shown in Fig. 4.

From the comparison of the angular distributions shown in Figs. 1 and 4 it is seen that the deformations of the angular distribution caused by statistical fluctuations imitate sufficiently well a large number of the experimentally observed cases of the "two-center" angular distribution. From the calculations it further follows that the number of randomly chosen angular distributions that imitate the "two-center" model make up 15 — 20% of the total number of showers for which the number of shower particles is $n_s = 10 - 20$. This figure is in approximate agreement with the experimentally observed fraction of "two-center" angular distributions of shower particles, which, according to the data given by Power,[7] is ~ 20%.

Hence the obtained results indicate, at least, that the greater part of the experimentally observed cases of a "two-center" angular distribution of shower particles can be explained by natural statistical fluctuations. Of course, the comparison of the calculated and experimental data is basically of a qualitative character. At the same time, it is obvious that any reliable evidence in favor of the existence of a "two-center" mechanism for the production of explosive showers can be obtained only by a fuller space — energy analysis of the showers. Proof of the "two-center" mechanism of shower production based only on the analysis of the angular distribution of the shower particles is quite difficult, since it is necessary to take into account correctly the influence of statistical fluctuations, which is possible only by substantially increasing the available experimental data.

In conclusion the authors express their gratitude to I. I. Gurevich for his constant interest in this work, to N. A. Lobachev for help in the calcula-

tions. We also wish to thank G. Cocconi and M. Miesowicz for sending us preprints of their work prior to publication.

---

[1] Ciok, Coghen, Gierula, Holynski, Jurak, Miesowicz, and Saniewska, Nuovo cimento **10**, 741 (1959).

[2] Z. Koba and S. Takagi, Nuovo cimento **10**, 755 (1959).

[3] K. Niu, Nuovo cimento **10**, 994 (1959).

[4] Burmeister, Lanius, and Meier, Nuovo cimento **11**, 12 (1959).

[5] G. Cocconi, Phys. Rev. **111**, 1699 (1958).

[6] O. Piccioni, 1958 Annual Internation Conference on High Energy Physics at CERN, Geneva, 1958, p. 75.

[7] C. F. Powell, Report at the 9th International Conference on High Energy Physics, Kiev, July, 1959.

[8] A. P. Mishakova and B. A. Nikol'skiĭ, JETP (U.S.S.R.) **37**, 1594 (1959), Soviet Phys. JETP **10**, 1130 (1960).

Translated by E. Marquit
288

SOVIET PHYSICS JETP VOLUME 11, NUMBER 5 NOVEMBER, 1960

# *COULOMB SCATTERING OF CHARGES IN A STRONG MAGNETIC FIELD*

YU. N. BARABANENKOV

Moscow State University

Submitted to JETP editor November 9, 1959

J. Exptl. Theoret. Phys. (U.S.S.R.) 38, 1512-1514 (May, 1960)

Coulomb scattering of charges in a strong magnetic field, when the impact parameter is much greater than the Larmor radius, is considered. The solution of the problem indicates that the collisions cannot change the plasma electric (ion) distribution function, which is symmetric with respect to the velocity component transverse to the magnetic field.

As is well known, a sufficiently strong magnetic field can affect the process of charge collisions in a plasma. This problem was discussed by E. Lifshitz[1] on the basis of the equation of Landau, and by Belyaev[2,3] on the basis of the equation of Bogolyubov. We want to demonstrate a somewhat different, rather graphic approach to the problem under discussion. At the basis of this approach lie very well-known representations of the drift of Larmor loops in crossed fields. In the present research, the problem of two charged particles is considered.

Thus, we consider two charges interacting according to Coulomb's law and located in a magnetic field. The magnetic field will be considered to be homogeneous and constant in time. Moreover, we shall assume that it is strong. This means that the two conditions

$$(ewH/c)/(e^2/R^2) \gg 1, \qquad R/\rho_L \gg 1, \tag{1}$$

are satisfied, where w is the velocity component of the charge transverse to the magnetic field, $\rho_L$ is the Larmor radius, R is the impact parameter. The equations of motion of the charges have the form

$$m_1 \ddot{\mathbf{x}}_1 = \frac{e_1}{c}[\dot{\mathbf{x}}_1 \times \mathbf{H}] + e_1 e_2 \mathbf{F}, \qquad \mathbf{F} = \mathbf{x}/x^3,$$
$$m_2 \ddot{\mathbf{x}}_2 = \frac{e_2}{c}[\dot{\mathbf{x}}_2 \times \mathbf{H}] - e_1 e_2 \mathbf{F}, \qquad \mathbf{x} = \mathbf{x}_1 - \mathbf{x}_2. \tag{2}$$

Here **F** is the strength of the Coulomb interaction of two unit positive charges. Under the conditions (1), we can simply (2), making use of the method of rapidly changing phase shift.[4]

As a result, we get

$$\dot{w}_1 = \dot{w}_2 = 0, \tag{3}$$

$$\dot{\mathbf{x}}_\perp = \frac{c(e_1 + e_2)}{H^2}[\mathbf{F}_\perp \times \mathbf{H}],$$
$$\dot{\mathbf{y}}_\perp = \frac{c(m_1 e_2 - m_2 e_1)}{H^2(m_1 + m_2)}[\mathbf{F}_\perp \times \mathbf{H}] \tag{4}$$

$$\ddot{x}_3 = (e_1 e_2/\mu) F_3, \qquad \ddot{y}_3 = 0, \tag{5}$$

where the index 3 denotes the coordinate axis parallel to the magnetic field, $\mu$ is the reduced mass of the charges. Equations (3) — (5) have a simple meaning. Each charge rotates around the magnetic field in a Larmor ring with speed $w_i$ ($i = 1, 2$). The centers of the Larmor rings (in the case of a strong magnetic field, it is the custom to call them guiding centers) move along, and perpendicular to, the magnetic field. Equations (4) describe the motion of the guiding centers perpendicular to the field, while Eqs. (5), the motion along the field. As in (2), $\mathbf{x} = \mathbf{x}_1 - \mathbf{x}_2$, but now $\mathbf{x}_1$ and $\mathbf{x}_2$ refer to the guiding centers and not the charge; $\mathbf{y} = (m_1\mathbf{x}_1 + m_2\mathbf{x}_2)/(m_1 + m_2)$ is the center of mass of the guiding centers. We note that Eqs. (3) — (5) could be written down directly from elementary considerations on the drift velocity of the guiding center in crossed fields.

We proceed to analysis of Eqs. (3) — (5). First of all, according to (3), the velocities of the Larmor rotation of the charges in the scattering process do not change. Further, from the first of Eqs. (4), we find $x_\perp \equiv R = \text{const}$, i.e., the projection of the distance between the guiding centers on the plane perpendicular to the magnetic field is a constant quantity. Finally, an interesting integral of the motion follows from (4): the "electric" center of gravity of the guiding centers:

$$\mathbf{z} = (e_1\mathbf{x}_1 + e_2\mathbf{x}_2)/(e_1 + e_2) = \text{const}.$$

We obtain the following picture of the motion of the guiding centers. Each guiding center moves along a helix lying on the surface of a right circular cylinder. The axis of the cylinder is parallel to the magnetic field and always passes through the electric center of gravity. The displacements of the guiding centers as a result of scattering can be found from the following formulas:

$$\Delta \mathbf{x}_{\perp}^{(1)} = \frac{e_2}{e_1 + e_2} \Delta \mathbf{x}_{\perp}, \qquad \Delta \mathbf{x}_{\perp}^{(2)} = -\frac{e_1}{e_1 + e_2} \Delta \mathbf{x}_{\perp},$$

$$\Delta \mathbf{x}_{\perp} = \frac{1}{H} [\mathbf{H} \times \mathbf{x}_{\perp}^{(0)}] \sin \Delta\varphi - 2\mathbf{x}_{\perp}^{(0)} \sin^2 \frac{\Delta\varphi}{2},$$

$$\Delta\varphi = -\frac{c(e_1 + e_2)}{HR^3} \int_{-\infty}^{\infty} \left(1 + \frac{x_3^2}{R^2}\right)^{-3/2} dt. \tag{6}$$

Here the index zero denotes the initial instant of time. In order to compute $\Delta\varphi$ — the angle of turning of the vector $\mathbf{x}_{\perp}$ as the result of scattering — it is necessary to solve the preliminary equation (5). As usual, we obtain the energy integral

$$\mu u^2/2 + e_1 e_2 (R^2 + x_3^2)^{1/2} = \text{const} = \mu u_0^2/2, \tag{7}$$

where $u = \dot{x}_3$. Two important consequences follow from (7). In the first place, unlike charges travel alongside one another, without changing their velocities. In the second place, for like charges there exists a critical impact parameter $R_c = 2e_1e_2/\mu u_0^2$. For $R > R_c$, the identical charges travel alongside one another, similar to the unlike charges, without changing their speeds. If now $R < R_c$, then the charges approach each other up to some minimum distance, after which they recoil backwards, like elastic spheres in a head-on collision.

We shall now apply these results to the case of a plasma. We obtain the following important conclusion: if, at a certain moment of time, the electron (or ion) distribution function is an even function of the transverse (to the magnetic field) velocity, an arbitrary function of the longitudinal velocity, and is homogeneous in space, then it does not change with time. The constancy of the distribution with respect to the transverse velocities follows directly from (3). The constancy relative to the longitudinal velocity is somewhat more complicated. We shall consider electrons as an example. From what has been said above, it is clear that their distribution function can change only upon collisions with other electrons. But in the collision of two electrons moving along the field, they exchange velocities, since their masses are the same. In this case the distribution function cannot change. In order to make the latter circumstance clearer, we recall the Boltzmann collision integral. The integrand is proportional to the difference $f(u_1') f(u_2') - f(u_1) f(u_2)$. If $u_1' = u_2$, $u_2' = u_1$, then the integral vanishes identically. We note that the conclusion which we have reached is in agreement with the result of Lifshitz and Belyaev on the problem of relaxation in a plasma: these authors showed that the collisions with an impact parameter larger than the Larmor radius make no contribution to the relaxation process.

In conclusion, I take the opportunity to express my thanks to S. Temko and Yu. Klimontovich for discussion of the research.

---

[1] E. M. Lifshitz, JETP 7, 390 (1937)

[2] S. T. Belyaev, Сб. Физика плазмы (Collection: Plasma Physics), Acad. Sci. Press, 3, 1958, p. 50.

[3] S. T. Belyaev, ibid.

[4] N. N. Bogolyubov and Yu. Mitropol'skiĭ, Асимптотические методы в теории нелинейных колебаний, (Asymptotic Methods in the Theory of Non-linear Vibrations) Fizmatgiz, 2nd ed., 1958.

Translated by R. T. Beyer
289

# *ON TRANSITIONS BETWEEN HYPERFINE STRUCTURE LEVELS IN MU-MESIC ATOMS*

A. E. IGNATENKO

Joint Institute for Nuclear Research

Submitted to JETP editor November 13, 1959

J. Exptl. Theoret. Phys. (U.S.S.R.) **38**, 1515-1517 (May, 1960)

The possibility of an experimental verification of the existence of transitions between hyperfine structure levels in mesic atoms is considered. A convenient method, in the case of mesic atoms possessing nuclear spins $J > 1/2$, is shown to be the measurement of the precession frequency of the mesic atoms.

THE question of the existence of transitions between the hyperfine structure levels is of great interest in the investigation of the effects of the hyperfine structure in $\mu$-mesic atoms. In fact, a theoretical analysis of these effects, which manifest themselves in the capture of polarized mesons,[1-3] is always carried out for the case of isolated mesic atoms. Actually, however, an experimental verification of the predictions of the theory is possible only when the mesic atoms are produced and stopped in the medium Yet the presence of the medium can complicate the situation. Thus, for example, while the hyperfine structure states with $F = J + 1/2$ and $F = J - 1/2$ form in the case of isolated atoms an incoherent mixture, transitions can occur between them in certain cases in a medium. In particular, in liquid hydrogen one observes the phenomenon of meson "jump" from one proton to another with simultaneous transition into the lower hfs state.[4-6] Attention was called in references 7 and 8 to the need of accounting for the influence of the medium on the hfs effects on other substances. For example, two types of transitions are possible in metals, accompanied either by conversion on the conduction electrons or by magnetic dipole radiation. The expressions for the probabilities of the corresponding transitions $w_k$ and $w_p$ have the following form:[7]

$$w_k \approx 10\left(\frac{1}{137}\right)^6 Z\left(\frac{m_e}{m_\mu}\right)^3 \frac{m_\mu c^2}{\hbar}, \qquad (1)$$

$$w_p \approx 10\left(\frac{1}{137}\right)^{13} Z_{eff}^9 \left(\frac{m_\mu}{m_p}\right)^3 \frac{m_\mu c^2}{\hbar}. \qquad (2)$$

It is obvious that if the medium is not a metal, there will be no transitions of type $w_k$.

In this article we shall touch upon the question of experimental verification of the existence of the transitions. One of the methods,[8] proposed for the detection of transitions, consists of investigating the curvature K of the $\mu^-$-meson decay curve. Thus, with the A-V interaction universal and in the presence of transitions in metals having nuclear magnetic moment $\mu_N > 0$ and $Z \geq 13$, the value of K should be negative if the meson capture takes place by a separate "super-shell" proton of the nucleus. The preliminary results of an experiment[8] with aluminum have shown that $K < 0$. However, the results of this experiment alone cannot be interpreted uniquely in favor of the existence of transitions, since there is no direct experimental proof at present of the universality of interaction in the process $\mu^- + p = n + \nu$, or of the assumption that meson capture in aluminum is on the "super-shell" proton of the nucleus. Yet a direct detection of the transitions would add to the arguments in favor of interpreting such experiments to mean that in the process $\mu^- + p = n + \nu$ the constants of the A and V interactions have different signs.[8] We wish to call attention in the present paper to one possibility of direct experimental verification of the existence of transitions, consisting of a study of the polarization of mesons in mesic atoms of a definite type. The suggestion consists essentially of the following. Estimates of the values of $w_k$ and $w_p$ with the aid of formulas (1) and (2) for different values of Z show that $w_p$ (whose value at small Z in many orders of magnitude smaller than $\Lambda$, the total meson-absorption probability) becomes of the same order of magnitude as $\Lambda$ when $Z_{eff} \geq 30$. As regards $w_k$, it becomes equal to $\Lambda$ even at small Z. Thus, for aluminum[7] $w_k = 4 \times 10^5\ \text{sec}^{-1}$, $w_p = 1 \times 10^3\ \text{sec}^{-1}$, and $\Lambda = 1.2 \times 10^6\ \text{sec}^{-1}$.

It is obvious that the existence of transitions will also affect the magnitude of the polarization of mesons in mesic atoms of metals, as well as of non-metals with $Z_{\text{eff}} \geq 30$. Therefore the polarization in substances having different properties but the same values of nuclear spin J may be different. A measure of the transition probability will be the difference between the value of the polarization, obtained experimentally, and that calculated[2] for isolated mesic atoms.

It would seem best to use for the proposed experiments substances with $J = \frac{1}{2}$ and $\mu_N > 0$. Actually, such mesic atoms can be produced in states $F = 1$ and $F = 0$. In the case of the lower state $F = 0$, the mesons become depolarized. The upper state $F = 1$ "remembers" the spin direction (no depolarization takes place). Each of the states is characterized by its own value of g, the gyromagnetic ratio. If the polarization is determined by measuring the asymmetry of the decay electrons,[9] the curve for the precession of the spins of the mesic nuclei in a magnetic field, observed in this case, will be very simple, corresponding to either $F = 1$ or $F = 0$. In addition, since the degree of polarization P of a meson on the K shell, averaged over two hfs states, is[2]

$$P = \tfrac{1}{6} P_0 [1 + 2/(2J + 1)^2]$$

(here $P_0$ is the degree of polarization of the meson beam), the value of P will be greatest for substances with $J = \frac{1}{2}$. Unfortunately, experiments with such substances cannot be performed in practice. The point is that among the substances with $J \neq 0$ and small Z, in which the quantities $w_k$ and $\Lambda$ are comparable, there are no metals with $J = \frac{1}{2}$. One might think that phosphorus and silver would be "accessible" and convenient objects of investigation. True, both substances have $J = \frac{1}{2}$ and differ greatly in their properties, silver being a metal and phosphorus not. In the case of phosphorus, therefore, the investigated transitions will play an insignificant role,[6] owing to the small values of $w_k$ and $w_p$, whereas for silver they will play the predominant role. However, results of experiments with phosphorus and silver cannot be interpreted uniquely. The reason is that in mesic nuclei of silver, with $\mu_N < 0$, the transitions will be from the state $F = 0$ to the state $F = 1$. Consequently, in the case of phosphorus and silver, the experimentally expected precession curves will belong to mesic nuclei which are only in the state $F = 1$, and consequently the value of polarization will be the same.

It becomes possible to observe the transitions if substances with $J > \frac{1}{2}$ are used and the precession frequency of the mesic nuclei is measured in the experiment instead of the polarization. Actually, in this case the precession curve observed experimentally[6] in the absence of transitions will be complex, namely a superposition of spin precessions mesic nuclei in two hfs states with $F \neq 0$. In the presence of transitions the curve will be simple, corresponding to the spin precessions of mesic nuclei in the lower state only. As is well known,[10] at small values of the polarization P the precession frequencies can be measured with greater accuracy than the values of P.[11] In the method proposed above, it is best to use substances with equal values of $J > \frac{1}{2}$, but with different signs of $\mu_N$, such as lithium and beryllium. In the presence of transitions, such mesic nuclei, being in the lower state, will precess with different frequencies in spite of having equal values of J. It must be noted that the foregoing discussions hold only when $w_k$ and $w_p$ are sufficiently large compared with $\Lambda$ and with the probability of the $\mu - e$ decay. We are now carrying out experiments with such nuclei for the purpose of detecting the transitions.

The author is grateful to Ho Tso-Hsiu, V. B. Belyaev, and B. N. Zakhar'ev for numerous discussions and continuous interest in the work.

---

[1] Bernstein, Lee, Yang, and Primakoff, Phys. Rev. **111**, 313 (1958).

[2] H. Uberall, Hyperfine Splitting Effects in the Capture of Polarized $\mu^-$ Mesons, Preprint, Carnegie Inst. Tech., 1959.

[3] É. I. Dolinskiĭ, Dissertation, Res. Inst. Nuc. Phys. Moscow State Univ. 1959.

[4] S. S. Gershteĭn, JETP **34**, 463 (1958), Soviet Phys. JETP **7**, 318 (1958).

[5] Ignetenko, Egorov, Khalupa, and Chultém, JETP **35**, 894 (1958), Soviet Phys. JETP **8**, 621 (1959).

[6] Egorov, Ignatenko, and Chultém, JETP **37**, 1517 (1959), Soviet Phys. JETP **10**, 1077 (1960).

[7] H. Primakoff, Revs. Modern Phys. **31**, 802 (1958).

[8] V. Telegdi, Phys. Rev. Lett. **3**, 59 (1959).

[9] Garwin, Lederman, and Weinrich, Phys. Rev. **105**, 1415 (1957).

[10] Lundy, Sens, Swanson, Telegdi, and Yovanovich, Phys. Rev. Lett. **1**, 38 (1958).

[11] Ignatenko, Egorov, Khalupa, and Chultém, JETP **35**, 1131 (1958), Soviet Phys. JETP **8**, 792 (1959).

Translated by J. G. Adashko
290

SOVIET PHYSICS JETP VOLUME 11, NUMBER 5 NOVEMBER, 1960

# THE POLARIZATION OF THE BETA-RAY ELECTRONS FROM ORIENTED RaE

A. Z. DOLGINOV and N. P. POPOV

Leningrad Physico-Technical Institute, Academy of Sciences, U.S.S.R.

Submitted to JETP editor November 24, 1959

J. Exptl. Theoret. Phys. (U.S.S.R.) 38, 1518-1524 (May, 1960)

A formula is obtained for the polarization vector of the electrons emitted in the $\beta$ decay of RaE nuclei whose spins are oriented in an external field. A region of possible values of the nuclear matrix elements is determined on the basis of the experimental data relating to the shape of the spectrum and the longitudinal polarization of the $\beta$ particles. These values are used to calculate the polarization of the $\beta$ particles from oriented RaE. The dependence of the polarization on the assumed radius of the nucleus is considered. It is shown that the transverse polarization of the $\beta$ particles is very sensitive to possible nonconservation of time parity.

## 1. INTRODUCTION

THE $\beta$-decay transition of RaE is a first-forbidden transition ($1^- \rightarrow 0^+$). As is well known, in the overwhelming majority of cases the shape of the $\beta$-ray spectrum for first-forbidden transitions with $\Delta j = 1$ is the same as for allowed transitions. The point here is that the factor that modifies the allowed shape of the spectrum consists of several terms, and those that depend on the energy are usually small in comparison with those that are proportional to the nuclear charge and do not depend on the energy. The spectrum of RaE is an exception to the general rule — its shape differs markedly from that of an allowed spectrum. To explain this anomaly, in earlier papers[1] a special assumption has been made about the values of the nuclear matrix elements of RaE. If these values are such that the large terms in the correction factor cancel each other, then the small terms which depend on the energy will play the dominant role and the shape of the spectrum will be different from the allowed shape. The matrix elements depend on the structure of the nucleus, and such a cancellation can occur only in exceptional cases.

In connection with the unusual shape of the spectrum of RaE, Alikhanov, Eliseev, and Lyubimov[2] have supposed that the longitudinal polarization of the $\beta$-ray electrons is also anomalous and different from the value v/c. A theoretical treatment of this question has been given in a paper by Geshkenbeĭn, Nemirovskaya, and Rudik,[3] who took into account the nonconservation of spatial parity in $\beta$ decay and also the possible nonconservation of time parity. Alikhanov, Eliseev, and Lyubimov[2] have determined the longitudinal polarization of the $\beta$ particles of RaE experimentally and have compared it with the predictions of the theory. This comparison has allowed a rather accurate determination of an upper limit on the possible nonconservation of time parity. Further improvement of this value involves not only experimental difficulties but also the necessity in the interpretation of the experiments of taking into account a number of corrections which are hard to estimate, since they depend on the structure of the nucleus.

We shall show that the difficulties in the interpretation of the experiments can be avoided if we study the transverse polarization of the electrons emitted by oriented RaE nuclei. With conservation of time parity the degree of polarization in the direction $\mathbf{n} \times \mathbf{n}_0$ does not exceed 2 percent. Here $\mathbf{n} = \mathbf{p}/|\mathbf{p}|$, $\mathbf{p}$ being the momentum of the $\beta$ particle; $\mathbf{n}_0$ is the direction of dominant orientation of the nuclear spins. Within the accuracy of the existing experiments [$\arg(C_V/C_A) \sim 3°$, see later discussion], for nonconservation of time parity the degree of polarization reaches 45 percent. In addition we repeat the analysis of the experimental data relating to the spectrum and longitudinal polarization of the $\beta$ particles, with corrections included that were not dealt with in the previous papers.

## 2. THE POLARIZATION OF THE $\beta$-RAY ELECTRONS

A general expression for the polarization of the $\beta$ particles emitted by oriented nuclei in first-forbidden transitions has been obtained in reference 4. In the special case of a $1^- \rightarrow 0^+$ transition the polarization is given by the formula

$$\zeta = \{\mathbf{n}\,[-a_0 v/c + a_1 \langle\mu\rangle \cos\vartheta + a_2 \langle\mu^2\rangle P_2(\cos\vartheta)] + \mathbf{n}_1 a_3 \langle\mu\rangle \sin\vartheta + \mathbf{n}_2 [a_4 \langle\mu\rangle \sin\vartheta + a_5 \langle\mu^2\rangle \sin 2\vartheta]\}\,[W_{\mathbf{nn}_0}]^{-1}, \tag{1}$$

$$W_{\mathbf{nn}_0} = 1 - b_0 \langle\mu\rangle \cos\vartheta - b_1 \langle\mu^2\rangle P_2(\cos\vartheta), \tag{2}$$

$$\mathbf{n}_1 \parallel [\mathbf{n}\times\mathbf{n}_0],\quad \mathbf{n}_2 \parallel [\mathbf{n}_1\times\mathbf{n}],\quad \cos\vartheta = \mathbf{nn}_0,$$

$$\langle\mu\rangle = \sum_{\mu=-1}^{1} \mu w(\mu),\quad \langle\mu^2\rangle = \sum_{\mu=-1}^{1} (3\mu^2 - 2)\, w(\mu). \tag{3}$$

$\mu$ is the projection of the spin of the nucleus on the axis $n_0$; $w(\mu)$ is the probability of a given value of $\mu$; $W_{nn_0}$ is the angular distribution of the $\beta$ particles emitted by the oriented RaE. The explicit form of the coefficients $a_i$ and $b_i$ is presented in Appendix I.* They depend on the energy of the $\beta$ particle, on the $\beta$-decay interaction constants, and on two ratios of nuclear matrix elements x and y defined by

$$x = i\varepsilon_V \int \mathbf{r} / \varepsilon_A \int [\sigma\times\mathbf{r}],\qquad y = \varepsilon_V \int \alpha / \varepsilon_A \int [\sigma\times\mathbf{r}],$$

$$\varepsilon_V^2 = |C_V|^2 + |C_V'|^2,\qquad \varepsilon_A^2 = |C_A|^2 + |C_A'|^2, \tag{4}$$

x and y are real quantities; $C_A$, $C_A'$, $C_V$, and $C_V'$ are the $\beta$-decay interaction constants. In the theory of the two-component neutrino $C_V = C_V'$, $C_A = C_A'$. We shall deal mainly with the case of the VA interaction, which is evidently confirmed by experiment, and shall show only at the end how to go over to the ST interaction. $\int \mathbf{r}$, $\int \alpha$, and $\int \sigma\times\mathbf{r}$ are nuclear matrix elements of the $\beta$-decay transition.

The spectrum of RaE is of the form

$$N(E)\,dE = (G^2/2\pi^3)\, F(Z, E)\, pE\, (E_0 - E)^2\, C(E)\, dE, \tag{5}$$

where G is the Fermi interaction constant, F(Z, E) is the Fermi function, and C(E) is the correction factor for the spectrum.

In the diagram the dashed curves show the region of spread of the experimental points C(E). The main inaccuracy is that associated with the determination of the limiting energy of the spectrum:[6] $3.26\ mc^2 \lesssim E_0 \lesssim 3.32\ mc^2$. The solid curves are the theoretical values for certain possible values of x and y.

The formulas of Appendices I and II have been used to calculate the coefficients $a_i$ and $b_i$ that appear in Eq. (1) for the values of x and y fitted in this way to the shape of the spectrum; the values of the coefficients so obtained are shown in Appendix III, Table I. Agreement cannot be obtained with values of x and y that differ much from those given in the tables.

The finite size of the nucleus was taken into account in the calculation of the coefficients $a_i$, $b_i$. A uniform volume distribution of charge in the nucleus was assumed for two possible values of the nuclear radius, $r_0 = 1.2$ and $r_0 = 1.5$, where $R = r_0 A^{1/3} \times 10^{-13}$ cm and A = 210 for RaE.* The limiting energy $E_0$ of the spectrum was taken to be 3.26 $mc^2$. $a_0$ is the coefficient of the departure of the longitudinal polarization of the $\beta$ particles of unoriented RaE from the value v/c. Table II of Appendix III shows the experimental values of $a_0$ available at present from the data of various authors.

## 3. DISCUSSION OF THE RESULTS

An examination of the curves of C(E) and the values for $a_0$ shows that the shape of the spec-

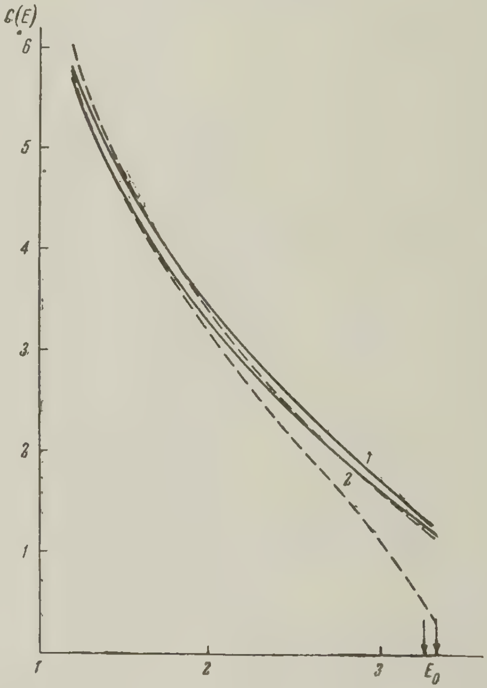

The dashed lines bound the region of the experimental values of the form factor C(E). The solid curves are calculated for the following possible values of the parameters x and y: 1 – x = 1, y = 30.5, $r_0$ = 1.2; 2 – x = 1. y = 25.1, $r_0$ = 1.5.

---

*The coefficients $b_i$ have been calculated independently of us by Geshkenbeĭn, Nemirovskaya, and Rudik.[5]

*In the approximation $(\alpha Z)^2 \ll 1$ a surface distribution of charge in the nucleus is equivalent to a volume distribution with the radius of the nucleus increased by 20 percent. This approximation is not valid for RaE (Z = 83), but nevertheless by increasing the radius of the nucleus and choosing new values of x and y that fit the shape of the spectrum we get a result corresponding to a distribution of charge in the nucleus that is close to a surface distribution with the original value of the radius of the nucleus.

trum and the size of the longitudinal polarization as observed experimentally can be best described with values of x in the range 0.67 — 1 and corresponding values of y that depend on the radius of the nucleus. These values do not depart too far from those that have been obtained by other authors.

The possible amount of nonconservation of time parity obtained by Geshkenbeĭn and others[3] agrees with the results of our work. A change of the assumed nuclear radius has a marked effect on the quantities x and y, but we can always take values of x and y that satisfy all the experimental data without resorting to the hypothesis of a considerable nonconservation of time parity. The inaccuracy associated with the determination of $E_0$ affects the values of $a_i$ and $b_i$ mainly near the limit of the spectrum. For example, when we replace $E_0 = 3.26$ by $E_0 = 3.32$ the value of $a_0$ at $E = 3.0$ decreases by 9 percent for $x = 0.2$ and by 14 percent for $x = 1.2$. At $E = 2.0$, however, the maximum change of $a_0$ for permissible values of x does not exceed 3 percent.

We see from the tables that the change of the longitudinal polarization is of the same order of magnitude as the transverse polarization in the direction $[\mathbf{n} \times \mathbf{n}_0] \times \mathbf{n}$. For conservation of time parity the transverse polarization in the direction $\mathbf{n} \times \mathbf{n}_0$ is very small. For example, for $E = 1.2$ the coefficient $a_3$ is equal to 2 percent.

It is a remarkable fact, however, that $a_3$ depends sharply on a possible nonconservation of time parity. If we write $C_A = aC_V e^{i\theta}$, then if the angle $\theta$ that gives the phase shift between the A and V interactions is 3° (which is within the limits of error of the existing experiments), the coefficient $a_3$ reaches a value of 45 percent. Therefore we can recommend the study of the transverse polarization of the $\beta$ particles from oriented RaE as one of the most sensitive ways of testing the law of conservation of time parity.

The polarization formula (1) is valid for nuclei oriented in any way (for example, by the method of Gorter and Rose). For nuclei aligned by the method of Bleaney or Pound there remain only the terms proportional to the quadrupole polarization of the nuclei. In this case the amount of longitudinal polarization will differ from that of unoriented RaE by not more than 15 percent. There can be a transverse polarization only in the direction $[\mathbf{n} \times \mathbf{n}_0] \times \mathbf{n}$. In the special case $x = 0.5$ the coefficients $a_2$, $a_5$, and $b_1$ are equal to zero. Thus in this case with aligned nuclei there can be only a longitudinal polarization of the $\beta$ particles, of an amount that agrees exactly with the polarization of the $\beta$ particles from unoriented RaE.

We can make an estimate of the corrections from the third degree of forbiddenness. Using an estimate for the matrix elements of the third order in forbiddenness that is clearly too high

$$\varepsilon_V \int \alpha r^2 \Big/ \varepsilon_A \int [\sigma \times \mathbf{r}] \leqslant R^2 \varepsilon_V \int \alpha \Big/ \varepsilon_A \int [\sigma \times \mathbf{r}] \approx \left(\frac{1}{50}\right)^2 y \qquad (6)$$

and keeping the largest term in the expression for the correction, we get

$$a_i' = \frac{a_i C(E) + 2\,|G(E, R)|\,\sqrt{a_i C(E)}}{C(E) + 2\,|G(E, R)|\,\sqrt{C(E)}}, \qquad (7)$$

where the $a_i'$ are the corrected values and the $a_i$ the original values of the coefficients in Eq. (1), and

$$G(E, R) = \frac{2q}{15}\frac{\alpha Z}{R}\frac{\varepsilon_V}{\varepsilon_A} \int \alpha r^2 \Big/ \int [\sigma \times \mathbf{r}]. \qquad (8)$$

The $b_i'$ and $b_i$ are related in a similar way.

It follows from Eqs. (7) and (8) that the third-forbidden terms make their largest contribution to the soft part of the $\beta$-ray spectrum. Their total contribution is small. At $E = 1.2$ the coefficient $a_0$ is decreased by 2 percent.

The writers are grateful to K. A. Ter-Martirosyan, who informed them about earlier papers[2,3] before their appearance in print and called attention to the problem of RaE.

## APPENDIX I

Analytical form of the functions $a_i$, $b_i$ for the VA interaction:

$$\begin{aligned}
a_0 C(E)\, pE^{-1} = {} & x^2 [\beta_{VV} (M_0' + 2L_1' - \tfrac{2}{3} qN_0' \\
& + \tfrac{1}{3} q^2 L_0') - \tfrac{2}{3} q\beta_{VV}' N_0''] + y^2 \beta_{VV} L_0' + \beta_{AA} (M_0' + \tfrac{1}{2} L_1' \\
& + \tfrac{2}{3} qN_0' + \tfrac{1}{6} q^2 L_0') + \tfrac{2}{3} q\beta_{AA}' N_0'' \\
& + 2y [\beta_{VA} (N_0' + \tfrac{1}{3} qL_0') - \beta_{VA}' N_0''] \\
& + 2x [\beta_{VA} (M_0' - L_1') + \tfrac{2}{3} q\beta_{VA}' N_0''] \\
& + 2xy [\beta_{VV} (N_0' - \tfrac{1}{3} qL_0') + \beta_{VV}' N_0''],
\end{aligned}$$

$$\begin{aligned}
b_0 C(E) = {} & x^2 \{\beta_{VV} [M_0' - 2M_1' + L_1' - \tfrac{2}{3} q (N_0' - N_1')] \\
& - 2\beta_{VV}' [M_2' + \tfrac{1}{3} q (N_0'' - N_2')]\} + \beta_{AA} [M_0' + M_1' + \tfrac{1}{4} L_1' \\
& + \tfrac{1}{3} q (2N_0' + N_1') + \tfrac{1}{12} q^2 L_0'] \\
& + \beta_{AA}' [M_2' + \tfrac{1}{3} q (2N_0'' + N_2')] \\
& + y^2 \beta_{VV} L_0' + y [\beta_{VA} (2N_0' + N_1' + \tfrac{2}{3} qL_0') - \beta_{VA}' (2N_0'' + N_2')] \\
& + x [\beta_{VA} (2M_0' - M_1' - L_1' - qN_1' - \tfrac{1}{3} q^2 L_0') \\
& - \beta_{VA}' (3M_2' - \tfrac{4}{3} qN_0'' + \tfrac{1}{3} qN_2')] \\
& + 2xy [\beta_{VV} (N_0' - N_1' - \tfrac{1}{3} qL_0') + \beta_{VV}' (N_0'' - N_2')],
\end{aligned}$$

$$a_2 C(E) = x^2[\beta_{VV}(2M_1' + L_1' - \tfrac{2}{3} qN_1') + \beta_{VV}'(2M_2' - \tfrac{2}{3} qN_2')]$$
$$+ \beta_{AA}(\tfrac{1}{4} L_1' - M_1' - \tfrac{1}{3} qN_1') - \beta_{AA}'(M_2' + \tfrac{1}{3} qN_2')$$
$$- y(\beta_{VA} N_1' + \beta_{VA}' N_2') + x[\beta_{VA}(M_1' - L_1' + qN_1')$$
$$+ \beta_{VA}'(3M_2' + \tfrac{1}{3} qN_2')] + 2xy(\beta_{VV} N_1' + \beta_{VV}' N_2').$$

We get C(E), $b_1$, and $a_1$ from $a_0C(E)pE^{-1}$, $a_2$, and $b_0$, respectively, if in the latter expressions we make the replacements

$$(M_i', L_i', N_i') \to (M_i, L_i, N_i),\ \beta_{ii'} \to \alpha_{ii'},\ \beta_{ii'}' \to \alpha_{ii'}',\ N_0'' \to 0.$$

We get $a_4$ from $a_1$ by the replacements

$$M_0 \to \overline{M}_0,\ L_0 \to \overline{L}_0,\ N_0 \to \overline{N}_0,\ L_1 \to -2\overline{L}_1,$$
$$M_1 \to -\tfrac{1}{2}\overline{M}_1,\ N_1 \to -\tfrac{1}{2}\overline{N}_1,$$
$$M_2 \to -\tfrac{1}{2}\overline{M}_2 \text{ and } N_2 \to -\tfrac{1}{2}\overline{N}_2.$$

We get $a_5$ from $\frac{1}{2}a_2$ by the replacements

$$M_1' \to \tfrac{3}{2}\overline{M}_1',\ N_1' \to \tfrac{3}{2}\overline{N}_1',\ N_2' \to \tfrac{3}{2}\overline{N}_2',$$
$$\overline{M}_2' \to \tfrac{3}{2}\overline{M}_2' \text{ and } L_1' \to 0.$$

We get $a_3$ from $b_0$ by the replacements

$$M_1' \to -\tfrac{1}{2}M_1',\ L_1' \to 2L_1',\ N_1' \to -\tfrac{1}{2}N_1',\ M_2' \to -\tfrac{1}{2}\overline{M}_2',$$
$$N_2' \to -\tfrac{1}{2}\overline{N}_2',\ \beta_{ii'} \to \beta_{ii'}' \text{ and } \beta_{ii'}' \to -\beta_{ii'}.$$

$$\alpha_{ii'} = \mathrm{Re}(C_i C_{i'}^* + C_i' C_{i'}'^*)/\varepsilon_i\varepsilon_{i'},$$
$$\alpha_{ii'}' = \mathrm{Im}(C_i C_{i'}^* + C_i' C_{i'}'^*)/\varepsilon_i\varepsilon_{i'},$$
$$\beta_{ii'} = \mathrm{Re}(C_i C_{i'}'^* + C_i' C_{i'}^*)/\varepsilon_i\varepsilon_{i'},$$
$$\beta_{ii'}' = \mathrm{Im}(C_i C_{i'}'^* + C_i' C_{i'}^*)/\varepsilon_i\varepsilon_{i'},$$
$$\varepsilon_i^2 = C_i{}^2 + C_i'{}^2,\ \alpha_{ii} = 1,\ \alpha_{ii}' = \beta_{ii}' = 0.$$

For the case of the ST interaction we must make the following replacements in the formulas presented above: in $\beta_{ii'}$ and $\beta_{ii'}'$ replace indices A → T; in the terms in $x^2$, x, and 1 replace V → S; in the terms in $y^2$, xy, and y replace V → T; also replace $a_2 \to -a_2$, $b_0 \to -b_0$, $q \to -q$, and let

$$x = i\varepsilon_S \int \beta \mathbf{r} \Big/ \varepsilon_T \int \beta[\sigma \times \mathbf{r}],\quad y = \int \beta\alpha \Big/ \int \beta[\sigma \times \mathbf{r}].$$

## APPENDIX II

Values of the functions $M_i$, $L_i$, etc., as functions of the energy of the β particle and the radius of the nucleus, as found for a volume charge distribution in the nucleus:

$$M_0 = \frac{2\pi}{9EpF}\left\{\left[0.95(W-1)^2 - \frac{3\alpha Z}{5R}(W-1) + \left(\frac{3\alpha Z}{10R}\right)^2\right]a^2_{1/2\,-1/2}\right.$$
$$\left. + \left[0.95(W+1)^2 - \frac{3\alpha Z}{5R}(W+1) - \left(\frac{3\alpha Z}{10R}\right)^2\right]a^2_{1/2\,1/2}\right\},$$

$$L_0 = \frac{2\pi\cdot 0.88}{EpF}(a^2_{1/2\,-1/2} - a^2_{1/2\,1/2}),$$

$$L_1 = \frac{2\pi\cdot 0{,}93}{EpF}(a^2_{3/2\,-1/2} + a^2_{3/2\,1/2}),$$

$$N_0 = -\frac{2\pi}{3EpF}\left\{\left[0.92(W-1) - \frac{3\alpha Z}{10R}\right]a^2_{1/2\,-1/2}\right.$$
$$\left. + \left[0.92(W+1) - \frac{3\alpha Z}{10R}\right]a^2_{1/2\,1/2}\right\}$$

$$M_0' = \frac{4\pi}{9EpF}\left[0.95\varkappa^2 - \frac{3\alpha Z}{5R}W + \left(\frac{3\alpha Z}{10R}\right)^2\right]a_{1/2\,1/2}a_{1/2\,-1/2}\cos\delta_0,$$

$$L_0' = \frac{4\pi\cdot 0{,}88}{EpF}a_{1/2\,1/2}a_{1/2\,-1/2}\cos\delta_0,\quad L_1' = \frac{4\pi\cdot 0{,}93}{EpF}a_{3/2\,1/2}a_{3/2\,-1/2}\cos\delta_1,$$

$$N_0' = -\frac{4\pi}{3EpF}\left(0.92W - \frac{3\alpha Z}{10R}\right)a_{1/2\,1/2}a_{1/2\,-1/2}\cos\delta_0,$$

$$N_0'' = -\frac{3.68\pi}{3EpF}a_{1/2\,1/2}a_{1/2\,-1/2}\sin\delta_0,$$

$$M_1 = \frac{2\pi}{3EpF}\left\{\left[0.94(W-1) - \frac{3\alpha Z}{10R}\right]a_{1/2\,-1/2}a_{3/2\,1/2}\cos\delta_2^+\right.$$
$$\left. + \left[0.94(W+1) - \frac{3\alpha Z}{10R}\right]a_{1/2\,1/2}a_{3/2\,-1/2}\cos\delta_2^-\right\},$$

$$N_1 = -\frac{1.8\pi}{EpF}(a_{1/2\,-1/2}a_{3/2\,1/2}\cos\delta_2^+ + a_{1/2\,1/2}a_{3/2\,-1/2}\cos\delta_2^-).$$

We get $M_1'$ and $N_1'$ from $M_1$ and $N_1$, respectively, if we replace $a_{3/2,1/2}$ by $a_{3/2,-1/2}$ and conversely, and take $\delta_3^\pm$ instead of $\delta_2^\pm$. $M_2$, $N_2$, $M_2'$, and $N_2'$ differ from $M_1$, $N_1$, $M_1'$, and $N_1'$, respectively, by replacement of $\cos\delta_1^{\mp}$ by $\sin\delta_1^{\mp}$.

We get $\overline{M}_0$, $\overline{L}_0$, $\overline{N}_0$ from $M_0$, $L_0$, $N_0$ by the replacement $a^2_{1/2\ 1/2} \to -a^2_{1/2\ 1/2}$, and we get $\overline{M}_1$, $\overline{N}_1$ from $M_1$, $N_1$ by replacing $\cos\delta_2^-$ by $-\cos\delta_2^-$.

$$\delta_0 = \delta_{1/2\,-1/2} - \delta_{1/2\,1/2},\ \delta_1 = \delta_{3/2\,1/2} - \delta_{3/2\,-1/2},\ \delta_2^\pm = \delta_{1/2\,\mp 1/2} - \delta_{3/2\,\pm 1/2},$$
$$\delta_3^\pm = \delta_{1/2\,\mp 1/2} - \delta_{3/2\,\mp 1/2},\ W = E + \frac{3}{2}\frac{\alpha Z}{R},\ \varkappa^2 = W^2 - 1,$$
$$p^2 = E^2 - 1,\ q = E_0 - E.$$

$a_{j\lambda}$ and $\delta_{j\lambda}$ are tabulated in the work of Sliv and Volchok[7] for $r_0 = 1.2$ and $r_0 = 1.5$. F is the Fermi function, which is tabulated in the work of Dzhelepov and Zyryanova.[8] If we neglect the change of the electron wave function inside the nucleus, $M_0$, $L_0$, $L_1$, and $N_0$ coincide with the functions determined by Konopinski and Uhlenbeck.[9] Corrected for the finite size of the nucleus, but for different values of Z, these functions have been tabulated in reference 8.

## APPENDIX III

The values of $a_i$ and $b_i$ in Table I are calculated for $r_0 = 1.2$. A change of $r_0$ can be compensated by a suitable change of y. The values of y obtained from the data on the shape of the β-ray spectrum for $r_0 = 1.2$ and $r_0 = 1.5$ are given in Table III. It was found that the quantities $a_i$ and $b_i$ calculated with these values of y were practically identical for the two values of $r_0$, being a

**TABLE I.** Calculated values of the coefficients $a_i$ and $b_i$

| $E$ / $x$ | 1,2 | 1,5 | 2,0 | 3,0 | 1,2 | 1,5 | 2,0 | 3,0 |
|---|---|---|---|---|---|---|---|---|
| | $a_0$ | | | | $b_0$ | | | |
| 0.2 | 0.84 | 0.85 | 0.86 | 0.89 | 0.41 | 0.44 | 0.68 | 0.61 |
| 0.5 | 0.80 | 0.82 | 0.81 | 0.84 | 0.38 | 0.39 | 0.64 | 0.70 |
| 0.67 | 0.78 | 0.80 | 0.79 | 0.81 | 0.35 | 0.35 | 0.63 | 0.74 |
| 1.0 | 0.74 | 0.76 | 0.74 | 0.75 | 0.30 | 0.28 | 0.59 | 0.75 |
| 1.2 | 0.72 | 0.74 | 0.70 | 0.71 | 0.28 | 0.18 | 0.54 | 0.71 |
| | $a_1$ | | | | $a_4$ | | | |
| 0.2 | 0.93 | 0.82 | 0.89 | 0.85 | 0.37 | 0.58 | 0.65 | 0.93 |
| 0.5 | 0.89 | 0.78 | 0.89 | 0.98 | 0.17 | 0.50 | 0.65 | 1.01 |
| 0.67 | 0.86 | 0.74 | 0.93 | 1.05 | 0.02 | 0.60 | 0.66 | 1.06 |
| 1.0 | 0.76 | 0.69 | 0.89 | 1.07 | —0.40 | 0.63 | 0.70 | 1.08 |
| 1.2 | 0.70 | 0.55 | 0.87 | 1.08 | —0.58 | 0.42 | 0.64 | 1.11 |
| | $b_1$ | | | | $a_2$ | | | |
| 0.2 | 0.010 | 0.026 | 0.057 | 0.148 | 0.016 | 0.035 | 0.069 | 0.167 |
| 1.0 | —0.010 | —0.029 | —0.062 | —0.124 | —0.027 | —0.047 | —0.089 | —0.175 |
| 1.2 | —0.011 | —0.035 | —0.071 | —0.103 | —0,028 | —0.062 | —0.112 | —0.181 |
| | $a_5$ | | | | | | | |
| 0.2 | 0.016 | 0.031 | 0.056 | 0.122 | | | | |
| 1.0 | —0.012 | —0.032 | —0.084 | —0.220 | | | | |

**TABLE II.** Experimental values of $a_0$

| $E$ | $a_0$ | $E$ | $a_0$ |
|---|---|---|---|
| 1.23 | 0.69±0.04 [10] | 1.57 | 0.66±0.06 [10] |
| 1.24 | 0.733±0.06 [2] | 1.76 | 0.725±0.06 [2] |
| 1.30 | 0.75±0.04 [10] | 2.28 | 0.69±0.10 [11] |
| 1.41 | 0.75±0.04 [10] | | |

**TABLE III**

| $x$ | $y$ | |
|---|---|---|
| | $r_0 = 1.2$ | $r_0 = 1.5$ |
| 0.2 | 19.2 | 16.0 |
| 0.5 | 23.5 | 19.5 |
| 0.67 | 25.9 | 21.4 |
| 1.0 | 30.5 | 25.1 |
| 1.2 | 33.2 | 27.3 |

**TABLE IV**

| $E$ / $x$ | 1,2 | 1,5 | 2,. | 3,0 |
|---|---|---|---|---|
| 0.2 | 0.84 | 0.85 | 0.85 | 0.83 |
| 0.5 | 0.80 | 0.81 | 0.81 | 0.75 |
| 0.67 | 0.78 | 0.79 | 0.78 | 0.69 |
| 1.0 | 0.74 | 0.74 | 0.72 | 0.60 |
| 1.2 | 0.71 | 0.71 | 0.68 | 0.55 |

bit different only at the limit of the spectrum.

As an example, values of $a_0$ for $r_0 = 1.5$ are shown in Table IV.

---

[1] M. Yamada, Progr. Theoret. Phys. **10**, 252 (1953). Fujita, Yamada, Matumoto, and Nakamura, Progr. Theoret. Phys. **20**, 287 (1958).

[2] Alikhanov, Eliseev, and Lyubimov, JETP **35**, 1061 (1958), Soviet Phys. JETP **8**, 740 (1959).

[3] Geshkenbeĭn, Nemirovskaya, and Rudik, JETP **36**, 517 (1959), Soviet Phys. JETP **9**, 360 (1959).

[4] A. Z. Dolginov, Nuclear Phys. **5**, 512 (1958). A. Z. Dolginov and N. P. Popov, JETP **36**, 529 (1959), Soviet Phys. JETP **9**, 368 (1959).

[5] Geshkenbeĭn, Nemirovskaya, and Rudik, Nuclear Phys. **13**, 60 (1959).

[6] E. A. Plassmann and L. M. Langer, Phys. Rev. **96**, 1593 (1954).

[7] L. A. Sliv and B. A. Volchok, Таблицы кулоновских фаз и амплитуд с учетом конечных размеров ядра. (Tables of Coulomb Phase Shifts and Amplitudes, Corrected for the Finite Size of the Nucleus), U.S.S.R. Acad. Sci. Press, Moscow-Leningrad, 1956.

[8] B. S. Dzhelepov and L. N. Zyryanova, Влияние электрического поля атома на бета-распад. (Effect of the Electric Field of the Atom on Beta Decay), U.S.S.R. Acad. Sci. Press, Moscow-Leningrad, 1956.

[9] E. J. Konopinski and G. E. Uhlenbeck, Phys. Rev. **60**, 308 (1941).

[10] Wegener, Bienlein, and Issendorff, Phys. Rev. Letters **1**, 460 (1958).

[11] Geiger, Ewan, Graham, and MacKenzie, Phys. Rev. **112**, 1684 (1958).

Translated by W. H. Furry
291

# ON THE CALCULATION OF SCATTERING PHASE SHIFTS

V. K. PETERSON

Moscow State University

Submitted to JETP editor November 26, 1959

J. Exptl. Theoret. Phys. (U.S.S.R.) 38, 1525-1527 (May, 1960)

A method for the calculation of the phase shifts of particles in a centrally symmetric potential field is proposed. The case where the phase shift can be expressed in the form of a series in powers of a constant characterizing the dimensions of the potential well is considered.

As is well known, the problem of the scattering of particles in a centrally symmetric potential field reduces to solving an equation of the type

$$d^2u/dx^2 + [k^2 + W(x) + U(x)]\,u(x) = 0 \qquad (1)$$

with the conditions

$$u(0) = 0, \quad u_{\mathrm{as}} = \sin(kx + \delta(x) + \eta).$$

Here we assume that $W(x)$ is a function of $x$ for which [with $U(x) \equiv 0$] the two independent solutions with the asymptotic behavior[1]

$$v_{1\,\mathrm{as}} = \sin(kx + \delta(x)), \qquad v_{2\,\mathrm{as}} = \cos(kx + \delta(x))$$

are known. An example of such a function is

$$W(x) = -l(l+1)\,x^{-2} - 2\alpha k x^{-1};$$

in this case

$$\delta(x) = -\tfrac{1}{2}\pi l + \arg\Gamma(l + 1 + i\alpha) - \alpha\ln 2kx.$$

Problems of such a type with a complex potential occur, in particular, in the nuclear optical model calculations. For small $k$ this involves complicated numerical computations.[2,3] A general method of solving these problems was developed by Nemirovskiĭ.[4] Below we shall propose a different method in which the phase $\eta$ is sought in the form of a power series in $U_0$ [$U(x) = U_0 f(x)$]. The method can be applied successfully in the region of intermediate and high energies.

We shall seek the solution of Eq. (1) in the form

$$u(x) = [1 - D(x)]\Big\{v_1(x)\cos\int_0^x \Phi(x')\,dx' + v_2(x)\sin\int_0^x \Phi(x')\,dx'\Big\}, \qquad (2)$$

Assuming $D(\infty) = 0$ and $\Phi(\infty) = 0$, we obtain

$$\eta = \int_0^\infty \Phi(x)\,dx.$$

Substituting expression (2) in Eq. 1 and setting the coefficients of the sine and cosine equal to zero, we obtain, after some transformation, equations for the determination of D and Φ:

$$D'' - \beta'\beta^{-1}D' + \beta^2\,[(1 - D)^{-3} + D - 1] = U(x)\,(1 - D),$$
$$\Phi = \beta\,[(1 - D)^{-2} - 1], \qquad (3)$$

where $\beta = k(v_1^2 + v_2^2)^{-1}$. With $W(x) = -l(l + 1)x^{-2}$ we have for $l = 0, 1$

$$\beta_0 = k, \qquad \beta_1 = k^3x^2\,(1 + k^2x^2)^{-1}.$$

Equation (3) can be written in the integral form

$$D(x) = \int_\infty^x K(x, x')\{U(x')(1 - D(x')) - \beta^2(x')[(1 - D(x'))^{-3} - 3D(x') - 1]\}\,dx',$$

$$K(x, x') = \tfrac{1}{2}\sin\Big(2\int_{x'}^x \beta(x_1)\,dx_1\Big)\beta^{-1}(x'). \qquad (4)$$

If $|D(x)| \ll 1$, $(1 - D)^{-3}$ can be expanded into a series in powers of D:

$$(1 - D)^{-3} - 3D - 1 = \frac{1}{2}\sum_{n=2}^{\infty}(n + 1)(n + 2)\,D^n(x).$$

In first approximation we obtain

$$D_1(x) = \int_\infty^x K(x, x')\,U(x')\,dx'.$$

If $|D_1(x)| \ll 1$, we can seek $D(x)$ in the form of a power series in $U_0$:

$$D(x) = \sum_{n=1}^{\infty} D_n(x). \qquad (5)$$

Introducing the recurrence relations

$$D_{n1} = D_n, \qquad D_{nm} = \sum_{q=1}^{n-m+1} D_q D_{n-q,\,m-1}$$

($D_{nm}$ is proportional to $U_0^n$), we obtain equations for the determination of the $D_n(x)$ $(n > 1)$:

$$D_n(x) = -\int_{\infty}^{x} K(x, x') \Big\{ U(x') D_{n-1}(x') + \frac{1}{2} \beta^2(x') \sum_{m-2}^{n} (m+1)(m+2) D_{nm}(x') \Big\} dx'.$$

$\Phi(x)$ can also be expressed in the form of a power series in $U_0$:

$$\Phi(x) = \beta(x) \sum_{n=1}^{\infty} \sum_{m=1}^{n} (m+1) D_{nm}(x). \qquad (6)$$

If the series (6) converges in the interval $(0, \infty)$ we have

$$\eta = \sum_{n-1}^{\infty} \int_{0}^{\infty} \beta(x) \sum_{m=1}^{n} (m+1) D_{nm}(x)\, dx.$$

For a potential well of the form $U(x) = U_0 e^{-x}$ we find

$$D_1(x) = \frac{U_0}{1+4k^2} e^{-x}, \qquad D_2(x) = \frac{-U_0(1+10k^2)}{(1+4k^2)^2(4+4k^2)} e^{-2x}, \ldots$$

Thus we obtain for $U_0 = 2$, $k^2 = 1$, which corresponds to the scattering of a neutron with energy 20.5 Mev by a potential well of depth 41 Mev which decreases by the factor $e^{-1}$ at the distance $10^{-13}$ cm,

$$D(x) = 0.4\, e^{-x} - 0.22 e^{-2x} + 0.06585 e^{-3x} - 0.00331 e^{-4x} - 0.00244 e^{-5x} - 0.00053 e^{-6x} + 0.00046\, e^{-7x} + \ldots,$$

$$\eta = 0.8000 + 0.0200 - 0.0468 + 0.0005 + 0.0078 - 0.0003 - 0.0016 + \ldots \approx 0.780.$$

For larger k the convergence is faster; in the region of small k, on the other hand, D(x) can be obtained in the form (5) only in some interval $(x_0, \infty)$, if we use the above-mentioned form of the potential well. Beyond that the problem must be solved numerically.

If $U(x) = \text{const}$ for $x < a$, we can use the method of joining of the wave functions. In this case we seek $u(x)$ for $x > a$ in the form

$$u(x) = [1 - D(x)] \Big\{ v_1 \cos\Big(\eta_0 + \int_a^x \Phi(x')\, dx'\Big) + v_2 \sin\Big(\eta_0 + \int_a^x \Phi(x')\, dx'\Big) \Big\};$$

$\eta_0$ is determined by the boundary conditions at $x = a$.

---

[1] N. F. Mott and H. S. W. Massey, The Theory of Atomic Collisions, Oxford, 1949.

[2] P. É. Nemirovskiĭ, JETP **32**, 1143 (1957), Soviet Phys. JETP **5**, 932 (1957).

[3] Luk'yanov, Orlov, and Turovtsev, JETP **35**, 750 (1958), Soviet Phys. JETP **8**, 521 (1959).

[4] P. É. Nemirovskiĭ, JETP **30**, 551 (1956), Soviet Phys. JETP **3**, 484 (1956).

Translated by R. Lipperheide
292

SOVIET PHYSICS JETP VOLUME 11, NUMBER 5 NOVEMBER, 1960

# *POLARIZATION OF THE HYDROGEN ATOM IN THE GROUND STATE BY THE FIELD OF A POINT CHARGE*

V. P. SHMELEV

Moscow State University

Submitted to JETP editor November 27, 1959

J. Exptl. Theoret. Phys. (U.S.S.R.) **38**, 1528-1533 (May, 1960)

The dipole moment p of a hydrogen atom in the ground state, induced by a positive charge e, is considered as a function of the distance between the charge and the atomic nucleus (Fig. 2). The proton and the hydrogen atom in this state do not form a stable system. The stability of the proton-electron-positron quasimolecule is investigated with the aid of the solution thus obtained.

## 1. THE HYDROGEN ATOM IN THE FIELD OF A POINT CHARGE e

THE appearance of a dipole moment in the hydrogen atom is considered by us as a problem involving the motion of an electron in the field of two fixed positive charges e. Let the nucleus of the hydrogen atom a be fixed at the origin of the coordinate system, and let the charge e be at a point b a distance R along the z axis. We denote by $r_a$ and $r_b$ the respective distances from the electron to these points. It is now necessary to find a solution of the Schrödinger equation with potential

$$U_1 = -e^2/r_a - e^2/r_b,$$

which corresponds to the ground state of the hydrogen atom polarized by a charge e located at a distance R from it.

The given problem is solved by the same methods used for the well-known problem of two centers in the case of the hydrogen molecule. Only the boundary conditions change for $R \to \infty$; whereas the wave function of the ionized molecule of hydrogen changes, as $R \to \infty$, into a symmetric combination of hydrogen atoms at the points a and b, in our case the wave function goes over into a hydrogen atom with the nucleus at the point a. If we introduce the elliptic coordinates

$$\xi_0 = (r_a + r_b)/R, \qquad \eta_0 = (r_a - r_b)/R, \tag{1}$$

then we can separate the variables in the Schrödinger equation with potential $U_1$:

$$\Psi(r_a, r_b) = X(\xi_0)\,Y(\eta_0), \tag{2}$$

$$\frac{d}{d\xi_0}\left[(\xi_0^2 - 1)\frac{dX}{d\xi_0}\right] + [-\lambda^2\xi_0^2 + 2R\xi_0 + A]\,X = 0, \tag{2a}$$

$$\frac{d}{d\eta_0}\left[(\eta_0^2 - 1)\frac{dY}{d\eta_0}\right] + [-\lambda^2\eta_0^2 + A]\,Y = 0, \tag{2b}$$

where $\lambda = R\sqrt{|E|}/2$, while A denotes the separation constant.[1]

Here and below, the energy E is expressed in Rydbergs ($1\ \mathrm{Ry} = e^2/2a_0$), the distance R in Bohr radii, $a_0$, and the electron charge e is set equal to unity.

Let us fix the boundary conditions as $R \to \infty$. If the electron remains with the charge a, then upon removal of the point b to infinity along the z axis, the elliptical coordinates of (1) go over into parabolic coordinates

$$\xi_0 \to \mu/R + 1, \qquad \eta_0 \to \nu/R - 1,$$

where $\mu = r_a - z_a$, $\nu = r_a + z_a$. Equations (2a) and (2b) transform into the equations for a hydrogen atom at the point a in parabolic coordinates. In order that the solution $\Psi = X(\mu)\,Y(\nu)$, corresponding to the ground state of the hydrogen atom, exist for $R \to \infty$, it is necessary to require that

$$\lim_{R\to\infty} E(R) = -1 \quad \text{or} \quad \lim_{R\to\infty} \lambda(R) = R/2;$$

$$\lim_{R\to\infty} A(R) = |E|\,R^2/4 - R$$
$$= \lambda^2 - 2\lambda + b_0 + b_{-1}/\lambda + b_{-2}/\lambda^2 + \ldots$$

Then we get the limiting values for the functions X and Y at large R:

$$X(\xi_0) \approx C_1(R)\,e^{-\lambda\xi_0}, \qquad Y(\eta_0) \approx C_2(R)\,e^{-\lambda\eta_0}, \tag{3}$$

i.e., $\Psi$ transforms into the function of an isolated hydrogen atom:

$$\lim_{R\to\infty} \Psi(\xi_0, \eta_0) = e^{-\lambda(\xi_0+\eta_0)} = e^{-r_a}.$$

For $R \to 0$, Eqs. (2) go over into the equation of a helium atom in spherical coordinates,[1] while the parameter A takes on one of the values $A = -l(l+1)$. For the ground state $l = 0$, we have

$A(0) = 0$. Such a definition of the limits for R equal to $\infty$ and 0 is based on the well-known theorem that, for an adiabatic change of the parameters of the system (R changes from $\infty$ to zero), the number of its quantum state (energy level) does not change.[2]

We now turn to Eqs. (2), which we shall solve under the boundary conditions (3). Both Eqs. (2a) and (2b) have the same characteristic equation relative to the singular points $+1$ and $-1$, one multiple root of which is $\rho = 0$. Consequently, for example at the point $+1$, each equation has one finite solution and one that is logarithmically divergent. The boundary conditions at the other point in each of the equations are different: $X(\xi_0)$ is bounded in the region $1 \leq \xi_0 < \infty$ and $Y(\eta_0)$ in the region $-1 \leq \eta_0 \leq +1$. The usual method of solution of Eqs. (2) is the following: initially, for a given $\lambda$, one finds a value of the parameter $A(\lambda)$ for which the mentioned solution $Y(\eta_0)$ exists [we note that Eq. (2b) does not depend explicitly on R]. When the parameter A is found as a function of $\lambda$, it is substituted in Eq. (2a), and then such an R is sought for which the solution $X(\xi_0)$ exists, bounded in the region $1 \leq \xi_0 \leq \infty$. The energy is then determined from the condition $\lambda^2 = -ER^2/4$.

Whereas only even or odd solutions of Eq. (2b) are obtained in the problem of the hydrogen molecule, $Y(\eta_0)$ in our case has no symmetry with respect to $\eta_0$. Therefore it is necessary to use the method of solution of the spheroidal equation (2b), developed by Wilson[3] for the general case. For this purpose, we make the substitution

$$Y(\eta_0) = e^{-\lambda\eta_0} y(\eta_0), \qquad x = \eta_0 - 1, \qquad \mu = A - \lambda(2 + \lambda)$$

in Eq. (2b). A solution that is finite at the point $x = 0$ $(\eta_0 = +1)$ is sought in the form of a series

$$y(x) = \sum_{m=0}^{\infty} a_m x^m,$$

which leads to the recurrence relation

$$a_{m+1} = -u_m(\mu, \lambda, m)\, a_m + v_m(\mu, \lambda, m)\, a_{m-1}. \tag{4}$$

The eigenvalue $\mu$ is then determined from the condition that the solution must be finite at the other singular point $x = -2$ $(\eta_0 = -1)$.

The coefficients $a_m$ are determined from the infinite set of linear homogeneous equations (4), so that the vanishing of the determinant is necessary. It has been shown[3,4] that the condition of the vanishing of the infinite determinant of the system (4) is equivalent to the vanishing of the following infinite continued fraction:

$$0 = u_0 + \cfrac{v_1}{u_1 + \cfrac{v_2}{u_2 + \cfrac{v_3}{u_3 + \dots}}}\,. \tag{5}$$

The elements of the continued fraction $u_m$ and $v_m$ are the coefficients of the system of equations (4), while $u_0 = \mu/2$. Wilson[3] proposed to find the values of $\mu_i(\lambda)$ for which the solutions $Y(\eta_0)$ exist, bounded at the point $\eta_0 = -1$, as roots of Eq. (5). This is possible only in the case of the convergence of the infinite continued fraction (5). The fraction converges[4,3] in the case when just those roots of $\mu_i(\lambda)$ of the equation $\Delta(1, u_m, -v_m) = 0$ which correspond to the indicated solutions $Y(\eta_0)$ are substituted in the functions $u_m(\mu, \lambda, m)$ and $v_m(\mu, \lambda, m)$.

We shall seek the root $\mu(\lambda)$ which vanishes for $\lambda = 0$. It corresponds to a state with the lowest energy level.[1] In the case of small $\lambda$, we can find for it a power series in $\lambda$ by making use of the method of successive approximations suggested by Wilson:[3]

$$\mu = -2\lambda - \frac{2}{3}\lambda^2 + \frac{4^3}{3\cdot 5^3}\lambda^4 + \dots$$

Then the following series holds for $A(\lambda)$ in the case of small $\lambda$:

$$A(\lambda) = \frac{1}{3}\lambda^2 + \frac{4^3}{3\cdot 5^3}\lambda^4 + \frac{4^4}{3^4\cdot 5^4}\lambda^5 + \dots \tag{6}$$

For $\lambda \to 0$, the function $A(\lambda)$ coincides with the same parameter for the hydrogen molecule;[3] there, the series contains only even powers of $\lambda$, and the first term is $\lambda^2/3$.

The values of the root $\mu(\lambda)$ for large $\lambda$ are found from the finite continued fraction made up of the first few elements $u_m$ and $v_m$. Their number is larger the larger the value of $\lambda$. To calculate the continued fraction, it is convenient to use the results set forth in the monograph by Perron;[4] the fraction (5) is classified as "limiting periodic."

After finding the values of A for a number of values of $\lambda$, we find the value of R for each pair of numbers A and $\lambda$ as eigenvalues of (2a). Teller[1] suggested a variational principle for this problem, in which the test function $X(\xi_0) = \exp(-\lambda\xi_0)$ is a sufficiently good approximation. In the problem for the conditional extremum

$$\delta I = \delta \int_1^{\infty} \{(\xi_0^2 - 1)X'^2 + (\lambda^2\xi_0^2 - A)X^2\}\, d\xi_0, \qquad \int_1^{0} 2\xi_0 X^2 d\xi_0 = 1$$

the quantity R is a Lagrange multiplier, which is found from the condition

$$R = \min\left\{ I \Big/ \int_1^\infty 2\xi_0 X^2 d\xi_0 \right\}.$$

It is useful to write the wave function $Y(\eta_0)$ in the form

$$Y(\eta_0) = e^{-\lambda\eta_0}(a_0 + a_1\eta_0 + a_2\eta_0^2 + \ldots) \approx e^{-\gamma\eta_0},$$

where $\gamma(R) = \lambda(R) - \delta(R)$, $\lim_{R\to\infty}\delta = 0$. Then $\gamma(R)$ is determined from the condition of the minimum of the functional

$$S(\gamma) = \int_{-1}^{+1} \{(\eta_0^2 - 1) Y'^2 + (\lambda^2\eta_0^2 - A) Y^2\} d\eta_0.$$

Since $A(\lambda)$ is already determined, this is a problem of an absolute extremum. For large $\lambda$, the derivative $dS/d\gamma$ vanishes if $A = \lambda^2 - 2\lambda + 1$ (here, $\gamma = \lambda$). The condition $\delta S = 0$ is satisfied for small $\lambda$ also, if $A(\lambda)$ is taken from the series (6). Such a simplified expression

$$\Psi(\xi_0, \eta_0) = \exp(-\lambda\xi_0 - \gamma\eta_0)$$

is similar to the wave function of the ionized hydrogen molecule obtained by Guillemin and Zener,[5] also from a variational principle. For large R, it is convenient to write it in the form $\Psi = e^{-r_a} e^{\delta\eta_0}$. The result is that the spherically symmetric electron shell of the hydrogen atom is somewhat elongated in the direction of large $\eta_0$, i.e., toward the charge $+e$.

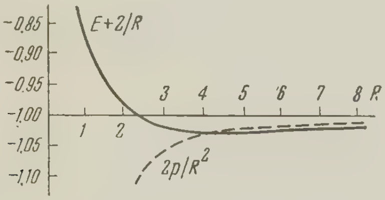

FIG. 1

The solid line in Fig. 1 gives the curve of the electron energy $E = -4\lambda^2/R^2$ combined with the energy of separation of the charge e from the nucleus of the atom, i.e., the energy $E + 2/R$. The resultant curve does not form a deep potential well; its maximum depth of 0.03 is reached for $R = 4$; the system goes over into the much deeper level of the hydrogen molecule only if the proton is entirely removed from the atom.

In order to find the dipole moment of the hydrogen atom induced by the charge e, we write down the normalized function $\Psi$. Here it is convenient to use the coordinates

$$\xi = \xi_0 R = r_a + r_b, \qquad \eta = \eta_0 R = r_a - r_b \tag{7}$$

and introduce the notation used in reference 5:

$$\alpha = 2\lambda / R, \qquad \beta = 2\gamma / R.$$

Normalization of the wave function depends on R:

$$\Psi(\xi, \eta) = C(R) f(R, \xi, \eta),$$
$$f(R, \xi, \eta) = \exp(-\alpha\xi/2 - \beta\eta/2). \tag{8}$$

The condition of normalization in the coordinates (7) has the form

$$\tfrac{1}{4}\pi C^2(R) J(R) = 1, \qquad J(R) = \frac{1}{R}\int_R^\infty d\xi \int_{-R}^{+R} d\eta\, (\xi^2 - \eta^2) f^2. \tag{9}$$

The function $J(R)$ increases monotonically from $J(0) = \frac{1}{2}$ to $J(\infty) = 4$. Then Eq. (9) determines the normalizing factor $C(R)$. The dipole moment of the hydrogen atom in the state (8) is determined as

$$-p = \frac{\pi C^2}{4R} \iint r_a \cos\theta\, (\xi^2 - \eta^2) f^2 d\xi\, d\eta,$$

where $\theta$ is the angle between $r_a$ and R. Integrating over $d\xi$ and $d\eta$, we get the dipole moment $p(R)$ as a function of the distance between the charge e and the nucleus of the atom. From the graph of $p(R)$ in Fig. 2, it is seen that this dipole moment is a short-range effect. In Fig. 1, the broken line shows the energy of interaction of the dipole p and the charge e, equal to $2p/R^2$. Beginning with $R = 4$, this energy is very close to the curve $E + 2/R$.

## 2. STABILITY OF THE PROTON-ELECTRON-POSITRON QUASIMOLECULE

By using the given solution, we shall try to find such a state of the proton, electron and positron system $(pe^-e^+)$, which should dissociate into a positron and a hydrogen atom. For this purpose, we use the variational method employed earlier by the author[6] for the calculation of such a state of the system $(pe^-e^+)$, which dissociates into a proton and a positronium atom: $p + (e^+e^-)$. Here also, the system is treated in the adiabatic approximation, with a fixed positron, but now its state is determined by the wave function (8), and not by the function of the hydrogen molecule. We seek a wave function of the system $(pe^-e^+)$ in the form

$$\psi(r, \xi, \eta) = \Phi(r) F(r, \xi, \eta), \tag{10}$$

where $F(r, \xi, \eta)$ corresponds to the function $\Psi(\xi, \eta)$, which is determined by means of (8),

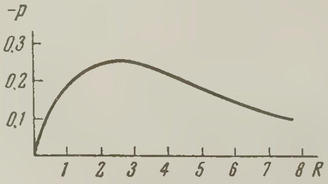

FIG. 2

only the parameter R is replaced by the variable r — the coordinate of the positron. The function $F(r, \xi, \eta)$ is normalized to unity in the coordinates $\xi$, $\eta$, as is shown in (9). The wave function of the positron, $\Phi(r)$, remains arbitrary; its value must be determined from the condition of the minimum of the functional

$$S = \iiint L\left(r, \xi, \eta, \frac{\partial\psi}{\partial r}, \frac{\partial\psi}{\partial\xi}, \frac{\partial\psi}{\partial\eta}, \psi\right) d\tau,$$

where the Lagrangian function of the system $(pe^-e^+)$ and the element of volume $d\tau$ in the coordinates $r$, $\xi$, $\eta$ are given in reference 6. Substituting the function (10) in this integral, and integrating over the coordinates $\xi$ and $\eta$, we arrive at the isoperimetric variational problem

$$\delta S = \delta \int_0^\infty \left(\frac{d\Phi^*}{dr}\frac{d\Phi}{dr} + U(r)\,\Phi^*\Phi\right) r^2\,dr, \quad \int_0^\infty \Phi^*\Phi r^2\,dr = 1 \tag{11}$$

by the same means as previously.[6] Here, the potential $U(r)$ is a function of r, expressed both directly in terms of r and also by $\alpha(r)$ and $\beta(r)$;

$$\begin{aligned} U(r) = {} & \left(\frac{2}{r} + \frac{\alpha^2 + 5\beta^2 - 2\alpha\beta}{4}\right) + \frac{1}{4rJ}\left(\frac{d\alpha}{dr}\frac{\partial}{\partial\alpha} + \frac{d\beta}{dr}\frac{\partial}{\partial\beta}\right)^2 (rJ) \\ & - \left(\frac{1}{2J}\frac{dJ}{dr}\right)^2 + \frac{8}{rJ}\frac{e^{-\alpha r}}{\alpha\beta}\left\{\left(r + \frac{1}{\alpha}\right)\left(\frac{\alpha^2 - \beta^2}{2\alpha} - 2\right)\sinh\beta r \right. \\ & + \frac{\alpha - \beta}{4}\left[\frac{d\alpha}{dr}\left(\frac{r^2}{\alpha} + \frac{3r}{\alpha^2} + \frac{3}{\alpha^3} + \frac{r^2}{2\beta} + \frac{r}{\alpha\beta} + \frac{1}{\alpha^2\beta}\right)\right. \\ & \times\left(\cosh\beta r - \frac{\sinh\beta r}{\beta r}\right) + \frac{d\beta}{dr}\left(r + \frac{1}{\alpha}\right)\left[\left(\frac{2}{\alpha\beta} + \frac{3}{\beta^2}\right)\right. \\ & \left.\left.\left.\times\left(\cosh\beta r - \frac{\sinh\beta r}{\beta r}\right) - \left(\frac{r}{\alpha} + \frac{r}{\beta}\right)\sinh\beta r\right]\right]\right\}. \end{aligned} \tag{12}$$

The function $J(R)$ is determined by Eq. (9). For $r \to 0$, the potential $U(r)$ increases according to Coulomb's law. Taking it into account that $\alpha(\infty) = \beta(\infty) = 1$, we find the limit at infinity:

$$\lim_{r\to\infty} U = -1,$$

toward which $U(r)$ tends according to the exponential law $re^{-br}$.

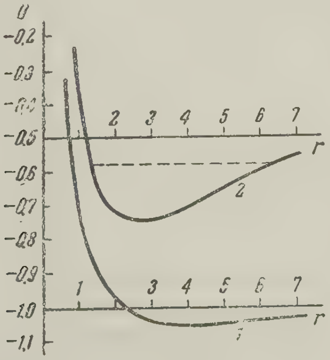

FIG. 3

The variational problem (11) corresponds to the Schrödinger equation with the potential energy (12), and its Lagrangian multiplier corresponds to the eigenvalue of the energy $E_n$. The potential (12) is plotted in Fig. 3 (curve 1). The maximum depth of $U(r)$ is equal to $-1.05$ and is reached at $r = 4$. However, the "free energy" amounts to $-0.05$. In the same drawing, we have plotted the curve (term) for the state of the system $(pe^-p^+)$ which we found earlier (curve 2), which dissociates into a proton and a positronium atom.[6] This curve has the limit $-\frac{1}{2}$ for $r \to \infty$, and a depth of the potential well equal to $-0.26$. The depth of the potential well, $-0.05$, of the new term (12) is insufficient for the existence of stationary states of positronium. All attempts at changing $\alpha(r)$ and $\beta(r)$ arbitrarily (variation) have failed to make any appreciable increase in this depth. Therefore, although the application of the variational principle still does not prove the absence of stationary states, it is nevertheless very probable that there are none. The positron could be kept in the potential well (12) if its mass were four times greater. In order to find the energy of the system $(pe^-e^+)$, Ore[7] took the wave function of the ionized hydrogen molecule $H_2^+$, and then decreased the mass of one of its protons. By a variational method, he found that this system would exist had the mass of the proton amounted to 4.5 m (m = mass of electron). The results obtained by us furnish a basis for assuming that this result of Ore is final. Thus, it is necessary to regard the lowest state of the system $(pe^-e^+)$ as the state found earlier[7] with energy $E = -0.563$. This state is stable, inasmuch as the new term (12) does not overlap the first, i.e., there is no predissociation.

In conclusion, the author expresses his deep gratitude to his supervisor, Prof. A. A. Sokolov, and also to Prof. V. I. Gol'danskiĭ.

---

[1] E. Teller, Z. Physik **61**, 458 (1930).

[2] M. Born and V. Fock, Z. Physik **51**, 165 (1928); A. Lenard, Ann. of Phys. **6**, 261 (1959).

[3] A. H. Wilson, Proc. Roy. Soc. (London) **A118**, 617, 635 (1928).

[4] O. Perron, Die Lehre von den Kettenbruchen, **2**, Stuttgart, 1957.

[5] V. Guillemin and C. Zener, Proc. Nat. Acad. Sci. USA **15**, 314 (1929).

[6] V. P. Shmelev, JETP **37**, 458 (1959), Soviet Phys. JETP **10**, 325 (1960).

[7] A. Ore, Phys. Rev. **73**, 1313 (1948).

Translated by R. T. Beyer

SOVIET PHYSICS JETP VOLUME 11, NUMBER 5 NOVEMBER, 1960

# *THE THOMAS-FERMI MODEL OF THE ATOM WITH QUANTUM AND EXCHANGE CORRECTIONS*

N. N. KALITKIN

Submitted to JETP editor December 3, 1959

J. Exptl. Theoret. Phys. (U.S.S.R.) **38**, 1534-1540 (May, 1960)

Quantum and exchange corrections to the energy and the chemical potential of the Thomas-Fermi atom are derived and numerical calculations of thermodynamical functions for a cold atom are presented. The extrapolation of the model into the region of normal densities is considered. The calculations are compared with the experimental data.

## 1. INTRODUCTION

ONE of the models used for the description of the behavior of matter at high temperatures and pressures is the statistical Thomas-Fermi model of the atom (abbreviated TF model),[1,2] which is the quasi-classical approximation to the method of the self-consistent field. The inclusion of exchange effects in the Thomas-Fermi-Dirac (TFD model)[1,3] represents a refinement of this approximation. However, the TFD model is not consistent, since here the exchange effects are computed exactly within a quasi-classical framework, i.e., one considers the exchange effects of all orders, but neglects the quantum corrections. The more rigorous treatment of the quantum effects with the help of the Weizsäcker equation[4,5] involves considerable methodological difficulties and leads to arduous numerical calculations.

The TF model with quantum and exchange corrections (abbreviated TFC model) has been considered by a number of authors.[5-8] In the present paper we calculate corrections to the potential, the energy, and the chemical potential of the atom within the framework of this model and present the numerical results of these calculations for the compressed atom at zero absolute temperature.

## 2. THE ATOM AT ARBITRARY TEMPERATURES

The operator corresponding to the single particle density matrix for a nondegenerate Fermi gas has the form

$$\hat{\rho}(\mathbf{r}, \hat{\mathbf{p}}) = 2(2\pi\hbar)^{-3}[1 + \exp\{(\hat{H} - \mu)/kT\}]^{-1}, \qquad (1)$$

where $\hat{H}$ is the Hamiltonian of the electron in the Hartree-Fock field. The magnitude of the chemical potential $\mu$ is determined by the total energy of the system, which, according to the self-consistent field approximation, is equal to

$$E = \int \hat{H}\hat{\rho}\,d\mathbf{p}\,d\mathbf{r} - \frac{e^2}{2}\int \rho(\mathbf{r}_1)\,\rho(\mathbf{r}_2)\,|\,\mathbf{r}_1 - \mathbf{r}_2\,|^{-1}\,d\mathbf{r}_1\,d\mathbf{r}_2. \qquad (2)$$

Kirzhnits[5] has shown that expression (1) satisfies the system of TFD equations written in operator form

$$\Delta\varphi(\mathbf{r}) = -4\pi Ze\delta(\mathbf{r}) + 4\pi e\int \hat{\rho}(\hat{H})\,d\mathbf{p},$$

$$\hat{H} = \hat{\mathbf{p}}^2/2m - e\varphi(\mathbf{r}) - 2\pi\hbar^2 e^2\int \hat{\rho}(\hat{H}')\,|\,\mathbf{p} - \mathbf{p}'\,|^{-2}\,d\mathbf{p}'. \qquad (3)$$

The zeroth approximation to this system is, of course, the TF equation.* Using the rules for the computation of a function of a sum of noncommuting arguments, we can expand Eqs. (1) to (3) in powers of $\hbar^2$ (see references 5 to 7) and obtain corrections of arbitrary order to the equations of the TF model.

We shall denote the quantum and exchange corrections of first order by the symbols $\delta_1$ and $\delta_2$, respectively. We introduce the dimensionless potential function of the TF model and the quantum and exchange corrections to it:†

$$\xi(\mathbf{r}) = [e\varphi(\mathbf{r}) + \mu]/kT,$$

$$\delta_i\xi(\mathbf{r}) = [e\delta_i\varphi + \delta_i\mu]/kT$$
$$= (e/3\pi\sqrt{2a_0kT})\,[I'_{1/2}(\xi)\,\delta_{1i} + u_i(\mathbf{r})]. \qquad (4)$$

The corrections to the potential satisfy the following equation and boundary conditions:[8]

$$\Delta u_i(\mathbf{r}) - \sqrt{32kT/\pi^2e^2a_0^3}\,I'_{1/2}(\xi)\,u_i(\mathbf{r}) = \sqrt{32kT/\pi^2e^2a_0^3}\,\Psi'_i(\xi),$$
$$(ru_i)_{r=0} = 0, \qquad (du_i/dr)_{r=r_0} = 0. \qquad (5)$$

Here we use the following notation for the Dirac functions and their combinations:

---

*Not the TFD equation, since the exchange term in the Hamiltonian is itself a correction of order $\hbar^2$.

†Here $\delta_{11}$ is the Kronecker symbol, which separates out the quantum correction.

$$I_k(\xi) = \int_0^\infty \frac{x^k dx}{1 + \exp(x - \xi)},$$

$$\Psi_1(\xi) = I_{1/2}(\xi)\, I'_{1/2}(\xi), \quad \Psi_2(\xi) = 6 \int_{-\infty}^{\xi} [I'_{1/2}(x)]^2 dx.$$

Since we assume that the potential vanishes at the boundary of the atom in any approximation, it follows from (4) that the corrections to the chemical potential of the atom and to the potential of the self-consistent field have the form

$$\delta_i\mu = \frac{e}{3\pi}\sqrt{kT/2a_0}\,\{I'_{1/2}(\xi(r_0))\,\delta_{1i} + u_i(r_0)\}, \tag{6}$$

$$e\delta_i\varphi(r) = \frac{e}{3\pi}\sqrt{kT/2a_0}\,\{I'_{1/2}(\xi(r))\,\delta_{1i} + u_i(r)\} - \delta_i\mu. \tag{7}$$

The calculation of the correction to the energy leads to a divergent volume integral: as is known, one cannot compute the quantum correction of Weizsäcker with the help of the quasi-classical electron density. However, the divergence is related to the region near the nucleus which is not affected by the external conditions (temperature and pressure). The divergent terms therefore cancel out in the calculation of the difference of the energies of the atom under different external conditions. The remaining finite expression represents the correction to the energy of excitation of the atom and has the following form:

$$\delta_i E = \frac{e}{3\pi}\sqrt{\frac{kT}{2a_0}}\, Z u_i(0)$$
$$+ \frac{1}{3\pi^3}\left(\frac{kT}{ea_0}\right)^2 \int_V \left[\frac{1}{2} u_i I_{1/2}(\xi) + \Psi_i(\xi)\right] dr + C(Z), \tag{8}$$

where C(Z) is chosen such that the energy of the unexcited atom is zero. This still leaves the correction to the binding energy of the atom undetermined.

In the region where the electron density is nearly uniform we can obtain[8] explicit expressions for the thermodynamical quantities in terms of the boundary conditions. Denoting the correction due to the non-uniformity by the symbol $\delta_n$, we find for the energy of the uniform distribution and the correction to it:

$$E_0 = ZkT I_{3/2}(\xi_0)/I_{1/2}(\xi_0), \quad \delta_n E = -3\sqrt[3]{36\pi} Z^2 e^2/10 V^{1/3},$$
$$\delta_i E = -(Ze/3\pi)\sqrt{kT/2a_0}\left[\frac{3}{2}\Psi'_i(\xi_0)/I'_{1/2}(\xi_0)\right.$$
$$\left. - \Psi_i(\xi_0)/I_{1/2}(\xi_0)\right], \tag{9}$$

where $\xi_0$ is determined by the equation

$$Z/V = (2kT/e^2 a_0)^{3/2} I_{1/2}(\xi_0)/2\pi^2. \tag{9a}$$

## 3. THE COLD ATOM

For the description of the compressed atom at zero absolute temperature we go to the limit T → 0 in Eqs. (5) to (8) (for $\mu > 0$), using the asymptotic Dirac functions:

$$I_k(\xi) \to \xi^{k+1}/(k+1), \quad \Psi_1(\xi) \to \frac{2}{3}\xi^2,$$
$$\Psi_2(\xi) \to 3\xi^2 \text{ for } \xi \to +\infty. \tag{10}$$

Since the asymptotic functions $\Psi_i$ of (10) differ only by numerical factors, the quantum and exchange corrections also differ only by the numerical factor 9/2 at absolute zero. For simplicity we shall consider in the following only the sum of the quantum and exchange corrections of first order.

For a complete description of the TFC model we must use the equations of the TF model[1,2] and the expression for the corrections to the pressure.[8] For convenience of calculation we make the following change of coordinates:

$$x = r/r_0, \quad \Phi(x)/x = \xi(r)/\xi(r_0),$$
$$\psi(x)/x = u_i(r)/u_i(r_0) \tag{11}$$

and go to the limit as above. The equations and boundary conditions for the dimensionless potential then take the form

$$\Phi''(x) = \alpha\Phi^{3/2}(x)/\sqrt{x}, \quad \Phi(1) = \Phi'(1) = 1,$$
$$\Phi(0) \equiv \Phi_0 = Ze^2/r_0\mu,$$
$$\psi''(x) - \frac{3}{2}\alpha\sqrt{\Phi(x)/x}\,\psi(x) = \beta\psi(x),$$
$$\psi(1) = \psi'(1) = 1, \quad \psi(0) = 0, \tag{12}$$

where

$$\alpha = r_0^2\mu^{1/2}/e(\varkappa a_0)^{3/2},$$
$$\beta = 11\alpha\sqrt{\mu/kT}/[u_1(r_0) + u_2(r_0)], \quad \varkappa = (9\pi^2/128)^{1/3}.$$

Transforming expression (8) with the help of equations analogous to the virial theorem in the TF model, we obtain the following expressions for the thermodynamical quantities and the corrections to them:

$$ZV = \frac{4\pi(\varkappa a_0)^3}{3}\alpha^2\Phi_0, \qquad \frac{\mu}{Z^{4/3}} = \frac{e^2}{\varkappa a_0}(\alpha\Phi_0^2)^{-2/3},$$
$$\frac{P}{Z^{10/3}} = \frac{e^2}{10\pi(\varkappa a_0)^4}(\alpha\Phi_0^2)^{-5/3},$$
$$\frac{E}{Z^{7/3}} = \frac{e^2}{\varkappa a_0}\left[C_\infty + \frac{\alpha^{1/3}}{\Phi_0^{7/3}}\left(\frac{2}{35} + \frac{3}{7}\frac{\Phi_0\Phi'_0}{\alpha}\right)\right],$$
$$\frac{\delta\mu}{Z^{2/3}} = \frac{e^2}{16\varkappa^2 a_0}(\alpha\Phi_0^2)^{-1/3}\left[1 + \frac{11\alpha}{\beta}\right],$$
$$\frac{\delta P}{Z^{8/3}} = \frac{11e^2}{64\pi\varkappa^5 a_0^4}(\alpha\Phi_0^2)^{-4/3}\left[\frac{1}{2} + \frac{\alpha}{\beta}\right],$$
$$\frac{\delta E}{Z^{5/3}} = -\frac{11e^2}{32\varkappa^2 a_0}\left[\delta C_\infty + \frac{\alpha^{2/3}}{\Phi_0^{5/3}}\int_0^1 \Phi^2(x)\,dx\right], \tag{13}$$

where $C_\infty$ and $\delta C_\infty$ are chosen such that the energy and its correction become zero for an infinite atom. The potential and its correction are obtained from the formulas

| $ZV$, Å³ | $Z^{-10/3}P$, dyne/cm² | $-Z^{-8/3}\delta P$, dyne/cm² | $Z^{-7/3}E$, erg/atom | $-Z^{-5/3}\delta E$, erg/atom | $Z^{-4/3}\mu$, erg/atom | $-Z^{-2/3}\delta\mu$, erg/atom |
|---|---|---|---|---|---|---|
| .21078 (−3) | .30412 (20) | .55306 (18) | .93547 (−8) | .33829 (−9) | .16304 (−7) | .40323 (−9) |
| .16483 (−2) | .95892 (18) | .35577 (17) | .22487 | .16484 | .40907 (−8) | .20328 |
| .62812 | .99762 (17) | .59598 (16) | .86759 (−9) | .10162 | .16545 | .13021 |
| .24391 (−1) | .98523 (16) | .96937 (15) | .31962 | .60883 (−10) | .65539 (−9) | .82860 (−10) |
| .10168 (0) | .83186 (15) | .14178 | .10592 | .34219 | .24384 | .51432 |
| .26456 | .15396 | .38603 (14) | .48388 (−10) | .22544 | .12418 | .37294 |
| .41652 | .68308 (14) | .20691 | .32843 | .18279 | .89717 (−10) | .31984 |
| .12101 (1) | .97281 (13) | .46674 (13) | .12584 | .10759 | .41143 | .22194 |
| .23973 | .26900 | .17537 | .65214 (−11) | .74094 (−11) | .24603 | .17472 |
| .47555 | .71642 (12) | .64075 (12) | .32458 | .49412 | .14493 | .13671 |
| .96270 | .17573 | .21958 | .15111 | .31355 | .82608 (−11) | .10536 |
| .13114 (2) | .93461 (11) | .13558 | .10637 | .25350 | .64171 | .93704 (−11) |
| .18739 | .44521 | .76876 (11) | .70018 (−12) | .19622 | .47699 | .81629 |
| .26012 | .22241 | .45150 | .47082 | .15345 | .36136 | .71718 |
| .35927 | .11094 | .26452 | .31471 | .11924 | .27360 | .62966 |
| .50824 | .51816 (10) | .14712 | .20138 | .89897 (−12) | .20178 | .54579 |
| .71602 | .24067 | .81334 (10) | .12772 | .67196 | .14848 | .47232 |
| .10150 (3) | .10857 | .43883 | .79167 (−13) | .49348 | .10798 | .40623 |
| .14862 | .44678 (9) | .22005 | .46147 | .34716 | .75705 (−12) | .34310 |
| .20701 | .20338 | .11914 | .28453 | .25264 | .55259 | .29519 |
| .28687 | .92408 (8) | .63314 (9) | .17445 | .18273 | .40306 | .25373 |
| .41240 | .37795 | .31923 | .99690 (−14) | .12582 | .28188 | .21358 |
| .61577 | .13804 | .14472 | .52758 | .82059 (−13) | .18841 | .17576 |
| .81519 | .67390 (7) | .82305 (8) | .33418 | .60277 | .14142 | .15292 |
| .11248 (4) | .29238 | .42611 | .19569 | .41916 | .10127 | .12997 |
| .15950 | .11650 | .20604 | .10808 | .27959 | .70084 (−13) | .10859 |
| .22919 | .44137 (6) | .95619 (7) | .05754 | .18152 | .47534 | .89791 (−12) |
| .31529 | .18559 | .48144 | .03266 | .12297 | .33613 | .75746 |
| .42552 | .81345 (5) | .25034 | .01901 | .84621 (−14) | .24167 | .64401 |
| .86918 | .10973 | .51008 (6) | .00505 | .33762 | .10845 | .43378 |
| .16984 (5) | .16014 (4) | .11035 | .00140 | .13790 | .50220 (−14) | .29640 |
| .39330 | .13569 (3) | .15450 (5) | .00026 | .04310 | .18711 | .18164 |
| .23448 (6) | .60040 (0) | .20455 (3) | .00001 | .00321 | .21402 (−15) | .61776 (−13) |
| .90408 | .88368 (−2) | .70377 (1) | .00000 | .00041 | .39591 (−16) | .26638 |
| .44188 (7) | .56275 (−4) | .12372 (0) | .00000 | .00004 | .52385 (−17) | .97086 (−14) |

The numbers in the table represent decimal fractions to be multiplied by the power of ten indicated in parentheses)

$$e\varphi(r) = \mu\left[\Phi(x)/x - 1\right],$$

$$e\delta\varphi(r) = Z^{-2/3}\mu\left[\delta\Phi(x)/x - \delta\Phi(1)\right],$$

$$\delta\Phi(x) = \frac{(\alpha\Phi_0^2)^{1/3}}{16\varkappa}\left[\sqrt{x\Phi(x)} + \frac{11\alpha}{\beta}\psi(x)\right]. \tag{14}$$

Expanding (12) in a power series in the parameter $\alpha$, we find the asymptotic expressions for the case of high compression:

$$\Phi(x) = x + \alpha\left(\tfrac{1}{6}x^3 - \tfrac{1}{2}x + \tfrac{1}{3}\right) + O(\alpha^2),$$

$$\Phi_0 = \tfrac{1}{3}\alpha + \tfrac{1}{20}\alpha^2 + O(\alpha^3), \qquad \psi(x) = x + O(\alpha^2),$$

$$\alpha = \left(r_0\sqrt[3]{3Z}/\varkappa a_0\right)\left(1 - r_0\sqrt[3]{3Z}/20\varkappa a_0 + \ldots\right),$$

$$\beta = -\frac{3}{2}\alpha\left(1 - \frac{1}{20}\alpha\right) + O(\alpha^3). \tag{15}$$

The asymptotic values of the thermodynamic quantities will not be quoted here; they are easy to obtain by substituting (15) in (13).

## 4. SOLUTION OF THE EQUATIONS

It is known that the TF equation has a universal form. If we take ZV and $Z^{-4/3}T$ for the unknown variables and $Z^{-10/3}P$, $Z^{-7/3}E$, and $Z^{-4/3}\mu$ for the functions of these variables, the equations do not contain Z in any other fashion than the one indicated. If we further introduce the functions $Z^{-8/3}\delta P$, $Z^{-5/3}\delta E$, and $Z^{-2/3}\delta\mu$ this universality is extended to the equations for the corrections of first order. This circumstance greatly facilitates the numerical calculations, since any solution of the TFC equations can be used for all elements; we recall that the TFD equation or the Weizsäcker equation have to be solved separately for each element.

The numerical integration of (12) was performed on the computer "Strela." The computations were carried up to values of the compression for which the relations (15) are applicable with an accuracy of $10^{-3}$ to $10^{-4}$. The calculations for very rarefied matter (up to $r_0Z^{1/3} \approx 100$ A) led to the following values for the constants $C_\infty$ and $\delta C_\infty$:

$$C_\infty = 0.6806018678, \quad \delta C_\infty = -0.615434693.$$

The calculated thermodynamical quantities are given in the table.* The tables listing the shapes of the potentials for the various values of the radius of the atom are omitted for lack of space.

---

*Our values for the charge of the electron and the Bohr radius, $e = 4.80286 \times 10^{-10}$ cgs esu and $a_0 = 0.529172$ A, are somewhat different from those used by Latter.[2]

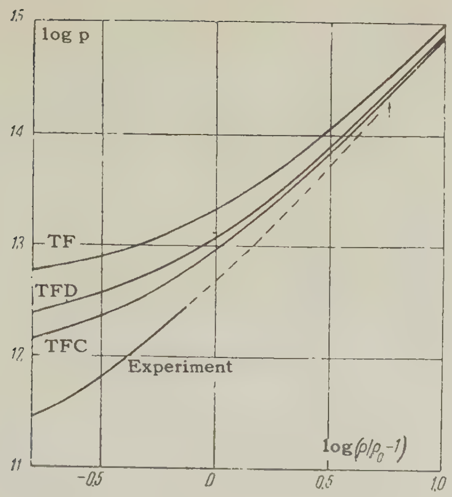

FIG. 1

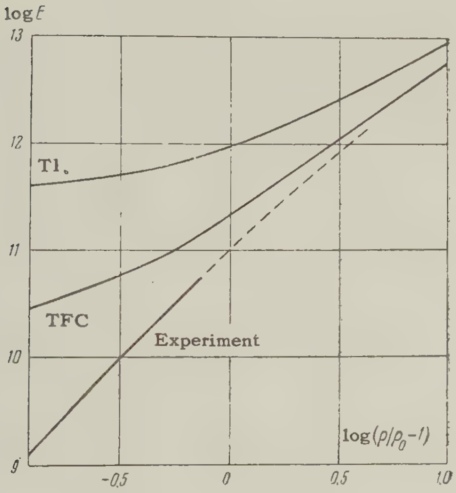

FIG. 2

## 5. DISCUSSION OF THE RESULTS

Let us compare the results of our calculations with the experimental data of Al'tshuler et al.[9] on the compressibility of iron. Figures 1 and 2 show the theoretical and experimental curves for the pressure and the energy[*] (P is in dyne/cm$^2$ and E in erg/g). It is seen that the TFC model reproduces the experimental curves better than the TF and TFD models. The Weizsäcker model gives much lower pressures;[†] this is due to the fact that the coefficient of the correction term used by Gombas is ten times too large (see reference 5). The dotted curves represent the extrapolation of the experimental curves into the region where the correction to the pressure calculated by the TF model amounts to 30% (arrow in Fig. 1). These extrapolated curves, which go over into the curves of the TFC model, apparently describe (with an accuracy of 10 to 15%) the compressibility of iron at pressures which have not yet been attained by experiment.[*]

In the region of normal densities where it is impossible to neglect the shell structure of the atom and where the approximation of spherical cells and the self-consistent field method become inaccurate, the TFC model is, in general, not applicable. However, in contrast to the TF model, the TFC model does describe qualitatively some properties of solid matter, so that the discussion below has some significance.

The corrections to the thermodynamical quantities are negative and go to zero more slowly for $V \to \infty$ than the uncorrected quantities. Therefore the corrected pressure becomes zero for some finite density $\rho_0(Z)$. By virtue of the thermodynamical relation $P = -(\partial E/\partial V)_{T=0}$ the energy has a minimum for this density;[†] the value of this mini-

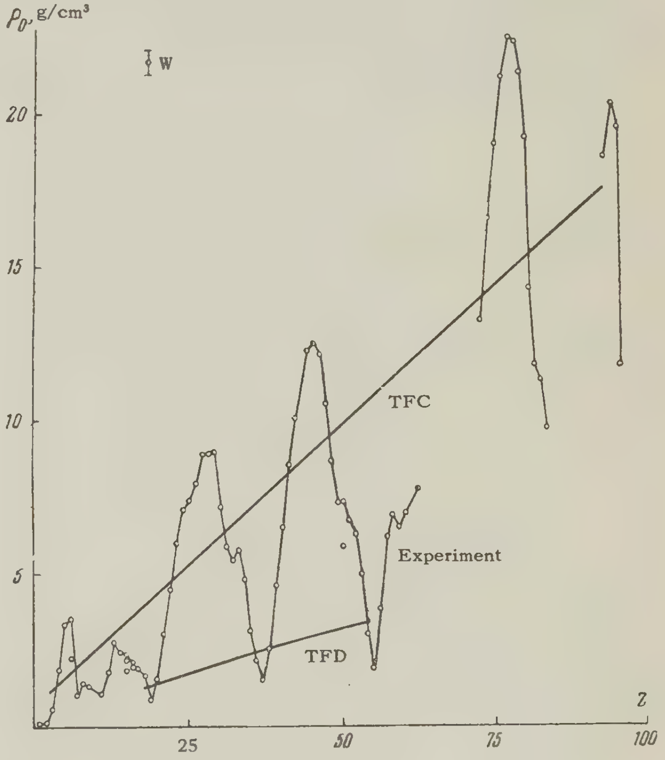

FIG. 3

---

[*] The energy in the TFC model was reckoned from the minimum (see below), which is equal to –5.488 ev/atom relative to the energy of the cold infinite atom.

[†] The corresponding curves are not shown in Figs. 1 and 2, since the points obtained by Gombas[4] lie beyond the limits of the graphs.

[*] It was pointed out by Ya. B. Zel'dovich that the occurrence of a phase transition in the unknown region may complicate the picture.

[†] Since the dependence of the corrections on Z is different from that of the uncorrected quantities, the binding energy and the density of the uncompressed matter are obtained separately for each element from the data of the table.

mum gives the binding energy of solid matter in our model.

Figure 3 shows the experimental and theoretical dependence of the density of the uncompressed matter on the charge of the nucleus. The TFC model, in which the dependence of the physical quantities on Z is monotonic, is not adequate for the explanation of the behavior of the experimental curves. It does, however, describe the average dependence of the density on the charge better than the TFD model. The reasons for the sharp disagreement between experiment and the results of the Weizsäcker model (point W in the figure) were discussed earlier.

In conclusion we note that the numerical calculations of Kompaneets and Pavlovskiĭ,[6] who obtained the correction to the potential for the infinite cold atom, are not sufficiently accurate for distances from the nucleus larger than $rZ^{1/3} = 2$ A. Furthermore, reference 6 contains a printing error: the quantity shown in the figure is not $y(x)$, as indicated in the paper, but $y(x)/8(6\pi)^{2/3}$.

I express my sincere gratitude to A. A. Samarskiĭ and V. Ya. Gol'din for proposing this problem and for constant attention to this work, to D. A. Kirzhnits for valuable comments, and to I. A. Govorukhina for carrying out many of the numerical calculations.

---

[1] Feynman, Metropolis, and Teller, Phys. Rev. **75**, 1561 (1949).

[2] R. Latter, Phys. Rev. **99**, 1854 (1955); J. Chem. Phys. **24**, 280 (1956).

[3] N. Metropolis and J. R. Reitz, J. Chem. Phys. **19**, 555 (1951). K. Cowan and J. Ashkin, Phys. Rev. **105**, 144 (1957).

[4] P. Gombas, Acta Phys. Acad. Sci. Hung. **8**, 321 (1958).

[5] D. A. Kirzhnits, JETP **32**, 115 (1957), Soviet Phys. JETP **5**, 64 (1957).

[6] A. S. Kompaneets and E. S. Pavlovskiĭ, JETP **31**, 427 (1956), Soviet Phys. JETP **4**, 328 (1957).

[7] S. Golden, Phys. Rev. **105**, 604 (1957).

[8] D. A. Kirzhnits, JETP **35**, 1545 (1958), Soviet Phys. JETP **8**, 1081 (1959).

[9] Al'tschuler, Krupnikov, Ledenev, Zhuchikhin, and Brazhnik, JETP **34**, 874 (1958), Soviet Phys. JETP **7**, 606 (1958).

Translated by R. Lipperheide
294

SOVIET PHYSICS JETP VOLUME 11, NUMBER 5 NOVEMBER, 1960

# *COULOMB EXCITATION OF NUCLEI BY HEAVY IONS, ACCOMPANIED BY EMISSION OF GAMMA QUANTA*

B. N. KALINKIN

Joint Institute for Nuclear Research

Submitted to JETP editor December 4, 1959

J. Exptl. Theoret. Phys. (U.S.S.R.) **38**, 1541-1543 (May, 1960)

We consider Coulomb excitation of high single-nucleon levels in the nucleus, due to bombardment of the latter with heavy ions of energies lower than the Coulomb barrier. The value of the cross sections thus obtained indicates that an experimental proof of the existence of such levels may be feasible.

IN reactions due to Coulomb excitation of nuclei, one observes most frequently collective excitations corresponding to rotational and vibrational degrees of freedom. Most experiments pertain to a study of the lower levels (lower than 1 Mev). This circumstance is explained by the fact that the accelerated ions employed are protons, deuterons, and low-energy $\alpha$ particles. As the ion energy is increased, one can hope to obtain higher excited states of nuclei. In this case, however, the energy is found to be considerably higher than the Coulomb barrier, and other reactions due to nuclear interaction become possible and make the investigations difficult.

In view of modern advances in technique, it becomes feasible to accelerate heavy ions (up to iron ions[1]). Naturally, the use of such ions will make it possible to raise considerably the region of investigated levels of the Coulomb-excited nuclei (approximately 6 or 7 Mev). From this point of view it is interesting to investigate the Coulomb excitation of a nucleus by a heavy ion, followed by emission of a relatively high-energy photon (6 or 7 Mev).

This process can be analyzed using the shell model, i.e., within the framework of single-nucleon excitations. It is well known that earlier calculations for this process, in the region of low excitations, could not yield satisfactory results because the experimental probabilities of radiative nuclear transitions deviated greatly from the probabilities calculated theoretically on the basis of the independent-particle model. This is understandable, for the collective aspects of the nucleus play an important role at low excitations. However, as shown by the author in a paper on resonance scattering of $\gamma$ quanta by nuclei,[2] in the energy interval of interest to us a decisive role is played by single-nucleon transitions. The theory developed in reference 2 agrees satisfactorily with experiment. This circumstance gives some grounds for using the shell model to estimate the cross sections for the process indicated above.

By way of a specific example, we consider the Coulomb excitation of $Pb^{208}$ by the $Ne^{20}$ ion. The Coulomb barrier has in this case an approximate order of magnitude of 130 Mev. Let the kinetic energy of the ion be approximately 100 to 120 Mev. The nucleus can go into the ground state, emitting a 6-Mev $\gamma$ quantum, if, for example, a neutron electric-dipole transition $2f_{7/2} \rightarrow 2g_{9/2}$ is realized in the excitation. The energy lost by the ion to excitation of the nucleus is nearly $1/20$. Under these conditions, the excitation process can be considered from the classical point of view.

Using the theory of the Coulomb excitation of nuclei in this approximation,[3,4] we can calculate the total cross section. The reduced probability B(E1) (with allowance for the filling of the corresponding shell), has the following form

$$B(E1) = \frac{3\varepsilon^2}{4\pi}\left|\int \varphi_f^* r \varphi_i r^2 dr\right|^2 (2L_i + 1)$$

$$\times (2L_f + 1) \,|\, (L_i 100 \,|\, L_f 0) \,|^2 W^2 (L_i J_i L_f J_f, {}^1\!/_2 1).$$

Here $\epsilon$ is the effective charge of the nucleon (in our case $\epsilon \approx 0.4$), $(L_i 100 \mid L_f 0)$ is the Clebsch-Gordan coefficient, W is the Racah function, while $\varphi_i$ and $\varphi_f$ are the radial parts of the nucleon wave functions in the initial (ground) and final (excited) states, respectively. We borrow the expressions for $\varphi_i$ and $\varphi_f$ from reference 2. They are exact solutions of the approximate Schrödinger equation, with allowance for the smearing of the nuclear boundaries, and have the form

$$\varphi_i = r^{-1} N_i \, 2\alpha_i (r - r_0^i) \exp\left[-\alpha_i^2 (r - r_0^i)^2 / 2\right],$$

$$\varphi_f = r^{-1} N_f 2\alpha_f (r - r_0^f) \exp\left[-\alpha_f^2 (r - r_0^f)^2 / 2\right],$$

where N is a normalization factor; $\alpha$ and $r_0$ are parameters determined when solving the equation.

The matrix element in B(E1) can be determined numerically. It is found to be approximately $5.6 \times 10^{-13}$ cm. The total cross section for Coulomb excitation of the single-nucleon level $2g_{9/2}$ in the $Pb^{208}$ nucleus by the $Ne^{20}$ ion (100 to 120 Mev) is approximately $2 \times 10^{-2}$ mb.

As the ion energy is decreased, the cross section diminishes practically exponentially.

If $Pb^{208}$ nuclei are bombarded with much heavier ions, for example, $Fe^{56}$ (Coulomb barrier ~ 360 Mev), then at an approximate energy of 300 Mev (direct contact between the nuclei becomes possible at higher energy), the cross section is $\sigma = 0.01$ mb.

Assuming that the reverse transition is also pure electric-dipole, and using the general theory of angular correlation (see reference 5 and also 3), we can calculate the angular distribution of the $\gamma$ quanta for the case $Ne^{20} + Pb^{208}$.

Its form is

$$W(\vartheta) = 1 - 0.064\, P_2(\cos \vartheta_\gamma).$$

Analogously we can obtain the cross section for the Coulomb excitation for the case of single-nucleon transitions of the electric-quadrupole type. A specific example is the transition $1h_{11/2} \rightarrow 2f_{7/2}$ in $Pb^{208}$ (transition energy 3.5 Mev).

Using the method indicated above to determine the wave functions, we can calculate the matrix element $\langle r^2 \rangle_{if}$ to be approximately $20.2 \times 10^{-26}$ cm$^2$. We then obtain for $Ne^{20}$ ions with approximate energy 120 Mev, $\sigma = 0.24$ mb. For ions with approximate energy 200 Mev, the cross section is found to be 0.67 mb.

The calculated cross sections appear to be sufficiently large. It is therefore advantageous to set up experiments for the purpose of analyzing the high excited levels of nuclei.

The author is indebted to S. M. Polikanov for useful discussions.

---

[1] G. N. Flerov, (Proc. of Conf. on Reactions with Multiply-Charged Ions), Joint Inst. Nuc. Res., 1959.

[2] B. N. Kalinkin, JETP **36**, 1438 (1959), Soviet Phys. JETP **9**, 1022 (1959).

[3] Alder, Bohr, Huus, Mottelson, and Winther, Revs. Modern Phys. **28**, 432 (1958).

[4] K. Alder and A. Winther, Kgl. Dan. Vid. Selsk. Mat.-Fys. Medd. **31**, No. 1, 1956.

[5] L. C. Biedenharn and M. E. Rose, Revs. Modern Phys. **25**, 729 (1953).

Translated by J. G. Adashko
295

SOVIET PHYSICS JETP VOLUME 11, NUMBER 5 NOVEMBER, 1960

# THE MOTION OF A PISTON IN A CONDUCTING MEDIUM

R. V. POLOVIN

Physico-Technical Institute, Academy of Sciences, Ukrainian S.S.R.

Submitted to JETP editor December 4, 1959; resubmitted February 17, 1960

J. Exptl. Theoret. Phys. (U.S.S.R.) 38, 1544-1555 (May, 1960)

We consider magnetohydrodynamic waves which arise when a piston moves in a perfectly conducting medium in the presence of a magnetic field. If the transverse velocity component of the piston exceeds the velocity of sound in the undisturbed medium, then a magnetic field is generated; in this case, the magnetic pressure becomes comparable with the hydrostatic pressure. At supersonic velocities, a vacuum is formed between the piston and the medium (cavitation). Compared with ordinary hydrodynamics, additional cases of cavitation appear when the piston moves with supersonic velocity in the direction perpendicular to the normal, and also when the piston moves in, if the angle between its velocity vector and the normal to its surface exceeds 70° (for an ideal gas with $\gamma = 5/3$). Increase of the piston velocity component perpendicular to the normal decreases the drag. When cavitation occurs, the drag is four times less than in the case of motion of the piston in the direction normal to its surface.

## I: INTRODUCTION

THE motion of a magnetohydrodynamic medium under the action of an ideally conducting piston moving in it with constant velocity was considered by Bazer[1] (for a piston moving perpendicularly to the normal, and in a longitudinal magnetic field), by Lyubarskiĭ and Polovin[2] (for motion of the piston along the normal), and by I. Akhiezer and Polovin[3] (for subsonic velocities of the piston). The special case of the problem of a piston in the absence of a longitudinal magnetic field was considered by Golitsyn.[4]

In the present paper we consider the problem of a piston in the case of an arbitrary direction of the magnetic field and for an arbitrary (constant) piston velocity. It is also assumed that the unperturbed magnetic field is small, so that the Alfvén velocity is

$$U = H/\sqrt{4\pi\rho} \ll c, \qquad (1.1)$$

where $c = \sqrt{\gamma p/\rho}$ is the velocity of sound (the medium satisfies the equation of state of an ideal gas with an adiabatic exponent $\gamma$). The left side of the medium is bounded by an ideally conducting piston located in the plane $x = 0$.

At the moment $t = 0$, the piston begins to move with constant velocity $\mathbf{u}$. Since the problem involves no parameter of the dimensionality of length, the motion of the medium will be self-similar. This means that all quantities depend only on the ratio $x/t$. Here the motion of the medium is characterized by a succession of shock and self-similar waves traveling one after the other. It is important to note that the problem of finding these waves has a unique solution only if the existence of evolutionary shock waves is assumed.[5,6]

Only in certain special cases, when slow shock waves are absent, can the piston problem be solved without account of the evolution condition. (This is connected with the fact that fast shock waves are always evolutionary.) Precisely this case has been considered by Bazer.[1]

The impossibility of the existence of nonevolutionary shock waves in magnetohydrodynamics* was shown by Akhiezer, Lyubarskiĭ and Polovin,[9,10] by Kontorovich, [11] and by Syrovat-skiĭ.[12]

There are three types of evolutionary discontinuities that move relative to the fluid — fast and slow shock waves and Alfvén discontinuities. Moreover, there are two types of continuous solutions — fast and slow self-similar magnetoacoustic waves.[13,14]

Shock waves are compression waves,[15-17] while self-similar waves are rarefaction waves.[14,18,19] The velocities of these waves are such that only the fast waves (shock or self-similar) can go ahead, followed by the Alfvén discontinuity, and, finally, by the slow waves (shock or self-similar). If it is also taken into account that several of these waves can exist at the same time, then a large number of qualitatively different motions of the medium are realizable for various piston velocities.

---

*In ordinary hydrodynamics, these ideas were first advanced by Landau and Lifshitz[7] and by Courant and Friedrichs.[8]

The following boundary conditions are satisfied on the surface of an ideally conducting piston: $v_x = u_x$, $v_y = u_y$, $v_z = u_z$, where **v** is the velocity of medium and **u** is the velocity of piston.

For sufficiently large amplitude of the rarefaction wave, the density of the medium in back of the wave vanishes — cavitation sets in. In this case the boundary conditions

$$\rho = 0,\ H_x(u_y - v_y) - H_y'(u_x - v_x) = 0,$$
$$H_x(u_z - v_z) - H_z(u_x - v_x) = 0 \qquad (1.2)$$

are satisfied on the boundary with the vacuum.

We shall limit ourselves to the most interesting case, in which the magnetic field, the velocity of the piston, and the normal to its surface lie in a single plane (the xy plane). The values of $v_z$ and $H_z$ will be equal to zero in this case not only in the undisturbed medium, but also in all the resultant waves. Therefore, the Alfvén discontinuity can rotate the magnetic field only by 180°. We shall set the undisturbed velocity of the medium $v_0$ equal to zero. For definiteness, we shall assume that the components of the undisturbed magnetic field $H_{0x}$ and $H_{0y}$ are positive. We shall neglect dissipative processes.

The types of waves that are produced as the piston moves depend on its velocity $(u_x, u_y)$. This dependence is shown in the drawing (the abscissa and ordinate are the longitudinal and transverse components of the velocity of the piston, $u_x$ and $u_y$, respectively). The letters $Y^+$ $Y^-$, $P^+$, $P^-$, and A denote respectively the presence of a fast and a slow shock wave, a fast and a slow rarefaction wave (self-similar), and an Alfvén discontinuity. For a sufficiently large amplitude of the slow rarefaction wave, the density of the medium in back of the wave vanishes — cavitation begins. In comparison with ordinary hydrodynamics, in which cavitation sets in when the piston is moved out with a velocity exceeding $2c_0/(\gamma - 1)$ ($c_0$ is the velocity of sound in the undisturbed medium), in magnetohydrodynamics cavitation sets in at lower piston velocities, provided the velocity of motion of the piston in the transverse direction is sufficiently large.

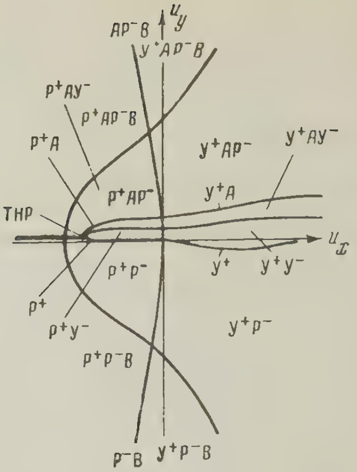

Waves due to the motion of a piston. The longitudinal component of the piston velocity $u_x$ is plotted along the abscissa, and the transverse component $u_y$ is plotted along the ordinate. The letters $Y^+$, $Y^-$, $P^+$, $P^-$, A, and B denote the presence of fast and slow shock waves, fast and slow rarefaction waves, an Alfvén discontinuity, and the formation of a vacuum. THP is the point of maximum rarefaction realizable in the fast self-similar wave.

If the piston moves only in the transverse direction, then cavitation sets in when the piston velocity is 3.67 times the velocity of sound in the undisturbed medium (for $\gamma = 5/3$; this result was obtained earlier by Bazer[1]). Cavitation begins also in the case when the piston moves into the medium and simultaneously moves in the transverse direction. If the piston moves in with supersonic velocity, cavitation begins when the angle between the vector velocity of the piston and its normal to the surface reaches 70° ($\gamma = 5/3$). (We note that in this case the difference between the velocity of displacement of the medium — vacuum boundary and the velocity of the piston is very small.) The presence of cavitation is marked in the drawing by the letter B.

In contrast with the slow rarefaction wave, cavitation is impossible in the fast rarefaction wave. If the Alfvén velocity in the undisturbed medium is much less than the velocity of sound, then at the maximum amplitude of the fast rarefaction wave the Alfvén velocity behind it comes close to the velocity of sound. The point of maximum rarefaction achieved in the fast self-similar wave is denoted by the letters THP in the drawing. It should be noted that upon satisfaction of the condition (1.1), the density of the medium at the point of maximum rarefaction will be very small.

At supersonic transverse piston velocity $u_y$, generation of a magnetic field takes place, i.e., the growth of the magnetic field from an infinitesimally small to finite values; in this case the magnetic pressure becomes comparable with the hydrostatic pressure or exceeds it. At supersonic velocities of insertion $(u_x)$ and sliding $(u_y)$ of the piston, the magnetic field generated is directly proportional to $u_x$.

An increase in $u_x$ generally leads to an increase in the amplitude of the shock wave and to a decrease in the amplitude of the self-similar wave. An exception to this rule occurs in the region $Y^+ Y^-$ for supersonic piston velocities. Upon increase in the value of $u_x$, a redistribution of the amplitudes of the fast and slow shock waves takes place; the increase of the amplitude of the fast shock wave is accompanied by a certain decrease in the amplitude of the slow shock wave.

## 2. SELF-SIMILAR WAVES

The change in the magnetohydrodynamic quantities in self-similar waves is determined by the differential equation first obtained by Friedrichs (see reference 1):

$$\frac{dq_\pm}{ds} = \frac{1}{\theta}\frac{(1-q_\pm)q_\pm^2}{1-sq_\pm^2}, \qquad \theta = \gamma/(2-\gamma),\ q_\pm = U_\pm^2/c^2,$$

$$U_\pm = \{U^2 + c^2 \pm \sqrt{(U^2+c^2)^2 - 4U_x^2c^2}\}^{1/2}/\sqrt{2}, \quad (2.1)$$

c is the speed of sound, **U** is the Alfvén velocity, and $s = c^2/U_x^2 = 4\pi\gamma p/H_x^2$ is the dimensionless pressure; the plus and minus signs in the equations for $q_\pm$ and $U_\pm$ correspond to the fast and slow self-similar waves, respectively.

The transverse magnetic field $H_y$ is determined by the formula

$$H_y = H_x\{(1-q_\pm)(1-sq_\pm)/q_\pm\}^{1/2}\operatorname{sign} H_{1y}, \quad (2.2)$$

where $H_{1y}$ is the transverse magnetic field ahead of the wave.

The longitudinal and transverse components of the velocity of the liquid are determined by the differential equations

$$dv_x/ds = c\sqrt{q_\pm}/\gamma s, \quad (2.3)$$

$$\frac{dv_y}{ds} = \mp\frac{c}{\gamma s}\sqrt{\frac{1-q_\pm}{1-sq_\pm}}\operatorname{sign} H_{1y}. \quad (2.4)$$

Equations (2.3) and (2.4) are valid only when the wave is propagated in the positive direction of the x axis and $H_x > 0$. The upper sign in Eqs. (2.4) corresponds to the fast wave, the lower to the slow wave.

In the fast waves, the inequalities

$$sq_+ \geqslant 1,\ q_+ > 1,\ sq_\pm^2 > 1, \quad (2.5)$$

are satisfied, and in the slow waves, the inequalities

$$sq_- \leqslant 1,\ q_- < 1,\ sq_-^2 < 1. \quad (2.6)$$

It follows from (2.1), (2.5), (2.6) that $q_\pm$ always decreases in self-similar waves.

If the Alfven velocity is much less than the velocity of sound, then $q_-$ and $q_+$ satisfy the relations:

$$q_- = 1/s \ll 1, \quad (2.7)$$

$$q_+ - 1 \equiv \xi_+ = U_y^2/c^2 \ll 1. \quad (2.8)$$

Since $q_-$ decreases, satisfaction of the inequality (2.7) ahead of the slow wave brings about satisfaction of this inequality over the entire slow wave, although in this case the inequality (1.1) can be violated (because of the increase of the transverse magnetic field and the decrease of the density in the slow self-similar wave[18,19]). In exactly the same way, fulfillment of the inequality (2.8) in front of the fast wave brings about satisfaction of this inequality over the entire fast wave.

Let us now consider some limiting cases of self-similar waves, which we shall need in what follows.

1) The slow self-similar wave in the case in which the inequality (2.7) is satisfied. It follows from Eq. (2.1) that

$$q_- = \theta/[(\theta+1)s_1 - s], \quad (2.9)$$

$$H_{2y} = \sqrt{\frac{2}{\gamma}}\left\{1 - \frac{s_2}{s_1}\right\}^{1/2} c_1\sqrt{4\pi\rho_1}\operatorname{sign} H_{1y}, \quad (2.10)$$

$$\Delta_- v_x = -U_{1x}(2\gamma)^{-1/2}\int_{s_2/s_1}^{1}\sigma^{-(\gamma+1)/2\gamma}d\sigma/\sqrt{1-\sigma/(\theta+1)}, \quad (2.11)$$

$$\Delta_- v_y = -\frac{c_1}{\gamma}\int_{s_2/s_1}^{1}\sigma^{-(\gamma+1)/2\gamma}\sqrt{\frac{1-\sigma/(\theta+1)}{1-\sigma}}\,d\sigma\operatorname{sign} H_{1y}. \quad (2.12)$$

Here $\Delta_- \mathbf{v} = \mathbf{v}_2 - \mathbf{v}_1$. The index 1 refers to the region ahead of the wave, the index 2 to the region behind the wave.

2) The slow self-similar wave;

$$1 - q_{2-} \equiv \xi_{2-} \ll 1;\ s_1 \approx 1. \quad (2.12a)$$

In this case the inequality $\xi_- \equiv 1 - q_- \ll 1$ is satisfied over the entire wave. [Violation of (2.7), and consequently of (1.1) takes place as a consequence of the change of magnetohydrodynamic quantities in the fast wave moving ahead of the slow wave.] In this case the values of $\xi_-$, s, $\Delta_- v_x$, $\Delta_- v_y$ are determined by the expressions

$$\xi_- \equiv 1 - q_- \quad (2.13)$$

$$s = 1 - [\gamma/(\gamma-1)]\,\xi_-^\theta/\xi_{1-}^{\theta-1} + \xi_-\gamma/(\gamma-1), \quad (2.14)$$

$$\Delta_- v_x = -2c_1[1 - (s_2/s_1)^{(\gamma-1)/2\gamma}]/(\gamma-1), \quad (2.15)$$

$$\Delta_- v_y = -\frac{c_1}{\gamma s_1^{(\gamma-1)/2\gamma}}\int_{\xi_{2-}}^{\xi_{1-}} s^{-(\gamma+1)/2\gamma}\sqrt{\frac{1-q_-}{1-sq_-}\frac{ds}{d\xi_-}}\,d\xi_-\operatorname{sign} H_{1y}. \quad (2.16)$$

The index 1 refers to the region ahead of the wave, the index 2 to the region behind the wave.

3) The fast self-similar wave.

$$\xi_+ \equiv q_+ - 1 \ll 1, \tag{2.17}$$

$$s = 1 + s_0 \xi_+^\theta / \xi_{0+}^\theta - \gamma \xi_+ / (\gamma - 1), \tag{2.18}$$

$$\Delta_+ v_x = -2c_0 \left[1 - (s_1 / s_2)^{(\gamma-1)/2\gamma}\right] / (\gamma - 1), \tag{2.19}$$

$$\Delta_+ v_y = \frac{c_0}{\gamma s_0^{(\gamma-1)/2\gamma}} \int_{\xi_{1+}}^{\xi_{0+}} s^{-(\gamma+1)/2\gamma} \sqrt{\frac{1-q_+}{1-sq_+} \frac{ds}{d\xi_+}}\, d\xi_+. \tag{2.20}$$

The index 0 refers to the region ahead of the wave, the index 1 to the region behind the wave.

It follows from Eq. (2.18) that cavitation ($s = 0$) is impossible on the fast self-similar wave. The maximum rarefaction possible in this wave takes place for $sq_+ = 1$; the corresponding value of $\xi_{1+}$ is

$$\xi_{1+} = \xi_{0+} \left[\xi_{0+} / (\gamma - 1) s_0\right]^{1/(\theta-1)}, \quad s_1 \approx 1. \tag{2.21}$$

The value of the integral (2.20) depends weakly on the behavior of the function under the integral when $\xi_+ \approx \xi_{1+}$. Therefore, the expression for $\Delta_+ v_y$ can be simplified:

$$\Delta_+ v_y = U_{0y} \left(\frac{U_{0x}}{c_0}\right)^{1/\gamma} \cdot \frac{1}{\gamma} \int_{s_1}^{s_2} s^{-(\gamma+1)/2\gamma} (s-1)^{-(\gamma-1)/\gamma} ds. \tag{2.22}$$

However, Eq. (2.22) is not suitable for calculation of the derivative $dv_{1y}/dv_{1x}$ in the vicinity of the point of maximum rarefaction (2.21).

## 3. SHOCK WAVES

1) 180° Alfvén discontinuity.

The jumps in the velocity and the magnetic field are determined by the expression

$$\Delta_A v_y = 2U_{1y}, \quad \Delta_A H_y = -2H_{1y}. \tag{3.1}$$

The index 1 refers to the region ahead of the discontinuity. The jumps of the other quantities are equal to zero.

2) Fast shock wave.

Under condition (1.1) discontinuities will be the same as without a magnetic field:

$$c_1 = \{c_0^2 + (\gamma - 1)^2 v_{1x}^2 / 4 + [(c_0^2 + (\gamma - 1)^2 v_{1x}^2 / 4)^2 + (\gamma - 1)^2 (\gamma v_{1x}^4 / 4 + c_0^2 v_{1x}^2 / 2) - c_0^4]^{1/2}\}^{1/2}, \tag{3.2}$$

$$\rho_1 = \rho_0 \{[(c_1^2 - c_0^2) / (\gamma - 1)] + v_{1x}^2 / 2\} / \{[(c_1^2 - c_0^2) / (\gamma - 1)] - v_{1x}^2 / 2\}. \tag{3.3}$$

The index 0 refers to the region in front of the wave, the index 1 to the region behind the wave.

For high-intensity shock waves, $v_{1x} \gg c_0$, Eqs. (3.2), (3.3) take the form

$$c_1 = v_{1x} \sqrt{\gamma (\gamma - 1)/2}, \quad \rho_1 = \rho_0 (\gamma + 1) / (\gamma - 1). \tag{3.4}$$

3) Slow shock wave.

With the satisfaction of the inequality (1.1), the discontinuities of the magnetohydrodynamic quantities on a slow shock wave of low intensity, $\Delta_- \rho \ll \rho$, are determined by the relations:[3]

$$\Delta_- v_x = U_{1x} \Delta_- \rho / \rho_1, \quad \Delta_- p = c_1^2 \Delta_- \rho,$$
$$\Delta_- v_y = U_{1y} \left(1 \mp \sqrt{1 - 2c_1^2 \Delta_- \rho / U_{1y}^2 \rho_1}\right),$$
$$\Delta_- H_y = H_{1y} \left(-1 \pm \sqrt{1 - 2c_1^2 \Delta_- \rho / U_{1y}^2 \rho_1}\right). \tag{3.5}$$

The index 1 refers to the region in front of the wave. The same formulas are obtained also for a slow self-similar wave of low intensity, with the positive sign in front of the radical corresponding to the self-similar wave. In evolutionary waves, the transverse magnetic field $H_y$ does not change sign;[17] therefore, in Eqs. (3.5) the upper sign corresponds to evolutionary waves, and the lower sign corresponds to non-evolutionary waves. This means that only in evolutionary shock waves will the relations between the discontinuities of the magnetohydrodynamical quantities (in first approximation in $\Delta_- \rho$) be the same as in self-similar waves. We shall henceforth write the upper sign in front of the radical for the formulas (3.5).

## 4. SINGLE RAREFACTION WAVE

1) Slow wave (see the lines $P^-$ and $AP^-$ in the drawing).

The parametric equation of the lines $P^-$ and $AP^-$ has the form ($s_1$ is the parameter)

$$u_x = -U_{0x} (2\gamma)^{-1/2} \int_{s_1/s_0}^{1} \sigma^{-(\gamma+1)/2\gamma} d\sigma / \sqrt{1 - \sigma (\theta + 1)^{-1}}, \tag{4.1}$$

$$u_y = \mp c_0 \gamma^{-1} \int_{s_1/s_0}^{1} \sigma^{-(\gamma+1)/2\gamma} d\sigma \left[[1 - \sigma / (\theta + 1)] / (1 - \sigma)\right]^{1/2}. \tag{4.2}$$

The line $P^-$ corresponds to the upper sign in Eq. (4.2); the line $AP^-$ corresponds to the lower sign. For $s_1 = 0$, cavitation sets in; in this case the velocity of the piston is

$$u_x = -U_{0x} f(\gamma), \quad u_y = \mp c_0 g(\gamma), \tag{4.3}$$

$$f(\gamma) = (2\gamma)^{-1/2} \int_0^1 \sigma^{-(\gamma+1)/2\gamma} d\sigma / \sqrt{1 - \sigma (\theta + 1)^{-1}}, \tag{4.4}$$

$$g(\gamma) = \gamma^{-1} \int_0^1 \sigma^{-(\gamma+1)/2\gamma} d\sigma \left[[1 - \sigma / (\theta + 1)] / (1 - \sigma)\right]^{1/2}. \tag{4.5}$$

To calculate $f(\gamma)$ and $g(\gamma)$, the radicals in Eqs. (4.4), (4.5) must be expanded in series:

$$f(\gamma) = \sqrt{2\gamma} \left[\frac{1}{\gamma - 1} + \frac{1}{2(\theta + 1)(3\gamma - 1)} + \frac{1}{8(\theta + 1)^2 (5\gamma - 1)} + \cdots\right], \tag{4.6}$$

$$g(\gamma)=\frac{\sqrt{\pi}\,\Gamma((\gamma-1)/2\gamma)}{\gamma\Gamma((2\gamma-1)/2\gamma)}\left[1-\frac{1}{2(\theta+1)}\frac{\gamma-1}{2\gamma-1}\right.$$
$$\left.-\frac{1}{8(\theta+1)^2}\frac{\gamma-1}{2\gamma-1}\frac{3\gamma-1}{4\gamma-1}-\ldots\right], \qquad (4.7)$$

where $\Gamma(p)$ is the gamma function. For $\gamma = 5/3$, we get

$$f(^5/_3)=2.78,\quad g(^5/_3)=3.67. \qquad (4.8)$$

The value of $q_{2-}$ at the point where $s_2 = 0$ is given by

$$q_{2-}=\gamma q_{1-}/2. \qquad (4.9)$$

The magnetic field is determined by the formula

$$H_{2y}=\pm\sqrt{2/\gamma}\,c_0\sqrt{4\pi\rho_0}. \qquad (4.10)$$

2) Slow wave with cavitation (the line of separation between the regions $P^+P^-B$ and $Y^+P^-B$ or $P^+AP^-B$ and $Y^+AP^-B$ in the drawing).

The equation of the line of separation has the form

$$u_x\mp\sqrt{\gamma/2}\,U_{0x}u_y/c_0+[f(\gamma)-\sqrt{\gamma/2}\,g(\gamma)]\,U_{0x}=0, \qquad (4.11)$$

The upper and lower signs correspond to the absence and presence of an Alfvén discontinuity. The line in the $u_x$, $u_y$ plane corresponding to the slow rarefaction wave has a kink at the point (4.3), where cavitation begins;

$$\text{before cavitation: } du_y/du_x=\mp c_0/U_{0x};$$

$$\text{with cavitation: } du_y/du_x=\mp\sqrt{2/\gamma}\,c_0/U_{0x}. \qquad (4.12)$$

3) Fast rarefaction wave (the line $P^+$ in the drawing).

The parametric equation of the line $P^+$ is determined by Eqs. (2.19), (2.22), in which $\Delta_+v_x = u_x$; $\Delta_+v_y = u_y$; the parameter is the quantity $s_1$. At the point $u_x = u_y = 0$ we have $du_y/du_x = -U_{0x}U_{0y}/c_0^2$, in accord with reference 3. At the point of maximum rarefaction (2.21)

$$u_x=-\frac{2c_0}{\gamma-1}\left(1-s_0^{-(\gamma-1)/2\gamma}\right),$$

$$u_y=U_{0y}(U_{0x}/c_0)^{1/\gamma}h(\gamma), \qquad (4.13)$$

$$h(\gamma)=\Gamma\left(\frac{\gamma-1}{2\gamma}\right)\Gamma\left(\frac{1}{\gamma}\right)\Big/\gamma\Gamma\left(\frac{\gamma+1}{2\gamma}\right). \qquad (4.14)$$

For $\gamma = 5/3$ we have $h(5/3) = 3.52$.

The value of $du_y/du_x$ in the vicinity of the point of maximum rarefaction (2.21) cannot be determined from (2.22); use must be made of the more exact expression (2.20), from which it follows that

$$du_y/du_x=-\sqrt{(1-q_+)/(1-sq_+)}. \qquad (4.14a)$$

At the point of maximum rarefaction we obtain $du_y/du_x = -\infty$.

4) Fast rarefaction wave with an Alfvén discontinuity (the line $P^+A$ in the drawing).

The line $P^+A$ in the plane $u_xu_y$ is determined by parametric equations expressed in terms of the parameter $s_1$, with $u_x = \Delta_+v_x$ determined by (2.19), and $u_y$ by

$$u_y=2U_{0x}\xi_{1+}\left\{\frac{s_0}{\xi_{0+}}\left(\frac{\xi_{1+}}{\xi_{0+}}\right)^{\theta-1}-\frac{1}{\gamma-1}\right\}^{1/2}\left(\frac{s_0}{s_1}\right)^{1/2\gamma}+\Delta_+v_y, \qquad (4.15)$$

where $\Delta_+v_y$ is in turn determined by Eq. (2.22), or, more exactly, by Eq. (2.20). The point of maximum rarefaction, as before, is determined by Eqs. (2.21) and (4.13). At the point $u_x = 0$, $u_y = 2U_{0y}$, we have $du_y/du_x = U_{0y}/c_0$, which coincides with reference 3; at the point of maximum rarefaction, $du_y/du_x = +\infty$.

## 5. A SINGLE SHOCK WAVE

1) Slow shock wave (the lines $Y^-$ and $AY^-$ in the drawing).

In the $u_xu_y$ plane the lines $Y^-$ and $AY^-$ are described by the equation[3]

$$u_x+U_{0x}\,u_y(u_y-2U_{0y})/2c_0^2=0. \qquad (5.1)$$

2) Fast shock wave (the line $Y^+$ in the drawing).

The equation of the line $Y^+$ in the $u_xu_y$ plane has the form

$$u_y=-U_{0x}U_{0y}u_x^3/\{[(c_1^2-c_0^2)/(\gamma-1)]^2-u_x^4/4\}, \qquad (5.2)$$

where $c_1$ is determined by (3.2), in which $v_{1x}$ must be replaced by $u_x$. For $u_x \gg c_0$, Eq. (5.2) is greatly simplified:

$$u_y=-4U_{0x}U_{0y}/(\gamma^2-1)\,u_x. \qquad (5.3)$$

3) Fast shock wave with Alfvén discontinuity (the line $Y^+A$ in the drawing).

In the $u_xu_y$ plane the line $Y^+A$ is determined by the equation

$$u_y+U_{0x}U_{0y}u_x^3/\{[(c_1^2-c_0^2)/(\gamma-1)]^2$$
$$-u_x^4/4\}=2U_{0y}(\rho_1/\rho_0)^{1/2}, \qquad (5.4)$$

where $c_1$ and $\rho_1$ are determined by (3.2) and (3.3) ($v_{1x} = u_x$). In the limiting case $u_x \gg c_0$, Eq. (5.4) takes the form

$$u_y+4U_{0x}U_{0y}/(\gamma^2-1)\,u_x$$
$$=2U_{0y}[(\gamma+1)/(\gamma-1)]^{1/2}. \qquad (5.5)$$

## 6. TWO RAREFACTION WAVES

1) The cavitation line $P^+P^-$ or $P^+AP^-$ (the line of separation between the regions $P^+P^-$ and $P^+P^-B$ or $P^+AP^-$ and $P^+AP^-B$ in the figure).

The equation of the cavitation line for $u_y$: $|u_y|/c_0 \gg g(\gamma)(U_{0x}/c_0)^{4/(5-\gamma)}$ has the form

$$u_x = -\frac{2c_0}{\gamma-1} \mp \frac{2}{\gamma-1}\frac{|u_y|}{g(\gamma)} - U_{0x} f(\gamma)\left[\frac{c_0 g(\gamma)}{|u_y|}\right]^{1/(\gamma-1)}. \qquad (6.1)$$

For $|u_y|$ close to $h(\gamma)U_{0y}(U_{0x}/c_0)^{1/\gamma}$: $|u_y - U_{0y}(U_{0x}/c_0)^{1/\gamma}h(\gamma)| \ll U_{0x}(U_{0x}/c_0)^{-1/\gamma}$, the equation of the cavitation lines has the form

$$u_x = -2c_0/(\gamma-1). \qquad (6.1a)$$

2) Line of separation between the regions $P^+P^-$ and $P^+AP^-$.

From qualitative considerations of the topological structure of the regions in the drawing, given in reference 3, it follows that the quantity $u_y$ is determined on the line of separation between the regions $P^+P^-$ and $P^+AP^-$ as the maximum velocity of the medium, $v_{2y}$, obtained for a given value of $u_x$ by means of two rarefaction waves ($P^+$ and $P^-$). In this case the wave $P^+$ passes through the point of maximum rarefaction (2.21).

The equation of the line of separation has the form

$$u_y = U_{0y}(U_{0x}/c_0)^{1/\gamma}h(\gamma). \qquad (6.2)$$

The transverse magnetic field $H_{2y}$ vanishes on the line of separation. At the point of intersection of the lines of separation of regions $P^+P^-$ and $P^+AP^-$ with the cavitation lines, $s_2$ vanishes; at this point $u_x = \mp 2c_0/(\gamma - 1)$.

3) The line of separation between the regions $P^+P^-B$ and $P^+AP^-B$.

The equation of the line of separation follows from (1.2):

$$u_y = U_{0y}(U_{0x}/c_0)^{1/\gamma}h(\gamma). \qquad (6.3)$$

## 7. TWO SHOCK WAVES

The value of $u_y$ on the line of separation between the regions $Y^+Y^-$ and $Y^+AY^-$ is determined as the maximum value of $v_{2y}$ obtained in the waves $Y^+Y^-$ (for a given value of $u_x$), or as the minimum value of $v_{2y}$ obtained in the waves $Y^+AY^-$. The problem of the motion of the magnetohydrodynamic medium has a unique solution only when $\max v_{2y}|_{Y^+Y^-} = \min v_{2y}|_{Y^+AY^-}$. In satisfying these relations it is necessary to exclude from consideration non-evolutionary shock waves. Since the distance between the lines $Y^+$ and $Y^+A$ is small in comparison with the velocity of sound, the slow shock wave will have a small amplitude. We can therefore make use of (3.5). The equation of the line of separation between the regions $Y^+Y^-$ and $Y^+AY^-$ has the form

$$u_y + U_{0x}U_{0y}u_x^3/\{[(c_1^2 - c_0^2)/(\gamma-1)]^2 - (u_x^4/4)\} = U_{0y}(\rho_1/\rho_0)^{1/2}, \qquad (7.1)$$

where the values of $c_1$ and $\rho_1$ are determined by Eqs. (3.2) and (3.3). For $u_x \gg c_0$, Eq. (7.1) is simplified:

$$u + \frac{4U_{0x}U_{0y}}{(\gamma^2-1)u_x} = U_{0y}\left(\frac{\gamma+1}{\gamma-1}\right)^{1/2}. \qquad (7.1a)$$

The region $Y^+Y^-$ is bounded below in the drawing by the line $Y^+$, determined for $u_x \gg c_0$ by Eq. (5.3), on which the amplitude of the slow shock wave $Y^-$ vanishes. Since the value of $u_y$ determined by Eq. (5.3) is an increasing function of $u_x$, an increase in the longitudinal velocity of the piston $u_x$ for fixed transverse velocity $u_y$ brings about a decrease in the amplitude of a slow shock wave. In this case, of course, the amplitude of the fast shock wave increases, for as the piston velocity increases the magnetic field begins to play a smaller role, and in the limiting case $u_x/c_0 \to \infty$ the shock waves become the same as in the absence of a magnetic field. In this case the amplitude of the slow wave for $U_0 \ll c_0$ tends to zero.

## 8. COMBINATION OF SHOCK WAVES AND RAREFACTION WAVES

1) Fast shock wave and slow self-similar wave without cavitation (regions $Y^+P^-$ and $Y^+AP^-$ in in the drawing).

The value of $s_2$ on the surface of the piston, for given $u_x$ and $u_y$, is determined from the relation

$$u_y = \mp c_1\gamma^{-1}\int_{s_2/s_1}^{1}\sigma^{-(\gamma+1)/2\gamma}\{[1-\sigma/(\theta+1)]/(1-\sigma)\}^{1/2}d\sigma, \qquad (8.1)$$

where $c_1$ is determined by Eq. (3.2), in which we set $v_{1x} = u_x$; $\rho_1$ and $H_{2y}$ are determined by Eqs. (3.3) and (2.10); $s_1 = s_0(c_1/c_0)^{2\gamma/(\gamma-1)}$. The upper sign in Eq. (8.1) corresponds to the region $Y^+P^-$, the lower to the region $Y^+AP^-$.

2) Fast shock wave and self-similar wave on the cavitation line (the line separating the regions $Y^+P^-$ and $Y^+P^-B$, and also $Y^+AP^-$ and $Y^+AP^-B$ in the drawing).

The transverse velocity of the piston is determined by the relation $u_y = \mp g(\gamma)c_1$, where $c_1$ is determined by Eq. (3.2) ($v_{1x} = u_x$). For $u_x = 0$, we obtain the formula of Bazer:[1] $u_y = \mp g(\gamma)c_0 \approx \mp 3.67\, c_0$ for $\gamma = 5/3$. The slope of the cavitation line at $u_x = 0$ is determined by $du_y/du_x = \mp(\gamma - 1)/g(\gamma)/2 \approx \mp 1.2$ for $\gamma = 5/3$, and for $u_x \gg c_0$ by the expression $du_y/du_x = \pm g(\gamma)[\gamma(\gamma$

$- 1)/2]^{1/2} \approx \mp 2.7 \approx \pm \tan 70°$ for $\gamma = 5/3$. The transverse magnetic field on the boundary with the piston is equal to $H_{2y} = \pm(2/\gamma)^{1/2}(4\pi\rho_0)^{1/2} c_0$.

The upper sign in the above formulas corresponds to the absence of an Alfvén discontinuity, the lower sign corresponds to the combination $Y^+AP^-$.

3) Strong shock wave and weak self-similar wave with cavitation (the regions $Y^+P^-B$ and $Y^+AP^-B$ in the drawing).

For a given $u_x$ and $u_y$, the velocity of the medium $v_{2x}$ on the voundary with the piston or with the vacuum (in the case of cavitation) is determined by the relation

$$v_2 = u_x + (\gamma/2)^{1/2}(U_{1x}/c_1)[|u_y| - c_1 g(\gamma)], \qquad (8.1a)$$

where $U_{1x} = H_x(4\pi\rho_1)^{-1/2}$, $\rho_1 = \rho_0 (c_1/c_0)^{2/(\gamma - 1)}$, and $c_1$ is expressed in terms of $v_{1x}$ with the aid of Eq. (3.2); in turn, $v_{1x}$ and $v_{2x}$ are related by $v_{1x} = v_{2x} + U_{1x} f(\gamma)$. Solving the resultant equation for $v_{2x}$, we find all the remaining magnetohydrodynamical quantities. In the particular case of shock waves of large amplitude $(c_1 \gg c_0)$ in the presence of cavitation, we find

$$\begin{aligned} v_{2x} &= \tfrac{1}{2}\{u_x - U_{0x} f(\gamma)[(\gamma-1)/(\gamma+1)]^{1/2} \\ &\quad - U_{0x} g(\gamma)[\gamma(\gamma-1)/2(\gamma+1)]^{1/2}\} \\ &\quad + \{\tfrac{1}{4}u_x^2 + \tfrac{1}{2}U_{0x}u_x f(\gamma)[(\gamma-1)/(\gamma+1)]^{1/2} \\ &\quad - U_{0x}u_x g(\gamma) - [\gamma(\gamma-1)/2(\gamma+1)]^{1/2} \\ &\quad + U_{0x}|u_y|(\gamma-1)^{-1/2}\}^{1/2}, \end{aligned} \qquad (8.2)$$

$$H_{2y} = - v_{2x}[4\pi\rho_0(\gamma+1)]^{1/2} \operatorname{sign} u\ . \qquad (8.3)$$

For $u_x = 0$, Eqs. (8.2) and (8.3) go over into the formulas obtained by Bazer.[1]

If the longitudinal velocity of the piston is not small, $U_{0x}|u_y| \ll u_x^2$, it follows from Eq. (8.2) that the velocities $v_{2x}$ and $u_x$ are close to one another:

$$v_{2x} - u_x = U_{0x}(\gamma+1)^{-1/2}u_x^{-1}\{|u_y| - [\gamma(\gamma-1)/2]^{1/2} g(\gamma)u_x\}. \qquad (8.3a)$$

In this case the generated magnetic field is proportional to the longitudinal velocity of the piston

$$H_{2y} = - u_x[4\pi\rho_0(\gamma+1)]^{1/2} \operatorname{sign} u_y. \qquad (8.3b)$$

## 9. RESISTANCE FORCE

The relations obtained make it possible to determine the resistance force F produced when the piston moves uniformly with velocity $(u_x, u_y)$. This force consists of two components: a longitudinal component $F_x$, the drag, and a transverse component $F_y$, the lifting force. We limit ourselves to the case of a fast shock wave of high amplitude, accompanied by a slow rarefaction wave.

The force acting on a certain element of area is none other than the momentum flux through this element. Making use of Eq. (51.8) of Landau and Lifshitz[20] for the momentum flux density tensor, we obtain for the most interesting case, $u \gg c_0$ and $U_{0x}|u_y| \gg u_x^2$, an expression for the drag,

$$-F_x = \frac{\gamma+1}{2}\rho_0 u_x^2\left(\frac{2\sigma_2^{1/\gamma}}{\gamma-1} + 1\right), \qquad (9.1)$$

where the quantity $\sigma_2$ is determined from the equality

$$\int_{\sigma_2}^{1} \sigma^{-(\gamma+1)/2\gamma}\left\{\left[1 - \frac{\sigma}{\theta+1}\right]\Big/(1-\sigma)\right\}^{1/2} d\sigma = \left(\frac{2\gamma}{\gamma-1}\right)^{1/2}\frac{|u_y|}{u_x}, \qquad (9.1a)$$

in the absence of cavitation; $\sigma_2 \equiv 0$ in the presence of cavitation.

The lifting force has the form

$$\begin{aligned} -F_y &= (\gamma+1)\rho_0 u_x u_y \sigma_2^{1/\gamma}/(\gamma-1) \\ &\quad + \sqrt{\gamma+1}\sqrt{1-\sigma_2}\,\rho_0 U_{0x} u_x \operatorname{sign} u_y. \end{aligned} \qquad (9.2)$$

It follows from Eq. (9.1) that for a fixed value of $u_x$, the drag decreases with increasing $|u_y|$. The value of the drag on the cavitation line is $(\gamma + 1)/(\gamma - 1)$ times smaller than for $|u_y| \ll u_x$. Upon further increases $|u_y|$, the value of the drag does not change.

The author expresses his gratitude to A. I. Akhiezer and G. Ya. Lyubarskiĭ for a number of valuable suggestions.

---

[1] J. Bazer, Astrophys. J. **128**, 686 (1958).

[2] G. Ya. Lyubarskiĭ and R. V. Polovin, Dokl. Akad. Nauk SSSR **128**, 684 (1959), Soviet Phys.-Doklady **4**, 977 (1960).

[3] I. A. Akhiezer and R. V. Polovin, JETP **38**, 529 (1960), Soviet Phys. JETP **11**, 383 (1960).

[4] G. S. Golitsyn, JETP **35**, 776 (1958), Soviet Phys. JETP **8**, 538 (1959).

[5] P. Lax, Comm. Pure Appl. Math. **10**, 537 (1957).

[6] K. I. Babenko and I. M. Gel'fand, Научные докл. высшей школы, серия физ.-мат. наук, (Sci. Notes of the Colleges, Math. Phys. Ser.) No. 1, 12 (1958).

[7] L. D. Landau and E. M. Lifshitz, Механика сплошных сред (Mechanics of Continuous Media), Gostekhizdat, 1953, p. 405.

[8] R. Courant and K. Friedrichs, Supersonic Flow and Shock Waves (Russ. transl.) IIL, 1950, p. 215.

[9] Akhiezer, Lyubarskiĭ, and Polovin, JETP **35**, 731 (1958), Soviet Phys. JETP **8**, 507 (1959).

[10] G. Ya. Lyubarskiĭ and R. V. Polovin, JETP **36**, 1272 (1959), Soviet Phys. JETP **9**, 902 (1959).

[11] V. M. Kontorovich, JETP **35**, 1216 (1958), Soviet Phys. JETP **8**, 851 (1959).

[12] S. I. Syrovat-skiĭ, JETP **35**, 1466 (1958), Soviet Phys. JETP **8**, 1024 (1959).

[13] Akhiezer, Lyubarskiĭ, and Polovin, Ukr. fiz. zhurn. **3**, 433, (1958), J. Tech. Phys. (U.S.S.R.) **29**, 933 (1959), Soviet Phys. Tech. Phys. **4**, 849 (1959).

[14] A. G. Kuli'kovskiĭ, Dokl. Akad. Nauk SSSR 121, 987 (1958), Soviet Phys.-Doklady **3**, 743 (1958).

[15] S. V. Iordanskiĭ, Dokl. Akad. Nauk SSSR **121**, 610 (1958), Soviet Phys.-Doklady **3**, 736 (1958).

[16] R. V. Polovin and G. Ya. Lyubarskiĭ, JETP **35**, 510 (1958), Soviet Phys. JETP **8**, 351 (1958).

[17] R. V. Polovin and G. Ya. Lyubarskiĭ, Ukr. fiz. zhurn. **3**, 571 (1958).

[18] G. Ya. Lyubarskiĭ and R. V. Polovin, JETP **35**, 509 (1958), Soviet Phys. JETP **8**, 351 (1959).

[19] G. Ya. Lyubarskiĭ and R. V. Polovin, Ukr. fiz. zhurn. **3**, 567 (1958).

[20] L. D. Landau and E. M. Lifshitz, Электродинамика сплошных сред, (Electrodynamics of Continuous Media), Gostekhizdat, 1957.

Translated by R. T. Beyer
296

SOVIET PHYSICS JETP VOLUME 11, NUMBER 5 NOVEMBER, 1960

# *PREPARATION OF POLARIZED HYDROGEN TARGETS*

L. N. ROZENTSVEǏG* and M. YA. AZBEL'

Physico-Technical Institute, Academy of Sciences, U.S.S.R.

Submitted to JETP editor December 7, 1959

J. Exptl. Theoret. Phys. (U.S.S.R.) **38**, 1556-1558 (May, 1960)

A method is proposed for obtaining polarized hydrogen targets.

In recent years several nuclear investigations have been carried out with macroscopic samples in which the nuclei were oriented. It would be of great interest for elementary particle physics to obtain polarized hydrogen targets, but the known methods of polarizing the nuclei in macroscopic samples are unsuitable, except for the obvious but at present unfeasible "brute force" method based on the combination of an extremely strong magnetic field H and a very low temperature $T \lesssim \mu_p H/k$.

However a detailed theoretical examination[1] of the paramagnetic resonance of the conduction electrons in massive metallic samples and of the related nuclear polarization changes the usual notions about the possibilities of the Overhauser method[2] and about the choice of an optimal mode. The following statements are essential for the remainder of this paper.

1. It is claimed by Overhauser[2] that the method allows one to polarize only very small samples (the thickness d must be of the order of the skin depth $\delta \sim 10^{-4}$ cm). Azbel', Gerasimenko, and Lifshitz[1], however, have shown that the limiting thickness of an effectively polarized sample is considerably greater. If the constant magnetic field is not strictly parallel to the metal surface, then

$$d \sim \delta_{eff} \sim v\sqrt{t_0 T_s}, \tag{1}$$

where v is the average speed of the electrons on the Fermi surface, $t_0$ is the average relaxation time of the electrons without spin flip, and $T_s$ is the same but with spin flip. For pure lithium, e.g., at liquid-helium temperature [$v \sim 10^8$ cm/sec, $t_0 \sim 10^{-11}$ sec, $T_s \sim 3 \times 10^{-7}$ sec (reference 3)] an estimate gives $d \sim 1$ mm. For the polarization of so thick a sample, an rf field

$$H_1 \gtrsim \frac{2\pi v}{c^2 |Z|} \sqrt{t_0 / T_s}\, H_0, \tag{2}$$

is required, and the power absorbed on a unit surface will be of the order

$$Q \gtrsim \frac{1}{|Z|} \left(\frac{H_0 v}{2c}\right)^2 \frac{t_0}{T_s}, \tag{3}$$

where Z is the surface impedance of the metal, and $H_0$ is the intensity of the constant magnetic field perpendicular to the surface.

We note that the effective removal of the heat generated in the sample is entirely possible for thicknesses $d \sim 1$ mm.

2. In reference 1 there is predicted the phenomenon of selective transparency of metal foils in paramagnetic resonance: the dependence of the transmission coefficient k on the field $H_0$ has a resonant character, which is pronounced for $\delta \ll d \ll \delta_{eff}$. The resonant value of k is

$$k_m \sim (\chi T_s c^3 |Z|^2 / 2\pi d)^2, \tag{4}$$

($\chi$ is the magnetic susceptibility of the metal), and the width of the resonance curve $k(H_0)$ is given by

$$\Delta H / H_0 \sim 1 / \omega T_s. \tag{5}$$

These features of the phenomenon under consideration suggest the possibility of polarizing hydrogen dissolved in a metal foil. As is known, hydrogen is soluble in metals of the transition group and forms intrusion-type hydrides possessing metallic properties and a regular structure. If it were possible to polarize protons "embedded" in the lattice of a metal, such a foil could be used as a polarized hydrogen target. The scattering on protons is reliably separated from scattering on metal nuclei, if coincidences between the scattered particle and the recoil proton are registered, or if the scattered particles are discriminated according to energy.

The question about the feasibility of the method proposed here and about the choice of the most suitable metal can be decided only after an experimental study of the relevant physical properties of the hydrides. Below we outline a program of measurements.

For the foil under investigation (whose thickness must be small compared with $\delta_{eff}$), the surface impedance $Z(H_0)$ and the transmission coefficient $k(H_0)$ will be determined as functions of the constant magnetic field $H_0$. We obtain $T_s$ and the ratio $t_0/T_s$ according to formulas (3) and (5). Knowing $t_0$ and $T_s$, we determine the thickness $\delta_{eff}$ of the polarized layer according to (1). It is possible to check the data thus obtained by measuring the transmission coefficient through the polarized sample. The observed selective transparencies of the sample afford an additional method of controlling the polarization P, which can be determined from the formula of Sec. 5 of reference 1.

---

*Deceased.

All the above statements obtain also for polarized deuterium and tritium targets.

We note a single difficulty which E. K. Zavoĭskiĭ brought to our attention. If the constant magnetic field is not strictly perpendicular to the metal surface, then the magnetic induction will depend on the depth, inasmuch as the nuclear polarization damps out with depth. If the magnetic field of the nuclei is so large that

$$H_{\text{nuc}} P(0)/H_0 \gtrsim 1/\omega T_s,$$

then by increasing the depth it is possible for the basic condition of resonance to be violated, and the polarization will be considerably smaller than predicted in reference 1. In order to avoid this, one can use either a constant field that is strictly perpendicular to the metal surface (then div B = 0, and B, normal to the surface, does not depend on depth; the induction obviously determines the resonant frequency) or a constant field so strong that the change in resonant frequency at the depth $\delta_{eff}$ would be small or of the order of the half-width of the resonance curve $k(H_0)$.

Estimates of the permissible angular deviation $\alpha$ from perpendicularity in the first case and of the magnitude of the field in the second case can be obtained from the formulas of reference 1. For the angle $\alpha$ we find

$$\alpha < H_0/\omega T_s H_{\text{nuc}} P(0),$$

and for the magnitude of $H_0$ under fulfillment of condition (2)

$$P(0) - P(\delta_{eff}) < \frac{H_0}{\omega T_s H_{\text{nuc}}}, \qquad \frac{\mu H_0}{kT} > e \ln \frac{2|e| T_s H_{\text{nuc}}}{m_0 c I},$$

where $\omega$ is the frequency of the rf field, $H_{\text{nuc}}$ is the magnetic field of the nuclei at full polarization, I is the nuclear spin, and P(0) is the polarization at the surface (see reference 1).

---

[1] Azbel', Gerasimenko, and Lifshitz, JETP **32**, 1212 (1957), Soviet Physics JETP **5**, 986 (1957).

[2] A. W. Overhauser, Phys. Rev. **89**, 689 (1953), Phys. Rev. **92**, 411 (1953).

[3] Griswold, Kip, and Kittel, Phys. Rev. **88**, 951 (1952). G. Feher and A. F. Kip, Phys. Rev. **95**, 1343 (1954), Phys. Rev. **98**, 337 (1955).

Translated by J. Heberle
297

SOVIET PHYSICS JETP VOLUME 11, NUMBER 5 NOVEMBER, 1960

# INVESTIGATION OF THE SPECTRA OF NEUTRONS EMITTED IN THE DISINTEGRATION OF DEUTERONS BY PROTONS

V. V. KOMAROV and A. M. POPOVA

Institute of Nuclear Physics, Moscow State University

Submitted to JETP editor December 8, 1959

J. Exptl. Theoret. Phys. (U.S.S.R.) **38**, 1559-1563 (May, 1960)

We calculate the energy spectra of neutrons emitted at 0 and 180 deg in the c.m.s. from the reaction p + d → p + p′ + n, at an approximate total reaction energy of 4 Mev, with pair interaction of the nucleons in the final state taken into account. Applications of this method to the calculation of the energy distributions of reaction products when several particles are emitted are considered from the standpoint of clarifying the role of interactions of particles in final states.

Two maxima, one at the upper boundary of the spectrum and one at a neutron energy ~ 0.7, have been observed[1,2] in the spectrum of neutrons from the reaction p + d → p + p′ + n, emitted at zero degrees to the direction of incident 8.9-Mev protons. These maxima can be attributed to the interaction between the nucleons produced in the final state.[3] This spectrum of neutrons from the reaction p + d → p + p′ + n was investigated theoretically by Heckrotte and McGregor,[4] but only with allowance for the interaction between two protons in the final state, and in the approximation of a zero proton interaction radius, so that the form of the neutron spectrum could not be fully explained.

In the present paper we calculate the energy distributions from the reactions (p + d) emitted at 0 and 180 deg to the direction of the incident protons in the c.m.s., for a total reaction energy of approximately 4 Mev. It is assumed in the calculation that two out of three nucleons produced in the reaction interact with each other. Thus, the three-body problem is reduced to a two-body problem, that of a virtual biproton and a deuteron, which symbolize pairs of nucleons interacting in the final state. (The use of the terms "virtual particle" does not imply their existence.) The interaction between nucleons was taken into account accurately, and its parameters were taken from the experimental data on nucleon-nucleon scattering. The Born approximation was used to account for the interaction between the third nucleon and the virtual particle.

It must be noted that, strictly speaking, the use of the Born approximation is not justified at such low energies. However, this approximation has been used successfully in that energy region for the investigation of the angle and energy distributions in stripping which is quite similar to the process investigated here.[5] One can therefore expect the use of the Born approximation for the interaction of a pair of particles with small relative momenta and a third particle to yield in this case angle and energy distributions that are close to the real ones.

The orbital momentum of the relative motion of the proton and deuteron in the investigated disintegration of a deuteron by protons was assumed to be zero, for a total reaction energy of 4 Mev. The orbital momentum of the relative motion of the nucleons produced by the reaction, joined in a virtual biproton and deuteron, is also assumed to be zero. Then, by virtue of the conservation of the total momentum of the system and of the exclusion principle, the total momentum of the system can be either $J = \frac{1}{2}$ or $J = \frac{3}{2}$, and the spin of the virtual particles can be either $S = 0$ or $S = 1$. Consequently, the differential cross section of the disintegration of the deuteron by protons should be determined by the expression

$$\frac{d\sigma}{dE_n d\Omega_n} = \frac{M_n M_0}{(2\pi\hbar^2)^2} \frac{\rho(E_n)}{k_0} \left\{ \frac{2}{3} |H_1|^2 + \frac{1}{3} |H_2|^2 + \frac{1}{3} |H_3|^2 \right\}, \tag{1}$$

where $M_0$ and $M_n$ are the reduced masses of the incident proton and of the neutron produced by the reaction, $\rho(E_n)$ is the density of the neutron energy states, $H_1$, $H_2$, and $H_3$ are the matrix elements of the transition, corresponding to $J = \frac{3}{2}$, $s = 1$; $j = \frac{1}{2}$, $s = 1$; and $j = \frac{1}{2}$, $s = 0$.

The general form of the matrix element of the transition is

$$H = \langle (1 - P_{13}) \psi_f \chi_f | V_{pp} + V_{pn} \ | \psi_i \chi_i \rangle, \tag{2}$$

where $(1 - P_{13})$ is the particle rearrangement operator. Expansion of the expression for H leads to six integrals, of which two correspond to the formation of a virtual biproton ($I_{pp}$) and four to the formation of a virtual deuteron ($I_{pn}$). Since the spin state of the two interacting protons can be only singlet in this case, while the spin states of the interacting proton and neutron can be singlet and triplet, the matrix elements $H_1$ and $H_2$ include integrals $I_{pn}^t$ corresponding to a triplet interaction of a neutron and a proton in the final state, while $H_3$ can contain integrals $I_{pp}^S$ and $I_{pn}^S$, corresponding to the formation of virtual particles in the singlet state.

The integral $I_{pp}$ is written in the form

$$I_{pp} \sim \int \varphi_{2p}(\rho)\, \chi_{2p}\, \varphi(\mathbf{r}_n)\, \chi_n (V_{pp} + V_{pn})\, \psi_d \chi_d\, \psi(\mathbf{r}_p)\, \chi_p d\tau, \qquad (3)$$

where $\psi_d$ is the internal wave function of the deuteron, taken in the form of a Hulthen function; $\psi(\mathbf{r}_p)$ and $\varphi(\mathbf{r}_n)$ are the wave functions of the incoming proton and the emitted neutron, taken in the form of plane waves; $\chi_d$ and $\chi_p$ are the spin functions of the deuteron and the incident protons; $\chi_{2p}$ and $\chi_n$ are the spin functions of two protons in the singlet state and a neutron; $\varphi_{2p}(\rho)$ is the wave function of the relative motion of two protons, taken with allowance for their scattering by each other in the singlet states.

If the nuclear interaction of the two protons is chosen in the form of a potential well with $\rho_0 = 2.65 \times 10^{-13}$ cm, the radial part of the wave function $\varphi_{2p}(\rho)$ assumes the following form for $\rho < \rho_0$:

$$\varphi_{2p}^{(1)}(\rho) = A\rho^{-1} \sin k\rho,$$

where **k** is the wave vector of the relative motion of two protons within the potential well. For $\rho > \rho_0$, account was taken of the Coulomb interaction of the two protons, and

$$\varphi_{2p}^{(2)}(\rho) = G(f\rho) + \cot\delta\, F(f\rho),$$

where $G(f\rho)$ and $F(f\rho)$ are Coulomb functions, and $\cot\delta$ is a factor that takes nuclear interaction into account. The coefficient A and the absolute value of the wave value **k** are determined by making the logarithmic derivatives of the functions $\varphi_{2p}^{(1)}(\rho)$ and $\varphi_{2p}^{(2)}(\rho)$ continuous at $\rho = \rho_0$. Variation of the parameter $\rho_0$ from $2.4 \times 10^{-13}$ to $2.8 \times 10^{-13}$, values known from experiments on proton-proton scattering, does not change substantially the magnitude and form of the differential cross section of the reaction. In Eq. (3) $V_{pp}$ and $V_{pn}$ are the potentials of interaction between the incoming proton and the nucleons of the deuteron, $V_{pn}$ was taken in the form of a $\delta$ function, while $V_{pp}$ was chosen in the form of a potential well of radius $\rho_0 = 2.65 \times 10^{-13}$ cm. It was impossible to take $V_{pp}$ in the form of a $\delta$ function in this case, since $\varphi_{2p}(\rho)$ depends on the same parameter $\rho$. Since we deal with S waves only in this analysis, the choice of the type of interaction, $V_{pp}$ or $V_{pn}$, is immaterial, for it is determined only by the one parameter — the scattering length.

For the case of interaction of a neutron and proton in the singlet or triplet final state, i.e., in the case of production of a virtual deuteron, the integrals $I_{pn}$ have the form

$$I_{pn} \sim \int \varphi_{pn}(\rho)\, \chi_{pn}\, \varphi(\mathbf{r}_{p'})\, \chi_{p'} (V_{pp} + V_{pn})\, \psi_d \chi_d \psi(\mathbf{r}_p)\, \chi_p d\tau, \qquad (4)$$

where $\varphi_{pn}(\rho)$ is the wave function of the relative motion of a proton and neutron, taking into account scattering in the triplet or singlet states.

If the interaction between the proton and neutron is chosen in the form of a potential well with $\rho_0 = 2.65 \times 10^{-13}$ cm, the radial part of $\varphi_{pn}(\rho)$ has the form

$$\varphi_{pn}^{(1)}(\rho) = A'\rho^{-1} \sin k'\rho, \qquad \rho < \rho_0;$$

$$\varphi_{pn}^{(2)}(\rho) = 2\sqrt{\pi}\,(f\rho)^{-1} \sin f\rho + 4\pi f(\theta)\, \rho^{-1} e^{if\rho}, \qquad \rho > \rho_0,$$

where $f(\theta)$ is the amplitude of scattering of a proton by a neutron in the singlet or triplet states;[6] A and k′ are determined by making the logarithmic derivatives of the functions $\varphi_{pn}^{(1)}(\rho)$ and $\varphi_{pn}^{(2)}(\rho)$ continuous at $\rho = \rho_0$. The potential $V_{pp}$ in the integrals $I_{pn}$ was chosen in the form of a $\delta$ function, while $V_{pn}$ was chosen either in the form of a $\delta$ function for $\varphi_{pn}(\rho)$ independent of the coordinates of the incident proton, or in the form of a potential well with $\rho_0 = 2.65 \times 10^{-13}$ cm for $\varphi_{pn}(\rho)$ dependent on the coordinates of the incident proton.

Calculation has shown that the integrals $I_{pn}^t$, which take into account the triplet interaction of the neutron with the proton in the final state, are much smaller than the integrals $I_{pn}$ corresponding to the interaction in the singlet state. Consequently, the differential cross section of the reaction should be determined by the square of the matrix element $H_3$ and can be written in the form $d\sigma = d\sigma_{pn} + d\sigma_{pp} + d\sigma_{interf}$.

Figure 1 shows the experimental c.m.s. spectrum of the neutrons from the reaction p + d → p + p′ + n, emitted at zero degrees to the direction of the incident 8.9-Mev protons.[1,2] Figure 2 shows the experimental c.m.s. spectrum of the neutrons from the reaction d + p → p + p′ + n, emitted at zero degrees to the direction of the incident 18.6-Mev deuterons.[2] This last spectrum can be considered as a spectrum of neutrons emitted at 180 deg to the direction of the incident protons from the reaction p + d → p + p′ + n, since the total energy of either reaction is of order 4 Mev. The figures show also

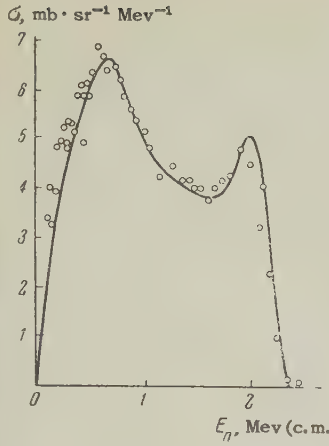

FIG. 1. Spectrum of neutrons (c.m.s.) produced at a zero angle in the (p + d) reaction by incoming 8.9-Mev protons. The points are the experimental data of reference 1, and the curve is calculated in the present work.

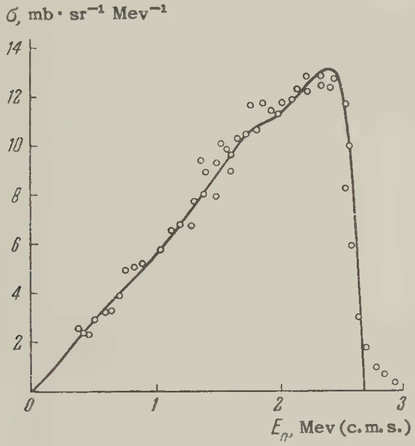

FIG. 2. Spectrum of neutrons (c.m.s.) produced at a zero angle in the (d + p) reaction by incoming 18.6-Mev deuterons. The points are the experimental data of reference 2, and the curve is calculated in the present work.

the neutron energy spectra, calculated in the present paper, for neutrons from the reaction $p + d \rightarrow p + p' + n$, emitted at 0 and 180 deg to the direction of the incoming protons, for the corresponding total reaction energies.

The calculated spectrum of the neutrons emitted at zero degrees has two maxima, like the experimental one. The position and shape of the maximum at 0.7 Mev neutron energy is determined essentially by the contribution of $d\sigma_{pn}$ to $d\sigma$, i.e., by the interaction between the neutron and the proton in the final singlet state. The maximum at the upper boundary of the neutron spectrum is determined by the contribution of $d\sigma_{pp}$ to $d\sigma$, i.e., by the interaction of two protons in the final singlet state. The maximum at $E_n \approx 0.7$ Mev is considerably broader and higher than the maximum at the upper boundary of the neutron spectrum. This may be due to the high probability of pickup of a neutron (deuteron) by the incoming proton and their emission forward.

The spectrum of the neutrons emitted at 180 deg has one maximum at the upper boundary. The form of this spectrum, as shown by calculation, is determined completely by $d\sigma_{pp}$, i.e., by the production of a virtual biproton in the singlet state, emitted forward.

The ratio of the areas under the experimental points is

$$\frac{d\sigma}{d\Omega}(180°)\Big/\frac{d\sigma}{d\Omega}(0°) = 1{,}8 \pm 0.3,$$

while the same ratio under the corresponding theoretical curves is 1.75. This is evidence that the angular distributions of the products of reactions accompanied by emission of several particles can be calculated by the foregoing method.

Because of isotopic invariance, one can expect the c.m.s. spectrum of protons from the reaction $n + d \rightarrow p + n + n'$, emitted at zero degrees to the direction of the incident protons of energy ~10 Mev to have two maxima, like the corresponding neutron spectrum from the reaction $p + d \rightarrow p + p' + n$. The first maximum, at a proton energy of approximately 0.7 Mev, should correspond to the interaction between the neutron and proton in the final singlet state, while the second, that at the upper boundary of the spectrum, should correspond to the interaction between two neutrons in the final singlet state. However, great interest attaches to an experimental investigation of the spectrum of protons from the reaction $n + d \rightarrow n + n' + p$, emitted at zero degrees, since its theoretical analysis by the method given above yields the neutron-neutron scattering length.

The method developed in the present paper and in references 3 and 7 can be used to analyze the spectra of the products of the reactions (d + d), (d + T), (d + $He^4$), (T + T), and similar reactions, in order to explain the role of interaction of the products of these reactions in the final state and the possibility of the existence of excited states of $He^4$, $He^5$, and $Li^5$.

In conclusion, the authors thank S. S. Vasil'ev, A. S. Davydov, and Yu. M. Shirokov for an evaluation of this work, and also N. A. Vlasov and B. V. Rybakov for great interest in the work and for numerous discussions.

---

[1] Nakada, Anderson, Gardner, McClure, and Wong, Phys. Rev. **110**, 594 (1958).

[2] Vlasov, Kalinin, Rybakov, and Sidorov, Proc. Intl. Conf. on Nuclear Physics, Paris, 1958.

[3] A. B. Migdal, JETP **28**, 3 (1955), Soviet Phys. JETP **1**, 2 (1955).

[4] W. Heckrotte and M. McGregor, Phys. Rev. **111**, 593 (1958).

[5] A. G. Sitenko, Usp. Fiz. Nauk **67**, 377 (1959), Soviet Phys. - Uspekhi **2**, 195 (1959).

[6] V. V. Komarov and A. M. Popova, JETP **36**, 1574 (1959), Soviet Phys. JETP **9**, 1118 (1959).

[7] V. V. Komarov and A. M. Popova, JETP **38**, 253 (1960), Soviet Phys. JETP **11**, 184 (1960).

Translated by J. G. Adashko
298

SOVIET PHYSICS JETP VOLUME 11, NUMBER 5 NOVEMBER, 1960

# *MAGNETIC BREMSSTRAHLUNG OF A CONFINED PLASMA*

K. N. STEPANOV and V. I. PAKHOMOV

Physico-Technical Institute, Academy of Sciences, Ukrainian S.S.R.

Submitted to JETP editor December 9, 1959

J. Exptl. Theoret. Phys. (U.S.S.R.) **38**, 1564-1568 (May, 1960)

Magnetic bremsstrahlung of a high-temperature plasma located in a strong magnetic field is considered.

AN investigation of the magnetic bremsstrahlung of electrons of a high-temperature plasma is of interest in connection with the problem of controllable thermonuclear reactions (energy balance in a thermonuclear reaction, microwave diagnostics of plasma).

In the present paper we consider magnetic bremsstrahlung from a confined plasma under conditions where the magnetic pressure $p_H$ is considerably greater than the pressure of the electron gas $p_e$. The condition $p_H \gg p_e + p_i$ ($p_i$ is the pressure of the ion gas) is necessary to create equilibrium plasma configurations and to ensure their stability (plasma ring stabilized by a strong magnetic field,[1] stellarator,[2] etc.).

A plasma electron in a magnetic field **H**, moving in a helix along a magnetic force line, radiates electromagnetic waves of frequency

$$\omega = s\omega_H / (1 - v_\parallel n_j \cos\theta / c), \quad s = 1, 2, \ldots, \tag{1}$$

where $\omega_H = eH/mc$ is the gyrofrequency for the electron; e, m and $v_\parallel$ are the charge, mass, and projection of the electron velocity **v** on the direction of the magnetic field; $n_j$ are the refractive indices of the two normal waves (ordinary and extraordinary) that can propagate in the plasma; and $\theta$ is the angle between the direction of propagation of the wave and the magnetic field. The $n_j$ are defined by the well-known expressions

$$n_{1,2}^2 = (-B \pm \sqrt{B^2 - 4AC})/2A, \quad A = 1 - u - v + uv\cos^2\theta,$$
$$B = (2 - v)u - 2(1 - v)^2 - uv\cos^2\theta,$$
$$C = (1 - v)[(1 - v)^2 - u], \tag{2}$$

where $v = \Omega^2/\omega^2$, $u = \omega_H^2/\omega^2$, $\Omega = (4\pi e^2 n_0/m)^{1/2}$ is the Langmuir frequency for the electrons, and $n_0$ is the number of electrons per unit volume.

We assume that $\beta = v_t/c = (T_e/mc^2)^{1/2} \ll 1$, where $T_e$ is the temperature of the electron gas. In addition, we assume that the electromagnetic waves corresponding to the first harmonics of (1), for which $n_j^2 > 0$, can propagate in the plasma. This takes place when $\Omega/\omega \lesssim 1$. In this case $n_j \sim 1$, so that $\omega \approx s\omega_H$ in (1). Thus, the total radiation per unit volume of plasma is found to consist of individual lines near the frequencies $\omega_H$, $2\omega_H$, ..., which are Doppler-broadened with a half-width $\Delta\omega \sim s\omega_H \beta \cos\theta$. For large values of $s$ ($s \gtrsim 1/\beta$) the neighboring harmonics coalesce, and when $\omega \gg \omega_H/\beta$ the radiation spectrum becomes continuous. Our analysis pertains only to the case of non-overlapping harmonics. The case when the major fraction of the radiation intensity of the confined plasma occurs at the frequencies $\omega$ corresponding to overlapping harmonics was considered by Trubnikov[3,4] (the case of large plasma dimensions and high temperatures). He considered radiation in the direction $\theta = \pi/2$, when there is no ordinary (non-relativistic) Doppler effect and relativistic effects must be taken into account.

We note that inhomogeneities in the magnetic field lead to additional line broadening. We shall assume that the inhomogeneities in the magnetic field are sufficiently small, $\Delta H/H \lesssim \beta$, so that the magnetic field can be considered homogeneous.

Electromagnetic waves with frequencies close to $s\omega_H$ are strongly absorbed in a high-temperature plasma[5] (cyclotron absorption, due to the presence of thermal motion of the plasma electrons). The distance in which the intensity of the electric field of a plane electromagnetic wave of frequency $\omega \approx s\omega_H$ is reduced by a factor e = 2.7 ... is

$$l_s = ƛ/\varkappa_s, \quad ƛ = c/s\omega_H, \tag{3}$$

where $\kappa_s$ is the imaginary part of the complex index of refraction (damping factor).

When $s = 2, 3, \ldots$ and $s^2\beta^2 n_j^2 \sin^2\theta \ll 1$, the propagation of an electromagnetic wave in a plasma is characterized by the dielectric-permittivity tensor

$$(\varepsilon_{ij}) = \begin{pmatrix} \varepsilon_{11} & \varepsilon_{12} & 0 \\ -\varepsilon_{12} & \varepsilon_{11} & 0 \\ 0 & 0 & \varepsilon_{33} \end{pmatrix}, \qquad \varepsilon_{ij} = \varepsilon^{(0)} + \varepsilon_{ij}^{(1)}, \tag{4}$$

where $\epsilon_{ij}^{(0)}$ are certain konwn expressions for $\epsilon_{ij}$, obtained without allowance for the thermal motion of the electrons. The small additions $\epsilon_{ij}^{(1)}$, which cause the cyclotron absorption of the waves, are

$$\varepsilon_{11}^{(1)} = i\varepsilon_{12}^{(1)} = 2i\sigma_s, \qquad \varepsilon_{33}^{(1)} \approx 0;$$

$$\sigma_s = \frac{\sqrt{\pi}\, s^{2s-2} \sin^{2s-2}\theta\ \Omega^2}{2^{s+3/2} s! \cos\theta\, \omega_H^2} (\beta n)^{2s-3} e^{-z_s^2}, \qquad z_s = \frac{1 - s\omega_H/\omega}{\sqrt{2}\beta n \cos\theta}.$$

If the frequency $\omega$ is determined by expression (1), then $z_s = v_{||}/\sqrt{2v_t}$. Taking (4) into account, we readily find

$$\begin{aligned} \varkappa_s &= \sigma_s n_j (1 - u)(2C + Bn_j^2)^{-1} \\ &\times \Big\{ n_j^4 \sin^2\theta - (1 - v)(1 + \cos^2\theta) n_j^2 \\ &+ 2\left(1 - \frac{v}{1-u} + \frac{v\sqrt{u}}{1-u}\right)(1 - v - n_j^2 \sin^2\theta)\Big\}. \end{aligned} \tag{5}$$

We must put $n = n_j$ in the right half of (5). In order of magnitude,

$$l_s = a_s ƛ (\omega/\Omega)^2 \beta^{-(2s-3)} e^{-z_s^2}, \tag{6}$$

where, for the first harmonics, $a_s \sim 1$.

When $s = 1$, the tensor $\epsilon_{ij}$ is

$$\varepsilon_{11} = i\sigma + 1 - v/4, \quad \varepsilon_{12} = \sigma - iv/4 - \alpha,$$

$$\varepsilon_{22} = i\sigma + 1 - v/4 - 2i\alpha,$$

$$\varepsilon_{33} = 1 - v + \varepsilon_{33}', \quad \varepsilon_{33}' = \frac{v \sin^2\theta}{\sqrt{2}\cos\theta} \beta n z_1 (1 + i\sqrt{\pi} z_1 w(z_1)),$$

$$\varepsilon_{13} = \varepsilon_{31} = -i\varepsilon_{23} = i\varepsilon_{32} = \frac{v\sin\theta}{2\cos\theta}(1 + i\sqrt{\pi} z_1 w(z_1)),$$

$$\sigma = \sqrt{\frac{\pi}{8}} \frac{v w_1(z_1)}{\beta n \cos\theta}, \quad \alpha = \beta^2 \sigma n^2 \sin^2\theta,$$

$$w(z) = e^{-z^2}\left(1 + \frac{2i}{\sqrt{\pi}} \int_0^z e^{t^2} dt\right). \tag{7}$$

The damping factor $\kappa_1$ can be determined in two limiting cases. If $v|w(z_1)|/\beta n_j \cos\theta \gg 1$ and $\theta^3 \gg \beta$, then*

$$\varkappa_1 = \operatorname{Re} \sqrt{\frac{2}{\pi}} \frac{\beta\cos\theta}{v w(z_1)} Q (2n^2 \sin^2\theta - 2 + 2v - \sin^2\theta)^{-1},$$

$$\begin{aligned} Q &= n^4 \left[1 - v\left(\cos^2\theta + \frac{1}{4}\sin^2\theta\right) + 2\varepsilon_{13}\cos\theta\sin\theta\right] \\ &+ n^2 [\varepsilon_{13}(v - 2)\cos\theta\sin\theta + (1 + \cos^2\theta)(\varepsilon_{13}^2 - (1 - v) \\ &\times (1 - v/4) - i\sigma\varepsilon_{33}') - \sin^2\theta (1 - v/2)] \\ &+ i\sigma\varepsilon_{33}'(2 - v) + (1 - v)(1 - v/2) + \varepsilon_{13}^2 (v - 2). \end{aligned} \tag{8}$$

In order of magnitude, $l_1 \sim l_1 \sim (ƛ/\beta) \exp (v_{||}^2/2v_T^2)$. The refractive index $n_j$ is determined in this case by Eq. (2), in which we must put $u = 1$. If $\theta^3 \lesssim \beta$, then the electromagnetic wave of frequency $\omega \approx \omega_H$ is strongly damped: $n \sim \kappa \sim \beta^{-1/2}$ when $|1 - \omega_H/\omega| \lesssim \beta^{2/3}$.

If $v \ll 1$ and $v|w(z_1)|/\beta \cos\theta \ll 1$ (low-density plasma), we have $n_j = 1$ and

$$\varkappa_1 = \sqrt{\frac{\pi}{2}} \frac{v \exp(-z_1^2)}{4\beta\cos\theta} (1 + \cos^2\theta). \tag{9}$$

With this

$$l_1 \sim \beta ƛ (\omega^2/\Omega^2) \exp (v_{||}^2/2v_T^2).$$

Using Kirchhoff's law and expressions (5), (8), and (9) for the absorption coefficients, we can determine the radiating ability of the plasma, after which one can readily estimate the energy of the magnetic bremsstrahlung from a confined plasma. A clearer estimate is obtained, however, in the following manner. The radiation intensity of an individual plasma electron, for the harmonics $s = 2, 3, \ldots,$ is[6]

$$w_s = b_s(\theta) \frac{s^4 n_j^3}{(s!)^2 2^{2s}} w \left(\frac{v_\perp}{c} s n_j \sin\theta\right)^{2s-2}, \tag{10}$$

where $b_s(\theta) \sim 1$, $v_\perp$ is the electron-velocity component perpendicular to **H**, and $w = 2e^2\omega_H^2 v_\perp^2/3c^2$ is the intensity of radiation of the electron in vacuum.

Since the radiation of an electron of velocity $v$ is absorbed at a distance $l_s = l_s(v_{||})$, the contribution of the $s$-th harmonic to the radiation intensity will be produced by electrons in the layer $l_s < L$, where $L$ is the plasma dimension. We shall assume that when $v_{||} \gg 2v_t$ we have $l_s \gg L$. The number of such electrons is exponentially small, and their contribution to the overall intensity of the $s$-th harmonic can be disregarded. Therefore the overall intensity of the $s$-th harmonic from a unit plasma surface will be on the order of $W_s \sim \overline{w_s l_s} n_0$, where $\overline{w_s l_s}$ is the value of $w_s l_s$ averaged over the Maxwellian distribution. The integration over $v_{||}$ is carried out here up to the velocity $v_{lim}$, for which $l_s(v_{lim}) \sim L$, i.e., $v_{lim}^2 \sim 2v_t^2 ln\ (L\Omega^2\beta^{2S-3}/ƛ\omega^2 a_s)$; $v_{lim}$ is of order of several times $v_t$. It is precisely the value of $v_{lim}$ which determines the line width of the radiation emitted from the plasma: $\Delta\omega \sim s\omega_H v_{lim} c^{-1} \cos\theta$. When $z_s = 0$ $(\omega = s\omega_H)$ the line intensity reaches a maximum corresponding to the radiation from the surface of an absolutely black body. Thus

$$W_s = q_s \frac{m\beta^3 s^3 \omega_H^3}{4\pi^3} \frac{v_{lim}}{v_T} \sim \frac{\omega^2 T_e}{8\pi^3 c^2} \Delta\omega, \tag{11}$$

where $q_s \sim 1$.

---

*The expression for $\kappa_1$, derived in reference 5 for $|z_1| \ll 1$, does not include terms proportional to $\varepsilon_{13}$.

The radiation intensity of the electron at the first harmonic is determined by the following expressions

$$w_1 = \tfrac{2}{3} w (1 + \cos^2\theta) \text{ for } v\,|w(z_1)|/\beta \cos\theta \leqslant 1, \qquad (12)$$

$$w_1 \sim w\beta^2 \text{ for } v\,|w(z_1)|/\beta n_j \cos\theta \gg 1. \qquad (13)$$

The result (13) was obtained by Ginzburg and Zheleznyakov[7] (see also reference 8). However, since the expression used in reference 7 for the tensor $\epsilon_{ij}$ does not take the thermal motion of the electrons into account, the results of that paper pertain only to electrons with velocities $v_{\|} \gg \sqrt{2}v_t$. Taking (12), (13) and (8), (9) into account, we obtain also expression (11), from which it follows that the intensity of radiation from a unit plasma surface depends very little (logarithmically) on the density, and is proportional to $T^{3/2}$ and $H^3$.

Let, for example, $n_0 \sim 10^{13}\,\text{cm}^{-3}$, $H \sim 10^4$ Gauss, $T \sim 5$ kev, and $L \sim 10^2$ cm. In this case $\Omega/\omega_H \sim 1$, $\beta \sim 0.1$, $\lambda\!\!\!^{-} \sim 0.1$ cm, $l_1 \sim l_2 \sim 1$ cm, $l_3 \sim 10^2$ cm, and $W_{1-3} \sim 10^2 - 10^4$ erg-sec$^{-1}$ cm$^{-2}$. The energy released in a nuclear reaction in a DT mixture is in this case $W_{\text{nuc}} \sim 10^3$ erg-sec$^{-1}$ cm$^{-3}$. Thus, with the reactor size $L$ ranging from 10 to 100 cm, the energy released in the nuclear reaction is greater than the energy carried away by the magnetic bremsstrahlung.

The radiation intensities corresponding to different harmonics depend on $n_0$ to an equal degree (if the logarithmic dependence is disregarded). This is due to the fact that the drop in the intensity of radiation from a single electron due to increasing $s$ is offset by the increase in $l_s$ due to the increase in the number of electrons radiated to the outside. Expressions (11) are valid up to $s = s^*$, where $l_{s^*} \sim L$. For $s \geq s^* + 1$ we have $l_s \gg L$, and instead of (11) we obtain

$$W_s \sim \overline{w}_s L n_0. \qquad (14)$$

It is obvious that $W_s \sim W_{s^*}\beta^{2(s-s^*)} \ll W_{s^*}$ for $s > s^*$.

The presence of density inhomogeneities, which are particularly large on the boundary between the plasma and the vacuum, will cause the rays to be reflected and curved. In addition, for $s$ such that $l_s \sim L$, the value of $W_s$ will depend on the plasma configuration. An accounting of these circumstances is essential for an accurate determination of the coefficients $q_s$.

Expression (11) and the estimate given show that even in strong magnetic fields the energy lost to magnetic bremsstrahlung is not very large in thermonuclear reactors using the DT reaction. This is explained primarily by the fact that when $v|w(z_1)|/\beta n \cos\theta \gg 1$ the intensity of radiation of the first harmonic in the plasma decreases by a factor $1/\beta^2 \gg 1$ compared with the intensity of radiation in vacuum. Secondly, the radiation of the first harmonics is strongly absorbed in the plasma.

In conclusion, we consider the question of the intensity of thermal radiation near resonant frequencies* $\omega \approx \omega_{1,2}$, where

$$\omega_{1,2}^2 = \tfrac{1}{2}(\Omega^2 + \omega_H^2) \pm \tfrac{1}{2}[(\Omega^2 + \omega_H^2) - 4\Omega^2\omega_H^2\cos^2\theta]^{1/2}.$$

When $\omega \rightarrow \omega_{1,2}$ the coefficient $A = (1 - \omega_1^2/\omega^2) \times (1 - \omega_2^2/\omega^2)$ tends to zero, and one of the refractive indices (2) tends to infinity:

$$n^2 = -B/A \gg 1. \qquad (15)$$

However, (15) can be used only when $1 \gg |A|^2 \gg \beta^2$. In the general case $|A| \ll 1$ and the value of $n^2$ is (see reference 5 and also reference 9)

$$n^2 = [-A \pm \sqrt{A^2 - 4\beta^2 A_1 B}]/2\beta^2 A_1 B \gg 1,$$

$$A_1 = -3v\left[\cos^4\theta(1-u) + \frac{6-3u+u^2}{(1-u)^2}\cos^2\theta\sin^2\theta + \frac{\sin^4\theta}{1-4u}\right]. \qquad (16)$$

When $1 \gg |A|^2 \gg \beta^2$, one of the refractive indices (16) turns into (15). The second refractive index describes the plasma wave. The damping factor is

$$\varkappa = -n(P+R)(4\beta^2 A_1 n^2 + 2A)^{-1}(1-u), \qquad (17)$$

where

$$P = \sqrt{\pi} v z_0 \sum_{s=-\infty}^{\infty} \frac{\mu^{|s|}}{2^{|s|}|s|!} e^{-z_s^2}\left(\frac{s^2\sin^2\theta}{\mu} + 2z_s^2\cos^2\theta\right), \qquad (18)$$

$$R = \nu(1 + 2uv(1-u)^{-2}\sin^2\theta), \qquad (19)$$

where $\mu = \beta^2 n^2 u^{-1}\sin^2\theta \ll 1$, and $\nu$ is the electron-ion collision frequency. The individual terms of (18) are in general of different order of magnitude, and the largest of these should be taken in the sum (18). In the derivation of (16) and (17) it is assumed that $\kappa \ll n$ and $\beta^2 n^2 \ll 1$.

The direction of beam propagation, i.e., the direction of the energy flux transferred by the plane wave with wave vector **k**, is not the same as **k** in an anisotropic medium. If the angle between **H** and **k** is $\theta$, then the angle $\xi$ between the beam and **H** is determined from the following equation[10]

$$\frac{1}{n(\theta)}\frac{\partial n(\theta)}{\partial\theta} = \tan(\xi - \theta).$$

The absorbing ability of the medium (the damping coefficient of the energy flux along the beam) is

---

*This question was considered by Ginzburg and Zheleznyakov.[7]

$$\alpha(\xi, \omega) = 2\omega c^{-1}\varkappa(\theta, \omega)\cos(\theta - \xi).$$

In the preceding estimate of the energy flux we disregarded the difference between $\alpha$ and $2\omega\kappa/c$, for this difference is small when $\omega$ is not close to $\omega_{1,2}$. However, when $\omega \approx \omega_{1,2}$, the quantity $n^{-1}dn/d\theta$ is very large, so that the difference $|\theta - \xi|$ is close to $\pi/2$

$$\frac{1}{n}\frac{\partial n}{\partial\theta} \approx \frac{uv\cos\theta\sin\theta}{A + 2\beta^2 A_1 n^2} = \tan(\theta - \xi) \approx \frac{1}{\cos(\theta - \xi)} \gg 1.$$

Therefore $\alpha$ is much less than $2\omega\kappa/c$:

$$\alpha(\xi, \omega) = 2\varkappa\frac{\omega}{c}\frac{A + 2\beta^2 A_1 n^2}{uv\cos\theta\sin\theta}. \qquad (20)$$

If the dimensions of the plasma are sufficiently large, then the plasma radiates like a "black" body when $\omega = \omega_{1,2}$. The width of the radiation spectrum can be estimated from the condition $\alpha(\xi, \omega_{1,2} + \Delta\omega) L = 1$ (it is assumed that the plasma is transparent when $\omega$ is not close to $\omega_{1,2}$ or to $s\omega_H$, i.e., $\alpha(\omega) L \ll 1$). The intensity of radiation will be $W(\xi) = I_0|\Delta\omega|$, where $I_0 = \omega^2 T_e/8\pi^3 c^2$. The question of the emergence of the energy of the plasma wave from the plasma calls for a separate consideration.

The authors are deeply grateful to A. I. Akhiezer, M. A. Leontovich, and Ya. B. Faĭnberg and their associates for a discussion of the work and for useful advice.

[1] S. I. Braginskiĭ and V. D. Shafranov, Second Geneva Conference, Papers by Soviet Scientists, I, p. 221.

[2] L. Spitzer, Phys. of Fluids **1**, 253 (1958).

[3] B. A. Trubnikov and A. E. Bazhanova, Физика плазмы и проблема управляемых термоядерных реакций (Plasma Physics and Controllable Thermonuclear Reactions), vol. 3, Acad. Sci. Press, 1958, p. 121.

[4] B. A. Trubnikov, Dokl. Akad. Nauk SSSR **118**, 913 (1958), Soviet Phys.-Doklady **3**, 136 (1958).

[5] A. G. Sitenko and K. N. Stepanov, JETP **31**, 642 (1956), Soviet Phys. JETP **4**, 512 (1957). K. N. Stepanov, JETP **35**, 283 (1958), Soviet Phys. JETP **8**, 195 (1959).

[6] V. Ya. Éidman, JETP **34**, 131 (1958), Soviet Phys. JETP **7**, 91 (1958).

[7] V. L. Ginzburg and V. V. Zheleznyakov, Изв. вузов МВО СССР, Радиофизика (News of the Colleges, Radiophysics) **1**, 59 (1958).

[8] R. Q. Twiss and J. A. Roberts, Austr. J. Phys. **2**. No 3, 424 (1958).

[9] B. N. Gershman, JETP **24**, 659 (1953).

[10] S. M. Rytov, Теория электрических флуктуаций и теплового излучения (Theory of Electric Fluctuations and Thermal Radiation), Acad. Sci. Press, M., 1953.

Translated by J. G. Adashko
299

SOVIET PHYSICS JETP VOLUME 11, NUMBER 5 NOVEMBER, 1960

# *ANOMALIES OF ELECTRON CHARACTERISTICS OF A METAL IN THE HIGH PRESSURE REGION*

I. M. LIFSHITZ

Physico-Technical Institute, Academy of Sciences, Ukrainian S.S.R.

Submitted to JETP editor December 12, 1959

J. Exptl. Theoret. Phys. (U.S.S.R.) 38, 1569-1576 (May, 1960)

A peculiar "electron transition" due to variation of the topology of the Fermi surface during its continuous deformation may occur in metals at high pressures. At the point of such a transition, the electron-state density near the boundary surface, and the electron dynamics also possesses some peculiar features which lead to anomalies of the electron characteristics of the metal (thermodynamic and kinetic). The most characteristic anomalies in the vicinity of the "electron transition" point at low temperatures are investigated. The possibility of an ismorphic first-order transition near the "electron transition" point is discussed.

## INTRODUCTION

In connection with the peculiar features of the energy spectrum of conduction electrons in metal, characteristic anomalies of thermodynamic and kinetic quantities can take place at low temperatures in the region of high pressures. The nature of this phenomenon consists of the following.

As is well known, the electron state density $\nu(\epsilon) = dN(\epsilon)/d\epsilon$ of conduction electrons is connected with the form of the constant energy surfaces in momentum space, $\epsilon(p) = \epsilon$. Those values of the energy $\epsilon = \epsilon_k$, for which the topology of these surfaces changes [for example, an open surface changes to a closed surface by disruption of a "neck" (Fig. 1a), or a new split-off region of surface appears (Fig. 1b)], correspond to peculiarities of the surface density $\nu(\epsilon)$. At the same time the "critical" surface $\epsilon(p) = \epsilon_k$ contains singular points, near which the electron dynamics has an unusual character.

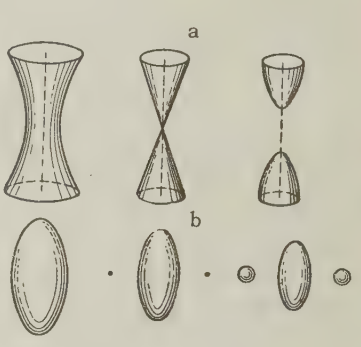

FIG. 1. a – Disruption of the "neck" of a Fermi surface, b – appearance of a new-detached region.

Generally speaking, the value of $\epsilon_k$ is located sufficiently far from the chemical potential of the electrons $\zeta$, and one can ascertain the presence of singular points $\epsilon_k$ only by the x-ray spectrum. However, if there exists any continuously changing parameter whose variation causes the difference $\zeta - \epsilon_k$ to pass through zero (i.e., changes the topology of the Fermi boundary surface), then the peculiarities of the spectrum density $\nu(\epsilon)$ and the electron dynamics close to the "critical" surface $\epsilon(p) = \epsilon_k$ lead to singular anomalies of thermodynamic and kinetic characteristics of the electron gas in the metal.

Deformation of the lattice, and in particular hydrostatic compression at high pressures, can serve as such a continuous parameter. It is well known that at high pressures the anisotropy of a large number of properties is reduced, and therefore one can expect that a Fermi surface of the "corrugated cylinder" type, which is characteristic for layered structures, should go over, by gradual deformation, into a closed surface [even if the total number of electrons in the conduction band is constant (see Fig. 2a, b, c)]. It appears that other examples of variation of the topology of the Fermi surface are possible. It should be emphasized that a change of the topology of the Fermi surface is not connected with a change in the symmetry of the lattice, and therefore does not correspond to a phase transition of second order.

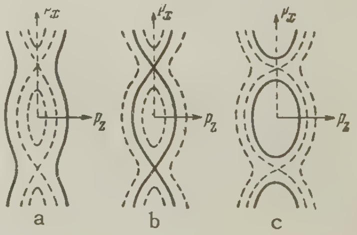

FIG. 2. Gradual transition of an open surface of the "corrugated cylinder" type into a closed band.

On the other hand, the primitive lattice can cease to be thermodynamically stable up to the approach to the "critical" Fermi surface, so that the phase transition of first order takes place before the anomaly connected with the variation of topology.* However, since the time of electron "attuning" in the deformation of the lattice is shorter than the time of realignment of the lattice in the phase transition, similar anomalies can be observed even in short-lived metastable states. Therefore, in what follows, the problem of stability or metastability of a state close to the point of variation of the topology of the Fermi surface can be disregarded.

Another parameter — the concentration of impurities or components in an alloy — would appear to change the chemical potential $\zeta$ in the Fermi surface strongly; however, for an irregular lattice, the very concept of a Fermi surface loses its exact meaning, owing to the absence of translational symmetry; therefore the singularity of $\nu(\epsilon)$ is smeared out and is practically absent.

We shall investigate below the properties of the metal near the singular point of an "electron transition" (variation of the topology of the Fermi surface). We shall begin with the case of zero temperature, at which the thermodynamic characteristics possess singularities connected with the singularities $\nu(\epsilon)$. These singularities fade away with increase in temperature; the corresponding estimates are given at the end of the first section.

## 1. ANOMALIES OF THERMODYNAMIC QUANTITIES

The state density is determined by the equation

$$\nu(\varepsilon) = (2\pi)^{-3}V \int\limits_{\varepsilon(\mathbf{p})=\varepsilon} d\Omega_{\mathbf{p}} / |\nabla_{\mathbf{p}}\varepsilon|. \qquad (1)$$

$V$ is the volume of the metal and $d\Omega_p$ is the element of surface area of $\epsilon(\mathbf{p}) = \epsilon$ in $\mathbf{p}$-space. Close to the singular point $\mathbf{p}_0$ on the "critical" surface, $\epsilon(\mathbf{p})$ has the form

$$\varepsilon(\mathbf{p}) = \varepsilon_k + p'^2\varphi(\mathbf{n}), \quad \mathbf{p} - \mathbf{p}_0 = \mathbf{p}' = p'\mathbf{n}, \qquad (2)$$

where $\mathbf{n}$ is a unit vector.

In the simplest case, when there is no degeneracy at the singular point $p' = 0$, we obtain by suitable choice of axes

$$\varepsilon(\mathbf{p}) = \varepsilon_k \pm p_1'^2/2m_1 \pm p_2'^2/2m_2 \pm p_3'^2/2m_3. \qquad (2a)$$

If the signs of $p_i'^2$ are identical, then a new surface recess appears at the point $\mathbf{p} = \mathbf{p}_0$; if these signs are different, then the neck is disrupted at this point (see Fig. 1,a, b).

It is easy to demonstrate that the state density close to the point $\epsilon_k$ is $\nu(\epsilon) = \nu_0(\epsilon) + \delta\nu$, where $\nu_0(\epsilon)$ is a smooth function and $\delta\nu$ differs from zero only on one side of the point $\epsilon_k$ — on the side where the number of recesses of the surface $\epsilon(\mathbf{p}) = \epsilon$ is large:

$$\delta\nu = \begin{cases} 0; \\ \alpha|\varepsilon - \varepsilon_k|^{1/2}, \quad \alpha \sim N/\zeta^{3/2} > 0. \end{cases} \qquad (3)$$

In what follows, to be specific, we shall assume that the number of surface recesses increases for $\epsilon > \epsilon_k$. In this case, for a total number of states $N(\epsilon) = N_0(\epsilon) + \delta N$, we have

$$\delta N = \begin{cases} 0, & \varepsilon < \varepsilon_k \\ \frac{2}{3}\alpha(\varepsilon - \varepsilon_k)^{3/2}, & \varepsilon > \varepsilon_k. \end{cases} \qquad (4)$$

Correspondingly, we have for the thermodynamic potential $\Omega$,

$$\Omega(\zeta) = \Omega_0(\zeta) + \delta\Omega, \quad \delta\Omega = -\int_0^\infty \frac{\delta N\, d\varepsilon}{1 + \exp[(\varepsilon - \zeta)/T]}$$

($T$ is the temperature in ergs) or, setting $\epsilon - \epsilon_k = x$, $\zeta - \epsilon_k = z$:

$$\delta\Omega = -\frac{2\alpha}{3}\int_0^\infty \frac{x^{3/2}\, dx}{1 + \exp[(x - z)/T]}. \qquad (5)$$

At low temperatures, $T \ll |z|$, we obtain

$$\delta\Omega = \begin{cases} -(\sqrt{\pi}/2)\alpha T^{5/2}\exp(-|z|/T), & z < 0, \\ -\frac{4}{15}\alpha z^{5/2} - (\pi^2/6)\alpha T^2 z^{1/2}, & z > 0. \end{cases} \qquad (6)$$

For $T = 0$,

$$\delta\Omega = \begin{cases} 0, & z < 0, \\ -\frac{4}{15}\alpha z^{5/2}, & z > 0. \end{cases} \qquad (7)$$

This means that the second derivatives of $\Omega$ at the point of "electron transition" $z = 0$ have a vertical break, while the third derivatives go to infinity as $z^{-1/2}$.

Inasmuch as the number of conduction electrons must be considered constant (at least in the vicinity of the point $\zeta = \epsilon_k$), it is useful to employ the free energy $F(T, v)$ per electron. In this case the volume $v$ is a parameter connected with the applied pressure; $\epsilon_k = \epsilon_k(v)$ is a direct function of the volume $v$ and the chemical potential $\zeta$ is also a function of $v$ by by virture of the contancy of the number of particles:*

---

*Evidently, such is the case in the so-called isomorphic transition, where the parameters of the lattice undergo a discontinuous change in one and the same type of structure (see below, page 1133).

$$N(\zeta, v) = 1. \tag{8}$$

Denoting by $v_k$ the volume at which the variation of the topology of the Fermi surface begins (i.e., $z = \zeta - \epsilon_k = 0$), we have

$$N_0(\varepsilon_k(v_k), v_k) = 1. \tag{9}$$

From (8) and (9), we get

$$z = \gamma(v - v_k), \quad \gamma = -(\partial N_0/\partial v + \nu_0 d\varepsilon_k/dv)/\nu_0. \tag{10}$$

Writing the free energy F in the form

$$F = F_0 + \delta F,$$

where $F_0$ is the smooth part of the free energy plotted against the density $\nu_0(\epsilon)$, it is easy to be convinced that $\delta F$ is quantitatively equal to the irregular contribution $\delta\Omega$, expressed in the variables v and T. Thus $\delta F$ is given by Eqs. (6) and (7), where one must set $z = \gamma(v - v_k)$. Then, as $T \to 0$

$$\delta \frac{C}{T} = -\delta \frac{\partial^2 F}{\partial T^2} = \begin{cases} 0, & z < 0, \\ (\pi^2/3)\alpha z^{1/2}, & z > 0; \end{cases} \tag{11}$$

$$\delta \frac{1}{T}\frac{\partial p_e}{\partial T} = -\frac{1}{T}\delta \frac{\partial^2 F}{\partial T\,\partial v} = \begin{cases} 0, & z < 0, \\ (\pi^2/3)\alpha\gamma z^{-1/2}, & z > 0. \end{cases} \tag{12}$$

$$\delta \frac{\partial p_e}{\partial v} = -\delta \frac{\partial^2 F}{\partial v^2} = \begin{cases} 0, & z < 0, \\ \alpha\gamma^2 z^{1/2}, & z > 0; \end{cases} \tag{13}$$

The expression (11) represents the anomaly of the electron specific heat C for $z > 0$:

$$C/T = (C/T)_0\{1 + \alpha z^{1/2}/\nu_0\}.$$

The expression (12) gives the anomaly of the coefficient of electron compressibility. The total pressure in the metal is made up of the electron pressure and the pressure $p_L$ of the lattice "core" of the metal, which frequently compensates it. However, inasmuch as the lattice part of the compressibility $\partial p_L/\partial v$ is continuous at the point $z = 0$,† then the peculiarity of the total coefficient of compressibility is given by the same expression (see Fig. 3a).

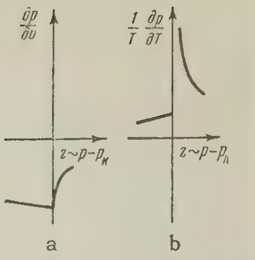

FIG. 3. a – Anomaly of the coefficient of compressibility close to the singular point $z = 0$, b – anomaly of the thermal coefficient of the pressure near the point $z = 0$.

Finally, as seen from (13), the strongest singularity is possessed by the thermal coefficient of pressure $\partial p/\partial T$ (Fig. 3b). Considering that at low pressures it is the electron part of the thermal coefficient of pressure that plays the fundamental role, we have for the smooth part of $\partial p/\partial T$:

$$(\partial p/\partial T)_0 = AT, \quad A = (\pi^2/3)\,\partial\nu_0/\partial v.$$

Thus, in the region of the anomaly,

$$\left(\frac{\partial p}{\partial T}\right)_v = AT\left\{1 + \alpha\gamma z^{-1/2}/2\frac{\partial\nu_0}{\partial v}\right\}, \quad z > 0. \tag{14}$$

The same sort of singularity is possessed by the coefficient of thermal expansion $(\partial v/\partial T)_p = -(\partial p/\partial T)_v/(\partial p/\partial v)_T$:

$$\left(\frac{\partial v}{\partial T}\right)_p = \frac{AT}{\varkappa_0}\left\{1 + \alpha\gamma z^{-1/2}/2\frac{\partial\nu_0}{\partial v}\right\}, \quad \varkappa_0 = -\left(\frac{\partial p}{\partial v}\right)_0. \tag{15}$$

To be able to consider the anomalies in all the formulas (6) — (15) on a pressure scale, it suffices to assume that $p - p_k = -\kappa_0(v - v_k)$ and, consequently,

$$z = \gamma(v - v_k) = (\gamma/\varkappa_0)(p_k - p). \tag{16}$$

In this case, it is convenient to estimate the coefficients $\gamma$, $\gamma/\kappa_0$ and the critical pressure p by expressing them in terms of the original difference of the energy $z_0 = (\zeta - \epsilon_k)_0$ (for zero pressure), and also of the critical deformation $(v_0 - v_k)/v_0$, for which the transition

$$|z| = |z_0|\,|p - p_k|/p_k, \quad p_k = \varkappa_0|v_0 - v_k|,$$

$$|\gamma| = |z_0|/|v_0 - v_k| \tag{17}$$

exists.

Naturally, the expressions (17) are only estimates, since the linear relations between p, $v - v_0$ and $z - z_0$ are violated in the large interval of deformations. If we set $|v_0 - v_k|/v_0 \sim 0.05$ to 0.1 for critical deformation, then $p_k \sim 5 \times 10^4$ to $10^5$ kg/cm².*

Equations (11) — (15) are valid for $T \ll |z|$. Thus, for finite temperatures, the singularities of all the thermodynamic quantities are lessened. The width of the temperature lessening of the anomaly will be $\Delta z \sim T$; on the pressure scale this gives

---

*In the case of several intersecting zones, $N(\zeta, v)$ is the total number of particles in all the zones.

†It may turn out that the part of the "lattice" binding energy, brought about by the conduction electrons, has a singularity at the point $z = 0$ of the same character as that of $\Omega_0$; this would give an insignificant contribution to $\partial p/\partial v$, which does not change any of the results qualitatively.

*It can be thought that less symmetric deformations (for example, uniform compression or tension) greatly change the geometry of the Fermi surface and require smaller stresses. In particular, violation of the initial symmetry of the crystal for such appropriately small deformations can lead to a splitting of the surface at the points of unavoidable self-intersection (for terms of identical symmetry) and lines of accidental intersection (for terms of different symmetry).

$$\Delta p / p_k = T / | z_0 | = T / | \zeta - \varepsilon_k |_{p=c*} \qquad (18)$$

As follows from Eq. 12, the negative quantity $(\partial p/\partial v)_0 = -\kappa_0$ obtains a positive increment $\sim z^{1/2}$ in the region of the anomaly. If as a result, $p(v)$ ceases to be a monotonic function and becomes positive at some point $\partial p/\partial v$, then an isomorphic phase transition of first order takes place with a discontinuity in the volume. Writing the expansion of $\partial p/\partial v$ for small $z > 0$ and $T \to 0$:

$$\partial p / \partial v = -\varkappa_0 + \alpha\gamma^2 z^{1/2} - \varkappa_1 z, \qquad (18a)$$

we establish the fact that the region of instability $(\partial p/\partial v > 0)$ can exist for the condition $\alpha\gamma^2 > 2\sqrt{\kappa_0 \kappa}$, and lies to the right of the point $z = 0$ in the interval

$$\alpha\gamma^2 - \sqrt{(\alpha\gamma^2)^2 - 4\varkappa_0\varkappa_1} < 2\varkappa_0 z < \alpha\gamma^2 + \sqrt{(\alpha\gamma^2)^2 - 4\varkappa_0\varkappa_1}. \qquad (19)$$

Here the point of "electron transition," $z = 0$, lies itself in the region of metastability or stability.

Since the singularity at the point $z = 0$ is reduced at finite temperatures, one should not call the "electron transition" at the point $z = 0$ a phase transition; in this connection we always speak of "anomalies" at the point $z = 0$, although in the terminology of Ehrenfest one could tentatively call such anomalies at $T = 0$ "transitions of the $2\frac{1}{2}$ order," since the second derivatives of the thermodynamic potentials have a singularity $\sim z^{1/2}$, and the third derivatives have a singularity $\sim z^{-1/2}$.

To conclude this section, we determine the anomaly of spin paramagnetism at $T = 0$. In an external magnetic field, the spin magnetic moment will be

$$M = \mu \{N(\zeta + \mu H) - N(\zeta - \mu H)\},$$

$$N_+ + N_- = \text{const},$$

while the magnetic susceptibility $\chi = \partial M/\partial H$ has the form

$$\chi = \{\nu(\zeta + \mu H) + \nu(\zeta - \mu H)\}\mu^2 = \chi_0 + \{\delta\nu(z + \mu H) + \delta\nu(z - \mu H\}\mu^2,$$

$$\chi_0 = \mu^2 \{\nu_0(\zeta + \mu H) + \nu_0(\zeta - \mu H)\},$$

$$\delta\nu(z) = \begin{cases} 0, & z < 0, \\ \alpha z^{1/2}, & z > 0. \end{cases}$$

Then

$$\delta\chi = \begin{cases} 0, & z + \mu H < 0, \quad z - \mu H < 0, \\ \alpha(z + \mu H)^{1/2}, & z + \mu H > 0, \quad z - \mu H < 0, \\ \alpha(z - \mu H)^{1/2}, & z + \mu H < 0, \quad z - \mu H > 0, \\ \alpha(z + \mu H)^{1/2} + \alpha(z - \mu H)^{1/2}, & z + \mu H > 0, \quad z - \mu H > 0 \end{cases} \qquad (20)$$

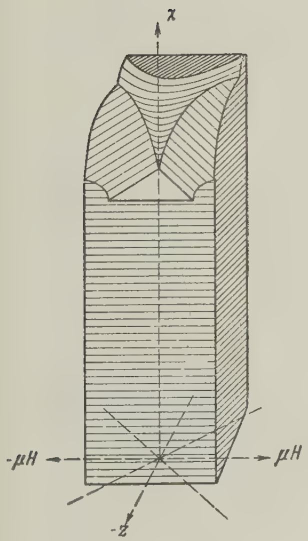

FIG. 4. Anomaly of the paramagnetic susceptibility close to the point $z = 0$.

(see Fig. 4).

However, the actual picture is somewhat further complicated by the superposition of quantum diamagnetism, which we have not taken into account here.

## 2. ANOMALIES OF GALVANOMAGNETIC CHARACTERISTICS

The anomalies of the kinetic coefficients (for example, the coefficient of heat conduction and electrical conductivity, viscosity, sound absorption, etc.) are connected both with the singularities of the state density $\nu(\epsilon)$ and of the thermodynamic quantities, and with the singularities of the electron dynamics on the critical surface. So far as the first part of the phenomenon is concerned, this leads, as also in the case of thermodynamic quantities, to singularities of the type $|z|^{-1/2}$ and $|z|^{1/2}$. For example, inasmuch as the absorption coefficient of sound $\chi_1$ is connected with the derivative of the sound velocity $c$ with respect to the density, while $c^2 \sim \partial p/\partial v$, we can expect that

$$\delta\chi_1 \sim \delta(\partial^2 p/\partial v^2) \sim |z|^{-1/2}.$$

In the present paper we shall not consider the detailed theory of anomalies of kinetic coefficients in the vicinity of the transition point $z = 0$. We shall only investigate the case in which the entire effect is fundamentally determined by a change in the electron dynamics. This takes place for the electrical resistance in strong magnetic fields if an open surface at the point $z = 0$ is converted into a closed one (or vice versa).

For definiteness, we shall assume that the initial open surface of the "corrugated cylinder"[1] type at the point $z = 0$ goes over into closed regions by means of a disruption of the neck (see Fig. 2a, b). As was shown in references 1 and 2, the asymptotic character of the electrical resistance in a strong magnetic field depends materially on the topology of the Fermi surface, and is determined by the presence or absence of open trajectories of the electrons. The latter are obtained by the intersection of the Fermi surface with the plane perpendicular to the magnetic field ($p_z$ – const., $z$ is the direction of the magnetic field). For closed surfaces there are no such open trajectories, and the resistance in strong fields generally tends toward saturation* (to $\rho_\infty$; in order of magnitude, $\rho_\infty \sim \rho_0$). For an open surface of the corrugated-cylinder type, open trajectories are obtained for the direction of the magnetic field perpendicular to the axis of the cylinder; this leads to an unlimited growth of the resistance: $\rho \sim H^2$. We shall investigate precisely this case.

We begin the calculation of the resistance in the vicinity of the point $z = 0$ with the determination of the conductivity tensor $\sigma_{ik}$. For $z > 0$, by assumption, the surface is closed. This means that the conductivity has the form[1]

$$\sigma_{ik}^{(0)} = \begin{vmatrix} \gamma^2 a_{xx} & \gamma a_{xy} & \gamma a_{xz} \\ \gamma a_{yx} & \gamma^2 a_{yy} & \gamma a_{yz} \\ \gamma a_{zx} & \gamma a_{zy} & a_{zz} \end{vmatrix}, \quad \gamma = H_0/H \ll 1, \tag{21}$$

where $H_0$ is the characteristic magnetic field, in which the period of precession of the electron is equal to its path length; the $a_{ik}$ have the order of magnitude of the conductivity in the absence of the magnetic field.

For $z < 0$, a contribution is added to the value of $\sigma_{ik}^{(0)}$ from the open trajectories. Choosing the $x$ axis along the corrugated cylinder, we can write down the dispersion law close to the singular point $p_0$ on the surface $\epsilon(p) = \epsilon_k$ in the form

$$\varepsilon = \varepsilon_k + p_x'^2/2m_1 - p_y'^2/2m_2 - p_z'^2/2m_3, \quad \mathbf{p}' = \mathbf{p} - \mathbf{p}_0. \tag{22}$$

The contribution $\delta\sigma_{ik}$ from the open trajectories is proportional to its relative share, i.e., the thickness of the layer of the open trajectories $\Delta p_z$ ($\Delta p_z$ is the width of the neck in the corrugated cylinder in Fig. 2).

According to (22),

$$\Delta p_z = m_3^{1/2} |z|^{1/2}.$$

Thus, taking into account the form of the conductivity tensor in the presence of open trajectories along the $x$ axis [see reference 1, Eq. (29) and reference 2, Eq. (16)], we have

$$\delta\sigma_{ik} = \left|\frac{z}{\zeta}\right|^{1/2} \begin{vmatrix} \gamma^2 b_{xx}, & \gamma b_{xy}, & \gamma b_{xz} \\ \gamma b_{yx}, & b_{yy}, & b_{yz} \\ \gamma b_{zx}, & b_{zy}, & b_{zz} \end{vmatrix}. \tag{23}$$

Retaining the principal terms in $\gamma$ and $z$, we can write for the total conductivity (for $z < 0$):

$$\sigma_{ik} = \sigma_{ik}^0 + \delta\sigma_{ik}$$

$$= \begin{vmatrix} \gamma^2 a_{xx} & \gamma a_{xy} & \gamma a_{xz} \\ \gamma a_{yx} & \gamma^2 a_{yy} + \left|\frac{z}{\zeta}\right|^{1/2} b_{yy} & \gamma a_{yz} + \left|\frac{z}{\zeta}\right|^{1/2} b_{yz} \\ \gamma a_{zx} & \gamma a_{zy} + \left|\frac{z}{\zeta}\right|^{1/2} b_{zy} & a_{zz} \end{vmatrix}, \tag{24}$$

where $b_{ik} = b_{ik}(z)$. Then, for the resistance along the $x$ axis,

$$\rho = (\sigma^{-1})_{xx} = \frac{a_{yy} a_{zz} - a_{yz} a_{zy}}{|a_{xy}|^2 a_{zz}} + \frac{b_{yy}(z)}{|a_{xy}|^2} \left|\frac{z}{\zeta}\right|^{1/2} \left(\frac{H}{H_0}\right)^2. \tag{25}$$

To make clear the dependence of $b_{yy}$ on $z = \zeta - \epsilon_k$, it is necessary to take into account that the velocities $v_x$ and $v_y$ are very small ($v\perp \sim p'$) on open trajectories close to the singular point $\mathbf{p}' = 0$, and that the time of motion close to this point on the curve $\epsilon = \epsilon_k$ diverges logarithmically [see reference 3, Eq. (3.15)]:

$$T \sim \int dp_x / v_y \sim \ln(\varepsilon - \varepsilon_k).$$

Therefore, the fundamental contribution to the mean velocity $\bar{v}_y$ is given by the motion near this point; this leads to the following estimate of $\bar{v}_y$:

$$v_y \sim v / \ln(|z|/\zeta),$$

$v$ = velocity of the electron far from the singularity.

Inasmuch as the contribution to the conductivity $\sigma_{yy}$ made by the open trajectories contains the factor $\overline{v_y^2}$ (see reference 2), then

$$b_{yy} \sim a / \ln(\zeta/|z|). \tag{26}$$

Finally, we obtain

$$\frac{\rho}{\rho_0} = \begin{cases} A + B\dfrac{|z|^{1/2}}{\zeta^{1/2}}\left(\dfrac{H}{H_0}\right)^2 \Big/ \ln\dfrac{\zeta}{|z|}, & z < 0, \\ A, & z > 0, \end{cases} \tag{27}$$

where $A$ and $B$ are constants of the order of unity.

---

*The case in which the electrons and holes are equal in number is an exception.

The anomaly of the pressure derivative of the resistance is especially sharp:

$$\frac{1}{\rho_0}\,\delta\,\frac{d\rho}{dp} = \frac{Bz_0}{2\,|z|^{1/2}\,\zeta^{1/2}\,p_k}\left(\frac{H}{H_0}\right)^2 \Big/ \ln\frac{\zeta}{|z|}. \qquad (28)$$

Attention must be given to one characteristic circumstance: while the anomalies of the thermodynamic quantities are located in the region $z > 0$ (i.e., to the right of the point of "electron transition," $z = 0$), the anomaly of the resistance lies in the region $z < 0$ (i.e., to the left of the point $z = 0$).*

As follows from the estimates (18), all the anomalies are more marked at low temperatures; however, the effect exists even in the region of very high temperatures. As far as the anomalies of resistance in a magnetic field are concerned, the entire effect is essentially a low temperature one, since it takes place only when the radius of curvature of the trajectory of the electron in the magnetic field is much less than its mean free path.

[1] Lifshitz, Asbel, and Kaganov, JETP **31**, 63 (1956), Soviet Phys. JETP **4**, 41 (1957).

[2] I. M. Lifshitz and V. G. Peschanskiĭ, JETP **35**, 1251 (1958), Soviet Phys. JETP **8**, 875 (1959).

[3] I. M. Lifshitz and M. I. Kaganov, Usp. Fiz. Nauk **69**, 419 (1959), Soviet Phys.—Uspekhi **2**, 831 (1960).

Translated by R. T. Beyer
300

---

*A much weaker anomaly of the resistance due to thermodynamic parameters takes place also for $z > 0$.

SOVIET PHYSICS JETP VOLUME 11, NUMBER 5 NOVEMBER, 1960

# *ON THE ELECTROMAGNETIC PROPERTIES OF A RELATIVISTIC PLASMA*

V. P. SILIN

Submitted to JETP editor December 14, 1959

J. Exptl. Theoret. Phys. (U.S.S.R.) 38, 1577-1583 (May, 1960)

We considered the dielectric constant for a relativistic electron-ion plasma, taking spatial dispersion into account. We obtained expressions for the screening radius and the skin-depth. Both undamped and weakly damped plasma oscillations were considered.

1. Relativistic plasma has recently drawn more and more the attention of physicists, as witness the number of papers devoted to the theory of a relativistic electron plasma.[1-7] The present communication is devoted to a consideration of the electromagnetic properties of an electron-ion plasma characterized by a complex dielectric constant that takes spatial dispersion into account. We shall in the following not take into account the dissipation caused by the collisions between particles.

2. In a medium with spatial dispersion — the simplest example of which is a plasma — the connection between the induction and the electrical field strength is well known to be (see, for instance, reference 8) nonlocal both in time and in space. We have, namely, for an infinite uniform medium

$$D_i(\mathbf{r}, t) = \int d\mathbf{r}' \int_{-\infty}^{t} dt' \hat{\varepsilon}_{ij}(\mathbf{r}-\mathbf{r}', t-t')\, E_j(\mathbf{r}', t'). \qquad (1)$$

We take for the dielectric constant tensor the quantity

$$\varepsilon_{ij}(\omega, \mathbf{k}) = \int d\mathbf{r}\, e^{-i\mathbf{k}\mathbf{r}} \int_{0}^{\infty} dt\, e^{i\omega t} \hat{\varepsilon}_{ij}(\mathbf{r}, t). \qquad (2)$$

It is necessary also to define the induction of the electric field. We shall not use in the following the concept of the magnetic field strength, so that we take for $\mathbf{D}$ the definition

$$\mathbf{D}(\mathbf{r}, t) = \mathbf{E}(\mathbf{r}, t) + 4\pi \int_{-\infty}^{t} dt' \mathbf{j}(\mathbf{r}, t').$$

These relations define a dielectric constant that takes spatial dispersion into account.

In the case of an isotropic system, the dielectric-constant tensor can be written in the form[2]

$$\varepsilon_{ij}(\omega, \mathbf{k}) = (\delta_{ij} - k_i k_j / k^2)\, \varepsilon^{tr}(\omega, k) + (k_i k_j / k^2)\, \varepsilon^{l}(\omega, k).$$

Such a tensor enables us to write down many electromagnetic properties of the medium. In particular, the transverse field oscillations are defined by the condition

$$c^2 k^2 - \omega^2 \varepsilon^{tr}(\omega, k) = 0, \qquad (3)$$

and the longitudinal oscillations by the condition

$$\varepsilon^{l}(\omega, k) = 0. \qquad (4)$$

The conventional dielectric constant corresponds to the limit of the longitudinal and transverse dielectric constants for $k = 0$

$$\varepsilon(\omega) = \lim_{k=0} \varepsilon^{l}(\omega, k) = \lim_{k=0} \varepsilon^{tr}(\omega, k).$$

The concept of a screening radius for the interaction is of great importance to the description of the interaction between particles. Such a concept has a simple physical meaning only in the case of a static field, and is thus defined through the limit of $\epsilon_{ij}$ for $\omega = 0$. The limit of the longitudinal dielectric constant is then finite. The screening radius for the longitudinal interaction is therefore defined by the equation

$$\lim_{k=0} \lim_{\omega/k=0} k^2 (\varepsilon^{l} - 1) = r_{\text{scr}}^{-2}.$$

It is necessary to let $\omega$ tend to zero first, and afterwards take the limit $k \to 0$. This means that one can only speak about a screening radius at large distances, where the decrease of the field is characterized by an exponential law.*

We must finally discuss still one more characteristic of the electromagnetic properties, also determined by the dielectric constant. In the limit $\omega/k \to 0$, the skin depth is a characteristic distance in the variation of the transverse field. When the mean free path can be assumed to be infinite, the anomalous skin-effect occurs. The transverse dielectric constant can then be written in the form*

---

*In the language of the theory that uses Green functions to describe many-particle systems, the different limits of $\varepsilon$ when $k/\omega \to 0$ and when $\omega/k \to 0$ correspond to different limits of the field Green functions in the time and space regions for small k and $\omega$. A similar situation occurs also for the vertex part and also for the two-particle Green function, as was noted by Landau.[9]

$$\varepsilon^{tr} = (4\pi i/\omega)\,\sigma^{tr}(k), \qquad \sigma^{tr} = C/k,$$

where C is a constant which depends on the actual properties of the plasma. One easily sees from this and from Eq. (3) that the skin depth of the transverse field is equal to

$$\delta = (2c^2/\pi C\omega)^{1/3}.$$

We go now over from these general considerations to a discussion of the dielectric-constant tensor and of the quantities that determine this tensor for a relativistic plasma.

**3.** We shall use Vlasov's self-consistent field approximation to obtain the dielectric-constant tensor of a relativistic plasma. We have then for a description of the electron and ion distributions (see, for instance, references 2, 3, 5, and 7)

$$\frac{\partial f_{\mathrm{el}}}{\partial t} + \mathbf{v}_{\mathrm{el}}\frac{\partial f_{\mathrm{el}}}{\partial \mathbf{r}} + e\left(\mathbf{E} + \frac{1}{c}[\mathbf{v}_{\mathrm{el}}\times\mathbf{B}]\right)\frac{\partial f_{\mathrm{el}}}{\partial \mathbf{p}} = 0,$$
$$\frac{\partial f_{\mathrm{i}}}{\partial t} + \mathbf{v}_{\mathrm{i}}\frac{\partial f_{\mathrm{i}}}{\partial \mathbf{r}} - Ze\left(\mathbf{E} + \frac{1}{c}[\mathbf{v}_{\mathrm{i}}\times\mathbf{B}]\right)\frac{\partial f_{\mathrm{i}}}{\partial \mathbf{p}} = 0. \qquad (5)$$

$f_{\mathrm{el}}$ and $f_{\mathrm{i}}$ are here the electron and ion distribution functions, $\mathbf{v}_{\mathrm{el}}$ and $\mathbf{v}_{\mathrm{i}}$ the velocities of the corresponding particles, and Z the ionic charge. The electrical charge and current densities are equal to

$$\rho = e\int d\mathbf{p}\,(f_{\mathrm{e}} - Zf_{\mathrm{i}}), \qquad \mathbf{j} = e\int d\mathbf{p}\,(\mathbf{v}_{\mathrm{el}}f_{\mathrm{el}} - Z\mathbf{v}_{\mathrm{i}}f_{\mathrm{i}}).$$

We can obtain the dielectric constant from the linearized transport equations, in which we retained in the last term only the equilibrium distribution function, as we assume that there is no constant magnetic field. Moreover, it is necessary to take retardation into account when we determine the dielectric constant. In that case, if we have at time $t_0$ a given non-equilibrium addition $\delta f(\mathbf{r}, \mathbf{p}, t_0)$ to the distribution function, we have at time t

$$\delta f_{\mathrm{el}}(\mathbf{r}, \mathbf{p}, t) = \delta f_{\mathrm{el}}(\mathbf{r} - \mathbf{v}_{\mathrm{el}}(t - t_0), \mathbf{p}, t_0)$$
$$-\frac{\partial f^0_{\mathrm{el}}}{\partial \mathbf{p}}e\int_{t_0}^{t} dt'\,\mathbf{E}(\mathbf{r} - \mathbf{v}_{\mathrm{el}}(t - t'), t'). \qquad (6)$$

Here $f^0_{\mathrm{el}}$ is the electron equilibrium distribution function. The solution of the transport equation for the ions has a similar form.

Assuming the interaction to be switched on adiabatically infinitely far back in time, we have from (6)

$$\delta f_{\mathrm{el}}(\mathbf{r}, \mathbf{p}, t) = -\frac{\partial f^0_{\mathrm{el}}}{\partial \mathbf{p}}e\int_{-\infty}^{t} dt'\,\mathbf{E}(\mathbf{r} - \mathbf{v}_{\mathrm{el}}(t - t'), t'). \qquad (7)$$

Using (3) and (7) we get

$$\varepsilon_{ij}(\omega, \mathbf{k}) = \delta_{ij} + \frac{4\pi e^2}{\omega}\int d\mathbf{p}\left\{\frac{v_{\mathrm{el}\,i}}{\omega - \mathbf{k}\mathbf{v}_{\mathrm{el}}}\frac{\partial f^0_{\mathrm{el}}}{\partial p_j} + Z^2\frac{v_{\mathrm{i}\,i}}{\omega - \mathbf{k}\mathbf{v}_{\mathrm{i}}}\frac{\partial f^0_{\mathrm{i}}}{\partial p_j}\right\}. \qquad (8)$$

The dielectric constant tensor (8) was obtained by us as a function of the real arguments $\omega$ and $\mathbf{k}$. In accordance with the fact that we are dealing with a retardation, the contour for integration over the momenta must be arranged such that the pole $\omega = (\mathbf{k}\cdot\mathbf{v})$ of the integrand on the right hand side of (8) is encircled from below.[10]

From (8) we have

$$\varepsilon(\omega) = 1 - \frac{4\pi e^2}{3\omega^2}\int d\mathbf{p}\left\{f^0_{\mathrm{el}}\frac{\partial \mathbf{v}_{\mathrm{el}}}{\partial \mathbf{p}} + Z^2 f^0_{\mathrm{i}}\frac{\partial \mathbf{v}_{\mathrm{i}}}{\partial \mathbf{p}}\right\},$$
$$r_{\mathrm{scr}}^{-2} = -4\pi e^2\int d\mathbf{p}\,\{f^{0\prime}_{\mathrm{el}} + Z^2 f^{0\prime}_{\mathrm{i}}\},$$
$$C = -\frac{\pi e^2}{2}\int d\mathbf{p}\left\{f^{0\prime}_{\mathrm{el}}v_{\mathrm{el}}\delta\left(\frac{\mathbf{k}\mathbf{v}_{\mathrm{el}}}{kv_{\mathrm{el}}}\right) + Z^2 f^{0\prime}_{\mathrm{i}}v_{\mathrm{i}}\delta\left(\frac{\mathbf{k}\mathbf{v}_{\mathrm{i}}}{kv_{\mathrm{i}}}\right)\right\}. \qquad (9)$$

We have taken it into account here that the equilibrium distribution functions are functions of the energy; the prime indicates a derivative with respect to the energy.

**4.** Let the electrons be ultrarelativistic. Their contribution to the dielectric constant will then be of the form

$$\delta\varepsilon_{\mathrm{el}\,ij}(\omega, \mathbf{k}) = \frac{4\pi e^2 c}{\omega}\int d\mathbf{p}\,\frac{\partial f^0_{\mathrm{el}}}{\partial p}\frac{p_i p_j}{p^2}\frac{1}{\omega - c\mathbf{k}\mathbf{p}/p}. \qquad (10)$$

We have then for the longitudinal and transverse dielectric constants

$$\delta\varepsilon^{l}_{\mathrm{el}}(\omega, k) = \frac{4\pi e^2}{ck^2}A\left\{1 + \frac{\omega}{2ck}\ln\left|\frac{\omega - ck}{\omega + ck}\right| + \frac{i\pi\omega}{4ck}\left(\frac{ck - \omega}{|ck - \omega|} + 1\right)\right\}, \qquad (11)$$

$$\delta\varepsilon^{tr}_{\mathrm{el}}(\omega, k) = \frac{\pi e^2}{ck\omega}A\left\{-\frac{2\omega}{ck} + \left[1 - \left(\frac{\omega}{ck}\right)^2\right]\ln\left|\frac{\omega - ck}{\omega + ck}\right| + \right.$$
$$\left. + \frac{i\pi}{2}\left[1 - \left(\frac{\omega}{ck}\right)^2\right]\left(\frac{ck - \omega}{|ck - \omega|} + 1\right)\right\},$$

$$A \equiv c\,(\partial N_{\mathrm{el}}/\partial\mu_{\mathrm{el}}) \equiv -\int d\mathbf{p}\,\partial f^0_{\mathrm{el}}/\partial p. \qquad (12)$$

In the case of a Boltzmann electron distribution $[(f \sim \exp(-cp/\kappa T_{\mathrm{el}})]$ we get

$$A = cN_{\mathrm{el}}/\kappa T_{\mathrm{el}}, \qquad (13)$$

where $N_{\mathrm{el}}$ is the number of electrons per unit volume,* $\kappa$ is Boltzmann's constant, and $T_{\mathrm{el}}$

---

*In the case of a quantum-mechanical system, the limit of the dielectric constant as $\omega/k \to 0$ contains terms $\sim(k/\omega)^2$, which lead to diamagnetism. One can easily understand this from the definition of the magnetic permeability[2] $\mu(\omega, k)$:

$$1 - \mu^{-1}(\omega, k) = (\omega^2/c^2k^2)(\varepsilon^{tr} - \varepsilon^{l}).$$

*In the case where there is an equilibrium number of electron-positron pairs, $N_{\mathrm{el}} = 0.183\,(\kappa T_{\mathrm{el}}/\hbar c)^3$.

the electron temperature. For the case where the electron gas is degenerate we have $A = 3N_{el}/p_0$, where $p_0 = (3\pi^2)^{1/3}\hbar N_{el}^{1/3}$ is the limiting momentum of the Fermi distribution.[*] Equations (11) and (12) are similar to the ones occurring in the theory of a degenerate nonrelativistic electron gas. The reason for this is that, both in the case of the ultrarelativistic gas and in the case of the nonrelativistic degenerate electron gas, the particles determining the dielectric constant have all the same velocity, the velocity of light in our case and the velocity on the Fermi surface in the case of a degenerate Fermi gas.

The limiting characteristics of $\epsilon(\omega)$, $r_{scr}^{-2}$, and C following from Eqs. (11) and (12) are of the form

$$\delta\varepsilon_{el}(\omega) = -\frac{4\pi e^2 c}{3\omega^2}A, \quad \delta(r_{scr}^{-2})_{el} = \frac{4\pi e^2}{c}A, \quad \delta C_{el} = \frac{\pi e^2}{4}A. \tag{14}$$

For nonrelativistic particles, and we consider the ions to be such particles, the contribution to the dielectric constant is well known to be

$$\delta\varepsilon_{i\,ij}(\omega, \mathbf{k}) = \frac{4\pi e^2 Z^2}{\omega M}\int dp\,\frac{p_i}{\omega - \mathbf{kp}/M}\frac{\partial f_i^0}{\partial p_j},$$

where M is the ionic mass. In particular we have for a Maxwell distribution of the ions

$$\delta\varepsilon_i^l(\omega, k) = \frac{\omega_{0i}^2}{k^2}\frac{M}{\varkappa T_i}\left\{1 + \frac{\omega}{k}\sqrt{\frac{M}{2\varkappa T_i}}\frac{1}{\sqrt{\pi}}\int\frac{dx e^{-x^2}}{x - (\omega/k)\sqrt{M/2\varkappa T_i}}\right\}, \tag{15}$$

$$\delta\varepsilon_i^{tr}(\omega, k) = \frac{\omega_{0i}^2}{k\omega}\sqrt{\frac{M}{2\varkappa T_i}}\frac{1}{\sqrt{\pi}}\int\frac{dx e^{-x^2}}{x - (\omega/k)\sqrt{M/2\varkappa T_i}}, \tag{16}$$

where $\omega_{0i}^2 = 4\pi e^2 Z^2 N_i/M$, and where the pole of the integrand is encircled from below.

From (15) and (16) we have the following equations which are analogous to Eqs. (14)

$$\delta\varepsilon_i(\omega) = -\frac{\omega_{0i}^2}{\omega^2}, \quad \delta(r_{scr}^{-2})_i = \frac{4\pi e^2 Z^2 N_i}{\varkappa T_i},$$

$$\delta C_i = \frac{\omega_{0i}^2}{4}\sqrt{\frac{M}{2\pi\varkappa T_i}}. \tag{17}$$

Comparing Eqs. (14) and (17) we see that if the electrons have a Boltzmann distribution, the extra contribution to $\epsilon(\omega)$ is determined by the electrons in each case where the condition $\kappa T_{el} \ll Mc^2$ is satisfied. In order that the same be true for the skin depth, it is necessary that the condition $\kappa T_{el} \ll \sqrt{Mc^2\kappa T_i}$ be satisfied. It is evident that this condition is violated when $T_{el} \gtrsim 10^3 T_i$. Finally, for the screening radius the situation is the same as in the nonrelativistic case, namely

$$r_{scr}^{-2} = (4\pi e^2/\varkappa T_{el})[1 + ZT_{el}/T_i].$$

This is due to the fact that in the nonrelativistic limit the screening is independent of the mass of the particles, but the difference in the relativistic case lies essentially in the dependence of the mass on the velocity. We note that the conditions under which the electromagnetic properties of the plasma are determined by the electrons or by the ions are completely similar for ultrarelativistic Fermi-Dirac electrons; we must only use $cp_0/3$ instead of $\kappa T_{el}$.

5. We turn now to a consideration of the propagation of electromagnetic waves in a relativistic plasma.

In a nonrelativistic isotropic plasma the motion of the particles and accordingly the change, reflecting this motion, of the spatial dispersion of the dielectric constant influences the propagation of transverse waves only weakly. In our case the particle velocity is very large and the part played by the spatial dispersion therefore increases. This is clear from the following relations for the transverse waves, obtained from (3) by assuming that the electron energy is small compared to the rest mass energy of the ions.[*]

$$\omega^2 = \frac{4}{3}\pi e^2 cA + \frac{4}{5}c^2k^2 \quad \text{if } \omega \gg ck, \tag{18}$$

$$\omega^2 = 2\pi e^2 cA + c^2k^2 \quad \text{if } \omega \to ck. \tag{19}$$

Indeed, in the case of Eq. (18), taking the motion of the particles into account changes the term proportional to $k^2$ by 20%. In the case of Eq. (19), however, the constant term is changed by a factor of one and a half by taking into account the spatial dispersion. Because the phase velocity of the transverse waves is greater than the velocity of light and is equal to it in the limiting case of infinitely short waves, the transverse waves are not damped. We can thus drop the imaginary parts when substituting (12) and (16) into (3).

We turn now to longitudinal waves. Two modes of natural vibrations, the so-called plasma and acoustical branches are possible, as in the case of a nonrelativistic plasma.[11] We consider first the plasma oscillations. In this case one can easily see from (4), (14), and (17) that in the long-wave case the frequency tends to a limit equal to[†]

$$\omega_0 = (4\pi e^2 A/3 + \omega_{0i}^2)^{1/2}. \tag{20}$$

---

[*] The dielectric constant of a degenerate relativistic electron gas was considered in a paper by Lindhard.[2]

[*] In the nonrelativistic case the equation

$$\omega^2 = \omega_{0\,el}^2 + c^2k^2, \text{ where } \omega_{0\,el}^2 = 4\pi e^2 N_{el}/m$$

corresponds to Eqs. (18) and (19).

[†] Assuming that the electron energy is small compared with the rest-mass energy of the ions, we have $\omega^2 = (4/3)\pi e^2 cA + (3/5)c^2k^2$ in the region $ck \ll \omega_0$.

It follows from this that as $k \rightarrow 0$ the phase velocity increases without limit.

It is well known that in the long-wave region, where the phase velocity is greater than the velocity of light, there is no damping.[4] As long as we can speak about ultrarelativistic electrons, i.e., as long as we can neglect the difference between their velocity and the velocity of light, the minimum phase velocity of the longitudinal plasma waves is also the same as the velocity of light. Indeed, we have in the short-wave limit ($kc \gg \omega_0$) from (4), (11), and (15);

$$\omega = ck\left\{1 + 2\exp\left[-\frac{ck^2}{2\pi e^2 A} - 2 + \frac{\omega_{0i}^2}{2\pi e^2 cA}\right]\right\}. \tag{21}$$

The damping is then, of course, also equal to zero. However, to be able to apply Eq. (21) to the case of a Boltzmann plasma, the electron temperature must satisfy the condition

$$\varkappa T_{\mathrm{el}} \geqslant mc^2 \ln (ck/\omega_0).$$

It is thus necessary for short wavelengths, where this condition is violated, to take into account the fact that the particle velocity is different from the velocity of light. In other words it is no longer possible to use Eq. (10), obtained for ultrarelativistic electrons.

Since, however, the average thermal velocity of the particles in an ultrarelativistic gas differs only very little from the velocity of light, the minimum phase velocity will also differ little from the light velocity. One can, namely, use (8) to verify that this difference is of the order of magnitude of $c(mc^2/\kappa T_{\mathrm{el}})^2$. It is also important that the number of electrons with velocities appreciably different from the average thermal velocity be very small, i.e., that there be a small spread in electron velocities. This leads to the fact that when the phase velocity of the plasma wave tends to its minimum value the damping turns out to be relatively small, namely $\gamma/\omega \sim (mc^2/\kappa T_{\mathrm{el}})^2$.

The second branch of longitudinal vibrations — acoustical waves — is only possible in a plasma because of the spatial dispersion of the dielectric constant. This should already be evident from the fact that the velocity of such waves can be small compared with the electron velocity. This last fact leads to the occurrence of damping caused by the electrons. The Cerenkov mechanism of damping of the oscillations in a plasma occurs when there is some group of particles for which the condition $(\mathbf{k} \cdot \mathbf{v}) = \omega$ is satisfied. In our case the electron velocity differs little from the light velocity; if, however, the sound velocity is small compared to the light velocity, only a small part of the electrons, moving nearly perpendicularly to the direction of the propagation of sound, will take part in the absorption of the vibrations. Similarly, if the phase velocity of the wave is appreciably larger than the average thermal velocity of the ions, only a small group of ions which have velocities much higher than the thermal ones will be involved in the absorption of sound. Under such circumstances where a small part of the particles in the plasma is involved in the absorption, one can expect the damping of sound to turn out to be relatively small.

If the electron velocities have a Boltzmann distribution the velocity of sound turns out to be small compared with the average velocity and at the same time large compared with the thermal velocity of the ions, when $Mc^2 \gg Z\kappa T_{\mathrm{el}} \gg \kappa T_{\mathrm{i}}$. We get then from (4), (11), and (15) for the velocity of sound

$$v_s = \omega/k = \sqrt{Z\varkappa T_{\mathrm{el}}/M}. \tag{22}$$

Equation (22) is the same as the corresponding formula for the sound velocity obtained in the nonrelativistic plasma theory (see reference 12). This is understandable, as the sound velocity in that case is independent of the electron mass.

If the electron distribution is a Fermi-Dirac one, the condition similar to those under which Eq. (22) is valid in the Boltzmann case is determined by the inequalities $Mc^2 \gg Zp_0c \gg \kappa T_{\mathrm{i}}$. We have then

$$v_s = \sqrt{Zp_0c/3M}. \tag{23}$$

The contributions from the electrons and the ions add up for the absorption of sound waves of a velocity determined by Eqs. (22) and (23). The electron part of the logarithmic decrement is connected with the sound frequency by the relation

$$\gamma_{\mathrm{el}} = \frac{\pi}{4}\frac{v_s}{c}\omega. \tag{24}$$

We note that such an absorption of sound in a plasma is very similar to the absorption of sound by electrons in a metal in the low-temperature region, which has been extensively studied recently both theoretically and experimentally.

The ionic part of the logarithmic decrement is determined by the expression

$$\gamma_{\mathrm{i}} = \omega\sqrt{\pi}\left(\frac{Mv_s^2}{2\varkappa T_{\mathrm{i}}}\right)^{3/2}\exp\left(-\frac{Mv_s^2}{2\varkappa T_{\mathrm{i}}}\right), \tag{25}$$

the structure of which shows that for this part we can essentially use the results of the nonrelativistic theory.[13]

We emphasize that to be able to apply Eqs. (24) and (25) it is also necessary that the Cerenkov dissipation of the sound wave be the basic one, as the entire foregoing analysis does not take into account the usual dissipation mechanism, which is connected with collisions.

---

[1] Yu. L. Klimontovich, Dokl. Akad. Nauk SSSR **87**, 927 (1952).

[2] J. Lindhard, Kgl. Danske Videnskab. Selskab, Mat.-fys. Medd. **28**, No 8 (1954).

[3] S. T. Belyaev and G. I. Budker, Dokl. Akad. Nauk SSSR **107**, 807 (1956), Soviet Phys.-Doklady **1**, 218 (1956).

[4] P. C. Clemmow and A. J. Willson, Proc. Roy. Soc. (London) **A237**, 117 (1956).

[5] P. C. Clemmow and A. J. Willson, Proc. Cambridge Phil. Soc. **53**, 222 (1957).

[6] V. M. Galitskiĭ and A. B. Migdal, Физика плазмы (Plasma Physics) **1**, Acad. Sci. Press, (1958) p. 161.

[7] B. A. Trubnikov, Физика плазмы (Plasma Physics) **3**, 1958, p. 104.

[8] B. L. Ginzburg, JETP **34**, 1593 (1958), Soviet Phys. JETP **7**, 1096 (1958).

[9] L. D. Landau, JETP **35**, 97 (1958), Soviet Phys. JETP **8**, 70 (1959).

[10] L. D. Landau, JETP **16**, 574 (1946), J. Phys. (U.S.S.R.) **10**, 25 (1946).

[11] V. P. Silin, JETP **23**, 649 (1952).

[12] G. V. Gordeev, JETP **27**, 19 (1954).

[13] L. M. Kovrizhnykh, JETP **37**, 1692 (1959), Soviet Phys. JETP **10**, 1198 (1960).

Translated by D. ter Haar
301

SOVIET PHYSICS JETP VOLUME 11, NUMBER 5 NOVEMBER, 1960

# *ROTATION OF THE SPIN OF A RELATIVISTIC PARTICLE WITH A MAGNETIC MOMENT MOVING IN AN EXTERNAL FIELD*

V. S. POPOV

Submitted to JETP editor December 15, 1959

J. Exptl. Theoret. Phys. (U.S.S.R.) **38**, 1584-1588 (May, 1960)

The problem of the rotation of the spin is solved for a relativistic particle that has a magnetic dipole moment and moves in an external electromagnetic field. The angular velocity of the rotation of the spin is determined in the rest system of the particle, which is rigidly fixed to its trajectory (analog of the Frenet axis system for a four-dimensional curve). The results obtained are significant for experiments made to measure the magnetic and electric moments of elementary particles.

LET us consider the problem of the change of the polarization of a particle with arbitrary spin s and magnetic dipole moment $\mu = g(e\hbar/2mc)\mathbf{s}$ under the action of an external electromagnetic field. It is assumed that the field is a macroscopic field, i.e., that the motion of the particle in the field obeys the laws of classical mechanics:[1]

$$du_\mu/d\tau = (e/mc)\, F_{\mu\nu}u_\nu. \tag{1}$$

The spin operator is uniquely defined only with respect to spatial rotations in the rest system, and various relativistic generalizations of this operator are possible. We shall use the spin pseudovector $\hat{s}_\mu = -\frac{1}{2} i\epsilon_{\mu\nu\lambda\rho}M_{\nu\lambda}p_\rho$,[2] which coincides with the nonrelativistic spin operator in the rest system of the particle. For the average value of $\hat{s}_\mu$ one can obtain the equation (cf. reference 3)

$$ds_\mu/d\tau = (e/mc)\left[\tfrac{1}{2}gF_{\mu\nu}s_\nu + \left(\tfrac{1}{2}g - 1\right)u_\mu F_{\alpha\beta}u_\alpha s_\beta\right], \tag{2}$$

where g is the gyromagnetic ratio and $u_\mu$ is the four-velocity. The polarization is essentially a three-dimensional vector defined in the rest system of the particle. Therefore after solving the equation (2) one must translate the four-vector $s_\mu$ into the rest system. The direct solution of the equation (2) is cumbersome even in the simplest case of a uniform magnetic field. Therefore we shall find the angular velocity of the rotation of the spin directly in the rest system.

Let us introduce four axes $\eta^\alpha$ ($\alpha = 0, 1, 2, 3$) rigidly connected with the trajectory (which is regarded as a curve in the four-dimensional Minkowski space). The four unit vectors $\eta^\alpha$ are the four-dimensional analog of the Frenet axes. They obey the equations

$$d\eta^\alpha_\mu/d\tau = \varkappa_{\alpha\beta}\eta^\beta_\mu, \qquad \eta^\alpha_\mu\eta^\beta_\mu = g_{\alpha\beta};$$
$$g_{\alpha\beta} = 0 \quad (\alpha \neq \beta), \qquad g_{00} = -1, \qquad g_{11} = g_{22} = g_{33} = 1. \tag{3}$$

We shall construct the vectors $\eta^\alpha$ in the following way. Suppose the vectors $u_\mu$, $\dot{u}_\mu$, $\ddot{u}_\mu$, $\dddot{u}_\mu$ are linearly independent (the dot denotes differentiation with respect to the proper time $\tau$). Then we set

$$\eta^\alpha_\mu = \sum_{\beta=0}^{\alpha} C_{\alpha\beta}d^\beta u_\mu/d\tau^\beta,$$

where the coefficients $C_{\alpha\beta}$ are found from the conditions of orthogonality and normalization. It follows from this that $\kappa_{\alpha\beta} \neq 0$ only for $\beta = \alpha \pm 1$, i.e., the curvature tensor has the form

$$\varkappa_0 = \varkappa_{01} = \varkappa_{10}, \qquad \varkappa_1 = \varkappa_{12} = -\varkappa_{21},$$
$$\varkappa_2 = \varkappa_{23} = -\varkappa_{32}$$

(the other components of the tensor $\kappa_{\alpha\beta}$ are all zero). For the unit vectors $\eta^\alpha_\mu$ we get the following expressions:

$$\eta^0_\mu = u_\mu, \quad \eta^1_\mu = C_1\dot{u}_\mu, \quad \eta^2_\mu = C_2\left(\ddot{u}_\mu - \tfrac{1}{2}\dot{p}p^{-1}\dot{u}_\mu - pu_\mu\right),$$
$$\eta^3_\mu = C_3\varepsilon_{\mu\nu\lambda\rho}u_\nu\dot{u}_\lambda\ddot{u}_\rho, \tag{4}$$

where

$$C_1 = p^{-1/2}, \quad C_2 = \left(p^2 + q - \tfrac{1}{4}\dot{p}^2p^{-1}\right)^{-1/2}, \quad C_3 = -iC_1C_2;$$
$$p = \dot{u}_\mu\dot{u}_\mu, \qquad q = \ddot{u}_\mu\ddot{u}_\mu. \tag{5}$$

Substituting Eq. (5) in Eq. (3), we find the connection of $C_i$ with the curvatures $\kappa_{\alpha\beta}$:

$$C_1 = \varkappa_0^{-1}, \quad C_2 = \varkappa_0^{-1}\varkappa_1^{-1}, \quad C_3 = -i\varkappa_0^{-2}\varkappa_1^{-1}. \tag{6}$$

The spin four-vector $s_\mu$ can be expressed in terms of the vectors $\eta^i_\mu$ ($i = 1, 2, 3$), since $s_\mu u_\mu = 0$. Let

$$s_\mu = \sum_{i=1}^{3} \sigma_i \eta_\mu^i;$$

it follows from Eq. (2) that

$$d\boldsymbol{\sigma}/d\tau = [\boldsymbol{\Omega}\times\boldsymbol{\sigma}],$$

where

$$\Omega_{ij} = -\varkappa_{ij} - g\,(e/2mc)\,F_{\mu\nu}\eta_\mu^i\eta_\nu^j, \qquad (7)$$

and $\boldsymbol{\Omega}$ is the vector of the angular velocity of the rotation of the polarization $\boldsymbol{\sigma}$ in the rest system we have chosen (the system of axes $\eta^i$). From Eqs. (4) and (6) it is clear that $k_{ij}$ and $\eta_\mu^i$ can be expressed in terms of the four-velocity $u_\mu$ and its derivatives, which are determined by the field $F_{\mu\nu}$. Therefore to find $\boldsymbol{\Omega}$ we need first to determine the trajectory of the particle, i.e., to solve (1).

Let us consider the case in which $\mathbf{E} = 0$ but $\mathbf{H}$ is an arbitrary function of the coordinates (and the time). Using the equations of motion (1), we can obtain the following expression for the components of $\boldsymbol{\Omega}$:

$$\Omega_1 = u_0\Delta^{-2}\,[\dot{\varepsilon}\cos\theta + (1+\varepsilon\sin\theta)\,\dot{\theta}],$$

$$\Omega_2 = -\tfrac{1}{2}\,g\Omega_L\Delta^{-1}u_0\varepsilon\,\mathrm{tg}\,\theta,$$

$$\Omega_3 = \left(\tfrac{1}{2}\,g - 1\right)\Omega_L\Delta - \tfrac{1}{2}\,g\Omega_L\Delta^{-1}\varepsilon\,(\varepsilon + \sin\theta); \qquad (8)$$

here

$$\varepsilon = \frac{mc}{e}\,\frac{[\dot{\mathbf{H}}\times\mathbf{H}]\,\boldsymbol{\nu}}{H^3\cos^2\theta}, \quad \Omega_L = \left|\frac{eH}{mc}\right|,$$

$$\Delta = (1 + u^2\cos^2\theta + 2\varepsilon\sin\theta + \varepsilon^2)^{1/2},$$

$\boldsymbol{\nu}$ is the direction of the velocity of the particle, and $\theta$ is the "pitch angle" of the trajectory, defined by the condition $\boldsymbol{\nu}\cdot\mathbf{H} = \sin\theta$. It is obvious that $\epsilon$ is a parameter that characterizes the degree of inhomogeneity of the magnetic field.

Starting from the formulas (5), we can determine the positions of the unit vectors $\eta_\mu^i$ in the laboratory coordinate system (l. s.) at each instant of time:

$$\eta_\mu^1 = \{\varkappa_0^{-1}\,[\boldsymbol{\Omega}_L\times\mathbf{u}];\,0\},$$

$$\eta_\mu^2 = \varkappa_0^{-1}\varkappa_1^{-1}\{[\dot{\boldsymbol{\Omega}}_L\times\mathbf{u}] + (\boldsymbol{\Omega}_L\times\mathbf{u})\,\boldsymbol{\Omega}_L - (1 + u^2\cos^2\theta)\,\Omega_L^2\mathbf{u}$$

$$- ([\boldsymbol{\Omega}_L\times\mathbf{u}]\,[\dot{\boldsymbol{\Omega}}_L\times\mathbf{u}]/|\,[\boldsymbol{\Omega}_L\times\mathbf{u}]\,|^2)\,[\boldsymbol{\Omega}_L\times\mathbf{u}];\;\; -i\varkappa_0^2u_0\},$$

$$\eta_\mu^3 = \{-u_0\Omega_L\varkappa_1^{-1}(\xi\mathbf{H}/H + \varepsilon\mathbf{u}/u);\;\; -iu\Omega_L\varkappa_1^{-1}(\varepsilon + \sin\theta)\}. \qquad (9)$$

The curvatures $\kappa_0$, $\kappa_1$ that appear here are given by

$$\varkappa_0 = |\,[\boldsymbol{\Omega}_L\times\mathbf{u}]\,|, \quad \varkappa_1 = \Omega_L\Delta; \quad \xi = e/|e|, \quad \boldsymbol{\Omega}_L = -(e/mc)\,\mathbf{H}.$$

In a uniform magnetic field we must set $\epsilon = 0$, $\theta = \mathrm{const}$, so that we have

$$\boldsymbol{\Omega} = \left\{0,\,0,\,\left(\tfrac{1}{2}\,g - 1\right)\Omega_L\sqrt{1 + u^2\cos^2\theta}\right\}.$$

The electron then moves in a spiral with a constant pitch angle $\theta$ ($u_z = u\sin\theta$, if the $z$ axis is the axis of the spiral). It follows from Eq. (9) that the vectors $\eta^i$ are in fixed positions with respect to the accompanying Frenet vectors $\mathbf{t}$, $\mathbf{n}$, $\mathbf{b}$ of the electron trajectory. In the rest system defined by the axes $\eta^i$ the polarization vector precesses around the axis $\eta^3$, and the angular velocity is zero for $g = 2$. For the vector $\eta^3$ in the laboratory system we have

$$\eta_\mu^3 = \left\{\frac{u_0}{\sqrt{1 + u^2\cos^2\theta}}\,(-\mathbf{t}\sin\theta + \mathbf{b}\cos\theta);\right.$$

$$\left. -i\,\frac{u\sin\theta}{\sqrt{1 + u^2\cos^2\theta}}\right\}.$$

If the polarization was longitudinal initially (at $t = 0$), then after a certain time it becomes transverse. This time is given by

$$T = \frac{2u_0}{(g/2 - 1)\,\Omega_L\sqrt{1 + u^2\cos^2\theta}}$$

$$\times \arcsin\left(\sqrt{1 + u^2\cos^2\theta}/\sqrt{2}\,u_0\cos\theta\right)$$

(from the point of view of clocks in the laboratory system).

The polarization will be longitudinal at the times

$$2\pi n\left[\left(\tfrac{1}{2}\,g - 1\right)\Omega_L\sqrt{1 + u^2\cos^2\theta}\right]^{-1} \qquad (n = 0, 1, 2, \ldots)$$

and transverse at the times

$$2\pi n\left[\left(\tfrac{1}{2}g - 1\right)\Omega_L\sqrt{1 + u^2\cos^2\theta}\right]^{-1} \pm T.$$

Assuming $u \ll 1$, $\theta \ll 1$ and neglecting quantities of the orders $u^2\theta^2$ and $\theta^4$, we get

$$T \approx (\pi/(g-2)\,\Omega_L)\,(1 + 0.64\theta^2),$$

i.e., in the nonrelativistic region the time of transition from longitudinal to transverse polarization does not depend on the speed of the particle. Measurement of this time gives a possibility for determining the gyromagnetic ratio g.[4] If high accuracy is to be obtained the angle of rotation of the spin must be large. One achieves this by bounding the region of uniform field by magnetic traps at its two ends, so that the particle is reflected and passes back and forth between the traps many times, while being essentially in a uniform field. Then, however, one must examine the additional rotation of the spin on reflection from a trap, and the effects of unavoidable inhomogeneities of the field. This can be done conveniently by starting with the equations (8).

As is well known, the existence of an electric dipole moment of an elementary particle is in contradiction with CP or T invariance. With a slight modification, the experiment considered here gives a possibility for an experimental test of the vanishing of the electric moment.[4] Let us write down the equation of motion of the spin for a particle that has both magnetic and electric dipole moments:

$$\frac{ds_\mu}{d\tau} = \frac{e}{mc}\left\{\left(\frac{g}{2}F_{\mu\nu} + \frac{f}{2}\widetilde{F}_{\mu\nu}\right)s_\nu + u_\mu\left[\left(\frac{g}{2} - 1\right)F_{\alpha\beta} + \frac{f}{2}\widetilde{F}_{\alpha\beta}\right]u_\alpha s_\beta\right\}. \qquad (10)$$

Equation (10) is the only possible equation linear in $s_\mu$ that together with Eq. (1) satisfies the conditions

$$d(s_\mu u_\mu)/d\tau = d(s_\mu^2)/d\tau = 0$$

In the nonrelativistic case Eq. (10) has the form

$$ds/dt = -(e/2mc)\{g[\mathbf{H}\times\mathbf{s}] + f[\mathbf{E}\times\mathbf{s}]\},$$

from which it is clear that the magnetic and electric moments of the particle are $\mu = g(e\hbar/2mc)\mathbf{s}$, $\mathbf{p} = f(e\hbar/2mc)\mathbf{s}$. The tensor $\widetilde{F}_{\mu\nu}$ that appears in Eq. (10) is the dual tensor of the electromagnetic field:

$$\widetilde{F}_{\mu\nu} = \tfrac{1}{2} i\varepsilon_{\mu\nu\lambda\rho}F_{\lambda\rho}.$$

Let the unit vectors $\eta_\mu^\alpha$ be determined as before from Eqs. (5) and (6). The angular velocity of the rotation of the spin in the axes $\eta^i$ is given by

$$\Omega_{ij} = -[\varkappa_{ij} + (e/2mc)(gF_{\mu\nu} + f\widetilde{F}_{\mu\nu})\eta_\mu^i\eta_\nu^j]. \qquad (11)$$

We get from this for the case of a uniform magnetic field

$$\Omega = \{-\tfrac{1}{2}f\Omega_L u\cos\theta,\ 0,\ (\tfrac{1}{2}g - 1)\Omega_L\sqrt{1 + u^2\cos^2\theta}\}.$$

The electric dipole moment leads to the appearance of a component $\Omega_1$, i.e., to an additional rotation of the spin around the principal normal **n** of the Frenet axis system. If, however, $|f| \ll |g/2 - 1|$, the component $\Omega_3$ that comes from the magnetic moment is much larger than $\Omega_1$ and makes measurement of f difficult. A method in which the rotation of the spin because of the anomalous magnetic moment is compensated seems more attractive.[4]

For this purpose one has only to apply in addition to the uniform magnetic field (along the z axis) a radial electric field $E_r = a/r$ (in a cylindrical coordinate system). It can be shown that as before it is possible for the particle to move along a spiral, but with altered frequency and radius. The positions of the axes $\eta^i$ in the cylindrical coordinate system are then given by the formulas

$$\eta^1 = \{-1, 0, 0; 0\},$$

$$\eta^2 = \{0, \xi\Delta, -\Delta^{-1}u^2\sin\theta\cos\theta; -i\Delta^{-1}u_0 u\cos\theta\},$$

$$\eta^3 = \{0, 0; -\xi u_0\Delta^{-1}; -i\xi\Delta^{-1}u\sin\theta\},$$

$$\Delta = (1 + u^2\cos^2\theta)^{1/2}, \quad \xi = e/|e|.$$

Here we have taken the axes in the order r, $\varphi$, z, t, and the z axis is directed along the magnetic field H.

In these axes the angular velocity of the spin precession is

$$\Omega = \left\{-f\frac{\Omega_L u\cos\theta}{2(1+x)},\ g\Omega_L\xi\frac{x}{1+x}\frac{u^2\sin\theta\cos\theta}{2u_0\Delta},\ \times\frac{\Omega_L}{1+x}\left[\left(\frac{g}{2} - 1\right)\Delta + \frac{gx}{2\Delta}\right]\right\},$$

where $x = (ea/mc)(u_0/u^2\cos^2\theta)$. If a is measured in volts, then $x = 1.96 \cdot 10^{-6}au_0/u^2\cos^2\theta$. By a suitable choice of the electric field we can make the component $\Omega_3$ equal to zero; to do this we must choose $x = x_0 = -(g-2)g^{-1}(1 + u^2\cos^2\theta)$. On each reflection from a trap the angle $\theta$ changes sign. We note that $\Omega_1$ is an even function of $\theta$, and $\Omega_2$ is an odd function of $\theta$; therefore after one complete cycle of motion between the traps the rotation of the spin comes only from the component

$$\Omega_1 = -f\frac{\Omega_L u\cos\theta}{2(1+x_0)} = -\frac{fg}{4}\frac{\Omega_L u\cos\theta}{1 - (g/2 - 1)u^2\cos^2\theta}.$$

Measurement of the spin precession frequency $\Omega_1$ offers a method for determining the gyroelectric ratio f.

In conclusion I express my gratitude to V. V. Vladimirskiĭ for suggesting this topic and for a discussion of the results, and also to A. S. Shapiro for his interest in the work.

---

[1] L. D. Landau and E. M. Lifshitz, Теория поля, (The Classical Theory of Fields), Gostekhizdat, 1948. [Transl. Addison-Wesley, 1951]

[2] Yu. M. Shirokov, JETP 21, 748 (1951).

[3] Bargmann, Michel, and Telegdi, Phys. Rev. Letters 2, 435 (1959).

[4] Nelson, Shupp, Pidd, and Crane, Phys. Rev. Letters 2, 492 (1959).

Translated by W. H. Furry
302

SOVIET PHYSICS JETP VOLUME 11, NUMBER 5 NOVEMBER, 1960

# *SLOWING-DOWN TIME OF NONEQUILIBRIUM CURRENT CARRIERS IN SEMICONDUCTORS*

O. N. KROKHIN and YU. M. POPOV

P. N. Lebedev Physics Institute, Academy of Sciences, U.S.S.R.

Submitted to JETP editor December 17, 1959

J. Exptl. Theoret. Phys. (U.S.S.R.) **38**, 1589-1592 (May, 1960)

Slowing-down times are derived for electrons and holes which are not in thermal equilibrium with the semiconductor lattice. It is shown that account of degeneracy does not affect the slowing-down time appreciably.

A determination of the slowing-down time of nonequilibrium current carriers in semiconductors is of prime importance in the design of quantum-mechanical semiconductor generators and amplifiers.[1] Negative losses are possible in a semiconductor only if the time of production of a negative temperature in the semiconductor (slowing-down time) is shorter than the lifetime of the fast electrons and holes produced by the external excitation. We consider the nonequilibrium (fast) carriers to be electrons* (holes) having an initial energy $\epsilon_0$ considerably in excess of the average thermal or degeneracy energy (if the gas is degenerate), but not exceeding the threshold energy $\epsilon_i$ of impact ionization of the valence band. In crystals that are sufficiently pure and regular, the slowing down of the electron is due to scattering by lattice vibrations, i.e., the impurities and imperfections can be disregarded in the slowing down.

We start with a derivation of the kinetic equation for the distribution function of the electrons in the crystal, with allowance for the Fermi degeneracy of the electron gas, since it becomes significant in the final stages of the slowing down. We leave out of the kinetic equation the term that describes collisions between electrons, since such a process does not lead directly to the process of interest to us, the reduction in the average electron energy.

The kinetic equation for f(p) has the form (see reference 2)

$$\frac{\partial f(\mathbf{p})}{\partial t} = \sum_{\mathbf{q}} \{ -\rho_a(\mathbf{q}) f(\mathbf{p}) [1 - f(\mathbf{p}+\mathbf{q})] + \rho_e(\mathbf{q}) f(\mathbf{p}+\mathbf{q}) [1 - f(\mathbf{p})] - \rho_e(\mathbf{q}) f(\mathbf{p}) [1 - f(\mathbf{p}-\mathbf{q})] + \rho_a(\mathbf{q}) f(\mathbf{p}-\mathbf{q}) [1 - f(\mathbf{p})] \}. \qquad (1)$$

Here $\rho_e$ and $\rho_a$ are the probabilities of emission and absorption of a phonon with momentum q and energy $\hbar\omega_q$. We consider the slowing down of electrons in the absence of an electric field. Naturally, in this case $f(\mathbf{p}) \equiv f(\epsilon)$, where $\epsilon = p^2/2m$ is the electron energy and m the electron effective mass.

Following the usual procedure and changing from summation over **q** to integration over d**q**, we expand the integrals in the right half of (1) in powers of the small quantity $\hbar\omega_q/\epsilon(p)$, and obtain*

$$\frac{\partial f(\varepsilon)}{\partial t} = \frac{1}{p} \frac{\partial}{\partial \varepsilon} \left\{ G(\varepsilon) \left[ f(\varepsilon)(1 - f(\varepsilon)) + \eta(\varepsilon) \frac{\partial f(\varepsilon)}{\partial \varepsilon} \right] \right\},$$

$$G(\varepsilon) = \frac{Vm}{2\pi\hbar^4} \int_0^{2p} B(q)\, \hbar\omega_q q\, dq,$$

$$G(\varepsilon)\, \eta(\varepsilon) = \frac{Vm}{4\pi\hbar^4} \int_0^{2p} B(q) (\hbar\omega_q)^2 (2n_q + 1)\, q\, dq, \qquad (2)$$

where B(q) is the square of the electron-phonon interaction matrix element, $n_q$ is the number of phonons of energy $\hbar\omega_q$, and V is the volume of the crystal.

The time of collision between the electron and the lattice, $\tau$, is given by

$$\tau^{-1} = \frac{v}{l} = \frac{Vm}{4\pi\hbar^4 p^3} \int_0^{2p} B(q) (2n_q + 1)\, q^3 dq, \qquad (3)$$

where v is the electron velocity and $l$ is the mean free path. Multiplying (2) by $\epsilon\rho(\epsilon)$, where $\rho(\epsilon)$ is the density of electron states with energy $\epsilon$

$$\rho(\varepsilon) = 4\pi (2\pi\hbar)^{-3} V (2m)^{3/2} \varepsilon^{1/2},$$

and integrating over the energy of the electron, we obtain

$$\frac{dE}{dt} = -\int_0^{\infty} \frac{\rho(\varepsilon)}{p} G(\varepsilon) \left\{ f(\varepsilon)[1 - f(\varepsilon)] + \eta(\varepsilon) \frac{\partial f}{\partial \varepsilon} \right\} d\varepsilon. \qquad (4)$$

---

*We shall discuss henceforth only conduction electrons, although all the results are equally valid for the holes of the valence band.

*In the absence of degeneracy, (2) becomes identical with the equation obtained by Davydov, Stratton, and Keldysh.[3]

Here E is the average electron energy. The first term in the integral of (4) describes the energy lost by the electrons through spontaneous emission of phonons. The second term describes the diffusion of the electrons in energy space. As can be seen from what follows, in the scattering of an electron by the acoustic lattice vibrations, allowance for the second term in the integral of (4) leads to a logarithmic singularity in the time of establishment of equilibrium between the electrons and the lattice. Confining ourselves to an examination of the slowing down of electrons to energies exceeding the lattice temperature, we disregard for the time being the second term of (4).

We consider the slowing down of an individual electron, without allowance for degeneracy. In this case

$$f(\varepsilon)\,\rho(\varepsilon)=\delta(\varepsilon-E). \tag{5}$$

1. For acoustic phonons we have[4]

$$G(\varepsilon)=16m^3C^2\varepsilon^2/9\pi\hbar^4Mn_0,\quad 1/\tau=4C^2m^2kTv/9\pi\hbar^4Mn_0u^2, \tag{6}$$

where $C^2$ is the interaction constant, n the density of the lattice atoms, M the mass of the lattice atom, u the velocity of sound, T the lattice temperature, and k Boltzmann's constant. Using (5) and (6), we obtain from (4)

$$dE/dt=-a_0E^{3/2}. \tag{7}$$

expressed in terms of the free path $l_{ac}$ in scattering by acoustic lattice vibrations, $a_0$ is given by

$$a_0=2\,(2m)^{1/2}u^2/l_{\text{ac}}(T)\,kT. \tag{8}$$

The time to slow down from an energy $E_0$ to E is

$$t=(2/a_0)\,(E^{-1/2}-E_0^{-1/2}). \tag{9}$$

We note that the slowing-down time t depends on two constants of the semiconductor — mobility and velocity of sound.

When $E_0 \gg E$, the time to slow down to energies corresponding to T ~ 300°K is $t \sim 4.5\times10^{-10}$ sec for n-type germanium (w ~ 3600 cm$^2$. $^{-1}$sec$^{-1}$ at room temperature and $u \sim 4.94\times10^5$ cm/sec), and $t \sim 5.1\times10^{-11}$ sec for n-type silicon (w ~ 1200 cm$^2$ v$^{-1}$ sec$^{-1}$, $u \sim 8.5\times10^5$ cm/sec).

The ratio of the time to slow down from $E_0$ to E, with $E_0 \gg E$, in two differenct semiconductors x and y is

$$t_x/t_y=w_xu_y^2/w_yu_x^2,$$

where w is the mobility.

2. We proceed to examine the slowing down of a fast electron by the optical lattice vibrations of a valence simiconductor. In this case (2) and (4) hold when the electron energy $E \gg \hbar\omega_0$, where $\hbar\omega_0$ is the energy of the optical phonon ($\hbar\omega_0 \approx kT_D$, where $T_D$ is the Debye temperature).

Then[4]

$$G(\varepsilon)=D^2K^2m^2\varepsilon/\pi\hbar^2Mn_0,\quad \tau^{-1}=D^2K^2m^2v/2\pi\hbar^4Mn_0\hbar\omega_0, \tag{10}$$
$$dE/dt=-(K^2D^2m^{3/2}/\sqrt{2}\pi n_0M\hbar^2)\,E^{1/2},$$

where K is the reciprocal-lattice vector, and $D^2$ is the constant of interaction with the optical phonons, analogous to $C^2$. The time to slow down from $E_0$ to E is

$$t_{\text{op}}=(2^{3/2}\pi Mn_0\hbar^2/K^2D^2m^{3/2})\,(E_0^{1/2}-E^{1/2}). \tag{11}$$

Comparison of the time of slowing down by optical and acoustical phonons yields, for $C^2 \approx D^2$,

$$t_{\text{op}}/t_{\text{ac}}\approx mu^2/kT_D\approx10^{-2}.$$

Negative temperatures can be produced in the semiconductor only when the electrons of the conduction band and the holes of the valence band become degenerate as they are slowed down by the crystal lattice. As is well known, the degeneracy is connected with the temperature (average energy) and density of the electron gas. Reduction of the average electron-gas energy to low values increases greatly the slowing-down time, so that the electrons can recombine prior to production of the negative temperature. It is therefore sensible to confine oneself to not too low average electron energies, but to increase their density.* As shown by Fröhlich and Paranjape,[2] the exchange energy is more intense in inter-electron collisions than in collisions with acoustic phonons, even at an electron density $n \approx 10^{14}$cm$^{-3}$ (when $T < T_D$ and $\epsilon < kT_D$, the interaction with the optical phonon is insignificant).

Thus, at the electron densities necessary to obtain negative temperatures, the form of the distribution function can be assumed known:

$$f(\varepsilon)=(e^{(\varepsilon-\mu)/k\Theta}+1)^{-1}, \tag{12}$$

where $\mu$ is the Fermi level and $\Theta$ the temperature of the electron gas. The slowing-down process becomes a reduction in the temperature $\Theta$ to the lattice temperature T. We have determined earlier the electron slowing-down time without account of degeneracy or of the second term of the right half of (4). We now obtain from (4) the time required for the electron gas temperature to change from $\Theta_0$ to $\Theta$, taking interaction with acoustical phonons only into account.

Using (12), we obtain in the usual manner from (4)

---

*The electron density need, however, not yield a negative dielectric constant in the frequency range of interest.

$$\partial E/\partial t = -2a_0(\Theta - T)\overline{E^{1/2}},$$

$$\overline{E^{1/2}} = \int_0^\infty \varepsilon^{1/2}\rho(\varepsilon) f(\varepsilon)\, d\varepsilon. \tag{13}$$

Equation (13) is a differential equation for $\Theta(t)$ and can be integrated in terms of elementary functions in the case of sufficiently strong degeneracy, when we can put $\mu/k\Theta \gg 1$. Applying in this case the usual procedure of expanding the integrals[5] for $E$, $\overline{E^{1/2}}$ and $\mu$, we obtain

$$\Theta\partial\Theta/\partial t = -(3a_0/k\pi^2\mu_0^{1/2})(\Theta - T)\left[\mu_0^2 + \tfrac{1}{6}\pi^2k^2\Theta^2\right],$$

$$2m\mu_0 = (\pi\hbar)^2(3n/\pi)^{2/3}. \tag{14}$$

Integrating (14) we obtain

$$t = \frac{k\pi^2}{3a_0\mu_0^{3/2}}\left(1 + \frac{\pi^2k^2T^2}{6\mu_0^2}\right)^{-1}\left\{T \ln \frac{(\Theta_0 - T)(1 + \pi^2k^2\Theta^2/6\mu_0^2)^{1/2}}{(\Theta - T)(1 + \pi^2k^2\Theta_0^2/6\mu_0^2)^{1/2}} + \frac{\sqrt{6}\mu_0}{\pi k}\left[\tan^{-1}\left(\frac{\pi k}{\sqrt{6}\mu_0}\Theta_0\right) - \tan^{-1}\left(\frac{\pi k}{\sqrt{6}\mu_0}\Theta\right)\right]\right\}. \tag{15}$$

The first term in the bracket of (15), which results from allowance for the second term in the right half of (4), does logarithmically to infinity as $\Theta \to T$. This is equivalent to an infinite time to establish equilibrium between the electrons and the lattice. When $\Theta \gg T$, the logarithm in (15) can be neglected, and the slowing-down time becomes

$$t \approx (k\pi^2/3a_0\mu_0^{3/2})(\Theta_0 - \Theta). \tag{16}$$

In comparing the slowing-down time with and without allowance for degeneracy [see Eq. (9)], it is convenient to replace the temperature in (16) by the average electron energy $\epsilon$, hence $(\Theta_0 \gg \Theta)$

$$t \approx (2\pi/5a_0\varepsilon^{1/2})(\varepsilon_0/\varepsilon - 1)^{1/2},$$

$$\varepsilon \approx \tfrac{3}{5}\mu_0, \quad \varepsilon_0 \approx \tfrac{3}{5}\mu_0\left(1 + \tfrac{5}{12}\pi^2k^2\Theta_0^2/\mu_0^2\right).$$

In this case, in spite of the different forms of (9) and (16), the times are of the same order of magnitude.

Let us point out that there is no need for considering the slowing down of a degenerate electron gas by optical phonons, for in the cases of interest to us the average electron energy at which degeneracy becomes important is less than $\hbar\omega_0$. Thus, the electron gas slows down in a semiconductor in two stages: first by the optical lattice vibrations to energies $\sim\hbar\omega_0$, in a short time, given by (11), and then by the acoustic vibrations in a considerably longer times, in accordance with (9) and (16). Consequently, the time required to produce negative temperatures is determined essentially by the slowing-down of the electrons from energies $\hbar\omega_0$ to energies corresponding to the necessary degree of degeneracy with allowance for interactions with acoustic lattice vibrations only.

In conclusion, the authors are grateful to N. G. Basov for discussing the result of this work and for valuable remarks.

---

[1] Basov, Vul, and Popov, JETP **37**, 587 (1959), Soviet Phys. JETP **10**, 416 (1960).

[2] H. Frohlich and B. V. Paranjape, Proc. Phys. Soc. **B69**, 21 (1956).

[3] B. I. Davydov, JETP **7**, 1069 (1937). R. Stratton, Proc. Roy. Soc. **242**, 355 (1957). L. V. Keldysh, JETP **37**, 713 (1959), Soviet Phys. JETP **10**, 509 (1960).

[4] F. Seitz, Phys. Rev. **73**, 549 (1948).

[5] L. D. Landau and E. M. Lifshitz, Статистическая физика (Statistical Physics), M-L., Gostekhizdat, 1951.

Translated by J. G. Adashko
303

# *SINGLE-PHOTON ANNIHILATION AND ELECTRON-PAIR CREATION IN A MEDIUM*

G. S. SAAKYAN

Erevan State University

Submitted to JETP editor December 16, 1959

J. Exptl. Theoret. Phys. (U.S.S.R.) **38**, 1593-1596 (May, 1960)

Single-photon annihilation and electron-pair creation $e^+ + e^- \rightleftarrows \gamma$ can occur in a dispersive medium with a refractive index less than unity. For such processes to occur, the photon energy must lie within the interval $2m \leq \omega \leq N^{1/3}$, where m is the electron rest-mass energy, and N the electron density in the medium. In this paper we have evaluated the probability for such processes. This effect is similar in its physics to the Vavilov-Cerenkov effect. The processes discussed are the dominant ones in the energy range $2m < \omega < 10m$.

1. If no outside particles are involved, the creation of an electron-positron pair by a $\gamma$ quantum and, conversely, the transformation of a pair into one quantum,

$$e^+ + e^- \rightleftarrows \gamma \tag{1}$$

is impossible in vacuo because of the momentum conservation law. It is, however, easy to check that the momentum conservation law is observed for the processes (1) in a dispersive medium with refractive index $n(\omega) < 1$:

$$\mathbf{k} = \mathbf{p}_1 + \mathbf{p}_2; \quad \omega = E_1 + E_2; \ k = \omega n(\omega), \tag{2}$$

and these phenomena can thus occur.

The energies of the quanta involved in the processes (1) must have not only a lower bound, but also an upper one. The upper limit of the energy of the quanta is determined by the obvious requirement $\lambda \gtrsim l$, where $\lambda = 1/\omega$ is the wavelength divided by $2\pi$, and $l$ the mean distance between particles. It is evident that when $\lambda < l$ the concepts of a continuous medium and of a refractive index independent of the position cease to be correct. Thus, if the average interparticle distance is $l \sim N^{-1/3}$, where N is the number of electrons per unit volume, the applicability of the "refractive index" concept will impose on the photon energy a limit: $\omega \lesssim l^{-1} \approx N^{1/3}$, whence it follows that the threshold for pair formation must correspond to a particle density of the order of $N \gtrsim 8\lambda_C^{-3} \approx 1.4 \times 10^{32}\ \text{cm}^{-3}$, where $\lambda_C = 1/m$ is the electron Compton wavelength divided by $2\pi$.

Such high densities of matter are not even assumed to exist in the interior regions of the sun or other normal stars. However, the possibility of the existence, in the central regions of white dwarfs, of matter with a density of the order of nuclear densities or even higher has often been discussed in the literature.[1-3] The idea of the existence of a hyper-dense state of matter ("prestellar matter") has particularly been emphasized by Ambartsumyan.[4]

For the processes (1) to occur in a dispersive medium, the photon energy must therefore satisfy the condition

$$2m \lesssim \omega \lesssim N^{1/3}. \tag{3}$$

The temperature of the medium plays here an important role.[5] At sufficiently low temperatures we are dealing with a strongly degenerate electron gas in which the process $\gamma \rightarrow e^+ + e^-$ is forbidden by the Pauli principle. We shall evaluate in the following the probability for a single-photon annihilation and for the creation of electron pairs, assuming that all the necessary conditions for the occurrence of these phenomena in a medium exist in nature.

2. We consider first pair production by a $\gamma$ quantum. We have for the matrix element for such a process[6-8]

$$S_{if}^{(1)} = -e\left(\frac{\mu}{2\alpha\omega n^2 V}\right)^{1/2} \int \overline{\psi}_1 \gamma_\nu e^{i\widetilde{k}\widetilde{x}} \widetilde{\psi}_2 \, d^4x, \tag{4}$$

where $n^2 = \epsilon\mu$, V is the normalization volume, $\gamma_\nu$ is the component of the matrix $\widetilde{\gamma}$ in the direction of the polarization of the photon (a tilde indicates a four-dimensional vector), $\widetilde{k} = (\mathbf{k}, i\omega)$ is the four-momentum of the photon, $\psi_1$ and $\psi_2$ are the electron and positron wave functions,

$$\psi_1 = \frac{u_1(\mathbf{p}_1)}{\sqrt{V}} \exp\{i\widetilde{p}_1 \widetilde{x}\}, \ \psi_2 = \frac{u_2(\mathbf{p}_2)}{\sqrt{V}} \exp\{-i\widetilde{p}_2 \widetilde{x}\}, \tag{5}$$

and, finally

$$\alpha = 1 + (\omega/n)\, dn/d\omega. \tag{6}$$

Using (5) we get from (4) for the transition probability per unit time

$$dW = \frac{\mu e^2}{(2\pi)^2\, 2\alpha\omega n^2} \left| \bar{u}_1(\mathbf{p}_1)\, \gamma_\nu u_2(-\mathbf{p}_2) \right|^2 \delta(\tilde{k} - \tilde{p}_1 - \tilde{p}_2)\, d^3p_1\, d^3p_2. \tag{7}$$

We average next over the polarization of the quantum, sum over the spin components of the electron and the positron, also integrate over the positron momentum, and get from (7)

$$dW = \frac{\mu e^2}{(2\pi)^2\, 2\alpha\omega n^2} \frac{E_1E_2 + m^2 - p_1p_2\cos\theta_1\cos\theta_2}{E_1E_2}$$
$$\times\delta(\omega - E_1 - E_2)\, d^3p_1, \tag{8}$$

where $\theta_1$ is the angle between $\mathbf{p}_1$ and $\mathbf{k}$; $\theta_2$ is the angle between $\mathbf{p}_2$ and $\mathbf{k}$, and $d^3p_1 = 2\pi p_1 E_1 dE_1 \sin\theta_1\, d\theta_1$.

We must still integrate over the electron momentum. Integration over $\theta_1$ in (8) is equivalent to the substitution

$$\delta(\omega - E_f)\sin\theta_1\, d\theta_1 \rightarrow E_2/kp_1,$$

where $E_f = E_1 + E_2$ is the energy of the final state of the system

$$E_f = E_1 + (E_1 + k^2 - 2kp_1\cos\theta_1)^{1/2}.$$

We get as a result

$$dW = \frac{\mu e^2}{4\pi\alpha\omega^2 n^3}(E_1E_2 + m^2 - p_1p_2\cos\theta_1\cos\theta_2)\, dE_1. \tag{9}$$

$E_2$, $\theta_1$, and $\theta_2$ are now functions of $E_1$

$$\cos\theta_1 = E_1/np_1 - k(1-n^2)/2n^2p_1,$$
$$\cos\theta_2 = E_2/np_2 - k(1-n^2)/2n^2p_2. \tag{10}$$

Eliminating $\theta_1$, $\theta_2$, and $E_2$ from (9) we get

$$dW = \frac{\mu e^2}{4\pi\alpha\omega^2 n^5}\left[(n^2-1)(\omega E_1 - E_1^2) + n^2m^2 + \frac{1-n^4}{4}\omega^2\right] dE_1. \tag{9$'$}$$

Integrating (9′) over $E_1$ between the limits $m$ and $\omega - m$ we get the total probability of annihilation of a photon accompanied by the formation of an electron pair

$$W = \frac{\mu e^2}{4\pi\alpha\omega^2 n^5}(\omega - 2m)$$
$$\times(1-n^2)\left[\frac{1}{12}(\omega-2m)^2 + \frac{1}{4}n^2\omega^2 + \frac{n^2}{1-n^2}m^2\right]. \tag{11}$$

To obtain the total probability of creation of a pair by a quantum per unit path length we must divide (11) by the phase velocity of the light, $1/n$.

In order to get the complete picture of the probability evaluated here, one must know the dispersion law for very high densities of matter. This problem was considered by the present author in reference 5. It was shown there that at very high temperatures $\kappa T > mc^2$, when the electron gas is non-degenerate ($\kappa$ is Boltzmann's constant),

$$1 - n^2 \approx \frac{2.4\pi e^2}{m\omega^2}\left(\frac{mc^2}{\kappa T}\right)^2 N,$$

where $N$ is the electron density in the medium (here in the usual units). When, however, the electron gas is degenerate ($\kappa T < mc^2$),

$$1 - n^2 \approx 3c^2N^{2/3}/137\omega^2.$$

Using these formulae for $n$ and taking it into account that for the process under consideration we have practically $N \sim 8\lambda_C^{-3}$, we verify easily that the last term within the square brackets in (11) is appreciably larger than the first two. The pair-creation probability is thus of the order of magnitude

$$W \approx \frac{m}{137\omega}\left(1 - \frac{2m}{\omega}\right)\lambda_C^{-1}, \tag{11$'$}$$

where we have omitted the factors $\mu$, $\alpha$, and $n^2$, which are of the order of unity.

The pair-creation probability for $\gamma$ quanta (by the usual mechanism, i.e., in the field of a nucleus) is equal to $W_0 = Z^2\Phi N$, where $N$ is the density of nuclei and $Z^2\Phi$ the total pair-creation cross section. For the electron densities considered here, the nuclei break up into separate nucleons (neutron stars) so that we must put $Z = 1$. For photon energies $\omega = 3m$, $5m$, $10m$, $20m$, and $100m$ we have[9] $\Phi/(5.8\times10^{-28}) \approx 0.49$, 3.5, 11, 21, and 46. Taking it into account that $N \sim (\omega/c)^3$ and comparing these data with (11′), we find $W/W_0 \approx 2700$, 146, 7.66, 0.63, and 0.0023, respectively.

In the energy range $2m < \omega < 10m$ the probability $W$ is thus appreciably larger than the probability $W_0$.

**3.** We turn now to a consideration of the single-photon electron-positron annihilation process. We have, by analogy with (4), for the matrix element of this process

$$S_{if}^{(1)} = -e\left(\frac{\mu}{2\alpha\omega n^2 V}\right)^{1/2}\int \bar{\psi}_2\gamma_\nu e^{-i\tilde{k}\tilde{x}}\psi_1\, d^4x. \tag{12}$$

Integrating (12) over the four-dimensional volume we find

$$S_{if}^{(1)} = -(2\pi)^4 eV^{-3/2}(\mu/2\alpha\omega n^2)^{1/2}\bar{u}_2$$
$$\times(-\mathbf{p}_2)\gamma_\nu u_1(\mathbf{p}_1)\,\delta(\tilde{p}_1 + \tilde{p}_2 - \tilde{k}), \tag{13}$$

where $\tilde{\mathfrak{p}}_1$ and $\tilde{\mathfrak{p}}_2$ are the four-momenta of the electron and the positron.

The matrix elements (4) and (12) are Hermitian conjugates. The summation of the square of the modulus of the matrix elements over the polarization of the photon and of the electrons leads thus to the same result for the pair creation and annihilation processes (principle of detailed balancing). The probabilities for these processes are, however, not the same since the statistical weights of the final states are different. Taking this into account we get for the transition probability per unit time the formula

$$dW' = \frac{\pi\mu e^2}{V\alpha\omega n^2}\,\frac{E_1E_2 + m^2 - p_1p_2\cos\theta_1\cos\theta_2}{E_1E_2}\,\delta(\tilde{k} - \tilde{p}_1 - \tilde{p}_2)\,d^3k, \tag{14}$$

where $\theta_1$ and $\theta_2$ have the same meaning as before and are determined by Eqs. (10). Integrating (14) over the photon momentum we get

$$dW' = \frac{\pi\mu e^2}{V\alpha\omega n^2}\,\frac{E_1E_2 + m^2 - p_1p_2\cos\theta_1\cos\theta_2}{E_1E_2}\,\delta(\omega - E_1 - E_2). \tag{15}$$

The formula obtained here leads to one pair of particles in the volume V under consideration, where we have assumed that the electron and the positron have strictly well defined momenta.

We determine now the probability for the annihilation of a positron of given energy $E_2$ by all electrons in the medium with energies within the range $(E_1, E_1 + dE_1)$ and with arbitrary directions of motion. To do this we must multiply (15) by the electron distribution function

$$VN_1(E_1, \theta, \varphi)\,dE_1\sin\theta\,d\theta\,d\varphi \tag{16}$$

and integrate over the angles. $\theta$ is here the angle between the directions of motion of the colliding particles. When integrating one must take the dependence of $\omega$ on the angle $\theta$ into account.

We assume that the angular distribution of the electrons in the medium is isotropic, which in actual fact is always true. Using (10) and (16) we get then from (15)

$$dW' = \frac{\pi\mu e^2}{2n^2}\Big[n^2m^2 + \frac{1-n^4}{4}\,\omega^2 - (1-n^2)\,E_1E_2\Big]\frac{N_1(E_1)\,dE_1}{E_1E_2p_1p_2}, \tag{17}$$

where $N_1(E_1)\,dE_1$ is the number of electrons with energies within the range $(E_1, E_1 + dE_1)$ per unit volume. The total probability that a positron with energy $E_2$ is annihilated per unit time is equal to

$$W' = \frac{\pi\mu e^2}{2E_2p_2}\int\Big[n^2m^2 + \frac{1-n^4}{4}\,\omega^2 - (1-n^2)\,E_1E_2\Big]\frac{N_1(E_1)\,dE_1}{E_1p_1n^2}. \tag{18}$$

The lower limit of the integral is equal to m and the upper one to ∞ if the electron gas in the medium is non-degenerate (case of very high temperatures) or to the Fermi energy if the electron gas is strongly degenerate (case of low temperatures).

At sufficiently high temperatures, $T > 10^{10}$ °K, there will be a large number of positrons in the medium.* It is thus of interest to determine the total probability for the annihilation of an electron of given energy $E_1$. The corresponding equations for electrons can be obtained from (17) and (18) by replacing in them the electron distribution function by the positron distribution function $N_2(E_2)\,dE_2$.

---

[1] J. R. Oppenheimer and G. M. Volkoff, Phys. Rev. **55**, 374 (1939).

[2] L. D. Landau and E. M. Lifshitz, Статистическая физика, (Statistical Physics), Gostekhizdat, 1951, [Statistical Physics, Pergamon, London, 1958].

[3] S. Chandrasekhar, An Introduction to the Study of Stellar Structure, Chicago University Press, 1939.

[4] V. A. Ambartsumyan, Izv. Akad. Nauk Arm. SSR **11**, 9 (1958).

[5] G. S. Saakyan, JETP **38**, 843 (1960), Soviet Phys. JETP **11**, 610 (1960).

[6] A. I. Akhiezer and V. B. Berestetskiĭ, Квантовая электродинамика (Quantum Electrodynamics) 2nd edition, Fizmatgiz, 1959.

[7] K. M. Watson and J. M. Jauch, Phys. Rev. **75**, 1249 (1949).

[8] M. I. Ryazanov, JETP **32**, 1244 (1957), Soviet Phys. JETP **5**, 1013 (1957).

[9] W. Heitler, The Quantum Theory of Radiation, Oxford University Press, 1954.

Translated by D. ter Haar
304

---

*See reference 2, p. 335.

SOVIET PHYSICS JETP VOLUME 11, NUMBER 5 NOVEMBER, 1960

# *ON THE AMOUNT OF ACCELERATED PARTICLES IN AN IONIZED GAS UNDER VARIOUS ACCELERATING MECHANISMS*

A. V. GUREVICH

P. N. Lebedev Physics Institute, Academy of Science, U.S.S.R.

Submitted to JETP editor December 21, 1959

J. Exptl. Theoret. Phys. (U.S.S.R.) 38, 1597-1607 (May, 1960)

The kinetic equation is solved for a system of particles interacting according to Coulomb-law conditions where the presence of the accelerating mechanism makes the distribution function non-stationary in the high-velocity range, i.e., when the accelerating mechanism leads to continuous acceleration of particles whose energy is greater than the injection energy. The value of the particle flux is determined.

1. Great attention is being paid of late, in connection with investigations of the origin of cosmic rays and corpuscular radiation from the sun, to the analysis of various mechanisms of acceleration in an ionized gas. Under consideration, for example, is Fermi's statistical mechanism of acceleration, by which the ion energy increases through collisions with clouds of charged particles. In this case, if the free path L between two collisions of an ion with the clouds is constant (independent of the ion energy $\epsilon$), and if the ion acquires during each impact an average energy $(2/3)\ Mv_c^2$ (where M is the ion mass and $v_c$ the average cloud velocity), then the energy transferred to the ion by the accelerating mechanism over a time $\Delta t$ is

$$\Delta\varepsilon_+ = \frac{2}{3}\, Mv_c^2\, \frac{\sqrt{2\varepsilon/M}}{L}\, \Delta t.$$

Within the same time, the particle loses, by interaction with other ions of the plasma, an energy $\Delta\epsilon_- = (\epsilon - 3kT/2)\,\nu(\epsilon)\,\Delta t$, where $\nu(\epsilon)$ is the collision frequency. As is well known, the collision frequency of the particles interaction in Coulomb-law diminishes rapidly with increasing energy, $\nu(\epsilon) = \nu_0\,(kT/\epsilon)^{3/2}$, where

$$\nu_0 = \nu(kT) = \frac{4\pi Ne^4}{(kT)^{3/2}\, M^{1/2}} \ln\left(\frac{kTD}{e^2}\right) \tag{1}$$

is the collision frequency of a particle of average (thermal) energy (e is the ion charge, N the ion density, and D the Debye radius). Thus, the change in ion energy, due to the Fermi statistical acceleration mechanism, is given by

$$\frac{d\varepsilon}{dt} = \frac{2}{3}\, Mv_c^2\, \frac{\sqrt{2\varepsilon/M}}{L} - \nu_0\left(\varepsilon - \frac{3}{2}kT\right)\left(\frac{kT}{\varepsilon}\right)^{3/2}, \tag{2}$$

from which we see directly that only when

$$\varepsilon < \varepsilon_{in} = 3\nu_0 L\, (kT)^{3/2}/2\sqrt{2}\, v_c^2\, M^{1/2}$$

will the ion energy tend to a stationary value. When $\epsilon > \epsilon_{in}$ it increases continuously with time, and in collisions with other ions the particle loses only a small part of the energy it acquires from the clouds. $\epsilon_{in}$ is usually called the injection energy. It is clear that when the injection energy is close to the average thermal ion energy ($\epsilon_{in} \sim kT$), all particles are immediately accelerated. If $\epsilon_{in} \gg kT$, on the other hand, only a small part of the particles become accelerated, those with sufficiently large energies $\epsilon > \epsilon_{in} \gg kT$.

When $\epsilon_{in} \gg kT$, the acceleration mechanism is logically called "weak." We shall consider here only weak accelerating mechanisms. Since a weak acceleration mechanism transfers to the ions, over the mean free time $1/\nu_0$, an energy which is small compared with the thermal energy kT, the action of a weak acceleration mechanism cannot cause the distribution function to deviate considerably from equilibrium (Maxwellian). In the range of high energies, however, the mean free time is large, and the effect of a weak acceleration mechanism can be substantial. Furthermore, when $\epsilon > \epsilon_{in}$ the particle energy increases with time, so that the particle energy distribution in this region is essentially not in equilibrium.

Collisions cause the energy of certain particles to increase from the main equilibrium value to the injection value. The particles then leave (escape) the main region and are accelerated. The order of magnitude of the number of particles escaping per unit time $\Delta t$ is, naturally,

$$\Delta N \sim \nu\, \Delta t N\, (\varepsilon_{in}), \tag{3}$$

where $N(\epsilon_{in})$ is the number of particles with energies ranging from $\epsilon_{in} - kT$ to $\epsilon_{in}$. It appears natural at first glance to assume, in estimating the value of $N(\epsilon_{in})$, that the distribution function is Maxwellian up to $\epsilon = \epsilon_{in}$. We would obtain then

$$\Delta N \sim \nu \Delta t N_0 \exp\{-\varepsilon_{in}/kT\}. \tag{3a}$$

We shall see below that the acceleration mechanism changes the character of the velocity distribution in the region $\epsilon \sim \epsilon_{in}$ so much that expressions of type (3) are utterly inapplicable for estimates of the number of escaping particles.

At the same time, the number of escaping particles, and consequently the number of accelerated particles, is one of the basic characteristics of the acceleration mechanism. Therefore the question of the flux of escaping particles and its dependence on the parameters that characterize the acceleration mechanism, the plasma, and the accelerating particles themselves is of considerable interest.

The present paper is devoted to a solution of the corresponding problem.* In Sec. 2 we develop a method for finding a weakly-nonstationary solution of the kinetic equation. A general expression is obtained for the flux of escaping particles. This solution is analyzed in Sec. 3 for ions accelerated in a plasma by the statistical Fermi acceleration mechanism.

**2.** We consider first, for the sake of simplicity, a system of identical particles, interacting in accordance with the Coulomb law and subject to a weak statistical acceleration mechanism. The equation for the velocity distribution function of these particles has the form

$$\frac{\partial f}{\partial \tau} - \frac{1}{u^2}\frac{\partial}{\partial u}\left\{\left(\frac{1}{u} + u^2\alpha(u)\right)\frac{\partial f}{\partial u} + f\right\} = 0. \tag{4}$$

Allowance is made here for the fact that the statistical acceleration mechanism does not have a preferred direction in velocity space; the distribution function can therefore depend only on the modulus of the velocity $v$ and on the time $t\,[f = f(v, t)]$. In addition, we use in (4) the dimensionless variables

$$u = v/\sqrt{kT/M}, \qquad \tau = t\nu_0, \tag{5}$$

where $\nu_0$ is the collision frequency, determined by Eq. (1), while $T$ is the system temperature ($T$ is considered henceforth constant in time; this is meaningful only in the case of a weak acceleration mechanism).* Finally, the function $\alpha(u)$ describes the effect of the acceleration mechanism on the particles. Thus, if the mean free path $L$ of the particle between two collisions with the clouds is independent of its velocity, then

$$\alpha(u) = \alpha_0 u, \qquad \alpha_0 = {}^2/_3\, v_c^2 / \nu_0 L \sqrt{kT/M}. \tag{6}$$

The parameter $\alpha_0$ is very simply connected with the injection energy $\epsilon_{in}$, $\alpha_0 = kT/\sqrt{2}\,\epsilon_{in}$; in the case of a weak acceleration mechanism, $\alpha_0$ is always much less than unity.

## STATIONARY SOLUTION

Solving Eq. (4) under stationary conditions ($\partial f/\partial\tau = 0$), we have

$$(1/u + u^2\alpha(u))\,\partial f/\partial u + f = -S_0, \tag{7}$$

where $S_0$ is the total flux of the particles through the surface $u = \text{const}$ in velocity space.† Hence

$$f = C_0 \exp\left\{-\int_0^u \frac{u\,du}{1 + u^3\alpha(u)}\right\} - S_0, \tag{8}$$

where the constant $C_0$ is determined by the normalization condition

$$\int_0^\infty u^2 f\,du = N_0. \tag{8a}$$

The flux $S_0$ can differ from zero in the entire velocity space only if a source is located at the origin.

In the absence of such a source we have for $\alpha(u) = \alpha_0 u$ [see Eq. (6)]

$$f = C_0 \exp\left\{-\int_0^u \frac{u\,du}{1 + \alpha_0 u^4}\right\}. \tag{9}$$

The distribution function (9) tends to a constant value as $u \to \infty$: $f(\infty) = C_0 \exp(-\pi/4\sqrt{\alpha_0})$. It cannot satisfy, naturally, the normalization condition (8a). This means that there exists no stationary distribution in this case, as should be

---

*An analysis of the question of the number of accelerating ions in a plasma in a case of the Fermi acceleration mechanism is treated by Parker.[1] He did not obtain, however, correct expressions for the flux of the escaping particles. We note also that Parker disregarded the interaction with electrons, which fundamentally affects the flux of escaping ions (see Sec. 3 of the present paper).

*We note that (4) holds, strictly speaking, only for particles much faster than thermal ($u^2 \gg 1$). In the vicinity of $u \sim 1$, the terms that describe collisions between particles should be written down in somewhat more complicated form (see reference 2). It is easy to verify, however, that this is of no importance to us, for in the case of an acceleration mechanism only the region of high velocities is of importance.

†Equation (4) can be written in the form $\partial f/\partial\tau + \operatorname{div} S = 0$, from which it is clear that $S = \int S d\sigma$ (integration over the region $u = \text{const}$) is actually the particle flux in velocity space.

(see Sec. 1). We note that if $\alpha(u) = \alpha_0 u^{\lambda}$, then no normalizable stationary distribution exists for $\lambda < -1$, and the particles do not escape in this case. A similar conclusion is reached by analysis of Eq. (2), where the acceleration of particles for $\Delta\epsilon_+ \sim \epsilon^{\lambda/2}$ is possible only if $\lambda > -1$.

We note in conclusion that in the general case when the equation for the function f has the form

$$\frac{\partial f}{\partial \tau} - \frac{1}{u^2}\frac{\partial}{\partial u}\left(A(u)\frac{\partial f}{\partial u} + B(u)f\right) = 0, \tag{10}$$

the stationary solution (with flux $S_0$) is given by

$$f = C_0 \exp\left\{-\int_0^u \frac{B(u)}{A(u)}du\right\}$$
$$- S_0 \exp\left\{-\int_0^u \frac{B(u)}{A(u)}du\right\}\int_0^u \frac{dv}{A(v)}\exp\left\{\int_0^v \frac{B(t)}{A(t)}dt\right\}. \tag{11}$$

## STEADY-STATE QUASI-STATIONARY SOLUTION

We have noted earlier that only the particles whose energy exceeds the injection energy $\epsilon_{in} = kT/\sqrt{2}\ \alpha_0$ are accelerated. The number of such particles in the case of a weak acceleration mechanism, i.e., at sufficiently small $\alpha_0$, is very small. The state of the main mass of the particles, whose energy is less than the injection energy $\epsilon_{in}$, is almost stationary. In fact, were it not for the escape ($\alpha_0 \to 0$, that is, $\epsilon_{in} \to \infty$), this would be in general a stationary state [see Eq. (9)]. Since $\alpha_0 \neq 0$, the energy of certain particles increases to $\epsilon_{in} = kT/\sqrt{2}\ \alpha_0$, and they leave the main region. At sufficiently small $\alpha_0$, this flux of escaping particles is naturally very weak [see Eq. (3)]. Therefore, although the main state does change with time, its change is very slow, quasi-stationary. The flux of particles from the main region to the acceleration region also changes slowly.*

It was also indicated in Sec. 1 that the influence of a weak acceleration mechanism on particles with energies close to thermal is insignificant. Therefore, in solving Eq. (4) for the case of a weak Fermi acceleration mechanism (6), it is convenient to single out first the region (I) in which the velocities are $u \sim 1$ ($0 \leq u \leq u_1$), and where the effect of the acceleration mechanism can be neglected in first approximation. In region I, Eq. (4) becomes

$$\frac{\partial f^{\rm I}}{\partial \tau} - \frac{1}{u^2}\frac{\partial}{\partial u}\left(\frac{1}{u}\frac{\partial f^{\rm I}}{\partial u} + f^{\rm I}\right) = 0. \tag{12}$$

The boundary $u_1$ is subject to the condition that the acceleration mechanism be weak when $u \leq u_1$, i.e., $\alpha_0 u_1^3 \ll 1/u_1$. On the other hand, it is necessary that the number of particles which are not in the mean region be negligibly small, i.e., $u_1^3 \exp(-u_1^2/2) \ll 1$. At sufficiently small $\alpha_0$ (if $\alpha_0^{-3/4} \exp\{-1/2\cdot\sqrt{\alpha_0}\} \ll 1$), both conditions can be satisfied.

It must also be considered that escape causes the total number of particles in the main region I to be variable, i.e., although the flux $S = u^{-1}\partial f^{\rm I}/\partial u + f^{\rm I}$ vanishes on the boundary $u = 0$ (there are no sources), the flux of particles through the boundary $u = u_1$ is different from zero, $S = -S_0$. At sufficiently small $\alpha_0$, as indicated above, this flux should be weak ($S_0 \ll N_0$), so that the distribution function in the main region should be close to stationary. As a result, it is natural to seek the solution of Eq. (4) by the method of successive approximations, $f^{\rm I} = f_1^{\rm I} + f_2^{\rm I} + \ldots$, neglecting in first approximation the time variation of $f^{\rm I}$, i.e., assuming it to be quasi-stationary. We then obtain instead of (4) the following system of equations for $f_1^{\rm I}, f_2^{\rm I}, \ldots$

$$\frac{1}{u^2}\frac{\partial}{\partial u}\left(\frac{1}{u}\frac{\partial f_1^{\rm I}}{\partial u} - f_1^{\rm I}\right) = 0, \qquad \frac{1}{u^2}\frac{\partial}{\partial u}\left(\frac{1}{u}\frac{\partial f_2^{\rm I}}{\partial u} + f_2^{\rm I}\right) = \frac{\partial f_1^{\rm I}}{\partial \tau}, \ldots \tag{13}$$

From the first equation of (13) we find that, in first approximation, the distribution function in the main region is Maxwellian:

$$f_1^{\rm I} = C^{\rm I}\exp\{-u^2/2\}, \tag{14}$$

as should be. The constant $C^{\rm I}$ is determined from the normalization condition

$$N = \int_0^{u_1} f_1^{\rm I} u^2\,du = C^{\rm I}\int_0^{u_1} u^2 \exp\{-u^2/2\}\,du,$$

where N is the total number of particles with velocity $u \leq u_1$.* Since we have assumed that $u_1$ is sufficiently large, so that terms of order $u_1^3 \exp(-u_1^2/2)$ can be neglected, we get

---

*The time variation of the distribution function in the case of the weak acceleration mechanism considered here is so to speak analogous to the leakage of water from a large reservoir through a very small hole. It is clear that all the water will leak out after an infinite time, i.e., there is no perfectly stationary state, but the level of the water in the reservoir changes very slowly. The escape flux itself soon reaches a definite value, which can subsequently change only slowly (quasi-stationarily) with a change in the overall level of water in the reservoir.

*Since the system under consideration is supposed to be homogeneous in coordinate space, N can be taken to mean both the number of particles in the medium and their density in coordinate space.

$$C^{\mathrm{I}} = \sqrt{\frac{2}{\pi}}\, N = \sqrt{\frac{2}{\pi}} \left( N_0 - \int\limits_0^{\tau} S_0 \, d\tau \right). \tag{14a}$$

Here $N_0$ is the total number of particles in the system, and $S_0$ is the flux of particles escaping from the main region I through the surface $u = u_1$.

In the next higher approximation we obtain

$$\frac{1}{u^2} \frac{\partial}{\partial u} \left\{ \frac{1}{u} \frac{\partial f_2^{\mathrm{I}}}{\partial u} + f_2^{\mathrm{I}} \right\} = - S_0 \sqrt{\frac{2}{\pi}} \exp \left\{ - \frac{u^2}{2} \right\}. \tag{15}$$

Let us integrate this equation, recalling that on the boundary $u = 0$ the flux $S = u^{-1} \partial f_2^{\mathrm{I}} / \partial u + f_2^{\mathrm{I}}$ vanishes. We then have

$$S = - S_0 \sqrt{\frac{2}{\pi}} \int\limits_0^u v^2 \exp \left\{ - \frac{v^2}{2} \right\} dv,$$

i.e., the flux $S$ increases (in absolute value) with increasing $u$ from $0$ when $u = 0$ to $S_0$ when $u = u_1$, as should be. It is interesting that when $u > 1$ the flux rapidly approaches $S_0$ and remains practically unchanged with increasing $u$. The flux is thus independent of the choice of the boundary $u_1$ (provided $u_1 \gg 1$).

Integrating further Eq. (15), we readily obtain also the function $f_2^{\mathrm{I}}$

$$f_2^{\mathrm{I}} = C_2 e^{-u^2/2} - \sqrt{\frac{2}{\pi}}\, S_0 \int\limits_0^u t^2 e^{-t^2/2} \, dt + \sqrt{\frac{2}{\pi}}\, S_0 \frac{u^3}{3} e^{-u^2/2}. \tag{16}$$

The constant $C_2$ is determined here by the normalization condition $\int\limits_0^u f_2^{\mathrm{I}} u^2 du = 0$. It is important to note that at sufficiently large $u \gg 1$ the function $f_2^{\mathrm{I}}$ tends to a constant value, independent of u: $f_2^{\mathrm{I}} \rightarrow -S_0$. In particular, on the boundary of the region under consideration we have $f_2^{\mathrm{I}}(u_1) = -S_0$.

In region II ($u_1 \leq u \leq u_2$) the influence of the acceleration mechanism must already be accounted for. It is important, however, that through this region passes a constant particle flux $-S_0$, which is independent of $u$ (as shown above, the flux is produced in the region $u \sim 1$ and is practically independent of u when $u \gg 1$). Solving Eq. (4) in region II by the same method as in region I, we find that the distribution function in region II is of the form [cf. Eq. (8)]

$$f^{\mathrm{II}} = C^{\mathrm{II}} \exp \left\{ - \int\limits_0^u \frac{u \, du}{1 + \alpha_0 u^4} \right\} - S_0. \tag{17}$$

The constant $C^{\mathrm{II}}$ is determined from the condition of continuity of the distribution function on the boundary $f^{\mathrm{I}}(u_1) = f^{\mathrm{II}}(u_1)$, i.e.,

$$\sqrt{\frac{2}{\pi}}\, N \exp \left\{ - \frac{u_1^2}{2} \right\} - S_0 = C^{\mathrm{II}} \exp \left\{ - \int\limits_0^u \frac{u \, du}{1 + \alpha_0 u^4} \right\} - S_0. \tag{18}$$

Therefore, considering that $\alpha_0 u^4 \ll 1$, we get $C^{\mathrm{II}} = N \sqrt{2\pi}$. Thus, the steady-state solution in region II is

$$f^{\mathrm{II}}(u) = \sqrt{\frac{2}{\pi}}\, N \exp \left\{ - \int\limits_0^u \frac{u \, du}{1 + \alpha_0 u^4} \right\} - S_0. \tag{17a}$$

It is important here that as $u$ increases $f^{\mathrm{II}}(u)$ tends to a constant value independent of $u$,

$$f^{\mathrm{II}}(\infty) = \sqrt{\frac{2}{\pi}}\, N \exp \left\{ - \int\limits_0^{\infty} \frac{u \, du}{1 + \alpha_0 u^4} \right\} - S_0 = \sqrt{\frac{2}{\pi}}\, N \exp \left\{ - \frac{\pi}{4 \sqrt{\alpha_0}} \right\} - S_0. \tag{19}$$

We have thus determined the distribution functions in regions I and II. In the case of a weak flux $S_0 \ll N$, the resulting expression (14)—(17) is almost stationary, and changes with time only to the extent that the number of particles changes in the main region, $N = N_0 - \int\limits_0^{\tau} S_0 d\tau$. The only unknown in (14)—(17) is the flux $S_0$, which can be determined from the normalization condition. In fact, the total number of particles passing from region I to region II during the time $\tau$ is $\int\limits_0^{\tau} S_0 d\tau$. The total change in the normalization integral of the distribution function over the entire region $u > u_1$ should obviously be equal to this quantity,

$$\Delta N = \int\limits_{u_1}^{\infty} u^2 [f(u, \tau) - f(u, 0)] \, du = \int\limits_0^{\tau} S_0 \, d\tau, \tag{20}$$

where $f(u, 0)$ is the initial (Maxwellian) distribution function. From this we can obtain the flux $S_0$. We first consider that the quasi-stationary distribution (17a) is valid up to the boundary $u = u_2$. The boundary itself, naturally, moves with increasing $\tau$ towards higher values of $u$, at which the quasi-stationary distribution function $f^{\mathrm{II}}$ becomes a constant quantity, $f^{\mathrm{II}}(\infty)$ [see Eq. (19)]. Consequently, at sufficiently large $\tau$, i.e., at sufficiently large $u_2$, the number of particles in the stationary region II alone ($\Delta N^{\mathrm{II}}$) is given by

$$\Delta N^{\mathrm{II}} = \int\limits_{u_1}^{u_2} f^{\mathrm{II}} u^2 \, du \gtrsim \int\limits^{u_2} f^{\mathrm{II}}(\infty) u^2 \, du = f^{\mathrm{II}}(\infty) u_2^3 / 3. \tag{20a}$$

We now determine the time variation of the boundary of the steady-state quasi-stationary distribution $u_2$. In the region of large $u$ ($u > \sqrt{\epsilon_{\mathrm{in}}/kT} \sim 1/\sqrt{\alpha_0}$) the collisions are insignificant and the distribution function changes only because of the effect of the acceleration mechanism on the particle. Equation (4) obviously assumes in this region the form

$$\frac{\partial f}{\partial \tau} - \frac{1}{u^2}\frac{\partial}{\partial u}\left(\alpha_0 u^3 \frac{\partial f}{\partial u}\right) = 0. \qquad (21)$$

The boundary $u_2$ of the quasi-stationary region obviously changes with time like the average velocity $\bar{u} = 1/\Delta N \int\limits_{u_1}^{\infty} u^3 f(u, \tau)\, du$. From (21) we obtain for $\bar{u}$ the equation $d\bar{u}/d\tau = 3\alpha_0$ or $\bar{u} = \bar{u}_0 + 3\alpha_0\tau$. Consequently, $u_2$ also increases with time in proportion to $\tau$:

$$u_2 = u_{20} + 3\alpha_0\tau, \qquad (22)$$

where $u_{20} \sim \sqrt{\epsilon_{in}/kT} \sim 1/\sqrt{\alpha_0}$. Substituting now (22) in (20a), we find that for sufficiently large $\tau\ (\tau \gg \alpha_0^{-3/2})$

$$\Delta N^{\mathrm{II}} \approx f^{\mathrm{II}}(\infty)\, u_2^3/3 = 9\alpha_0^3\tau^3 f^{\mathrm{II}}(\infty).$$

We now assume that the number of particles in the quasi-stationary region II $(u_1 \le u \le u_2)$ in no case exceeds $\Delta N$, the total number of particles in the entire region $u \ge u_1$, i.e.,

$$\Delta N^{\mathrm{II}} \approx 9\alpha_0^3\tau^3 f^{\mathrm{II}}(\infty) \leqslant \Delta N = \int\limits_0^{\tau} S_0\, d\tau.$$

Since the steady-state flux $S_0$ is almost stationary (it can only decrease slowly with increasing $\tau$), it follows from this inequality that

$$f^{\mathrm{II}}(\infty) \leqslant \bar{S}_0\, (3\alpha_0^{3/2}\tau)^{-2},$$

where $\bar{S}_0$ is the average value of $S_0$. It is clear therefore that the steady-state value is $f^{\mathrm{II}}(\infty) = 0$ (time to establish steady state $\Delta\tau \gtrsim \alpha_0^{-3/2}$):

$$f^{\mathrm{II}}(\infty) = \sqrt{\frac{2}{\pi}}\, N \exp\left\{-\int\limits_0^{\infty} \frac{u\,du}{1+\alpha_0 u^4}\right\} - S_0 = 0.$$

Consequently

$$S_0 = \sqrt{\frac{2}{\pi}}\, N \exp\left\{-\int\limits_0^{\infty} \frac{u\,du}{1+\alpha_0 u^4}\right\} = \sqrt{\frac{2}{\pi}}\, N \exp\left\{-\frac{\pi}{4\sqrt{\alpha_0}}\right\}. \qquad (23)$$

The ion density $N$ is determined here by the equation

$$dN/dt = -S_0\nu_0 = -\nu_0 N \exp\{-\pi/4\sqrt{\alpha_0}\},$$

in the solution of which, naturally, it is necessary to take into account the fact that $\nu_0$ and $\alpha_0$ depend on $N$.

Thus, in the system considered of identical particles interacting in accordance with a Coulomb law and under the influence of a weak $(\alpha_0 \ll 1)$ Fermi acceleration mechanism, the quasi-stationary distribution established after a time

$$\Delta\tau \gg \alpha_0^{-3/2} \qquad (24)$$

is*

$$f(u, \tau) = \sqrt{\frac{2}{\pi}}\, N(\tau)\left[\exp\left\{-\int\limits_0^{u} \frac{u\,du}{1+\alpha_0 u^4}\right\} - \exp\left\{-\int\limits_0^{\infty} \frac{u\,du}{1+\alpha_0 u^4}\right\}\right]. \qquad (25)$$

The condition for the existence of a quasi-stationary distribution (25) is written here in the form $S_0\Delta\tau \ll N$, or

$$\alpha_0^{-3/2} \exp\{-\pi/4\sqrt{\alpha_0}\} \leqslant 1, \qquad (26)$$

This condition is always satisfied at sufficiently small $\alpha_0\,(\alpha_0 \ll 10^{-2})$. It is easy to see that the other requirements stipulated above during the solution process are also satisfied if conditions (24) and (26) are satisfied.

It is interesting to note that the distribution function (25) differs from the stationary distribution function (9) only by a constant (second term in the square brackets), which determines precisely the value of the flux of escaping particles. The distribution function (25), unlike the stationary distribution function (9), vanishes as $u \to \infty$.

## FLUX OF ESCAPING PARTICLES

The steady-state flux of the escaping particles, as is clear from (23), is

$$dN/dt = \sqrt{2/\pi}\, N\nu_0 \exp\{-\pi/4\sqrt{\alpha_0}\}. \qquad (23a)$$

Comparing this exact expression for the first flux with the "elementary" formula (3), obtained under the assumption that the distribution function is Maxwellian up to the injection energy,

$$dN/dt \sim N\nu \exp\{-\varepsilon_{in}/kT\} = N\nu \exp\{-1/\sqrt{2}\,\alpha_0\}, \qquad (3b)$$

we see that the difference between them is very great. It is important that this difference is not only quantitative but also qualitative (a different dependence on the parameter $\alpha_0$ which characterizes the acceleration mechanism). The reason is that the region in which the acceleration mechanism begins to influence substantially the form of the distribution function is much closer to the injection energy, and consequently the distribution function at $\epsilon \approx \epsilon_{in}$ is much different from Maxwellian. In fact, the region in which the substantial deviation of the distribution function from Maxwellian begins is determined, as is clear from (9) and (25), by the condition $\alpha_0 u^4 \sim 1$ or $\epsilon \sim \epsilon_{in}/\sqrt{\alpha_0} \ll \epsilon_{in}$. From a comparison of (3a) with the exact formula (23a) it is seen that actually the elementary formula is never applicable.

---

*Strictly speaking, the distribution (14)–(16) is valid in region I, but in considering the distribution function itself (and not the flux) we can neglect the difference between the distribution (14)–(16) and (25). It must also be noted that condition (24) indicates only the time required to establish quasi-stationary distribution (25), up to injection energies $u \sim \alpha_0^{-1/2}$. The time to establish the distribution (25) is accordingly greater at higher energies: $\Delta\tau \sim u^3 \gg \alpha_0^{-3/2}$.

The solution obtained for the special form of acceleration mechanism (6) can be readily extended to cover more general cases. In particular, if the equation for the distribution function has the general form (10), then the expression for the steady-state flux (at a weak acceleration mechanism) has the form

$$S_0 = \sqrt{2/\pi}\, N \left[ \int_0^\infty \frac{du}{A\,(u)} \exp\left\{ \int_0^u \frac{B\,(v)}{A\,(v)} \quad \right\} \right] . \tag{27}$$

In particular, if $B(u) = 1$, then

$$S_0 = \sqrt{\frac{2}{\pi}}\, N \exp\left\{ -\int_0^\infty \frac{du}{A\,(u)} \right\}. \tag{27a}$$

When $A(u)$ has a value $1/u + \alpha_0 u^3$, formula (27a) naturally coincides with (23). The distribution function in this general case is

$$f\,(u, \tau) = \sqrt{\frac{2}{\pi}}\, N\,(\tau) \exp\left\{ -\int_0^u \frac{B\,(u)}{A\,(u)}\, du \right\} \left[ 1 - \int_0^u \frac{dv}{A\,(v)} \right.$$

$$\left. \times \exp\left\{ \int_0^v \frac{B\,(t)}{A\,(t)}\, dt \right\} \Big/ \int_0^\infty \frac{dv}{A\,(v)} \exp\left\{ \int_0^v \frac{B\,(t)}{A\,(t)}\, dt \right\} \right]. \tag{28}$$

It is seen from (27) that one can distinguish two essentially different cases in which the flux of escaping particles is different from zero: either $A(u)$ increases much faster than $B(u)$ as $u \to \infty$ (as in the example considered above), or the function $B(u)$ vanishes at a certain $u_c$ and subsequently becomes negative.* In the latter case, for a weak acceleration mechanism, $u_c$ is always much greater than unity. It is consequently possible to carry out the integration in (27) (by the saddle-point method). We then find that

$$S_0 = \frac{1}{\pi} N \left( B \frac{dA}{du} - A \frac{dB}{du} \right)^{1/2}_{u = u_c} \exp\left\{ -\int_0^{u_c} \frac{B\,(u)}{A\,(u)}\, du \right\}, \tag{27b}$$

where the velocity $u_c$ is determined by the condition $B(u_c) = 0$.

3. A weak Fermi acceleration mechanism in a plasma changes significantly only the velocity distribution of the ions. The acceleration mechanism hardly affects the electron distribution function, which can therefore be considered Maxwellian. The equation for the ion distribution function, with allowance for interactions between the ions and with the electrons, has the form

$$\frac{\partial f}{\partial \tau} - \frac{1}{u^2} \frac{\partial}{\partial u} \left\{ \left( \frac{1}{u} + \frac{1}{u} \gamma^2 G \left( \frac{u}{\sqrt{2}\gamma} \right) \right.\right.$$

$$\left.\left. + u^2 \alpha\,(u) \right) \frac{\partial f}{\partial u} + \left( 1 + \gamma^2 G \left( \frac{u}{\sqrt{2}\gamma} \right) \right) f \right\} = 0. \tag{29}$$

Here $u = v/\sqrt{kT/M}$ and $\tau = \nu_{0i} t$, where $T$ is the plasma temperature and $\nu_{0i}$ is the collision frequency for the ions (1), assuming single collisions for simplicity. The terms containing $\gamma$ describe the interaction between the ions and the electrons. Here $\gamma^2 = M/m$ ($m$ is the electron mass) and

$$G\,(x) = \frac{2}{\sqrt{\pi}} \left( \int_0^x e^{-z^2}\, dz - x e^{-x^2} \right). \tag{29a}$$

At small $x \ll 1$ we have $G(x) = 4x^3/3\sqrt{\pi}$; at large $x \gg 1$ we have $G(x) = 1 - 2xe^{-x^2}/\sqrt{\pi}$. Values of the function $G(x)$ for $x \sim 1$ are given, for example, in reference 2. Finally, the term with $\alpha(u)$, as above, describes the effect of the acceleration mechanism on the ions

$$\alpha\,(u) = \alpha_0 u^\lambda, \qquad \alpha_0 = {}^2\!/_3 v_c^2 / \nu_0 L \left( \sqrt{kT/M} \right) \sqrt{kT/M}. \tag{30}$$

All the quantities here are the same as in Sec. 2, except that a somewhat more general expression than (6) is used for $\alpha(u)$, making it possible to describe not only the case of a constant ion mean free path between two collisions with clouds, but also the case of an arbitrary power-law dependence of $L$ on the ion velocity $v$: $L(v) = Q_0 v^{1-\lambda}$

Using (23) and (27) for the steady-state flux of the escaping ions, we find that in our case

$$\frac{dN}{dt} = \nu_0 S_0 = \sqrt{\frac{2}{\pi}}\, N \nu_0 \left[ \int_0^\infty \frac{u\, du}{1 + \gamma^2 G\,(u/\sqrt{2}\gamma) + \alpha_0 u^{\lambda+3}} \right.$$

$$\left. \times \exp\left\{ \int_0^u \frac{-t\,[1 + \gamma^2 G\,(t/\sqrt{2}\gamma)]}{1 + \gamma^2 G\,(t/\sqrt{2}\gamma) + \alpha_0 t^{\lambda+3}} \right\} \right]^{-1}. \tag{31}$$

Considering that the principal role is played in this expression for $dN/dt$ by the exponential term, we can, integrating by parts, convert this term to

---

*This case is usually characteristic of guided acceleration mechanisms (for example, acceleration by means of an electric field, acceleration of particles in a plasma contained between two contracting walls, etc.). It should be noted that although one cannot assume in the analysis of guided acceleration mechanisms, as was done above, that the distribution function depends only on the absolute value of the velocity, nevertheless expressions of the type (27b) for the flux of the escaping particles hold in this case, too.

$$\frac{dN}{dt}=\sqrt{\frac{2}{\pi}}N\nu_0(1+\gamma^2\bar{G})\exp\left\{-\int_0^\infty\frac{u\,du\,(1+\gamma^2G\,(u/\sqrt{2}\gamma))}{1+\gamma^2G\,(u/\sqrt{2}\gamma)+\alpha_0u^{\lambda+3}}\right\}, \tag{32}$$

where $\bar{G}$ is a certain average value of the function $G(u/\gamma\sqrt{2})$; we shall show below that $\bar{G}$ is always equal to unity in the cases of interest to us.

Our principal problem is to analyze the form of the function

$$J\,(\gamma,\alpha_0,\lambda)=\int_0^\infty\frac{u\,du\,(1+\gamma^2G\,(u/\sqrt{2}\gamma)}{1+\gamma^2G\,(u/\sqrt{2}\gamma)+\alpha_0u^{\lambda+3}}$$
$$=2\gamma^2\int_0^\infty\frac{x\,dx\,(1+\gamma^2G\,(x))}{1+\gamma^2G\,(x)+2^{(\lambda+3)/2}\alpha_0\gamma^{\lambda+3}x^{\lambda+3}}. \tag{33}$$

We note first that when $\lambda \leq -1$ the function $J(\gamma, \alpha_0, \lambda)$ becomes infinite. This means that the flux of escaping ions is zero when $\lambda \leq -1$. In other words, in this case the distribution function is stationary, as it should be (see Sec. 2). We shall assume $\gamma^2 = M/m$ always to be a very large quantity. It is easy to see that we can consequently always neglect unity compared with the other terms in (33),* i.e., we can rewrite (33) as

$$J=2\gamma^2\int_0^\infty\frac{xG\,(x)\,dx}{G\,(x)+2^{(\lambda+3)/2}\alpha_0\gamma^{\lambda+1}x^{\lambda+3}}. \tag{33a}$$

It is now easy to obtain the essential limiting values of the function J, namely, when $p = 2^{(\lambda+3)/2}\alpha_0\gamma^{\lambda+1} \gg 1$,

$$J=\frac{2\gamma^2}{p}\int_0^\infty\frac{G\,(x)}{x^{\lambda+2}}dx=\frac{\gamma^{1-\lambda}}{\alpha_0}2^{-(1+\lambda)/2}q\,(\lambda),\qquad q\,(\lambda)=\int_0^\infty\frac{G\,(x)}{x^{\lambda+2}}dx, \tag{34}$$

where $\lambda < 2$. The numerical values of $q(\lambda)$ are listed in the table. In the second limiting case, when $p \ll 1$,

$$J=\frac{2\gamma^2}{p^{2/(\lambda+3)}}r\,(\lambda)=\left(\frac{\gamma^2}{\alpha_0}\right)^{2/(\lambda+3)]}r\,(\lambda).$$

The values of the function $r(\lambda)$ are also listed in the table, from which it is seen that the functions $q(\lambda)$ and $r(\lambda)$ differ little from each other. As $\lambda$ changes from $-0.5$ to 1, these functions change very little, and remain in fact close to unity.

| $\lambda$ | $q\,(\lambda)$ | $r\,(\lambda)$ |
|---|---|---|
| $-1.0$ | $\infty$ | $\infty$ |
| $-0.5$ | 2.04 | 2.07 |
| 0 | 1.13 | 1.21 |
| 0.5 | 0.93 | 0.92 |
| 1.0 | 1.0 | 0.78 |

It must be emphasized that only the first of the foregoing limiting cases is of prime significance. In fact, as can be seen from (32), the flux is proportional to $e^{-J}$, and when $p \lesssim 1$ the function J is greater than $\gamma^2$, where $\gamma^2 = M/m$ is always a very large quantity, on the order of $10^3$ to $10^5$. Consequently, only the first limiting case can be of practical interest, when $p \gg 1$ and the flux $S_0$ assumes sensible values at sufficiently large p. It is also easy to verify that $\bar{G}$, the mean value of $G(x)$ in the integral (32), is always close to unity.* Therefore, when calculating the flux of the escaping ions, we can always use the simple expression (34):

$$\frac{dN}{dt}=\sqrt{\frac{2}{\pi}}N\nu_0\gamma^2\exp\left\{-2^{-(1+\lambda)/2}q\,(\lambda)\frac{\gamma^{1-\lambda}}{\alpha_0}\right\}$$
$$=\sqrt{\frac{2}{\pi}}N\nu_0\frac{M}{m}\exp\left\{-C_0\frac{NT^{-(1+\lambda)/2}}{v_{06}^2M}\right\}, \tag{35}$$

$$C_0=3\pi e^4\,(2m)^{(1-\lambda)/2}q\,(\lambda)\,/\,Q_0k^{(\lambda+1)/2}\ln\,(kTD/e^2). \tag{35a}$$

It is seen therefore that if the cloud velocity $v_c^2$ is independent of the plasma parameters, the flux diminishes exponentially with increasing plasma density and increases with increasing plasma temperature.

It is also interesting that the flux of the escaping ions increases rapidly with increasing ion mass. It must be emphasized here, to be sure, that only singly-charged ions are considered. The flux of Z-fold ions is given by the same formulas, (35) and (35a), but the exponential term must be multiplied by $Z^2N_e/N_i$, and the term preceding the exponential must be multiplied by $N_e/Z^2N_i$.† It is clear therefore that the ion flux diminishes rapidly with increasing ion charge: the exponential term is proportional to $Z^2$ (if the number of multiply-charged ions is relatively small, so that $N_e \approx N_i$), or even to $Z^3$ (if all the ions are Z-fold ionized so that $N_e = ZN_i$).

---

*In other words, the basic decisive influence on the flux of the escaping ions is exerted by their interaction with the electrons and not with each other. This fact agrees with the well-known circumstance that the main energy losses of fast ions in a plasma are due to their interactions with electrons, and not with ions.

*In fact, as is clear from (31), $\bar{G}$ is determined by that region of the values of G(x), in which the quantity

$$\frac{\gamma^2G\,(x)\,x}{G\,(x)+px^{\lambda+3}}\exp\left\{2\gamma^2\int_0^x xG\,(x)\,/\,(G\,(x)+px^{\lambda+3})\,dx\right\}$$

has a maximum. This quantity always has a maximum at large x ($x_{max} \gg 1$). Therefore $\bar{G} = G(x_{max}) = 1$ [the function G(x) is close to unity for large x; see (29a)].

†We note also that the frequency of collisions between ions, $\nu_{0i}$, is proportional to $Z^4$ and the parameter $\tau = t\nu_{0i}$ changes accordingly.

The author is indebted to V. L. Ginzburg for interest in the work and to S. I. Syrovat-skiĭ for many valuable suggestions and comments.

---

[1] E. N. Parker, Phys. Rev. **107**, 830 (1957). E. N. Parker and D. A. Tidman, Phys. Rev. **111**, 1206 (1958).

[2] S. Chandrasekhar, Revs. Modern Phys. **15**, 1 (1943). A. V. Gurevich, JETP **37**, 304 (1959), Soviet Phys. JETP **10**, 215 (1960).

Translated by J. G. Adashko
305

SOVIET PHYSICS JETP VOLUME 11, NUMBER 5 NOVEMBER, 1960

# LIMITS OF APPLICABILITY OF THE WEAK-INTERACTION THEORY

B. L. IOFFE

Submitted to JETP editor December 21, 1959

J. Exptl. Theoret. Phys. (U.S.S.R.) **38**, 1608-1614 (May, 1960)

Weak interactions are assumed to conserve their form at high energies. Then, owing to the weak-interaction radiative corrections, the $\beta$-decay and $\mu$-decay vector interaction constants should become unequal and $\mu \to e + \gamma$ and $\mu \to 3e$ processes should appear. These radiative corrections are computed and, by comparison with experiment, the upper limit is established for the validity of the weak-interaction theory.

IN the study of weak interactions, it is of importance in principle to ascertain whether the weak interactions preserve their form of four-fermion interactions at high energies and, if this is not so, at what energies the interaction begins to assume a form appreciably different from that which it has at low energies. A direct answer to this question can be obtained in principle from experiment, by measuring the energy dependence of the cross sections of different weak processes (such as $\mu^+ + e^- \to \nu + \bar{\nu}$). If the form of the weak interaction does not change with increase in energy, then the cross sections of such processes ought to increase with the energy as $E^2$: $\sigma \sim g^2E^2$ [$E$ is the energy in the center of mass system (c.m.s.), $g$ is the constant of weak interaction: $g \approx 10^{-5}/M^2$, $M$ is the mass of the nucleon].

Another approach to the explanation of this problem is an analysis of the weak-interaction radiative corrections to the different effects observed at low energies. As is well known, the radiative effects in the case of four-fermion interaction diverge strongly, and if the weak interactions do not change their forms up to very high energies, then their contribution can be quite significant. Nor can we disregard a priori the possibility that the weak four-fermion interaction preserves its form up to such energies where it becomes effectively strong, so that the radiative corrections can, generally speaking, be shown to be of order unity. It is evident from dimensional considerations that a weak interaction becomes strong for energies $E \sim 1/\sqrt{g} \sim 10^3$ Bev. This means that, in the calculation of radiative corrections for weak interaction, the integration over the momentum of virtual particles must be carried out effectively up to momenta $\Lambda \sim 1/\sqrt{g}$. We shall assume that the weak interactions preserve their form up to momenta $\sim \Lambda$ and attempt to find an upper estimate for $\Lambda$ by analysis of the experimental data at hand.

In the calculation of radiative corrections, it is necessary to take into account only such interactions in which weakly-interacting particles participate [i.e., $\mu$-decay interaction and the interactions $(\bar{\mu}\nu)(\bar{\nu}\mu)$ and $(\bar{e}\nu)(\bar{\nu}e)$, if they exist]. In taking account of interactions involving strongly-interacting particles, the presence of a form factor makes the momenta of these particles in the intermediate state of order $M$, the mass of the nucleon. Consequently, the radiative corrections in such interactions will be less than or of the order of $gM^2 \sim 10^{-5}$, i.e., very small. For an estimate of $\Lambda$ it is appropriate to consider the following effects: the equality of the vector interaction constants in $\beta$ decay and $\mu$ decay, the decay $\mu \to e + \gamma$, and the decay $\mu \to 3e$.*

It is known experimentally that the vector-interaction constants in $\beta$ decay and $\mu$ decay are equal, to a very high degree of accuracy. Theoretically, however, this equality can be proved only by neglecting radiative corrections due to weak interaction. The connection between the bare and renormalized charges is different in $\beta$ and $\mu$ decays because of the presence of the form factor in the strongly-interacting particles. That is, in $\beta$ decay

$$g_\beta^2 = g_0^2 Z_{1\beta}^{-2} Z_2^2 / (2 - Z_2)^2, \tag{1}$$

and in $\mu$ decay,

$$g_\mu^2 = g_0^2 Z_{1\mu}^{-2} Z_2^4 / (2 - Z_2)^4. \tag{2}$$

Here $Z_{1\mu}$ and $Z_{1\beta}$ are the renormalizing factors for the vertex part in $\mu$ decay and $\beta$ decay and $Z_2$ is the renormalizing factor for the Green's function. The factor $1/(2 - Z_2)$ arises because of parity nonconservation [see reference 1, Eq. (2.14′)]. The renormalizing factors $Z_2$ are assumed to be equal for the $\mu$ meson, the electron, and the neutrino, inasmuch as we are interested in virtual-particle momenta which are proportional to $\Lambda$, when one can neglect all the masses. For strongly-interacting particles, $Z_2 = 1$. For different bare charges, the equality $g_\beta^2 = g_\mu^2$ can occur only when the ratio of the renormalizing factors in (1) and (2) is equal to unity, i.e.,

---

*The probability of the process $\mu^- + p \to e^- + p$ should be of the order of $g^2M^4$ of the probability of ordinary $\mu$ capture, inasmuch as integration over the intermediate states of strongly-interacting particles certainly enters into the matrix element of this process.

$$Z_{1\mu}^{-2}/Z_{1\beta}^{-2} = Z_2^{-2}(2 - Z_2)^2. \tag{3}$$

The radiative corrections entering into the expression for the renormalization of charge or amplitude of the decay $\mu \to 3e$ must be calculated by taking into account terms $\sim (g\Lambda^2)^n$ and discarding terms $(g\Lambda^2)^n(gm^2)^q$, where $q > 0$ ($m$ is one of the external masses of the electron or muon), inasmuch as the contribution of the latter terms is very small ($\sim 10^{-13}$). Therefore, in expressions for the matrix elements, one can neglect the masses of all particles, and also all the external momenta; that is, one can assume that $\hat{p} = 0$, for all external particles, so that a number of matrix elements vanish.

In fact, for example, let us consider the first correction to the vertex part in $\mu$ decay, corresponding to the diagram of Fig. 1; we shall show that the expression for it does not have the higher terms $\sim g(g\Lambda^2)$. Since the muon and the electron lines enter into the diagram of Fig. 1 at a single point, one can formally consider in the calculation the $\mu$-meson-electron field as an external field, described by the real vector

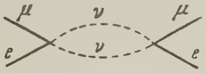

FIG. 1

$$A_\lambda = \bar{\psi}_\mu \gamma_\lambda (1 + \gamma_5)\psi_e + \bar{\psi}_e \gamma_\lambda (1 + \gamma_5)\psi_\mu,$$

which does not depend on the coordinates and the time by virtue of the conditions $\hat{p}_\mu = \hat{p}_e = 0$ (the notation is the same as in reference 1). Then, as is well known, the diagram of Fig. 1 determines the polarization operator of the field $A_\lambda$ and will be equal to (in the coordinate representation)

$$M = \mathrm{Sp}\,\{\gamma_\lambda G(x, x)\}, \tag{4}$$

where $G(x, y)$ is the Green's function of the neutrino in the external field $A_\lambda$ (since we neglect the masses of the particles, the axial interaction gives the same contribution as the vector interaction, and for brevity we shall not write it down). Starting out from the definition of the Green's function and the fact that the Hamiltonian of the interaction of the neutrino field with the field $A_\lambda$ admits of the transformation group

$$\psi'_\nu = e^{i\Phi}\psi_\nu, \qquad \bar{\psi}'_\nu = e^{-i\Phi}\bar{\psi}_\nu, \qquad \Phi = A_\lambda x_\lambda, \tag{5}$$

it is easy to show that the Green's function of the neutrino in the field of the constant vector $A_\lambda$ is equal to

$$G(x, y) = \exp\{i[\Phi(x) - \Phi(y)]\}\, G_0(x, y), \tag{6}$$

where $G_0(x, y)$ is the Green's function of the free neutrino field. Therefore, it follows that

$$G(x, x) = G_0(x, x), \tag{7}$$

$$M = 0. \tag{8}$$

As is evident from the proof, it is true not only in first order in $A_\lambda$ (which corresponds to the diagram of Fig. 1), but also in any order. This means that all the diagrams with neutrino loops and an arbitrary number of external electron and muon lines are equal to zero provided all the external electron and muon lines leave pairwise from a single point. We note that the internal lines can include electron and muon lines distributed in arbitrary fashion. The proof remains in force in this case; one need only formally separate the external vector field (for which (6) is equal to $G_0$, the Green's function in the absence of the field $A_\lambda$) and the quantum electron-muon field. It is also clear that the entire proof proceeds without change if the external field is that of the neutrino, while the loops are taken over the electron-muon field.

If the external particles are one charged particle and one neutral particle ($\mu$, $\nu$ or e, $\nu$), then it is impossible to carry out such a general proof. For example, let us consider the diagram of Fig. 2, which represents the first correction (in weak interaction) to $\beta$ decay. Just as in the preceding case, we can introduce the external constant vector

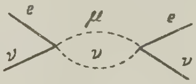

FIG. 2

$$A_\lambda = \bar{\psi}_e \gamma_\lambda (1 + \gamma_5)\psi_\nu,$$

which, however, will now be complex. Therefore, the Lagrangian will be invariant only relative to the group of infinitely small transformations (analogous to the group of transformations used in reference 2);

$$\psi = [1 - i(\tau^+\Phi + \tau\Phi^*)]\psi', \qquad \bar{\psi} = \bar{\psi}'[1 + i(\tau^+\Phi + \tau\Phi^*)].$$

$$\psi = \begin{pmatrix} \psi_\mu \\ \psi_\nu \end{pmatrix}, \qquad \tau = \sqrt{2}\begin{pmatrix} 0 & 1 \\ 0 & 0 \end{pmatrix}. \tag{9}$$

By means of (9), it is easy to obtain an expression for the Green's function of the muon-neutrino field with accuracy up to terms linear in $A_\lambda$:

$$\begin{aligned} G(x, y; A_\lambda) &= \langle 0|T(\psi(x), \bar\psi(y))|0\rangle = \langle 0|T\{[1-i(\tau^+\Phi(x) \\ &\quad + \tau\Phi^*(x))]\psi(x), \bar\psi(y)[1+i(\tau^+\Phi(y)+\tau\Phi^*(y))]\}|0\rangle \\ &= G_0(x, y) - i(\tau^+\Phi(x)+\tau\Phi^*(x))\, G_0(x, y) \\ &\quad + iG_0(x, y)(\tau^+\Phi(y)+\tau\Phi^*(y)) \\ &= G_0(x, y) - i\{\tau^+[\Phi(x)-\Phi(y)] \\ &\quad + \tau[\Phi^*(x)-\Phi^*(y)]\}\, G_0(x, y) \end{aligned} \tag{10}$$

(the latter equalities follow from the fact that $G_0$ must be diagonal in the indices of the muon and neutrino). Consequently, in this case, too,

$$G(x, x) = G_0(x, x)$$

and the polarization operator

$$\mathrm{Sp}\,\{\gamma_\lambda\tau^+G(x, x)\},$$

which determines the diagram of Fig. 2, also vanishes. Here again the result obtained remains valid if the internal part of the diagram of Fig. 2 is made more complicated in arbitrary fashion without changing the external points. However, diagrams with more than two external ends $(\bar e\nu)$ should generally no longer be equal to zero.

It follows directly from what has been shown that no corrections of first order in $g\Lambda^2$ to the vertex part are present in $\beta$ decay, inasmuch as they are described by a diagram similar to Fig. 2. In $\mu$ decay, the corrections of first order in $g\Lambda^2$ arise only in the case when, in addition to the interaction $(\bar\mu e)(\bar\nu e)$, one assumes the existence of the interactions $(\bar e\nu)(\bar\nu e)$ and $(\bar\mu\nu)(\bar\nu\mu)$. The corresponding diagrams for the vertex part will have the form of Fig. 3. Their calculation yields for the values of the renormalization of the vertex part $Z_{1\mu}^{-1}$:

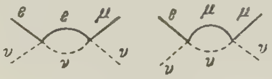

FIG. 3

$$Z_{1\mu}^{-1} = 1 + \sqrt{2}g\Lambda^2/\pi^2. \tag{11}$$

Since, in first order of $g\Lambda^2$, there is no renormalization of the Green's functions, $Z_2 = 1$ and $Z_{1\beta} = 1$, therefore

$$g_\beta^2/g_\mu^2 = 1 - 2\sqrt{2}g\Lambda^2/\pi^2. \tag{12}$$

Experimentally,[3,4] (with account of radiative corrections for the electromagnetic interaction[5,6]), the difference in the quantities $g_\beta^2$ and $g_\mu^2$ amounts to no more than 4 or 5 per cent. Hence an upper estimate for the cut-off limit

$$\Lambda \lesssim 120 \text{ Bev.} \tag{13}$$

is also obtained from (12). If the interactions $(\bar e\nu)(\bar\nu e)$ and $(\bar\mu\nu)(\bar\nu\mu)$ are absent, then the renormalization of the charge enters only in the approximation $g^2\Lambda^4$.* For its calculation, we note that in $\beta$ decay, for all diagrams for the vertex part except the chain type of Fig. 2, in the approximation $g\Lambda^2 \sim 1$ and, $g^2M^4 \ll 1$, the following relation holds, which is similar to Ward's theorem in electrodynamics,

$$\Gamma(0) = \bar u_e \left.\frac{\partial G^{-1}(p)}{\partial p_\lambda}\right|_{p=0} (1+\gamma_5)\,u_\nu \cdot \bar u_p\gamma_\lambda(1+a\gamma_5)\,u_n, \tag{14}$$

where $a = g_A/g_V$, $G(p)$ is the Green's function of the electron.

The proof of (14) follows directly from consideration of diagrams for the mass operator. For example, the correction $\sim g^2$ in the vertex part of Fig. 4 can be obtained by differentiation of the diagram of Fig. 5 for the mass operator. Chains of the type of Fig. 2 do not make a contribution to the renormalization of the vertex part, since they do not contain the higher term $\sim (g\Lambda^2)^n$. Therefore, we can assume that (14) holds for every vertex part. By using the connection between the unrenormalized and renormalized functions (see reference 1), we easily obtain

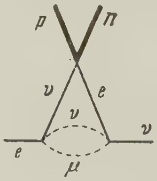

FIG. 4

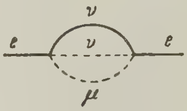

FIG. 5

$$Z_{1\beta} = Z_2/(2 - Z_2), \tag{15}$$

from (14), and, consequently, by Eq. (1), the constant of $\beta$ decay is not renormalized through weak interaction.

In $\mu$ decay in second approximation in $g\Lambda^2$, a relation similar to Ward's theorem also holds for the diagrams of Fig. 6:

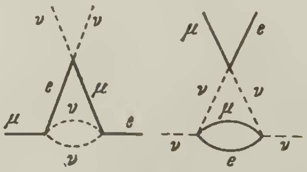

FIG. 6

---

*Renormalization of the charge in first approximation in $g\Lambda^2$ will also be absent if the signs of the interaction constants of $(\bar e\nu)(\bar\nu e)$ and $(\bar\mu\nu)(\bar\nu\mu)$ are opposite. Such a situation, however, contradicts the original assumption of Gell-Mann and Feynman[7] to the effect that all weak interactions arise as the products of the currents $j_\lambda j_\lambda^+$, $j_\lambda = (\bar e\nu) + (\bar\mu\nu) + \ldots$

$$\Gamma(0) = \bar{u}_\mu \frac{\partial G^{-1}(p)}{\partial p_\lambda}\Big|_{p=0} (1 + \gamma_5) u_e \cdot \bar{u}_\nu \frac{\partial G^{-1}(p)}{\partial p_\lambda}\Big|_{p=0} (1 + \gamma_5) u_\nu \tag{16}$$

(in higher orders in $g\Lambda^2$, the relation (16) will apply only for diagrams in which two external lines emerge from a single point, or diagrams which consist of two separate pieces which have the same general point). From (16) it is easy to demonstrate the relation

$$Z_{1\mu}^2 = Z_2^2/(2 - Z_2)^2, \tag{15$'$}$$

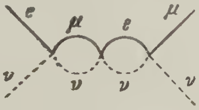

FIG. 7

whence it follows, in correspondence with (1), that the contribution of the diagrams of Fig. 6 to the renormalization is reduced to the contribution of the mass operator (all discussions of course are valid only with accuracy up to terms $\sim g^2\Lambda^4$). In addition to the diagrams of Fig. 6, the diagram of Fig. 7 enters into the vertex part; this diagram also determines the renormalization of charge in the approximation $g^2\Lambda^4$ [in the absence of the interactions $(\bar{\mu}\nu)(\bar{\nu}\mu)$ and $(\bar{e}\nu)(\bar{\nu}e)$]. Calculation of this diagram yields

$$Z_{1\mu}^{-1} = 1 + g^2\Lambda^4/2\pi^4, \tag{17}$$

so that

$$g_\beta^2/g_\mu^2 = 1 - g^2\Lambda^4/\pi^4. \tag{18}$$

From (18) we obtain for the upper estimate of the cut-off limit

$$\Lambda \lesssim 400 \text{ Bev} \tag{19}$$

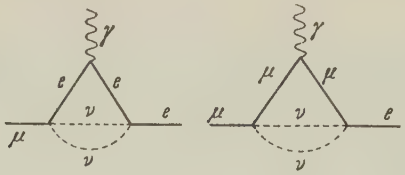

FIG. 8

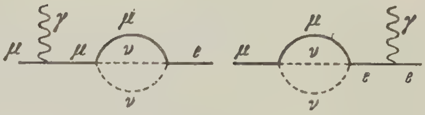

FIG. 9

We do not consider the decay $\mu \to e + \gamma$. It is well known (with great accuracy) from experiment that this process is absent. Therefore, we obtain a strong limitation on the quantity $\Lambda$, if we assume the existence of the interactions $(\bar{\mu}\nu)(\bar{\nu}\mu)$ and $(\bar{e}\nu)(\bar{\nu}e)$. In this case the amplitude of the decay $\mu \to e + \gamma$ is determined by diagrams of Fig. 8. Diagrams of the type Fig. 9 do not make a contribution to the real decay $\mu \to e + \gamma$, and are eliminated by the renormalization of the wave functions of the muon and the electron [because of the simultaneous presence of three types of interaction $(\bar{e}\nu)(\bar{\nu}e)$, $(\bar{\mu}\nu)(\bar{\nu}\mu)$, and $(\bar{\mu}\nu)(\bar{\nu}e)$, the wave function of the electron in the renormalization is expressed both in terms of the wave function of the electron and in terms of the wave function of the muon]. The probability of the decay $\mu \to e + \gamma$, computed for the diagrams of Fig. 8, is shown to be equal to (the calculations are carried out with logarithmic accuracy)

$$w_{e+\gamma} = \frac{8}{9(2\pi)^8} e^2 g^2 \Lambda^4 \left(\ln \frac{\Lambda^2}{\mu^2}\right)^2 \mu^5 \tag{20}$$

and the ratio of it to the probability of the decay $\mu \to e + \nu + \bar{\nu}$

$$w_{e+\nu+\bar{\nu}} = g^2\mu^5/192\pi^3 \tag{21}$$

amounts to

$$w_{e+\gamma}/w_{\mu+\nu+\bar{\nu}} = \frac{2}{3\pi^5} e^2 g^2 \Lambda^4 \left(\ln \frac{\Lambda^2}{\mu^2}\right)^2. \tag{22}$$

According to the experimental data of references 8 and 9, $w_{e+\gamma}/w_{+\nu+\bar{\nu}} < 2 \times 10^{-6}$. Substituting this value in (22), we get

$$\Lambda \lesssim 50 \text{ Bev} \tag{23}$$

The decay $\mu^\pm \to e^\pm + e^+ + e^-$ in the lowest approximation in $g\Lambda^2$ is described by the diagrams of Fig. 10, and can occur in the absence of the interactions $(\bar{\mu}\nu)(\bar{\nu}\mu)$ and $(\bar{e}\nu)(\bar{\nu}e)$. The ratio of the probability of the decay $\mu \to 3e$ to the probability of ordinary $\mu$ decay will be of the order of $g^4\Lambda^8$. An estimate of the cut-off value of $\Lambda$, obtained from the experimental value $w_{\mu\to 3e}/w_\mu \lesssim 10^{-6}$, is close to the estimate given by Eq. (19).

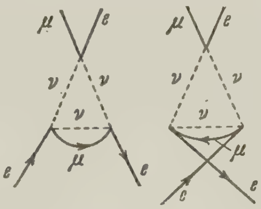

FIG. 10

All the foregoing estimates of the quantity $\Lambda$ were carried out on the basis of an analysis of the first approximations of perturbation theory. The values obtained for $\Lambda$ justified such a method of estimate, inasmuch as for $\Lambda \lesssim 100$ Bev the contribution of succeeding approximations should be small. The result of the calculation naturally depends on the concrete form of the cut-off. Therefore, the estimates used cannot be taken too literally: the inaccuracy in $\Lambda$ can reach the order of $\Lambda$ itself.

We note that the estimate (19) [but not (13)], which is based on the coincidence of the constants of $\beta$ decay and $\mu$ decay, holds even when there are two different neutrinos, namely, electron and muon. Therefore, making more precise (theoretically and experimentally) the coincidence of these constants should allow us to eliminate the hypothesis of a heavy vector meson (of mass ~ 100 M)[10].*

The author expresses his gratitude to I. Ya. Pomeranchuk and K. A. Ter-Martirosyan for useful discussions.

---

*In reference 10 a value of ~30 M was used for the value of the mass of the heavy vector meson. Actually, as has been noted by L. B. Okun', it ought to be $\approx\sqrt{4\pi e^2/g^2} \sim 100$ M.

[1] B. L. Ioffe, JETP **38**, 1263 (1960), Soviet Phys. JETP **11**, 911 (1960).

[2] B. L. Ioffe, JETP **34**, 1343 (1958), Soviet Phys. JETP **7**, 927 (1958).

[3] Swanson, Lundy, Telegdy, and Yovanovitch, Phys. Rev. Lett. **2**, 430 (1959).

[4] Fisher, Leontic, Lundby, Meunier, and Stroot, Phys. Rev. Lett. **3**, 349 (1959).

[5] S. Berman, Phys. Rev. **112**, 267 (1958).

[6] T. Kinoshita and A. Sirlin, Phys. Rev. **113**, 1652 (1959).

[7] R. Feynman and M. Gell-Mann, Phys. Rev. **109**, 193 (1958).

[8] Berley, Lee, and Bardon, Phys. Rev. Lett. **2**, 357 (1959).

[9] O'Keefe, Rigby, and Wormald, Proc. Phys. Soc. (London) **73**, 951 (1959).

[10] A. Salam and J. C. Ward, Nuovo cimento **11**, 568 (1959).

Translated by R. T. Beyer
306

SOVIET PHYSICS JETP VOLUME 11, NUMBER 5 NOVEMBER, 1960

# ON THE CONNECTION BETWEEN THE EXCITON BAND STRUCTURE AND THE NATURAL OPTICAL ACTIVITY OF CRYSTALS

YU. A. TSVIRKO

Kiev State University

Submitted to JETP editor December 18, 1958; resubmitted December 22, 1959

J. Exptl. Theoret. Phys. (U.S.S.R.) 38, 1615-1619 (May, 1960)

We have considered the structure of degenerate exciton bands in uniaxial crystals. We have obtained expressions for the dispersion of the optical activity which is caused by the intersection of the exciton energy surfaces.

## INTRODUCTION

PEKAR[1] has shown that if account is taken of the spatial dispersion of electromagnetic waves in a crystal in which there are excitons, one is led to new solutions of the Maxwell equations, which are essentially different from the previously known ones in the range of frequencies of the light which are near the exciton absorption frequency. Pekar[1,2] assumed the validity of the following expansion

$$\mathscr{E}(\mathbf{k}) = \mathscr{E}_0 + \frac{\hbar^2}{2}\sum_{ps} M_{ps}^{-1} k_p k_s + \ldots$$

for the exciton energy $\mathscr{E}(\mathbf{k})$ in the neighborhood of $\mathbf{k} = 0$ ($\mathscr{E}_0$ depends on the direction of the vector $\mathbf{k}$); this is always true for non-degenerate exciton bands, but not when degenerate bands intersect in the point $\mathbf{k} = 0$.

When electromagnetic waves are propagated along the principal optical axis of a uniaxial crystal only the exciton states that belong to degenerate bands contribute to the specific polarization.[1]

We shall show in the following, for crystals with symmetry groups $D_4^3$, $D_3^4$, $D_3^6$, ..., that the degenerate energy surfaces intersect at the point $\mathbf{k} = 0$ along the direction of the principal optical axis. These imply that there occur in $\mathscr{E}(\mathbf{k})$ terms linear in $\mathbf{k}$. Account of these terms when the $\mathscr{E}(\mathbf{k})$ surfaces intersect leads to a connection between the specific polarization and the electrical field different from the one given by Pekar.[1,2] This connection is significant in a wide range of light frequencies and causes a rotation of the plane of polarization of light in the crystal.

## 1. THE STRUCTURE OF A TWO-FOLD DEGENERATE EXCITON BAND OF A UNIAXIAL CRYSTAL FOR THE DIRECTION OF THE PRINCIPAL OPTICAL AXIS

We shall follow reference 1 and call an exciton any excited state of the crystal, the wave function of which is characterized by one continuous quantum number $\mathbf{k}$ and which is transformed upon application of a symmetry operator that commutes with the Hamiltonian according to the single-valued irreducible representation of the space group.

We shall everywhere consider $\mathbf{k} = (0, 0, k)$ to be a dimensionless wave vector within the interval $-\pi \le k \le \pi$.

As an example we shall study the behavior of $\mathscr{E}(k)$ for excitons in crystals with groups $D_4^3$ and $C_{4h}^1$. For $k = 0$ the wave functions $\psi_{11}(0)$ and $\psi_{21}(0)$, transforming as $x + iy$ and $x - iy$ respectively, correspond to the same energy $\mathscr{E}(0)$.

The matrices of the irreducible representations of the group $D_4^3$, obtained from the E representation of the group $C_4$ and constructed by Seitz' method,[3] are of the form

$$D_{1,2}(u_2) = \begin{pmatrix} 0 & 1 \\ 1 & 0 \end{pmatrix}, \qquad D_{1,2}(t) = \begin{pmatrix} \exp(ikt_3) & 0 \\ 0 & \exp(-ikt_3) \end{pmatrix},$$

$$D_1(\hat{4}_{00^1/_4}) = i\begin{pmatrix} \exp(ik/4) & 0 \\ 0 & -\exp(i3k/4) \end{pmatrix},$$

$$D_2(\hat{4}_{00^1/_4}) = -D_1(\hat{4}'_{00^1/_4}). \tag{1}$$

In the group there is an element $u_2$ which rotates the wave vector. $D_1$ and $D_2$ can therefore be brought to a real form.[4] Let $\psi_{11}(k)$ and $\psi_{12}(k)$ transform according to $D_1$, and $\psi_{21}(k)$ and $\psi_{22}(k)$ according to $D_2$. One can immediately verify that the functions

$$\xi_j = \frac{1}{\sqrt{2}}[\psi_{1j}(k) + \psi_{2j}(-k)], \quad \eta_j = \frac{i}{\sqrt{2}}[\psi_{1j}(k) - \psi_{2j}(-k)]$$

are transformed through real matrices. It is well known[5] that this leads to

$$\psi_{1j}^*(k) = e^{i\alpha}\psi_{2j}(-k). \tag{2}$$

If $\mathscr{E}_1(k)$ and $\mathscr{E}_2(k)$ belong respectively to the representations $D_1(k)$ and $D_2(k)$, it follows from (2) that

$$\mathscr{E}_1(k) = \mathscr{E}_2(-k). \tag{3}$$

For the group $C_{4h}^1$ (which contains an inversion) the matrices analogous to (1) have the form

$$D'_{1,2}(\sigma) = \begin{pmatrix} 0 & 1 \\ 1 & 0 \end{pmatrix}, \qquad D'_{1,2}(t) = \begin{pmatrix} \exp(ikt_3) & 0 \\ 0 & \exp(-ikt_3) \end{pmatrix}$$

$$D'_1(\hat{4}) = \begin{pmatrix} i & 0 \\ 0 & i \end{pmatrix}, \qquad D'_2(\hat{4}) = -D'_1(\hat{4}). \tag{4}$$

These representations can also be brought into real form, but now the functions

$$\frac{1}{\sqrt{2}}[\psi'_{11}(k) + \psi'_{22}(k)], \qquad \frac{i}{\sqrt{2}}[\psi'_{11}(k) - \psi'_{22}(k)], \ldots,$$

will be transformed according to a real representation; hence it follows that

$$\psi'^{*}_{11}(k) = e^{i\beta}\psi'_{22}(k), \qquad \psi'^{*}_{12}(k) = e^{i\beta}\psi'_{21}(k). \tag{5}$$

To the representation $D'_2(k)$ belong the complex conjugate (transposed) functions of the representation $D'_1(k)$, so that

$$\mathscr{E}'_1(k) = \mathscr{E}'_2(k). \tag{6}$$

If thus the group $C_4^1$ is supplemented with a plane perpendicular to the $\hat{4}$ axis, the degenerate bands are not split up when $k \neq 0$.

One can show that Eq. (3) is valid for degenerate exciton bands of crystals which possess other spatial symmetry groups with one axis of order higher than 2, provided that among the symmetry elements that change $k$ to $-k$ there is no inversion or a plane of reflexion. These groups are $D_n^j$, $C_n^j$ ($n = 3, 4, 6$), and others.

The expansion of the energy of the two-fold degenerate exciton bands in powers of $k$ is for uniaxial crystals of the form

$$\mathscr{E}_1(k) = \mathscr{E}_0 + \sum_n a_n k^n, \qquad \mathscr{E}_2(k) = \mathscr{E}_0 + \sum_n (-1)^n a_n k^n, \tag{7}$$

if Eq. (3) is satisfied.

Equation (3) is valid also for the electron bands of the same crystals if one neglects the spin-orbit interaction (see, for instance, reference 6), since we have used in deriving (3) only the definition of the exciton state, which can include also a spinless electron.

Pekar[1] considered the spatial dispersion of electromagnetic waves in a uniaxial crystal in the approximation $a_1 = 0$. We shall consider the case where $a_1 \neq 0$ and where the bands $\mathscr{E}_1(k)$ and $\mathscr{E}_2(k)$ intersect along the direction $(0, 0, k)$.

## 2. THE PROPAGATION OF A PLANE ELECTROMAGNETIC WAVE IN A UNIAXIAL DIELECTRIC CRYSTAL IN THE DIRECTION OF THE PRINCIPAL OPTICAL AXIS

Let $H$ be the energy operator of the crystal and $W$ the operator of the interaction energy of the crystal with the electromagnetic field.[*] We shall take the wave function of a crystal perturbed by the small alternating electrical field of the light wave in the form

$$\Psi = \Psi_0 + \sum_{q,s,k} C_{qs}(k)\psi_{qs}(k) + \ldots, \qquad |C_{qs}(k)| \ll 1, \tag{8}$$

where $\psi_{qs}(k)$ is the exciton-state wave function, $q$ the number of the irreducible representation of the space group, and $s$ the number of the function belonging to the $q$-th irreducible representation. All other excited states of the crystal will in the following be taken into account phenomenologically.

We shall neglect the difference between the magnetic induction and the magnetic field strength. This neglect enables us to write down the energy of the interaction of the crystal with the electromagnetic field in the form

$$W = -\frac{1}{c}\int \hat{\mathbf{P}}(\mathbf{r}')\,\mathbf{A}(\mathbf{r}'t)\,d\tau',$$

$$\mathbf{A}(\mathbf{r}t) = \mathbf{A}_0 \exp\{i(\varkappa z/d - \omega t)\} + \mathbf{A}_0^* \exp\{-i(\varkappa z/d - \omega t)\},$$

$$\mathbf{A}_0 = (\mathbf{A}_{0x}, A_{0y}, 0), \qquad \varkappa = n\omega d/c, \tag{9}$$

where $d$ is the lattice constant in the $z$ direction. The field $\mathbf{A}(\mathbf{r}, t)$ is assumed to be sufficiently smooth ($d \ll \lambda$). The coefficients $C_{qs}(k)$ are determined from the Schrödinger equation

$$\begin{aligned}[i\hbar\partial/\partial t - \mathscr{E}_q(k)]\,C_{qs}(k) \\ = -i\omega_q(k)c^{-1}V\langle qsk|\mathbf{P}(0)|0\rangle(\mathbf{A}_0\delta_{\varkappa,k}\exp(-i\omega t) \\ + \mathbf{A}_0^*\delta_{-\varkappa,k}\exp(i\omega t)).\end{aligned} \tag{10}$$

when we expand $\mathscr{E}_q(\kappa)$ in the power series (7) we retain the linear terms

$$\mathscr{E}_1(\varkappa) = \mathscr{E}_0 + \varkappa\partial\mathscr{E}_1/\partial k, \qquad \mathscr{E}_2(\varkappa) = \mathscr{E}_0 - \varkappa\partial\mathscr{E}_1/\partial k.$$

A cumbersome but elementary calculation leads to the following expression for the average specific dipole moment

$$\mathbf{P}(\mathbf{r}, t) = \int \hat{\mathbf{P}}(\mathbf{r})\,\Psi^*\Psi\,d\Omega.$$

In complex form

$$P_x = \beta_{xx}E_x + \beta_{xy}E_y,$$

$$\beta_{xx} = \beta_{yy} = \frac{a}{\omega_0}\left[\frac{\mathscr{E}_0 - \hbar\omega}{(\mathscr{E}_0 - \hbar\omega)^2 - (\varkappa\partial\mathscr{E}_1/\partial k)^2} + \frac{\mathscr{E}_0 + \hbar\omega}{(\mathscr{E}_0 + \hbar\omega)^2 - (\varkappa\partial\mathscr{E}_1/\partial k)^2}\right],$$

$$\beta_{yx} = \beta_{xy}^* = i\frac{a}{\omega_0}\frac{\partial\mathscr{E}_1}{\partial k}\varkappa\left[\frac{1}{(\mathscr{E}_0 - \hbar\omega)^2 - (\varkappa\partial\mathscr{E}_1/\partial k)^2} + \frac{1}{(\mathscr{E}_0 + \hbar\omega)^2 - (\varkappa\partial\mathscr{E}_1/\partial k)^2}\right],$$

$$\frac{a}{\omega_0} = \frac{V}{4}\left|\int [P_x(0) - iP_y(0)]\,\Psi_0\psi_{11}(0)\,d\Omega\right|^2. \tag{11}$$

We neglected in $\beta_{xy}$ corrections of the order $(d/\lambda)^2$. In deriving (11) we used the property (2) of the wave functions.

Let the condition $\kappa\partial\mathscr{E}_1/\partial k \ll \mathscr{E}_0 - \hbar\omega$ be satisfied for the frequency $\omega$. We can then neglect the small extra terms in the denominators of (11). We take the other excited states of the crystal into account by introducing $\epsilon'$ through $\mathbf{D} = \epsilon'\mathbf{E} + 4\pi\mathbf{P}$.

---

[*] Here and in the following we retain Pekar's notation.[1]

The specific rotation of the plane of polarization of the light $\rho$ can be obtained from (11) by the well-known equations of crystal optics[7]

$$\rho = \frac{K(\lambda^2+\lambda_0^2)}{(\lambda^2-\lambda_0^2)^2}, \qquad K = \frac{4\pi}{\hbar^2c^2}\frac{a}{\omega_0}\frac{\partial\mathscr{E}_1}{\partial k}\lambda_0^2 d, \qquad \frac{\lambda}{\lambda_0} = \frac{\mathscr{E}_0}{\hbar\omega}. \tag{12}$$

Expression (12) differs from the analogous equations obtained semi-phenomenologically by Agranovich and Rukhadze[8] and from Chandrasekhar's empirical formula,[9] because $\lambda_0^2$ appears in the numerator.

The classical analysis[8] of the optical activity disregards the extra terms of $\rho$, obtained by expanding the exciton transition frequency $\omega_q(k)$ (which occurs in the quantum mechanical expression for the oscillator strength) in powers of $d/\lambda$ [$\omega_q(k)$ is defined here by (10)]. Equation (12) is thus a natural way of making the equations obtained in reference 8 more exact.

Agranovich[10] obtained a dispersion relation of the form (12) without taking into account the intersection of the exciton bands. Equation (12) differs therefore from the corresponding dependence (12.2) of reference 10 not only in the meaning of the constants occurring in K but also in the range of applicability. In the case of uniaxial crystals, Eq. (12.2) of reference 10 is, for instance, applicable only for directions of the propagation of light which are different from the direction of the principal optical axis.

Chandrasekhar's formula[9] describes the dispersion of the optical activity of quartz well, but differs strongly from the experimental dependence $\rho(\lambda)$ in the wavelength range $\lambda \sim 0.4\mu$ for benzyl crystals.

Chandrasekhar's empirical formula is thus not universal, and can be applied only when $\lambda_0$ corresponds to an isolated absorption band. Equation (12) can also be applied when $\lambda_0$ corresponds to an isolated exciton absorption band, provided all other absorption bands are removed from the wavelength region under consideration.

As (12) is somewhat different from Chandrasekhar's expression, the parameters K and $\lambda_0$ in (12) will, of course, be different from the corresponding quantities in reference 9. One can, for instance, obtain for quartz satisfactory agreement with experiment if one chooses $K = 7.1$, $\lambda_0 = 0.081\,\mu$ ($\rho$ is expressed, as usual, in degrees per milimeter, and $\lambda$ in $\mu$). The parameter $\lambda_0$ must also occur in the formula for the dispersion of the refractive index $n_0(\lambda)$ of quartz. If we put $a = 3 \times 10^4$ and assume $\epsilon' = 1$ in (11), the expression for $n_0(\lambda)$, obtained from (11) by the usual methods [$n_0^2 - 1 = 1.4\lambda^2/(\lambda^2 - \lambda_0^2)$], as well as the expression for $\rho(\lambda)$, will differ by less than 1 or 2% from the experimental values, in a wide range of wave lengths $\lambda < 1\,\mu$.

The slight difference between the proposed expressions for $\rho$ and $n_0$ and the experimental ones may be caused by the fact that we have not taken into account virtual transitions to exciton states with $\lambda_0'$ lying within the infrared region, $\lambda_0' \sim 8.8\,\mu$ and $20\,\mu$. Taking these into account is especially important for $n_0(\lambda)$ when $\lambda > 1\,\mu$. We have also neglected other contributions to $n_0$ and $\rho$, connected with virtual transitions to nonexciton states, and also the contributions to the rotation, which were considered by Agranovich.[10]

Taking into account the approximate character of our expressions, we can use the numerical values of K and a only for an estimate of the width of the exciton band $\Delta\mathscr{E}$ in quartz, replacing $\partial\mathscr{E}/\partial k$ in (12) by $\Delta\mathscr{E}/2\pi$. We obtain as a result $\Delta\mathscr{E} \approx 0.8$ ev.

In the range of light frequencies near $\omega_0$ one can neglect the terms with $\mathscr{E}_0 + \hbar\omega$ in the numerators of (11).

The refractive indices for left-hand and right-hand circularly polarized waves, $E_y^{(r)} = iE_x^{(r)}$ and $E_y^{(l)} = -iE_x^{(l)}$, are determined from

$$(\varepsilon' - n^2)(\xi \pm n) - \frac{4\pi ac}{\omega_0^2\, d\partial\mathscr{E}_1/\partial k} = 0, \qquad \xi = \frac{\hbar c}{d\partial\mathscr{E}_1/\partial k}\,\frac{\omega-\omega_0}{\omega_0}, \tag{13}$$

where the upper and lower signs correspond to $n^{(r)}$ and $n^{(l)}$ (with $\partial\mathscr{E}_1/\partial k > 0$).

We show in the figure the frequency dependence of real and positive $n^{(r)}$ and $n^{(l)}$ for the following values of the parameters (cf. reference 1)

$$\hbar\omega_0 = 2\text{ev}, \qquad \varepsilon' = 2, \qquad \partial\mathscr{E}_1/\partial k = (2\pi)^{-1}\,\text{ev}, \qquad d = 5.29\ \text{A},$$
$$a = (e^2\hbar/2m)Nf, \qquad N = 6{,}76\cdot 10^{21}\text{cm}^{-3},$$

Such a behavior of the dependence $n(\omega)$ is qualitatively the same as the phenomenological dependence $n(\omega)$ obtained by Ginzburg[11] for a gyrotropic medium.

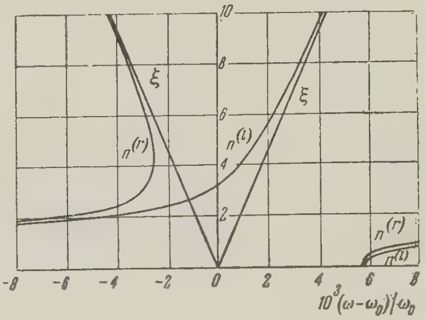

In the frequency range $\omega' < \omega < \omega''$ with

$$(\omega_0 - \omega')/\omega_0 \approx 2.51 \cdot 10^{-2};$$
$$(\omega'' - \omega_0)/\omega_0 \approx 5.75 \cdot 10^{-3}$$

only the $l$ wave has a real positive index of refraction, while the r waves have a complex index, $n_1^{(r)} = n_2^{(r)*}$. In an infinite medium the amplitudes of these two waves must be set equal to zero. In a semi-infinite crystalline medium $(z > 0)$ the r wave is exponentially damped when moving away from the surface. In the enantiomorphous modification of the crystal $(\partial \mathscr{E}_1/\partial k < 0)$, on the other hand, only the r wave will be propagated.

The author expresses his deep gratitude to Professor S. I. Pekar for his interest in this paper and for valuable discussions.

---

[1] S. I. Pekar, JETP **33**, 1022 (1957), **34**, 1176 (1958); Soviet Phys. JETP **6**, 785 (1958), **7**, 813 (1958).

[2] S. I. Pekar, JETP **36**, 451 (1959), **35**, 522 (1958); Soviet Phys. JETP **9**, 314 (1959), **8**, 360 (1959).

[3] F. Seitz, Ann. Math. **37**, 17 (1936).

[4] C. Herring, Phys. Rev. **52**, 361 (1937).

[5] E. Wigner, Nachr. Akad. Wiss. Göttingen, Math.-physik. Kl. 546 (1932).

[6] J. R. Reitz, Phys. Rev. **105**, 1233 (1957).

[7] M. Born, Optik, Berlin, 1933.

[8] V. M. Agranovich and A. A. Rukhadze, JETP **35**, 982 (1958), Soviet Phys. JETP **8**, 685 (1959).

[9] S. Chandrasekhar, Proc. Indian Acad. Sci. **A35**, 103 (1952); **A36**, 118 (1952); **A39**, 243 (1954).

[10] V. M. Agranovich, Оптика и спектроскопия (Optics and Spectroscopy) **2**, 739 (1957).

[11] V. L. Ginzburg, JETP **34**, 1593 (1958), Soviet Phys. JETP **7**, 1096 (1958).

Translated by D. ter Haar
307

SOVIET PHYSICS JETP VOLUME 11, NUMBER 5 NOVEMBER, 1960

# THE FORM FACTOR AND THE $\mu$ CAPTURE BY LIGHT NUCLEI WITH SPIN $\frac{1}{2}$

HO TSO-HSIU

Joint Institute for Nuclear Research

Submitted to JETP editor December 28, 1959

J. Exptl. Theoret. Phys. (U.S.S.R.) **38**, 1620-1626 (May, 1960)

Various processes of $\mu$ capture by light nuclei with spin $\frac{1}{2}$ without emission of neutrons or protons are investigated. The calculations show that the form factor gives a significant correction to the effects accompanying these processes.

## 1. INTRODUCTION

THERE has been a great deal of interest recently in studying the effect of the form factor on weak interaction processes.[1] The role of the form factor in the $\mu$ capture by light nuclei without emission of neutrons or protons has been investigated by several authors.[2] Strictly speaking, however, the formulas given by these authors are useful only for the description of a nucleus in the ground state with zero spin, since the rate of capture and the state of polarization of the nucleus in the final state depend to a great extent on the hyperfine structure of the $\mu$-mesic atoms, This circumstance was noted by Bernstein et al. and also by Shmushkevich.[3] It is therefore of interest to investigate the effect of the form factor on the process of $\mu$ capture without emission of neutrons with account of the hyperfine structure.

## 2. FORMULATION OF THE PROBLEM

The weak-interaction Hamiltonian including the form factor can be written in the form

$$H_W = \frac{1}{\sqrt{2}} G\overline{\Psi}_p (V_\alpha + A_\alpha)\Psi_n \overline{\Psi}_\nu \gamma_\alpha (1 + \gamma_5)\Psi_\mu,$$

$$V_\alpha = \gamma_\alpha + (\mu'/2m_p)\sigma_{\alpha\beta}K_\beta, \qquad A_\alpha = \lambda\gamma_\alpha\gamma_5 + (if'/m_\mu)\gamma_5 K_\alpha. \tag{1}$$

where

$$K = p_p - p_n; \qquad \sigma_{\alpha\beta} = -\tfrac{1}{2} i (\gamma_\alpha\gamma_\beta - \gamma_\beta\gamma_\alpha);$$

$\lambda$ is the ratio of the Gamow-Teller and Fermi coupling constants and is equal to 1.2 in the case of $\beta$ decay; the term involving $\mu'$ is the "weak magnetism" term [$\mu'$ is the sum of the anomalous gyromagnetic ratios, $\mu' = \mu_p - \mu_n - 1 = 3.7$ (reference 4)], and the term involving $f'$ represents an induced pseudoscalar (in order of magnitude $f'$ is equal to $8\lambda$ in the case of $\mu$ capture by a proton[5]).

If the $\mu$ meson is captured by a nucleus, the matrix element can be expressed in the form

$$\frac{G}{\sqrt{2}}\int d\tau \langle \nu | \gamma_\alpha (1+\gamma_5) | \mu\rangle \left\langle f \left| \sum_{i=1}^{A} \tau_i^{(-)} (V_\alpha + A_\alpha) \right| i \right\rangle \delta(\mathbf{r} - \mathbf{r}_i), \tag{2}$$

where $\nu$, $\mu$, f, and i are the wave functions of the neutrino, the $\mu$ meson, and of the final and the initial states of the nucleus, respectively; $\tau_i^{(-)}$ is an operator which converts a proton into a neutron, and $d\tau$ is the element of the nuclear volume.

Before the capture the $\mu$ meson is almost at rest, so that we may use the non-relativistic wave function of the $\mu$ meson. We also neglect the momentum of the protons in the initial state. As was shown by Primakoff and Ioffe,[2] this leads to an error which does not exceed a few percent. With these approximations the matrix element takes the form

$$\tfrac{1}{2} G \Big[ \langle v_\nu | 1 - \boldsymbol{\sigma}\mathbf{n} | v_\mu \rangle \langle f | \sum_{i=1}^{A} \tau_i^{(-)} (V - P\boldsymbol{\sigma}\mathbf{n}) e^{-i\mathbf{q}\mathbf{r}_i} \varphi_\mu | i \rangle$$
$$- \langle v_\nu | (1 - \boldsymbol{\sigma}\mathbf{n})\boldsymbol{\sigma} | v_\mu \rangle \langle f | \sum_{i=1}^{A} \tau_i^{(-)} A\boldsymbol{\sigma} e^{-i\mathbf{q}\mathbf{r}_i} \varphi_\mu | i \rangle \Big], \tag{3}$$

where $\mathbf{q}$ is the momentum of the neutrino, $\mathbf{n}$ is a unit vector in the direction of the momentum of the neutrino, $\varphi_\mu = \pi^{-1/2}(Z/a_\mu)^{3/2}\exp(-Zr/a_\mu)$ is the Coulomb wave function of the $\mu$ meson, $a_\mu = \hbar^2/m_\mu e^2$ is the Bohr radius of the $\mu$-mesic hydrogen atom, $v_\nu$ and $v_\mu$ are the spin wave functions of the neutrino and the $\mu$ meson, and

$$V = 1 + \tfrac{1}{2}\beta, \quad A = \lambda + \tfrac{1}{2}\mu\beta, \quad P = \tfrac{1}{2}\beta(f + \mu),$$
$$\beta = q/m_p, \qquad \mu = \mu' + 1, \qquad f = f' - \lambda. \tag{4}$$

Here we restrict ourselves to the calculation of the $\mu$ capture process by a nucleus with spin $\frac{1}{2}$. After the capture the nucleus goes into a state with spin $\frac{1}{2}$ or $\frac{3}{2}$ without emitting a neutrino. The $\mu$ meson is depolarized as it slows down and transfers part of its polarization to the nucleus during the formation of a definite state of the hyperfine structure. As it is well known that the hyperfine splitting of the ground state level in mesic hydrogen is appreciably larger than $\hbar/\tau$ ($\tau$ is the half-life of the $\mu$ meson), the states of the hyperfine structure are incoherent.

It was shown by Shmushkevich[6] that the corresponding density matrices for the initial states are

$$\rho_+ = \tfrac{1}{4}\left(1 + \varkappa\mathbf{j}\,(\boldsymbol{\sigma}_p + \boldsymbol{\sigma}_\mu) + \tfrac{1}{3}\,\boldsymbol{\sigma}_p\,\boldsymbol{\sigma}_\mu\right) \text{ (triplet state)},$$
$$\rho_- = \tfrac{1}{4}(1 - \boldsymbol{\sigma}_p\,\boldsymbol{\sigma}_\mu) \text{ (singlet state)}. \quad (5)$$

It is seen from (5) that in the triplet state the polarization vectors of the proton and the $\mu$ meson are identical and equal to $\kappa\mathbf{j}$. This implies that half of the polarization of the $\mu$ meson is transferred to the nucleus.

The theory proposed by Shmushkevich is, in a sense, confirmed by the latest experiments performed by Ignatenko et al.[7] They measured the polarization of a $\mu$ meson captured in the K shell of a phosphorus nucleus with spin $\frac{1}{2}$ and obtained the value 8.5%. This is exactly half the value of the polarization (~ 17%) of the $\mu$ meson in the capture by a nucleus with spin zero. Clearly, half of the polarization is in this case transferred to the nucleus.

Let us assume that the state of the mesic atom is a mixture of two possible states of the hyperfine structure. Then the density matrix before the capture is given by the formula ($b$ is the statistical weight of the singlet state)

$$\rho = (1-b)\,\rho_+ + b\rho_- = 1 + \boldsymbol{\xi}_p\,\boldsymbol{\sigma}_p + \boldsymbol{\xi}_\mu\,\boldsymbol{\sigma}_\mu + \varepsilon\boldsymbol{\sigma}_p\,\boldsymbol{\sigma}_\mu,$$

$$\varepsilon = \frac{1}{3}(1-4b), \qquad \boldsymbol{\xi}_p = \boldsymbol{\xi}_\mu = (1-b)\,\varkappa\mathbf{j}. \quad (6)$$

The value of $\boldsymbol{\xi}_\mu$ can be easily determined by measuring the asymmetry coefficient for the decay of the $\mu$ meson before capture. The quantity $b$ is equal to $\frac{1}{4}$ if we assume that the $\mu$ meson goes into the ground state and emits $\gamma$ rays. However, if there exists some mechanism which involves transitions between two states of the hyperfine structure, the value of $b$ is less than $\frac{1}{4}$. Its value can be estimated from the measured value of the asymmetry parameter of the $\mu$ meson, if we assume that the $\mu$ meson has the polarization predicted by the theory before this mechanism comes into effect, i.e., 8.5%, and then compare the theoretical value with the experimental one, since the transition from the triplet state to the singlet state involves an additional depolarization.

## 3. RESULTS OF THE CALCULATIONS

After the capture of the $\mu$ meson the nucleus goes over into a state with spin $\frac{1}{2}$ or $\frac{3}{2}$. Treating the transitions into either of these states separately and using the usual method of calculation, we can derive formulas for the transition probability, the angular distribution, the polarization of the nucleus in the direction of flight of the $\mu$ meson and of the recoil nucleus, and also for the angular correlation between $\nu - \beta$ and $\mu - \beta$. We shall give here the relatively simple formulas for the special case $\boldsymbol{\xi}_p = \boldsymbol{\xi}_\mu = \boldsymbol{\xi}$, $a = \frac{1}{4}$, $\epsilon = 0$; the formulas for the general case are given in the Appendix. The total transition probability is

$$W = (G^2Z^3/2\pi^2a_\mu^3)\,N_0q^2\,(1 - q/Am_p),$$
$$N_0 = (1+\beta)\,|M_F|^2 + (\lambda^2 + \tfrac{1}{2}\lambda\beta(2\mu - f))\,|M_{GT}|^2,$$
$$|M_F|^2 = \frac{1}{2J_i+1}\,\Big|\langle f|\sum_{i=1}^{A}\tau_i^{(-)}e^{i\mathbf{q}\mathbf{r}_i}\,\varphi_\mu|i\rangle\Big|^2,$$
$$|M_{GT}|^2 = \frac{1}{2J_i+1}\,\Big|\langle f|\sum_{i=1}^{A}\tau_i^{(-)}\boldsymbol{\sigma}e^{i\mathbf{q}\mathbf{r}_i}\,\varphi_\mu|i\rangle\Big|^2. \quad (7)$$

Ioffe has shown that the matrix elements $M_F$ and $M_{GT}$ can be expressed in terms of the matrix element for the $\beta$ decay in the following way:

$$M_F = M_F^\beta\,(1 - \tfrac{1}{6}q^2\langle r^2\rangle_e),$$
$$M_{GT} = M_{GT}^\beta\,(1 - \tfrac{1}{6}q^2\langle r^2\rangle_A), \quad (8)$$

where $\langle r^2\rangle_e$ and $\langle r^2\rangle_A$ are the square radii of the charge corresponding to the vector and pseudovector transitions. The numerical values of $M_F^\beta$ and $M_{GT}^\beta$ can be obtained from the experimental data on the $\beta$ decay, and $\langle r^2\rangle_e$ can be calculated with the help of the experimental data on the inelastic scattering of electrons by nuclei. Since the matrix element $\psi_f^*\sigma\psi_i$ has the same form as the matrix element for the magnetic dipole transition, $\langle r^2\rangle_A$ can be regarded as the square radius in the magnetic radiative transition of the nucleus corresponding to the same isotopic multiplet.

In the above-mentioned formulas we have neglected the contribution of the quadrupole moment, which, according to the calculations of Ioffe, does not exceed a few percent.[2]

The angular distribution of the neutrinos with respect to the direction of flight of the $\mu$ meson is given by the formula

$$W(\theta) = 1 - a\boldsymbol{\xi}\mathbf{n};$$
$$a = \frac{1+\beta-(2/\sqrt{3})\,[\lambda - (\beta/2)\,(f-\lambda)]\,\mathrm{Re}\,\rho + (\lambda^2 - \lambda\beta f)\,\rho^2/3}{1+\beta+[\lambda^2 + (\lambda\beta/3)\,(2\mu - f)]\,\rho^2}, \quad J' = {}^1/_2,$$
$$a = -\frac{2\lambda^2 + \lambda\beta\,(3\mu + f)}{3\lambda^2 + \lambda\beta\,(2\mu - f)}, \qquad J' = {}^3/_2. \quad (9)$$

Here $\rho = M_{GT}/M_F$, and $J'$ is the total angular momentum of the final state of the nucleus. It is seen from formula (9) that the coefficient of the angular distribution for the pure Gamow-Teller transition is independent of the matrix element, and the form factor gives rise to a large correction to the asymmetry coefficient. This means that we can determine the form factor by such an experiment. In a transition without change of spin of a nucleus with spin $\frac{1}{2}$ the coefficient of the angular distribution depends on the ratio of the matrix elements, which can be determined from the experimental data on $\beta$ decay.

The polarization of the nucleus in the direction of incidence of the $\mu$ meson is given by

$$W(m') = 1 + B(m'/j')\,\xi\mathbf{n}_j;$$

$$B = \frac{1+\beta+(2/\sqrt{3})[\lambda+(\beta/6)(3\lambda+2\mu-f)]\operatorname{Re}\rho+[\lambda^2+(\lambda\beta/3)(2\mu-f)]\rho^2/3}{1+\beta+[\lambda^2+(\lambda\beta/3)(2\mu-f)]\rho^2},$$

$$J' = {}^1/_2, \qquad B = 2, \quad J' = {}^3/_2; \tag{10}$$

$\mathbf{n}_j$ is the direction of polarization of the nucleus. In a pure Gamow-Teller transition the coefficient B is independent of the matrix element and of the coupling constants $\lambda$, $\mu$, and f. This has the consequence that we cannot obtain any information on the form factor by measuring the polarization in the direction of emission of the $\mu$ meson. Strictly speaking, this result is true only for the terms of lowest order in $\beta$. If terms involving $\beta^2$ are included, the correction amounts to 5 to 10%. This correction is given in the Appendix [formula (21)].

The polarization of the nucleus in the direction of emission of the neutrino is given by

$$W(m') = 1 + C(m'/J')\,\mathbf{n}\mathbf{n}_j + D\left(m'^2 - {}^5/_4\right)\left({}^1/_3 - (\mathbf{n}\mathbf{n}_j)^2\right);$$

$$C = {}^2/_3\,\frac{(\lambda^2+\lambda\mu\beta)\rho^2+\sqrt{3}[\lambda+(\beta/2)(\lambda-f)]\operatorname{Re}\rho}{1+\beta+[\lambda^2+(\lambda\beta/3)(2\mu-f)]\rho^2}, \qquad J' = {}^1/_2,$$

$$C = \frac{\lambda^2+\lambda\mu\beta}{\lambda^2+(\lambda\beta/3)(2\mu-f)}, \qquad J' = {}^3/_2,$$

$$D = 0, \qquad J' = {}^1/_2,$$

$$D = -\frac{(\beta\lambda/2)(\mu+f)}{\lambda^2+(\lambda\beta/3)(2\mu-f)}, \qquad J' = {}^3/_2. \tag{11}$$

In our case the angular correlation between $\mu$ and $\gamma$ is not of any great interest, since it is always isotropic and independent of whether we do or do not include a form factor. The angular correlation between $\nu$ and $\gamma$, on the other hand, depends on the form factor very strongly. Moreover, the latter case has the advantage that the strength of the correlation does not depend on the matrix element. Here we shall give the results for a number of special cases and leave the general formulas for the Appendix. Let $J_i$, $J'$, and $J_f$ be the spins of the initial, intermediate, and final states, respectively. Then the formulas for the angular correlation in the transition $J_i \rightarrow J' \rightarrow J_f$ are

$$\begin{aligned}
&1 - 3D\cos^2\theta/(3+D), && 0\rightarrow 1\rightarrow 0;\\
&1 + 3D\cos^2\theta/(6-D), && 0\rightarrow 1\rightarrow 1;\\
&1 - 3D\cos^2\theta/(30+D), && 0\rightarrow 1\rightarrow 2;\\
&1 - 3D\cos^2\theta/(6+2D), && {}^1/_2\rightarrow {}^3/_2\rightarrow {}^1/_2;\\
&1 + 6D\cos^2\theta/(15-D), && {}^1/_2\rightarrow {}^3/_2\rightarrow {}^3/_2;\\
&1 + 3D\cos^2\theta/(30-5D), && {}^1/_2\rightarrow {}^3/_2\rightarrow {}^5/_2.
\end{aligned} \tag{12}$$

Here $\theta$ is the angle between the directions of emission of the neutrino and the $\gamma$ quantum emitted by the excited nucleus. It is easily seen that the form factor gives a large contribution to the angular correlation. For example, in the transition $0 \rightarrow 1 \rightarrow 0$ the correlation is isotropic without the form factor, while the presence of the form factor leads to anisotropy in the angular correlations which may be as large as 50%.

The angular correlation between the $\mu$ meson and the electron is given by

$$\begin{aligned}
&W(\theta) = 1 + E\xi\mathbf{v}_e;\\
&E = 1 - \beta^2(f+\mu)^2/12\lambda^2, \quad 0\rightarrow 1\rightarrow 0,\\
&E = 2 - \beta^2(f+\mu)^2/12\lambda^2, \quad {}^1/_2\rightarrow {}^3/_2\rightarrow {}^1/_2,
\end{aligned} \tag{13}$$

where $\mathbf{v}_e$ is the velocity of the electron. Generally speaking, this correlation is difficult to observe, except in the case when the life time of the nucleus after capture is very small (for example, in the transitions $C^{12} \rightleftarrows B^{12}$, $C^{13} \rightleftarrows B^{13}$). It may therefore be possible to preserve the polarization of the nucleus after capture in an appropriate magnetic field. It is difficult to determine the form factor in this way, but the transition $\frac{1}{2} \rightarrow \frac{3}{2} \rightarrow \frac{1}{2}$ as well as the transition $0 \rightarrow 1 \rightarrow 0$ can be used for the purpose of finding out whether the nucleus is polarized by the meson and of determining the helicity of the $\mu$ mesons, since a different helicity of the $\mu$ meson leads to different signs in the angular correlations.

The author regards it as his obligation to thank Prof. Ya. A. Smorodinskiĭ for his interest in this work and a discussion of the results, and also Prof. Chou Huang-Yuan, Prof. I. S. Shapiro, and Chou Kuang-Chao for useful comments.

## APPENDIX

We give here the general formulas which are valid with an accuracy up to terms of order $\beta^2$. Even these formulas are, of course, not sufficiently accurate, since we neglected the momentum of the proton in the initial state. However, under certain circumstances, the terms $\sim\beta^2$ can become comparable with the terms of order $\beta$ in view of the large coefficient of the anomalous magnetic moment and of the pseudoscalar term. In the derivation of the formulas describing the angular distribution of the neutrino and of the $\gamma$ quanta for oriented nuclei we used the results of the work of Beretskiĭ et al.[8] and of Falkoff and Ling.[9]

### A. Transition ½ → ½

#### 1. Total transition probability

$$W = (G^2Z^3/2\pi^2a_\mu^3)\, q^2 (1 - q/Am_p)\, N_0, \qquad N_0 = (1 + \tfrac{1}{2}\beta)^2 |M_F|^2 + (\lambda^2 + \tfrac{1}{3}\lambda\beta(2\mu - f) + \tfrac{1}{12}\beta^2(2\mu^2 + f^2))\, |M_{GT}|^2$$

$$-2\varepsilon[\lambda^2 + \tfrac{1}{3}\lambda\beta(2\mu - f) - \tfrac{1}{12}\beta^2\mu(2f - \mu)]\, |M_{GT}|^2 - 2\sqrt{3}\varepsilon[\lambda + \tfrac{1}{6}\beta(3\lambda + 2\mu - f) + \tfrac{1}{12}\beta^2(2\mu - f)]\, \mathrm{Re}\, M_F M_{GT}. \tag{14}$$

#### 2. Angular distribution of the recoil nucleus

$$W(\theta) = 1 - \xi_p \mathbf{n} N_1/N_0 - \xi_\mu \mathbf{n} N_2/N_0, \qquad N_1 = \tfrac{2}{3}[(\lambda^2 + \lambda\mu\beta + \tfrac{1}{4}\mu^2\beta^2)\, |M_{GT}|^2 - \sqrt{3}(\lambda + \tfrac{1}{2}\beta(f - \lambda) - \tfrac{1}{4}\beta^2 f^2)\, \mathrm{Re}\, M_F M_{GT}],$$

$$N_2 = (1 + \tfrac{1}{2}\beta)^2 |M_F|^2 - \tfrac{1}{3}(\lambda^2 + \lambda\beta(2\mu + f) + \tfrac{1}{4}\beta^2(2\mu^2 - f^2))\, |M_{GT}|^2. \tag{15}$$

#### 3. Polarization of the nucleus in the direction of polarization of the $\mu$ meson

$$W(m') = 1 + \xi \mathbf{n}_j 2m' N_5/N_0 + \xi_\mu \mathbf{n}_j 2m' N_6/N_0; \qquad N_5 = (1 + \tfrac{1}{2}\beta)^2 |M_F|^2 - \tfrac{1}{3}(\lambda^2 + \tfrac{1}{3}\lambda\beta(2\mu - f) + \tfrac{1}{12}\beta^2(2\mu^2 + f^2))\, |M_{GT}|^2,$$

$$N_6 = -(2/\sqrt{3})\, [\lambda + \tfrac{1}{6}\beta(3\lambda + 2\mu - f) + \tfrac{1}{12}\beta^2(2\mu - f)]\, \mathrm{Re}\, M_F M_{GT} + \tfrac{2}{3}[\lambda^2 + \tfrac{1}{3}\lambda\beta(2\mu - f) - \tfrac{1}{12}\beta^2\mu(2f - \mu)]\, |M_{GT}|^2 \tag{16}$$

($m'$ is the magnetic quantum number of the nucleus in the final state).

#### 4. Polarization of the nucleus in the direction of flight of the neutrino

$$W(m') = 1 + \mathbf{n}\mathbf{n}_j 2m' N_4/N_0, \qquad N_4 = \tfrac{2}{3}[(\lambda^2 + \lambda\mu\beta + \tfrac{1}{4}\mu^2\beta^2)|M_{GT}|^2 + \sqrt{3}(\lambda + \tfrac{1}{2}\beta(\lambda - f) - \tfrac{1}{4}\beta^2 f)\mathrm{Re} M_F M_{GT}]$$

$$-\varepsilon[(1 + \tfrac{1}{2}\beta)^2 |M_F|^2 + \tfrac{1}{3}(7\lambda^2 - \beta\lambda(4\mu - 3f) + \tfrac{1}{3}\beta^2(2\mu^2 - 4\mu f + f^2))\, |M_{GT}|^2$$

$$+ (4/\sqrt{3})(\lambda + \tfrac{1}{2}\beta(\lambda + \mu) + \tfrac{1}{4}\beta^2\mu)\, \mathrm{Re}\, M_F M_{GT}]. \tag{17}$$

### B. Transition ½ → ³⁄₂

#### 1. Total transition probability

$$W = (G^2Z^3/2\pi^2a_\mu^3)\, N_0' q^2 (1 - q/Am_p), \qquad N_0' = [(1 + \varepsilon)(\lambda^2 + \tfrac{1}{3}\lambda\beta(2\mu - f) - \tfrac{1}{12}\beta^2\mu(2f - \mu) + \tfrac{1}{12}\beta^2(\mu + f)^2]\, |M_{GT}|^2. \tag{18}$$

#### 2. Angular distribution of the recoil nucleus

$$W(\theta) = 1 + \tfrac{1}{3}\xi_p \mathbf{n} N_1'/N_0' + \tfrac{1}{3}\xi_\mu \mathbf{n} N_2'/N_0', \quad N_1' = (\lambda^2 + \lambda\mu\beta + \tfrac{1}{4}\mu^2\beta^2)\, |M_{GT}|^2, \quad N_2' = (\lambda^2 + \lambda\beta(2\mu + f) + \tfrac{1}{4}\beta^2(2\mu^2 - f^2))\, |M_{GT}|^2. \tag{19}$$

#### 3. Polarization of the nucleus in the direction of polarization of the $\mu$ meson

$$W(m') = 1 + \tfrac{2}{3} m' \xi_p \mathbf{n}_j N_3'/N_0' + \tfrac{2}{3} m' \xi_\mu \mathbf{n}_j N_4'/N_0', \qquad N_3' = [\lambda^2 + \tfrac{1}{3}\lambda\beta(2\mu - f) + \tfrac{1}{12}\beta^2(2\mu^2 + f^2)]\, |M_{GT}|^2,$$

$$N_4' = [\lambda^2 + \tfrac{1}{3}\lambda\beta(2\mu - f) - \tfrac{1}{12}\beta^2\mu(2f - \mu)]\, |M_{GT}|^2. \tag{20}$$

If $\xi_p = \xi_\mu$, then

$$W = 1 + \tfrac{2}{3}[2 - \beta^2(f + \mu)^2/12(1 + \varepsilon)\lambda^2]\, m' \xi \mathbf{n}_j. \tag{21}$$

#### 4. Polarization of the nucleus in the direction of emission of the neutrino

$$W(m') = 1 + \tfrac{2}{3} m' \mathbf{n}\mathbf{n}_j N_5'/N_0' + (m'^2 - \tfrac{5}{4})[\tfrac{1}{3} - (\mathbf{n}\mathbf{n}_j)^2]\, N_6'/N_0', \quad N_5' = (1 + \varepsilon)(\lambda + \tfrac{1}{2}\mu\beta)^2 |M_{GT}|^2,$$

$$N_6' = -[(1 + \varepsilon)[\tfrac{1}{2}\beta\lambda(\mu + f) + \tfrac{1}{4}\beta^2(\mu^2 + f\mu)] - \tfrac{1}{8}\beta^2(\mu + f)^2]\, |M_{GT}|^2. \tag{22}$$

### C. Angular Correlation between the Neutrino and the $\gamma$ Quanta [W(m′) is given by (20)]

$$W(\theta) = \sum_{M_f, m'} W(m')\, P_{M_f, m'}(\theta), \qquad P_{M_f, m'}(\theta) = |\langle J_f, L, M_f, M \mid J', m'\rangle|^2 |E_L|^2 F_L^M(\theta) + |\langle J_f, L-1, M_f, M \mid J', m'\rangle$$

$$\times|^2 |M_{L-1}|^2 F_{L-1}^M(\theta) + \langle J_f, L, M_f, M \mid J', m'\rangle \langle J_f, L-1, M_f, M \mid J' m'\rangle (E_L M_{L-1}^* + \mathrm{c.c.})\, F_{L, L-1}^M(\theta);$$

$$F_L^M(\theta) = \frac{4\pi}{L(L+1)}[2M^2 |Y_L^M|^2 + (L + M)(L - M + 1)\, |Y_L^{M-1}|^2 + (L + M + 1)(L - M)\, |Y_L^{M+1}|^2],$$

$$F_{L, L-1}^M(\theta) = -4\pi[(2L + 1)(L^2 - M^2)/(2L - 1)L^2(L^2 - 1)]^{1/2} \times [2M\, |Y_{L-1}^M|^2 + (L - M - 1)\, Y_L^{M+1}|^2 - (L + M - 1)\, |Y_{L-1}^{M-1}|^2]. \tag{23}$$

### D. Angular Distribution of the Electrons in the Direction of Polarization of the $\mu$ Meson

$$W(\theta) = \sum_{m'} W(m')\,(1 + \overline{\beta}_{m'}\, v \cos\theta),$$

$$\overline{\beta}_{m'} = \{\Delta_{j',m'} + 2m'\,[j'\,(j'+1)]^{-1/2}\,\delta_{j_f,\,j'}\}\,[1 + |\rho'|^2\,\delta_{j_f,\,j'}]^{-1},$$

$$\Delta_{j',\,m'} = \begin{cases} m'/j', & j_f = j' - 1 \\ m'/j'(j'+1), & j_f = j' \\ -m'/(j'+1), & j_f = j' + 1 \end{cases} \qquad (24)$$

($j_f$ is the spin of the nucleus in the final state after the $\beta$ decay, $\rho' = M_F^\beta / M_{GT}^\beta$).

---

[1] Ya. A. Smorodinskiĭ, Usp. Fiz. Nauk **68**, 653 (1959), Soviet Phys. Uspekhi **2**, 557 (1959).

[2] B. L. Ioffe, JETP **37**, 159 (1959), Soviet Phys. JETP **10**, 113 (1960). Chou Kuang-Chao and V. Maevskiĭ, JETP **35**, 1581 (1958), Soviet Phys. JETP **8**, 1106 (1959). A. Fujii and H. Primakoff, Nuovo cimento **12**, 317 (1595).

[3] Bernstein, Lee, Yang, and Primakoff, Phys. Rev. **111**, 313 (1958). I. M. Shmushkevich, Nucl. Phys. **11**, 419 (1959).

[4] S. S. Gershteĭn and Ya. B. Zel'dovich, JETP **29**, 698 (1955), Soviet Phys. JETP **2**, 576 (1957). M. Gell-Mann, Phys. Rev. **111**, 362 (1958).

[5] M. L. Goldberger and S. B. Treiman, Phys. Rev. **111**, 354 (1958).

[6] I. M. Shmushkevich, JETP **36**, 953 (1959), Soviet Phys. JETP **9**, 673 (1959).

[7] Egorov, Ignatenko, and Chultém, Preprint, Joint Inst. Nuc. Res.

[8] Berestetsky, Ioffe, Rudik, and Ter-Martirosyan, Nucl. Phys. **5**, 464 (1958).

[9] D. S. Ling, Jr. and D. L. Falkoff, Phys. Rev. **76**, 1639 (1959).

Translated by R. Lipperheide
308

SOVIET PHYSICS JETP VOLUME 11, NUMBER 5 NOVEMBER, 1960

# *ON THE D MESON*

HSIEN TING-CH'ANG

Joint Institute for Nuclear Research

Submitted to JETP editor December 30, 1959

J. Exptl. Theoret. Phys. (U.S.S.R.) 38, 1627-1629 (May, 1960)

The processes most favorable for the production of D mesons are discussed. Experiments for the determination of the spin and the parity of the D meson are proposed.

1. Many of the existing classifications of elementary particles contain a free place. The scheme of Gell-Mann and Nischijima[1,2] leaves room for a meson with strangeness 2 and isotopic spin 0. The scheme of Salam and Polkinghorne[3] has a free spot for a $\tau$ particle, if we regard the $\tau$ and the $\theta$ as identical. In Sakata's model of elementary particles[4] one can construct the particles

$$D^+ = \frac{1}{\sqrt{2}}(pn - np)\,\bar{\Lambda}\bar{\Lambda}, \quad D^- = \frac{1}{\sqrt{2}}(\bar{p}\bar{n} - \bar{n}\bar{p})\,\Lambda\Lambda. \qquad (1)$$

In the Markov scheme[5] the analogous particle is represented by $(N\bar{\Xi})$.

On the other hand, evidence was recently found in the propane bubble chamber at Dubna for the existence of a heavy meson with mass ~ 750 Mev,[6] which decays according to the scheme

$$D^+ \to K^0 + \pi^+. \qquad (2)$$

It is of interest in this connection to investigate which reactions are the most appropriate for the further detection of the D meson and also which processes are most convenient for the study of the properties of this meson.

2. The D meson can be produced in the reaction

$$\pi + N \to D + 2K + N \qquad (3)$$

or in the reactions

$$K + N \to D + K + N, \qquad (4)$$

$$K + N \to D + \text{hyperon}, \qquad (5)$$

and also through annihilation of a nucleon with an antinucleon:

$$N + \bar{N} \to D^+ + D^-. \qquad (6)$$

We give the ratios of the probabilities of these reactions, calculated with the help of the statistical theory of the multiple production of particles (for the method of calculation see references 8 and 9):

$$\frac{\sigma(\pi^- + N \to D + 2K + N)}{\sigma(\pi^- + N \to \Xi + 2K)} \sim 3.2 \cdot 10^{-2}, \quad p_{\pi^-} = 7\ \text{Bev/c},$$

$$\frac{\sigma(K^+ + N \to D + K + N)}{\sigma(K^+ + N \to \pi + K + N)} \sim 3.3 \cdot 10^{-4}, \quad p_{K^+} = 2\ \text{Bev/c},$$

$$\frac{\sigma(K^+ + N \to D^+ + \Lambda)}{\sigma(K^+ + N \to K + N)} \sim 0.18. \quad p_{K^+} = 2\ \text{Bev/c},$$

$$\frac{\sigma(N + \bar{N} \to D^+ + D^-)}{\sigma(N + \bar{N} \to K^+ + K^-)} \sim 0.3, \quad p_{\bar{N}} = 0.$$

All momenta are given in the laboratory system of coordinates.

In the calculation we set $M_D/M_N = 0.8$ and assumed that the $\pi$ mesons and baryons are produced in a volume $V_\pi$ with radius $r_\pi = \hbar/m_\pi c = 1.4 \times 10^{-13}$ cm, while the K mesons and the D meson are produced in a smaller volume $V_K$ with radius $r_K = \hbar/m_K c = 0.4 \times 10^{-13}$ cm. If the experimental values of the last two ratios turn out to be smaller than the calculated ones, this may indicate that the D mesons are produced in a volume which is smaller than the corresponding volume for the K mesons.

The above-mentioned calculations show that the use of a $K^+$ meson beam is most convenient for the detection of the D meson.

It should be noted that the scheme of Salam and Polkinghorne also admits of the existence of the $D^0$ meson. One may expect that the $D^0$ meson decays according to the schemes

$$D^0 \to \pi^0 + K^0, \quad D^0 \to \pi^+ + K^-, \quad D^0 \to \pi^- + K^+,$$

| $s_D$ | $\Pi_D$ | $A$ | $B$ |
|---|---|---|---|
| 1 | 0 | —1 | 0 |
| 0 | —1 | 0 | 1 |
| 2<br>3 | —1<br>—1 | $^2/_5$ | $-^1/_5$ |
| 0<br>1<br>2 | 1<br>—1<br>1 | $>0\ (\neq {}^2/_5)$ | $\neq -{}^1/_5$ |

and its mass will be close to the masses of the $D^+$ and $D^-$ mesons. In the scheme of Gell-Mann and Nischijima this $D^0$ meson can be identified with the $\rho_0$ meson, whose existence has been the subject of wide discussion in recent times.

3. Information on the spin of the D meson can be obtained by measuring the angular correlation in the cascade process

$$K + N \rightarrow D + \text{hyperon}, \quad D \rightarrow K + \pi. \tag{7}$$

However, this correlation gives two possible integer values i and i+1 [for example, (0, 1) or (1, 2)] for the spin of the D meson, leaving the choice open.

If the reaction

$$D^- + \mathrm{He}^4 \rightarrow {}_\Lambda\mathrm{He}^4 + K^- \tag{8}$$

occurs and the angular distribution of $\mathrm{He}^4$ and $K^-$ is isotropic, one may conclude that the $D^-$ meson is a pseudoscalar (since the relative parity of $\Lambda$ and K is odd).[11] In the case of a nonisotropic distribution the spin and the parity of the $D^-$ meson cannot be determined uniquely from the data of this experiment.

More definite information on the spin and the parity of the D meson may be obtained from the study of the capture of the $D^-$ meson by the deuteron:

$$D^- + \text{deuteron} \rightarrow \Lambda^0 + \Lambda^0 \rightarrow 2p + 2\pi^-. \tag{9}$$

One should expect that the $D^-$ will be captured by the deuteron predominatly in the S state.[12] Then the angular correlation of the decay products of the two $\Lambda$ hyperons is equal to[13]

$$1 + \alpha^2 (A\,\mathbf{n}_1\mathbf{n}_2 + B(\mathbf{n}_1\mathbf{n})(\mathbf{n}_2\mathbf{n})),$$

where $\alpha$ is the asymmetry coefficient of the $\Lambda$ decay; $\mathbf{n}_1$ and $\mathbf{n}_2$ are unit vectors in the direction of the momenta of the decay products, referred to the rest systems of the first and second $\Lambda$ hyperons, respectively; $\mathbf{n}$ is a unit vector in the direction of the line connecting the two $\Lambda$ hyperons. The values of A and B, which depend on the spin $S_D$ and the parity $\Pi_D$ of the $D^-$ meson, are given in the table.*

The author thanks Prof. M. A. Markov, Prof. Wang Kang-Ch'ang, V. S. Barashenkov, L. G. Zastavenko, and M. I. Shirokov for valuable comments.

---

[1] M. Gell-Mann, Nuovo cimento Suppl. **4**, 448 (1953).

[2] T. Nakano and K. Nischijima, Progr. Theor. Phys. **10**, 581 (1953).

[3] A. Salam and J. C. Polkinghorne, Nuovo cimento **2**, 685 (1955).

[4] S. Sakata, Progr. Theor. Phys. **16**, 686 (1956).

[5] M. A. Markov, О систематике элементарных частиц (On the Systematics of Elementary Particles), U.S.S.R. Acad. Sci. Press (1955).

[6] Wang Kuang-Ch'ang, Report at the International High Energy Conference at Kiev, 1959.

[7] Barashenkov, Barbashev, and Bubelev, Nuovo cimento Suppl. **7**, 117 (1958).

[8] Hsien Ting-Ch'ang, JETP **38**, 289 (1960), Soviet Phys. JETP **11**, 209 (1960).

[9] L. G. Zastavenko, JETP **37**, 1319 (1959), Soviet Phys. JETP **10**, 939 (1960).

[10] R. K. Adair, Phys. Rev. **100**, 1540 (1955).

[11] Block, Brucker, Hughes, Kikuchi, Meltzer, Anderson, Pevsner, Harth, Leitner, and Cohn, Phys. Rev. Lett. **3**, 291 (1959).

[12] Day, Snow, and Sucher, Phys. Rev. Lett. **3**, 61 (1959).

[13] S. B. Treiman, Phys. Rev. **113**, 355 (1959).

[14] T. Yamanouchi and M. F. Kaplon, Phys. Rev. Lett. **3**, 283 (1959); T. Yamanouchi, preprint.

Translated by R. Lipperheide
309

---

*After this paper had been written, it became known to the author that after the Kiev Conference seven more cases have been found which can be interpreted as decays and reactions of $D^+$ mesons.[14]

SOVIET PHYSICS JETP VOLUME 11, NUMBER 5 NOVEMBER, 1960

# *COLLECTIVE EXCITATIONS OF NON-AXIAL EVEN-EVEN NUCLEI*

A. A. CHABAN

Moscow State University

Submitted to JETP editor December 30, 1959

J. Exptl. Theoret. Phys. (U.S.S.R.) 38, 1630-1636 (May, 1960)

The collectively excited states of non-axial even-even nuclei are investigated with account of the interaction between rotational and vibrational states.

DAVYDOV and Filippov[1] have calculated the collective energy levels of axially symmetric even-even nuclei with account of the interaction between rotational and vibrational states. The same authors[2] also investigated the rotational energy levels and the probabilities of transitions between them for the case of non-axial nuclei. The coupling between the vibrations and the rotation was not taken into account. In the present paper we study the collective excitations of the vibration-rotation type in non-axial even-even nuclei.

## 1. ENERGY LEVELS

We shall assume that the energy of the vibrations in the parameter of axial asymmetry, $\gamma$, is much larger than the energies of the collective rotation and of the vibrations in $\beta$. $\gamma$ can then be regarded as constant. According to the collective model of Bohr, the energy of the nucleus is made up of the following terms:

$$E_0 = \tfrac{1}{2}B\dot{\beta}^2 + \tfrac{1}{2}C\beta^2 + A\beta + \sum_{\chi} M_{\chi}^2/2I_{\chi}. \qquad (1)$$

The first two terms represent the kinetic and potential energy of the $\beta$ oscillations of the nucleus, respectively; $A\beta$ is the interaction of the external nucleons with the nuclear core, and is in first approximation proportional to $\beta$; the last term represents the energy of rotation of the nucleus, where $M_{\chi}$ is the projection of the classical angular momentum on the $\chi$ axis, and $I_{\chi}$ is the moment of inertia, which is given by the expression

$$I_{\chi} = 4B\beta^2 \sin^2(\gamma - 2\pi\chi/3).$$

In going from Eq. (1) to the corresponding quantum-mechanical equation, we have

$$\hat{H}\Psi = E_0\Psi, \qquad (2)$$

where

$$\hat{H} = -\frac{\hbar^2}{2B}\frac{1}{\beta^3}\frac{\partial}{\partial\beta}\beta^3\frac{\partial}{\partial\beta} + \frac{C\beta^2}{2} + A\beta + \hat{L},$$

$$\hat{L} = \sum_{\chi}\frac{\hbar^2}{2I_{\chi}}\Big(\hat{J}_{\chi} - \sum_{n}\hat{j}_{\chi}(n)\Big)^2, \qquad (3)$$

$\hat{J}_{\chi}$ is the projection of the total angular momentum of the nucleus on the $\chi$ axis, and $j_{\chi}(n)$ is the projection of the angular momentum of the n-th external nucleon.

The volume element in the space $(\beta, \theta_i)$ is written as

$$d\tau = G\beta^3 \sin\theta \, d\beta \, d^3\theta \qquad (4)$$

(G is a constant).

In the adiabatic approximation with respect to the one-nucleon states we can average the Hamiltonian operator (3) over the states of the external nucleons. If I is the sum of the spins of the external nucleons and $\Omega$ is its projection on the axis fixed in the nucleus, we can use the conditions of symmetry to obtain the wave function of the external nucleons in the form

$$\Psi_n = \sum_{I,\Omega} a_{I\Omega}\left(\Phi_{I\Omega} + (-1)^I \Phi_{I,-\Omega}\right), \qquad (5)$$

where $\Omega$ takes on only even values. The average value of the operator of the rotational energy is equal to

$$\langle \Psi_n | \hat{L} | \Psi_n \rangle = \hbar^2 D/6B\beta^2 + \sum_{\chi} \hbar^2\hat{J}_{\chi}^2/2I_{\chi},$$

$$\hbar^2 D/6B\beta^2 = \sum (\hbar^2/2I_{\chi}) \langle \Psi_n | \Big(\sum_{n}\hat{j}_{\chi}(n)\Big)^2 | \Psi_n \rangle,$$

so that, using Eq. (5),

$$\langle \Psi_n \Big| \sum_{n}\hat{j}_{\chi}(n) \Big| \Psi_n \rangle = 0.$$

We shall regard $\hbar^2 D/6B\beta^2$ as being included in the effective potential energy. Then the operator of the energy of rotation is $\sum_{\chi} \hbar^2 J_{\chi}^2/2I_{\chi}$. We seek the solution of Eq. (2) in the form of a product of the wave functions for the $\beta$ oscillations $(\Psi_{\beta})$ and for the collective rotation ($\Psi_{\text{rot}}$). For fixed $\beta$ we have

$$\sum_{\chi} \frac{\hbar^2 \hat{J}_\chi^2}{2I_\chi} \Psi_{\text{rot}} = \frac{\hbar^2}{4B\beta^2} \tilde{\varepsilon}_{J\lambda} \Psi_{\text{rot}}; \tag{6}$$

J is the total angular momentum, and $\lambda$ is the number of the solution for a given J. The quantities $\tilde{\epsilon}_{J\lambda}$ were obtained by Davydov and Filippov[2] using the symmetry conditions for $\Psi_{\text{rot}}$. With the help of their data we write Eq. (2) in the form

$$\left\{ -\frac{\hbar^2}{2B} \frac{1}{\beta^3} \frac{\partial}{\partial\beta} \beta^3 \frac{\partial}{\partial\beta} + V'(\beta) + \frac{\hbar^2}{4B\beta^2} \tilde{\varepsilon}_{J\lambda} \right\} \Psi_\beta = E_0 \Psi_\beta,$$

$$V'(\beta) = C\beta^2/2 + A\beta + \hbar^2 D/6B\beta^2. \tag{7}$$

Substituting the value $\Psi_\beta = U_{J\lambda}(\beta)/\beta^{3/2}$ in Eq. (7), we obtain the equation

$$\left\{ -\frac{\hbar^2}{2B} \frac{d^2}{d\beta^2} + V(\beta) + \frac{\hbar^2}{4B\beta^2} \tilde{\varepsilon}_{J\lambda} \right\} U_{J\lambda} = E_0 U_{J\lambda},$$

where the quantity

$$V(\beta) = V'(\beta) + 3\hbar^2/8B\beta^2$$

reaches a minimum in the point

$$\beta_0 = -A/C + \hbar^2 D/3BC\beta_0^3 + 3\hbar^2/4BC\beta_0^3.$$

Expanding $V(\beta)$ in a series in terms of $\beta_0$, we find

$$\left\{ -\frac{\hbar^2}{2B} \frac{d^2}{d\beta^2} + \frac{C_0}{2} (\beta - \beta_0)^2 + \frac{\hbar^2}{4B\beta^2} \tilde{\varepsilon}_{J\lambda} - \varepsilon \right\} U_{J\lambda} = 0,$$

$$\varepsilon = E_0 - V(\beta_0), \quad C_0 = C + \hbar^2 D/B\beta_0^4 + 9\hbar^2/4B\beta_0^4. \tag{8}$$

Equation (8) agrees with that obtained by Davydov and Filippov,[1] except that $J(J+1)$ is replaced by $\frac{3}{2}\tilde{\epsilon}_{J\lambda}$. [For $\gamma \to 0$ we have for the lowest level for a given J: $\frac{3}{2}\tilde{\epsilon}_{J\lambda} \to J(J+1)$].

The energy of rotation-vibration of the nucleus is determined by the equation

$$\varepsilon_\nu (J\lambda)/\hbar\omega_0 = (\nu + \tfrac{1}{2}) \sqrt{1 + \tfrac{3}{2} \tilde{\varepsilon}_{J\lambda}/\delta^4 \xi^4}$$

$$+ \tfrac{1}{2} \delta^2 (\xi - 1)^2 + \tilde{\varepsilon}_{J\lambda}/4\delta^2 \xi^2, \tag{9}$$

where

$$\delta = \beta_0 (BC/\hbar^2)^{1/4}, \quad \xi^3 (\xi - 1) = \tilde{\varepsilon}_{J\lambda}/2\delta^4, \quad \omega_0 = \sqrt{C_0/B}.$$

The quantity $\nu$ is found from the equation

$$H_\nu (-\delta_1 \xi) = 0 \text{ for } \delta_1 = \delta (1 + \tfrac{3}{2} \tilde{\varepsilon}_{J\lambda}/\delta^4 \xi^4)^{1/4}, \tag{10}$$

where

$$H_\nu (\zeta) = \frac{1}{2\Gamma(-\nu)} \sum_{k=0}^{\infty} \frac{(-1)^k}{k!} \Gamma\left(\frac{k-\nu}{2}\right) (2\zeta)^k$$

is a Hermite function of the first kind.

The unnormalized wave function $\Psi_\beta$ has the form

$$\Psi_\beta = \beta^{-3/2} e^{-\zeta^2/2} H_\nu (\zeta), \quad \zeta = \delta_1 (\beta/\beta_0 - \xi). \tag{11}$$

We shall be interested only in the excitation energy $E_{J\lambda} = \epsilon_{J\lambda} - \epsilon_{J=0}$. For large values of $\delta$ (usually already for $\delta > 3$) the correction to the energy due to the coupling of the rotation with the $\beta$ oscillations can be obtained with the help of an expansion in terms of the small parameter $1/\delta^4$. Then*

$$E_{J\lambda} = (\hbar^2/4B\beta_0^2) \tilde{\varepsilon}_{J\lambda} - F (\tilde{\varepsilon}_{J\lambda})^2 + M\tilde{\varepsilon}_{J\lambda},$$

$$F = \text{const}, \qquad M = \text{const}.$$

The quantity $\nu$ in Eq. (10) runs through an infinite sequence of discrete values. Each branch with J = 0 has its set of levels with spins 2, 3, 4, 6, etc. If $\delta > 2.5$, the lowest levels of the two lowest branches split up and we obtain a vibrational-rotational band (cf. reference 1).

We studied the quantities $R_\lambda(J) = E_{J\lambda}/E_1(2^+)$ as functions of $R_2(2) = E_2(2^+)/E_1(2^+)$. We considered the two lowest levels $4^+$, the first level $6^+$, and the level $3^+$ corresponding to the first band, and also the level $0^+$ of the second band. The results of the calculations for $R_1(6)$ and $R_1(4)$ are shown in Figs. 1 and 2. The points with $\delta = 0$, 1, 2, 3, 4, and $\infty$ and with $\gamma = 10$, 15, 22.5, and 30° are joined by curves. The curve with $\delta = \infty$ corresponds to the absence of the coupling between the rotation and the $\beta$ oscillations [the excitation of the $\beta$ oscillations is infinitely high as compared with $E_1(2^+)$]. It should be noted that $R(3)$ varies little for a given $R_2(2)$, i.e., the equality $E_1(2^+) + E_2(2^+) \approx E(3^+)$ is approximately conserved.

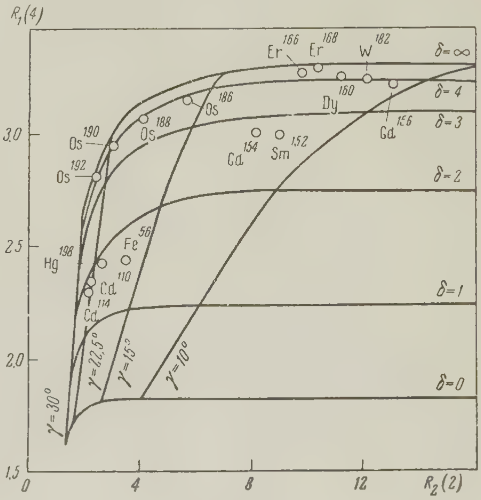

FIG. 1

---

*An empirical formula of this form (with M = 0) was proposed by Malman and Kerman (preprint) for the comparison of the theory of Davydov and Filippov[2] and of Davydov and Rostovskiĭ[3] with the experimental data.

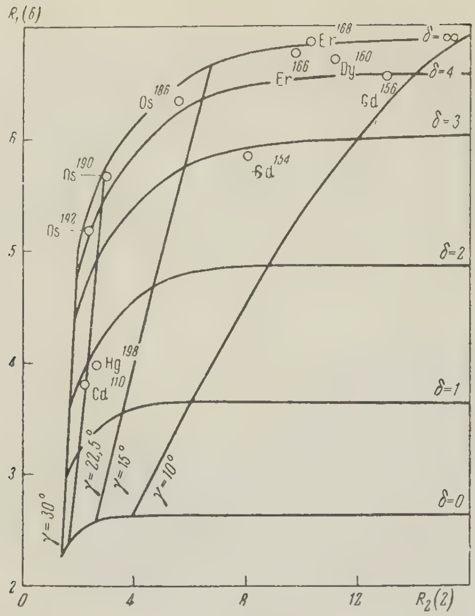

FIG. 2

The curves with small δ lie below the curves with larger δ for all levels; therefore, $R_\lambda(J)$ decreases if the coupling between the oscillations and the rotation is included.

## 2. PROBABILITIES OF QUADRUPOLE TRANSITIONS

The expression for the reduced probability for a quadrupole transition between the states Jλ and J′λ′ has the form

$$B(E2; J\lambda \to J'\lambda')$$
$$= \frac{5}{16\pi(2J+1)} \sum_{M,m,\mu} |(\Psi_{\mathrm{rot}}^{J'\lambda' m} \Psi_\beta^{J'\lambda'} | \hat{Q}_{2\mu} | \Psi_{\mathrm{rot}}^{J\lambda M} \Psi_\beta^{J\lambda})|^2,$$
$$\hat{Q}_{2\mu} = eQ_0 \frac{\beta}{\beta_0}\left(D_{\mu 0}^2 \cos\gamma + \frac{1}{\sqrt{2}}(D_{\mu 2}^2 + D_{\mu -2}^2)\sin\gamma\right),$$
$$Q_0 = \frac{3}{\sqrt{5\pi}} ZR^2\beta_0. \tag{12}$$

We rewrite Eq. (12) in the form

$$B(E2; J\lambda \to J'\lambda') = \widetilde{B}(E2; J\lambda \to J'\lambda')\,\beta_0^{-2}\,|\langle J'\lambda'|\beta|J\lambda\rangle|^2, \tag{13}$$

where $\widetilde{B}$ is a quantity which was computed in reference 2. The correction factor represents the matrix element of $\beta/\beta_0$ with respect to the functions $\Psi_\beta$. Using (11) and (4), we have

$$\langle i|\beta|j\rangle$$
$$= \int_0^\infty U_i(\beta)\,U_j(\beta)\,\beta d\beta \Big/ \left\{\int_0^\infty U_i^2(\beta)\,d\beta\right\}^{1/2} \left\{\int_0^\infty U_j^2(\beta)\,d\beta\right\}^{1/2}. \tag{14}$$

Here

$$U_i(\beta) = \exp(-\zeta_i^2/2)\,H_{\nu_i}(\zeta_i), \quad \zeta_i = (\delta_1)_i(\beta/\beta_0 - \xi_i).$$

For $\delta \to \infty$ we have $\nu_i \to 0$. In practice $\nu_i = 0$ for $\delta \geq 2$. ($\nu$ has the largest value in the case $J = 0$. If $J = 0$, $\delta = 2$, then $\nu = 0.02$.) For $\delta \geq 2$ the quantity $H_{\nu_i}$ can be replaced by $H_0 = 1$. Then expression (14) has a very simple form, which leads to the ratio ($\delta \geq 2$)

$$\frac{B(E2; 22 \to 21)}{B(E2; 22 \to 0)} = \mu\,\frac{\widetilde{B}(E2; 22 \to 21)}{\widetilde{B}(E2; 22 \to 0)};$$

$$\mu = \frac{\langle 21|\beta|22\rangle^2}{\langle 0|\beta|22\rangle^2} = \frac{(\delta_1)_1}{\delta}\exp\left\{2\left(\frac{b_{21}^2}{4a_{21}} - d_{21}\right)\right.$$
$$\left. - 2\left(\frac{b_{20}^2}{4a_{20}} - d_{20}\right)\right\}\left(\frac{b_{21}}{b_{20}}\right)^2\left(\frac{a_{20}}{a_{21}}\right)^3, \tag{15}$$

$$a_{ij} = \tfrac{1}{2}[(\delta_1)_i^2 + (\delta_1)_j^2], \quad b_{ij} = (\delta_1)_i^2\xi_i + (\delta_1)_j^2\xi_j,$$
$$d_{ij} = \tfrac{1}{2}[(\delta_1)_i^2\xi_i^2 + (\delta_1)_j^2\xi_j^2]. \tag{16}$$

The subscripts 0, 1, and 2 refer to the ground state, the lowest excited state with $J = 2$, and the second excited state with $J = 2$, respectively.

The most abundant group of nuclei experimentally has $\delta \sim 4$ and $10° \leq \gamma \leq 30°$. In this case $\mu \approx 1.015$ (it varies within the limits 1.013 and 1.017 for $\delta = 4$). For the second group $\delta \sim 2$ and $15° \leq \gamma \leq 30°$. Here $\mu \approx 1.2$ (it varies within the limits 1.20 and 1.23 for $\delta = 2$). If $\gamma \to 0$ for fixed δ, $\mu \to 0$; but this refers already to very small γ. If $\delta \to \infty$, then $\mu \to 1$, as should be expected ($\delta \to \infty$ corresponds to the absence of coupling between the β oscillations and the rotation). The correction due to the factor μ is thus important only for nuclei with $\delta \sim 2$. But here (as in the case of nuclei with $\delta \sim 4$) the change of γ on account of the coupling between the β oscillations and the rotation plays an incomparably greater role.

## 3. DISCUSSION OF THE RESULTS

The comparison of the theoretical results with experiment will be carried out in the following way. We determine δ and γ from the three levels $E_1(2^+)$, $E_2(2^+)$, and $E_1(4^+)$ with the help of Fig. 1, which shows the dependence of $R_1(4)$ on $R_2(2)$. It is here convenient to use curves with fixed values of δ and curves with fixed values of γ. With the help of the analogous curves computed for the dependence of $R_1(6)$ (see Fig. 2), $R_2(4)$, and $R_2(0)$ on $R_2(2)$ we can find $R_1(6)$, $R_2(4)$, and $R_2(0)$ from the known values of δ and γ. The results of the comparison with experiment are given in Table I (see also Figs. 1 and 2). The character of the interaction between the β oscillations and the rotation is apparently well accounted for by the calculations.

**TABLE I.** Energies of the excited states of the vibrational-rotational type*

| Nucleus | $E_1$ (2+), kev | $R_2$ (2) | $R$ (3) | $R_1$(4) | $R_2$ (4) | $R_1$ (6) | $R_2$ (0) | Reference |
|---|---|---|---|---|---|---|---|---|
| $Fe^{56}$ | 845 | 3.49 | 4.54 | 2.47 | 4.85 | | | [4] |
| | | | | 2.47 | 4.7 | 4.7 | 2.9 | |
| | | | | 3.09 | 6.2 | 5.94 | | |
| $Cd^{110}$ | 656 | 2.10 | 3.31 | 2.35 | | 3.80 | | [5,6] |
| | | | | 2.35 | 3.8 | 3.8 | 2.8 | |
| | | | | 2.78 | 5.5 | 5.23 | | |
| $Cd^{114}$ | 556 | 2.18 | | 2.30 | | | 2.35 | [7] |
| | | | | 2.30 | 3.8 | 3.7 | 2.7 | |
| | | | | 2.75 | 5.5 | 5.14 | | |
| $Sm^{152}$ | 121.8 | 8.92 | 10.14 | 3.01 | 11.68 | | 5.61 | [7,8] |
| | | | | 3.01 | 10.3 | 5.7 | 6.0 | |
| | | | | 3.31 | 11.3 | 6.80 | | |
| $Gd^{154}$ | 123.02 | 8.10 | 9.17 | 3.02 | | 5.84 | 5.52 | [7,8] |
| | | | | 3.02 | 9.6 | 5.7 | 6.2 | |
| | | | | 3.30 | 10.5 | 6.75 | | |
| $Gd^{156}$ | 89 | 13.01 | 14.00 | 3.24 | 15.34 | 6.56 | $\sim$8.09 | [7,8,9] |
| | | | | 3.24 | 14.9 | 6.5 | 13.6 | |
| | | | | 3.32 | 15.4 | 6.88 | | |
| $Dy^{160}$ | 86.6 | 11.16 | 12.11 | 3.27 | 13.35 | 6.70 | | [7,9] |
| | | | | 3.27 | 13.2 | 6.6 | $>14$ | |
| | | | | 3.32 | 13.6 | 6.86 | | |
| $Er^{166}$ | 80.7 | 9.76 | 10.67 | 3.29 | 11.87 | 6.76 | 18.12 | [7,10] |
| | | | | 3.29 | 12.0 | 6.7 | $>14$ | |
| | | | | 3.31 | 12.2 | 6.82 | | |
| $Er^{168}$ | 79.9 | 10.29 | 11.22 | 3.31 | 12.47 | 6.86 | | [9,10] |
| | | | | 3.31 | 12.7 | 6.8 | $>14$ | |
| | | | | 3.32 | 12.8 | 6.84 | | |
| $W^{182}$ | 100.9 | 12.11 | 13.20 | 3.26 | 14.68 | | | [7,8] |
| | | | | 3.26 | 14.0 | 6.6 | $>14$ | |
| | | | | 3.32 | 14.5 | 6.87 | | |
| $Os^{186}$ | 137.2 | 5.60 | 6.63 | 3.16 | 7.73 | 6.33 | | [8,10] |
| | | | | 3.16 | 7.7 | 6.2 | 11.4 | |
| | | | | 3.23 | 8.1 | 6.49 | | |
| $Os^{188}$ | 155.0 | 4.09 | 5.10 | 3.08 | 6.17 | | 7.01 | [7,8,10] |
| | | | | 3.08 | 6.3 | 5.8 | 12.1 | |
| | | | | 3.15 | 6.7 | 6.14 | | |
| $Os^{190}$ | 186 | 2.99 | 4.05 | 2.95 | 5.14 | 5.63 | | [8] |
| | | | | 2.95 | 5.6 | 5.5 | 11.2 | |
| | | | | 3.01 | 5.8 | 5.75 | | |
| $Os^{192}$ | 206 | 2.37 | 3.35 | 2.82 | | 5.17 | | [7,9] |
| | | | | 2.82 | 5.4 | 5.2 | $>14$ | |
| | | | | 2.84 | 5.5 | 5.34 | | |
| $Hg^{198}$ | 411.8 | 2.65 | | 2.43 | | 3.97 | 2.63 | [7,9] |
| | | | | 2.43 | 4.1 | 4.0 | 2.9 | |
| | | | | 2.92 | 5.6 | 5.53 | | |
| $Pu^{238}$ | 44.2 | 23.30 | 24.34 | 3.30 | | 6.86 | 21.15 | [7] |
| | | | | 3.30 | | 6.84 | $>14$ | |
| | | | | 3.33 | | 7.00 | | |

*For each element we list in the first row the experimental values, in the second row the theoretical values, and in the last row the values obtained when only the rotational excitations are taken into account.

In Table II we give the ratios of the reduced probabilities for the transitions $22 \rightarrow 21$ and $22 \rightarrow 0$. The effect of $\mu$ is not accounted for because of its smallness. Indeed, the change of the value of $\gamma$ on account of the coupling between the vibrations and the rotation plays a much larger role. But for nuclei with $\delta \sim 4$ even this effect does not change greatly the value found by Davydov and Filippov in reference 2 ($\gamma$ becomes somewhat smaller). For nuclei with $\delta \sim 2$ the value of $\gamma$ becomes appreciably smaller. The experimental data at our disposal are too inaccurate and very sparse in the region $\delta \sim 2$. They do not permit us to check the results of the theory with regard to the transition probabilities.

In conclusion I regard it my obligation to thank

TABLE II. Ratio of the reduced probabilities for quadrupole transitions from the second level 2 to the first level $2^+$ and from the second level $2^+$ to the ground state

| Nucleus | $\gamma$, degrees | $\gamma^*$, degrees | $B(E2;\ 22 \rightarrow 21)/(B(E2;\ 22 \rightarrow 0)$ | | |
|---|---|---|---|---|---|
| | | | Theory | Rotation only | Experiment |
| $Os^{186}$ | 15.9 | 16.5 | 3.05 | 3.30 | 2.5;5 [11] |
| $Os^{188}$ | 18.5 | 19.2 | 4.36 | 4.84 | 2.7 [3]<br>3.3 [11] |
| $Os^{190}$ | 21.9 | 22.2 | 7.8 | 8.3 | 9.7 [3]<br>5.6 [11] |
| $Os^{192}$ | 24.5 | 25 | 17.5 | 20.6 | 9.1 [3] |
| $W^{182}$ | 11.0 | 11.45 | 1.81 | 1.88 | 1.59 [2] |
| $Gd^{154}$ | 11.85 | 13.9 | 1.94 | 2.38 | 1.94 [3]<br>2.2 [11] |
| $Gd^{156}$ | 10.5 | 11.0 | 1.75 | 1.81 | 1.7 [11] |
| $Sm^{152}$ | 11.42 | 13.25 | 1.87 | 2.42 | 1.7 [2]<br>2.4 [11] |
| $Dy^{160}$ | 11.45 | 11.9 | 1.88 | 1.94 | 2.38 [2] |
| $Cd^{114}$ | 23.3 | 26.7 | 11.3 | 52 | 77.9 [2] |
| $Hg^{198}$ | 21.0 | 23.6 | 6.5 | 12.7 | 25 [2]<br>67 [9] |

*Rotation only.

Prof. A. S. Davydov for his constant attention to this work and for valuable remarks.

---

[1] A. S. Davydov and G. F. Filippov, JETP **33**, 723 (1957), Soviet Phys. JETP **6**, 555 (1958).

[2] A. S. Davydov and G. F. Filippov, JETP **35**, 440 (1958), Soviet Phys. **8**, 303 (1959). Nucl. Phys. **8**, 237 (1958).

[3] A. S. Davydov and V. S. Rostovskiĭ, JETP **36**, 1788 (1959), Soviet Phys. **9**, 1275 (1959). Nucl. Phys. **12**, 58 (1959).

[4] C. Sharp Cook, Nucl. Phys. **7**, 480 (1958).

[5] H. W. Taylor and W. R. Frisken, Phys. Rev. **114**, 127 (1959).

[6] Strominger, Hollander, and Seaborg, Revs. Modern Phys. **30**, 585 (1958).

[7] B. S. Dzhelepov and L. K. Peker, Схемы распада радиоактивных ядер (Decay Schemes of Radioactive Nuclei), U.S.S.R. Acad. Sci. Press, M.-L. (1958).

[8] B. S. Dzhelepov and L. K. Peker, Excited States of Deformed Nuclei, Joint Inst. Nuc. Res. Report R-288 (1959).

[9] E. P. Grigor'ev and M. P. Avotina, Report at the 10th Annual Conference on Nuclear Spectroscopy, Moscow, 1960; Izv. Akad. Nauk SSSR, Ser. Fiz. **24**, 3 (1960).

[10] Jacob, Mihelich, Harmatz, and Handley, Bull. Am. Phys. Soc. **3**, 558 (1958).

[11] Gregers Hansen, Nielson, and Sheline, Nucl. Phys. **12**, 389 (1959).

Translated by R. Lipperheide
310

# Letters to the Editor

## *SUPER-HEAVY ISOTOPES OF HYDROGEN AND HELIUM*

V. I. GOL'DANSKIĬ

P. N. Lebedev Physics Institute, Academy of Sciences, U.S.S.R.

Submitted to JETP editor January 16, 1960

J. Exptl. Theoret. Phys. (U.S.S.R.) **38**, 1637-1639 (May, 1960)

To estimate the stability of many isotopes (in particular $H^5$, $H^7$, and $He^8$) relative to the emission of neutrons, it is advantageous to use data on neutron pairing energy. Figure 1 shows the pairing energy $E_p$ [the difference between the binding energies of the (2m + 2)-nd and (2m + 1)-st neutrons] in the first six neutron layers (from $1s_{1/2}$ to $2s_{1/2}$) for the elements from hydrogen to potassium. It is obvious that the pairing energy is always less for nuclei with an odd number of protons (because the deuteron-like triplet pn bond is disturbed by pairing in an odd-odd nucleus). In the $p_{3/2}$ shell, which is filled in the nuclei $H^4$–$H^7$ and $He^5$–$He^8$, the pairing of the third and fourth neutrons gives a somewhat smaller energy gain (64—90%) than for the first neutron pair. Using these facts, we can present the following estimates.

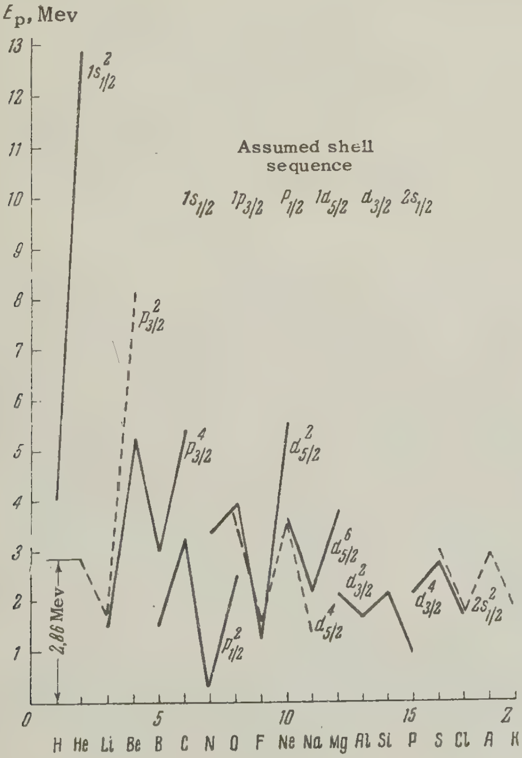

FIG. 1

$He^8$. The pairing energy does not exceed 2.86 Mev (the value for $He^6$, in which the first two places in the $p_{3/2}$ shell are filled). On the other hand, this energy is not less than 1.54 Mev (the value for $Li^9$). The necessary condition for the stability of $He^8$ is that the energy of the decay $He^7 \rightarrow He^6 + n$ be less than approximately 1.4 Mev, while the sufficient condition is that this energy not exceed approximately 0.8 Mev.

Comparing the masses of $Li^7$, $He^6$, and n and introducing a correction for the Coulomb interaction in $He^7$ $(1.2\,Z_{He}\,A^{-1/3})$, we readily find that the isotope $He^8$ can be stable if the first level $T = 3/2$ for $A = 7$ is not higher than 12.7 Mev, and is absolutely stable if this level is lower than 12 Mev. We know of a 12.4-Mev level[1] noted in the reaction $Li^7(\gamma\, n)Li^6$ (reference 2), but not observed for the transition $Li^7(\gamma\, t)He^4$. It is therefore natural to assign $T = 3/2$ to this level. If such a level with $T = 3/2$ exists, then the energy of the decay $He^7 \rightarrow He^6 + n$ is approximately 1.1 Mev, and the condition for the stability of $He^8$ reduces to having the pairing energy of the last two neutrons not less than approximately 2.2 Mev. Satisfaction of this condition, however, is far from obvious. It should be noted that Zel'dovich's conclusion[3] regarding the stability of $He^8$ was based on the assumption that the decay energies of $He^5$ and $He^7$ and the pairing energies of the first and second pair of neutrons in the $p_{3/2}$ shell are equal. Actually $He^7$ is not as strong as $He^5$, and pairing is less feasible in $He^8$ than in $He^6$. The problem of the stability of $He^8$ still remains open and should be resolved by experiment.

A possible method for finding $He^8$ is to observe the (n, 2p) reactions or the capture $(\pi^-, p)$ of slow negative pions in emulsions doped with $Be^9$ nuclei (the characteristic decay is $He \xrightarrow{8\beta^-} Li \xrightarrow{8\beta^-} Be^{8*} \rightarrow 2\alpha$).

We note, however, that in the $\beta^-$ decay of $He^8(0^+)$ the more probable is not the production of the ground state $(2^+)$ of $Li^8$, but of the excited state $(1^+$; 3.22 Mev), with subsequent emission of delayed neutrons $(Li^{8*} \rightarrow Li^7 + n)$.

$H^5$. In this case the pairing energy also does not exceed 2.86 Mev (the value for $He^6$, an even nucleus with the same number of neutrons). It is therefore obvious that for stability of $H^5$ the energy of the decay $H^4 \rightarrow H^3 + n$ must not exceed approximately 1.4 Mev. Comparing the masses of $He^4$, $H^3$, and n and introducing a correction for the Coulomb interaction in $He^4$ (~ 0.7 Mev),

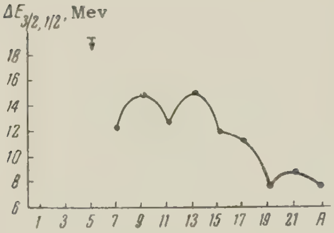

FIG. 2

we conclude that $H^5$ can be stable only if for the $\alpha$ particle the level with T = 1 lies below approximately 22 Mev. As is known, no such levels of $He^4$ have been observed in the energy range below 22 Mev, and this refutes the assumed[4] stability of $H^5$. We note that if the decay $H^5 \rightarrow H^4 + n$ requires (because of the pairing effects) the consumption of energy, the decay energy of $H^4$ cannot exceed 2.86 Mev. In this case the level with T = 1 should not be higher than approximately 23.4 Mev for $He^4$. However, extrapolation to hydrogen of the difference in the binding energy of the first and third neutrons leads to the conclusion that the energy of the decay $H^4 \rightarrow H^3 + n$ is so large, that the decay $H^5 \rightarrow H^4 + n$ becomes energetically feasible (to approximately 1.8 Mev). Then the upper limit of the T = 1 level for $He^4$ rises to approximately 25.2 Mev. These estimates (23.4 – 25.2 Mev) confirm the value of approximately 24 Mev given for the energy of this level in reference 5.

Stability of $H^5$ relative to the decay into $H^3$ and 2n agrees also with the energy of the first $T = 3/2$ level at A = 5: $\Delta E_{3/2\ 1/2} \lesssim 19.4$ Mev (arrow on Fig. 2). Blanchard and Winter[4] estimated this energy at 19.1 Mev. As is seen from Fig. 2, however, the data regarding $\Delta E_{3/2\ 1/2}$ cannot serve as a proof of the stability of $H^5$, for the case H–He–Li (transition from A = 5 to A = 7), which is magic in the number of protons, has an analogue in the case N-O-F (transition from A = 19 to A = 17) in which a sharper increase is observed in the energy of the first $T = 3/2$ level than in the other cases.

The collective data on the binding energies of neutrons and protons are also evidence in favor of the instability of $H^5$.

$\underline{H^7}$. If, however, $H^5$ is nevertheless stable, one would expect also the presence of a stable "superheavy" isotope of hydrogen $H^7$ (just as the presence of $He^6$ is proof of the existence of $He^8$).

In addition to searching for delayed neutrons in the reactions $Li^7(\gamma, 2p)$[6] or $H^3(H^3p)$, a possible method of verifying the existence of $H^5$ is to observe the reactions (n, 2p) or $(\pi^-, p)$ in emulsions doped with $Li^6$. If $H^7$ is stable, these nuclei could be observed in the reactions $Be^9(\pi^-, 2p)$ in the emulsions.

The author is grateful to Ya. B. Zel'dovich and A. A. Ogloblin for a discussion of this problem.

---

[1] F. Ajzenberg-Selove, and T. Lauritsen, Nucl. Phys. **11**, No. 1, 1959.

[2] J. Goldenberg and L. Katz, Phys. Rev. **95**, 471 (1954).

[3] Ya. B. Zel'dovich, JETP **38**, 1123 (1960), Soviet Phys. JETP **11**, 812 (1960).

[4] C. Blanchard and R. Winter, Phys. Rev. **107**, 774 (1957).

[5] Bogdanov, Vlasov, Kalinin, Rybakov, Samoĭlov, and Sidorov, Ядерные реакции при малых и средних энергиях (Nuclear Reactions at Small and Medium Energies), Acad. Sci. Press, 1958, pp. 7-15.

[6] G. Tautfest, Phys. Rev. **111**, 1162 (1958).

Translated by J. G. Adashko
311

---

# *CONNECTION BETWEEN OSCILLATION AND RATE OF LOSS OF CHARGED PARTICLES IN A CYLINDRICAL PLASMA OF LOW PRESSURE IN A LONGITUDINAL MAGNETIC FIELD*

A. A. ZAĬTSEV and M. Ya. VASIL'EVA

Moscow State University

Submitted to JETP editor January 21, 1960

J. Exptl. Theoret. Phys. (U.S.S.R.) **38**, 1639-1640 (May, 1960)

THE principal purpose of this investigation was to study the plasma oscillations in a longitudinal column in a constant longitudinal magnetic field. In addition, we investigated the diffusion current on the wall of the discharge tube and the effect of the magnetic field on the longitudinal potential gradient in the column. Such investigations have been attracting attention in recent years in connection with the question of the mechanism by which charged particles are displaced transversely to the magnetic flux lines in a magneto-ionic medium and with other problems in plasma dynamics.[1-4]

The discharge was produced in a cylindrical tube with an inside diameter of 2 cm and an interelectrode gap of 90 cm, filled with helium at 0.2 – 0.05 mm Hg. The anode current ranged from 50 to 350 ma. The positive column was homogeneous under these conditions. The degree of ionization of the gas did not exceed 0.1%. The discharge tube was placed in a solenoid with its cathode and anode ends projecting 25 and 15 cm respectively beyond the solenoid. The magnetic field was varied from 0 to 2.5 koe.

When there is no magnetic field, noise is generated in the discharge in a frequency range from $10^3$ to $10^6$ cps. A magnetic field amplifies this noise considerably and changes its spectrum. As the magnetic field is increased to a certain critical field value, oscillations are suddenly launched in the discharge, 10 or 15 times more intense than the maximum noise level at the pre-critical field. The corresponding amplitude of the electrode-voltage oscillations reaches 7 to 10 volts. The critical value of the field, above which oscillations are produced, is independent of the current and increases with increasing pressure, as can be seen from the following data:

| | | | | |
|---|---|---|---|---|
| p, mm Hg | 0.05 | 0.07 | 0.1 | 0.2 |
| $H_{cr}$, oe | 750 | 990 | 1400 | 1630 |

Simultaneous with the appearance of the intense oscillations is an abrupt decrease of the anode current by 5 to 8%. Probe measurements show (Fig. 1)

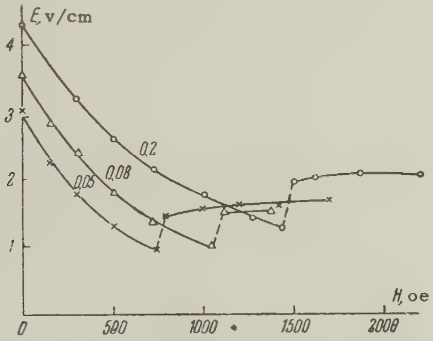

FIG. 1

that the oscillations are accompanied by an increase in the average value of the longitudinal potential gradient in the positive column located in a magnetic field (the numbers next to the curves give the pressure in mm Hg). If the magnetic field is less than critical, the increase in field reduces the potential gradient in accordance with the theory of paired collisions.[2,3] At fields exceeding the critical value, the curves exhibit an anomalous behavior. Figure 2 shows the current on the walls of the tube. The curves show clearly that the effective rate of diffusion loss of charged particles increases in a strong magnetic field.

The sudden occurrence and the irregular character of the oscillations is of interest. Orderly oscillations at frequencies of 80 — 140 kcs were noted only in a narrow range of variation of the magnetic field, near the critical value.

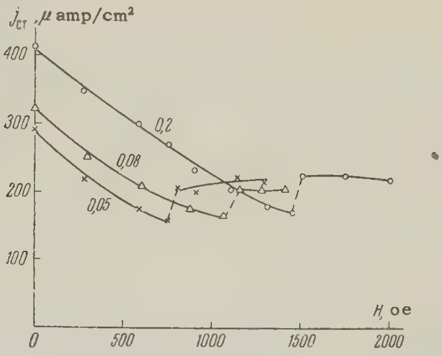

FIG. 2

Preliminary observations have shown that the potentials of probes located along the tube are delayed in time toward the anode. This delay indicates propagation of the oscillations toward the anode. The rate of propagation of the oscillations approaches, in order of magnitude, the drift velocity of the electrons. At the same time, a phase shift is observed in the fluctuations of the voltage between probes located on the axis and on the wall in the same cross section of the tube.

Under different conditions, moving layers may appear in the discharge. Under the conditions of Lehnert's experiments,[3] the moving layers produced oscillations of large amplitude in the absence of a magnetic field. These oscillations, however, changed neither the current on the wall nor the potential gradient in the column.

It is possible that the type of oscillations observed and the associated increase in the effective rate of diffusion loss of charged particles are the result of a macroscopic displacement of the plasma pinch in the magnetic field.

---

[1] W. Bostick and M. Levine, Phys. Rev. **97**, 13 (1955).

[2] A. Bikerton and A. Engel, Proc. Phys. Soc. **B69**, 468 (1956).

[3] W. Lehnert, Rep. Second Intern. Conf. on Peaceful Uses of Atomic Energy, Geneva, 1958.

[4] A. V. Zharinov, Атомная энергия (Atomic Energy) No. 7, 215, 220 (1959).

Translated by J. G. Adashko
312

## *INSTABILITY OF AN INDUCTION PINCH*

I. F. KVARTSKHAVA, K. N. KERVALIDZE, and Yu. S. GVALADZE

Submitted to JETP editor January 23, 1960

J. Exptl. Theoret. Phys. (U.S.S.R.) 38, 1641-1643 (May, 1960)

In a paper presented to the Fourth International Conference on Ionization Phenomena in Gases (Upsala, 1959), we considered a new type of instability, observed in pulsed compression of plasma in linear induction (theta) pinches.* The existence of such an instability was inferred from streak photographs of the discharge, taken through a narrow slit from the end of the chamber along the direction of its axis with the slit oriented along a chamber diameter. These photographs have shown that in some cases, following compression, plasma formations are ejected from the pinch surface, sometimes reaching the chamber walls.[1]

Further experiments in which the discharge was photographed with a SFR-2M high-speed camera operating in the "time-magnification" mode, mostly pertaining to the theta pinch, have disclosed a close connection between this effect and the azimuthal inhomogeneity of the radial velocities of the plasma during the compression process. It was found that in view of the presence of such an inhomogeneity, the contracting plasma layer is not cylindrical in form, as was assumed in our paper, as well as in papers by others, but is greatly deformed, assuming sometimes weird shapes. The photographs in these experiments were also taken from the ends of the chamber, sometimes in two modes simultaneously — in the "time-magnification" mode from one end by streak photography (through a narrow slit) from the other. The theta pinch was excited, as usual in an axially symmetrical magnetic field rapidly alternating in time, produced by discharging a capacitor into a single cylindrical turn. To avoid distortion of the photographs by reflection of the axial jets of the plasma at the ends of the chamber, the turn was located in the middle of the chamber, sufficiently far away from its ends.

The figure shows individual examples of the photographs obtained. Photographs a, b, c, d, and e (cylindrical chamber) and f and g (chamber with square cross section) pertain to the "time-magnification" mode. These photographs show the characteristic time variation of the shape of the pinch cross section. It is seen on analogous pictures, taken at a small angle to the camera axis, that the pinch (in any case, during the compression stage) retains the same shape of azimuthal section throughout its length. Picture e was obtained simultaneously with picture f, by streak photography through a narrow slit, and shows an eruption of a plasma formation from the surface of the pinch. Each of these photographs corresponds to a definite half cycle of current in the capacitor circuit. The exposures of the individual frames were 0.5 μsec. The time between neighboring frames was 2μ sec (a four-rowed system of lenses was used; we show here one of four rows of corresponding photographs). According to these pictures, an electrodeless vortical discharge is ignited at the start of the half cycle in the thin layer of gas adjacent to the chamber walls. Even before the plasma layer breaks away from the walls, its glow acquires a certain azimuthal inhomogeneity. During the breakaway and subsequent motion of the plasma, the brighter sections acquire smaller radial accelerations (velocities). As a result, the contracting plasma layer deviates considerably from a cylinder. In the initial stage of contraction, the pinch frequently assumes the shape of a polygon. In cylindrical chambers, the number of sides, their dimensions, and their relative orientations vary from experiment to experiment, or even from half cycle to half cycle of current in the same experiment. The expansion of the pinch after the maximum compression also proceeds with unequal radial velocity. The expansion figures produced are frequently similar to the contraction figures, and are turned by a certain angle in the azimuthal direction (photograph a). This is seen particularly clearly on figure h, where the angle is 45 deg. More complicated figures of motion are also observed. For example, on Figs.

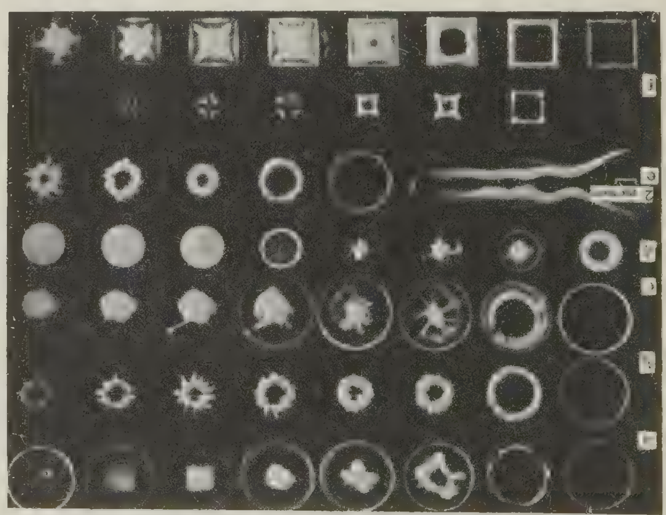

Experimental conditions

| Photograph | Initial voltage, kv | Capacitance, $\mu$f | Length of magnet turn, turn, cm | $H_z$ max $\times 10^6$ gauss | No. of current half-cycles | Working gas pressure, mm Hg | Dimensions of discharge chamber, cm | Material of discharge chamber wall |
|---|---|---|---|---|---|---|---|---|
| c | 30 | 90 | 55 | 12 | 1 | Air 0.1 | dia 27. $L = 100$ | Porcelain |
| d | 30 | 90 | 15 | 40 | 1 | Nitrogen 0.1 | dia 27. $L = 100$ | Porcelain |
| a | 30 | 90 | 15 | 40 | 2 | Helium 0.07 | dia 27. $L = 100$ | Porcelain |
| b | 30 | 60 | 22 | 43 | 1—2 | Helium 0.1 | dia 12. $L = 70$ | Glass |
| e | 30 | 180 | 55 | 18 | 1 | Helium 0.1 | dia 27. $L = 100$ | Porcelain |
| f | 30 | 180 | 55 | 18 | 1 | Helium 0.1 | dia 27. $L = 100$ | Porcelain |
| g | 30 | 90 | 15 | 40 | 1 | Air 0.1 | $22 \times 22 \times 50$ | Glass |
| h | 30 | 90 | 15 | 40 | 2 | Air 0.1 | $22 \times 22 \times 50$ | Glass |

b and d we see that meridional fin-like plasma jets emerge from the surface of the expanding pinch. Sometimes the fins are wavy, or else, as they approach the chamber walls, they are smoothly deflected in a common direction. In this case the jets acquire a certain rotary momentum relative to the central pinch. The plasma jets are frequently reminiscent of certain types of solar protuberances. In some cases the pinch is compressed in the form of a double layer of plasma (photograph c). Here, following the maximum compression of the central pinch, the plasma jets form "jumpers" with the still contracting outer sheath. We could discuss many other forms of plasma motion, but lack of space forces us to confine ourselves to these examples.

It should be noted that the observed effects vanish when the gas pressure increases. They do not appear, or at any rate are greatly attenuated, when the chamber has a small diameter (about 1 or 2 cm and less). In chambers with a rectangular cross section the shape of the pinch and its relative orientation are always fixed. This makes it possible to investigate the properties of the plasma not only by photography, but also by means of magnetic or electric probes and by other methods.

The main cause of the observed phenomena lies obviously in the magnetohydrodynamic nature of the motion of the plasma in magnetic fields. The azimuthal rotation of the figures of the expanding pinch relative to the contracting figures, indicates that a certain role is played in this process by reflection of shock waves from the magnetic fields enclosed by the plasma. From the character of the spatial variation of the pinch figures it follows that the plasma formations behave in magnetic fields like elastic bodies that are characterized by a "coefficient of elasticity" which is greatly dependent on the direction of the field. Experiment has shown that deformation of the plasma layer is greatly hindered along the field lines but develops readily perpendicular to the field, apparently with minimum energy loss.

Even a qualitative analysis of the presented data shows that the plasma is not in equilibrium when in the stage of maximum compression. Intense damped macroscopic motions, which lead to eruptive instabilities of the pinch, are excited rather weakly in the plasma. These instabilities apparently give rise to the main difficulty when attempts are made to produce a high-temperature plasma with the aid of pulse processes. The eruptive instabilities should be observed not only in linear but also in toroidal chambers, although they are more difficult to photograph in the latter.

In the present communication we give only a brief description of the main outlines of plasma motion in a theta pinch. A more detailed exposition of the results, including those for a linear pinch, and a discussion of the mechanism of the observed phenomena will be presented in a later paper.

---

*As is well known, the term linear pinch is used for a plasma column compressed by the magnetic field of its own current. A theta pinch is produced in a vortical discharge in a gas, in an axially-symmetrical magnetic field that builds up rapidly with time.

---

[1] Kvartskhava, Kervalidze, and Gvaladze, J. Tech. Phys. (U.S.S.R.) 30, 297 (1960), Soviet Phys.-Tech. Phys. 5, 274 (1960).

Translated by J. G. Adashko
313

# FARADAY EFFECT IN YTTRIUM GARNET AT INFRARED FREQUENCIES

G. S. KRINCHIK and M. V. CHETKIN

Moscow State University

Submitted to JETP editor February 13, 1960

J. Exptl. Theoret. Phys. (U.S.S.R.) **38**, 1643-1644 (May, 1960)

THE rotation of the plane of polarization when light passes through magnetized ferrite (Faraday effect) was measured in the visible region,[1] and also[2] in the near infrared region at a fixed wavelength $\lambda = 1\mu$. It was shown that in this region of the spectrum both the Faraday effect and the absorption of light by the ferrite are connected with the electron transitions. In this note we give the results of measurement of the Faraday effect in garnet ferrite of yttrium $Y_3Fe_5O_{12}$ with the wavelength varying from 0.94 to $9\mu$, that is, in the region where light absorption connected with electronic transitions ends and absorption due to lattice vibrations begins.

The experimental apparatus was a modification of that previously described for the investigation of the magneto-optical Kerr effect in the infrared region.[3] Polarized light passed through the sample and analyzer, which was oriented at 45 deg to the polarizer. The sample was a plate made of a single crystal of yttrium garnet 75 microns thick. The change in intensity of the transmitted light was measured with the specimen magnetized in a field of 3500 oe, from which one could readily calculate the specific rotation of the plane of polarization in degrees per centimeter. The figure shows the dependence of the Faraday effect on the wavelength of infrared light. Near the edge of the electronic-absorption band, at $\lambda \sim 1\mu$, the rotation of the plane of polarization drops off sharply. In the region of maximum transparency of the ferrite, and also in the region where the phonon absorption of light begins, the rotation remains approximately constant.

For non-ferromagnetic semiconductors, two causes of the rotation of the plane of polarization of infrared light have been discussed in detail:[4] 1) electronic transitions, at which the angle of rotation is proportional to $\lambda^{-2}$, 2) motion of free electrons, which leads to a rotation of the plane of polarization proportional to $\lambda^2$. The first reason can explain the sharp drop in the effect in the region of $1\mu$, where the angle of rotation is actually proportional to $\lambda^{-2}$. The second reason can explain neither the sign, nor the dependence on the wavelength, nor the value of the effect in the interval from 4 to $9\mu$, since the resistivity of the garnet is seven or eight orders of magnitude higher than the resistivity of the semiconductors in which the Faraday effect connected with free electrons is measured. It is possible that the considerable rotation of the plane of polarization of infrared light for $\lambda > 4\mu$, which is independent of the frequency, is observed only in ferromagnetic semiconductors and requires a special theoretical analysis.

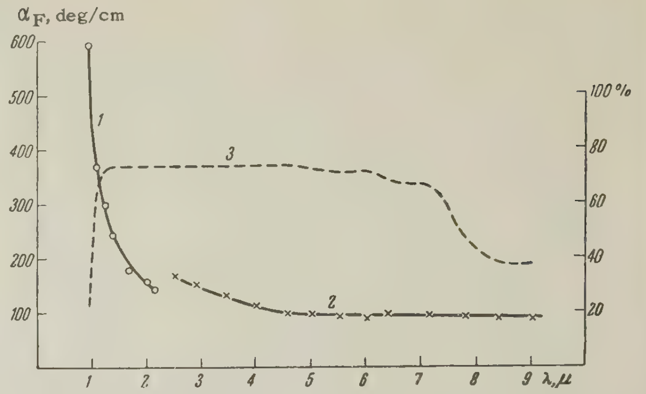

Faraday effect (left-hand scale) in yttrium garnet for infrared light. 1 – glass prism, 2 – prism of rock salt, 3 – transparency of plate of yttrium garnet 75 micron thick without correction for reflection (right-hand scale).

We note that in our experiments the intensity of the transmitted light at $\lambda \sim 1\mu$ was changed by the Faraday effect by approximately 30% when the specimen magnetization was reversed. This may be of practical interest for the construction of devices of the controllable-gyrator type or light-modulator type. At other wavelengths in the investigated range, by virtue of the great transparency of the garnet, one can also obtain comparable changes in the intensity, if the thickness of the specimen is increased.

We express deep gratitude to Professor A. G. Smolenskiĭ for providing us with the single crystal of yttrium garnet.

---

[1] J. F. Dillon, J. de Phys. **20**, 374 (1959).

[2] Sherwood, Williams, and Remeika, J. Appl. Phys. **30**, 217 (1959).

[3] G. S. Krinchik and R. D. Nuralieva, JETP **36**, 1022 (1959), Soviet Phys. JETP **9**, 724 (1959).

[4] V. Kimmel, Z. Naturforsch. **12a**, 1016 (1957). Smith, Moss, and Taylor, J. Phys. Chem. Solids **11**, 131 (1959).

Translated by J. G. Adashko

# *POLARIZATION OF RECOIL PROTONS FROM THE SCATTERING OF 300-Mev $\pi^-$ MESONS ON HYDROGEN*

I. M. VASILEVSKIĬ and V. V. VISHNYAKOV

Joint Institute for Nuclear Research

Submitted to JETP editor March 3, 1960

J. Exptl. Theoret. Phys. (U.S.S.R.) 38, 1644-1645 (May, 1960)

PHASE-SHIFT analysis of the differential cross sections of elastic scattering and scattering of $\pi^-$ mesons with charge exchange does not give a single-valued solution. As shown by Fermi,[1] the study of the polarization of recoil protons can be of aid in the choice between the different sets of phase shifts, since they give different angular distributions of polarization.

The polarization of recoil protons in $\pi^-$-p scattering has been measured thus far only in one work, on 223-Mev $\pi^-$ mesons.[2] The polarization was measured at two scattering angles of the $\pi^-$ mesons. Agreement was found with one set of phase shifts of the Fermi type, but the statistical accuracy did not allow the complete exclusion of one of the sets of the Yang type.

In this letter we present the preliminary results of the measurements of the polarization of recoil protons in the scattering of 300-Mev $\pi^-$ mesons on hydrogen. The measurements were carried out by means of a hodoscopic system of counters, the construction of which has been described earlier.[3,4]

When the scattered $\pi^-$ meson and recoil proton fall into the counters of the control system, a pulse is produced which triggers the hodoscope. In analyzing the photographs obtained, only those pictures were examined on which the process of elastic scattering of the $\pi^-$ meson was recorded, and cases of scattering of the proton in the carbon target and in the walls of the gas-discharge counters were chosen. We observed 305 cases of scattering, which were separated into three groups according to the direction of flight of the recoil proton from the hydrogen target. The results obtained are shown in the table, where the data have been summed over the volume of the chamber and are shown in such a way that all cases of scattering are taken as occurring in the chamber on the right. The polarization of the recoil protons was defined as

$$P = (N_L - N_R) / P_1 (N_L + N_R),$$

where $N_L$ and $N_R$ are the numbers of protons scattered to the left and to the right, $P_1$ is the analyzing power of the arrangement and was determined from the data of references 5 and 6. The direction of polarization was taken parallel to $\mathbf{k}_i \times \mathbf{k}_s$, where $\mathbf{k}_i$ is the momentum of the incident $\pi^-$ meson and $\mathbf{k}_2$ is the momentum of the scattered $\pi^-$ meson.

| Proton recoil angle (deg in lab) | $N_R$ | $N_L$ | $P$ |
|---|---|---|---|
| 15—23 | 43 | 48 | $0.12 \pm 0.20$ |
| 24—32 | 85 | 58 | $-0.45 \pm 0.19$ |
| 33—41 | 45 | 26 | $-\left(0.70^{+0.21}_{-0.32}\right)$ |

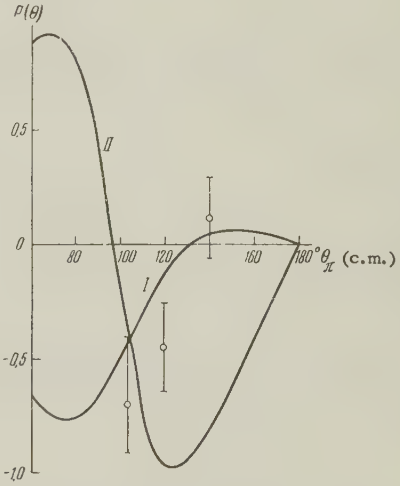

Curve I – set of phase shifts $\alpha_1 = 17.1°$, $\alpha_{11} = 11.4°$, $\alpha_{13} = -5.0°$. Curve II – set of phase shifts $\alpha_1 = 3.6°$, $\alpha_{11} = -22.3°$, $\alpha_{13} = 14.6°$.

The figure depicts the results of the present work and the polarization vs pion scattering angle curve for two sets of phase shifts obtained in reference 7. In the latter experiment it was found that the first set is the most probable. The experimental values of the polarization, as can be seen, are in satisfactory agreement with the first set of phase shifts and increase the probability that the sign of the phase shifts $\alpha_1$ and $\alpha_{11}$ is positive.

In conclusion, we express our gratitude to A. A. Tyapkin for help in this work and R. M. Sulyaev and L. I. Lapidus for constant interest in the work.

---

[1] E. Fermi, Phys. Rev. **91**, 947 (1953).

[2] Ashkin, Blaser, Burger, Kunze, and Romanowski, 1958 Annual International Conference on High Energy Physics at CERN, Geneva, 1958, p. 42.

[3] I. M. Vasilevskiĭ and V. V. Vishnyakov,

Приборы и техника эксперимента (Instrum. and Meas. Engg.) No. 2, 58 (1960).

[4] B. Pontecorvo, Report at International Conference on High Energy Physics at Kiev, 1959.

[5] J. M. Dickson and D. C. Salter, Nuovo cimento 6, 235 (1957).

[6] Alphonce, Johansson, and Tibell, Nuclear Phys. 3, 185 (1957).

[7] Zinov, Korenchenko, Polumordvinova, and Tentyukova, Preprint R-431, Joint Institute for Nuclear Research.

Translated by E. Marquit
315

---

## NON-RADIATIVE TRANSFORMATION OF THE $\mu$ MESON INTO AN ELECTRON

I. S. SHAPIRO

Submitted to JETP editor March 12, 1960

J. Exptl. Theoret. Phys. (U.S.S.R.) 38, 1646-1647 (May, 1960)

1. The process of non-radiative transformation of the $\mu$ meson into an electron in the Coulomb field of the nucleus,

$$\mu^- + A_Z \to A_Z^* + e^- \tag{1}$$

may occur with greater probability than the decay $\mu \to e + \gamma$, if the monopole form factor for the transition $\mu \to e$ is larger than the dipole form factor. Weinberg and Feinberg[1] quoted the example of the four-fermion interaction of the type $(\bar{e}\mu)(\bar{f}f)$ (where f is a charged particle) for which this situation may occur in principle. Steinberger and Wolfe[2] have made attempts to discover the process (1). According to their data the ratio of the probability of process (1) and the probability of the ordinary capture of $\mu$ mesons by the protons of the $Cu^{64}$ nucleus is $\leq 5 \times 10^{-4}$. These experimenters searched for the reaction (1) by registering the electrons with energies of about 100 Mev.

In this note we discuss a different method for detecting the reaction (1). Let us consider a $\mu$-mesic atom with a light even-even nucleus (for example, $C^{12}$, $O^{16}$, or $Ne^{20}$). In the 6 to 10 Mev region of the excitation energies these nuclei have excited states $0^+$ from which decay with emission of $\alpha$ particles takes place.[3] Our proposed method for the detection of the process (1) consists of registering the $\alpha$ particles of known energy emitted by nuclei which have been excited to the $0^+$ level as a consequence of reaction (1). The probability of this process can be calculated. It is equal to (in units where $\hbar = c = 1$)

$$W_{00}^{\mu e} = \frac{16}{9} \pi Z^3 \alpha^5 \mu (1 - 2\omega) \left| \mu^2 Q_0 \right|^2 \left| f_{E0} \right|^2. \tag{2}$$

Here $\omega$ is the excitation energy of the nucleus in units of the rest energy of the $\mu$ meson, $\mu$ (we assume that $\omega \ll 1$), $Q_0$ is the nuclear matrix element for the transition $0^+ \to 0^+$:

$$Q_0 = \left\langle A_Z^* 0^+ \middle| r^2 - \frac{1}{6} (\mu r)^2 \middle| A_Z 0^+ \right\rangle, \tag{3}$$

and $f_{E0}$ is the electric monopole form factor for the transition $\mu \to e$, which depends on the momentum transfer $q = p_e - p_\mu$ ($p_e$ and $p_\mu$ are the momenta of the electron and the $\mu$ meson) in the following fashion:

$$f_{E0}(q^2) = q^2 G(q^2), \quad \lim G(q^2) < \infty \quad \text{for} \quad q^2 \to 0. \tag{4}$$

It is convenient to compare $W_{00}^{\mu e}$ with the probability for the ordinary capture of $\mu^-$ mesons,

$$\mu^- + A_Z \to A_{Z-1} + \nu \tag{5}$$

(this type of reaction has now been relatively well studied in the case of $C^{12}$). The probability $W_{if}^{\mu\nu}$ for the process (5) has been calculated by a number of authors.[4,5] Using their result and formulas (2) and (4), we obtain

$$W_{00}^{\mu e} / W_{if}^{\mu\nu} = \frac{32}{9} \pi^3 \alpha^2 \left[ 1 + 2 (\omega' - \omega) \right] \eta \left| \mu^2 Q_0 \right|^2 / M_{if}. \tag{6}$$

Here $\omega'$ is the difference in energy of the nuclei $f(A_{Z-1})$ and $i(A_Z)$ (in the units $\mu$, $\omega' \ll 1$),

$$\eta = G^2(\mu^2)/g^2, \quad M_{if} = \lambda_F^2 \left| M_F^{if} \right|^2 + \lambda_{GT}^2 \left| M_{GT}^{if} \right|^2, \tag{7}$$

where g is the universal constant of the weak four-fermion interaction as determined from the decay time of the $\mu$ meson; $M_F^{if}$ and $M_{GT}^{if}$ are the Fermi and Gamow-Teller matrix elements for the allowed transition $i \to f$ including meson corrections and corrections for the finite wave length of the neutrino (see reference 4). In particular, formula (6) gives for the ratio of the probabilities of processes (1) and (5) for the $C^{12}$ nucleus

$$W(\mu^- + C^{12} \to C^{12*} + e) / W(\mu^- + C^{12} \to B^{12} + \nu) = 1.1 \cdot 10^{-2} \eta. \tag{8}$$

2. An effect which hinders the observation of reaction (1) (if the $\alpha$ particles are registered) is the Coulomb excitation of the nucleus of the $\mu$-mesic atom by the decay electrons from the $\mu^-$ meson. This effect, however, occurs relatively seldom owing to the smallness of the phase volume. The calculation leads to the following formula for

the probability of this effect:

$$W_{00}^{ee'} = \frac{2}{9}\frac{1}{192\pi^3} Z^3\alpha^5\mu^5\left(\frac{7}{20}-\omega\right)|\mu^2 Q_0'|^2 g^2. \qquad (9)$$

The ratio of the probabilities for the two effects is

$$W_{00}^{ee'}/W_{00}^{\mu e} = 2.36\cdot 10^{-3}\left(1-\frac{6}{7}\omega\right)\Big/\eta. \qquad (10)$$

(Here we neglected the small difference between $Q_0$ and $Q_0'$.) It is seen from (10) that this ratio becomes comparable to unity for $\eta \approx 3 \times 10^{-6}$, which is about $10^3$ times smaller than the upper limit for $\eta$ calculated by Weinberg and Feinberg from the data of Steinberger and Wolfe ($\eta \leq 4 \times 10^{-3}$).

I express my gratitude to M. Ya. Balats and Ya. B. Zel'dovich for an interesting discussion.

---

[1] S. Weinberg and G. Feinberg, Phys. Rev. Lett. **3**, 111 (1959).

[2] J. Steinberger and H. B. Wolfe, Phys. Rev. **100**, 1490 (1955).

[3] F. Ajzenberg-Selove and T. Lauritzen, Nucl. Phys. **11**, 1 (1959).

[4] B. L. Ioffe, JETP **37**, 159 (1959), Soviet Phys. JETP **10**, 113 (1960).

[5] H. Primakoff and A. Fujii, Nuovo cimento **12**, 327 (1959).

Translated by R. Lipperheide
316

---

# *POLARIZATION OF NUCLEI IN NONMETALLIC FERROMAGNETIC SUBSTANCES*

G. R. KHUTSISHVILI

Institute of Physics, Academy of Sciences, Georgian S.S.R.

Submitted to JETP editor March 13, 1960

J. Exptl. Theoret. Phys. (U.S.S.R.) **38**, 1647-1649 (May, 1960)

IN 1955 a method for polarizing the nuclei of ferromagnetic atoms was proposed by us[1] and simultaneously by Kurti and his co-workers.[2] The corresponding experiments on the anisotropy of $\gamma$ radiation have been made by a number of authors.[1-4] All of these experiments were made on ferromagnetic metals.

It would be interesting to make experiments of this type also in the case of nonmetallic ferromagnetic substances. As an example let us consider the case of a ferrite, i.e., a compound of the type $XO \cdot Fe_2O_3$, where X is a divalent metal ion. The ferrite is ferromagnetic if X is the ion of a divalent metal of the iron transition group (Fe, Co, Ni, Mn, Ti, Cu).* These ferrites have the reciprocal spinel structure. It is well known that in the spinel lattice there are one tetrahedral cation position A and two octahedral cation positions B for each molecule. In the case of the reciprocal spinel structure the $X^{++}$ ions occupy half the positions B, and the $Fe^{+++}$ ions occupy all the positions A and half the positions B.

We assume that the external magnetic field is larger than the saturation field. Then the specimen is a single domain. If furthermore the temperature is sufficiently low, the state will be close to the state of absolute saturation. We proceed further to apply the Néel model,[5] according to which each of the sublattices A and B is magnetized to saturation, with their magnetizations oppositely directed. Therefore the resultant magnetization is determined by the $X^{++}$ ions whose magnetic moments are directed along the external field. It follows that the fields exerted by the shells of $X^{++}$ ions on their nuclei will all have the same direction (parallel or antiparallel to the external field, depending on the sign of the hyperfine structure constant). At an extremely low temperature we get a considerable polarization of the X nuclei. The limiting degree of polarization (obtained if the Zeeman energy of the nuclear spin in the internal field caused by the ion shell is much larger than kT) will be equal to unity.

These considerations apply to the ferrites of Co, Ni, Mn, Ti, and Cu. It is easy to see that in these ferrites the iron nuclei will not be polarized, but only aligned. It is also obvious that in the ferrite of iron (i.e., in magnetite, $Fe_3O_4$) the limiting degree of polarization of the iron nuclei will be ⅓.

As a second example let us consider the case of a ferromagnetic garnet, i.e., a compound of the type $3X_2O_3 \cdot 5Fe_2O_3$, where X is the trivalent ion of a rare-earth element. A model analogous to the Néel model has been proposed to explain the properties of garnets[6,7] (cf. also reference 8). According to this model there are three types of positions for cations in a garnet, namely, in each molecule there are six so-called d positions, four a positions, and six c positions. The d and a positions are occupied by $Fe^{+++}$ ions, and the c positions by $X^{+++}$ ions. At low temperatures all the sublattices are magnetized to saturation, with the c and a sublattices magnetized parallel to each other, and the d sublattice magnetized in the opposite direction (with the total magnetization parallel to the external field). It is clear from this that at ultralow temperatures both the X nuclei and the iron nuclei will be polarized, and that the limiting degrees of polarization will be unity for the X nuclei and $-1/5$ for the iron nuclei.

Thus we see that by applying a magnetic field to a ferrite or garnet cooled to an ultralow temperature one can obtain polarization of the nuclei not only of ferromagnetic atoms, but also of many paramagnetic atoms.

Measurements of the nuclear polarization produced can be made by means of nuclear magnetic resonance, with the resonance frequency corresponding to the internal field.[9] In the case of radioactive nuclei the polarization can be observed by studying the angular anisotropy of the $\gamma$ radiation or the angular asymmetry of the $\beta$ radiation. The study of $\beta$ radiation is more advantageous, since it gives a possibility for direct determination of the degree of polarization of the nuclei.

Experiments of this kind can be made not only for the purpose of obtaining polarized nuclei, but also in order to study the properties of ferrites and garnets and of other nonmetallic ferromagnetic materials. In particular, such experiments can be made with so-called mixed ferrites and garnets, for which the structure problem has not yet been finally solved.

---

*This class also includes the ferrite of magnesium, which is ferromagnetic in spite of the fact that the $Mg^{++}$ ion is nonmagnetic.

---

[1] G. R. Khutsishvili, JETP **29**, 894 (1955), Soviet Phys. JETP **2**, 187 (1956).

[2] Grace, Johnson, Kurti, Scurlock, and Taylor, Communications at Conference on Low-temperature Physics, Paris, 1955.

[3] N. Kurti, J. phys. radium **20**, 141 (1959).

[4] Samoĭlov, Sklyarevskiĭ, and Stepanov, JETP **36**, 1366, 1944 (1959), **38**, 359 (1960); Soviet Phys. JETP **9**, 972, 1383 (1959), **11**, 261 (1960).

[5] L. Néel, Ann. phys. **3**, 137 (1948).

[6] F. Bertaut and F. Forrat, Compt. rend. **242**, 382 (1956).

[7] R. Pauthenet, Ann. phys. **3**, 424 (1958).

[8] K. P. Belov, Магнитные превращения, (Magnetic Transitions), Fizmatgiz, 1959.

[9] A. C. Gossard and A. M. Portis, Phys. Rev. Letters **3**, 164 (1959).

Translated by W. H. Furry

---

## *ON THE PROBLEM OF THE DIRECT RECONSTRUCTION OF THE ELASTIC-SCATTERING AMPLITUDE*

G. I. KOPYLOV and Z. D. LOMAKINA*

Joint Institute for Nuclear Research

Submitted to JETP editor March 18, 1960

J. Exptl. Theoret. Phys. (U.S.S.R.) **38**, 1649-1651 (May, 1960)

A paper by Puzikov, Ryndin, and Smorodinskiĭ[1] has dealt with the problem of the reconstruction of the scattering matrix. In particular, it contains a suggestion that phase-shift analysis be replaced by direct solution of the system of equations that follows from the unitarity condition.

We have made an attempt to find a method for solving this system for the simplest case of the scattering of spinless particles by a center of force. In this case one gets the following system of equations for the real part $R(\mu)$ and the imaginary part $I(\mu)$ ($\mu = \cos\vartheta$) of the scattering amplitude ($\sigma$ is the scattering cross section):

$$R^2(\mu) + I^2(\mu) = \sigma(\mu), \tag{1}$$

$$I(\mu) = \frac{k}{4\pi}\int\limits_{-1}^{1}\int\limits_{0}^{2\pi}[I(\mu'')I(\mu') + R(\mu')R(\mu'')]\,d\mu'd\varphi, \tag{2}$$

where

$$\mu'' = \mu\mu' + \sqrt{(1-\mu^2)(1-\mu'^2)}\cos\varphi. \tag{3}$$

It must be remarked that the choice of $I(\mu)$ and $R(\mu)$ as the unknown functions is to be preferred to the description of the complex amplitude by its absolute value and phase, which was suggested in reference 1. The latter description is unstable under small changes of the amplitude.

The system (1) — (2) was solved by Newton's method for functional equations.[2] Instead of the nonlinear equation (2) one gets for the correction $\xi(\mu)$ to the n-th approximation $I_n(\mu)$ the linear integral equation ($k = 1$)

$$\begin{aligned}\xi(\mu) + \frac{1}{2\pi}\iint \xi(\mu')\frac{R_n(\mu'')I_n(\mu') - R_n(\mu')I_n(\mu'')}{R_n(\mu')}\,d\mu'd\varphi \\ = -I_n(\mu) + \frac{1}{4\pi}\iint\Big[R_n(\mu'')R_n(\mu') + I_n(\mu')I_n(\mu'') \\ + R_n(\mu'')\frac{\sigma(\mu') - R_n^2(\mu') - I_n^2(\mu')}{R_n(\mu')}\Big]\,d\mu'd\varphi.\end{aligned} \tag{4}$$

The successive approximations for $I(\mu)$ and $R(\mu)$ are obtained from the formulas

$$I_{n+1} = I_n + \xi, \quad |R_{n+1}| = |\sigma - I_{n+1}^2|^{1/2}.$$

When $R_{n+1}(\mu)$ passes through zero the sign of $R_{n+1}(\mu)$ is fixed by the requirement of continuity of the derivative.

The integrals in Eq. (4) lose their meaning if $R_n(\mu')$ has zeroes $\mu_s$ in the interval $(-1, 1)$. To regularize the integrals we can use their principal values:

$$\Phi(R(\mu)) = \int_{-1}^{1} \frac{\varphi(\mu)}{R(\mu)} d\mu = \int_{-1}^{1} \left[ \frac{\varphi(\mu)}{R(\mu)} - \sum_s \frac{\varphi(\mu_s)}{(\mu-\mu_s) R'(\mu_s)} \right] d\mu + \sum_s \frac{\varphi(\mu_s)}{R'(\mu_s)} \ln \frac{1-\mu_s}{1+\mu_s}. \quad (5)$$

It was found that such applications of the theory of generalized functions assure convergence even in cases in which the numbers of zeroes of the solution and of the zeroth approximation are not the same (see diagram). Equation (4) was solved with an electronic computer by reducing it to an algebraic system of linear equations. The number of equations is then equal to the number of points used in the numerical-integration formula (that of Gauss) plus the number of zeroes of the real part of the scattering amplitude [cf. the factor $\varphi(\mu_s)$ in Eq. (5)]. In the examples solved the number of zeroes does not exceed three, and the number of points for the integration formula was six. As a rule the functions chosen as zeroth approximations were extremely far removed from the actual solutions of the system.

In spite of this, rapid convergence of the iteration process was found in seven out of the ten examples solved. The correction to the zeroth approximation, which was often larger in magnitude than $I_0(\mu)$ and $R_0(\mu)$ themselves, at once gave almost the correct value of $|R(\mu)|$. The next approximation led to the correct value of $I(\mu)$. Three or four approximations were usually enough to get three-figure accuracy (see diagram). The convergence is slower in the three examples in which either R or $R_0$ has no zeroes, i.e., in which the regularization by Eq. (5) either is unnecessary $(R_0 > 0)$ or leads to a $\Phi[R_0(\mu)]$ that differs sharply from $\Phi[R(\mu)]$ $(R > 0$, $R_0$ changes sign). In all ten examples the scattering amplitude in forward directions $(\mu > 0)$ was reconstructed with particularly high accuracy; the reconstruction for R was better than that for I.

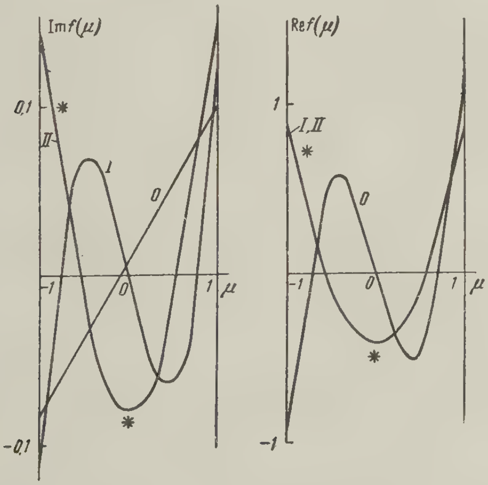

Convergence of the iteration process. Curves 0, I, II are respectively the zeroth, first, and second approximations, and * is the exact solution.

The numerical experiment which we have made allows us to hope that also in the more complicated case of scattering of particles with spin direct solution of the system of nonlinear equations can give the desired scattering matrix, bypassing phase-shift analysis.[1]

For a detailed exposition of the results of the present work, see reference 3.

The authors are grateful to R. M. Ryndin and L. A. Chudov for suggesting this problem.

---

*Staff member, Computation Center, Moscow State University.

---

[1] Puzikov, Ryndin, and Smorodinskiĭ, JETP **32**, 592 (1957), Soviet Phys. JETP **5**, 489 (1957); Nuclear Phys. **3**, 436 (1957).

[2] L. V. Kantorovich and G. P. Akilov, Функциональный анализ в нормированных пространствах, (Functional Analysis in Normalized Spaces), Fizmatgiz, 1959, Chapter 18.

[3] G. I. Kopylov and Z. D. Lomakina, Preprint P-505, Joint Institute for Nuclear Research, Dubna.

Translated by W. H. Furry
318

---

## *ELECTRONIC PARAMAGNETIC RESONANCE OF THE* $Ti^{3+}$ *ION IN CORUNDUM*

L. S. KORNIENKO and A. M. PROKHOROV

Institute of Nuclear Physics, Moscow State University

Submitted to JETP editor March 21, 1960

J. Exptl. Theoret. Phys. (U.S.S.R.) 38, 1651-1652 (May, 1960)

Up to recently, electronic paramagnetic resonance (e.p.r.) of the $Ti^{3+}$ ion was observed only in cesium-titanium alum.[1,2] The authors of these papers mentioned certain difficulties in the interpretation of the results obtained.

We observed e.p.r. of $Ti^{3+}$ ions, introduced isomorphically in the crystal lattice of corundum ($Al_2O_3$), at temperatures of liquid helium. The average concentration of the titanium ions in each of the three investigated samples was several hundredths atomic percent. The investigations were made at wavelengths near 3 cm.

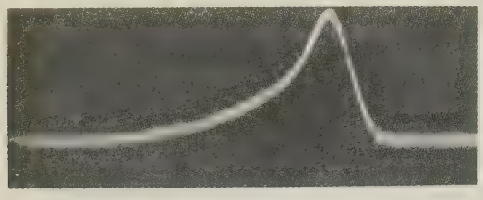

The e.p.r. line of the $Ti^{3+}$ ion in corundum for $\theta = 0°$ (the magnetic field increases to the right).

We observed one e.p.r. line, the shape of which had an unusual asymmetry with a steeper descent on the side of increasing magnetic field (see photograph). An investigation of the behavior of the line with varying angle $\theta$ between the directions of the permanent external magnetic field **H** and the trigonal axis of the electric field of the crystal has shown that the theoretical interpretation can be carried out with the aid of the spin Hamiltonian[3]

$$\hat{H} = g_{\parallel}\beta H_z\hat{S}'_z + g_{\perp}\beta(H_x\hat{S}'_x + H_y\hat{S}'_y),$$

where $g_{\parallel}$ and $g_{\perp}$ are the g factors in directions parallel and perpendicular to the trigonal axis of the crystal field, $\beta$ is the Bohr magneton, and $\hat{S}'$ is the effective-spin operator, with value $S' = \frac{1}{2}$.

The g factors, determined by the points of maximum line intensity, were found to be

$$g_{\parallel} = 1.067 \pm 0.001; \quad g_{\perp} \leqslant 0.1.$$

The estimate of $g_{\perp}$ was made by studying the dependence of the line position on the angle $\theta$ as the latter was varied from 0 to 67 deg. The e.p.r. line was studied here at magnetic field values from 6,000 to 16,000 oe, and the upper estimate of $g_{\perp}$ was chosen to obtain good agreement with the theoretical relationship $H = h\nu/g\beta$, where $g = (g_{\parallel}^2 \cos^2\theta + g_{\perp}^2 \sin^2\theta)^{1/2}$. This estimate of $g_{\perp}$ agrees with the extremely low density of the observed e.p.r. line of the $Ti^{3+}$ ion, the peak value of which at $\theta = 0$ deg is approximately equal to the peak intensity of the e.p.r. lines observed in the same specimens and produced by $Cr^{3+}$ and $Fe^{3+}$ ions at a concentration $10^3$ or $10^4$ times smaller than the concentration of the $Ti^{3+}$ ions. This is explained by the fact that when the high-frequency magnetic field is perpendicular to the external magnetic field the intensity of the absorption line is proportional to the square of the quantity

$$g' = g_{\parallel}g_{\perp}(g_{\parallel}^2\cos^2\theta + g_{\perp}^2\sin^2\theta)^{-1/2}.$$

The width of the e.p.r. line of the $Ti^{3+}$ ion in corundum at $\theta = 0°$, measured between points of maximum slope of the line at 4.2° K, was found to be 50 oe. The shape and the width of the line did not change as the temperature was reduced to 1.55° K. A study of the dependence of the line width (in oersteds) on the angle shows the presence of a considerable deviation from the law $\Delta H = h\Delta\nu/g\beta$, which in this case, assuming $\Delta\nu$ to be constant, can be represented with sufficient accuracy by $\Delta H = \text{const}/\cos\theta$. Actually, the line broadening was much faster, particularly at small values of $\theta$. A satisfactory explanation for this fact can be proposed by assuming for the individual ions a dispersion of order 0.5 to 1° in the directions of the trigonal axis of the crystal electric field, about a certain average direction. At all values of $\theta$, the line retained the characteristic asymmetric form.

When the specimen was heated, the line began to broaden noticeably with increasing temperature, starting with ~ 9° K. This enabled us to estimate the spin-lattice relaxation time $\tau_1$, for the indicated temperature, at approximately $5 \times 10^{-8}$ seconds. We also measure $\tau_1$ by the continuous-saturation method. If it is assumed that $g_{\perp} = 0.1$, the values of $\tau_1$ will be approximately $10^{-4}$ sec at 4.2° K and approximately $10^{-1}$ sec. at 1.55°K. As in the case of the $Co^{2+}$ in corundum,[4] $\tau_1$ has a rather strong temperature dependence at these temperatures. This has not yet been satisfactorily explained.

The authors express their sincere gratitude to R. P. Bashuk, A. S. Bebchuk, and A. A. Popova for preparation of samples for the investigation, and also to G. M. Zverev for useful discussions.

---

[1] D. Bijl, Proc. Phys. Soc. **A63**, 405 (1950).

[2] Bleany, Bogle, Cooke, Duffus, O'Brien, and Stevens, Proc. Phys. Soc. **A68**, 57 (1955).

[3] A. Abragam and M. H. L. Pryce, Proc. Roy. Soc. **A205**, 135 (1951).

[4] G. M. Zverev and A. M. Prokhorov, JETP **39**, 57 (1960), Soviet Phys. JETP **12**, in press.

Translated by J. G. Adashko
319

## *THEORY OF RESONANT INTERACTION OF GAMMA RAYS WITH CRYSTALS*

M. V. KAZARNOVSKIĬ

P. N. Lebedev Physics Institute

Submitted to JETP editor March 28, 1960

J. Exptl. Theoret. Phys. (U.S.S.R.) 38, 1652-1654 (May, 1960)

As Mössbauer has shown, the probability of elastic resonant interaction (without change of the quantum state of the crystal lattice) of gamma rays with nuclei in crystals contains the factor

$$f = \exp\left[g_\infty(T)\right],$$

where

$$g_\infty(T) = -2\sum_s \frac{(\mathbf{p}\mathbf{e}_s)^2}{2m\hbar\omega_s N}\left[\alpha\left(\frac{\hbar\omega_s}{kT}\right)+\frac{1}{2}\right], \quad \alpha(x) = \frac{1}{e^x-1}. \tag{1}$$

Here $\mathbf{p}$ is the momentum of the photon, $T$ is the temperature of the crystal, $m$ is the mass of the atoms in the crystal, $N$ is their density, and $\mathbf{e}_s$ and $\omega_s$ are the polarization and frequency, respectively, of the s-th phonon in the crystal.

Since f depends on $g_\infty(T)$ exponentially, an evaluation of the latter in the Debye approximation[1] is not always satisfactory. If, however, no correlation exists between the direction of the vector $\mathbf{e}_s$ and the frequency $\omega_s$ (as in crystals of cubic symmetry), then $g_\infty(T)$ can be more exactly calculated directly from the experimental data on the heat capacity at constant volume* (referred to a single atom)

$$C_v(T) = 3\frac{d}{dT}\int_0^\infty \nu(\omega)\hbar\omega\alpha\left(\frac{\hbar\omega}{kT}\right)d\omega, \tag{2}$$

where $\nu(\omega)$ is the spectrum of frequencies of the lattice vibrations. It is easy to verify that in this case

$$g_\infty(T) = -(E^2/2mc^2)\left[G_0 + G_1(T)\right], \quad E = pc,$$

$$G_0 = \int_0^\infty \frac{d\omega}{\hbar\omega}\nu(\omega), \qquad G_1(T) = 2\int_0^\infty \frac{d\omega}{\hbar\omega}\nu(\omega)\,\alpha\left(\frac{\hbar\omega}{kT}\right). \tag{3}$$

By direct substitution one obtains

$$G_0 = (\pi k)^{-2}\int_0^\infty C_v(T)\,dT/T^2. \tag{4}$$

By a method similar to that described in reference 3, one can show that

$$G_1(T) = \frac{2}{3}k^{-2}\sum_{n=1}^\infty \int_0^{T/n}\frac{dT'}{T'^2}\left(\frac{1}{T'}-\frac{n}{T}\right)\psi(T'),$$

$$\psi(T) = \sum_{n=1}^\infty \mu_n \int_0^{T/n} C_v(T')\,dT', \tag{5}$$

where $\mu_1 = 1$, $\mu_{n\pm1} = (-1)^l$ if n is the product of $l$ different prime numbers, and $\mu_n = 0$ in all remaining cases.

The values of $g_\infty(0)$ computed from the specific data[2,4] for $Ir^{191}$ (E = 129 kev) and $Zn^{67}$ (E = 93 kev)† are −2.75 and −5.6, respectively. From the experiments[5] on the resonant interaction of gamma rays in $Ir^{141}$ one obtains $g_\infty(0) = -3.0 \pm 0.3$.

In conclusion the author expresses his gratitude to A. V. Stepanov and F. L. Shapiro for helpful discussions.

---

*Strictly speaking, formula (2) gives only that part of $C_v$ which arises from the lattice vibrations. Therefore one should subtract the electronic heat capacity from the experimental values of $C_v$ before substitution into formulas (4) and (5). As is shown by the numerical calculation of $g_\infty(0)$ for $Ir^{191}$, however, the pertinent correction amounts to 3% in all, as the Debye temperature (in particular its dependence on T) varies considerably[2] in the calculation of this correction.

†As is known, $Zn^{67}$ can be used for measuring the red shift in the laboratory.

---

[1] R. L. Mössbauer, Z. Physik **151**, 124 (1958); Naturwiss. **45**, 538 (1958); Z. Naturforsch. **14a**, 211 (1959).

[2] K. Clusius and C. G. Losa, Z. Naturforsch. **10a**, 545 (1955).

[3] M. V. Kazarnovskiĭ, JETP **31**, 696 (1956), Soviet Phys. JETP **4**, 600 (1957).

[4] W. Eichenauer and M. Schulze, Z. Naturforsch. **14a**, 28 (1959).

[5] Craig et al., Phys. Rev. Lett. **3**, 221 (1959).

[6] Barit, Podgoretskiĭ, and Shapiro, JETP **38**, 301 (1960), Soviet Phys. JETP **11**, 218 (1960).

Translated by J. Heberle
320

---

## *NEW ISOTOPE* $Te^{115}$

I. P. SELINOV, N. A. VARTANOV, D. E. KHULELIDZE, Yu. A. BLIODZE, N. G. ZAĬTSEVA, and V. A. KHALKIN

Submitted to JETP editor March 29, 1960

J. Exptl. Theoret. Phys. (U.S.S.R.) 38, 1654 (May, 1960)

On the basis of the systematics of radioisotope half-lives, it was hypothesized that the unknown $Te^{115}$ isotope decays with $T \approx 7$ min, changing into the recently discovered isotope $Sb^{115}$ (T

= 32 min).[1] To observe the new isotopes, a tin foil enriched with $Sn^{112}$ (52.3%) was irradiated in a cyclotron by 21-Mev $\alpha$ particles. The foil and the chemically separated tellurium and antimony fractions were investigated with end-window counters and with a one-channel scintillation $\gamma$ spectrometer. In the tellurium fraction containing elemental tellurium (precipitated by tin chloride) there was observed an activity with T = 6 min belonging to the new isotope $Te^{115}$ formed in the reaction $Sn^{112}(\alpha, n)Te^{115}$.

In order to make a positive identification of this isotope, we carried out a fractional separation (in intervals of 5 min) of the isotope $Sb^{115}$ (T = 32 min) by precipitating the antimony with hydrogen sulfide from the solution containing the tellurium. After the activity of the antimony decreased, it was found that the half-life of $Te^{115}$, which is the parent of $Sb^{115}$, is 6.0 ± 0.5 min.

The authors express their gratitude to E. N. Khaprov and the cyclotron crew for irradiating the target.

---

[1] Selinov, Grits, Kushakevich, Bliodze, Vasil'ev, and Mikhaleva, Атомная энергия (Atomic Energy) No. 7, 547 (1959).

Translated by E. Marquit
321

# ON NEW STRANGE PARTICLES

B. PONTECORVO

Joint Institute for Nuclear Research

Submitted to JETP editor March 31, 1960

J. Exptl. Theoret. Phys. (U.S.S.R.) 38, 1654-1656 (May, 1960)

THE Gell-Mann systematics of elementary particles[1] provides for the possibility of the existence of as yet unknown baryons and mesons, in particular of particles $Z^+$ (T = 0, S = +1, baryon number N = 1) and $D^+$ (T = 0, S = +2, N = 0). At the present time there are strong arguments which indicate that the $Z^+$ baryon does not exist. In fact, if the mass of the $Z^+$ baryon is such that it can decay by the scheme $Z^+ \rightarrow \pi + N$, then it would have been found already without difficulty, and if its mass is close to that of the nucleon, it could be formed along with the $\Lambda$ particle in a reaction of the type $p + n \rightarrow Z^+ + \Lambda^0$, which is excluded by the experiments.[2]

At the conference on high-energy particle physics in Kiev, Wang Kang-Ch'ang and his co-workers[3] reported an interesting event of the interaction of a $\pi$ meson in a bubble chamber, which can be interpreted by assuming the existence of a new particle — a D particle with mass ~ 750 Mev, which decays by the scheme

$$D^+ \rightarrow K + \pi \begin{cases} K^0 + \pi^+ \\ K^+ + \pi^0. \end{cases}$$

If we identify this particle with the positive meson of strangeness +2 predicted by Gell-Mann, then the lifetime expected for the hypothetical D particle is of the order of $10^{-10}$ sec. In fact, the isotopic spin of the $(K\pi)$ system can be ½ or 3/2, so that the selection rule $\Delta T = ½$ cannot hinder the decay, as it does in the case of the decay of the $K^+$ meson.

It is assumed below that the lifetime of the hypothetical D particle does not exceed a few times $10^{-10}$ sec, so that it is not possible to get collimated beams of these particles by ordinary methods. Therefore it is desirable to look for new methods for detecting these particles. A special property of the new particle, which distinguishes it from all the well known particles, is that it decays with the emission of a K meson. This property can be used in the following way. Let us think of a target bombarded by high-energy particles. In the vacuum near the target K mesons will be produced by the decay of D particles, and these mesons can be registered after they have passed through a collimator that does not point toward the target. This method is reminiscent of that of Garwin, in which strange particles were studied by registering the $\gamma$ rays from the decay of $\pi^0$ mesons emitted "in vacuum" by strange particles (cf. e.g. reference 2).

The ratios of the intensities of K and $\pi$ mesons from the target and from the "vacuum" near the target are respectively characterized, roughly speaking, by the fractions of interactions in the target that lead to the production of the strange particles and the relative probabilities for production of D particles and ordinary strange particles. It is clear that if the probability of production of D particles is minute, then $(K/\pi)_{vac} \ll (K/\pi)_{targ}$.

If, for example, we assume that the number of D mesons produced is $\sim 10^{-4}$ of the number of interactions produced in the target by protons of energy ~ 10 Bev, and the number of K mesons is $\sim 10^{-2}$ of this number of interactions, then about 1 percent of the total K-meson beam has the D-particle nature. At a distance of several meters from the target the intensity of the K mesons that are of pure $\pi$-meson (sic) character, i.e., that are obtained under conditions in which the detector cannot see the target, will be $\sim 100\,\alpha$ times smaller than the intensity of the K mesons from the target. The factor $\alpha$ ($\gtrsim 10$) takes account of the loss of intensity caused by the fact that the K mesons from the D particles are emitted at some distance from the target.

Let us consider first the emission of $K^0$ mesons from D particles. As is well known, half of the neutral K mesons ($K_2^0$) have a lifetime $\sim 10^{-7}$ sec,[4] and can be detected at a distance of several meters from the target of the proton synchrotron under conditions of good collimation that assure that the detector cannot see the target. The shielding of the detector from the target must be massive. Unfortunately, the efficiency of detection of $K_2^0$ mesons is small, but calculation shows that with a proton synchrotron that has high intensity ($10^{10} - 10^{11}$ protons/pulse) the experiment is feasible with registration of the $K_2^0$ mesons by means of a large decay Wilson chamber, bubble chamber, or emulsion chamber. In the experimental arrangement we are considering the target is not visible, and therefore the main background will be due to photons from the decay of the $\pi^0$ mesons emitted by strange particles and to neutrons from the decay of strange particles.

It is convenient to secure registration of $K_2^0$ mesons in photographic plates by using the capacity of the $K_2^0$ mesons to produce hyperfragments.[5] Whatever method is used, one must measure the ratio $K_2^0/\pi^0$ from the target and from vacuum.

The registration of the $K^+$ mesons from $D^+$ particles ($D^+ \rightarrow K^+ + \pi^0$) decaying near the target is possible by means of an emulsion chamber or by electronic methods for registering particles. In this case also the criterion for the existence of D particles must be found in comparable values of $(K^+/\pi)_{\mathrm{targ}}$ and $(K^+/\pi)_{\mathrm{vac}}$.

In the planning of such experiments attention must be given to the fact that the K meson from the decay of a D particle with mass 750 Mev can be emitted at a large angle with the direction of the parent D particle only if the latter has a small energy. This complicates the problem of making the target invisible to the K-meson detector if the decaying D particles have energies larger than say 100 Mev (for $E_D = 100$ Mev the limiting angle of emission of K mesons is close to 43°, and the limiting angle decreases rapidly with decrease of the energy of the D mesons). We note, however, that the emission of "slow" mesons at large angles in collisions of protons with complex nuclei must be a relatively frequent phenomenon. We can judge this from the analogy with the case of emission of $K^0$ mesons at angle 90° by protons of energy 6 Bev (the average energy of the $K^0$ mesons is close to 50 Mev).[5] We remark that favorable conditions for the experiment correspond to a K-particle collimator that looks at a region near the target and above (or below) it. This arrangement decreases the background from the walls of the chamber and also is a convenient way to make possible the observation of K particles emitted at angles $\gtrsim 45°$ with the direction of the D particles.

In conclusion we remark that if the $D^+N$ forces are attractive, $D^+$ particles must form D nuclei, in which the D particle lives in nuclear matter up to its (quasi-free) decay. This is due to the fact that even in the presence of several nucleons there is no possibility of the D particle's experiencing strong-interaction processes.

It is a pleasure to thank V. I. Veksler, Chou Kuang-Chao, M. Ya. Danysh, and M. I. Podgoretskiĭ for interesting discussions.

---

[1] M. Gell-Mann, Suppl. Nuovo cimento **4**, 848 (1956).

[2] Balandin, Balashov, Zhukov, Pontecorvo, and Selivanov, JETP **29**, 265 (1955), Soviet Phys. JETP **2**, 98 (1956).

[3] Wang Kang-Ch'ang, Nineth Conference on the Physics of High-energy Particles, Kiev, 1959 (in press).

[4] Bardon, Lande, Lederman, and Chinowsky, Ann. of Phys. **5**, 156 (1958).

[5] Baldo-Ceolin, Dilworth, Fry, Greening, Huzita, Limentani, and Sichirollo, Nuovo cimento **6**, 130 (1957). Camerini, Fry, Baldo-Ceolin, Huzita, and Natali, Phys. Rev. **115**, 1048 (1959).

Translated by W. H. Furry
322